NASA Contractor Report 4461

Design, Analysis, and Testing of the Phase 1 CSI Evolutionary Model Erectable Truss

M. J. Gronet, D. A. Davis, D. H. Kuntz,
R. D. Brillhart, and E. M. Atkins

CONTRACT NAS1-19241
AUGUST 1992

NASA

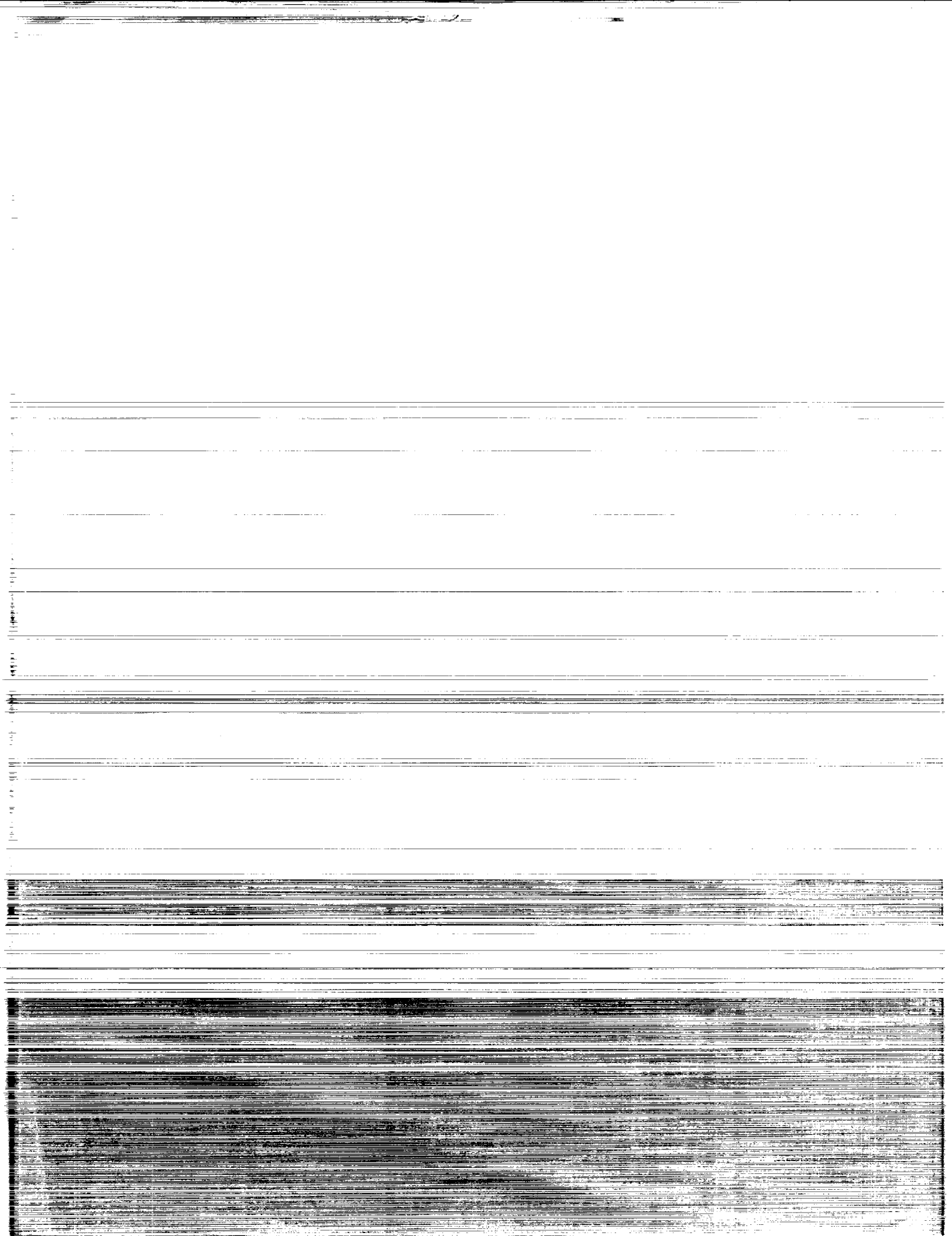

NASA Contractor Report 4461

Design, Analysis, and Testing of the Phase 1 CSI Evolutionary Model Erectable Truss

M. J. Gronet, D. A. Davis, and D. H. Kintis
Lockheed Missiles & Space Company, Inc.
Sunnyvale, California

R. D. Brillhart and E. M. Atkins
Structural Dynamics Research Corporation
San Diego, California

Prepared for
Langley Research Center
under Contract NAS1-19241

NASA
National Aeronautics and
Space Administration
Office of Management
Scientific and Technical
Information Program
1992

Table of Contents

APPENDICES

List of Acronyms

ADF	Associated Data File
AEC-Able	AEC-Able Engineering Company, Inc.
CBAR	NASTRAN Bar Element
CCW	Counter-Clockwise
CEM	CSI Evolutionary Model
CGM	Cross-Generalized Mass
CPU	Central Processing Unit
CSI	Controls-Structures Interaction
CW	Clockwise
DCDT	Direct Current Linear Variable Displacement Transducer
DEC	Digital Equipment Corporation
DOF	Degrees-of-Freedom
DSMT	Dynamic Scale Model Technology
EMF	Electromotive Force
FEM	Finite Element Model
FFT	Fast Fourier Transform
FRF	Frequency Response Function
HP	Hewlett Packard
IRS	Improved Reduction System
LaRC	Langley Research Center
LMSC	Lockheed Missiles & Space Company, Inc.
MAC	Modal Assurance Criterion
MIF	Mode Indicator Functions
MIMO	Multiple Input-Multiple Output
MMIF	Multivariate Mode Indicator Functions
NASA	National Aeronautics & Space Administration
OD	Outer Diameter
PC	Personal Computer
RMAC	Root Modal Assurance Criterion
SDRC	Structural Dynamics Research Corporation
SIMO	Single Input-Multiple Output
SS	Stainless Steel
SSD	Space Systems Division
TAM	Test-Analysis Model
UTM	Universal Test Machine
XO	Cross-Orthogonality

List of Symbols

Variables

E	Modulus of Elasticity
K	Stiffness
L	Length
M	Mass
W	Weight
ϕ	Mode Shape
η	Efficiency
ρ	Density
ω	Frequency

Subscripts

al	aluminum
eff	effective
j	joint
t	tube

Acknowledgements

The authors wish to acknowledge the LMSC, AEC-Able, and SDRC team members who contributed significantly to the success of this effort: Don Werner and Mark Tan (LMSC Dynamic Test Team), Jim Champagne, Roger Mihara, Doug Pensinger, and Ken Perry (LMSC Static Test Team); Bob Crawford, Ray Garza, Mike Evermen, and Pat Reyna (AEC-Able Design and Fabrication Team); Bill Robinson (LMSC Subcontracts), and Dave Hunt (SDRC Dynamic Test Team). The support and direction of Jerry Newsom, Rudeen Smith-Taylor, Brantley Hanks, Keith Belvin, Lucas Horta, Ken Elliott, and John Teter of NASA/LaRC is also gratefully acknowledged. The timely support of Sharon Harper is also sincerely appreciated.

1.0 EXECUTIVE SUMMARY

The NASA Langley Research Center has an ongoing program of focused research in the development of Controls-Structures Interaction (CSI) technology. To validate spacecraft advanced control design methodology and hardware implementation, an evolutionary testbed referred to as the CSI Evolutionary Model (CEM) has been developed. There are three planned phases for the CEM. The Phase 0 CEM (Figure 1-1) is based on a classic truss design containing uniform strut sizes, nominal sensor and actuator placement, and a controller design based on a fixed plant. The Phase 1 CEM is based on an integrated controller and structure design, whereby both structure and controller design variables are sized simultaneously. The overall structural geometry and actuator/sensor locations in the Phase 1 CEM are the same as in the Phase 0 CEM, with the exception that the truss strut stiffness and mass are tailored. Performance and stability comparisons will be made between the Phase 1 and Phase 0 designs in order to assess the benefits of integrated controller and structure design. While the Phase 0 and 1 CEM are both linear, time-invariant systems, the planned Phase 2 CEM will be designed to investigate appendage articulation for the study of time varying dynamics typical of multiple-payload platforms.

This report addresses the design, analysis, and testing of the Phase 1 CEM erectable truss structure performed under Contract NAS1-19241 to the NASA Langley Research Center.

1.1 BACKGROUND

In the integrated design analysis performed by NASA/LaRC using their CSI DESIGN Code[1,2], the CEM Phase 1 structure was divided into seven sections (Figure 1-2). Each of these sections contains three types of struts (Battens, Longerons, and Diagonals), resulting in a total of 42 strut stiffness and mass parameters. The 42 parameters are reduced to 21 design variables through the introduction of empirical curves which relate strut mass and stiffness. Constraints placed on the integrated design algorithm keep the total weight of the Phase 1 CEM at or below that of the Phase 0 CEM. The objective of the contracted effort discussed in this report was to design and fabricate a truss structure with parameters as close as reasonably possible to those resulting from the Phase 1 integrated design analysis.

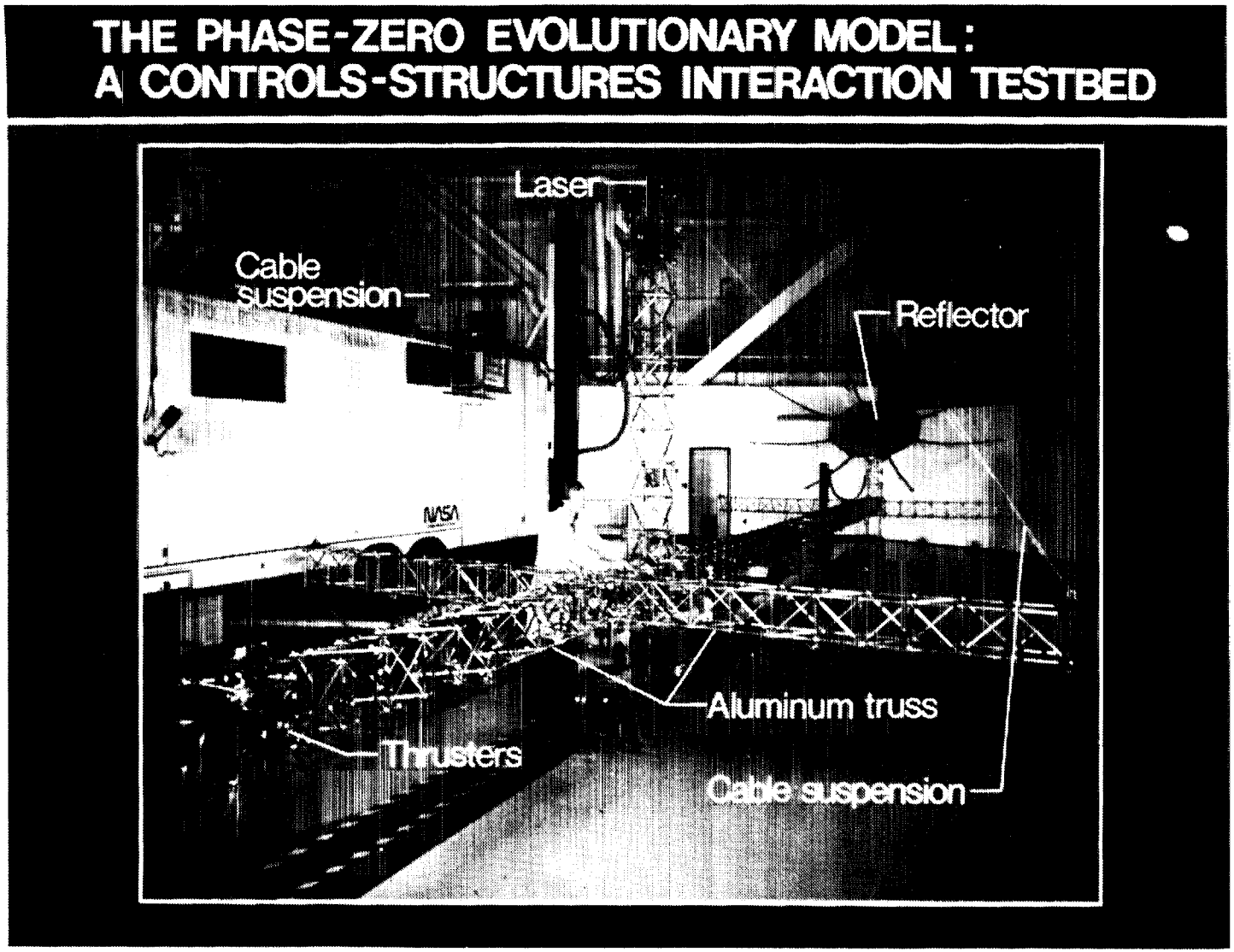

Figure 1-1 Phase 0 CSI Evolutionary Model

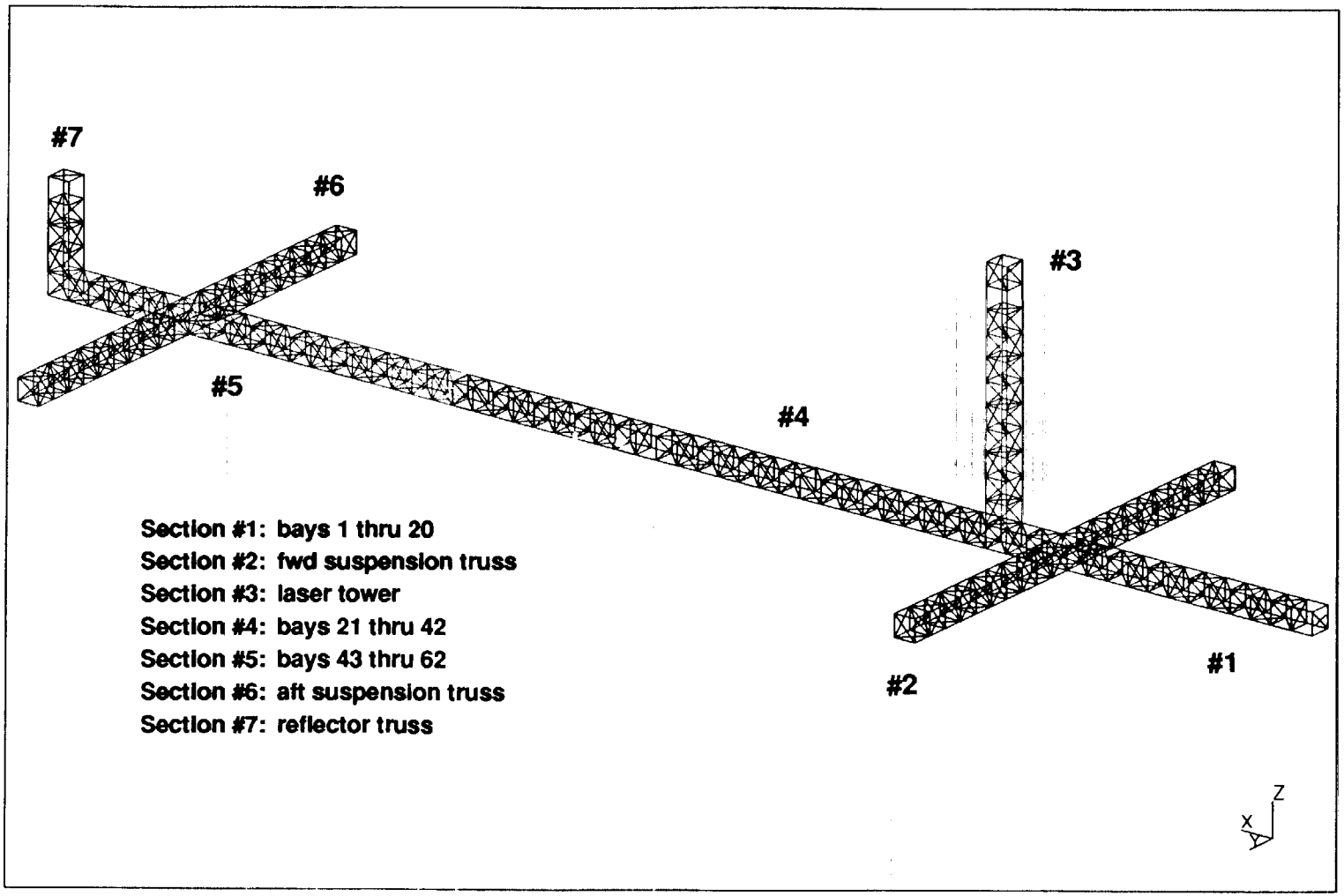

Figure 1-2 Phase 1 CEM Truss Sections

1.2 APPROACH

The approach for this task involved a rapid development, production, and test effort to complete the Phase 1 CEM structure. The effort started with an iterative development phase during which prototype struts were designed and fabricated by AEC-Able and tested by LMSC. At the completion of the development phase, empirical design curves for strut mass and stiffness were established. The baseline design features a single erectable joint that is used for all of the struts. The strut stiffness is tailored by changing the cross-sectional area of the strut tube. Once satisfactory struts were developed, the empirical design curves were input into the integrated design analysis using the NASA/LaRC CSI DESIGN Code. The results provided the tube sizing requirements for the production struts.

The fast-paced production and testing effort involved fabricating 1,799 struts and conducting 150 individual strut static tests, 8 truss section static tests, 8 truss section dynamic tests, and a modal test of the assembled CEM structure in less than four months. Figure 1-3 illustrates the tests that were conducted in order to quantify the CEM Phase 1 structural performance at the strut level, the 10-bay truss section level, and the assembly level. The strut and truss section tests were performed by LMSC in Sunnyvale, California, while the CEM assembly test was performed by SDRC in the Space Structure Research Laboratory at NASA/LaRC. All static tests were conducted over the load range of expected use, and the truss orientation and individual member locations were preserved throughout the different levels of testing. Testing of the hardware was conducted in parallel with the fabrication effort, beginning as each truss section came off the production line. Before delivery and assembly at NASA/LaRC, each strut was weighed and inspected, and all test data was referenced to the identification number marked on each strut. Pre-test analyses were conducted using analytical models provided by NASA/LaRC. After spot checks to validate the quality of the data, all test data was delivered to NASA/LaRC for analytical model correlation, which was outside the scope of the contracted effort.

1.3 SUMMARY

The CEM Phase 1 structure was fabricated, tested, and delivered on schedule. The test results indicate that the structure meets all functional requirements, and that the static and dynamic properties of the structure are predictable, well-characterized, and

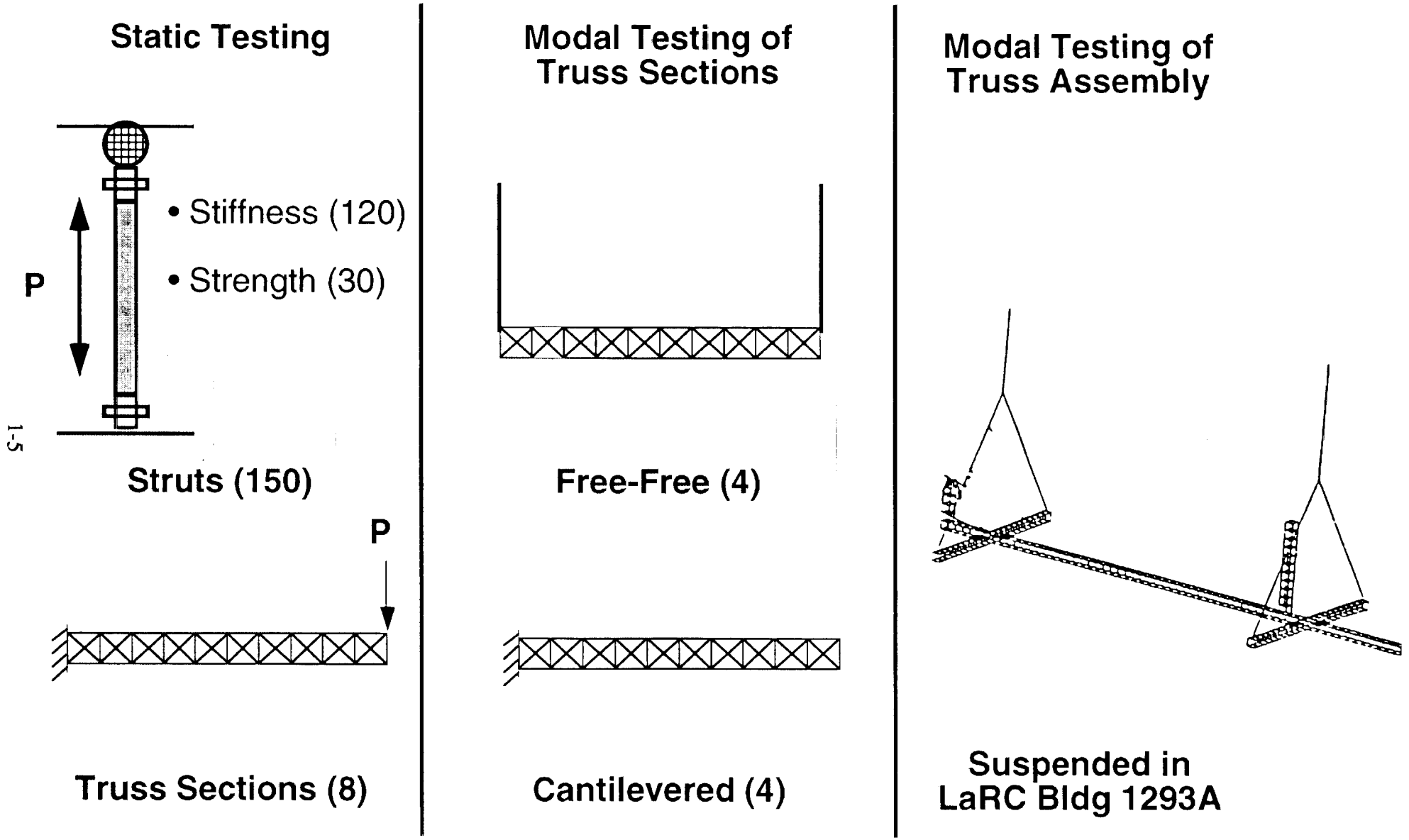

Figure 1-3 CEM Phase 1 Structural Testing

within the performance requirements established during the Phase 1 CEM integrated controller/structure design analysis.

All of the CEM Phase 1 strut sizes use a common erectable joint design which is based on a "pipe union" mechanism concept. This concept uses a nut that is torqued over a threaded tube to preload the connection (Figure 1-4). Four design and test iterations using different joint concepts were required to achieve a successful joint and strut design. It allows for any strut to be removed and replaced without disassembly of the other struts in a given truss bay. Due to the convergence of many of the strut design variables to the same values, the 21 different strut sizes were reduced to six unique strut designs: four longerons, one common batten, and one common diagonal. This resulted in four unique truss sections (sections 2, 6 & 7 are identical as well as 4 and 5). Assembly of the Phase 1 CEM structure in the NASA/LaRC Space Structures Research Laboratory was accomplished without difficulty in less than two days. Further details on the design description, key trades and lessons learned, and the quality assurance results are provided in Section 2.0.

One hundred twenty static stiffness tests and thirty strength tests were performed on individual struts to quantify their respective properties. The results indicate that the production struts generally meet or exceed the stiffness and weight requirements, as shown in Table 1-1. The small average errors (less than 1.3%) and standard deviations (less than 1.8%) in the test data indicate that the strut stiffness is very consistent over the sample size of 10 struts. Nonlinearities are on the order of +/- 1% of the average stiffness value over the desired load range. Repeatability tests show that the experimental uncertainty is on the order of 0.5% or less. The weight values for the struts indicate that the assembled Phase 1 CEM will weigh the same or slightly less than the Phase 0 CEM, as required. The strength test results indicate that a positive margin of safety exists for ultimate strength, using a factor of safety of two. Detailed information describing the struts stiffness and strength tests and the associated results is provided in Section 3.0.

Modal tests of 10-bay sections of the CEM Phase 1 truss were performed. Tests were conducted on the four unique CEM Phase 1 truss sections in both free-free and cantilevered configurations. Comparisons between the test data and analytical predictions using the updated measured weight and stiffness properties from the individual strut tests (Table 1-1) show that the frequencies and mode shapes of the truss are predictable and linear. Excellent agreement was obtained for the seven target modes for each truss section, consisting of the first and second bending mode pairs, the first and second torsion modes, and the first axial mode. For all eight tests, the average frequency error is only 2.7% for the bending and torsion modes and 5.1%

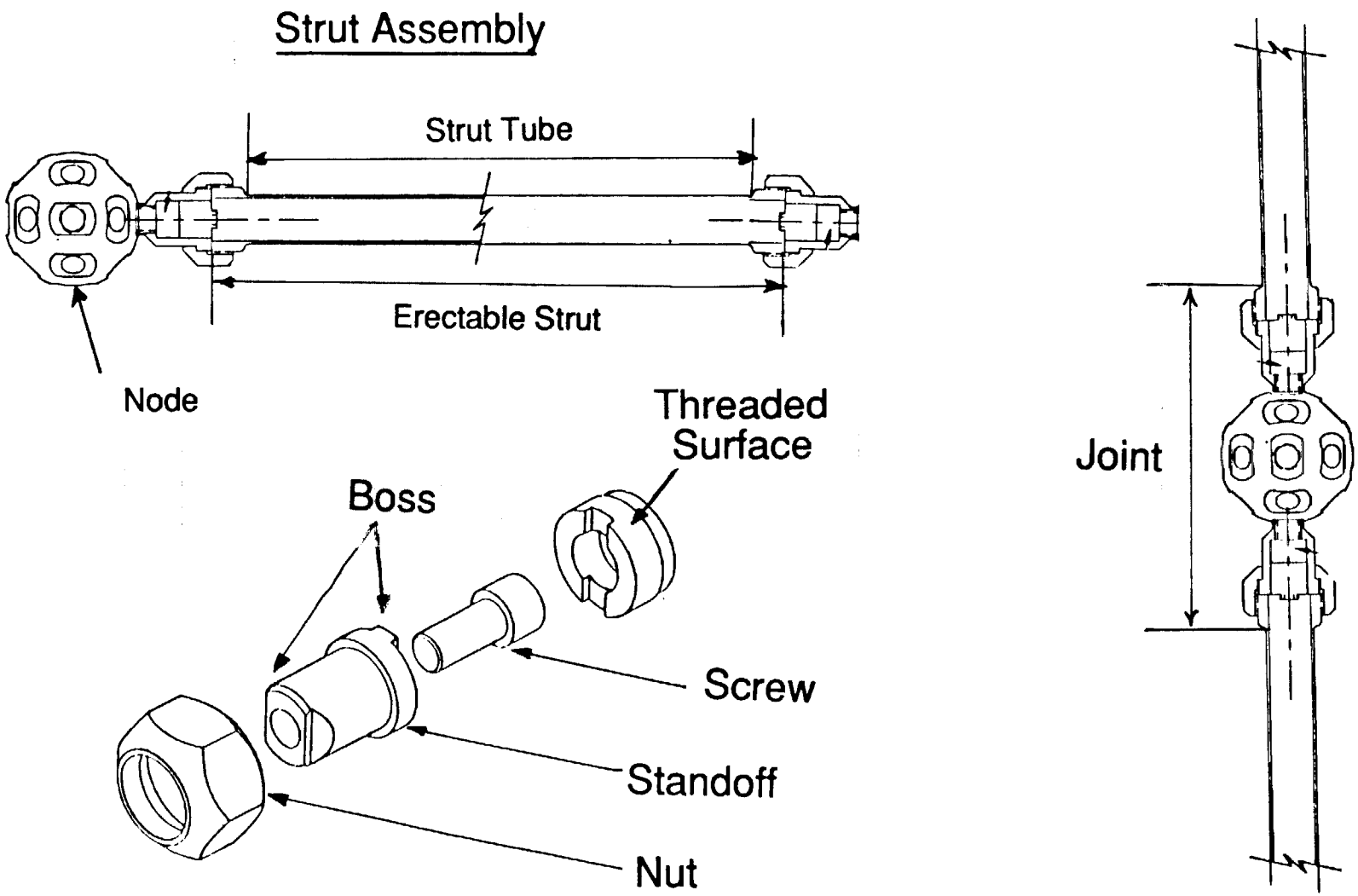

Figure 1-4 CEM Phase 1 Strut Design Features and Nomenclature

Table 1-1 CEM Phase 1 Strut Performance

SEC #	STRUT ID (Revised)	QTY with Spares	QTY Assy	Nominal Stiffness (lb/in)	Nominal Wt (lbs) (With 31% Node Ball)	Actual Stiffness (lb/in)	Actual Wt (lbs) (With 31% Node Ball)
Longerons							
1	1L	94	80	330,000	0.531	332,549	0.516
2	2L	94	80	85,387	0.276	99,125	0.272
3	3L	52	44	173,350	0.327	174,649	0.320
4	4L	104	88	260,300	0.411	264,236	0.402
5	4L	94	80	257,470	0.407	264,236	0.402
6	2L	94	80	95,226	0.280	99,125	0.272
7	2L	19	16	95,552	0.280	99,125	0.272
Battens							
1	B	99	84	81,898	0.274	97,359	0.269
2	B	94	80	82,951	0.274	97,359	0.269
3	B	52	44	82,155	0.274	97,359	0.269
4	B	104	88	81,797	0.274	97,359	0.269
5	B	94	80	80,792	0.273	97,359	0.269
6	B	94	80	80,941	0.274	97,359	0.269
7	B	19	16	81,432	0.274	97,359	0.269
Diagonals							
1	D	119	101	62,906	0.311	58,791	0.294
2	D	118	100	59,765	0.306	58,791	0.294
3	D	65	55	58,300	0.304	58,791	0.294
4	D	130	110	57,417	0.303	58,791	0.294
5	D	118	100	55,924	0.301	58,791	0.294
6	D	118	100	56,098	0.301	58,791	0.294
7	D	24	20	57,789	0.304	58,791	0.294

for the axial modes. Shape comparisons were near-perfect for all modes, with the exception of a few axial modes. This excellent agreement between the predicted and updated analytical models suggests that little model correlation is required, if any. Further information regarding the modal testing of the 10-bay truss sections is provided in Section 4.0.

Eight bending and torsional static tests were performed on the same four cantilevered 10-bay truss sections that were tested dynamically. The data is represented by tight, linear, and repeatable force-displacement curves characteristic of a well-preloaded, stiff, erectable structure with little or no hysteresis. Spot checks show that good agreement was achieved with analytical predictions obtained from models updated using the measured individual strut properties (Table 1-1), corroborating the results of the dynamic tests. Further information on the static 10-bay section tests is provided in Section 5.0.

Finally, a series of modal tests were conducted on the assembled CEM Phase 1 structure suspended in the Space Structures Research Laboratory at NASA/LaRC. The results of these tests show very good agreement between the pretest analysis modes and the test results. Frequency errors for the twenty-four primary flexible modes below 32 Hz are less than 6%, and cross-generalized mass values are greater than 90%. Substantially more modes, however, were identified in the test than in the pre-test efforts. This is believed to be the result of the modeling of the suspension cables. Because the cables are meshed as a single element, the pre-test model is incapable of predicting cable bending modes and their interaction with the test article. The modeling of the suspension cables should be updated during the planned post-test model correlation effort. Further information on the assembled CEM Phase 1 modal tests is provided in Section 6.0. Strut drawings, test setup information, and additional test data are included in the Appendices.

2.0 STRUT DESIGN

This section describes the individual CEM Phase 1 strut requirements, design, and the associated component materials and properties. Section 2.1 describes the strut requirements, many of which were derived from the results of integrated control-structure design analyses performed by NASA/LaRC using the CSI DESIGN Code. Section 2.2 describes the strut design features and some of the key design trades. Finally, Section 2.3 reviews the quality assurance data on production strut component tolerances and weights.

2.1 STRUT REQUIREMENTS

The geometry and truss configuration for the CEM Phase 1 truss are based on matching the CEM Phase 0 design. Thus, the Phase 0 and Phase 1 CEM bay size and diagonal pattern are identical, resulting in a longeron or batten strut length of 10.0 inches and a diagonal length of 14.142 inches. These dimensions are measured from the centroid of the Node Ball at each end of the strut.

Table 2-1 lists the stiffness, maximum weight, and load range requirements for the CEM Phase 1 struts corresponding to the seven different sections illustrated in Figure 1-2. Also included are the quantities required to assemble each section and the number of spares to be delivered. The nominal stiffness and weight requirements are derived from the results of integrated control-structure design optimization analyses performed by NASA/LaRC using the CSI DESIGN Code. The stiffness requirements include linearity over the associated load range as a desired goal. The weight requirements assume that 31% of the Node Ball weight is allocated to each strut. This percentage is derived from the repeatable elements of the truss configuration with the negligible exception of the seven exposed end faces of the truss.

The load range requirements are derived from the results of static finite element analyses of the suspended CEM Phase 1 configuration. They include an additional allocation of 300 lbs to account for dynamic loads. A factor of safety of two for ultimate strength of the struts is required. Note that some of the least stiff struts have the highest static loads.

Table 2-1 CSI Strut Requirements

SEC #	STRUT ID (Revised)	QTY with Spares	QTY Assy	Nominal Stiffness (lb/in)	Nominal Wt (lbs) (With 31% Node Ball)	Static Load Range (+/- lbs)	Total Load Range (+/- lbs)
Longerons							
1	1L	94	80	330,000	0.531	387	687
2	2L	94	80	85,387	0.276	823	1123
3	3L	52	44	173,350	0.327	22	322
4	4L	104	88	260,300	0.411	289	589
5	4L	94	80	257,470	0.407	419	719
6	2L	94	80	95,226	0.280	834	1134
7	2L	19	16	95,552	0.280	46	346
		551	468				
Battens							
1	B	99	84	81,898	0.274	792	1092
2	B	94	80	82,951	0.274	87	387
3	B	52	44	82,155	0.274	3	303
4	B	104	88	81,797	0.274	3	303
5	B	94	80	80,792	0.273	829	1129
6	B	94	80	80,941	0.274	88	388
7	B	19	16	81,432	0.274	1	301
		556	472				
Diagonals							
1	D	119	101	62,906	0.311	121	421
2	D	118	100	59,765	0.306	122	422
3	D	65	55	58,300	0.304	4	304
4	D	130	110	57,417	0.303	48	348
5	D	118	100	55,924	0.301	111	411
6	D	118	100	56,098	0.301	123	423
7	D	24	20	57,789	0.304	2	302
		692	586				
TOTALS		1799	1526				

The CEM Phase 1 strut functional requirements include the capability of (1) assembling the CEM Phase 1 structure and (2) the capability of removing any strut or struts from the assembled truss without having to take the entire truss bay apart. The latter capability is an improvement over the Phase 0 CEM. The latter capability also implies a requirement to provide sufficient access for a tool to be able to tighten or loosen any joint in the assembled CEM Phase 1 configuration.

2.2 STRUT DESIGN

During the development phase, six design and test iterations were required by the LMSC/AEC-Able team to meet all of the strut requirements described in the previous section. At the end of development, the resultant "pipe union IV" design was driven by a variety of factors, including cost and schedule time (Table 2-2). The stiffest strut (1L Longeron) provided the greatest challenge in terms of meeting the stiffness, weight, and linearity requirements. The highly-loaded but least stiff strut (Batten) provided the greatest challenge for strength. Only the final production design is described in this report.

Figures 2-1 and 2-2 show the design features and associated nomenclature. As a repeatable element of the truss, the strut assembly actually contains two half Node Balls (one at either end), but is shown equivalently as having one full Node Ball at one end. Two threaded connections at either end of the erectable strut are used to construct and preload the strut assembly. First, the Standoff is fastened to the Node Ball using the Screw. Second, the Standoff is connected to the end of the Erectable Strut by torquing the Nut over the threaded end of the Erectable Strut. Slots in the Node Ball and at the end of the Erectable Strut and bosses at either end of the Standoff provide torque restraints, reducing the number of assembly tools required. Torque values shown in Figure 2-1 are based on the NASA standard.

The joint components (Node Balls, Standoffs, Screws, and Nuts) are identical for all of the strut sizes outlined in Table 2-1. Because the stiffness and weight requirements for the 2L, 6L and 7L Longerons are very close, a single strut tube design was used, corresponding to the -2 item on the schedule in Figure 2-2. For the same reason, the 4L and 5L Longerons were designed as a single strut size (-4), as well as all of the Battens (-5) and Diagonals (-6). This reduction from 21 to 6 different strut sizes significantly reduced the cost and schedule time without impacting the Phase 1 CEM structural performance. Detailed drawings of the strut components are provided in Appendix A.

Table 2-2 CEM Phase 1 Strut Design Progression

Joint Design	Design Features						Improvements	Performance			
	Node OD, in	Node Mat'l	Node Wt, lb	Node Thread	Tube/Lug Joint	Joint Length	to Joint and/or Strut	Stiffness Range	η	Linearity	Strength
NASA/LaRC Button	1.6	AL6061	0.196	1/4-20	Bonded AL6061	7.684"	37% Increase in Eff vs DSMT Joint	X	X	X	√
Band-Clamp	1.4	AL6061	0.104	5/16-24	Welded AL6061	4.074"	Increased Joint & Strut Efficiency	X	√	√	-
Pipe Union I	1.4	AL6061	0.104	5/16-24	Welded AL6061	4.074"	Increased Joint & Strut Efficiency	X	√	√	-
Pipe Union II	1.4	AL7075		1/4-20	Welded AL6061	4.074"	Not Tested	-	-	-	-
Pipe Union III	1.5	AL7075	0.159	5/16-24 Alloy	Welded AL6061	4.197"	Ease of Assembly Wide Aeff Range Torque Restraint 303 SS Standoff	√	√	√	X
Pipe Union IV	1.5	AL7075	0.160	5/16-24 Alloy	1-Piece AL2024	4.072"	Improved Strut Tube Strength	√	√	√	√

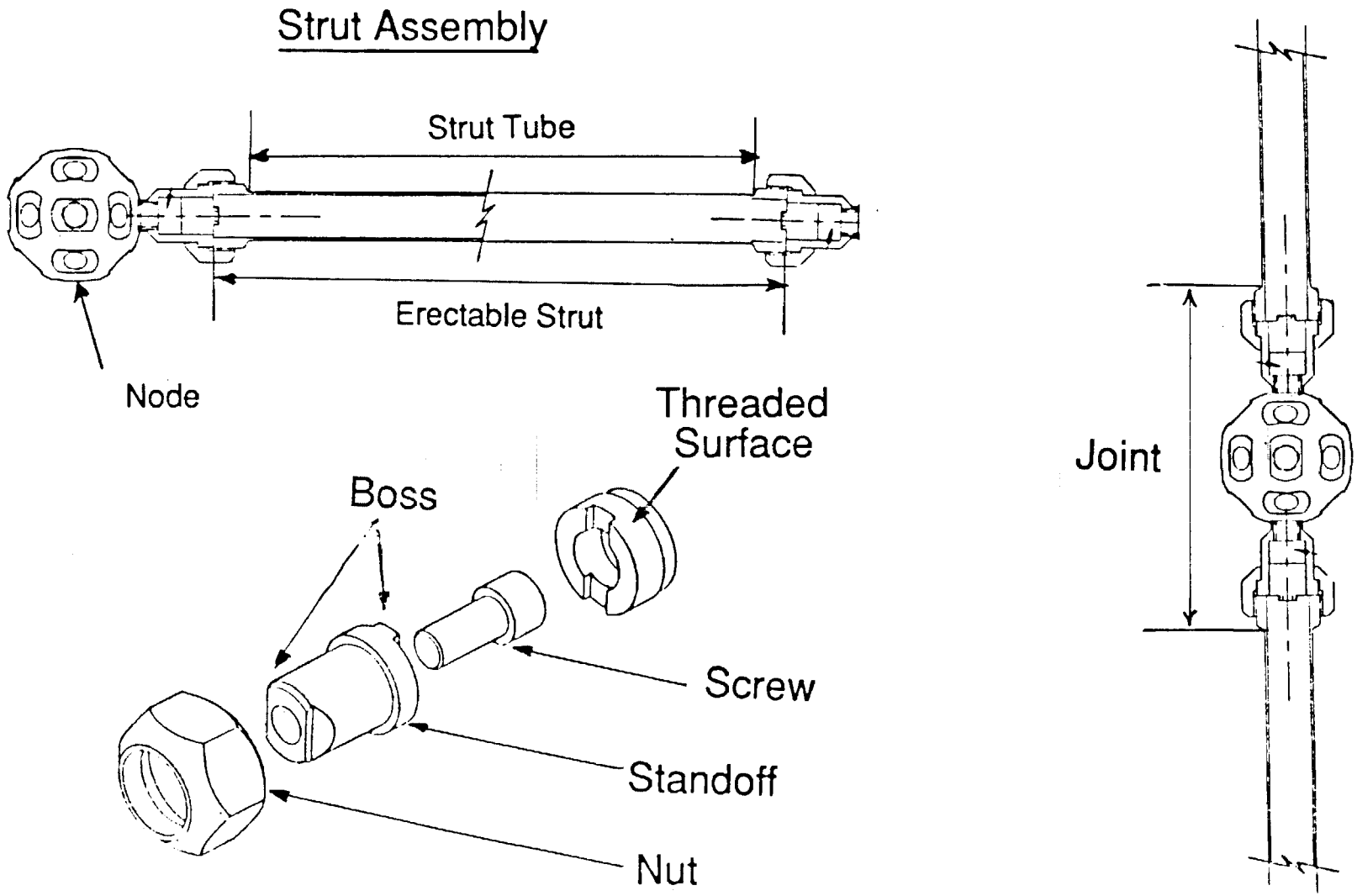

Figure 2-1 CEM Phase 1 Strut Design Features and Nomenclature

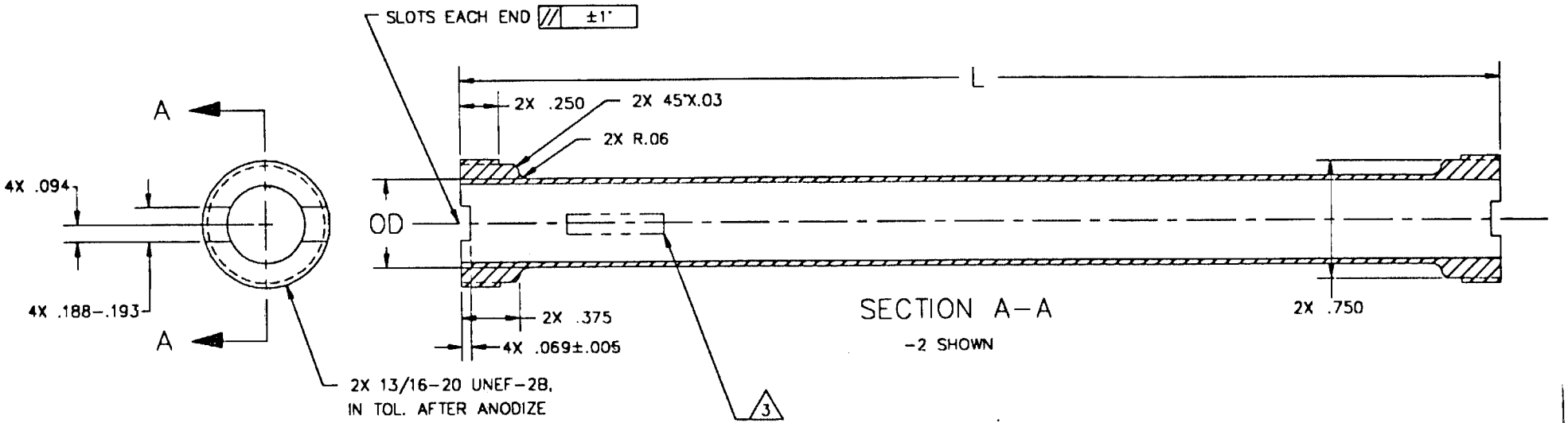

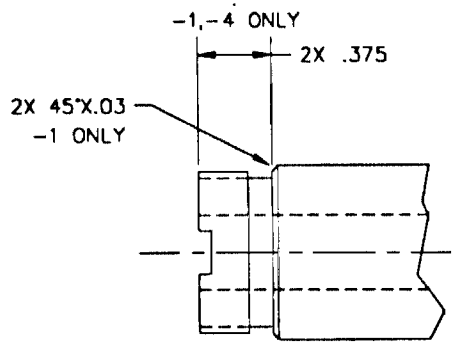

DETAIL, –1 AND –4

590–024 A

DASH NO.	OD ±.002	L ±.004	TUBE AREA (REF)
–1	STOCK(.875)	6.678	.491
–2	.587	6.678	.074
–3	.661	6.678	.147
–4	.787	6.678	.290
–5	.576	6.678	.064
–6	.579	10.820	.067

NOTES:

1. MATERIAL: 6061–T6 TUBING, .875 OD x .250 WALL (–1 ONLY).
   ALL OTHERS: 2024–T3 TUBING, .875 OD x .188 WALL.

Figure 2-2 One-Piece Erectable Strut Design

In order to evaluate the difficulty of achieving the specified stiffness requirements within the specified mass constraints, a non-dimensional figure-of-merit called the strut efficiency (η) was derived:

$$\eta = \frac{(K/W)_{eff}}{(K/W)_{al}} = \frac{(K/W)_{eff}}{(E/\rho L^2)_{al}} = \frac{(E/\rho)_{eff}}{(E/\rho)_{al}}$$

The efficiency is a measure of the effective specific stiffness of a strut or strut component expressed as a percentage of the specific stiffness of a reference material (in this case, aluminum). As shown in Figure 2-3, 100% efficiency for a strut corresponds to an unbroken element of constant cross section and constant mass per unit length. Because the stiffnesses along the strut are combined in series, non-uniform cross sections result in decreased effective specific stiffness. Additional causes of reduced η are non-structural weight and structural connections such as joints which have a stiffness knockdown factor. Thus, alternatively, the efficiency can be thought of as comparing the weight of an unbroken aluminum strut tube with that of a complete erectable strut of equivalent length and effective stiffness.

Some insight into the key design trades for achieving the strut stiffness and weight requirements can be gained by evaluating the strut efficiency expressed in terms of the efficiency, mass ratio, and length ratio properties of the joint and strut tube:

$$\frac{1}{\eta_{strut}} = \frac{1}{\eta j\ (mj/M)\ (L/Lj)^2} + \frac{1}{\eta t\ [1-(mj/M)]\ [L/(L-Lj)]^2}$$

Note that the nomenclature defined in Figure 2-1 is used, e.g., the joint is defined as the part of the strut which is *not* a constant tube cross section. Because of the mechanical breaks in the structure, the joint efficiency, η_j, is always less than 100% (50% is difficult to achieve in practice). The strut tube, however, does have a constant, unbroken cross section and therefore has an efficiency of 100% ($\eta_t = 1.0$). Therefore, the most efficient strut design would be to maximize the length and weight of the tube section relative to the joint section. While this is a rather obvious conclusion, the equation also shows that it is more important to minimize the joint length ratio than it is to minimize the joint mass ratio, as the length ratio appears as a quadratic term. With this in mind, strong emphasis was placed on reducing the joint/strut length ratio during the strut development.

- 100% Efficiency Corresponds to a Strut Composed of an Unbroken Bar with Uniform Cross Section and Constant Mass/Unit Length

- Mass-Related Causes of Reduced Strut Efficiency
  - Non-Uniform Mass Distribution Along Length of Strut
  - Non-Structural Weight or Material Which Does Not Contribute to Stiffness in the Load Path

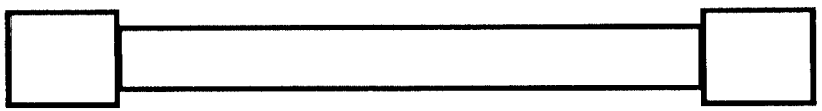

- Stiffness-Related Causes of Reduced Strut Efficiency
  - Joint Knockdown Factor
  - Non-Uniform Stiffness Distribution (Series Stiffness Equation)
  - Longer Relative Joint Length (Lj/Ltot)

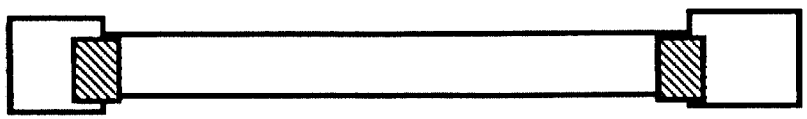

Figure 2-3 Physical Interpretation of Strut Efficiency

Other key design trades during the strut development include:

- Selecting the optimal Node Ball diameter to balance Node Ball stiffness, joint linearity, and joint weight objectives. Small changes in the Node Ball size have a dramatic impact on the joint weight.

- Use of a larger size, finer thread, higher strength 5/16-24 alloy Screw and high-strength Al7075 for the Node Ball to improve joint linearity via increased preload.

- Use of steel (303 SS) for the Standoff, allowing room for a larger screw without increasing the joint outer diameter (OD) or reducing the Standoff stiffness. Increasing the Standoff OD would have required an increase in the Node Ball OD (and weight) to provide access for the assembly tools. Since steel and aluminum have approximately the same specific stiffness, the efficiency is unchanged.

- Use of Al2024 for the one-piece Erectable Strut increases the yield strength for the less stiff struts. Machining this component in one piece on a lathe eliminates the need for a bond or weld at the connection of the lug and strut tube, thereby eliminating weld inspections or proof tests and reducing cost and schedule. The resultant lower parts count also reduces the strut tolerance stackup.

In order to meet the requirement for assembly of over 60 linear bays of truss, a tolerance stackup of 10 mils along the length of a single strut was established. This value was estimated, as the schedule time did not allow for 60 bays of development truss to be manufactured to validate the requirement. Also, 10 mils was considered a practical compromise in terms of manufacturing cost for numerical machining and the level of inspection required.

2.3 STRUT PROPERTIES

As part of the quality assurance plan, critical dimensions of parts were compared with the drawings and representative samples of all components were weighed. In addition, each individual Erectable Strut was weighed and measured for length. These values were recorded and referenced to the unique identification number marked on each strut.

The component weight results are displayed in Table 2-3. Overall, the weight results are very consistent. For the Node Ball, Standoff, Screw, and Nut, the maximum

Table 2-3 Component Weight Data

Component	Sample Size	Avg Weight (lbs)	Max Range (+/-lbs)
1L Strut	94	0.305	0.004
2L Strut	207	0.061	0.004
3L Strut	52	0.109	0.001
4L Strut	198	0.191	0.002
B Strut	556	0.058	0.004
D Strut	692	0.083	0.013
Node Ball	65	0.159	0.001
Standoff	65	0.045	0.001
Screw	65	0.02	0.001
Nut	65	0.016	0.001

Table 2-4 Strut Assembly Length Data

Strut Assembly	Length (in) (+/- .010)	Out of Tolerance			
		0 mil	1 mil	2 mil	3 mil
1L Strut	10.000	72	6	16	-
2L Strut	10.000	200	5	2	-
3L Strut	10.000	48	3	1	-
4L Strut	10.000	195	1	-	2
B Strut	10.000	534	11	8	3
D Strut	14.142	639	36	9	8
Subtotal		1688	62	36	13

deviation was on the order of the measurement error, or 0.001 lbs. For the 10 inch Longeron and Batten struts, the maximum deviation is also very small (0.001 to 0.004 lbs). For the 14.142 inch Diagonals, the maximum deviation was 0.013 lbs for a population of 692. The increased maximum deviation for the Diagonal is attributed to increased bending of the longer, thin-walled tube in response to the transverse cutting tool loads on the numerical lathe. Although not calculated, visual inspection of the data indicates that the standard deviation would be much less, as very few struts were counted at the maximum deviation. Adding the maximum weight deviations from the components yields a worst-case maximum weight deviation for the strut assembly ranging from 1.2% for the 3L Longerons to 4.2% for the Diagonals.

The strut length tolerance results are displayed in Table 2-4. While 93.8% of the struts met the 10-mil tolerance goal, some were a few mils beyond. The out-of-tolerance struts were of little consequence as the entire Phase 1 CEM structure was assembled at NASA/LaRC in less than two days, significantly less time than required for the Phase 0 CEM. The CEM assembly consisted of 1,526 struts and 3,052 joint connections which were accomplished without difficulty. Thus, the estimated 10-mil goal was conservative.

Overall, the CEM Phase 1 strut design meets the functional requirements. The performance of the strut design against the remaining requirements for stiffness, weight, linearity, and strength is discussed in the Section 3.4.

3.0 STRUT STATIC TESTS

This section describes the tests that were conducted by LMSC on individual CEM Phase 1 strut assemblies consisting of a Node Ball, two Standoffs, two Screws, two Nuts, and an Erectable Strut. The strut static test plan (Table 3-1) focuses on two principal objectives. The first is to quantify the stiffness of a representative population of the six different strut sizes over the load range each would expect to see in use. The second is to quantify the strength capabilities of the three smaller strut sizes where strength may be a concern. Supplemental repeatability tests were also conducted for the stiffest (1L Longeron) and least stiff (Batten) strut sizes to quantify the experimental uncertainty, including variations due to repeated strut assembly and disassembly. The following sections describe the test setup, test procedure, sample data, and results for the stiffness (3.1), repeatability (3.2), and strength (3.3) tests. Finally, the overall results of the strut testing activity are summarized in Section 3.4.

3.1 STRUT STIFFNESS TESTING

Tensile and compressive stiffness tests were conducted on 10 samples of each of the six different CEM Phase 1 struts. Table 3-1 specifies the load range (maximum tensile or compressive load) over which the tests were conducted. The load range for each strut size is based on the worst-case CEM Phase 1 static load plus an additional 300 lbs for dynamic loads. Table 3-1 also notes that not all of the strut hardware was always changed out for each strut test. For the less stiff 2L, 3L, Batten, and Diagonal struts, only the center erectable strut portion of the strut assembly is changed out. For the stiffer 1L and 4L struts, the entire strut assembly (including Node Ball, Standoffs, Screws, and Nuts) is changed out for each test. This is because the 1L and 4L strut tubes are stiff enough such that both the joint and strut tube flexibilities contribute significantly to the overall stiffness of the strut assembly. Changing out all of the components for these latter two strut sizes provides a more relevant statistical sample that includes the effect of manufacturing variances for the joint components.

3.1.1 Description of Strut Stiffness Test Setup

All of the strut stiffness testing was performed using an Instron Model 4501 Universal Testing Machine (UTM). Figures 3-1 and 3-2 illustrate the test setup. Deflection data

Table 3-1 CEM Phase 1 Strut Static Test Plan

Strut Size	Stiffness Tests			Strength Tests		
	Tension	Compression	Load Range (+/- lb)	Tension	Compression	Load Range (+/- lb)
1L	10†	10†	700	-	-	-
2L	10	10	1,150	5†	5†	4,000
3L	10	10	350	-	-	-
4L	10†	10†	750	-	-	-
B	10	10	1,150	5†	5†	4,000
D	10	10	450	5†	5†	4,000

† FOR EACH TEST SET-UP THESE STRUTS WERE PROVIDED WITH SEPARATE UNIQUE NODE BALL/STANDOFF ARRANGEMENTS

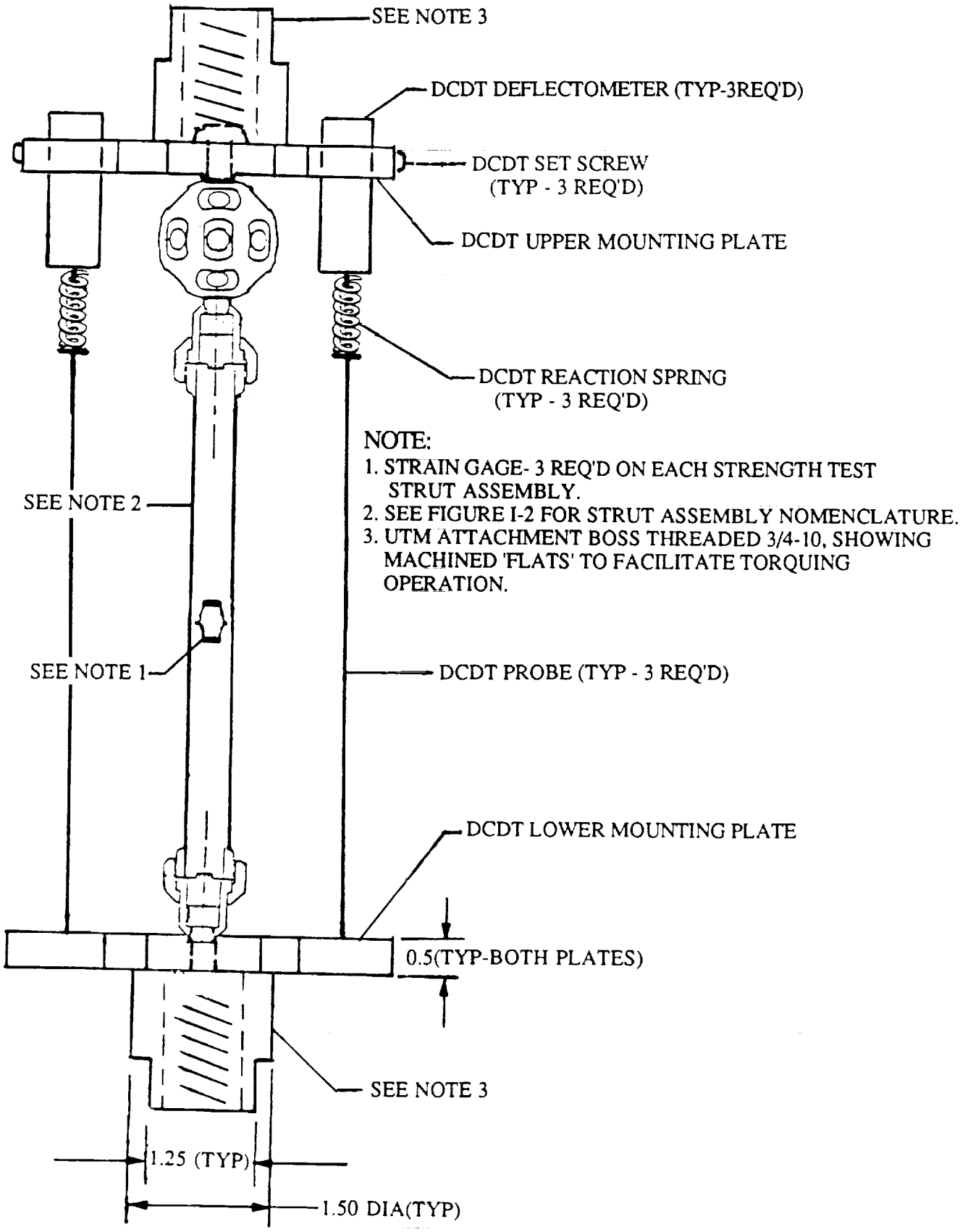

Figure 3-1 Schematic of Strut Static Test Setup in UTM

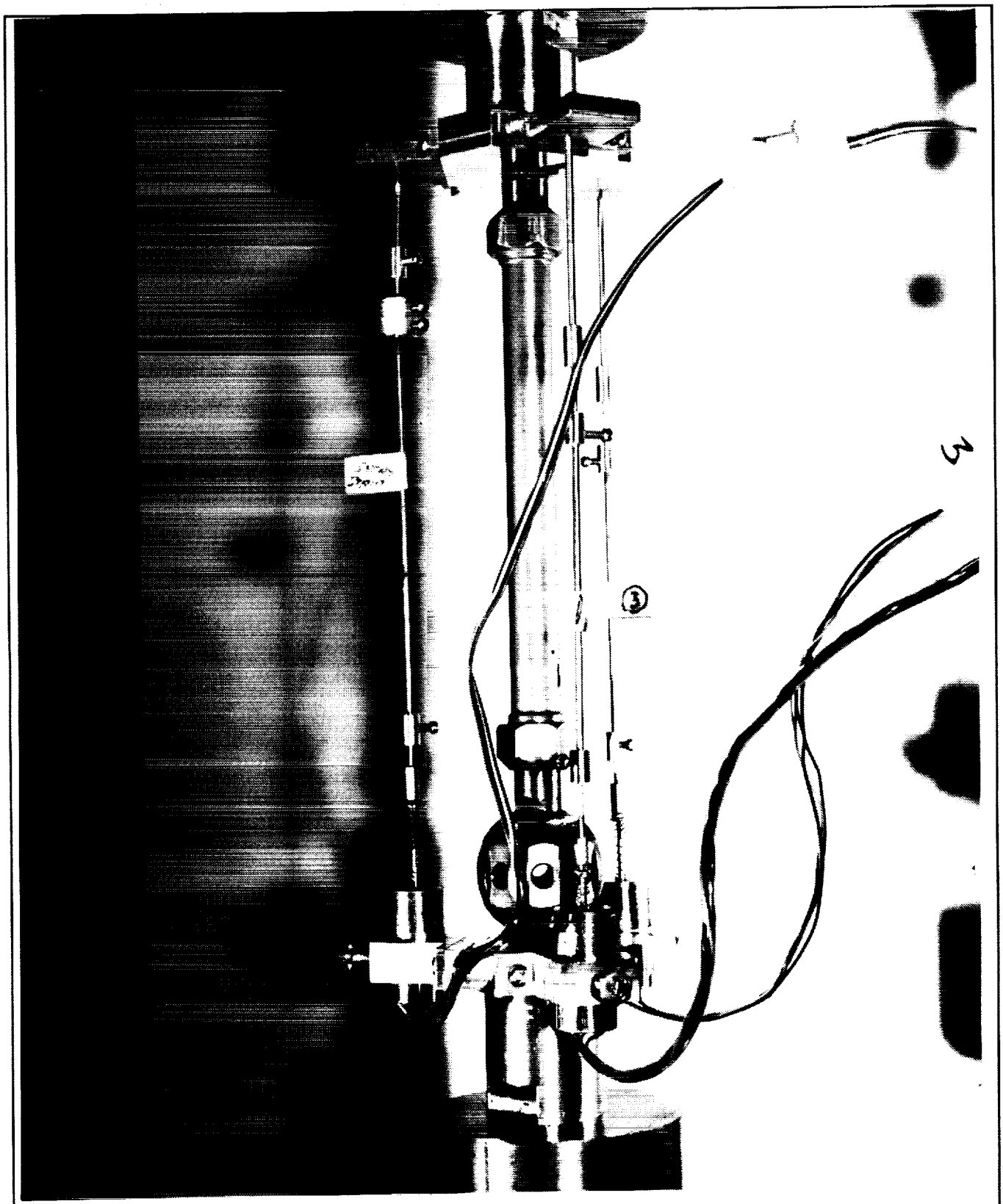

M8127F2Fig. 3-2

Figure 3-2 Longeron Strut Installed in UTM

for the strut assembly is obtained from three linear displacement transducers (G. L. Collins Model SS-103 DCDT's) mounted at 120° intervals around the specimen and supported by upper and lower DCDT mounting plates (Figure 3-3). Each DCDT mounting plate incorporates a UTM attachment boss on one side and a simulated strut interface fitting on the other side. The upper mounting plate contains a raised "grip" which fits into the recessed slot in the test article Node Ball, while the lower mounting plate contains a machined "slot" which secures the Standoff at the lower end of the test article. Both ends of the strut are fastened to the test apparatus using screws of the same size, material, thread pitch, and assembly torque as the Screw used in the CEM Phase 1 strut assembly (Figure 2-1). Tensile tests are conducted with universal joints in series with the specimen at either end (Figure 3-4). Compressive tests are conducted using a rigid adapter at the upper end and a spherical seat at the lower end (Figure 3-5).

Data acquisition for all testing was conducted using a Daytronic System 10. This system provided for data channels to be displayed on a monitor during testing and stored a desired rate.

Prior to testing the instrumentation was calibrated. For the DCDT's, a micrometer with 0.001 inch divisions was used for this purpose. In terms of performance, the UTM load cell has a resolution of 0.1 lbs while the DCDT's have a range of +/- 100 mils and a resolution of 0.1 to 0.01 mils in tension and 0.01 mils in compression.

3.1.2 Strut Test Assembly Procedure

An exploded view of the test article is provided in Figure 3-6. For each individual strut test, the test article and test apparatus were assembled using the following procedure:

- Treat threaded surfaces on Erectable Strut, Nuts, and Screws using Lubriplate No. 630 AA or equivalent
- Feed tapered end of Standoffs into and through threaded side of Nuts
- Use Screw to attach Standoff to lower DCDT plate and torque to 210 in-lbs
- Use vise and shims or Node Ball Tool (Holding Bar) to hold Node Ball while attaching Standoff to one end and upper DCDT plate to other end; torque both bolts to 210 in-lbs
- While reacting torque with Node Ball Tool inserted at 90° to strut axis, attach Nut to end of Erectable Strut and torque to 240 in-lbs
- While holding lower DCDT plate in vise, attach Nut to lower end of Erectable Strut and torque to 240 in-lbs

M8127F2Fig.3-3

Figure 3-3 Upper and Lower DCDT Mounting Plates

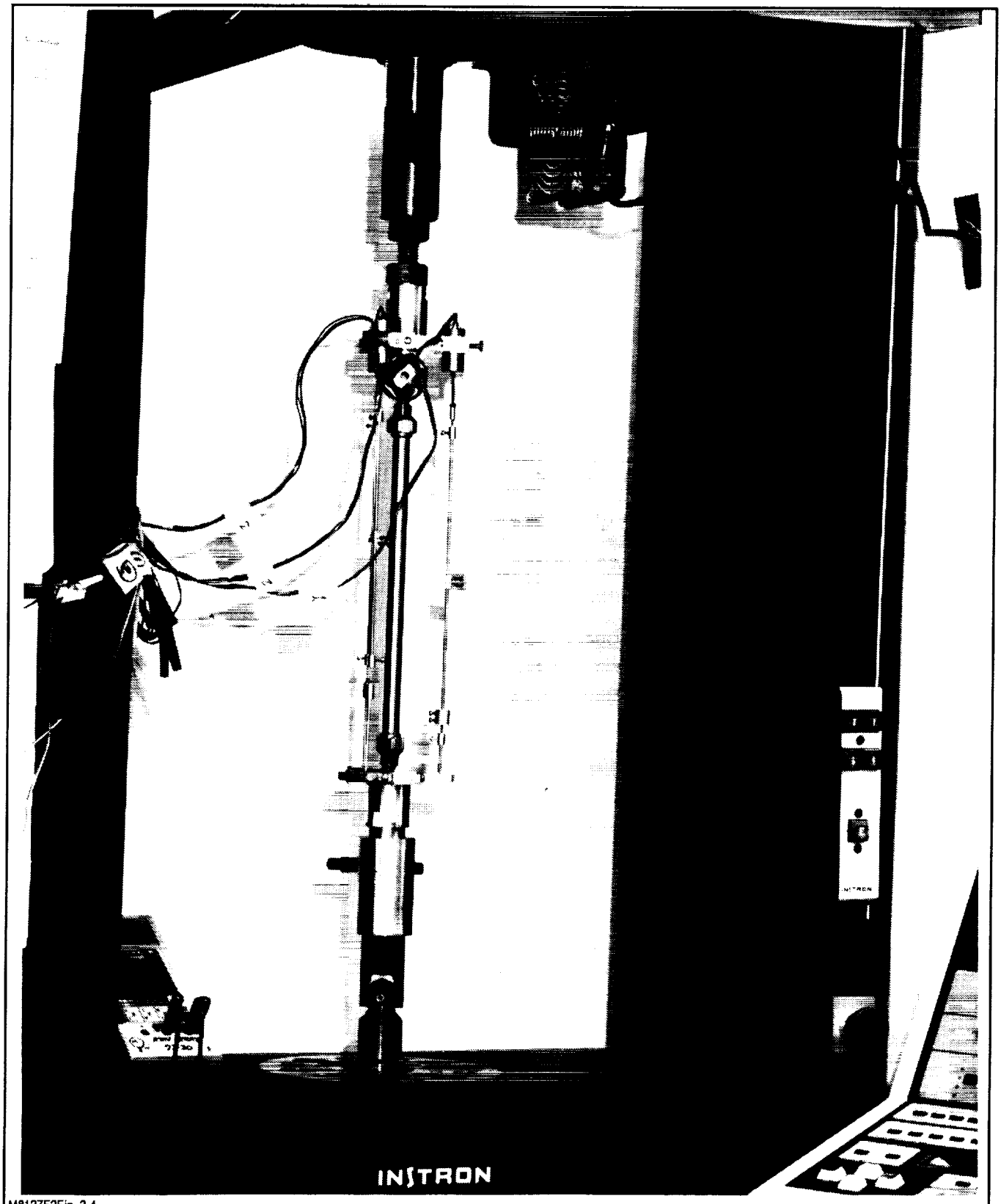

M8127F2Fig. 3-4

Figure 3-4 Diagonal Strut Tension Test Setup

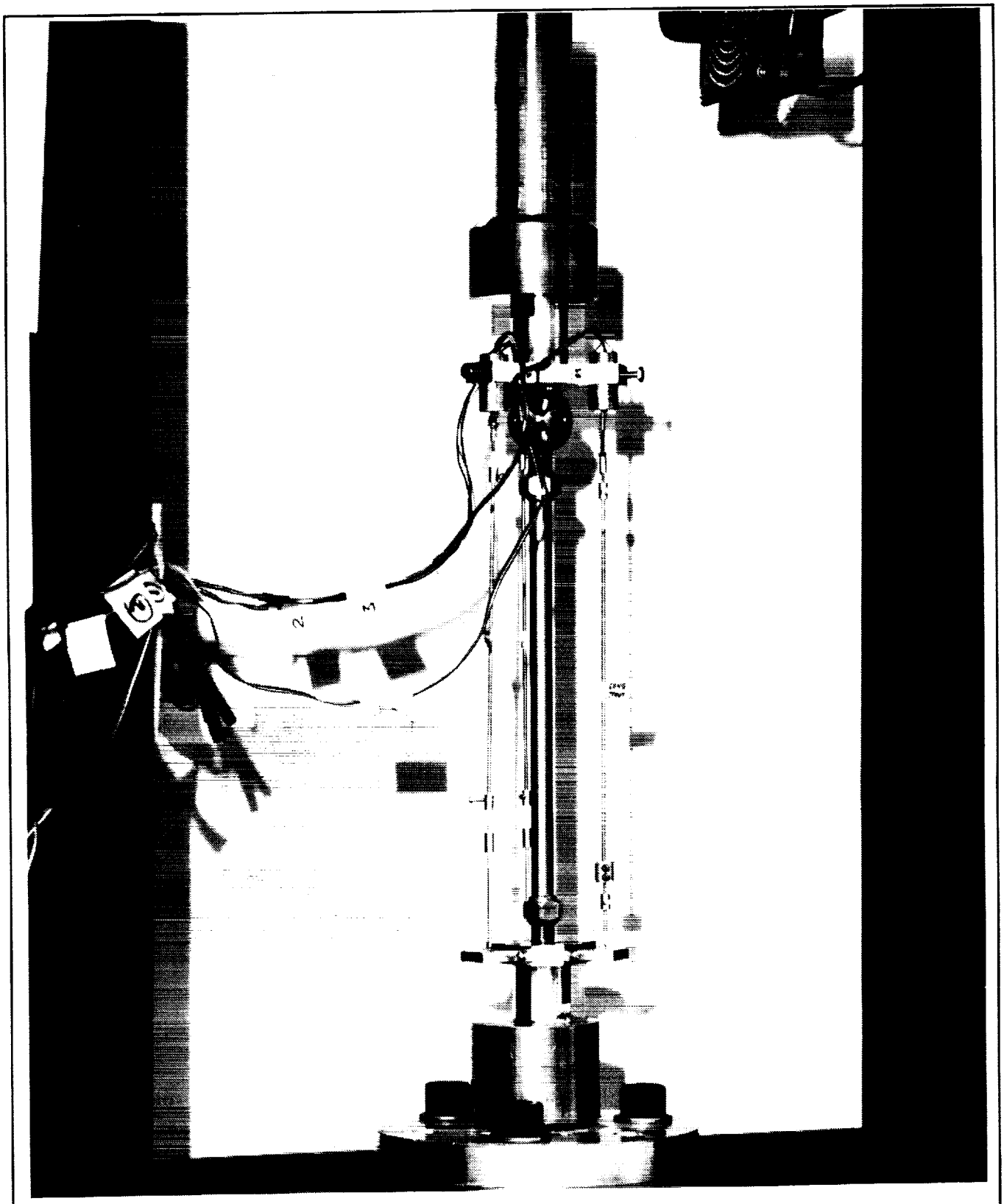

M8127F2Fig. 3-5

Figure 3-5 Diagonal Strut Compression Test Setup

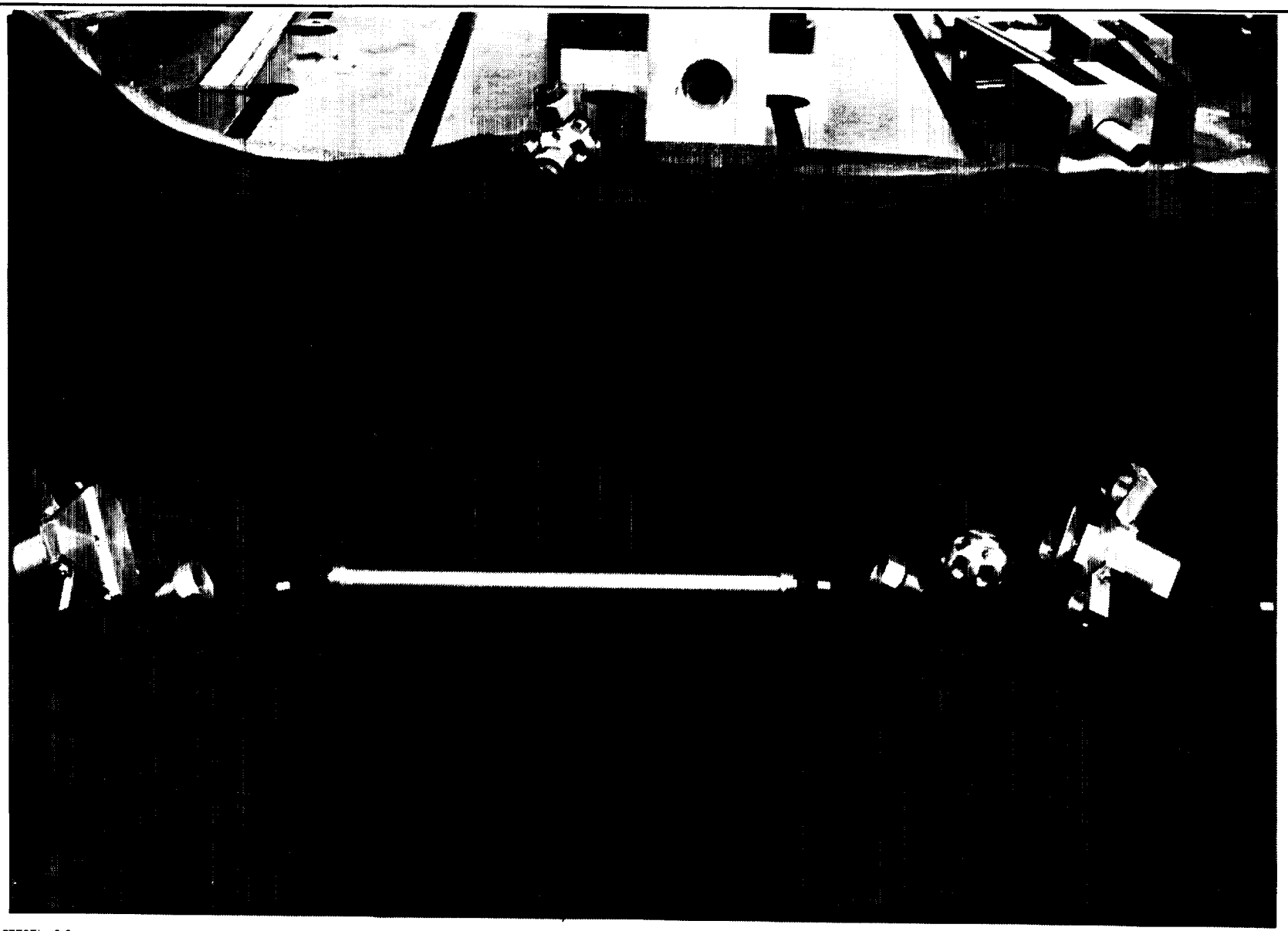

M8127F2Fig. 3-6

Figure 3-6 Components of Strut Test Assembly

- Thread upper and lower DCDT plates into Instron UTM
- Place DCDT's on mounting plates and make necessary wire connections
- Use reverse procedure for disassembly after test
- In cases where the Node Ball and Standoffs are not changed out between tests, re-check all 210 in-lb torques prior to re-assembly

During assembly, the appropriate Node Ball slot was used for the size of strut being tested, as indicated in Figure 3-7 and illustrated in Figures 3-2 and 3-4. Caution was also exercised while torquing the Nuts to avoid subjecting the strut tube to bending or torsion loads, particularly in the case of the less stiff (2L, 3L, B, and D) struts. For this reason, one should *never* restrain one end of the strut while torquing the other. The end of the strut assembly nearest the Nut being torqued should be restrained instead.

3.1.3 Test Procedure

The first step in the test procedure is to record the strut identification number marked on the strut tube. The next step is to zero the instrumentation and program the Instron UTM to ramp up to the desired maximum load, hold there briefly, and ramp back down to zero. A UTM crosshead rate of 0.05 in/min and a data acquisition rate of 2 Hz were typically used. The test sequence is initiated by pressing the start button and then proceeds automatically. At the completion of each test, the stored data is transferred to a PC and plots are made on an HP LaserJet II. After a review of the plots to screen out anomalies and check the return to zero, all data is transferred to a spreadsheet program and stored on a 3.5 inch floppy disk.

In the case of the stiffer 1L, 3L, and 4L struts, a linear regression was performed after each test as part of the anomaly screening. The smaller, 2 to 3 mil maximum deflections of these stiffer struts increased the sensitivity of the results to small misalignments of the strut assembly in the UTM. When necessary, individual strut tests were repeated until good, consistent data was obtained.

The stiffness tests outlined in Table 3-1 were not conducted in any particular order. Rather, the sequence was dictated by the availability of different components as they came off the production line.

3.1.4 Strut Stiffness Test Results

Most of the test data is characterized by very tight, repeatable, linear, force-displacement curves characteristic of a strut with stiff, highly-preloaded joints.

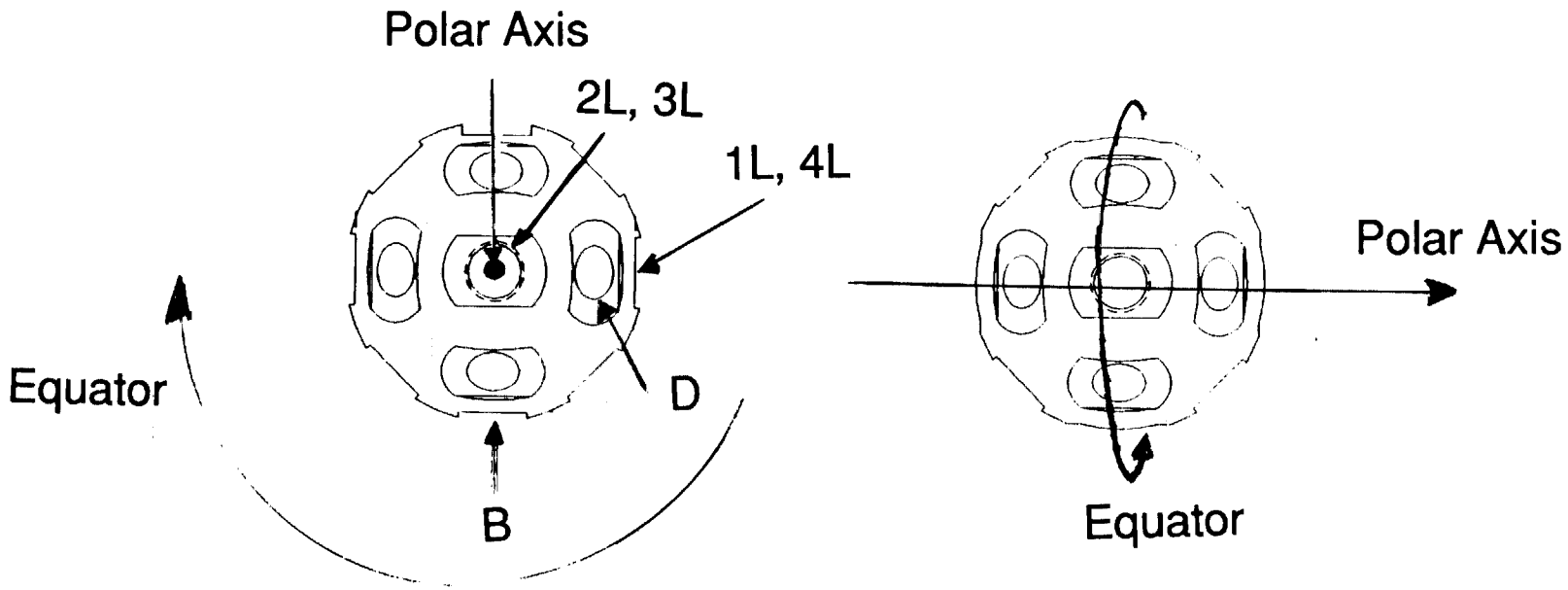

Figure 3-7 Node Ball Orientation for Various Strut Types

Representative samples of tensile and compressive stiffness data are provided in Figures 3-8 through 3-11.

The overall results of the stiffness tests are summarized in Table 3-2. Linear regressions were performed to determine the stiffness resulting from each strut test over the load range shown at the top of the table. In performing the regression, leading repeated zeroes, startup transients, and trailing repeated data points were deleted to avoid biasing the curve-fit. For each strut population, the average tensile stiffness, average compressive stiffness, and average combined tensile/compressive stiffness were determined. The corresponding average errors were also calculated. Note that in all cases, the average stiffness errors are low (less than 1.3%), and the average compressive stiffness is slightly greater than the average tensile stiffness.

Table 3-2 also lists the results of statistical analyses performed to determine the standard deviations for the tensile stiffness (0.42% - 1.65%), compressive stiffness (0.33% - 1.77%), and combined average tensile/compressive stiffness (0.21%- 0.94%) using a sample size of ten. The standard deviations are also shown for the sample size of twenty, containing the ten compressive and ten tensile stiffness tests for each strut size (1.31% - 2.03%). The fact that the standard deviation is greater for the sample size of twenty (tensile or compressive stiffness for each strut) than the sample size of ten (average tensile/compressive stiffness for each strut) indicates that the variation in stiffness from tension to compression is greater than the variation in stiffness within a particular tension or compression test series itself.

In the case of the highly-loaded Battens and 2L Longerons, some weak elastic nonlinearity was observed at higher loads (Figures 3-10 and 3-11). Additional regressions were performed over different load ranges to further characterize the nonlinearity. The results for the Battens and 2L Longerons are tabulated in Tables 3-3 and 3-4, respectively. They indicate a slight softening effect at higher tensile loads and a slight stiffening effect at higher compressive loads, both of which are on the order of 2.1% or less. In comparison to the average tensile or compressive stiffness over the entire 0 - 1150 lb load range, the softening and stiffening effects are less than 1.3% and 1.0%, respectively. This nonlinearity at high load was also observed during the strut developmental testing and is attributed to relaxation of the joint preload. Fortunately, the magnitude of the nonlinearity is small, and very few Batten and 2L Longerons are expected to see such high load levels in the actual CEM structure, as the high loads are very localized in a few critical areas.

Overall, the small average errors and small standard deviations attest to the degree of stiffness consistency in the production CEM Phase 1 erectable struts.

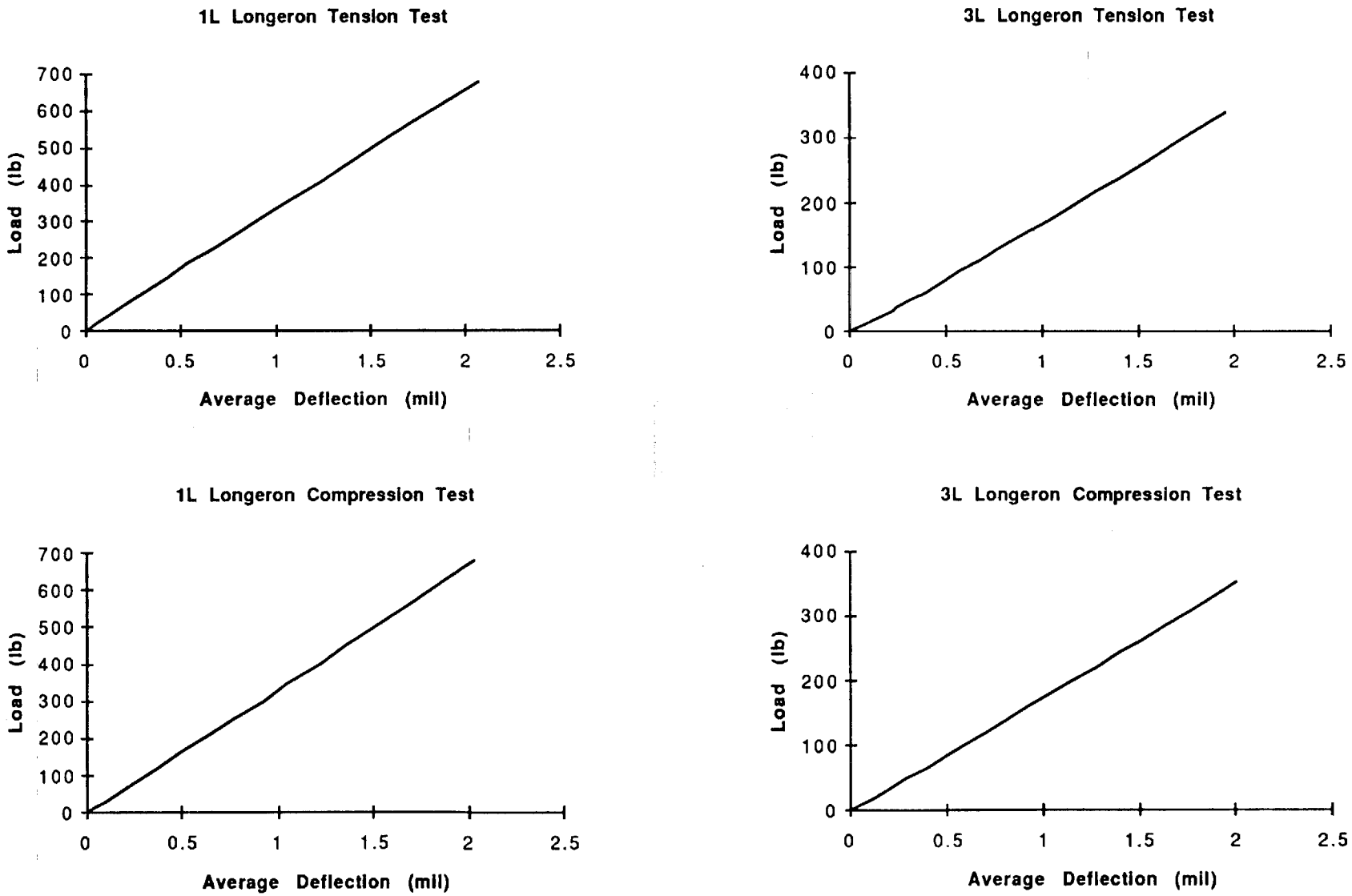

Figure 3-8 Typical 1L and 3L Longeron Stiffness Test Results

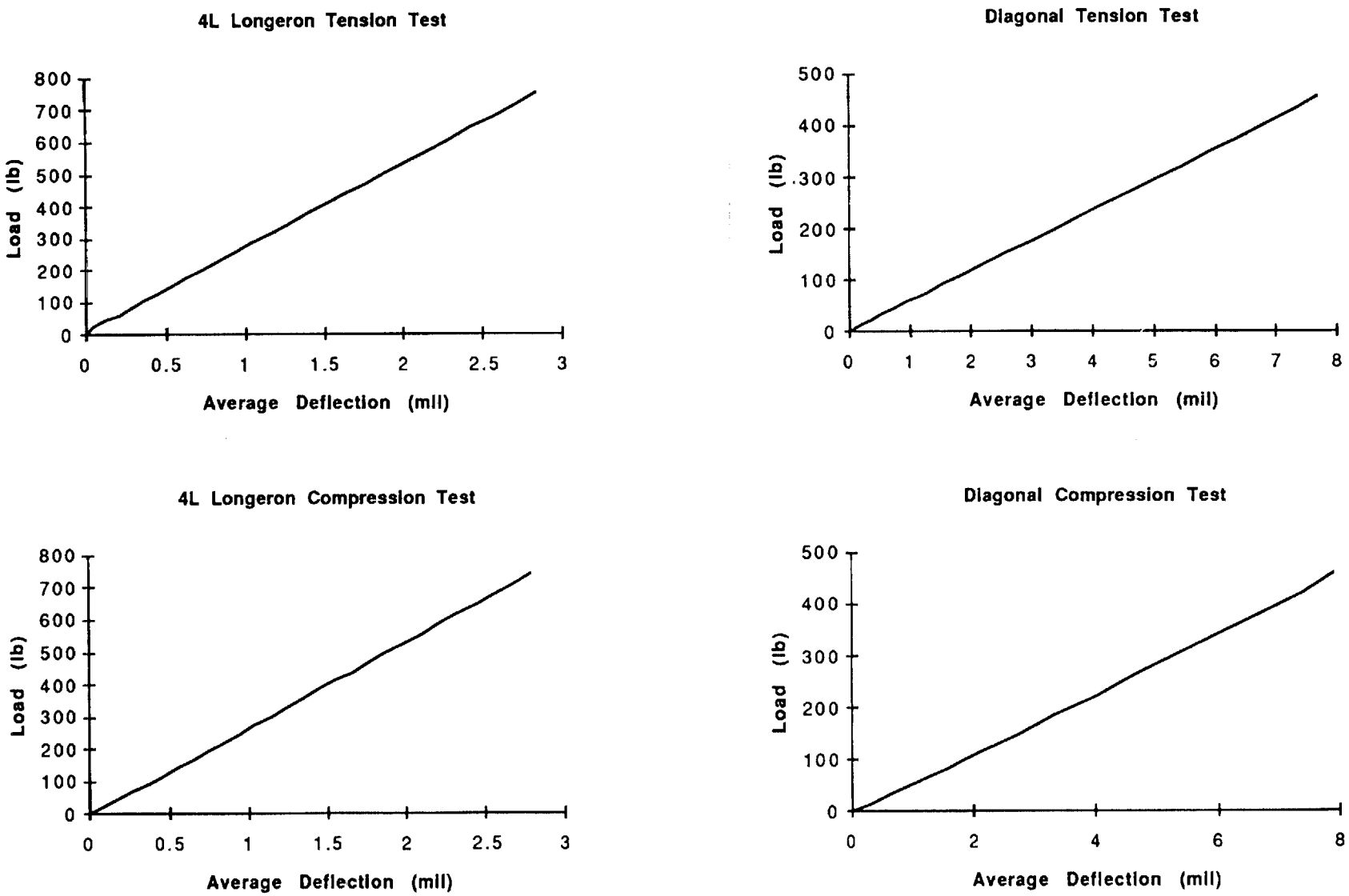

Figure 3-9 Typical 4L Longeron and Diagonal Stiffness Test Results

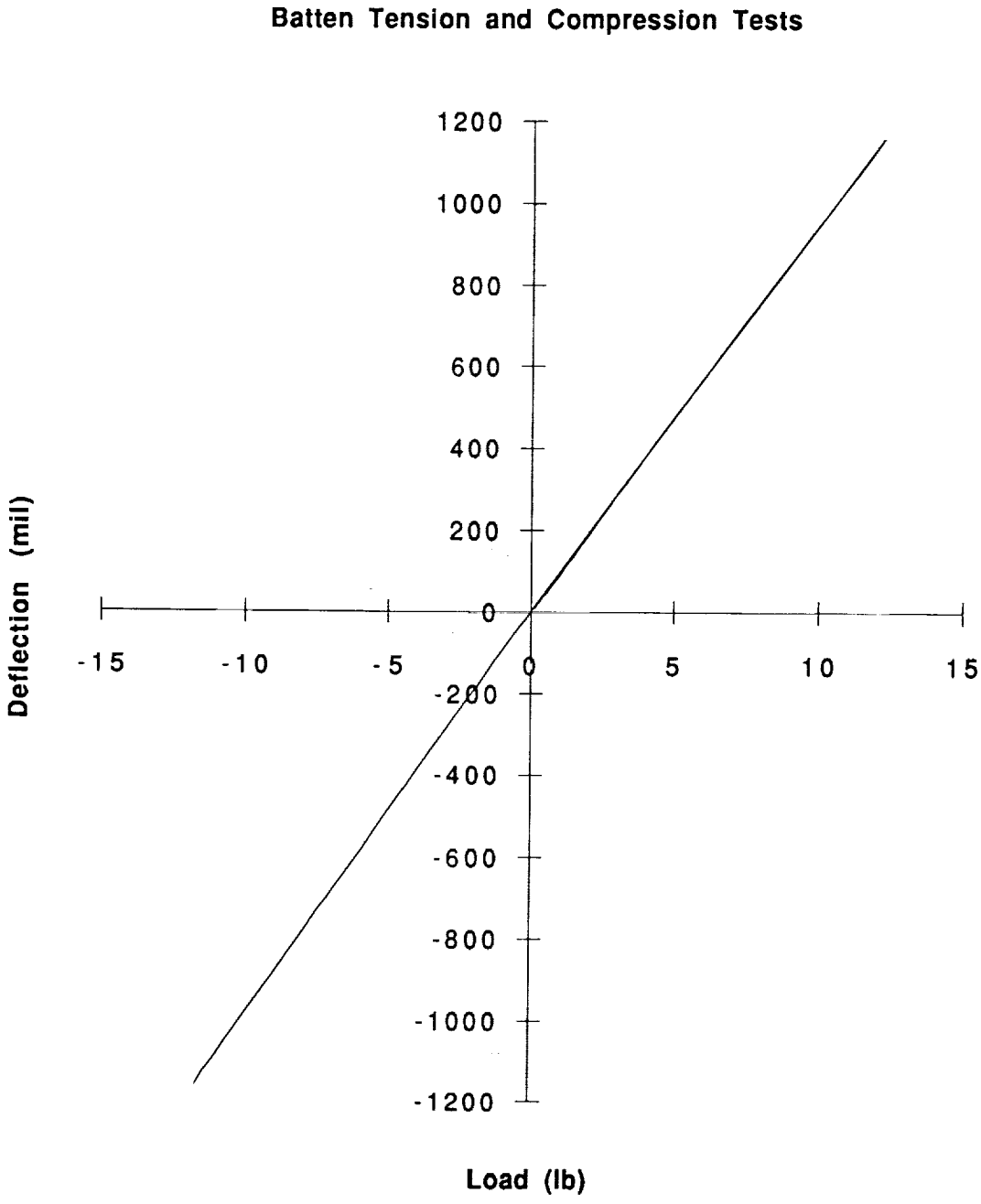

Figure 3-10 Typical Batten Tension and Compression Stiffness Test Results (Superimposed)

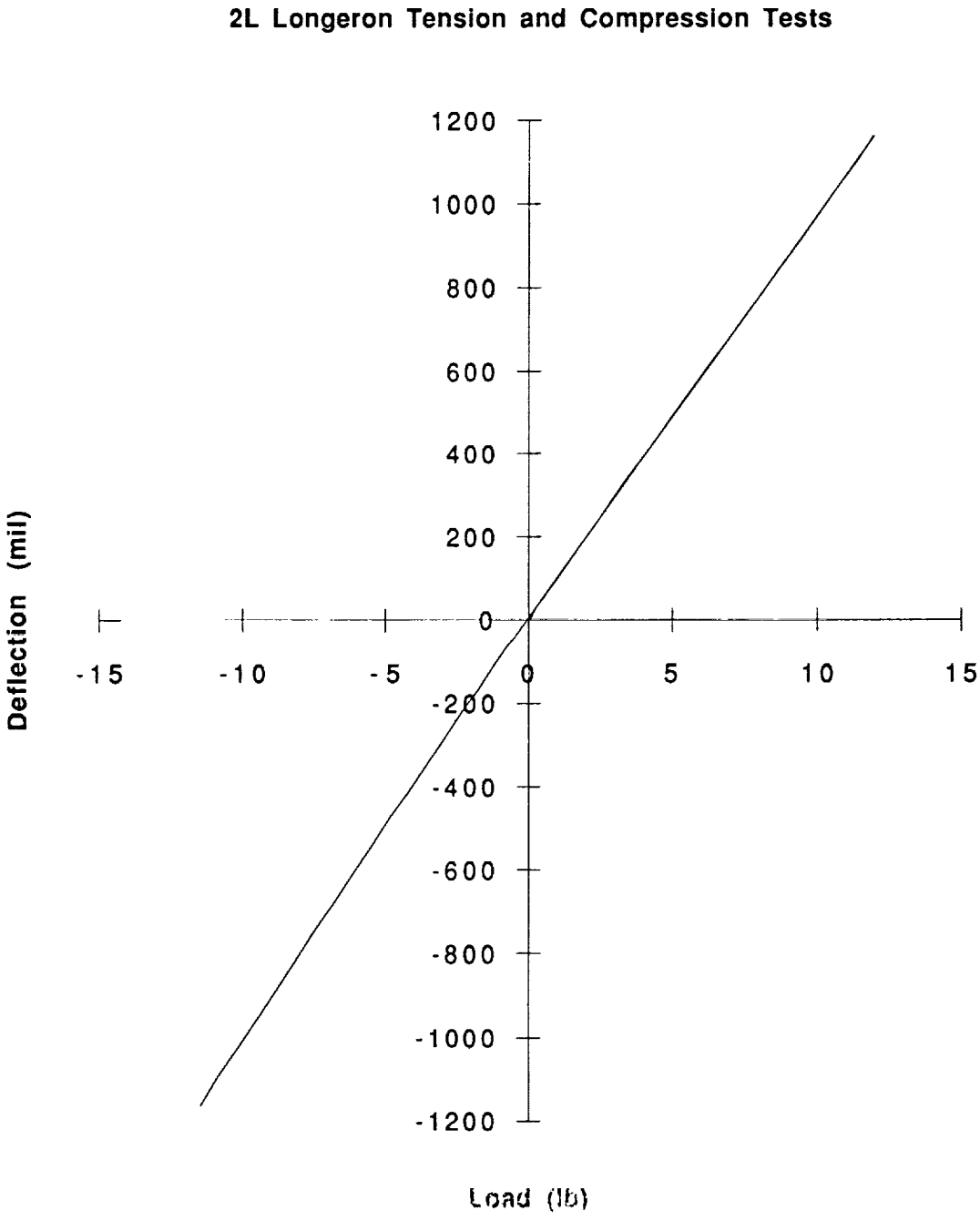

Figure 3-11 Typical 2L Longeron Tension and Compression Stiffness Test Results (Superimposed)

Table 3-2 Strut Stiffness Data Summary

STRUT	1L		2L		3L		4L		B		D	
PK LOAD	700 lbs		1,150 lbs		350 lbs		750 lbs		1,150 lbs		450 lbs	
LOAD DIR	T	C	T	C	T	C	T	C	T	C	T	C
1	326,705	336,030	98,165	100,002	171,660	177,497	261,509	267,890	95,179	99,572	59,184	59,162
2	331,041	323,805	98,179	100,172	170,842	176,307	258,814	261,996	95,527	99,024	58,937	57,901
3	326,151	341,726	96,521	101,196	172,022	177,850	260,009	266,032	94,822	99,163	58,743	58,667
4	326,875	341,587	-	-	170,150	177,786	259,502	264,916	95,894	99,395	58,260	58,762
5	322,074	336,016	97,440	102,061	176,453	176,617	260,414	265,529	95,756	98,694	58,418	59,142
6	328,480	340,630	96,926	100,508	176,097	176,030	259,181	268,879	95,529	98,980	58,580	57,956
7	326,967	338,812	96,905	101,407	167,716	177,124	263,637	269,139	95,893	99,160	58,544	59,802
8	324,545	339,683	97,078	101,258	169,884	176,310	261,184	267,858	96,062	98,574	58,301	61,447
9	329,763	341,210	96,832	101,311	175,016	178,601	268,741	269,263	96,003	99,321	58,504	58,793
10	331,219	337,661	96,470	101,821	172,488	176,530	263,394	-	95,911	98,711	58,516	58,204
Avg K*	**327,382**	**337,716**	**97,168**	**101,082**	**172,233**	**177,065**	**261,639**	**266,834**	**95,658**	**99,059**	**58,599**	**58,984**
Avg Err %	**0.67%**	**1.03%**	**0.52%**	**0.56%**	**1.29%**	**0.40%**	**0.83%**	**0.74%**	**0.33%**	**0.27%**	**0.36%**	**1.23%**
σ (10)	2,860	5,334	637	710	2,850	842	2,990	2,424	398	327	285	1,044
(%)	0.87%	1.58%	0.66%	0.70%	1.65%	0.48%	1.14%	0.91%	0.42%	0.33%	0.49%	1.77%
T/C Avg K	**332,549**		**99,125**		**174,649**		**264,236**		**97,359**		**58,791**	
Avg Err %	**0.62%**		**0.17%**		**0.66%**		**0.68%**		**0.16%**		**0.63%**	
σ (10)	2,609		283		1,465		2,486		204		491	
(%)	0.78%		0.29%		0.84%		0.94%		0.21%		0.83%	
σ (20)	6,742		2,117		3,214		3,769		1,781		771	
(%)	2.03%		2.14%		1.84%		1.43%		1.83%		1.31%	

*** Stiffness, Error, and Standard Deviation Data are in units of (lb/in)**

- Bad Test, Data Ignored

Table 3-3 Batten Nonlinearity Data

Load Direction	T	C	T	C	T	C
Load Range (lb)	0 - 1150	0 - 1150	0 - 500	0 - 500	500 - 1150	500 - 1150
Avg K (lb/in)	95,659	99,059	96,095	98,131	94,877	99,750
Stiffness Change (Relative to 0 - 1150)	-	-	0.5%	-0.9%	-0.8%	0.7%
Stiffness Change (Relative to 0 - 500)	-	-	-	-	-1.3%	1.7%

Table 3-4 2L Longeron Nonlinearity Data

Load Direction	T	C	T	C	T	C
Load Range (lb)	0 - 1150	0 - 1150	0 - 500	0 - 500	500 - 1150	500 - 1150
Avg K (lb/in)	97,168	101,082	98,126	99,799	96,087	101,851
Stiffness Change (Relative to 0 - 1150)	-	-	1.0%	-1.3%	-1.1%	0.8%
Stiffness Change (Relative to 0 - 500)	-	-	-	-	-2.1%	2.1%

Table 3-5 Repeatability Test Results

Strut	Batten	Batten	1L Longeron	1L Longeron
Load Direction	T	C	T	C
Load Range (lb)	0 - 1150	0 - 1150	0 - 700	0 - 700
Sample Size	1	1	1	1
No. Tests	10	10	10	10
Avg K Error (%)	0.10	0.07	0.22	0.51
Std Dev (%)	0.16	0.11	0.37	0.75

3.2 STRUT STIFFNESS REPEATABILITY TESTING

Supplemental stiffness tests were conducted on a single Batten and a single 1L Longeron strut to quantify the repeatability of the stiffness results. The results of these tests provide a measure of (1) the experimental uncertainty due to the test setup, (2) the experimental error, and (3) the repeatability of the joint preload resulting from the torquing operation during assembly. By testing the stiffest and least stiff struts, the experimental uncertainty can be bounded (the stiffest struts are the most difficult to test as well as the most sensitive to joint preload).

Ten compressive and ten tensile tests were conducted for each of the two struts over the appropriate load range, for a total of forty tests. Before each test, the test setup and strut were completely disassembled and re-assembled.

The regression results for the Batten and 1L Longeron tests are shown in Table 3-5. They show that the range of the experimental uncertainty for the struts is on the order of 0.07% to 0.51% in terms of average error and 0.11% to 0.75% in terms of standard deviation. Thus, the experimental uncertainty is slightly less than, but on the same order as, the average error shown in Table 3-2.

3.3 STRUT STRENGTH TESTING

Strength tests were conducted on the Batten and 2L Longeron struts because they are the highest-stressed members in the CEM Phase 1 structure, critically located at the intersection of the suspension truss and the main keel. Additional strength tests were conducted on the longer (14.142 inch) Diagonal struts primarily to evaluate compressive stability (buckling). Table 3-1 shows the strut strength test plan. Each of the three strut types was tested to a nominal 4,000 lbs in both tension and compression. As noted in the table, all of the component hardware for each strut size was changed out in its entirety before each tensile or compressive test.

The setup, instrumentation, assembly procedure, and test procedure for the strength tests are identical to those used in the stiffness tests (Section 3.1), with the exception that axial strains in the strut tube are monitored by three strain gages. Three Micro-Measurements CEA-13-125UW-350 gages were bonded to the strut tube midpoint at 120° intervals around the circumference using Micro-Measurements M-Bond 200. These gages had a gage factor of 2.15.

Figures 3-12 through 3-14 show typical strength test results for the 2L Longeron, Batten, and Diagonal, respectively. The force-displacement curves tended to reach a proportional limit at lower load levels than the force-strain curves. This is attributed to the loss of preload in the joint. For this reason, the onset of yield was determined as the proportional limit obtained from the force-strain data. This provides a conservative estimate of the yield value because plastic deformation has not yet occurred.

The strut strength test results are summarized in Table 3-6. Since no exact criterion for yield exists, both the onset (derived from the strain proportional limit) and the 0.2% plastic strain criteria are displayed in the table. The proportional limit for displacement is also shown, indicating the maximum load for stiffness linearity. The average onset yield values ranged from 1,913 lbs to 2,364 while the average 0.2% strain criterion yield values ranged from 2,577 to 3,665. In the case of the Diagonals, the lower 0.2% strain criteria for the struts in compression (compared with tension) indicates a buckling failure, which was observed during the testing. The compression failure modes for the other struts were observed to be a combination of squashing and bending.

Overall, the strut strength test results indicate that there is substantial load margin for the onset of yield. No destructive failures were observed during any of the tests, though a buckling instability of the diagonals was recorded around -2,500 lbs, yielding a positive margin of safety. The requirement of a positive margin of safety for ultimate strength using a factor of safety of 2.0 is satisfied for all struts.

3.4 STRUT STATIC TESTING SUMMARY

Overall, the production strut design generally meets or exceeds the stiffness and weight requirements, as shown in Table 3-7. The small average errors (less than 1.3%) and standard deviations (less than 1.8%) in the test data indicate that the strut stiffness is very consistent over the sample size of 10 struts. Nonlinearities in the less stiff, highly-loaded Batten and 2L longeron struts are on the order of 1% of stiffness when compared with the average stiffness over the 0 to 1,150 lb load range. Repeatability tests indicate that the experimental uncertainty is on the order of 0.5% or less for stiffness. The weight values for the struts indicate that the assembled Phase 1 CEM structure will weigh the same or slightly less than the Phase 0 CEM, as required.

Table 3-7 also shows the strut assembly efficiency (η) results (a relative measure of specific stiffness - see Section 2.2 for definition). The weighted average strut efficiency

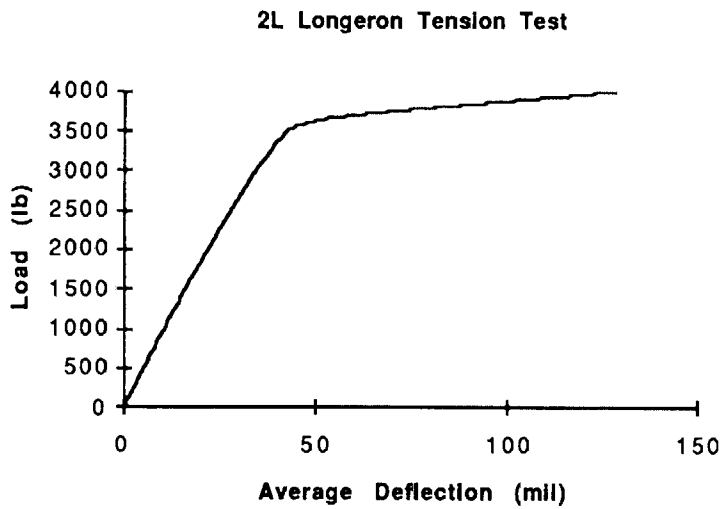

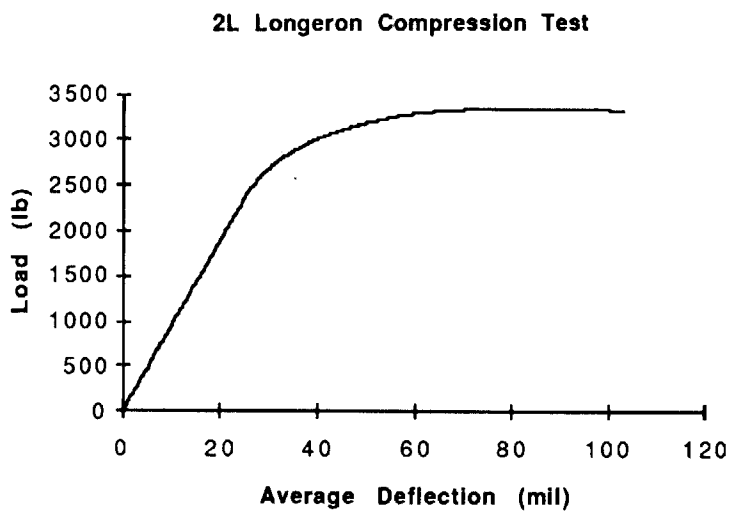

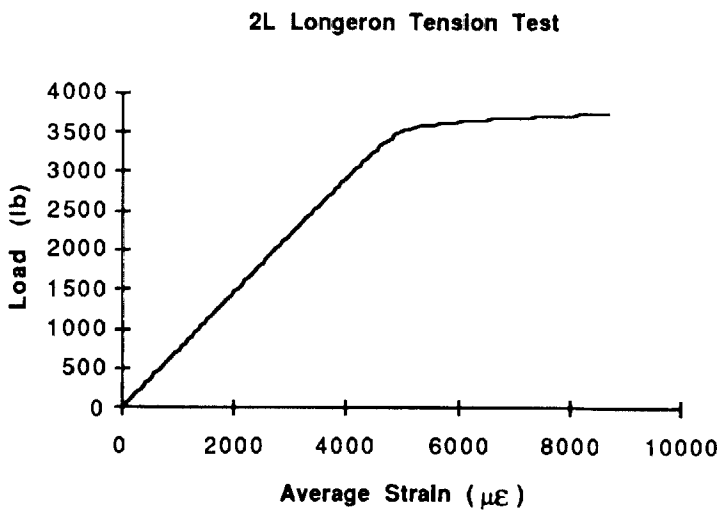

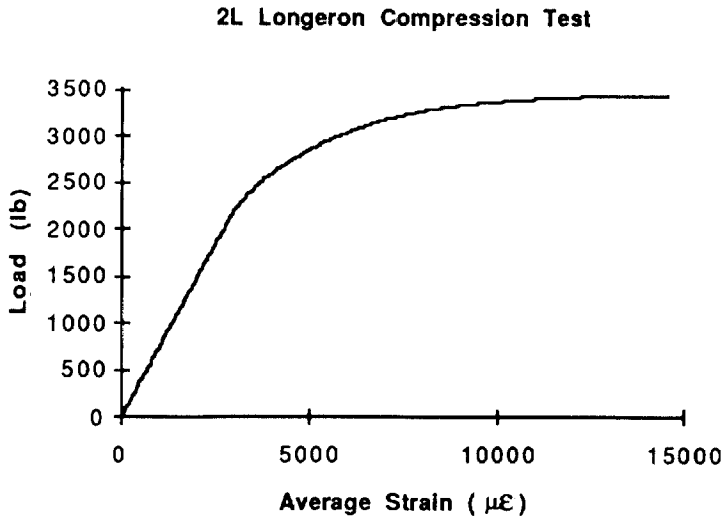

Figure 3-12 Typical 2L Longeron Strength Test Results

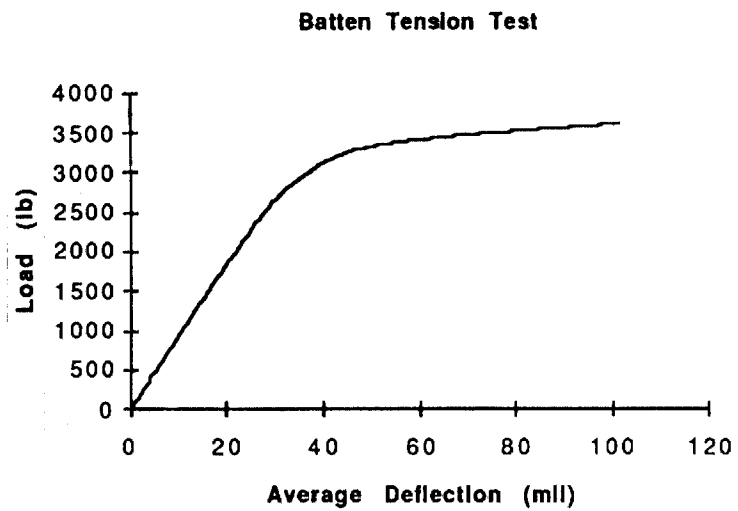

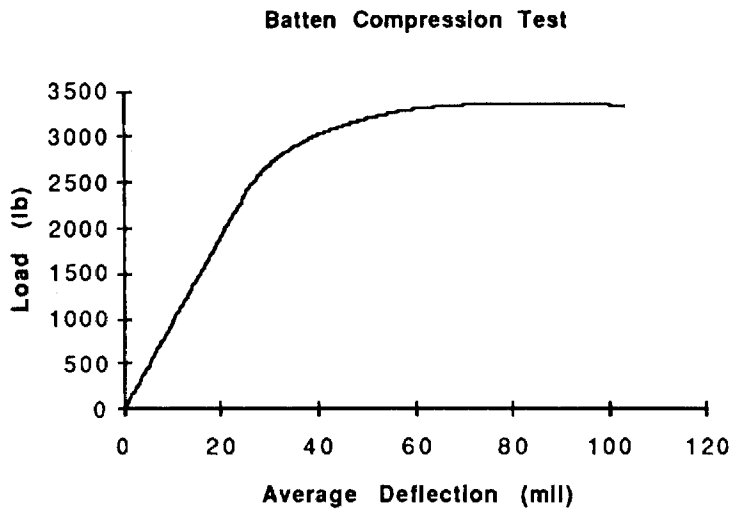

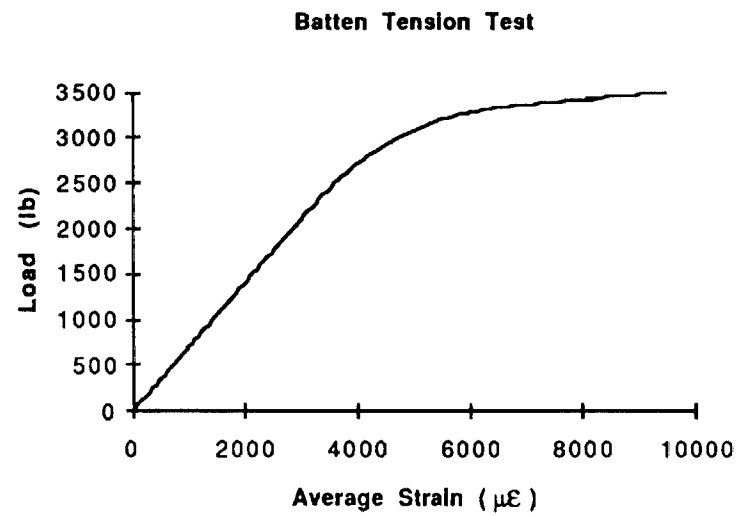

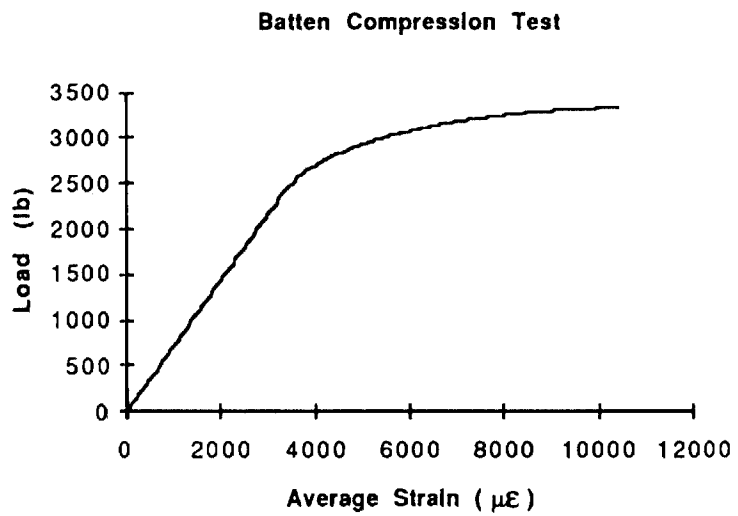

Figure 3-13 Typical Batten Strength Test Results

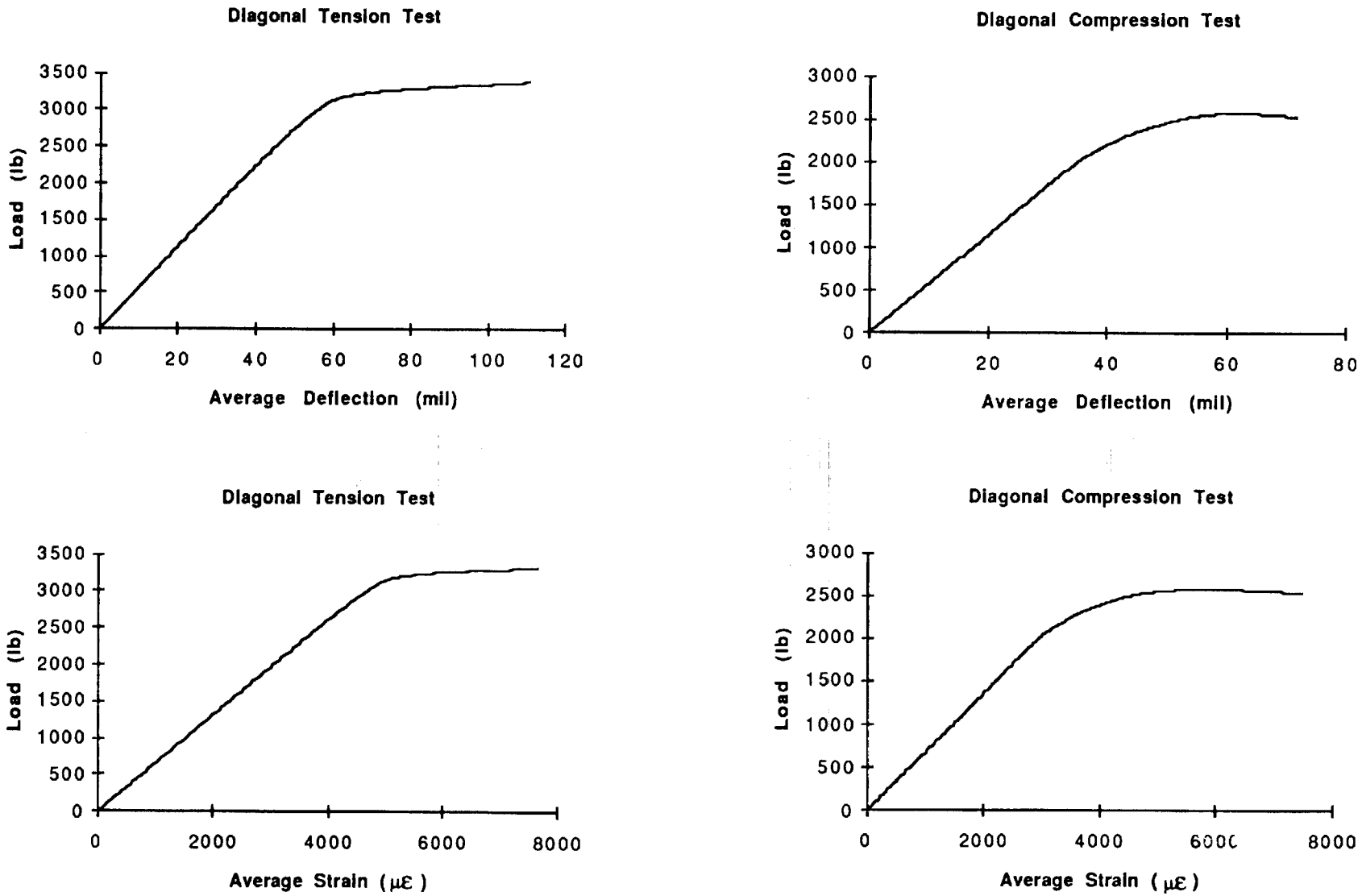

Figure 3-14 Typical Diagonal Strength Test Results

Table 3-6 Strut Strength Test Data Summary

STRUT ID	TEST TYPE	LOAD MAX (lbs)	LOAD @ YIELD Onset (lbs)	STRAIN @ YIELD Onset (με)	LOAD @ YIELD 0.2% (lbs)	STRAIN @ YIELD 0.2% (με)	LOAD @ Proport Limit (lbs)	DISP @ Proport Limit (mils)
2L161	T	4,056	2,602	3,456	3,774	7,000	1,925	19.67
2L016	T	4,035	1,933	2,663	3,640	7,041	1,480	15.73
2L018	T	3,999	2,358	3,238	3,673	7,052	1,544	16.07
2L020	T	4,091	2,125	2,958	3,623	7,081	1,940	23.47
2L034	T	4,021	2,803	3,900	3,617	7,052	1,597	17.40
Avg.		4,040	2,364	3,243	3,665	7,045	1,697	18.47
Std. Dev.		35	351	473	64	29	219	3.20
2L130	C	-3,275	-2,433	-3,093	-3,367	-6,265	-1,922	-18.92
2L011	C	-3,505	-2,073	-2,775	-3,211	-6,283	-2,027	-20.67
2L012	C	-3,560	-2,155	-2,892	-3,233	-6,354	-2,050	-21.13
2L013	C	-3,449	-2,120	-2,867	-3,065	-6,177	-2,117	-21.88
2L015	C	-3,524	-2,168	-2,904	-3,225	-6,313	-2,142	-22.02
Avg.		-3,463	-2,190	-2,906	-3,220	-6,278	-2,052	-20.92
Std. Dev.		112	141	116	107	66	86	1.25
B121	T	3,618	1,508	2,875	3,350	6,800	1,325	14.38
B122	T	3,669	2,116	3,067	3,366	6,875	1,350	14.42
B123	T	3,601	2,208	3,229	3,300	6,833	1,327	14.48
B124	T	3,633	2,100	3,054	3,317	6,775	1,583	17.17
B125	T	3,615	2,025	3,000	3,257	6,792	1,200	12.96
Avg.		3,627	1,991	3,045	3,318	6,815	1,357	14.68
Std. Dev.		26	278	128	43	40	139	1.53
B329	C	-2,891	-1,924	-2,900	-2,738	-6,125	-1,180	-13.40
B340	C	-2,981	-2,096	-3,133	-2,844	-6,275	-2,018	-22.40
B128	C	-3,372	-2,467	-3,463	-3,117	-6,375	-2,463	-26.13
B129	C	-3,294	-2,479	-3,454	-3,150	-6,375	-2,198	-23.00
B130	C	-3,344	-2,448	-3,452	-3,098	-6,371	-1,915	-20.73
Avg.		-3,176	-2,283	-3,280	-2,989	-6,304	-1,955	-21.13
Std. Dev.		224	257	255	186	109	480	4.74
D014	T	3,381	2,067	3,171	3,293	7,050	1,673	30.00
D015	T	3,357	1,899	2,875	3,233	6,873	1,400	24.75
D016	T	3,515	1,942	2,948	3,385	7,129	1,429	25.05
D017	T	3,425	1,557	2,373	3,283	8,000	1,467	26.05
D018	T	3,462	2,233	3,375	3,343	7,042	1,570	28.25
Avg.		3,428	1,940	2,948	3,307	7,219	1,508	26.82
Std. Dev.		63	250	377	58	447	113	2.25
D019	C	-2,581	-1,980	-2,935	-2,577	-5,810	-1,613	-27.83
D020	C	-2,752	-1,853	-2,740	-2,745	-6,046	-1,660	-28.10
D021	C	-2,565	-1,942	-2,908	-2,557	-5,833	-1,623	-28.33
D022	C	-2,494	-1,953	-2,896	-2,487	-5,708	-1,880	-33.03
D023	C	-2,523	-1,839	-2,792	-2,517	-5,821	-1,740	-30.93
Avg.		-2,583	-1,913	-2,854	-2,577	-5,844	-1,703	-29.64
Std. Dev.		101	63	84	100	124	111	2.27

Table 3-7 CEM Phase 1 Strut Performance

SEC #	STRUT ID (Revised)	QTY with Spares	QTY Assy	Nominal Stiffness (lb/in)	Nominal Wt (lbs) (With 31% Node Ball)	Actual Stiffness (lb/in)	Actual Wt (lbs) (With 31% Node Ball)	Strut Efficiency (η) (%)
Longerons								
1	1L	94	80	330,000	0.531	332,549	0.516	64.4
2	2L	94	80	85,387	0.276	99,125	0.272	36.4
3	3L	52	44	173,350	0.327	174,649	0.320	54.6
4	4L	104	88	260,300	0.411	264,236	0.402	65.7
5	4L	94	80	257,470	0.407	264,236	0.402	65.7
6	2L	94	80	95,226	0.280	99,125	0.272	36.4
7	2L	19	16	95,552	0.280	99,125	0.272	36.4
Battens								
1	B	99	84	81,898	0.274	97,359	0.269	36.2
2	B	94	80	82,951	0.274	97,359	0.269	36.2
3	B	52	44	82,155	0.274	97,359	0.269	36.2
4	B	104	88	81,797	0.274	97,359	0.269	36.2
5	B	94	80	80,792	0.273	97,359	0.269	36.2
6	B	94	80	80,941	0.274	97,359	0.269	36.2
7	B	19	16	81,432	0.274	97,359	0.269	36.2
Diagonals								
1	D	119	101	62,906	0.311	58,791	0.294	40.0
2	D	118	100	59,765	0.306	58,791	0.294	40.0
3	D	65	55	58,300	0.304	58,791	0.294	40.0
4	D	130	110	57,417	0.303	58,791	0.294	40.0
5	D	118	100	55,924	0.301	58,791	0.294	40.0
6	D	118	100	56,098	0.301	58,791	0.294	40.0
7	D	24	20	57,789	0.304	58,791	0.294	40.0

for the Phase 1 CEM structure is 42.9%, calculated using the number of struts of each type in the CEM Phase 1 structural assembly as the weighting factors. This is less than or equal to the corresponding 47.7% average strut efficiency for the CEM Phase 0 structure, as required to make valid comparisons between the Phase 1 and Phase 0 integrated control/structure performance.

The production strut design also meets the strength requirements. For the 30 strut strength tests conducted, ultimate failure was never observed below a factor of safety of 2.0, and significant margin exists for the onset of yield.

4.0 TRUSS SECTION DYNAMIC TESTS

Component modal tests on 10-bay truss sections of the NASA/LaRC CEM Phase 1 testbed were performed in the LMSC Space System Division (SSD) Structural Dynamics Lab located in Sunnyvale, California. The objective of these tests was to quantify the dynamic characteristics of individual truss sections and to provide data for NASA/LaRC to correlate the analytical models. Measured frequency, damping, and mode shape modal parameters for seven target modes were obtained for each truss section. The seven target modes were defined as the first and second bending mode pairs (B-1, B-2), the first and second torsion modes (T-1, T-2), and the first axial mode of the structure. Although difficulty was encountered in generating accurate test-analysis models using the Guyan reduction method, excellent test-analysis comparisons were obtained for the target modes.

This section discusses the test and analysis approach, followed by a discussion on pretest analysis, including the development of reduced test-analysis models. Next, descriptions of the test equipment, data acquisition/analysis software, and test methodology are presented. As a check of data quality, modal test results are compared with the finite element model predictions. A summary of the important findings and conclusions from the modal test series concludes this section.

4.1 APPROACH

The CSI Evolutionary Model consists of four unique truss sections referred to as Section-1, Section-2, Section-3, and Section-4. Both cantilevered and free-free modal tests were performed using ten bays of each section type resulting in the eight test configurations identified below.

TEST	CONFIGURATION
1.	Section-1 Cantilevered
2.	Section-1 Free-Free
3.	Section-2 Cantilevered
4.	Section-2 Free-Free
5.	Section-3 Cantilevered
6.	Section-3 Free-Free

7. Section-4 Cantilevered
8. Section-4 Free-Free

The cantilevered tests were conducted with the truss sections mounted to a steel base fixture as shown in Figure 4-1. The free-free tests were conducted with the truss structure suspended on four low frequency bungee cords as shown in Figure 4-2. Dynamically testing the truss sections using two different sets of boundary conditions provides additional information on the modal characteristics of the truss structure which can be beneficial during finite element model correlation.

The approach taken in choosing the appropriate 10-bay truss configuration for each section test was to duplicate selected truss sections contained in the assembled CEM model in terms of strut lacing pattern, coordinate system, node ball slot alignment, and applied gravity loading direction. This was accomplished by assembling each of the individual test sections to be identical to the representative 10-bay sections extracted from the system model (Figure 4-3). Representative sections were selected by defining the batten frames at the section-to-section interfaces as the fixed ends for the cantilevered modal tests. Defining the test sections in such a manner enabled the cantilevered modal tests to closely simulate the cantilevered truss configurations present in the assembled CEM with the exception of Section-4 which was located mid-span in the structure.

Configuring the test sections identical to the CEM system model allows for perfect integration of the test-verified 10-bay truss segments into the system level structure on a strut by strut basis during final assembly. Individual strut identification numbers were recorded for each test section as shown in Appendix B.

The gravity loading direction on the truss sections in the CEM model was preserved during modal testing for all sections except Section-3. This vertically aligned tower section was loaded by gravity in the longitudinal direction in the system model but was tested in a horizontal orientation for expediency.

Following each truss section modal test, the overall quality and consistency of the measured data was evaluated by comparing it with Finite Element Model (FEM) analytical predictions updated with individual strut static test results. Cross-orthogonality (XO), Root Modal Assurance Criteria (RMAC) and frequency error modal comparison criteria were used as defined in Figure 4-4. Post-test correlation of the finite element models for each truss section is outside of the scope of the contracted effort and is planned to be performed by NASA/LaRC.

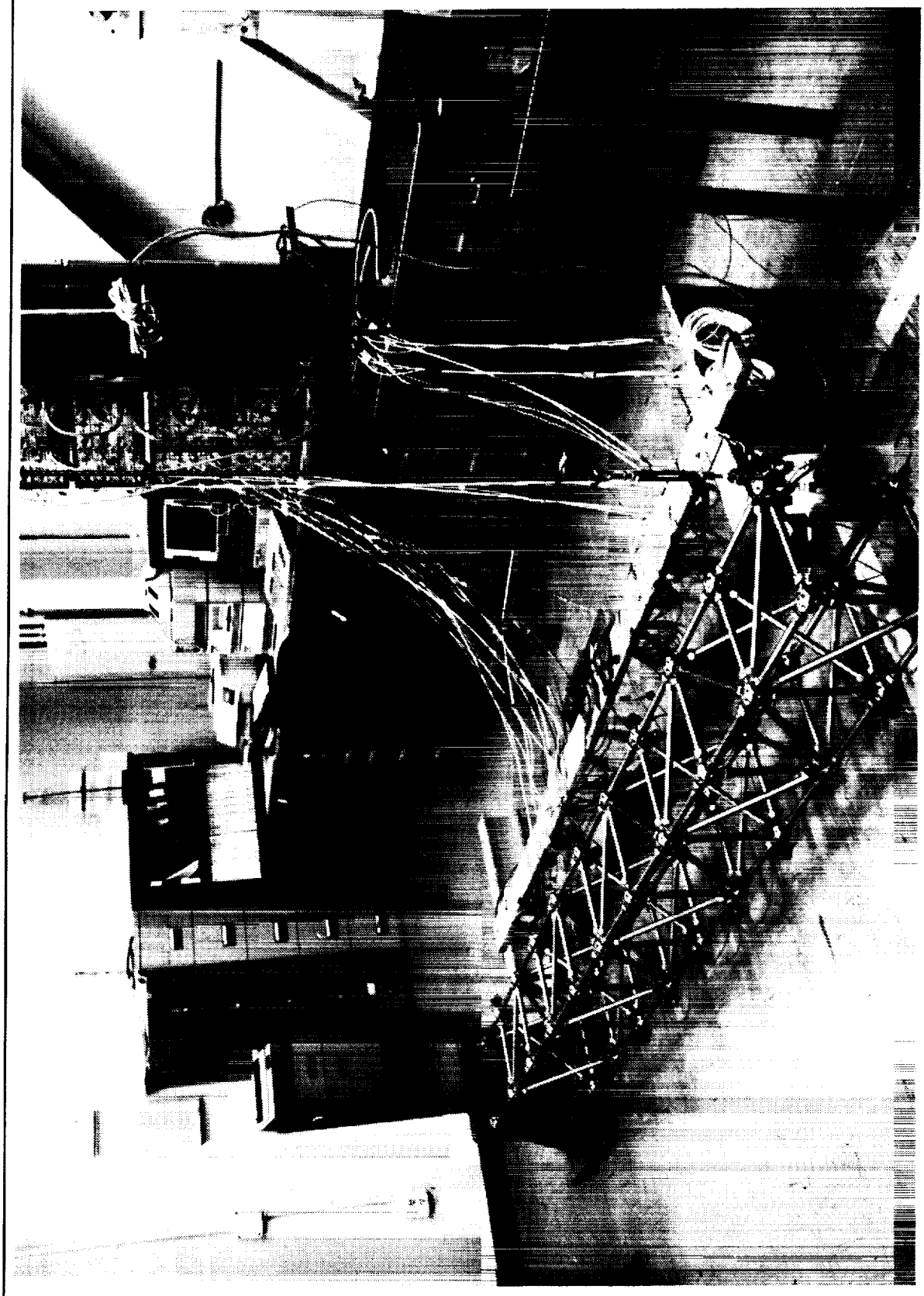

MB127F2Fig. 4-1

Figure 4-1 Cantilevered 10 Bay Truss Section Modal Test

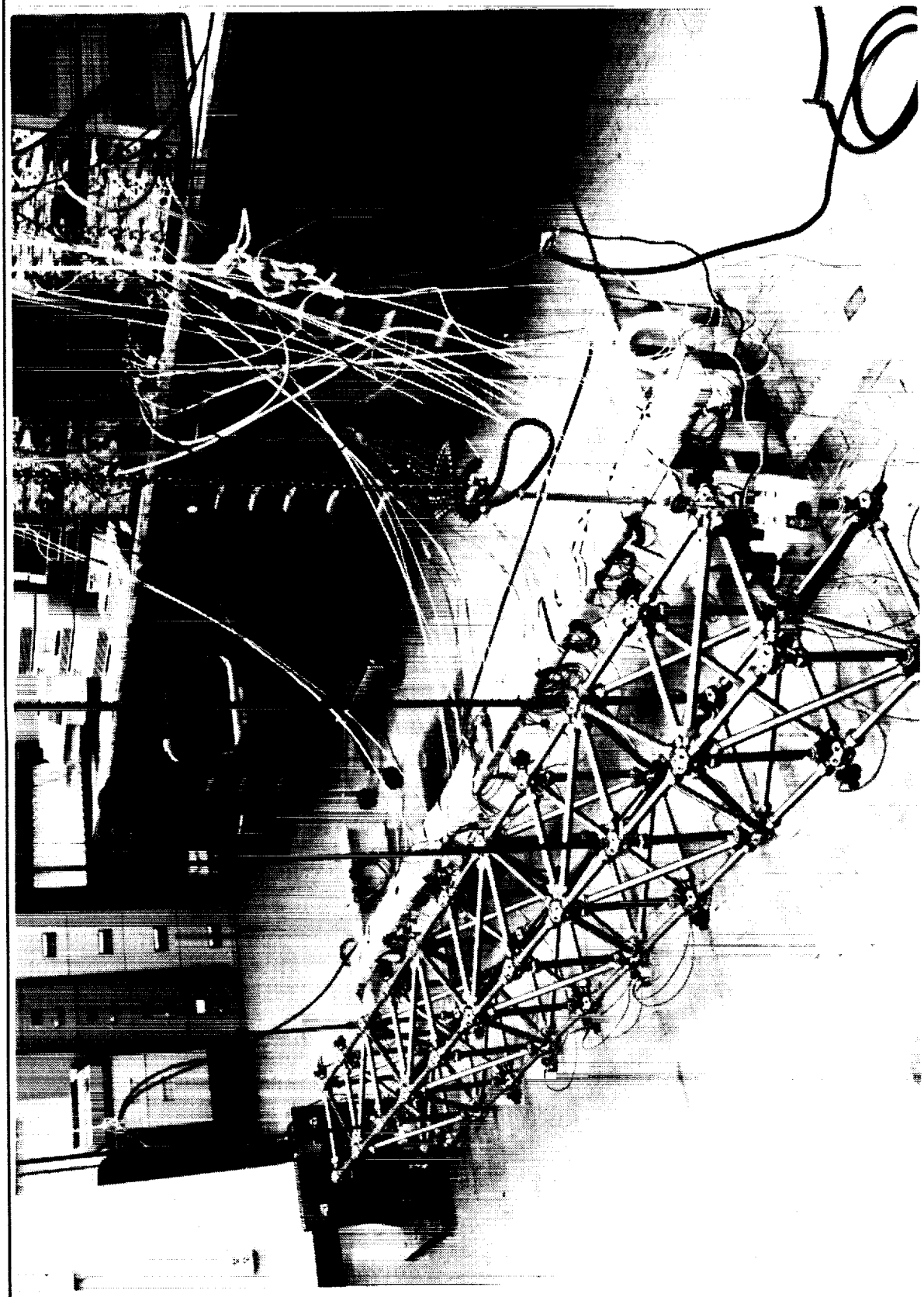

Figure 4-2 Free-Free 10 Bay Truss Section Modal Test

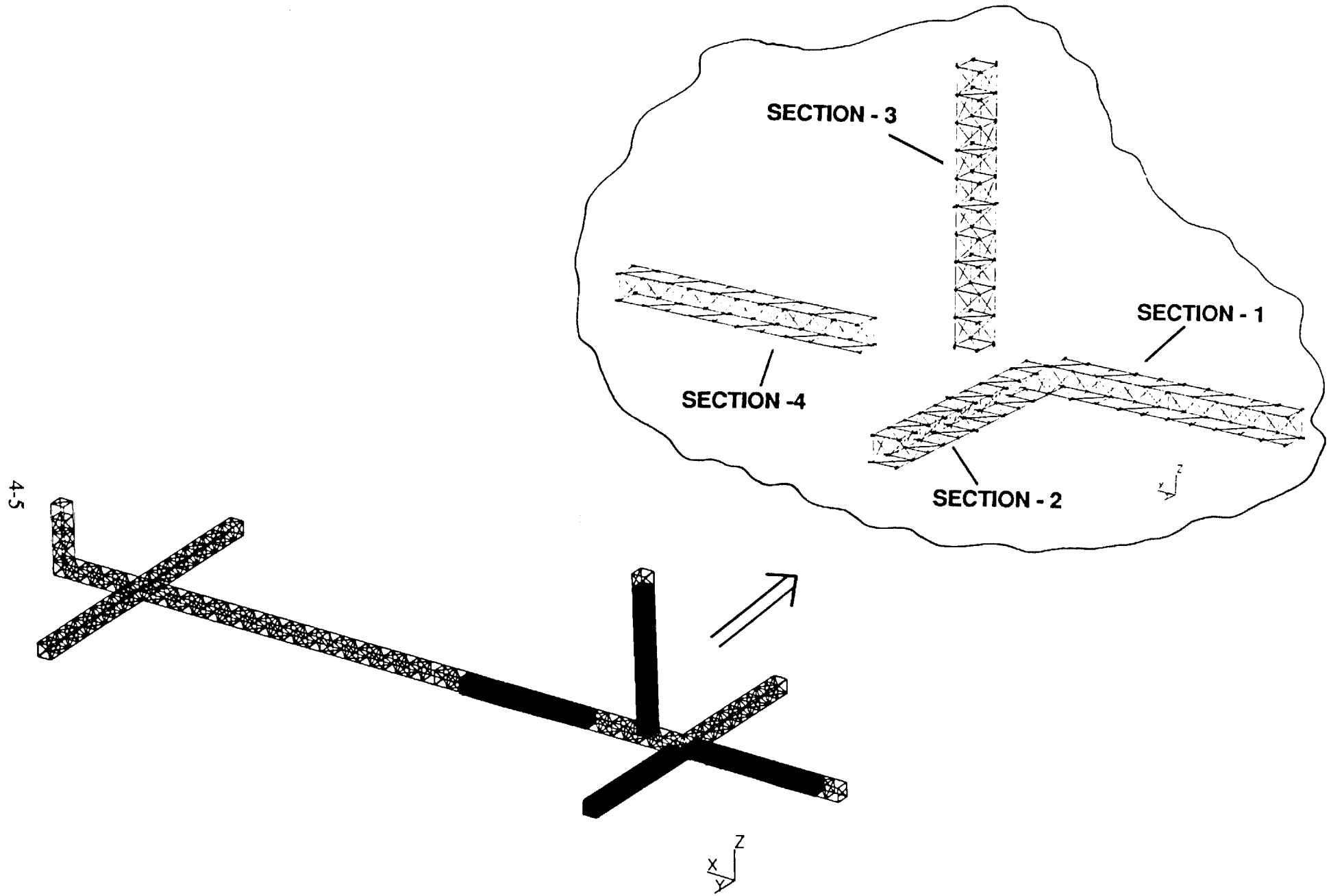

Figure 4-3 CEM Representative 10 Bay Test Sections

Basic Modal Comparison Criteria Are Frequency, RMAC, and XO

Root Modal Assurance Criterion

$$RMAC = \sqrt{\frac{[\phi_A^T \phi_B]^2}{[\phi_A^T \phi_A] \cdot [\phi_B^T \phi_B]}} = \cos\theta$$

RMAC = 1.0, Modes Are Identical
RMAC = 0.0, Modes Are Shape-Orthogonal

Cross-Orthogonality

$$XO = [\phi_A]^T [M] [\phi_B]$$

XO = 1.0, Modes Are Identical
XO = 0.0, Modes Are Mass-Orthogonal

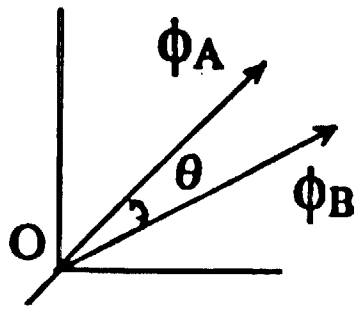

RMAC	θ^o
1.0	0.0
0.95	18.2
0.90	25.8

Notes:
XO Assumes Both Sets of Eigenvectors Are Orthonormalized
XO and RMAC Comparisons Are Weighted by the Number of Nodes
3-D Analogy Shows That Vector Dot Product (RMAC) is Based On A Sliding Scale

Figure 4-4 Modal Comparison Criteria

4.2 PRETEST ANALYSIS

Preliminary MSC/NASTRAN Version 66 finite element models of the four individual 10-bay truss sections were generated using the same model fidelity present in the existing system level CEM finite element model provided by NASA/LaRC. Grid points with concentrated masses were used to model the 44 Node Balls resulting in individual Longeron, Batten, and Diagonal struts being represented by single uniform CBAR elements with equivalent beam properties. Each strut assembly (including the joints) is modeled as a single element. Strut element mass properties were lumped at the Node Ball grid points using the coupled mass option in NASTRAN.

These preliminary models were used to determine the optimum set of the accelerometer measurements necessary to accurately quantify the truss dynamic behavior prior to the start of modal testing. Once the sensor set was defined, formal test-analysis models were generated based on updated finite element models which included instrumentation mass and offset effects as well as strut stiffness properties obtained from the static strut tests (Table 3-7).

4.2.1 Sensor Locations

To determine the locations and numbers of sensors needed to adequately describe the dynamic response of the test articles in both cantilevered and free-free configurations, preliminary Test-Analysis Models (TAM's) were generated using the Guyan static reduction procedure. A TAM is a reduced order analysis model whose Degrees-of-Freedom (DOF) are identical to the sensor DOF measured during a modal survey. The cross-orthogonality and frequency errors between the TAM and FEM are compared for the important modes as a means of evaluating the accuracy of the reduced model. Following testing, the TAM mass matrix is used to compute post-test cross-orthogonality between the test and analysis modes as well as to determine test mode orthogonality.

Preliminary TAM's were generated using the Section-2 cantilevered and free-free finite element models which are representative of all four test sections in terms of evaluating proposed instrumentation placement. Static reduction analyses were computed at several sets of selected Node Ball degrees-of-freedom in order to determine the optimum accelerometer locations. The modes used to evaluate the validity of the reduced models are the seven target modes listed earlier in the report. No instrumentation mass properties or offsets were included in the preliminary TAM models. Due to the large frequency separation between the suspension and elastic

modes for the free-free configuration, suspension system and gravity effects on the structure were considered negligible and thus not included in the analyses.

Two pretest requirements were defined as part of generating acceptable reduced models of the free-free and cantilevered test sections. The first was to maximize the accelerometer commonality between the two test configurations, which reduces the amount of instrumentation channel swap-out required. The second was to develop acceptable TAM's using no more than 44 measurement channels so the existing data acquisition system could simultaneously record all the data channels in a single pass. It was not desirable to record data in multiple passes since potential non-linear and time-variant effects may introduce inconsistencies between response data taken during different passes. In addition, acquiring the data in a single pass results in reduced testing time which was very important given the tight test schedule.

Tables 4-1a and 4-1b summarize the preliminary TAM results corresponding to the final accelerometer degrees-of-freedom set chosen for each test configuration. The cross-orthogonality and frequency comparisons between the TAM and FEM for the cantilevered case show excellent agreement for all seven target modes. The axial mode has the lowest cross-orthogonality and highest frequency error of 0.95 and 2.3%, respectively. This result is not surprising since the majority of the accelerometer DOF's measure vertical and lateral motion associated with bending and torsion modes and not pure axial motion. Similar results are evident in the free-free case where, again, the axial mode has the lowest cross-orthogonality and the highest frequency error.

In general, the free-free TAM is not as accurate as that generated for the cantilevered case. This result can be attributed to the fact that a first cantilevered bending mode shape represents only one-half of the first free-free bending mode shape for a classical truss structure. Thus, the spatial density of sensor DOF's for the cantilevered test is effectively twice that of the free-free test, resulting in a better reduced model.

Figure 4-5 illustrates the final overall accelerometer locations and degrees-of-freedom (tri-axial etc.) chosen for the modal tests based on the preliminary TAM results. The figure shows the accelerometer identification number, DOF's, and location as a function of truss batten frame number where the frames are viewed looking down the truss longitudinal axis from the fixed cantilevered end. The relative orientations of the batten frame diagonal struts shown in the figure are arbitrary. Individual coordinate systems used to model the truss sections are consistent with the CEM global coordinate system and are shown in Figure 4-6 for reference. A tabular listing of the information contained in Figure 4-5 is summarized in Table 4-2, which identifies the

Table 4-1a Preliminary Static TAM for Section-2 Cantilevered Test Without Accelerometer Weights

TAM MODE NO.	TAM FREQ (HZ)	XO	FEM MODE NO.	FEM FREQ (HZ)	FREQ ERROR (%)	DESCRIPTION
1	16.82	1.00	1	16.81	0.0	1st BENDING
2	17.22	1.00	2	17.21	0.0	1st BENDING
3	62.82	0.99	3	62.53	0.5	1st TORSION
4	84.51	0.99	4	83.99	0.6	2nd BENDING
5	89.09	0.99	5	88.63	0.5	2nd BENDING
6	171.79	0.98	6	170.14	1.0	AXIAL
7	189.55	0.95	7	185.23	2.3	2nd TORSION

Table 4-1b Preliminary Static TAM for Section-2 Free-Free Test Without Accelerometer Weights

TAM MODE NO.	TAM FREQ (HZ)	XO	FEM MODE NO.	FEM FREQ (HZ)	FREQ ERROR (%)	DESCRIPTION
7	93.44	0.97	7	93.15	0.3	1st BENDING
8	93.75	0.97	8	93.33	0.5	1st BENDING
9	123.00	0.89	9	121.53	1.2	1st TORSION
10	210.01	0.92	11	205.75	2.1	2nd BENDING
11	210.91	0.90	10	204.31	3.2	2nd BENDING
12	245.05	0.94	12	238.64	2.7	2nd TORSION
13	346.65	0.89	15	328.26	5.6	AXIAL

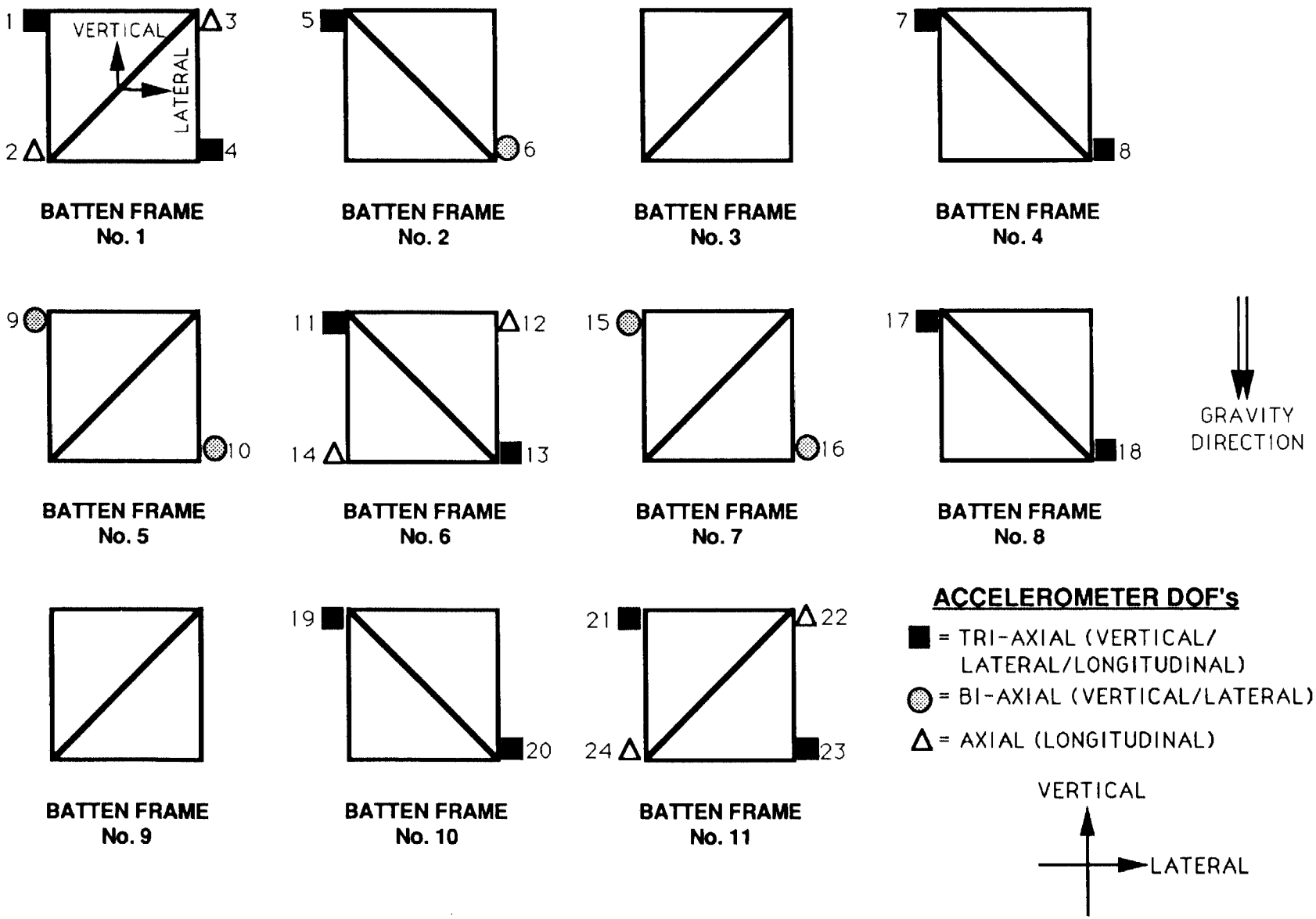

Figure 4-5 Overall Modal Test Accelerometer Locations

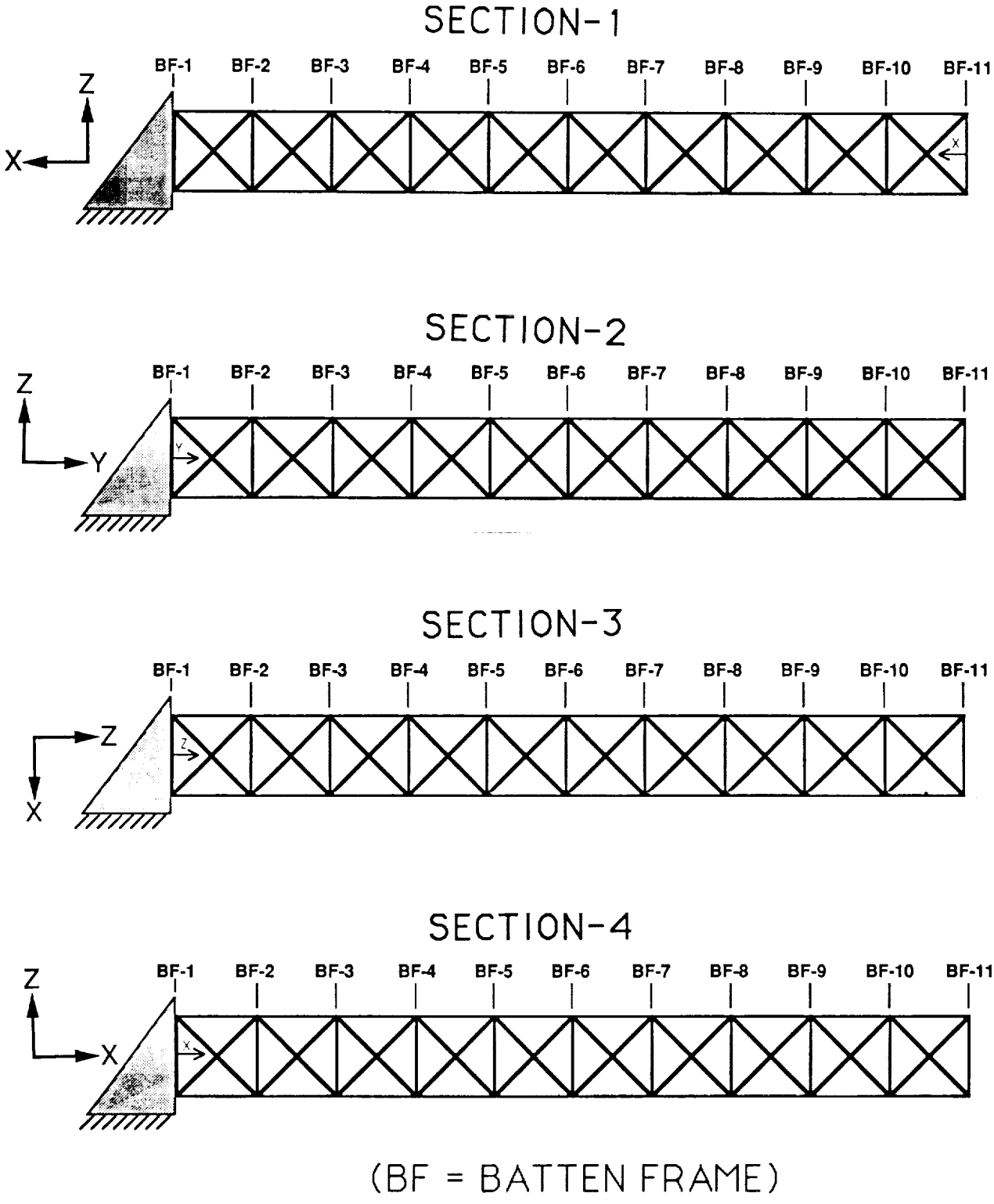

Figure 4-6 Modal Test Coordinate Systems

Table 4-2 Test vs FEM Accelerometer DOF Map

CANTILEVERED		FREE-FREE		
ACCEL NO.	DOF's	ACCEL NO.	DOF's	ACCELEROMETER FEM GRID NO.
1	-	1	Tri-Axial	X900
2	-	2	Axial	X901
3	-	3	Axial	X902
4	-	4	Tri-Axial	X903
5	Bi-Axial	5	Tri-Axial	X904
6	Bi-Axial	6	Bi-Axial	X906
7	Tri-Axial	7	Bi-Axial	X912
8	Tri-Axial	8	Bi-Axial	X914
9	Bi-Axial	9	Bi-Axial	X916
10	Bi-Axial	10	Bi-Axial	X918
11	Tri-Axial	11	Axial	X920
12	Axial	12	-	X921
13	Tri-Axial	13	Axial	X922
14	Axial	14	-	X923
15	-	15	Bi-Axial	X924
16	-	16	Bi-Axial	X926
17	Tri-Axial	17	Bi-Axial	X928
18	Tri-Axial	18	Bi-Axial	X930
19	Tri-Axial	19	Tri-Axial	X936
20	Tri-Axial	20	Bi-Axial	X938
21	Tri-Axial	21	Tri-Axial	X940
22	Axial	22	Axial	X941
23	Tri-Axial	23	Tri-Axial	X942
24	Axial	24	Axial	X943
TOTAL = 42		**TOTAL = 44**		

NOTES: *Tri-Axial = Vertical/Lateral/Longitudinal DOF's*

Bi-Axial = Vertical/Lateral DOF's

Axial = Longitudinal DOF

"X" = Truss Section Number (1,2,3, or 4)

Total Overall DOF = 55

FEM grid point corresponding to each accelerometer location. This test versus FEM degree-of-freedom map is needed when comparing test vs. FEM mode shape data.

All of the objectives and requirements associated with choosing the accelerometer locations for the modal tests were successfully met. Only 42 sensor DOF's were required to accurately capture the target modes in the cantilevered model while the maximum of 44 were chosen for the free-free model enabling the measured data to be recorded in a single pass. There was an overall combined total of 55 unique accelerometer DOF's between both test configurations, of which 31 were common. As a result, only a maximum of 13 accelerometer channels needed to be changed when converting from a cantilevered to free-free test set-up or vice versa. This reduced the potential for wiring errors and saved valuable set-up time in the test lab. All of the accelerometer instrumentation (55 channels) was mounted to each test article prior to the start of testing so that identical instrumentation hardware was present in each test configuration.

4.2.2 Finite Element Modeling

All of the truss section finite element models were generated using an identical grid numbering sequence relative to the cantilevered orientation of the truss sections. An example plot of the finite element model grid point numbering scheme is shown in Figure 4-7 using Section-1 for reference. Node Ball grids points were assigned X000 range values while accelerometer response grid points were assigned X900 range values with the "X" variable corresponding to the truss section number (1, 2, 3, or 4). By using this consistent and systematic grid numbering convention, only the "X" value needs to be changed when referring to different section models. This approach minimized the potential confusion associated with comparing test data versus FEM predictions for eight very similar modal tests.

Additional modeling simplifications were introduced by using the same identical MSC/NASTRAN bulk data deck for both the cantilevered and free-free finite element models of a truss section. This was made possible by the fact that all instrumentation weight was added to the structure prior to testing. Therefore, the only modeling differences between the two configurations are the boundary node conditions. A summary of the accelerometer weights included in the finite element models is shown in Table 4-3 as a function of FEM grid number. The combined instrumentation weight associated with the 55 accelerometer DOF's was 2.0134 lbs which is approximately 5% of the lightest test section weight.

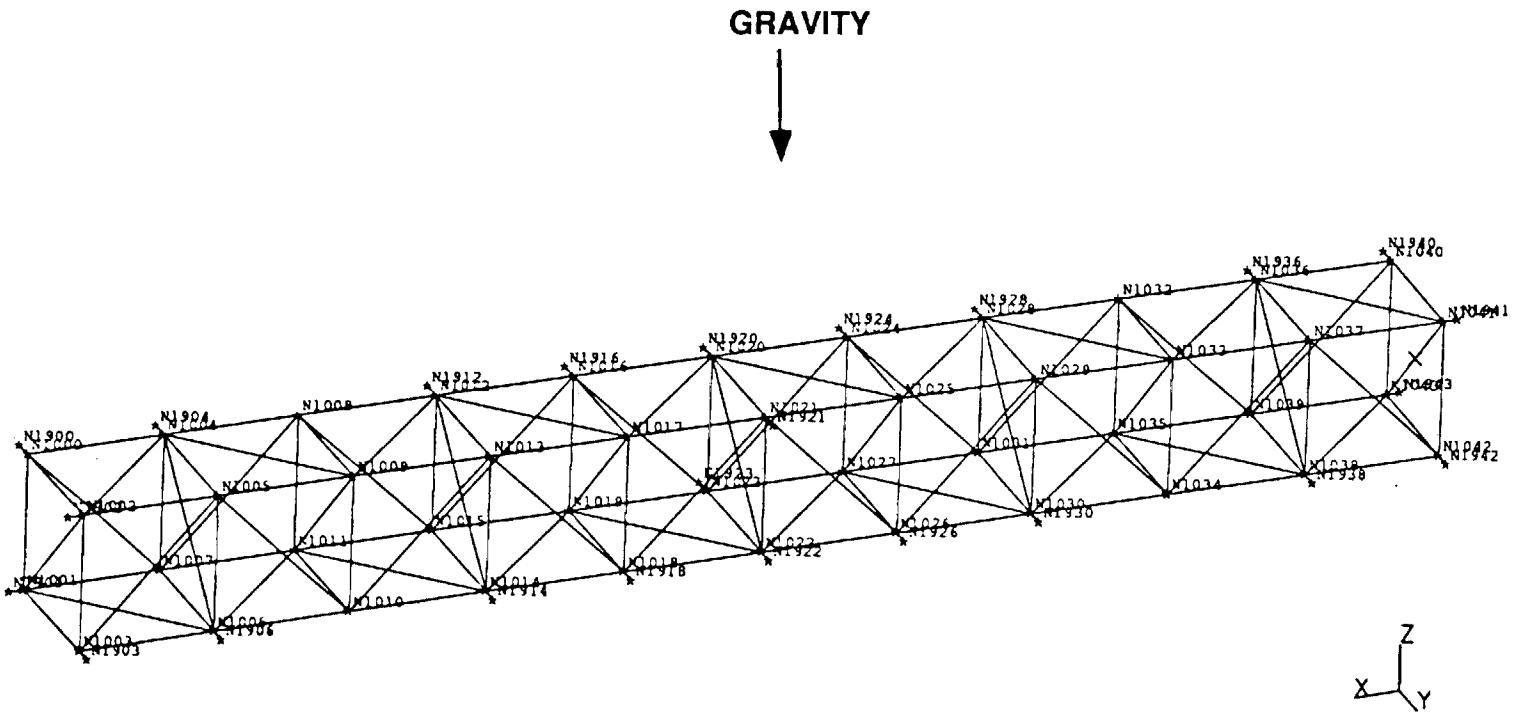

Figure 4-7 Section-1 FEM Mesh Plot With Grid Point Numbers

Table 4-3 Accelerometer Weights

ACCEL NO.	DOF's	ACCEL FEM GRID NO.	ACCEL WEIGHT (LBS)
1	Tri-Axial	X900	0.11268
2	Axial	X901	0.04414
3	Axial	X902	0.04414
4	Tri-Axial	X903	0.08435
5	Tri-Axial	X904	0.08435
6	Bi-Axial	X906	0.08435
7	Tri-Axial	X912	0.08435
8	Tri-Axial	X914	0.08435
9	Bi-Axial	X916	0.09954
10	Bi-Axial	X918	0.09954
11	Tri-Axial	X920	0.11268
12	Axial	X921	0.08640
13	Tri-Axial	X922	0.11268
14	Axial	X923	0.08640
15	Bi-Axial	X924	0.09954
16	Bi-Axial	X926	0.09954
17	Tri-Axial	X928	0.08435
18	Tri-Axial	X930	0.08435
19	Tri-Axial	X936	0.08435
20	Tri-Axial	X938	0.08435
21	Tri-Axial	X940	0.08435
22	Axial	X941	0.04414
23	Tri-Axial	X942	0.08435
24	Axial	X943	0.04414

NOTES: *Tri-Axial = Vertical/Lateral/Longitudinal DOF's*

Bi-Axial = Vertical/Lateral DOF's

Axial = Longitudinal DOF

"X" = Truss Section Number (1,2,3, or 4)

Total Accel DOF's = 55

Total Accel Weight = 2.0134 LBS

Several updates were made to the preliminary finite element models initially used for determining accelerometer locations. These changes were made to all four section models prior to computing final test-analysis models used in evaluating the modal test results. One of the more significant updates consisted of adding concentrated weight at the accelerometer FEM grid points in order to reflect the effect of instrumentation weight on dynamic response. These concentrated weights were placed at the physical transducer locations laterally offset approximately 1.5 inches from the Node Ball center.

A second important model update was the addition of actual strut effective area properties based on the strut static stiffness tests results presented in Section 3.0 of the report. All seven of the target mode frequencies are heavily coupled to strut axial stiffness, which explains the importance of accurately modeling the axial stiffness properties. A summary of the strut section properties used in the updated pretest finite element models is presented in Table 4-4. Table 4-5 shows the weight breakdown of the 10-bay section finite element models (free-free) on a component level with Section-1 being the heaviest and Section-2 the lightest. Complete MSC/NASTRAN mass property outputs are contained in Appendices C through F for the four truss test sections, respectively.

4.2.3 Test-Analysis Models

Reduced test-analysis models were computed for the free-free and cantilevered configurations of each truss section using the updated pretest finite element models. Analogous to the preliminary TAM analyses, the Guyan static reduction method was again employed but this time the reduction was performed at the sensor degrees-of-freedom (X900 grid points) corresponding to the actual measurement locations. This is different from the preliminary TAM which computed the static reduction at the Node Ball degrees-of-freedom (X000 grid points). The results of the computed TAM versus FEM comparisons for the seven target modes are shown in Tables 4-6 through 4-13 for all eight modal tests. Modal comparison criteria outlined in Figure 4-4 are used to evaluate the overall accuracy of the reduced models.

4.2.3.1 Closely Spaced Modes

Before interpreting the TAM results, it is important to note that the physical properties of the truss sections are extremely uniform and symmetric about the longitudinal axis of the structure which results in eigensolutions with closely spaced bending mode pairs. One of the consequences of performing the Guyan reduction at the actual sensor DOF's was the introduction of a mass moment of inertia bias in the TAM matrices due

Table 4-4 Pretest FEM Strut Properties

Strut Description	Effective Area (in^2)	Strut Weight (lbs)	Strut Length (in)	Node Weight (lbs)
S1 longeron	0.3326	0.467	10	0.159
S2 longeron	0.0991	0.223	10	0.159
S3 longeron	0.1747	0.271	10	0.159
S4 longeron	0.2640	0.353	10	0.159
Batten	0.0974	0.220	10	0.159
Diagonal	0.0831	0.245	14.142	0.159

- Strut weight and effective area include standoffs, nuts and screws
- Effective area assumes E=10.E+6 lb/in^2

Strut Description	Outer Radius Actual (in)	Inner Radius Actual (in)	Area Moment of Inertia (in^4)	Torsional Constant (in^4)
S1 longeron	0.438	0.188	0.027789	0.055579
S2 longeron	0.293	0.250	0.002736	0.005471
S3 longeron	0.330	0.250	0.006290	0.012580
S4 longeron	0.393	0.250	0.015703	0.031406
Batten	0.287	0.250	0.002314	0.004628
Diagonal	0.289	0.250	0.002442	0.004883

Table 4-5 FEM Section Weights Summary

SECTION NO.	LONGERONS (LBS)	DIAGONALS (LBS)	BATTENS (LBS)	NODE BALLS (LBS)	SENSORS (LBS)	TOTAL WEIGHT (LBS)
1	18.68	12.50	9.68	6.99	2.01	49.86
2	8.92	12.50	9.68	6.99	2.01	40.10
3	10.84	12.50	9.68	6.99	2.01	42.02
4	14.12	12.50	9.68	6.99	2.01	45.30

Table 4-6 TAM vs. FEM Cross-Orthogonality and RMAC Comparison for Updated Pretest Section-1 Cantilevered Truss Model

TAM MODE	TAM FREQ (HZ)	XO	LIN-COM XO	RMAC	LIN-COM RMAC	FEM MODE	FEM FREQ (HZ)	FREQ ERROR (%)	DESCRIPTION
1	24.86	0.93	1.00	0.93	1.00	1	24.84	0.1	1st BENDING
2	25.05	0.92	0.99	0.93	1.00	2	24.85	0.8	1st BENDING
3	57.39	0.99	0.99	1.00	1.00	3	57.10	0.5	1st TORSION
4	104.33	0.86	0.94	0.89	1.00	4	103.39	0.9	2nd BENDING
5	114.41	0.72	0.85	0.87	1.00	5	103.56	10.5	2nd BENDING
6	174.80	0.93	0.93	1.00	1.00	6	168.89	3.5	2nd TORSION
8	271.77	0.86	0.86	1.00	1.00	9	253.38	7.3	AXIAL

Table 4-7 TAM vs. FEM Cross-Orthogonality and RMAC Comparison for Updated Pretest Section-1 Free-Free Truss Model

TAM MODE	TAM FREQ (HZ)	XO	LIN-COM XO	RMAC	LIN-COM RMAC	FEM MODE	FEM FREQ (HZ)	FREQ ERROR (%)	DESCRIPTION
7	113.08	0.97	0.97	1.00	1.00	7	111.20	1.7	1st TORSION
8	129.41	0.81	0.91	0.86	1.00	8	127.13	1.8	1st BENDING
9	144.04	0.65	0.84	0.82	1.00	9	127.59	12.9	1st BENDING
10	230.20	0.87	0.87	1.00	1.00	10	215.33	6.9	2nd TORSION
11	245.29	0.61	0.71	0.75	0.98	11	234.81	4.5	2nd BENDING
12	312.42	0.35	0.72	0.75	0.91	12	236.56	32.1	2nd BENDING
22	569.74	0.44	0.44	0.64	0.64	31	480.89	18.5	AXIAL

Table 4-8 TAM vs. FEM Cross-Orthogonality and RMAC Comparison for Updated Pretest Section-2 Cantilevered Truss Model

TAM MODE	TAM FREQ (HZ)	XO	LIN-COM XO	RMAC	LIN-COM RMAC	FEM MODE	FEM FREQ (HZ)	FREQ ERROR (%)	DESCRIPTION
1	16.03	0.99	1.00	1.00	1.00	1	16.00	0.2	1st BENDING
2	16.40	0.99	1.00	1.00	1.00	2	16.37	0.2	1st BENDING
3	66.87	0.99	0.99	1.00	1.00	3	66.37	0.8	1st TORSION
4	82.23	0.83	0.92	0.89	1.00	4	80.05	2.7	2nd BENDING
5	88.52	0.79	0.93	0.87	1.00	5	84.14	5.2	2nd BENDING
6	177.22	0.80	0.80	1.00	1.00	6	159.74	10.9	AXIAL
8	204.80	0.91	0.91	1.00	1.00	9	196.21	4.4	2nd TORSION

Table 4-9 TAM vs. FEM Cross-Orthogonality and RMAC Comparison for Updated Pretest Section-2 Free-Free Truss Model

TAM MODE	TAM FREQ (HZ)	XO	LIN-COM XO	RMAC	LIN-COM RMAC	FEM MODE	FEM FREQ (HZ)	FREQ ERROR (%)	DESCRIPTION
7	89.20	0.86	0.96	0.88	1.00	7	88.48	0.8	1st BENDING
8	95.08	0.76	0.90	0.87	1.00	8	88.89	7.0	1st BENDING
9	132.10	0.96	0.96	1.00	1.00	9	129.27	2.2	1st TORSION
10	202.98	0.85	0.86	0.96	0.98	10	194.51	4.4	2nd BENDING
11	250.58	0.53	0.62	0.89	0.98	11	196.21	27.7	2nd BENDING
12	265.01	0.87	0.87	1.00	1.00	12	248.54	6.6	2nd TORSION
14	369.49	0.54	0.54	0.95	0.95	14	289.67	27.6	AXIAL

Table 4-10 TAM vs. FEM Cross-Orthogonality and RMAC Comparison for Updated Pretest Section-3 Cantilevered Truss Model

TAM MODE	TAM FREQ (HZ)	XO	LIN-COM XO	RMAC	LIN-COM RMAC	FEM MODE	FEM FREQ (HZ)	FREQ ERROR (%)	DESCRIPTION
1	20.49	0.89	1.00	0.89	1.00	1	20.48	0.1	1st BENDING
2	20.60	0.88	1.00	0.89	1.00	2	20.49	0.6	1st BENDING
3	60.37	0.99	1.00	1.00	1.00	3	60.03	0.6	1st TORSION
4	96.14	0.96	0.97	0.98	1.00	4	95.29	0.9	2nd BENDING
5	104.68	0.81	0.84	0.97	1.00	5	95.61	9.5	2nd BENDING
6	183.82	0.92	0.92	1.00	1.00	6	177.06	3.8	2nd TORSION
8	218.14	0.81	0.81	1.00	1.00	7	198.01	10.2	AXIAL

Table 4-11 TAM vs. FEM Cross-Orthogonality and RMAC Comparison for Updated Pretest Section-3 Free-Free Truss Model

TAM MODE	TAM FREQ (HZ)	XO	LIN-COM XO	RMAC	LIN-COM RMAC	FEM MODE	FEM FREQ (HZ)	FREQ ERROR (%)	DESCRIPTION
7	110.37	0.96	0.96	0.99	0.99	7	109.00	1.3	1st BENDING
9	121.00	0.96	0.96	0.98	0.98	8	109.51	10.5	1st BENDING
8	119.12	0.80	0.80	1.00	1.00	9	117.00	1.8	1st TORSION
10	230.80	0.90	0.90	1.00	1.00	10	220.01	4.9	2nd BENDING
11	239.98	0.50	0.50	0.98	0.98	12	225.56	6.4	2nd TORSION
12	297.78	0.87	0.87	1.00	1.00	11	223.49	33.2	2nd BENDING
19	454.03	0.38	0.38	0.65	0.65	19	354.41	28.1	AXIAL

Table 4-12 TAM vs. FEM Cross-Orthogonality and RMAC Comparison for Updated Pretest Section-4 Cantilevered Truss Model

TAM MODE	TAM FREQ (HZ)	XO	LIN-COM XO	RMAC	LIN-COM RMAC	FEM MODE	FEM FREQ (HZ)	FREQ ERROR (%)	DESCRIPTION
1	23.65	0.93	1.00	0.93	1.00	1	23.63	0.1	1st BENDING
2	23.81	0.92	0.99	0.93	1.00	2	23.64	0.7	1st BENDING
3	59.73	0.99	0.99	1.00	1.00	3	59.29	0.8	1st TORSION
4	103.59	0.87	0.94	0.90	1.00	4	102.48	1.1	2nd BENDING
5	113.10	0.73	0.85	0.88	1.00	5	102.69	10.1	2nd BENDING
6	229.50	0.92	0.92	1.00	1.00	6	175.30	4.2	2nd TORSION
8	254.21	0.85	0.85	1.00	1.00	9	235.74	7.8	AXIAL

Table 4-13 TAM vs. FEM Cross-Orthogonality and RMAC Comparison for Updated Pretest Section-4 Free-Free Truss Model

TAM MODE	TAM FREQ (HZ)	XO	LIN-COM XO	RMAC	LIN-COM RMAC	FEM MODE	FEM FREQ (HZ)	FREQ ERROR (%)	DESCRIPTION
7	117.94	0.96	0.96	1.00	1.00	7	115.52	2.1	1st TORSION
8	124.42	0.86	0.93	0.90	1.00	8	122.84	1.3	1st BENDING
9	138.93	0.69	0.82	0.87	1.00	9	123.14	12.8	1st BENDING
10	235.88	0.89	0.89	1.00	1.00	10	223.24	5.7	2nd TORSION
11	246.07	0.73	0.64	0.78	0.96	11	234.69	4.8	2nd BENDING
12	315.54	0.80	0.77	0.83	0.94	12	235.48	34.0	2nd BENDING
20	521.47	0.44	0.44	0.62	0.62	26	436.72	19.4	AXIAL

to the sensors being laterally offset from the Node Ball centers. Figure 4-2 clearly shows all the sensor blocks being offset from the truss in a lateral direction parallel to the floor, the only exceptions being the axial accelerometers at the ends of the truss. As a result of the sensor mass offset, the TAM did a poor job of predicting the closely spaced bending mode pairs at nearly equal natural frequencies for each section.

Inspection of the TAM vs. FEM comparison tables show frequency errors to be most pronounced in the free-free TAM's where sizeable frequency separations between the two second bending modes (B-2) resulted in frequency discrepancies as large as 34% with respect to the full FEM. This was not a concern with the preliminary TAM's since the reduction was performed at the Node Balls which are geometrically symmetric with respect to the centerline of the truss structure. Overall, the TAM's did an excellent job of predicting the frequency for both torsion modes and the first mode in each bending mode pair. However, large frequency errors in the TAM's occurred with the second bending mode in each closely spaced pair and the axial modes. Again, these errors are attributed to the performance of the static reduction at the offset sensor locations.

The limitations in using the Guyan reduction method are associated with the fact that the technique is based on the assumption that no forces act on the omitted degrees-of-freedom, which in the section models are the Node Balls. Since greater than 95% of the total mass of the truss structure is mathematically lumped at the non-instrumented Node Ball grid points for the final test-analysis models, it is a poor assumption for this type of model. This is the major cause of frequency and mode shape errors between the predicted TAM and FEM.

Even though performing the Guyan reduction at the sensor locations introduced deficiencies in the test-analysis models, it was decided to preserve the representative offset locations of the response degrees-of-freedom during the static reduction. Having sensors offset 1.5 inches from the node ball centers resulted in a rigid moment arm equivalent to 30% of the strut length (3 inches combined offset over 10 inch strut length) which is viewed as significant. The static reduction could have been performed at the Node Ball centers, but this would have incorrectly excluded the rigid body rotation contribution to the sensor translational motion.

Other static reduction techniques such as Improved Reduction System (IRS) developed by O'Callahan[3] do include the mass effects of the omitted DOF's which, in this case, might have eliminated the shortcomings associated with using the Guyan method. For programmatic and schedule reasons, these techniques were not explored during the pretest analysis effort. Since the acceptability of the chosen sensor locations was initially verified via the preliminary TAM's documented in Tables

4-1a and 4-1b, the primary purpose of generating the final section TAM's was to generate reduced mass matrices for possible use in post-test analyses.

Another important issue to be addressed before fully evaluating the TAM results is also related to the closely spaced bending modes. Motion of the predicted FEM closely spaced bending mode pairs was primarily in orthogonal off-axis directions not aligned with the principal truss lateral and vertical axes. In contrast, motion of the TAM bending mode pairs was principally along the lateral and vertical axes (0 and 90 degrees) of the truss structure. This anomaly can be attributed to the mass bias resulting from the static condensation at the sensor points. An example of this variation in mode shape is illustrated in Figure 4-8 which shows end views of the Section-1 free-free TAM and FEM first bending mode pairs along with the corresponding RMAC values. As a result of this behavior, typical cross-orthogonality and RMAC comparisons between the TAM and FEM mode shapes are not representative of the overall accuracy of the reduced bending modes.

4.2.3.2 Linear Recombination of Closely-Spaced Bending Mode Pairs

Linear recombination of the TAM bending mode pairs was necessary in order to obtain an apples-to-apples comparison between the full and reduced analysis modes. Because of the symmetrical dynamic behavior of the truss structure, the coefficients required to transform the TAM mode pairs consistent with the FEM modes could be estimated using the RMAC results. As described in Figure 4-4, in its simplest form the RMAC value represents the cosine of the angle between two modal vectors. A RMAC value of 1.00 (0.0 degrees) indicates the mode shapes are spatially identical, while a RMAC of 0.00 (90 degrees) indicates shape orthogonality. RMAC values are similar to cross-orthogonality values, but are not mass weighted and therefore are independent of the accuracy of the reduced mass matrix. Table 4-14 lists the transformation angles used in generating the revised TAM mode shapes for each test configuration.

Cross-orthogonality and RMAC values calculated using the linearly recombined TAM modes are presented in Tables 4-6 through 4-13. For the four cantilevered configurations, the RMAC values between the FEM and linearly combined TAM are exactly 1.00 for all seven target modes, indicating perfect mode shape correlation. The results are equally impressive for the first bending pair and first two torsion modes predicted for the free-free configurations. RMAC values for the free-free second bending mode pair are also quite good with values in the mid to high 0.90's range, the lowest being 0.91. Only the higher frequency free-free axial modes exhibit poor mode shape comparison between the TAM and FEM.

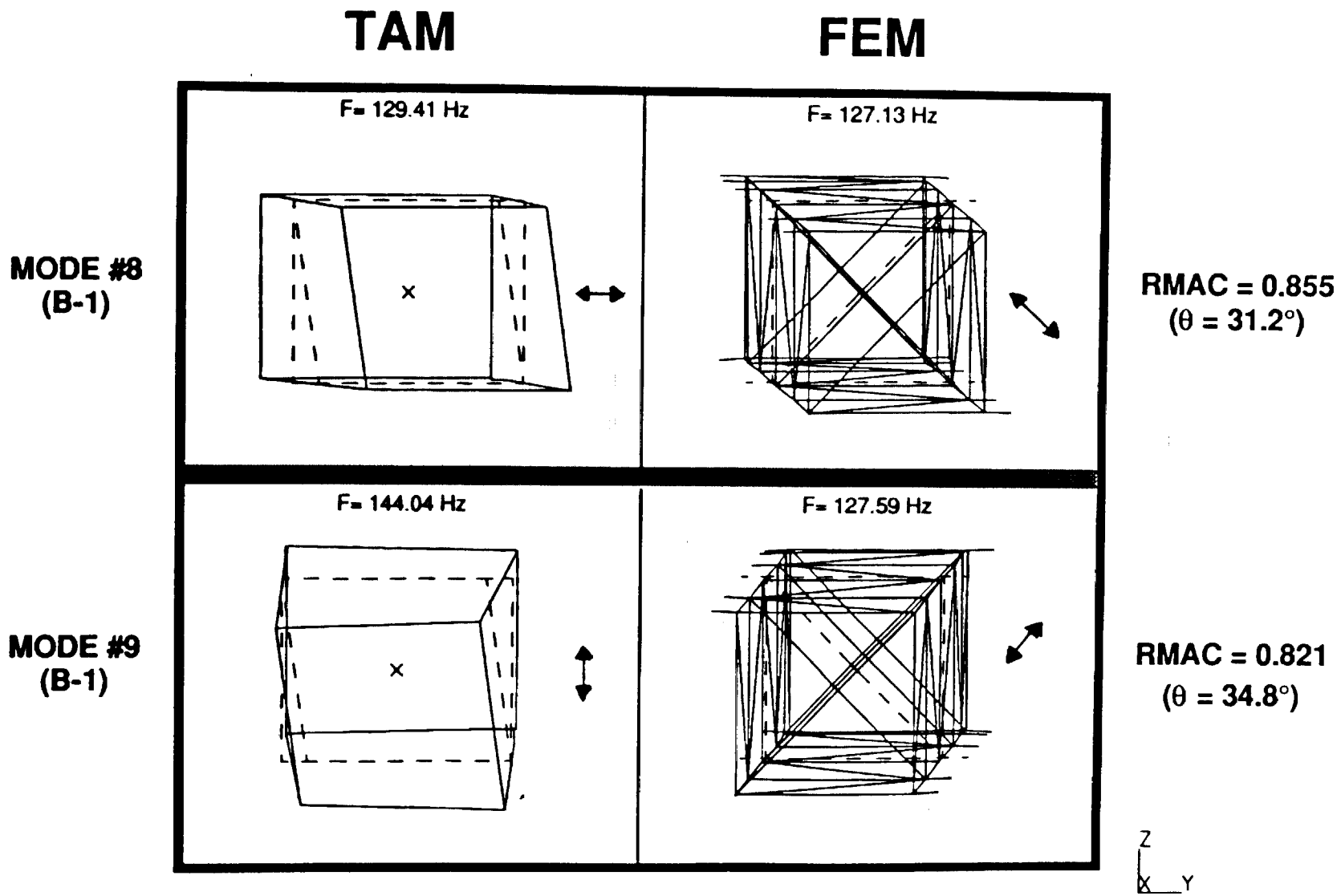

Figure 4-8 Comparison of Section-1 Free-Free TAM vs. FEM Closely Spaced Bending Mode Pairs

Table 4-14 TAM Bending Mode Pairs Linear Combination Angles Based on TAM vs. FEM RMAC Results

TRUSS CONFIGURATION	B-1 ANGLES (DEGREES)	B-2 ANGLES (DEGREES)
Section-1 Free-Free	33.1	41.4
Section-1 Cantilevered	21.0	29.0
Section-2 Free-Free	29.5	22.2
Section-2 Cantilevered	0.0	29.0
Section-3 Free-Free	0.0	0.0
Section-3 Cantilevered	27.6	13.2
Section-4 Free-Free	28.1	36.5
Section-4 Cantilevered	21.9	27.4

Results from the cross-orthogonality check computed using the linearly recombined TAM mode set were not as impressive as those obtained using RMAC. The sensitivity of the Guyan reduced matrices to the offset sensor mass points as discussed earlier resulted in a less than accurate reduced mass matrix representation of the truss structure which in turn affected the cross-orthogonality results. Fortunately, based on the excellent mode shape agreement (RMAC) between the TAM and FEM models for all eight section tests, it was concluded that the chosen set of sensor locations effectively captured the shape of the bending and torsion target modes regardless of the cross-orthogonality results. In theory, RMAC is equivalent to cross-orthogonality, given an identity mass matrix. Since the truss sections are such extremely uniform structures with constant mass weighting along their lengths, the RMAC calculation is nearly equivalent to the cross-orthogonality calculation for this case. The differences observed between the RMAC and XO values are due entirely to the use of an imperfect reduced mass matrix in the XO calculation.

An important outcome from the TAM versus FEM comparisons was the decision to emphasize the RMAC and frequency error comparisons when evaluating modal test data against finite element model predictions. Even though significant frequency errors associated with the TAM's exist, these errors are a product of the reduction process and therefore have no effect on FEM vs. test frequency comparisons. It was decided to use cross-orthogonality only as a secondary comparison because of the uncertainty associated with the Guyan reduced mass matrices.

4.3 TEST DESCRIPTION

The test objective of the modal surveys was to obtain the modal parameters (natural frequency, modal damping values, and mode shapes) for each of the four truss sections in the free-free and cantilevered configurations. Modal parameters were required for only the seven target modes of interest. Discussions on the test equipment, software tools, test procedure, and data analysis effort required to satisfy this test objective are presented.

4.3.1 Test Equipment

The test fixtures used during the modal test series consisted of a floor-anchored steel fixture shown in Figure 4-9 which was used as the fixed base for the cantilevered testing (Figure 4-1) and bungee cords which were used to support the free-free test sections (Figure 4-2). A modal survey of the anchored base fixture revealed that the first rigid body rolling mode on the concrete floor is at 204 Hz, which is higher than the

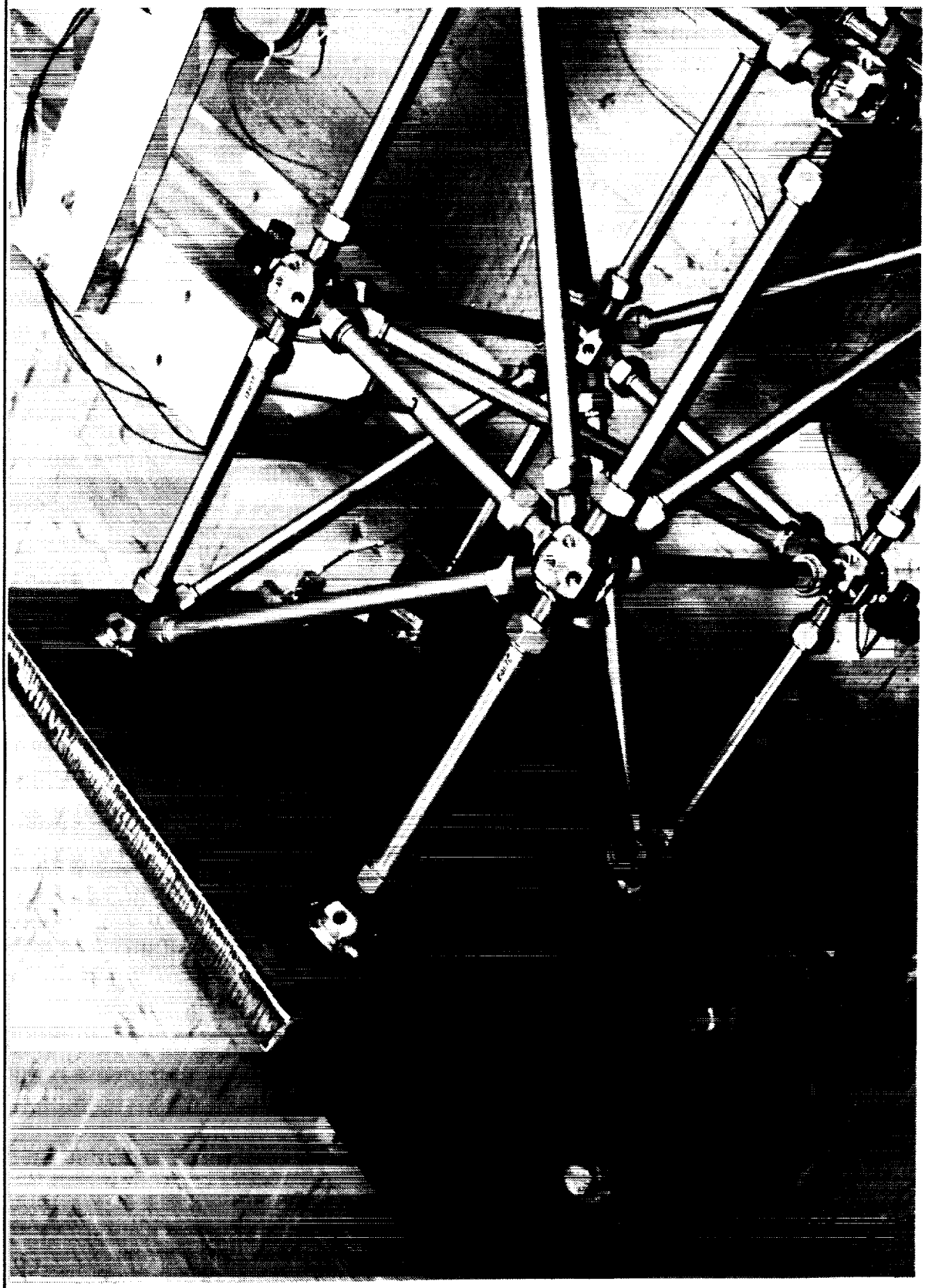

Figure 4-9 Base Fixture Used For Cantilevered Modal Tests

bending and torsion target modes measured during the cantilevered tests but lower than the axial mode for the two stiffest truss sections (Sections 1 and 4).

Bungee cords with a stretched length of ten feet were used to support the free-free test sections at four points. Estimated rigid body modes of the free-free sections ranged from 0.31 Hz to 1.51 Hz, well below the predicted frequencies for the first elastic free-free modes. The lowest frequency elastic mode measured during free-free testing was greater than 89 Hz resulting in an excellent minimum frequency separation of 60 to 1. The uncoupling of the rigid body and elastic modes is essential for obtaining high quality modal data. The combination of bungee cord flexibility and pendulum isolation effects was used to obtain the low rigid body frequencies.

A single four-pound Ling V203 shaker was used to excite the cantilevered test sections. For the free-free tests, two four-pound Ling V203 shakers were required to adequately excite the truss sections. The shaker stingers were attached to the test sections at end batten frame Node Balls in directions skewed to principal modal response directions in order to excite multiple target modes. A photo of the shaker set-up is displayed in Figure 4-10. Bungee cords were also used to suspend the shakers with the suspension modes of the shakers ranging from 0.3 Hz to approximately 3.0 Hz.

Test instrumentation used to measure input force and acceleration responses on the truss structure consisted of the following transducers:

1) Kistler 9712A5 low-impedance force transducers - 2 units.
2) Kistler 8630 and 8634 series low-impedance accelerometers - 55 units arranged in tri-axial, bi-axial, and uni-axial configurations.
3) Endevco 7701-100 piezoelectric accelerometers - 3 units used to monitor base fixture response during cantilevered section testing.

An example of a Kistler tri-axial accelerometer block mounted to a truss Node Ball during testing is shown in Figure 4-11.

The data acquisition/data analysis hardware system used for this test series was an HP-3565S. This included a Hewlett Packard (HP) work station and five data acquisition mainframes. The HP work station included the following equipment components:

1) HP 9000 319C+ CPU/Controller with 16 Mbytes of RAM
2) HP 7959B 302 Mbyte System Disk

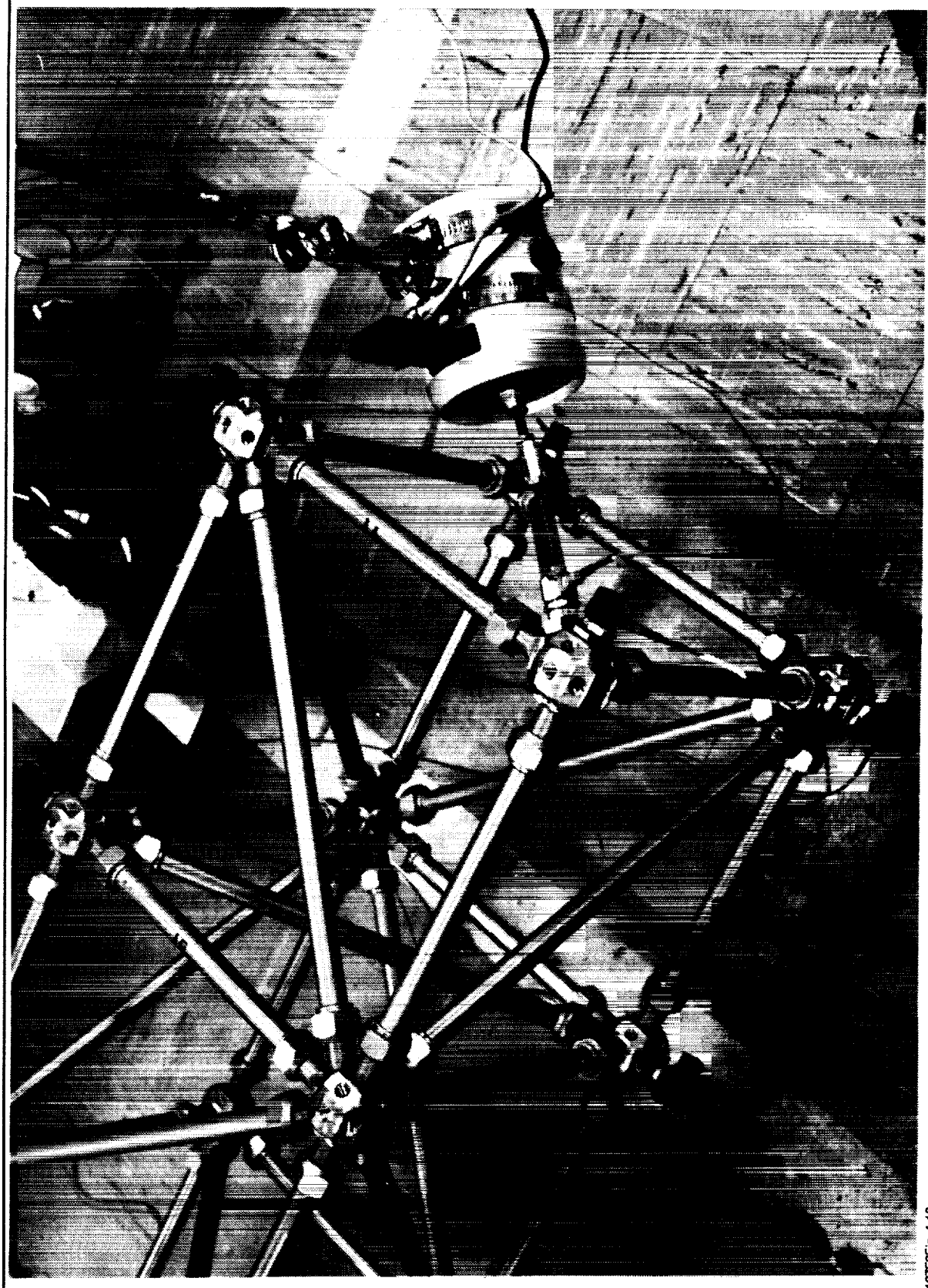

M8127F2Fig. 4-10

Figure 4-10 Typical Shaker/Stinger Set-up Used to Excite Truss Structure

Figure 4-11 Typical Tri-Axial Accelerometer Block Mounted to Truss Node Ball

3) HP 7957A 82 Mbyte Throughput Disk
4) HP 98785A Color Monitor
5) HP 33440A Laserjet Printer
6) HP 9144A Cartridge Tape Drive

The data acquisition mainframes contained input modules, source modules and a signal processor module. The input modules were used to power the low-impedance Kistler accelerometers and force gages as well as to acquire both low-impedance and piezoelectric transducer outputs. After performing the analog to digital conversion within each input module, the digitized data was transmitted from the input modules through the signal processor module to the CPU for data analysis, display, and disk storage. The two source modules generated the independent random analog signals which, after amplification, were used to drive the shakers.

4.3.2 Data Acquisition/Data Analysis Software

The HP-VISTA data acquisition and analysis and SDRC I-DEAS TDAS™ modal data analysis software packages are resident on the HP work station disk. During a typical modal test, the use of HP-VISTA enables the data to be processed, displayed, and stored to disk, and hard copies made of selected time histories and frequency response functions. With HP-VISTA the test engineer enters all instrumentation labels and calibration settings, shaker settings, and data processing parameters such as windows, frequency lines, and frequency spans. All through-put time histories and frequency response functions are saved in either HP-VISTA , universal file, or SDRC I-DEAS TDAS™ format. SDRC I-DEAS TDAS™ software is used to extract the measured natural frequencies, modal damping values, and mode shapes after the testing is completed.

4.3.3 Test Conduct

Prior to performing each section test, the 240 in-lb torque for each strut tube to Node Ball interface Nut was verified. Testing of a truss section with improperly torqued struts could introduce non-linearities in the measured response data. An additional pretest checkout was also performed to uncover potential problems with the instrumentation system prior to the start of each test. The proper working condition of each and every accelerometer used during a test was verified by exciting the truss structure with low level random excitation. A roving accelerometer was attached to each truss accelerometer and the two output signals compared to verify correct accelerometer number, orientation, sign convention, frequency response, and output level. This check was also useful in detecting damaged accelerometers and identifying

incorrectly connected channels since free-free and cantilevered tests required different instrument cable-acquisition system configurations.

The individual truss sections were subjected to continuous random excitation. The first set of tests were conducted in a base band mode with typical base band frequency ranges being 0 to 100 Hz, 0 to 200 Hz, and 0 to 400 Hz depending on the stiffness of the section being tested. It was discovered early in the test series that the first and second bending mode pairs are so closely spaced in frequency that the curve-fitting algorithms normally used could not extract the modes as accurately as desired. This led to performing additional random tests in the zoom mode. A typical zoom test range was 12.5 Hz with 400 frequency lines. As a result of using the zoom mode process, closely spaced bending modes were cleanly extracted from the response data. Appendices C through F contain the test logs for each truss section which summarize the various number of tests performed and the sets of frequency ranges used.

The continuous random responses from the input force gage(s) and the response accelerometers were windowed with a Hanning window prior to the Fast Fourier Transforms (FFT) calculations. Although the continuous random/Hanning window technique can result in possible errors in estimated damping, it was appropriate for this test because of the zoom processing employed for most modes. As described in Reference 4, improvements to the continuous random technique are the burst random with no window, or increased frequency resolution with zoom Fourier transforms. It was verified in tests on a lightly damped (0.2%) cantilevered structure in the laboratory that both techniques, when used in a zoom processing mode, resulted in modal damping estimates which only slightly differed, 2.08% vs. 2.04%.

Another advantage of continuous random/Hanning window is that overlap processing can be employed while it cannot be used with burst random/no window. The use of the latter technique results in increased testing time, which was critical for this test series. Even though burst random is generally the preferred technique, there are test situations where the continuous random/Hanning window approach can be used to obtain accurate results.

4.3.4 Test Data Acquisition/Analysis

All of the base band time history data was originally saved on the through-put disk during testing. After completing each test, the data was played back for FFT processing using the HP-VISTA software. The zoom data was analyzed directly with the HP-VISTA software and therefore was not saved on the through-put disk. Since all the tests were conducted using continuous random excitation, the time history data

was windowed with a Hanning window prior to the FFT calculation. An average of 30 samples were used in calculating the resulting frequency response functions. In some cases, overlap processing was also used in the data acquisition process to save time. The detailed modal testing parameters associated with each test are summarized in Appendices C through F. Immediately following each random test, the frequency response functions were converted from HP-VISTA format into SDRC I-DEAS TDAS™ Associated Data File (ADF) format using the HP Modal Data Manager program.

After completion of the random test series for a given test configuration, modal parameters were extracted using SDRC I-DEAS TDAS™ software. Modal parameters were generally extracted from the zoom modal test data due to the presence of the closely spaced bending mode pairs. The orthogonality of the extracted mode shapes was evaluated by computing the Modal Assurance Criteria (MAC) within TDAS. Modal extraction parameters used to generate the modal characteristics of each test configuration are presented in Appendices C through F. The names of the modal parameter files and the files containing the coordinates of the accelerometer locations are also included in these appendices .

4.4 MODAL TEST RESULTS

Immediately following each of the eight truss section modal tests, the quality of the measured target modes test data (Section 4.3) was verified using RMAC, frequency error, and cross-orthogonality comparisons with the predicted FEM normal modes (Section 4.2). These comparisons are also the first step in determining the degree of model correlation required in matching FEM modes with test data, if any. As previously detailed in Section 4.2, the major emphasis was placed on the RMAC and frequency error criteria in terms of evaluating test data versus FEM predictions. Due to the apparent uncertainty associated with the Guyan reduced mass matrices, cross-orthogonality comparisons were generated but used only as a secondary criteria.

4.4.1 Frequency Response Functions

Typical base band Frequency Response Functions (FRF's) generated from each of the eight modal surveys are shown in Figures 4-12 through 4-19. The FRF's are based on truss tip acceleration response as a function of applied force input at the truss tip. Inspection of the FRF's shows the strong presence of the seven target modes for each test configuration. Due to the closely spaced bending modes being at nearly the same frequency, the individual FRF peaks within a mode pair are not easily distinguishable

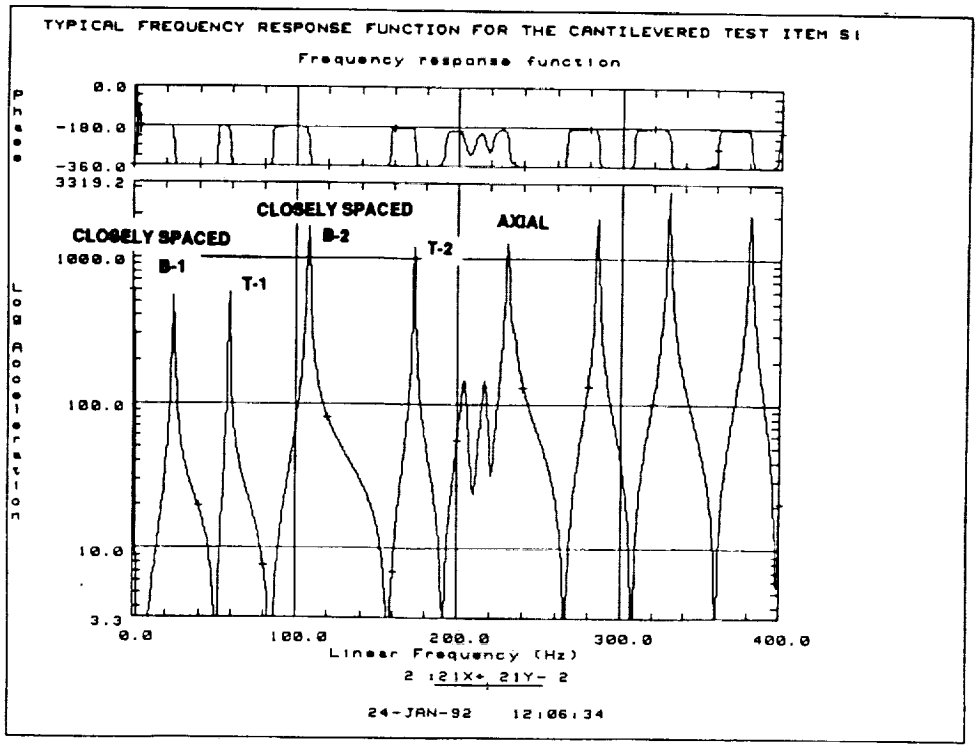

Figure 4-12 Typical Measured FRF From Section-1 Cantilevered Truss Modal Test

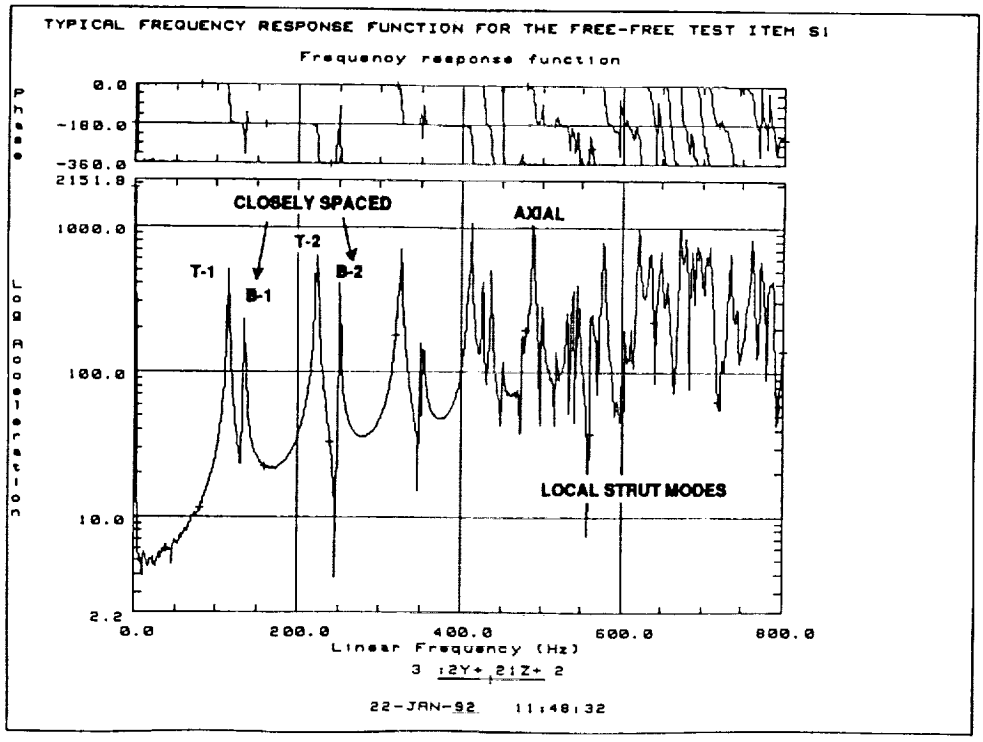

Figure 4-13 Typical Measured FRF From Section-1 Free-Free Truss Modal Test

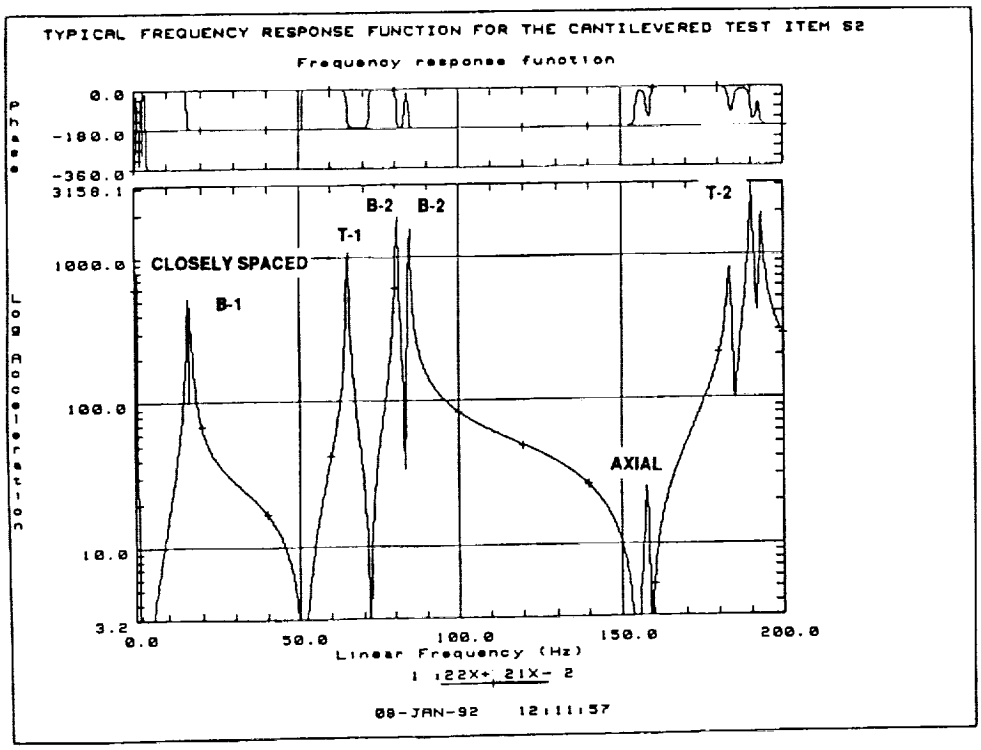

Figure 4-14 Typical Measured FRF From Section-2 Cantilevered Truss Modal Test

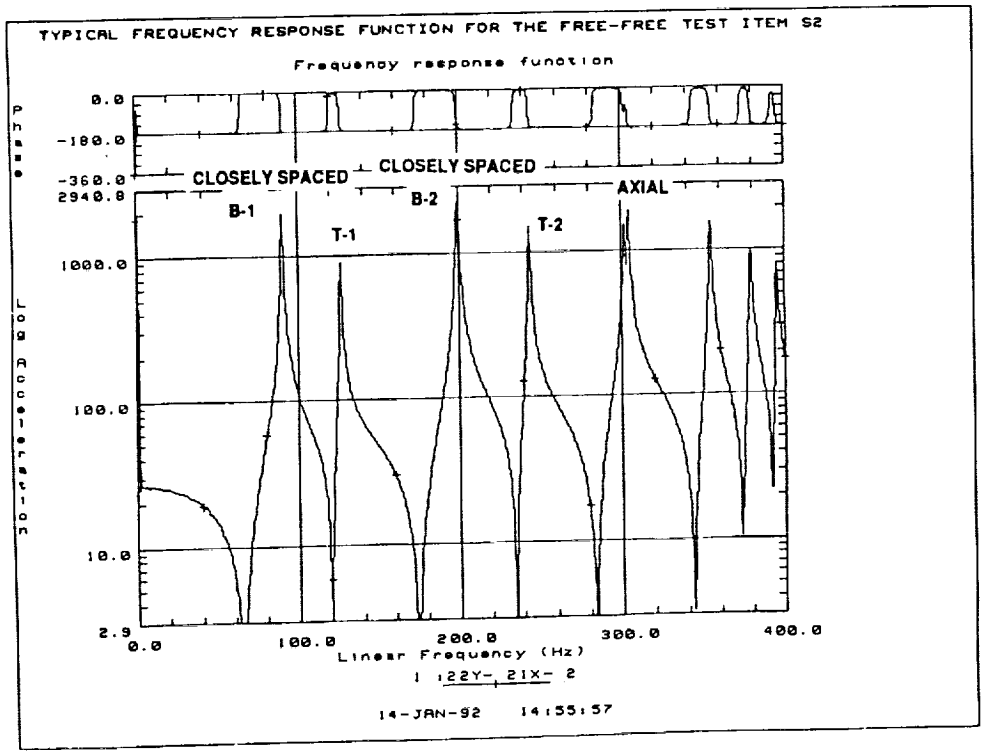

Figure 4-15 Typical Measured FRF From Section-2 Free-Free Truss Modal Test

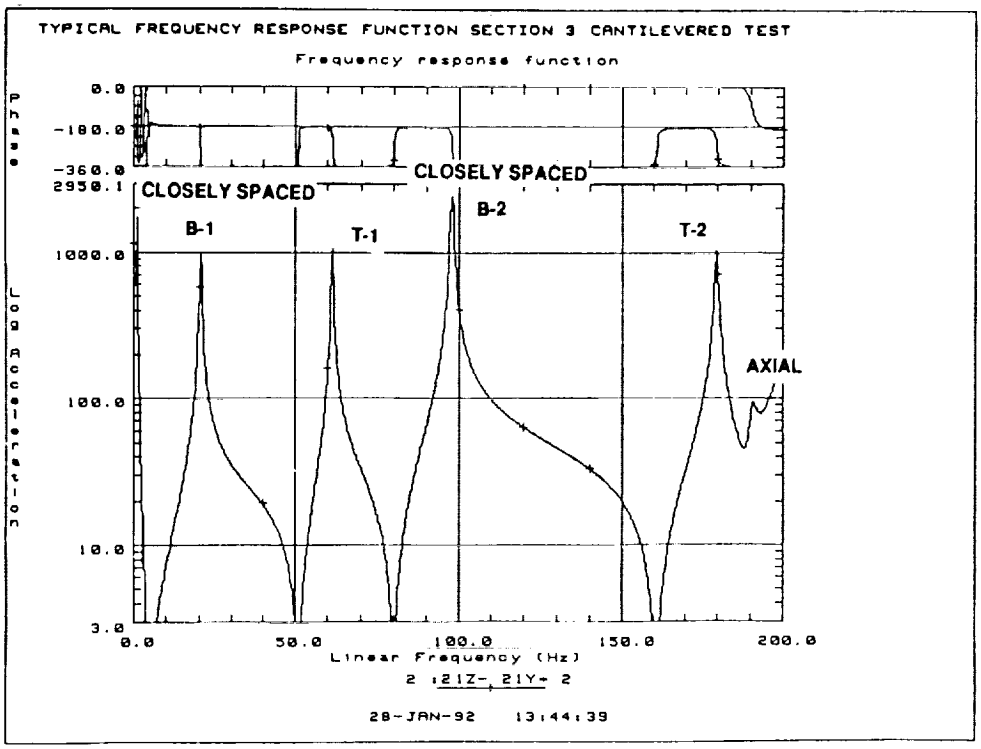

Figure 4-16 Typical Measured FRF From Section-3 Cantilevered Truss Modal Test

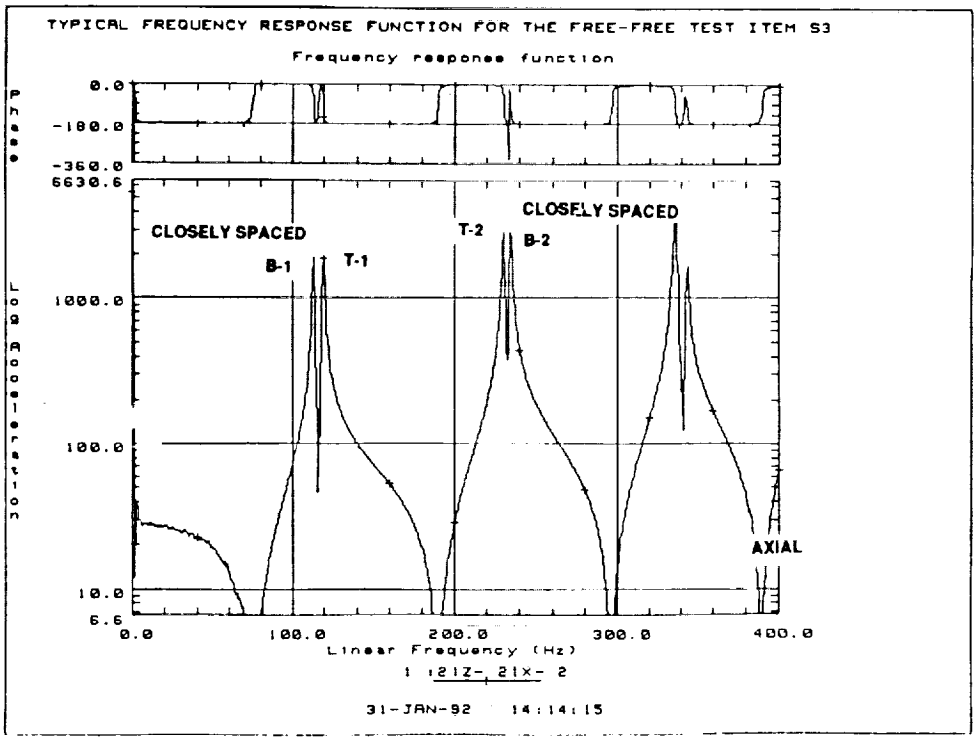

Figure 4-17 Typical Measured FRF From Section-3 Free-Free Truss Modal Test

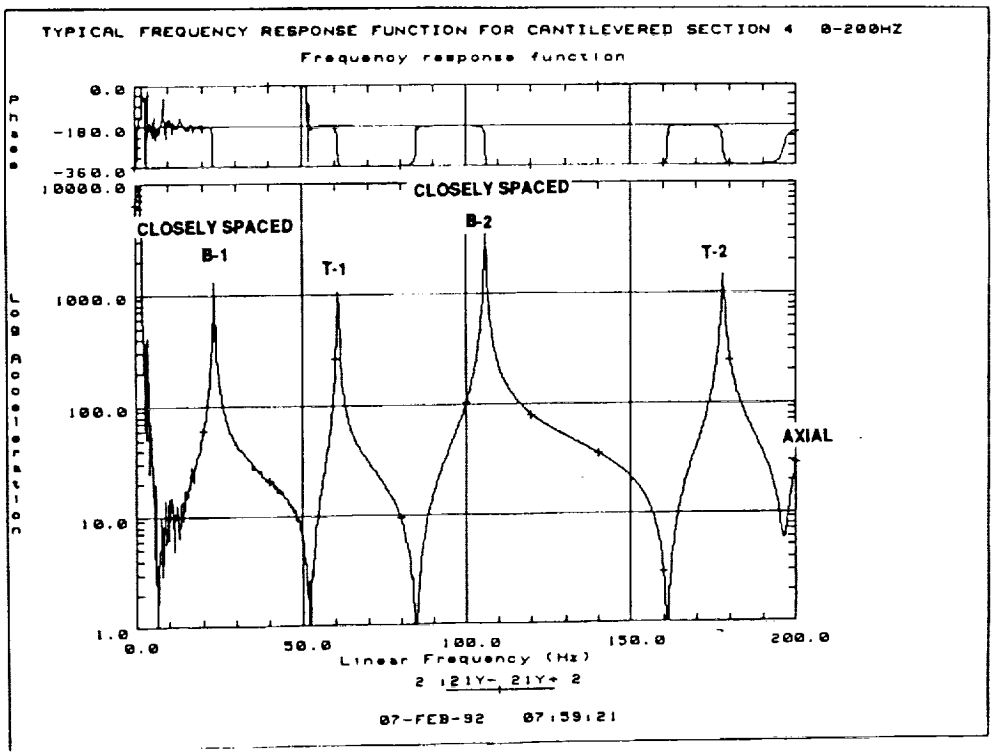

Figure 4-18 Typical Measured FRF From Section-4 Cantilevered Truss Modal Test

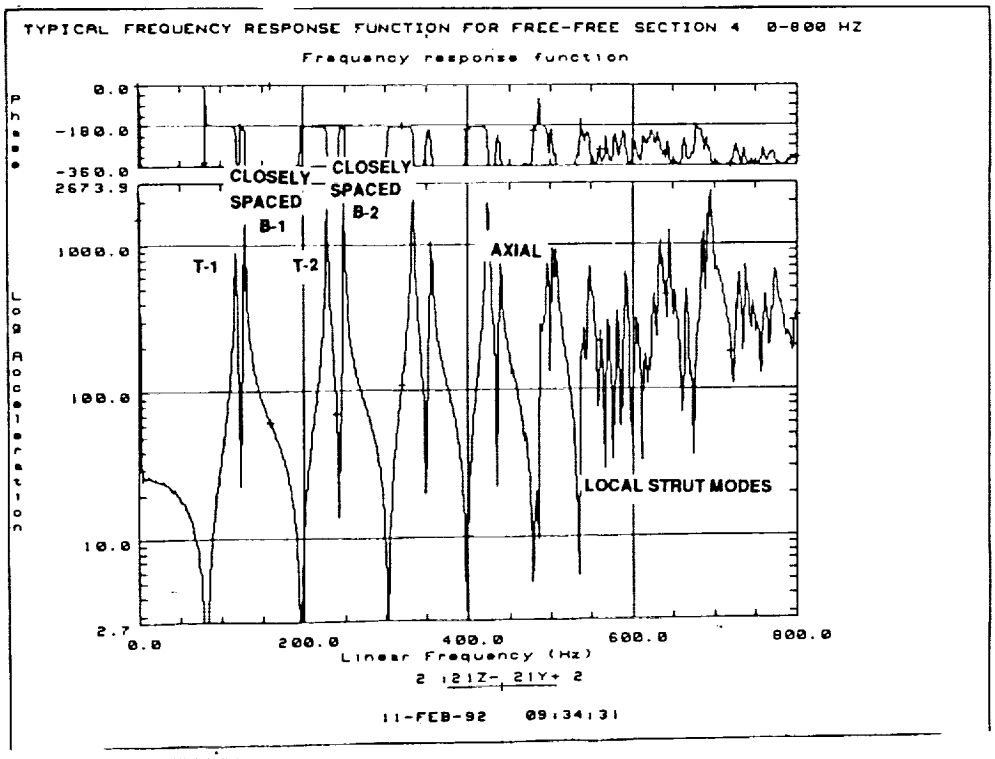

Figure 4-19 Typical Measured FRF From Section-4 Free-Free Truss Modal Test

given the resolution of the plots. Figure 4-20, which shows a higher resolution FRF plot of two closely spaced first bending modes (Section-3 cantilevered), demonstrates the clean separation within the mode pair. This data quality is representative of all of the closely spaced bending modes which resulted in the test modes being extracted with a high degree of confidence.

Higher order truss modes above 400 Hz can be observed in the Section-1 and Section-4 free-free FRF plots (Figures 4-13 and 4-19). These are believed to be associated with local strut bending . The first measured axial modes of these two truss sections are well above 400 Hz and may be coupled with the local strut bending modes, complicating the mode shape behavior.

4.4.2 Test Mode Modal Assurance Criterion Results

Shape orthogonality of the extracted test modes was computed using the Modal Assurance Criterion (MAC). The results are presented in Tables 4-15 through 4-22. For each of the eight modal tests, the off-diagonal terms between the seven target modes are significantly less than 0.100 which satisfies the criteria for orthogonal modes. The largest off-diagonal value computed between the target modes is 0.073 which strongly indicates that the measured mode shapes are uncoupled.

It should be noted that some of the MAC matrices contain extracted higher order bending modes which are not part of the target set. The orthogonality of these modes should be ignored since no attempt was made to accurately capture these higher order bending modes during the development of the pretest TAM's. Mass weighted mode shape orthogonality values computed using the pretest TAM mass matrices are not presented due to the uncertainty associated with the Guyan reduction.

4.4.3 Mode Shape and Frequency Error Comparisons

The results of the RMAC, cross-orthogonality, and frequency error comparisons between the measured test modes and updated pretest FEM normal modes are shown in Tables 4-23 through 4-30. As in the TAM vs. FEM comparisons in Section 4.2, linear recombination of closely spaced bending mode pairs was required in order to obtain an one-to-one orientation between the test and analysis modes. For this case, the transformation between the sets of modes was not a function of the model reduction process since the TAM modes were not involved. The observed frequency spacing of less than 1% within a pair of closely spaced modes indicates a very high sensitivity to small mass and stiffness perturbations in the truss structure. This is one possible explanation for the test modes being rotated with respect to the FEM modes.

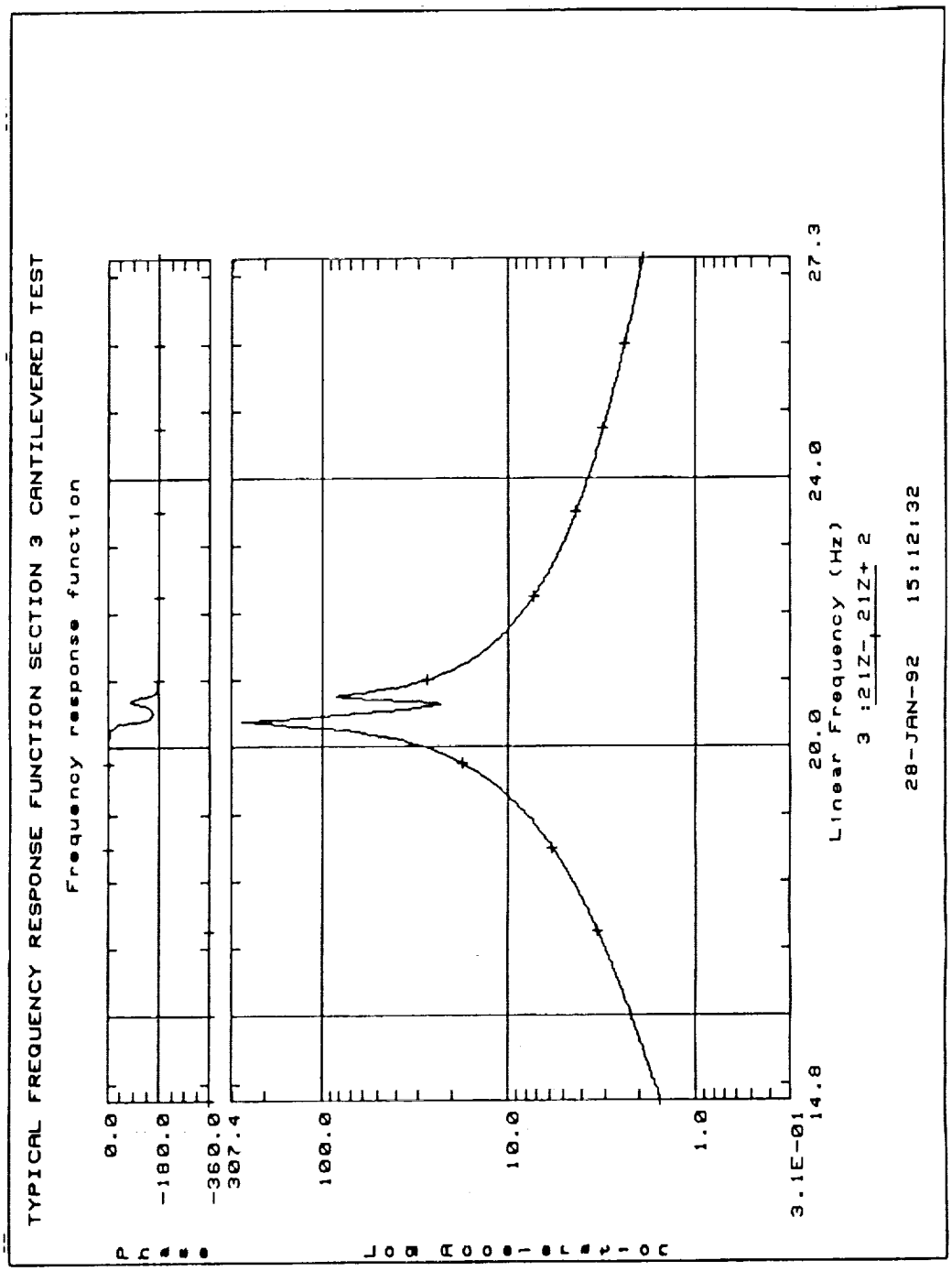

Figure 4-20 Closely Spaced First Bending Mode Pair Typical FRF Plot

Table 4-15 Modal Assurance Criteria (MAC) for Section-1 Cantilevered Truss Test Modes

	1	2	3	4	5	6	7	8	9
1	1.000	0.000	0.000	0.026	0.018	0.000	0.000	0.081	0.008
2	0.000	1.000	0.000	0.015	0.024	0.000	0.045	0.015	0.026
3	0.000	0.000	1.000	0.000	0.000	0.011	0.001	0.000	0.000
4	0.026	0.015	0.000	1.000	0.002	0.000	0.007	0.002	0.003
5	0.018	0.024	0.000	0.002	1.000	0.000	0.008	0.012	0.001
6	0.000	0.000	0.011	0.000	0.000	1.000	0.010	0.018	0.001
7	0.000	0.045	0.001	0.007	0.008	0.010	1.000	0.036	0.019
8	0.081	0.015	0.000	0.002	0.012	0.018	0.036	1.000	0.001
9	0.008	0.026	0.000	0.003	0.001	0.001	0.019	0.001	1.000

(TEST MODES 7 & 8 NOT TARGET MODES)

Table 4-16 Modal Assurance Criteria (MAC) for Section-1 Free-Free Truss Test Modes

	1	2	3	4	5	6	7
1	1.000	0.000	0.000	0.000	0.000	0.000	0.000
2	0.000	1.000	0.001	0.000	0.000	0.000	0.001
3	0.000	0.001	1.000	0.000	0.000	0.000	0.000
4	0.000	0.000	0.000	1.000	0.000	0.000	0.025
5	0.000	0.000	0.000	0.000	1.000	0.012	0.000
6	0.000	0.000	0.000	0.000	0.012	1.000	0.000
7	0.000	0.001	0.000	0.025	0.000	0.000	1.000

LARGEST OFF-DIAGONAL VALUE

Table 4-17 Modal Assurance Criteria (MAC) for Section-2 Cantilevered Truss Test Modes

	1	2	3	4	5	6	7	8	9
1	1.000	0.001	0.000	0.045	0.002	0.000	0.078	0.008	0.001
2	0.001	1.000	0.000	0.001	0.043	0.000	0.001	0.001	0.055
3	0.000	0.000	1.000	0.000	0.000	0.000	0.002	0.011	0.000
4	0.045	0.001	0.000	1.000	0.000	0.000	0.005	0.000	0.000
5	0.002	0.043	0.000	0.000	1.000	0.000	0.000	0.000	0.009
6	0.000	0.000	0.000	0.000	0.000	1.000	0.007	0.000	0.000
7	0.078	0.001	0.002	0.005	0.000	0.007	1.000	0.017	0.001
8	0.008	0.001	0.011	0.000	0.000	0.000	0.017	1.000	0.017
9	0.001	0.055	0.000	0.000	0.009	0.000	0.001	0.017	1.000

(TEST MODES 7 & 9 NOT TARGET MODES)

Table 4-18 Modal Assurance Criteria (MAC) for Section-2 Free-Free Truss Test Modes

	1	2	3	4	5	6	7	8	9
1	1.000	0.012	0.000	0.000	0.000	0.000	0.001	0.201	0.006
2	0.012	1.000	0.000	0.000	0.000	0.000	0.117	0.002	0.001
3	0.000	0.000	1.000	0.000	0.000	0.000	0.001	0.000	0.000
4	0.000	0.000	0.000	1.000	0.007	0.000	0.005	0.001	0.000
5	0.000	0.000	0.000	0.007	1.000	0.000	0.002	0.000	0.000
6	0.000	0.000	0.000	0.000	0.000	1.000	0.006	0.001	0.000
7	0.001	0.117	0.001	0.005	0.002	0.006	1.000	0.000	0.001
8	0.201	0.002	0.000	0.001	0.000	0.001	0.000	1.000	0.012
9	0.006	0.001	0.000	0.000	0.000	0.000	0.001	0.012	1.000

(TEST MODES 7 & 8 NOT TARGET MODES)

LARGEST OFF-DIAGONAL VALUE

Table 4-19 Modal Assurance Criteria (MAC) for Section-3 Cantilevered Truss Test Modes

	1	2	3	4	5	6	7
1	1.000	0.001	0.000	0.032	0.012	0.000	0.002
2	0.001	1.000	0.000	0.008	0.031	0.000	0.002
3	0.000	0.000	1.000	0.000	0.000	0.010	0.001
4	0.032	0.008	0.000	1.000	0.007	0.000	0.001
5	0.012	0.031	0.000	0.007	1.000	0.000	0.000
6	0.000	0.000	0.010	0.000	0.000	1.000	0.003
7	0.002	0.002	0.001	0.001	0.000	0.003	1.000

Table 4-20 Modal Assurance Criteria (MAC) for Section-3 Free-Free Truss Test Modes

	1	2	3	4	5	6	7
1	1.000	0.005	0.000	0.000	0.000	0.000	0.000
2	0.005	1.000	0.000	0.000	0.000	0.000	0.000
3	0.000	0.000	1.000	0.000	0.000	0.000	0.000
4	0.000	0.000	0.000	1.000	0.001	0.003	0.009
5	0.000	0.000	0.000	0.001	1.000	0.008	0.000
6	0.000	0.000	0.000	0.003	0.008	1.000	0.000
7	0.000	0.000	0.000	0.009	0.000	0.000	1.000

LARGEST OFF-DIAGONAL VALUE

Table 4-21 Modal Assurance Criteria (MAC) for Section-4 Cantilevered Truss Test Modes

	1	2	3	4	5	6	7
1	1.000	0.001	0.000	0.000	0.039	0.000	0.005
2	0.001	1.000	0.000	0.040	0.000	0.000	0.031
3	0.000	0.000	1.000	0.000	0.000	0.009	0.000
4	0.000	0.040	0.000	1.000	0.004	0.000	0.007
5	0.039	0.000	0.000	0.004	1.000	0.000	0.002
6	0.000	0.000	0.009	0.000	0.000	1.000	0.009
7	0.005	0.031	0.000	0.007	0.002	0.009	1.000

Table 4-22 Modal Assurance Criteria (MAC) for Section-4 Free-Free Truss Test Modes

	1	2	3	4	5	6	7
1	1.000	0.000	0.000	0.000	0.000	0.000	0.008
2	0.000	1.000	0.001	0.000	0.000	0.000	0.004
3	0.000	0.001	1.000	0.000	0.000	0.000	0.000
4	0.000	0.000	0.000	1.000	0.000	0.000	0.073
5	0.000	0.000	0.000	0.000	1.000	0.010	0.000
6	0.000	0.000	0.000	0.000	0.010	1.000	0.000
7	0.008	0.004	0.000	0.073	0.000	0.000	1.000

LARGEST OFF-DIAGONAL VALUE

C-2

Table 4-23 Test vs. Updated FEM Cross-Orthogonality and RMAC Comparison for Section-1 Cantilevered Truss Model

TEST MODE	TEST FREQ (HZ)	XO	LIN-COM XO	RMAC	LIN-COM RMAC	FEM MODE	FEM FREQ (HZ)	FREQ ERROR (%)	DESCRIPTION
1	24.20	0.73	0.99	0.74	1.00	1	24.84	2.6	1st BENDING
2	25.20	0.73	0.98	0.74	1.00	2	24.85	-1.4	1st BENDING
3	58.99	0.99	0.99	1.00	1.00	3	57.10	-3.2	1st TORSION
4	107.06	0.85	0.84	1.00	1.00	4	103.39	-3.4	2nd BENDING
5	107.85	0.94	0.96	1.00	1.00	5	103.56	-4.0	2nd BENDING
6	173.01	0.93	0.93	1.00	1.00	6	168.89	-2.4	2nd TORSION
9	234.01	0.76	0.76	0.81	0.81	9	253.38	8.3	AXIAL

Table 4-24 Test vs. Updated FEM Cross-Orthogonality and RMAC Comparison for Section-1 Free-Free Truss Model

TEST MODE	TEST FREQ (HZ)	XO	LIN-COM XO	RMAC	LIN-COM RMAC	FEM MODE	FEM FREQ (HZ)	FREQ ERROR (%)	DESCRIPTION
1	115.00	0.97	0.97	1.00	1.00	7	111.20	-3.3	1st TORSION
2	134.70	0.90	0.88	0.98	1.00	8	127.13	-5.6	1st BENDING
3	135.20	0.82	0.88	0.98	1.00	9	127.59	-5.6	1st BENDING
4	223.10	0.87	0.87	1.00	1.00	10	215.33	-3.5	2nd TORSION
5	250.45	0.67	0.61	0.94	1.00	11	234.81	-6.2	2nd BENDING
6	251.12	0.76	0.88	0.95	1.00	12	236.56	-5.8	2nd BENDING
7	488.17	0.61	0.61	0.85	0.85	30	480.89	-1.5	AXIAL

Table 4-25 Test vs. Updated FEM Cross-Orthogonality and RMAC Comparison for Section-2 Cantilevered Truss Model

TEST MODE	TEST FREQ (HZ)	XO	LIN-COM XO	RMAC	LIN-COM RMAC	FEM MODE	FEM FREQ (HZ)	FREQ ERROR (%)	DESCRIPTION
1	16.00	0.97	1.00	0.98	1.00	1	16.00	0.0	1st BENDING
2	16.45	0.98	1.00	0.98	1.00	2	16.37	-0.4	1st BENDING
3	65.24	0.98	0.98	1.00	1.00	3	66.37	1.7	1st TORSION
4	80.79	0.92	0.92	1.00	1.00	4	80.05	-0.9	2nd BENDING
5	84.63	0.94	0.94	1.00	1.00	5	84.14	-0.6	2nd BENDING
6	157.88	0.80	0.80	1.00	1.00	6	159.74	1.2	AXIAL
8	190.23	0.87	0.87	0.95	0.95	9	196.21	3.1	2nd TORSION

Table 4-26 Test vs. Updated FEM Cross-Orthogonality and RMAC Comparison for Section-2 Free-Free Truss Model

TEST MODE	TEST FREQ (HZ)	XO	LIN-COM XO	RMAC	LIN-COM RMAC	FEM MODE	FEM FREQ (HZ)	FREQ ERROR (%)	DESCRIPTION
1	89.88	0.96	0.95	1.00	1.00	7	88.48	-1.6	1st BENDING
2	90.02	0.89	0.91	0.99	1.00	8	88.89	-1.3	1st BENDING
3	126.45	0.96	0.96	1.00	1.00	9	129.27	2.2	1st TORSION
4	198.77	0.62	0.71	0.97	1.00	10	194.51	-2.1	2nd BENDING
5	199.51	0.87	0.83	0.99	1.00	11	196.21	-1.7	2nd BENDING
6	243.85	0.87	0.87	1.00	1.00	12	248.54	1.9	2nd TORSION
9	307.65	0.55	0.55	0.98	0.98	14	289.67	-5.8	AXIAL

Table 4-27 Test vs. Updated FEM Cross-Orthogonality and RMAC Comparison for Section-3 Cantilevered Truss Model

TEST MODE	TEST FREQ (HZ)	XO	LIN-COM XO	RMAC	LIN-COM RMAC	FEM MODE	FEM FREQ (HZ)	FREQ ERROR (%)	DESCRIPTION
1	20.37	0.72	1.00	0.72	1.00	1	20.48	0.5	1st BENDING
2	20.74	0.74	0.99	0.75	1.00	2	20.49	-1.2	1st BENDING
3	61.32	0.99	0.99	1.00	1.00	3	60.03	-2.1	1st TORSION
4	97.57	0.68	0.91	0.82	1.00	4	95.29	-2.3	2nd BENDING
5	97.92	0.86	0.91	0.87	1.00	5	95.61	-2.4	2nd BENDING
6	179.43	0.92	0.92	1.00	1.00	6	177.06	-1.3	2nd TORSION
7	190.62	0.78	0.78	0.95	0.95	7	198.01	3.9	AXIAL

Table 4-28 Test vs. Updated FEM Cross-Orthogonality and RMAC Comparison for Section-3 Free-Free Truss Model

TEST MODE	TEST FREQ (HZ)	XO	LIN-COM XO	RMAC	LIN-COM RMAC	FEM MODE	FEM FREQ (HZ)	FREQ ERROR (%)	DESCRIPTION
1	113.03	0.62	0.90	0.78	1.00	7	109.00	-3.6	1st BENDING
2	113.07	0.83	0.89	0.83	1.00	8	109.51	-3.1	1st BENDING
3	119.50	0.96	0.96	1.00	1.00	9	117.00	-2.1	1st TORSION
4	230.06	0.86	0.86	0.99	0.99	12	225.56	-2.0	2nd TORSION
5	232.84	0.90	0.87	0.99	0.99	10	220.01	-5.5	2nd BENDING
6	234.46	0.50	0.49	0.97	0.97	11	223.49	-4.7	2nd BENDING
7	382.35	0.51	0.51	0.95	0.95	19	354.41	-7.3	AXIAL

Table 4-29 Test vs. Updated FEM Cross-Orthogonality and RMAC Comparison for Section-4 Cantilevered Truss Model

TEST MODE	TEST FREQ (HZ)	XO	LIN-COM XO	RMAC	LIN-COM RMAC	FEM MODE	FEM FREQ (HZ)	FREQ ERROR (%)	DESCRIPTION
1	23.37	0.84	1.00	0.84	1.00	1	23.63	1.1	1st BENDING
2	23.93	0.84	0.99	0.85	1.00	2	23.64	-1.2	1st BENDING
3	60.69	0.98	0.98	1.00	1.00	3	59.29	-2.3	1st TORSION
4	105.51	0.58	0.83	0.74	1.00	4	102.48	-2.9	2nd BENDING
5	105.86	0.79	0.97	0.79	1.00	5	102.69	-3.0	2nd BENDING
6	177.78	0.91	0.91	1.00	1.00	6	175.30	-1.4	2nd TORSION
7	216.30	0.66	0.66	0.74	0.74	9	235.74	9.0	AXIAL

Table 4-30 Test vs. Updated FEM Cross-Orthogonality and RMAC Comparison for Section-4 Free-Free Truss Model

TEST MODE	TEST FREQ (HZ)	XO	LIN-COM XO	RMAC	LIN-COM RMAC	FEM MODE	FEM FREQ (HZ)	FREQ ERROR (%)	DESCRIPTION
1	118.00	0.96	0.96	1.00	1.00	7	115.52	-2.1	1st TORSION
2	128.30	0.89	0.87	0.95	1.00	8	122.84	-4.3	1st BENDING
3	129.02	0.79	0.89	0.95	1.00	9	123.14	-4.6	1st BENDING
4	228.55	0.89	0.89	1.00	1.00	10	223.24	-2.3	2nd TORSION
5	247.93	0.66	0.60	0.98	1.00	11	234.69	-5.3	2nd BENDING
6	249.45	0.79	0.85	0.99	0.99	12	235.48	-5.6	2nd BENDING
7	453.45	0.60	0.60	0.97	0.97	26	436.72	-3.7	AXIAL

Table 4-31 lists the transformation angles used in linearly combining the closely spaced FEM bending modes.

A review of the linearly combined RMAC results presented in Tables 4-23 through 4-30 for the eight truss test sections shows near-perfect mode shape correlation between the test and FEM bending and torsion target modes (B-1, B-2, T-1, T-2). For all four cantilevered tests, the bending and torsion mode RMAC values are a perfect 1.00. The free-free configuration results are equally impressive having 1.00 RMAC values for all bending and torsion modes except the second bending modes in Sections 3 and 4 whose values are above 0.97.

Comparison of test vs. FEM axial modes produces a wider spread in RMAC results with 5 out of the 8 values above 0.95, two in the 0.80 range, and a low of 0.74. In general, the axial test modes do not compare as well with the FEM as the bending and torsion modes. This result is not surprising since in all but one test the axial modes were the highest frequency mode where the potential for coupling with the local strut modes is the greatest. In addition, the majority of the accelerometers channels measured vertical and lateral response, and not pure axial motion. MSC/NASTRAN finite element mode shape plots of the seven target modes for each section test are contained in Appendices C through F which correspond to the four truss section types. Undeformed mesh plots which show the grid numbering used for each truss section are also included in the appendices.

Cross-orthogonality comparisons based on the Guyan reduced mass matrix were generated using the linearly combined mode set for completeness and are included in the tables for reference. Fortunately, as discussed previously in Section 4.2, the RMAC calculation is nearly equivalent to the cross-orthogonality calculations given the uniform mass distribution of the truss structure. Therefore, given the excellent results obtained using RMAC, the absence of quality cross-orthogonality data does not adversely effect the evaluation process.

Comparisons between the measured test and predicted FEM target mode frequencies show all of the frequency errors to be less than 6.2% for the bending and torsion modes with the overall average absolute frequency error for all eight tests excluding axial modes being only 2.7%. For the four cantilevered section tests, the largest individual frequency error for the non-axial modes is only 4.0% (Section-1) with an average error of just 1.9%. In general, the best frequency matches between test and FEM occur for the cantilevered tests. The best overall bending and torsion frequency matches considering both the cantilevered and free-free configurations are obtained

Table 4-31 FEM Bending Mode Pairs Linear Combination Angles Based on FEM vs Test RMAC Results

TRUSS CONFIGURATION	B-1 ANGLES (DEGREES)	B-2 ANGLES (DEGREES)
Section-1 Free-Free	10.9	19.4
Section-1 Cantilevered	42.3	0.0
Section-2 Free-Free	0.0	12.0
Section-2 Cantilevered	11.5	0.0
Section-3 Free-Free	36.4	11.5
Section-3 Cantilevered	42.7	32.3
Section-4 Free-Free	18.4	10.9
Section-4 Cantilevered	32.3	39.9

Table 4-32 Measured Modal Damping

TEST	B-1	T-1	B-2	T-2	AXIAL
SEC-1 CANT	0.18 / 0.18	0.17	0.19 / 0.15	0.13	0.31
SEC-1 F-F	0.15 / 0.14	0.16	0.10 / 0.08	0.11	0.13
SEC-2 CANT	0.13 / 0.10	0.27	0.15 / 0.13	0.20	0.27
SEC-2 F-F	0.12 / 0.16	0.15	0.15 / 0.10	0.09	0.08
SEC-3 CANT	0.16 / 0.18	0.13	0.18 / 0.17	0.19	0.58
SEC-3 F-F	0.20 / 0.14	0.14	0.10 / 0.13	0.13	0.13
SEC-4 CANT	0.14 / 0.16	0.15	0.17 / 0.12	0.20	0.69
SEC-4 F-F	0.11 / 0.16	0.23	0.10 / 0.08	0.14	0.11
AVERAGE	**0.15**	**0.17**	**0.13**	**0.15**	**0.29**

for the Section-2 tests (average error = 1.5%) while the largest frequency errors occur for the Section-1 tests (average error = 3.9%).

With regard to axial modes, measured test and predicted FEM frequencies differ by an average of 5.1% with the largest frequency error in any single test being 9.0%. The axial modes accounted for the largest target mode frequency error for five out of the eight tests performed.

Overall, the frequency comparisons between the test and updated pretest FEM modes for all eight tests are excellent, especially with regard to the bending and torsion modes. These frequency results, combined with the RMAC data already presented, corroborate the high quality of the measured modal test data. In addition, the near-perfect mode shape comparisons along with frequency errors generally well below 5% indicate the need for few adjustments in the post-test model correlation.

4.4.4 Modal Damping

Modal damping values extracted from the truss section test data (continuous random with Hanning window) are shown in Table 4-32 for each test. The B-1 and B-2 columns each contain two values corresponding to the closely spaced bending mode pairs. A value of 1.00 represents a critically damped structure. Measured damping values range from 0.10 - 0.20 with an average of 0.15 for the first bending modes and from 0.08 - 0.19 with an average of 0.13 for the second bending modes. Torsional modes exhibit damping levels similar to the bending modes with averages of 0.17 and 0.15 corresponding to the first and second modes, respectively. Only damping values associated with the axial modes show large variations between tests, ranging from as low as 0.08 to as high as 0.69 with the average being 0.29. The CEM Phase 1 truss sections are lightly damped typical of a truss with stiff, highly preloaded erectable joints.

4.4.5 Improved Reduction System (IRS) Method Test Case

As previously discussed in detail in both the pretest and post-test analysis sections of the report, the Guyan static reduction method was inadequate for developing accurate TAM's of the CSI truss section models. The primary reason for the overall poor TAM performance was the offsetting of the sensor masses from the Node Ball centers which resulted in the static reduction being performed at DOF's which accounted for less than 5% of the total structure mass. In theory, the Guyan method assumes that no forces act on the omitted DOF's (Node Balls), a poor assumption in this case. The

mass offset resulted in poor prediction of the closely spaced bending mode pair frequencies.

A static reduction technique referred to as the Improved Reduction System (IRS) method was identified as a possible solution to the TAM problem. It includes the mass effects of the omitted DOF's. Unfortunately, due to schedule constraints, evaluation of the IRS method could not be performed until after the full analysis cycle had been completed. With the post-test analysis milestones successfully met, limited resources were made available to investigate the benefits of using the IRS reduction method in place of the Guyan technique. The Section-1 Free-Free configuration FEM was chosen as the test case since its Guyan reduced model generated the largest errors during the pretest analysis.

Table 4-33 shows the results of computing the Section-1 Free-Free pretest TAM using the IRS method. All of the frequency errors between the IRS TAM and FEM are below 1% and all of the linearly combined cross-orthogonality values are above 0.90. These excellent results are a tremendous improvement over the Guyan TAM results shown previously in Table 4-7. The TAM generated using the IRS reduction method fully captured the dynamics of the CSI truss section including the nearly identical frequencies of the closely spaced bending mode pairs.

The newly generated IRS reduced mass matrix was used to compute test vs. FEM post-test cross-orthogonality values as shown in Table 4-34 for the same Section-1 test case. Comparison of these results with cross-orthogonality data computed earlier using the original Guyan reduced mass matrix (Table 4-24) indicates a significant improvement as a result of using the IRS method. Linearly combined cross-orthogonality values between test and FEM are all above 0.90 for the IRS case with the exception of a second bending (0.88) and the axial mode (0.84). In contrast, only one of the modes for the Guyan case has a cross-orthogonality greater than 0.90 and two of the modes are below 0.70.

Overall, the IRS static reduction method is significantly more accurate than the Guyan method in capturing the dynamics of the CSI truss section models with offset sensors. Performing the reduction at the offset sensor DOF's was not a problem for the IRS method. Though the IRS method is significantly better than the Guyan method, it was determined that there was no need to generate new reduced mass matrices using the IRS method in order to update the cross-orthogonality calculations as part of this report. The excellent agreement demonstrated between the FEM models and the measured modal test data using only the RMAC and frequency error criteria eliminated the need for improved cross-orthogonality calculations.

Table 4-33 TAM vs. FEM Cross-Orthogonality and RMAC Comparison for Updated Pretest Section-1 Free-Free Truss Model Using Improved Reduction System (IRS) Method

TAM MODE	TAM FREQ (HZ)	XO	LIN-COM XO	RMAC	LIN-COM RMAC	FEM MODE	FEM FREQ (HZ)	FREQ ERROR (%)	DESCRIPTION
7	111.20	1.00	1.00	1.00	1.00	7	111.20	0.00	1st TORSION
8	127.15	0.99	0.99	1.00	1.00	8	127.13	0.01	1st BENDING
9	127.63	0.99	0.99	1.00	1.00	9	127.59	0.03	1st BENDING
10	215.46	0.99	0.99	1.00	1.00	10	215.33	0.06	2nd TORSION
11	235.66	0.81	0.90	0.89	0.99	11	234.81	0.36	2nd BENDING
12	238.74	0.76	0.93	0.79	1.00	12	236.56	0.92	2nd BENDING
23	484.36	0.91	0.91	0.98	0.98	31	480.89	0.72	AXIAL

Table 4-34 Test vs. FEM Cross-Orthogonality Comparison for Updated Pretest Section-1 Free-Free Truss Model Using Improved Reduction System (IRS) Mass Matrix

TEST MODE	TEST FREQ (HZ)	XO	LIN-COM XO	RMAC	LIN-COM RMAC	FEM MODE	FEM FREQ (HZ)	FREQ ERROR (%)	DESCRIPTION
1	115.00	1.00	1.00	1.00	1.00	7	111.20	-3.3	1st TORSION
2	134.70	0.97	0.99	0.98	1.00	8	127.13	-5.6	1st BENDING
3	135.20	0.97	0.99	0.98	1.00	9	127.59	-5.6	1st BENDING
4	223.10	0.99	0.99	1.00	1.00	10	215.33	-3.5	2nd TORSION
5	250.45	0.85	0.88	0.94	1.00	11	234.81	-6.2	2nd BENDING
6	251.12	0.89	0.97	0.95	1.00	12	236.56	-5.8	2nd BENDING
7	488.17	0.84	0.84	0.85	0.85	30	480.89	-1.5	AXIAL

4.5 TRUSS SECTION DYNAMIC TEST SUMMARY

Dynamic testing of the four CSI truss sections in both the free-free and cantilevered configurations was successfully completed with measured frequency, damping, and mode shape modal parameters for the seven target modes used to fully describe the dynamic characteristics of each test section. Comparisons of test data versus updated FEM predictions show the truss structure dynamic behavior to be highly predictable and linear. Test modes were shown to be shape-orthogonal with all off-diagonal MAC terms less than 0.100.

The frequency and mode shape comparisons between the test and updated pretest FEM modes for all eight tests were excellent, especially with regard to the bending and torsion target modes. The near-perfect shape comparisons computed using RMAC combined with frequency errors generally well below 5% indicate the need for very few adjustments during the post-test model correlation, if any. Linear recombination of the closely spaced FEM bending mode pairs was necessary prior to computing RMAC values in order to obtain an apple-to-apples comparison between the test and analysis bending modes. Axial modes did not compare as well between test and analysis with an average frequency error of 5.1% and RMAC values below 0.95 for three out of the eight tests.

The Guyan reduction method used to compute the TAM's did not fully capture the dynamic behavior of the truss sections mainly because of the offset between the sensor DOF's and the truss Node Ball degrees-of-freedom. For this reason, the post-test cross-orthogonality values computed using the Guyan reduced mass matrix were ignored, and post-test comparisons were made using the RMAC criterion, which is independent of the accuracy of the reduced mass matrix. An improved static reduction technique referred to as the Improved Reduction System (IRS) was evaluated and found to be significantly more accurate than the Guyan reduction method when used on the CSI truss section models with offset sensors. Test versus FEM cross-orthogonality results computed using the IRS reduced mass matrix for a single test case fully corroborate the RMAC results used to demonstrate the excellent shape correlation.

5.0 TRUSS SECTION STATIC TESTS

This section describes the static tests that were conducted by LMSC on the four unique CEM Phase 1 truss sections. The purpose of the static truss section tests was to supplement the dynamic truss section testing with static test data that can be used in correlating the finite element models, if necessary. Bending and torsion tip loads were applied to 10-bay sections of truss in order to quantify their stiffness over the load range they would expect to see in use. The following sections describe the approach, test setup, test procedure, sample data, and results for these tests.

5.1 APPROACH

The truss section test plan is shown in Table 5-1. Eight bending and eight torsion tests were conducted on the same four cantilevered 10-bay truss sections that were tested dynamically in Section 4.0. In order to be consistent with the individual strut static tests, the truss section static tests were designed to exercise the struts over the same load range. As discussed in Section 3.1, the load range was established for each strut size by taking the absolute value of the worst-case CEM static load and adding 300 lbs to conservatively account for dynamic loads. Table 5-1 shows the desired peak Longeron and Diagonal struts loads and the associated maximum applied tip loads and moments used in the truss section tests. For the bending tests, different upward and downward tip shear loads were specified so that the combined effects of the tip load and the gravity loading did not exceed the desired Longeron load range. While the transition from upward to downward applied bending loads was accomplished continuously in the same truss test, the clockwise and counter-clockwise torsional loads were applied in separate, distinct tests.

All of the truss section static tests were conducted using EnerPak Model RD-93 hydraulic cylinders to apply the tip load through a loading plate affixed to the end of the truss. A strain gage bridge load cell was used to measure the applied load. Strut member strains were measured in the four Longerons and four Diagonals in the first truss bay located at the root of the cantilevered section. Displacements were measured at six locations at the mid-section and tip of the truss using Kaman Model KD2310-6U non-contact proximity sensors provided by NASA/LaRC. Additional DCDT displacement and rotation sensors were also used in specific instances to

Table 5-1 CEM Phase 1 Section Static Test Plan

BENDING

Test Section No.	Desired Longeron Load (lbs)	Peak Applied Upward Load (lbs)	Peak Applied Downward Load (lbs)
1	685	158	121
2	1140	241	225
3	325	84	58
4	735	170	149

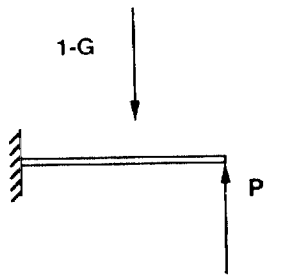

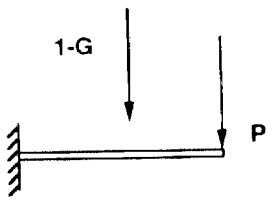

TORSION

Test Section No.	Desired Diagonal Load (in-lbs)	Peak Applied Torque CW (in-lbs)	Peak Applied Torque CCW (in-lbs)
1	425	7026	7002
2	425	6300	6150
3	425	6036	6054
4	425	7146	7074

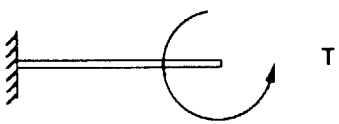

check out the test setup and validate that the test fixture was not moving. A Daytronic System 10 data acquisition system was used to collect the data.

5.1.1 Description of Truss Section Test Setup

The cantilevered 10-bay truss section static test setup is illustrated in Figure 5-1. This figure shows the entire test setup, including the test fixture consisting of two I-beams and the cantilever support base, the six Kaman sensors (K-1 through K-6), the hydraulic force actuators (L-1), and an extra DCDT (D-1).

Figure 5-2 shows the location of the eight truss struts where strains were measured, labelled A through H. Three strain gages were applied at strut tube mid-section at 120° intervals around the circumference of each strut member. Note that while the truss *face* location of the diagonals E, F, G, and H are uniquely determined in Figure 5-2, the *orientation* of the diagonals within the truss face are not. The orientation shown is appropriate for truss Sections-1, -3 and -4, but is reversed for Section-2 (see Appendix B for detailed maps of truss strut identification, location, and orientation). Table 5-2 lists the strut identification numbers and the associated gage factors for the strain gages. These particular struts were delivered to NASA/LaRC with the gages left on so that they may be used in suspended CEM assembly tests, if desired.

Figure 5-3 shows the location and sensing direction of the six Kaman proximity sensors. These sensors had a resolution of 0.1 mils. Three of the sensors are located on the batten frame at the mid-section of the truss (dividing bays five and six) and three are located at the tip of the truss behind the tip plate. Kaman sensors (1) and (4) measure deflections in the vertical direction while Kaman sensors (2), (3), (5), and (6) measure deflection in the transverse direction. Additional views of the Kaman sensor locations are provided in Figures 5-1 and 5-4. Figure 5-5 provides a close-up of the K-1 sensor installation. The 6-inch OD aluminum targets are bolted to the truss Node Balls such that the sensed surface is offset approximately 1.475 inches from the centroid of the Node Ball. The proximity sensors themselves are supported independently by fixturing, and are located 0.6 inches from the targets. Part of the K-3 sensor target is also visible in the lower part of the figure. Figure 5-5 also shows the attachment of the tip plate to the end of the truss and the bending load application fixture at the right of the photograph.

The bending and torsion load application fixtures are shown schematically in Figure 5-6. The tip shear load for bending is applied through a clevis pin attached to the 0.5 inch thick tip plate (Figures 5-6a and 5-7). The load application point is 3.35 inches from the plane formed by the centroids of the four Node Balls at the tip of the truss.

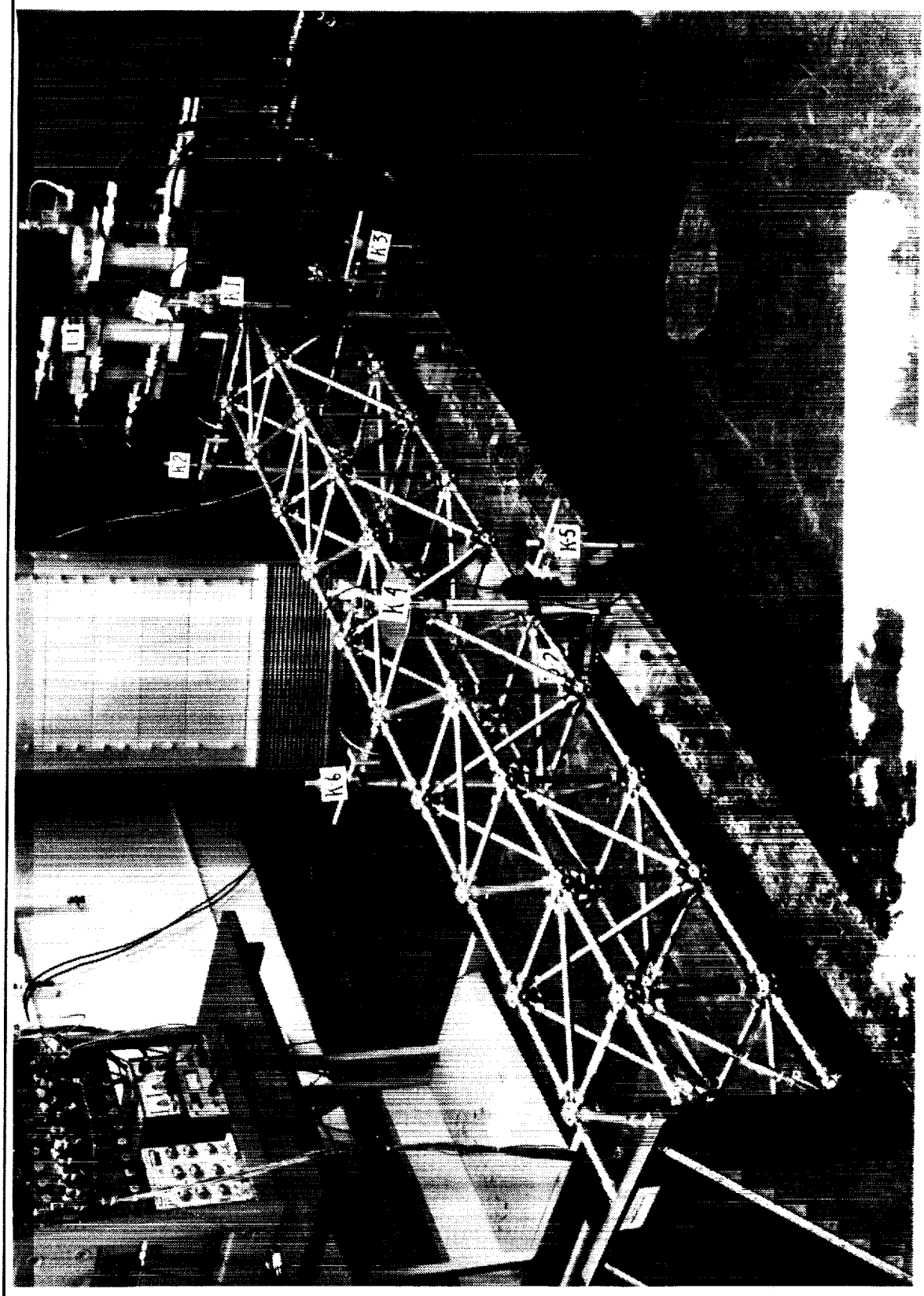

M8127F2Fig. 5-1

Figure 5-1 Truss Section Sensor Locations for Bending Tests

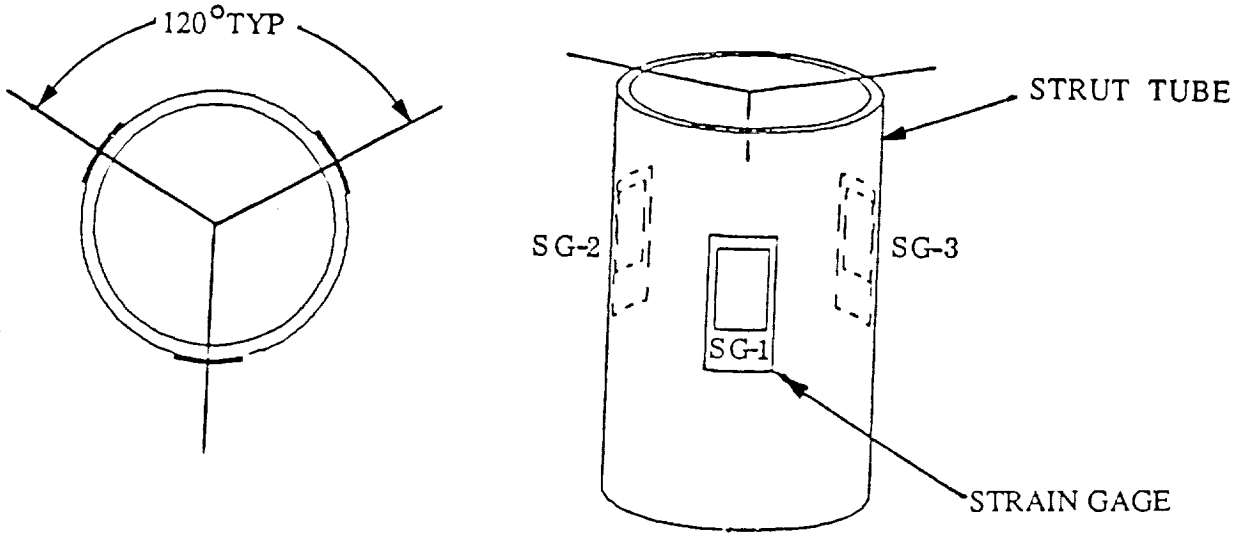

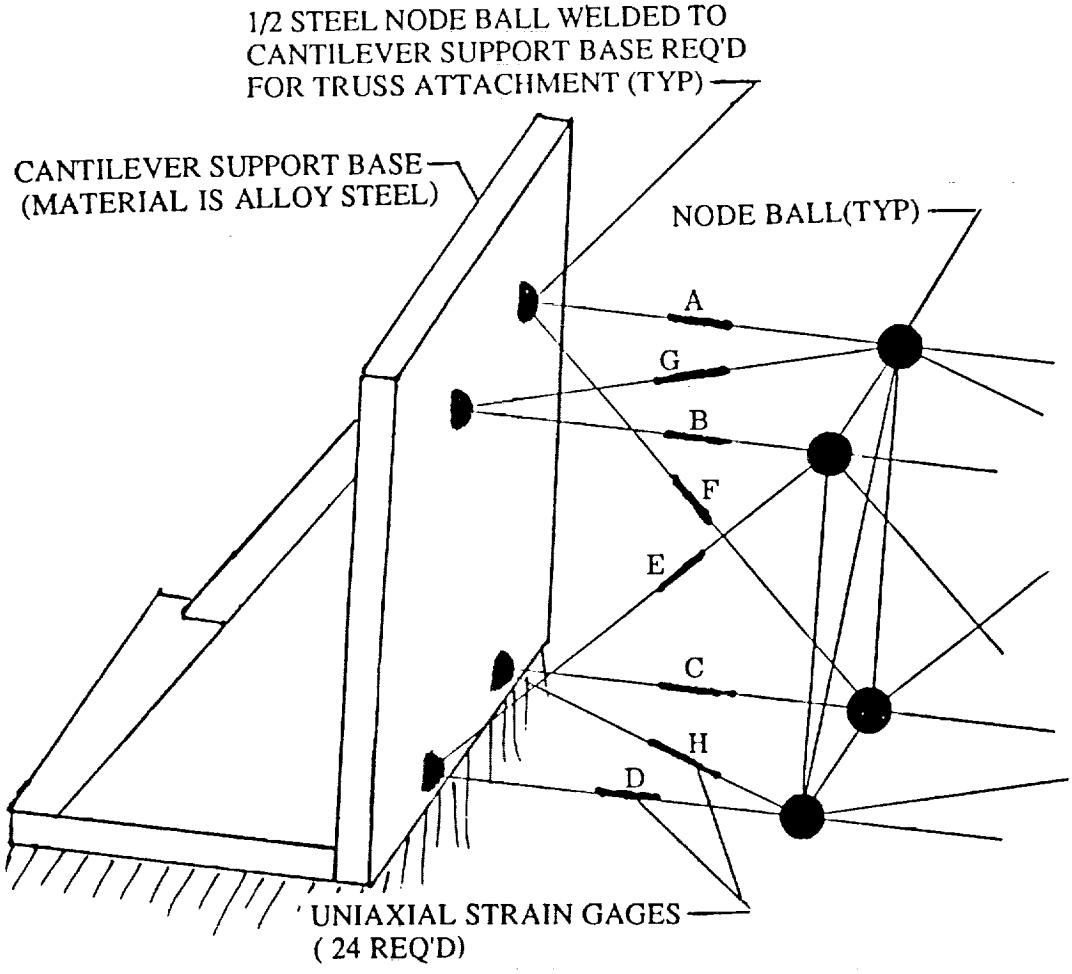

Figure 5-2 Strain Gage Location and Identification

Table 5-2 Strain Gage Strut Assignments

STRAIN GAGE NO.	TRUSS MEMBER	TRUSS SECTION STRUT IDENTIFICATION			
		TRUSS NO.1	TRUSS NO.2	TRUSS NO.3	TRUSS NO.4
SG-1, SG-2, SG-3	LONGERON (A)	1L052	2L081	3L042	4L013
SG-4, SG-5, SG-6	LONGERON (B)	1L050	2L102	3L031	4L026
SG-7, SG-8, SG-9	LONGERON (C)	1L051	2L104	3L049	4L005
SG-10, SG-11, SG-12	LONGERON (D)	1L057	2L101	3L033	4L037
SG-13, SG-14, SG-15	DIAGONAL (E) LEFT	D138	D121	D185	D010
SG-16, SG-17, SG-18	DIAGONAL (F) RIGHT	D300	D118	D149	D270
SG-19, SG-20, SG-21	DIAGONAL (G) TOP	D301	D111	D173	D256
SG-22, SG-23, SG-24	DIAGONAL (H) BOTTOM	D218	D106	D162	D198

MICRO-MEASUREMENTS STRAIN GAGES
IDENTIFICATION & GAGE FACTOR (GF)
AS APPLIED TO TRUSS SECTION STRUTS

TRUSS NO.	GAGE TYPE	GF	GAGES AFFECTED	STRUTS AFFECTED
1	CEA-13-125UW-350	2.15	ALL	ALL
2	CEA-13-125UW-350 CEA-13-125UW-120	2.135 2.12	1→9 & 13→24 10, 11, &12	ALL except 2L104
3	CEA-13-125UW-350	2.145	ALL	ALL
4	CEA-13-125UW-350	2.15	ALL	ALL

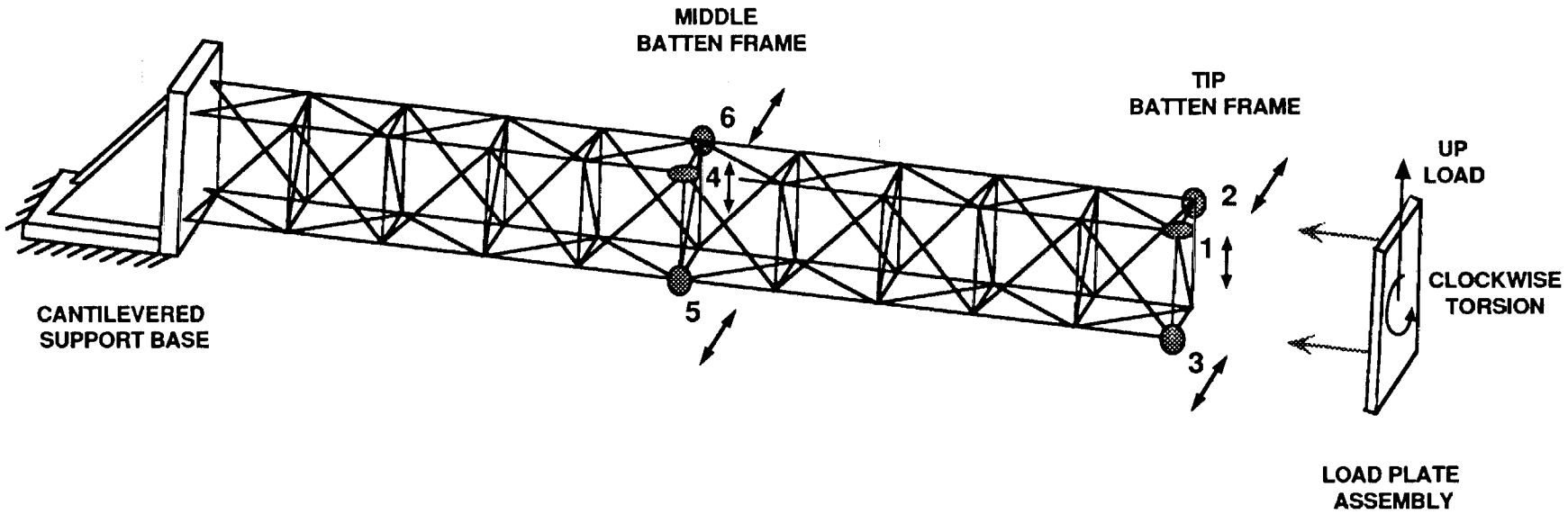

Figure 5-3. Kaman Sensor Locations and Sensing Directions

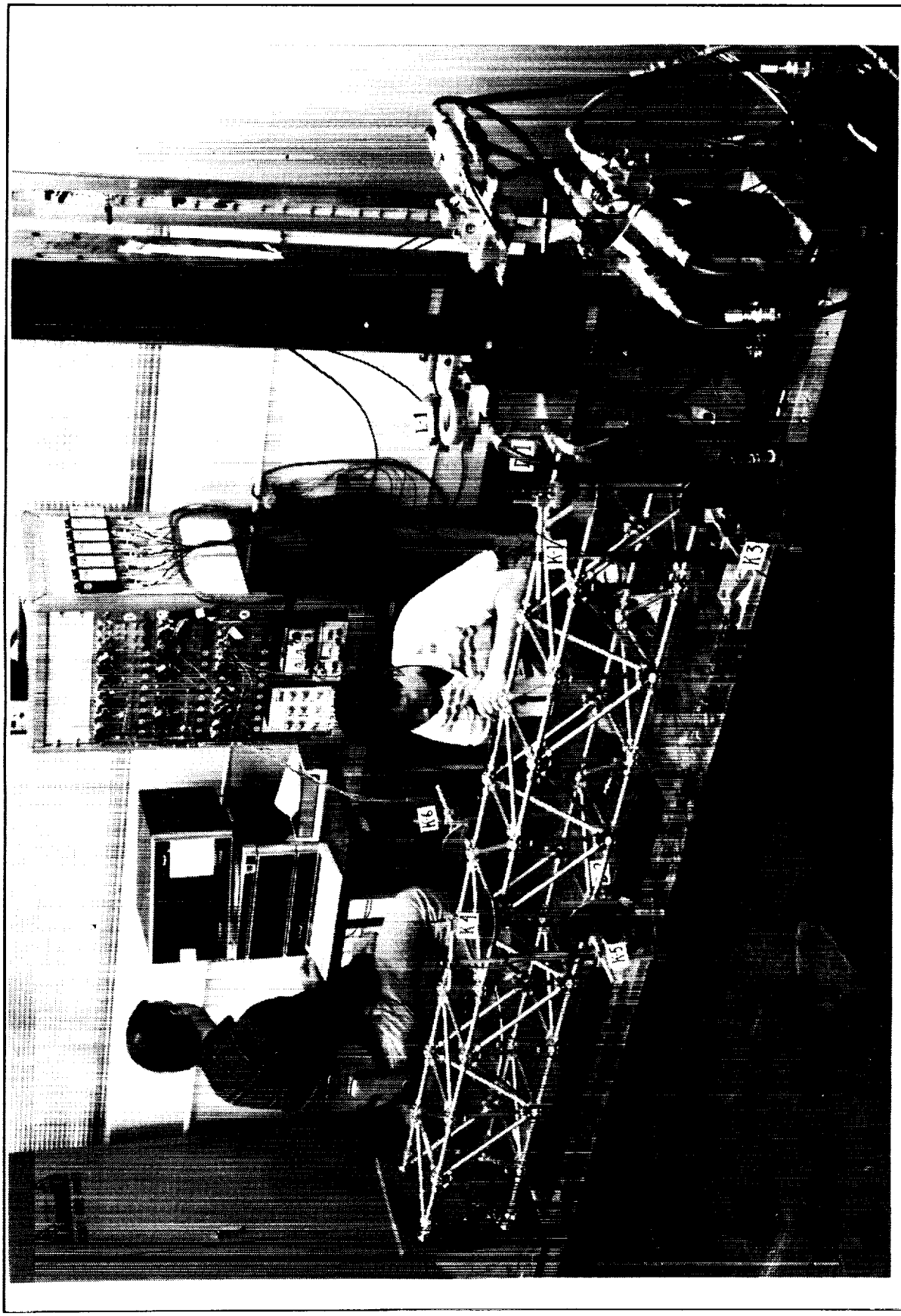

Figure 5-4 Reverse Angle View of Bending Test Sensor Locations

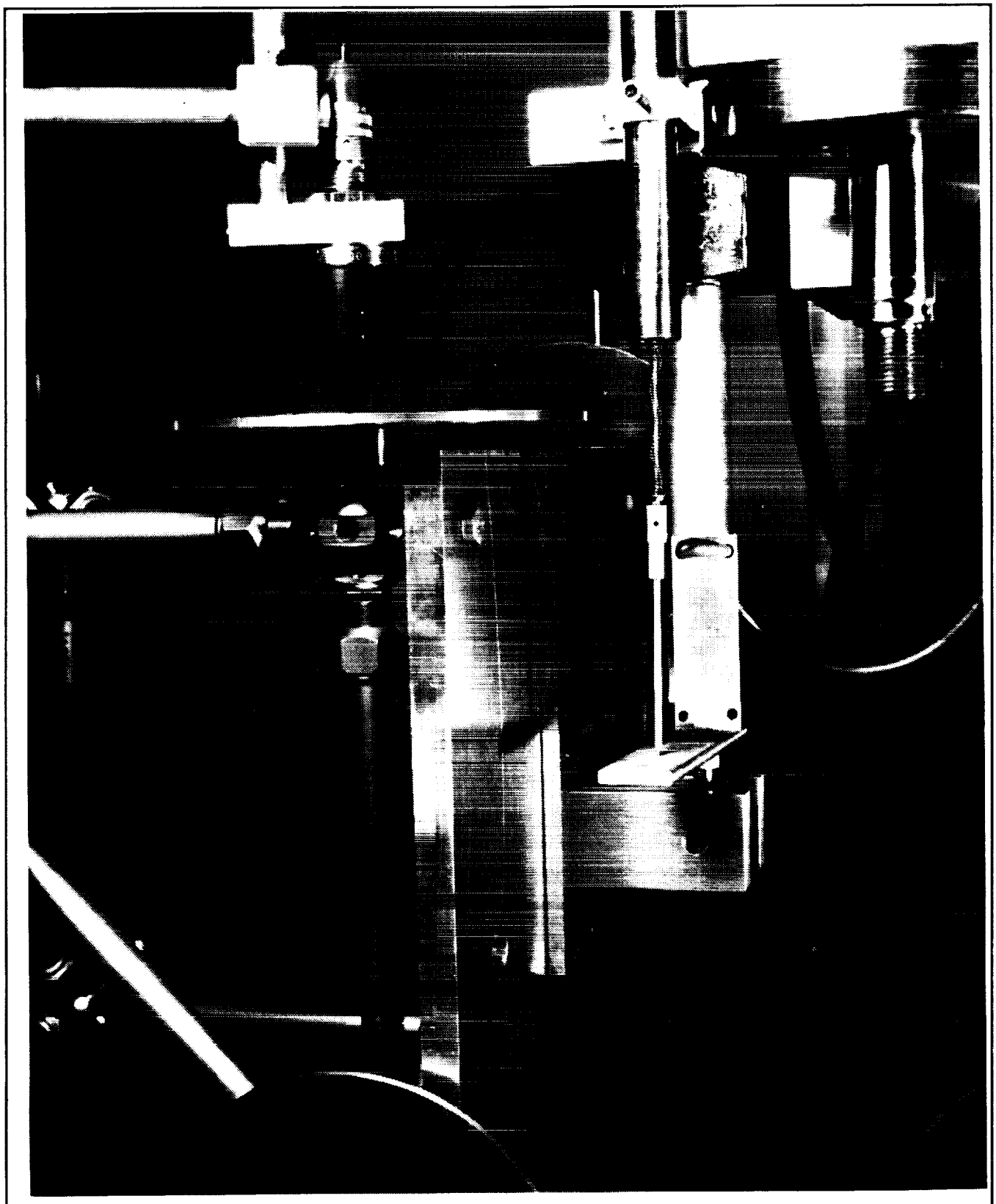

M8127F2Fig. 5-5

Figure 5-5 Applied Bending Load Fixture and Kaman Sensor No. 1

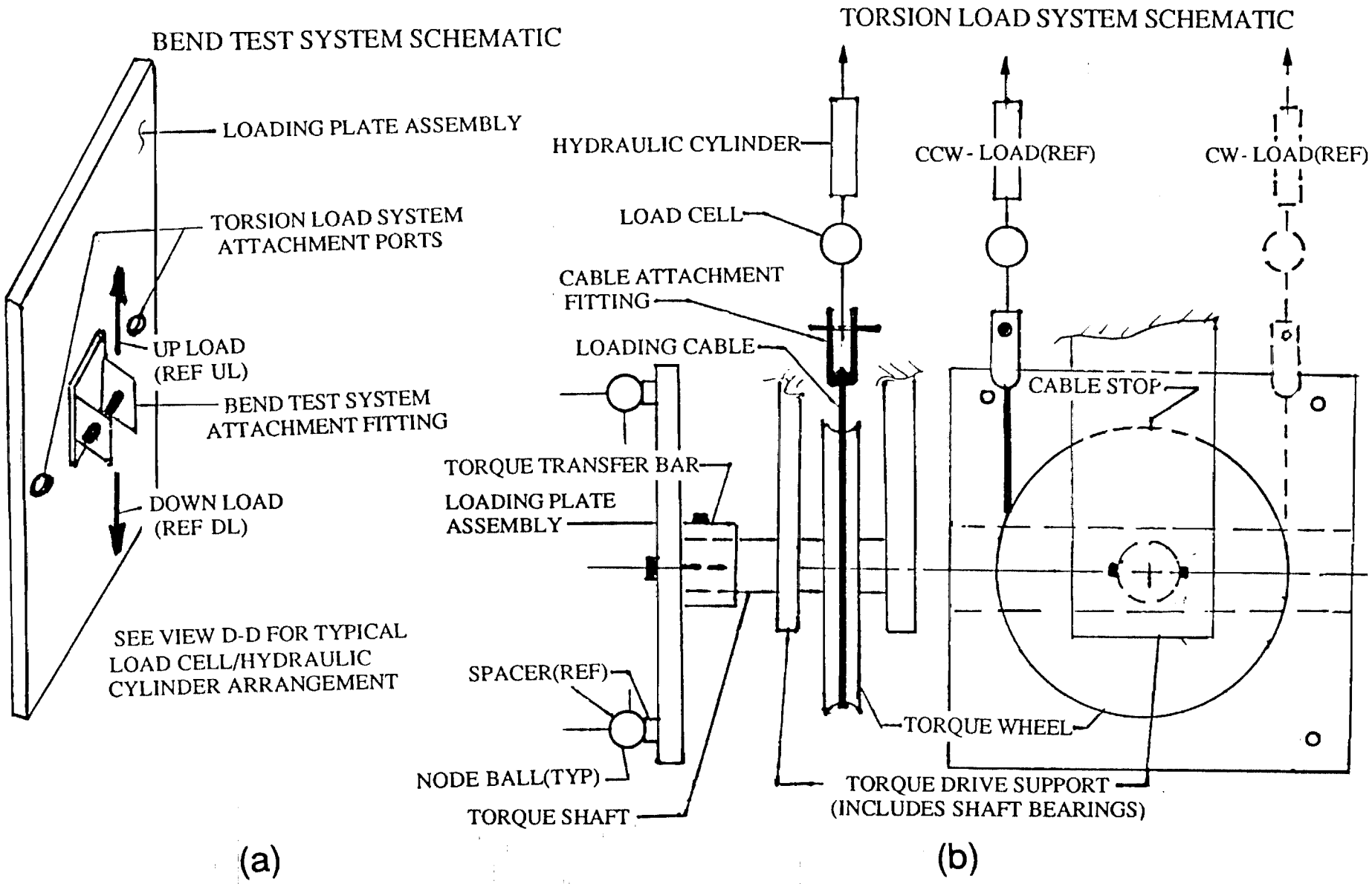

Figure 5-6 Bending and Torsion Load Application Fixtures

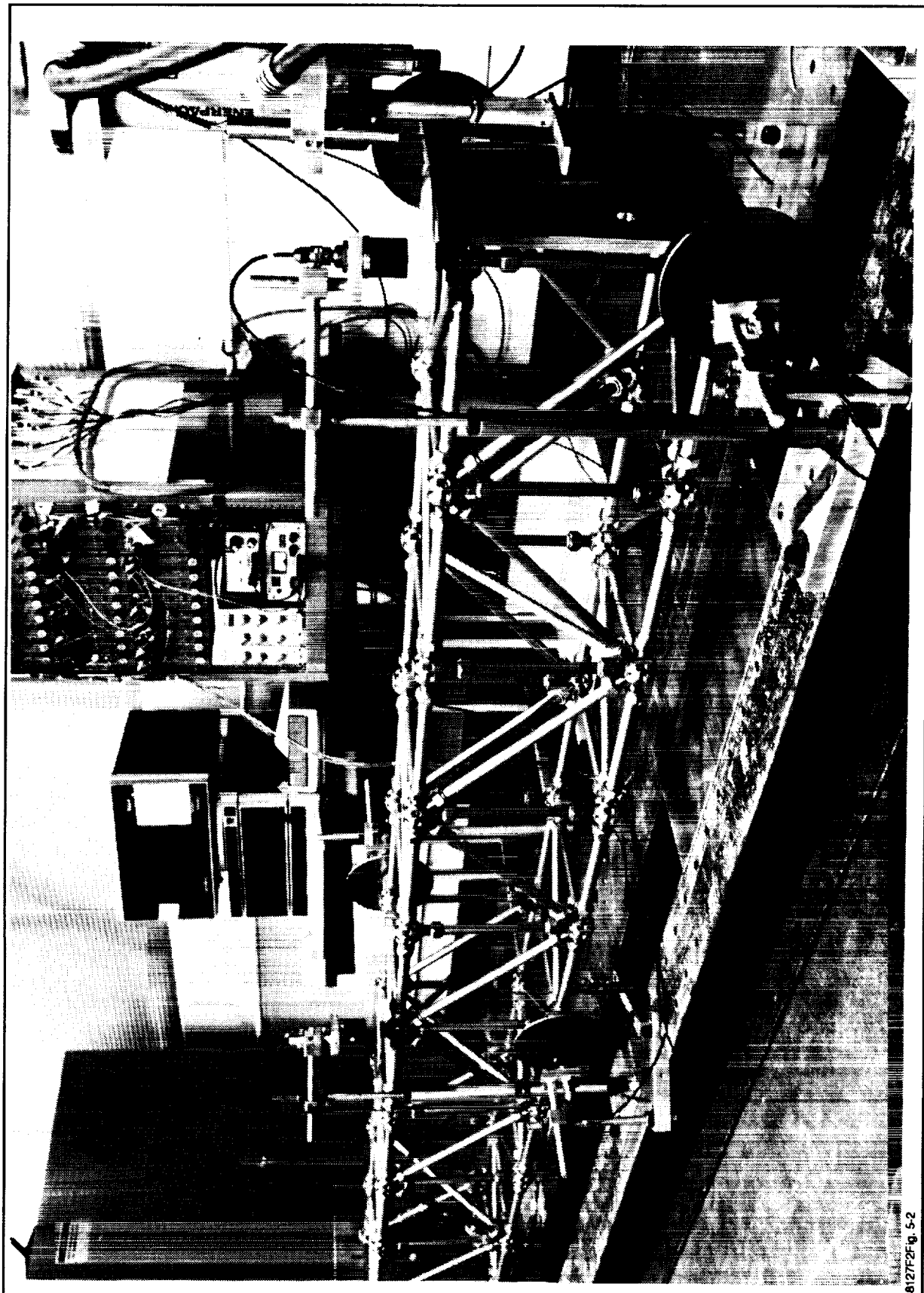

Figure 5-7 Bending Load Test Setup

The load cell is connected in series with the center hydraulic cylinder (Figure 5-8), and has a resolution of 0.1 lbs. The tip moment load for torsion is applied through a load cable in series with a load cell. The load cable is wrapped around the circumference of a 12-inch OD torque wheel which is supported on a bearing (Figure 5-6b). The load direction is changed from clockwise (CW) to counter-clockwise (CCW) by using either the right or left hydraulic cylinders shown in Figure 5-8 and changing the wrap direction of the loading cable. Further details of the CCW torsion test setup are provided in Figures 5-9 and 5-10.

5.1.2 Test Setup Assembly Procedure

Because the demanding schedule required that the dynamic and static truss section tests be conducted in parallel in separate facilities, the dynamic test setup could not be used for the static tests. Instead, the truss was assembled onto a duplicate cantilever base fixture identical to that used in the dynamic tests (see Section 4.0), but located in the LMSC Building 255 Structural Mechanics test laboratory. The individual member struts were located in the exact same positions within the truss, as indicated in Appendix B. In fact, only the four Longerons and four Diagonals which interface with the cantilever support base were disconnected for the transfer - the rest of the truss was left intact (Figure 5-11). Nonetheless, all strut Nuts were re-torqued to the specified 240 in-lbs prior to static testing in order to ensure that the proper preload level was maintained. Note also that during the assembly of the truss sections, the "equatorial" and "polar axis" orientations of the Node Ball (Figure 3-7) were maintained in the same directions as they would be on the assembled CEM Phase 1 structure.

The assembly procedure proceeds as follows:

A. Install Strain-Gaged Struts:

1. Install Standoffs (8 req'd) to the steel half section Node Balls on the Cantilever Support Base to match the Longeron and Diagonal Strut arrangement per Truss configuration per Figure 5-2. Torque Screws to 210 inch pounds.
2. Attach the strain-gaged Longeron and Diagonal Struts to the Support Base half Nodes using 2-turns of the required Nuts, but do not torque at this time

B. Position The Truss:

1. Place six leveling jacks (see Figure 5-12), three equally distributed on each 6-inch steel I-beam support

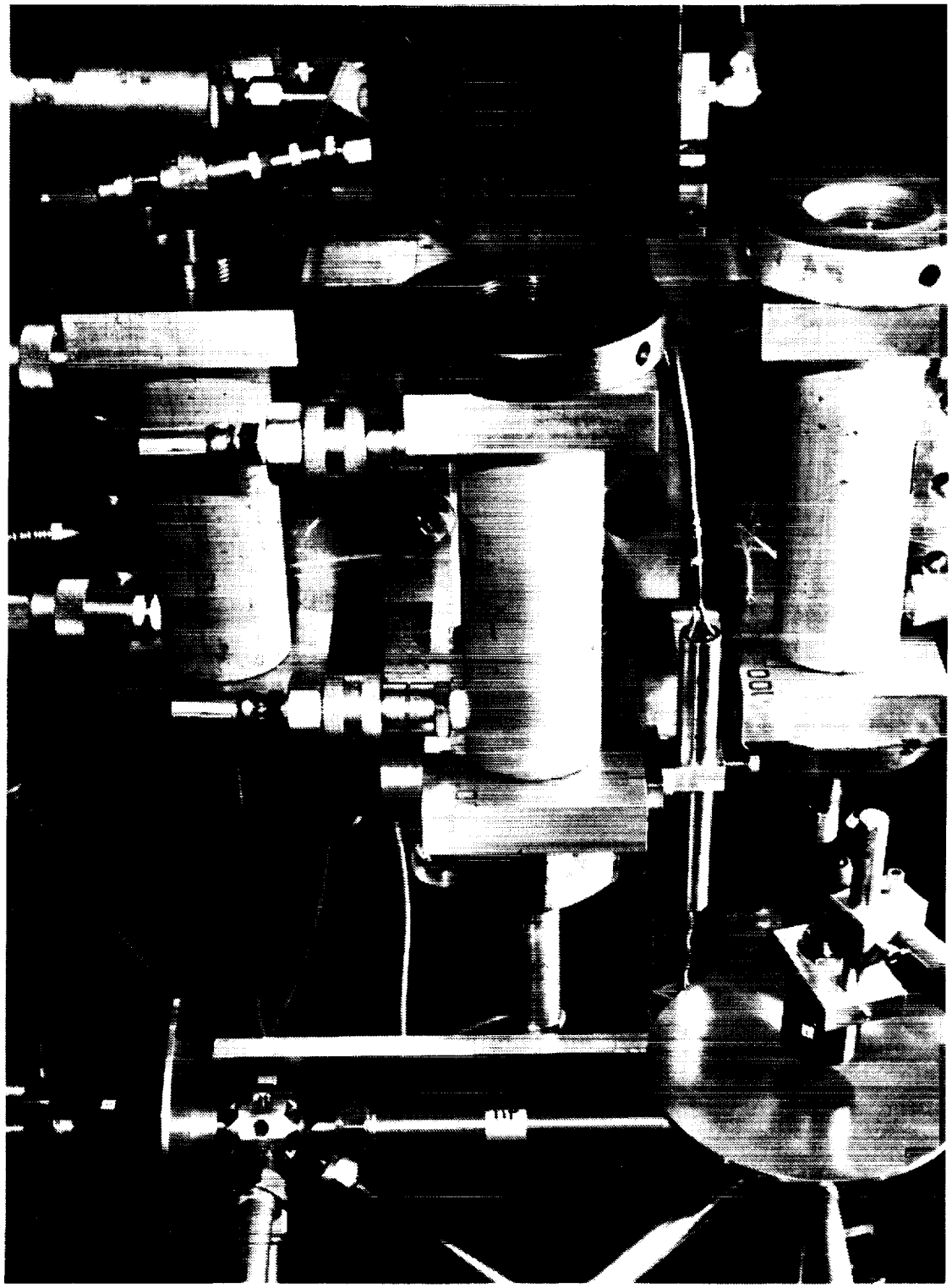

M8127F2Fig. 5-8

Figure 5-8 Hydraulic Cylinders for Applied Bending and Torsion Loads

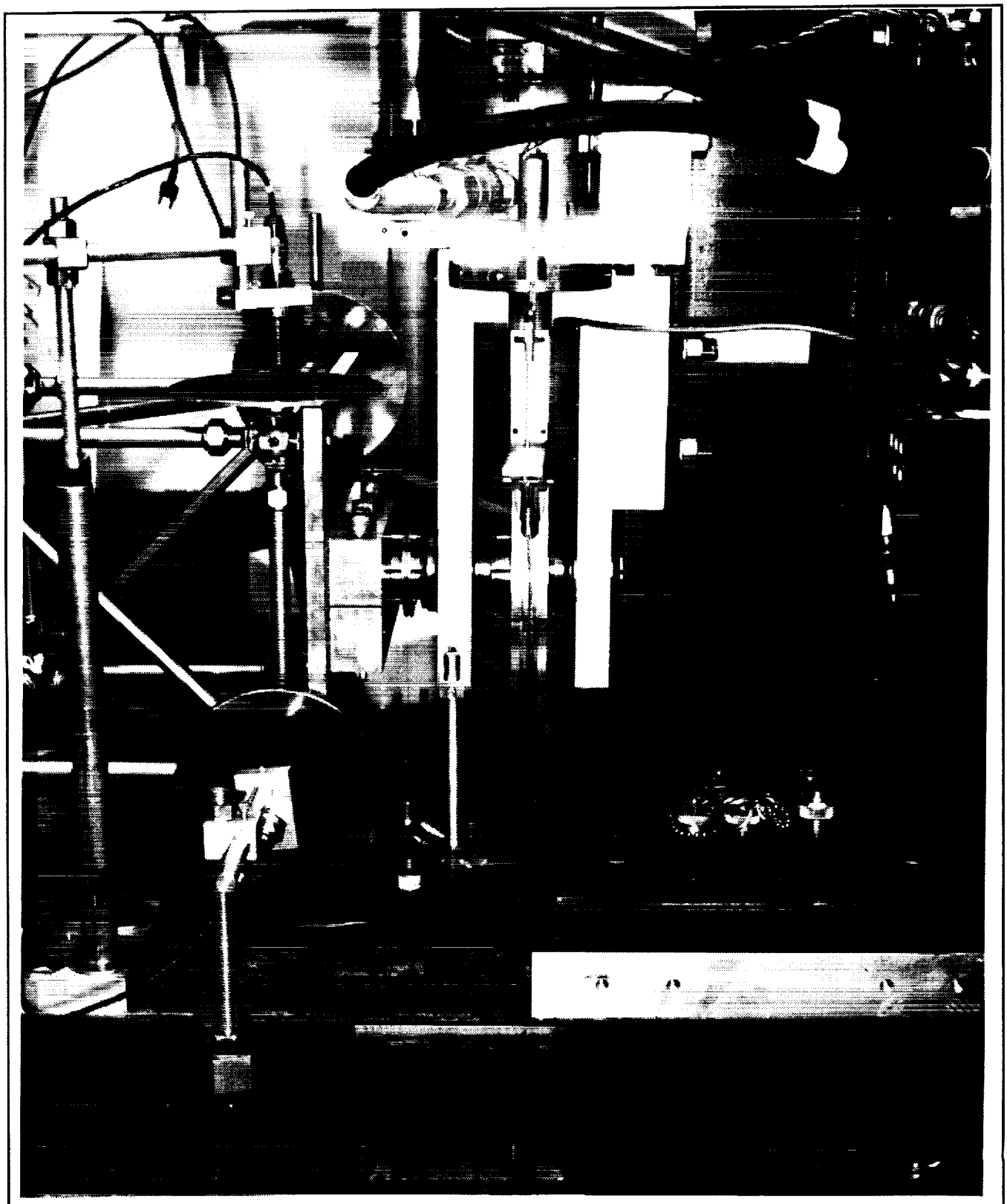

M8127F2Fig. 5-9

Figure 5-9 Side View of Torsion Load Application Fixture

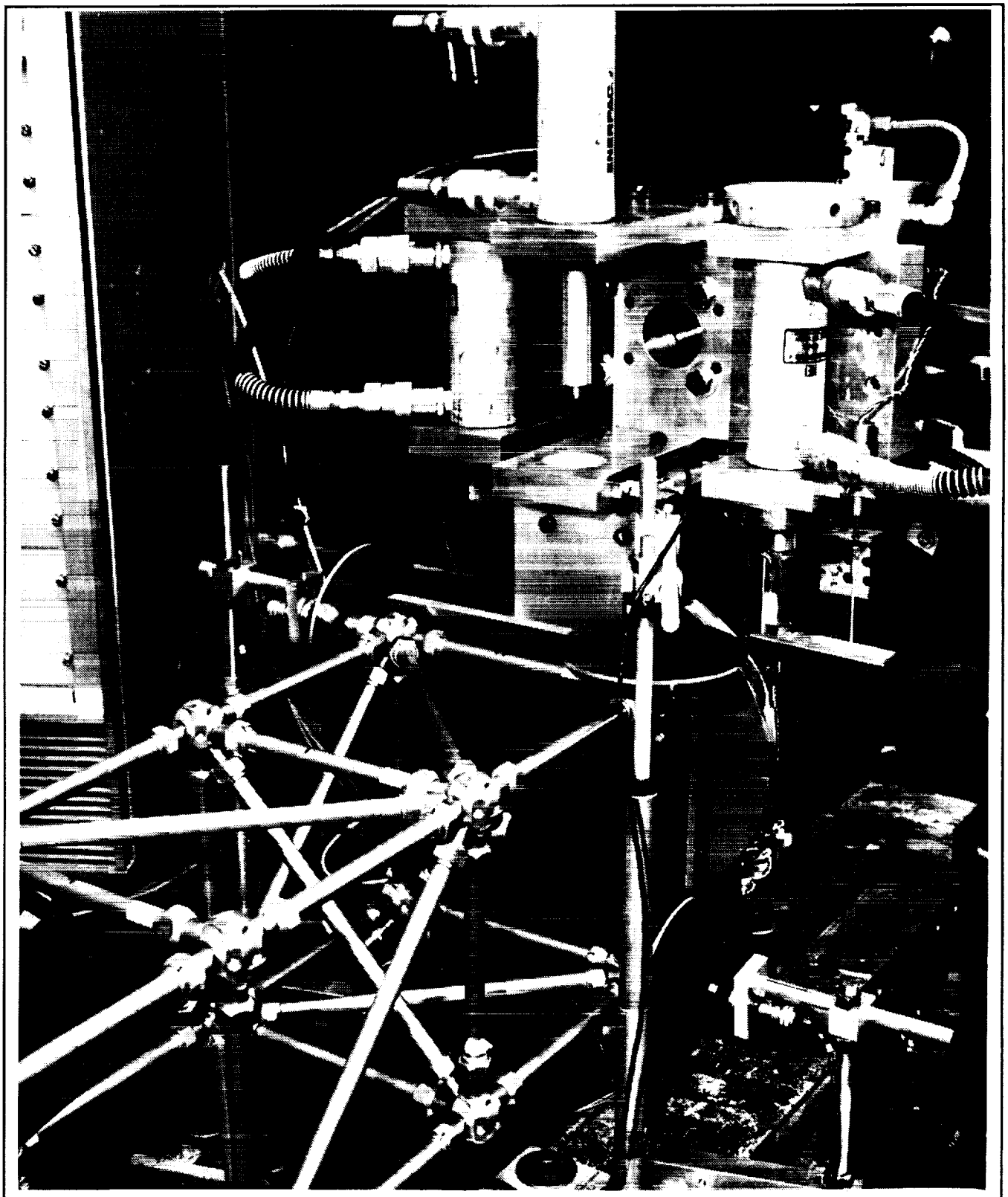

M8127F2Fig. 5-10

Figure 5-10 Torsion Test Setup for Counter-Clockwise Loading

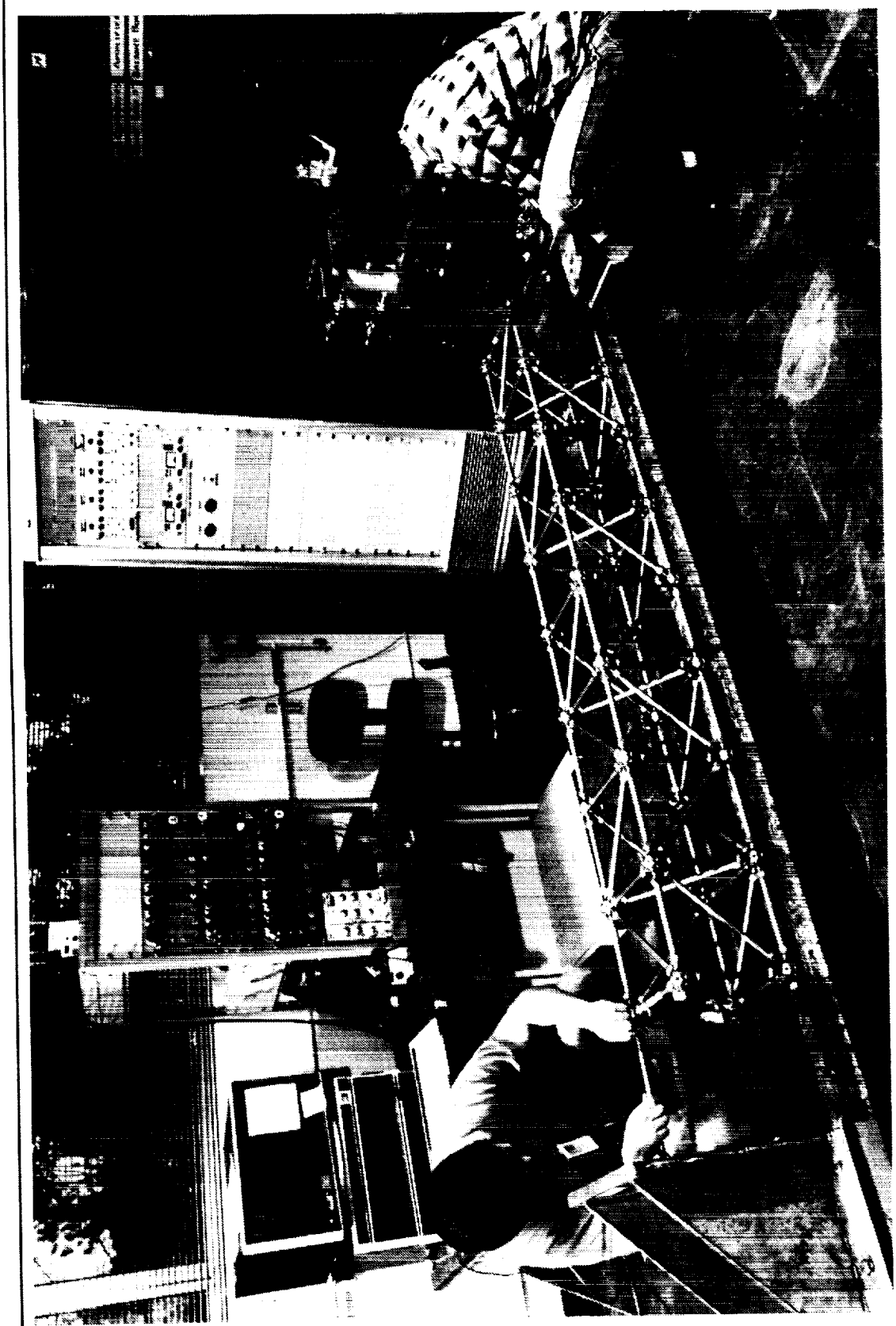

M8127F2Fig. 5-11

Figure 5-11 Truss Section in Process of Assembly

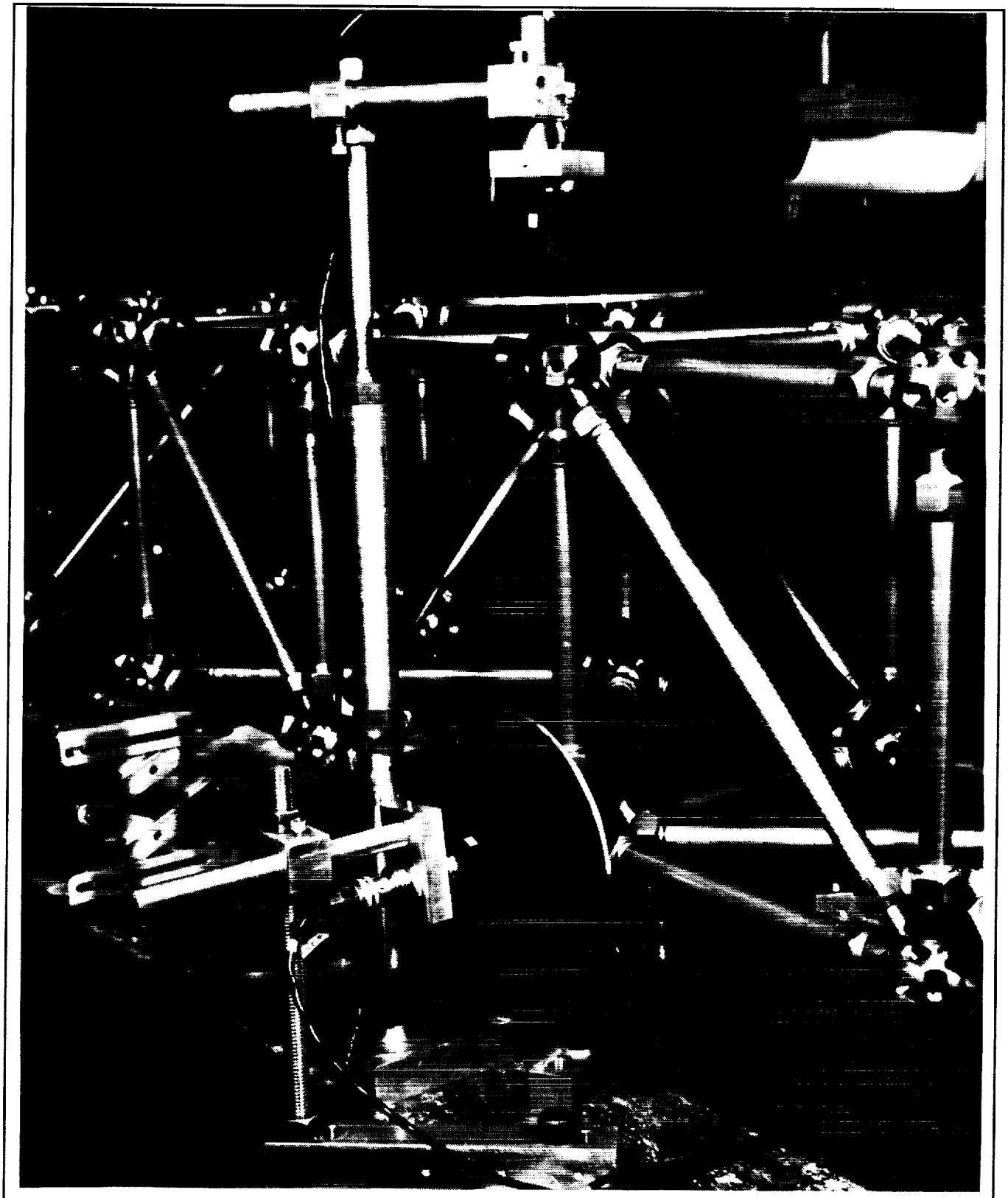

M8127F2Fig. 5-12

Figure 5-12 Typical Leveling Jack Support and Kaman No. 4 and 5

2. Place the partially assembled truss section on the leveling jacks (supporting it at the Node Balls) as close as practicable to the Cantilever Support Base, allowing for the lengths of the Longerons
3. Adjust the jacks until good alignment of the whole truss section is obtained.

C. Attach Partially Completed Truss Section

1. By a series of alignment moves bring the partially completed truss section into contact with the strain-gaged Longerons and Diagonals such that the Nuts can be finger threaded for two turns at a time until the truss is in its final position and all the Nuts are finger tight.
2. Complete the assembly by torquing each Nut to 240 in-lbs.

D. Attach Sensors & Actuators to Truss

1. Attach strain gage wiring
2. Attach tip plate (note truss should still be supported by jacks)
3. Attach Kaman sensor targets and center Kaman sensors above the targets
4. Attach bending or torsion actuator fixturing to truss tip plate

5.2 TRUSS SECTION TEST PROCEDURE

Prior to testing, the Kaman sensors are calibrated according to the manufacturer's instructions using the 0.5-inch and 1.0-inch ceramic spacers provided by NASA/LaRC. In addition, the ramp rate for the hydraulic cylinders is calibrated prior to connection to the truss. Next, the hydraulic cylinders are connected with the truss tip supported in the zero-deflection position. At this time, the jacks are removed from beneath the truss and the strain gages, Kaman sensors, and the load cell are zeroed. In this way, the effects of gravity are eliminated for the load cell and truss tip Kaman sensors, and minimized for the strain gage and mid-truss Kaman sensors.

Prior to each truss section bending or torsion test, a complete run-through of the test sequence is conducted at 50% load to checkout the test setup, verify the programming and operation of the Daytronic system, and establish the relationship between the strain in the struts at the root and the applied load. This relationship is then used to set the strain level corresponding to the peak load value and the 100% test is conducted automatically by issuing a start command to the Daytronic. Figure 5-13 shows the load profiles used in the bending tests while Figures 5-14 and 5-15 show the torque profiles

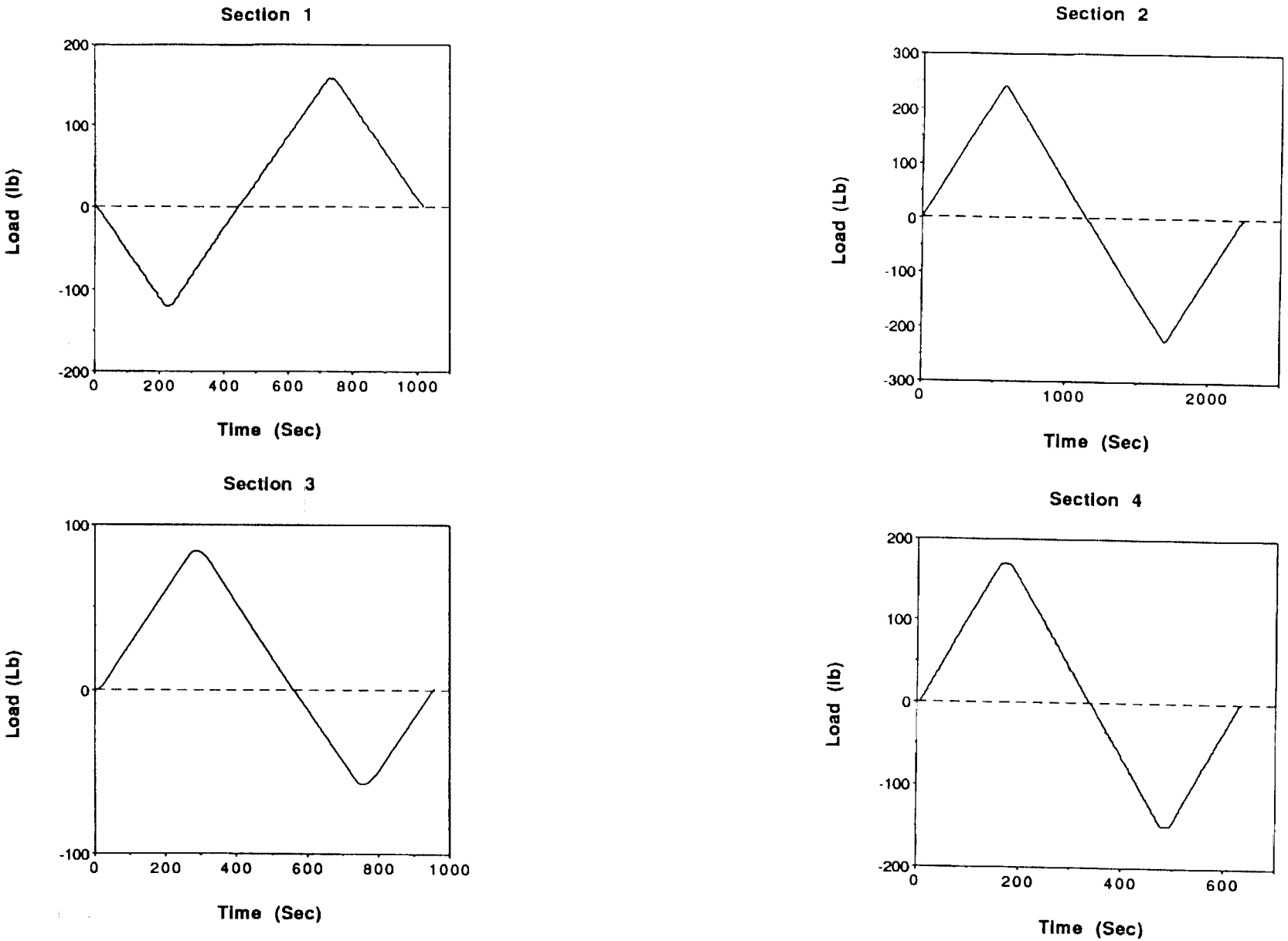

Figure 5-13 Load Profiles for Bending Tests

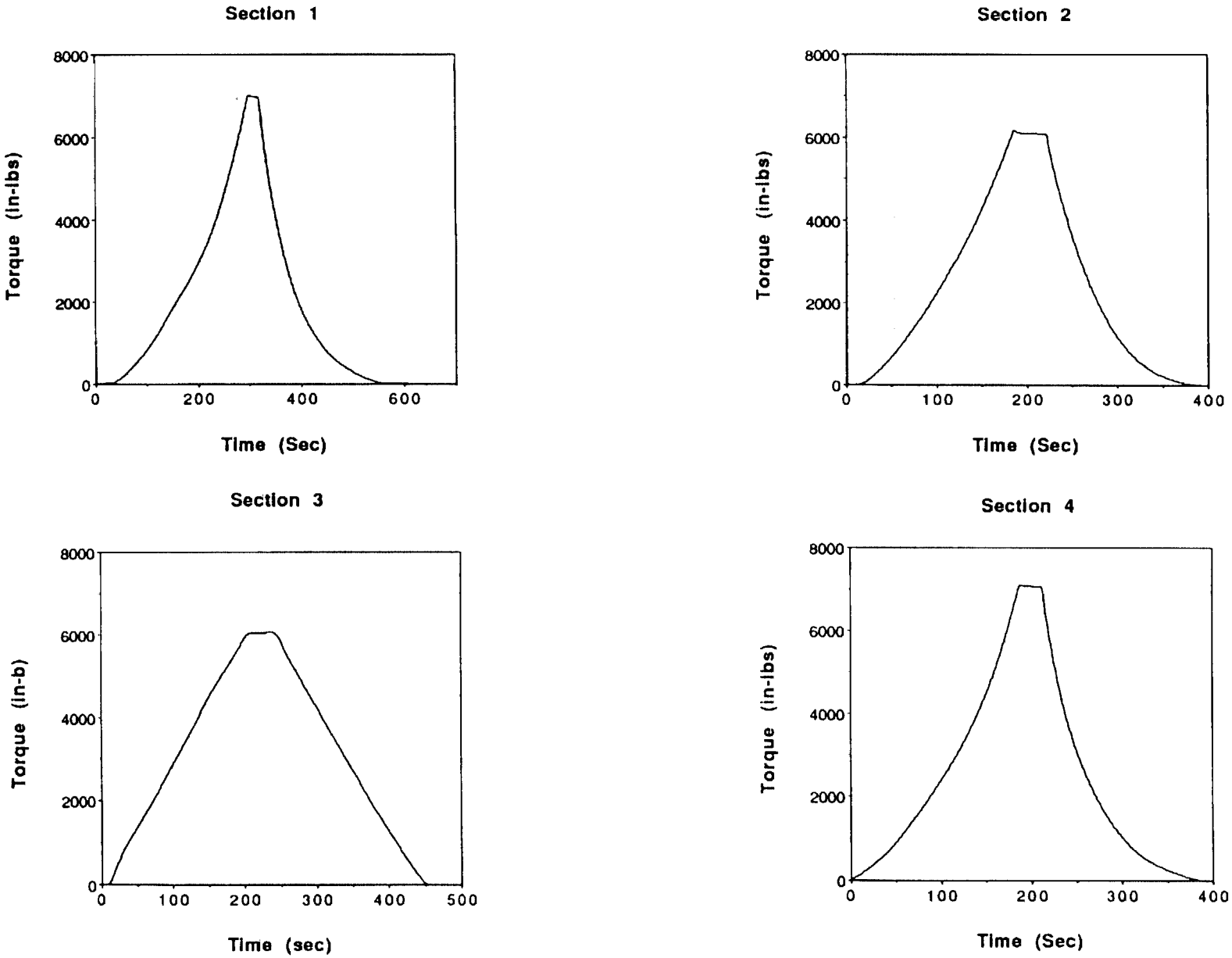

Figure 5-14 Load Profiles for Clockwise Torsion Tests

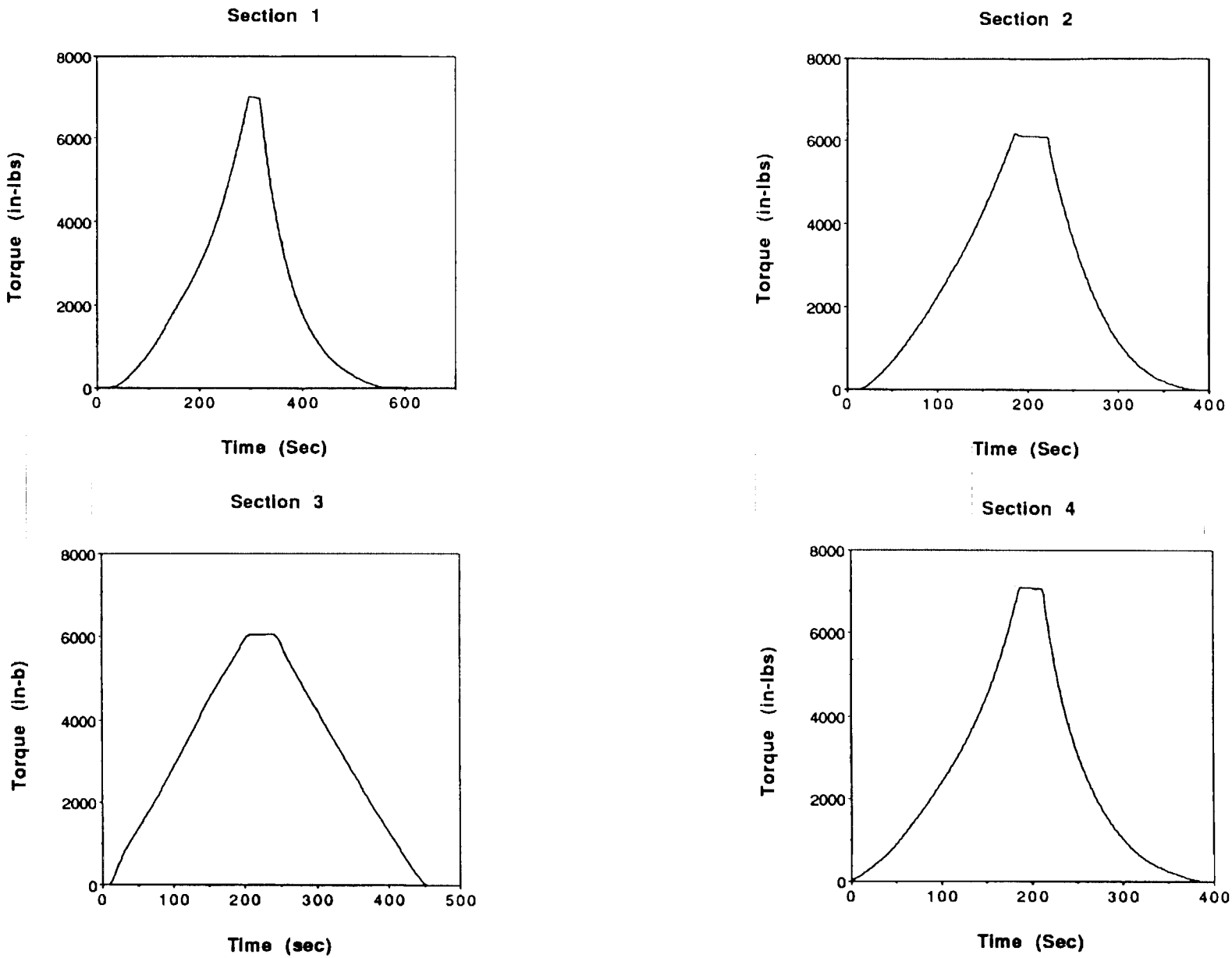

Figure 5-15 Load Profiles for Counter-Clockwise Torsion Tests

for the torsion tests. The different shape for the torque profile for Section-3 was obtained by using position control, rather than the force control used for the later tests.

5.3 TRUSS SECTION TEST RESULTS

Overall, the truss section test data is characterized by very tight, linear, and repeatable force-displacement curves characteristic of a well-preloaded erectable structure with little or no hysteresis. Since a large amount of data was taken (30 channels X 12 tests), this section will review the data from truss Section-4, which was typical of the data for all the truss sections. Data from truss Sections -1 through -3 is provided in Appendix G. Reduced data from all the tests (in terms of flexibility influence coefficients) is presented at the conclusion of this section in order to facilitate comparisons with analytical predictions and provide an overview of the overall performance.

Typical bending test data for truss Section -4 is provided in Figure 5-16. The K1 and K4 sensors are aligned with the direction of the applied loading. Note that K2, K3, K5 and K6 Kaman sensors typically registered on the order of only 5 - 10 mils of displacement, indicating that little or no out-of-plane motion occurred and that there was no bending-torsion coupling.

Typical counter-clockwise torsion test displacement data for truss Section-4 is provided in Figure 5-17. Note that all of the slopes are approximately the same for each sensor, which is indicative of a pure torsion response. This behavior was noted in all the counter-clockwise torsion data. For comparison, typical clockwise torsion test data for truss Section-4 is shown in Figure 5-18. In this case, the K1 and K3 slopes are approximately the same, but the K2 slope is different. This pattern suggests that some bending is occurring, and is characteristic of all the clockwise torsion data, with the exception of truss Section-3 (Figure 5-19).

Although model correlation was outside the scope of the contracted effort, some modeling was done in order to facilitate comparisons between predicted and test data, and thereby check the data quality. A finite element model was constructed using the updated truss member weight and stiffness properties resulting from the individual strut tests (Table 3-7). This model included appropriate geometric offsets (indicated by the circles in Figure 5-20) for the Kaman sensor targets and the load application point, including the tip plate. Unit tip shear and moment loads were applied to the analytical model and displacement results were obtained at the Kaman sensor locations. These

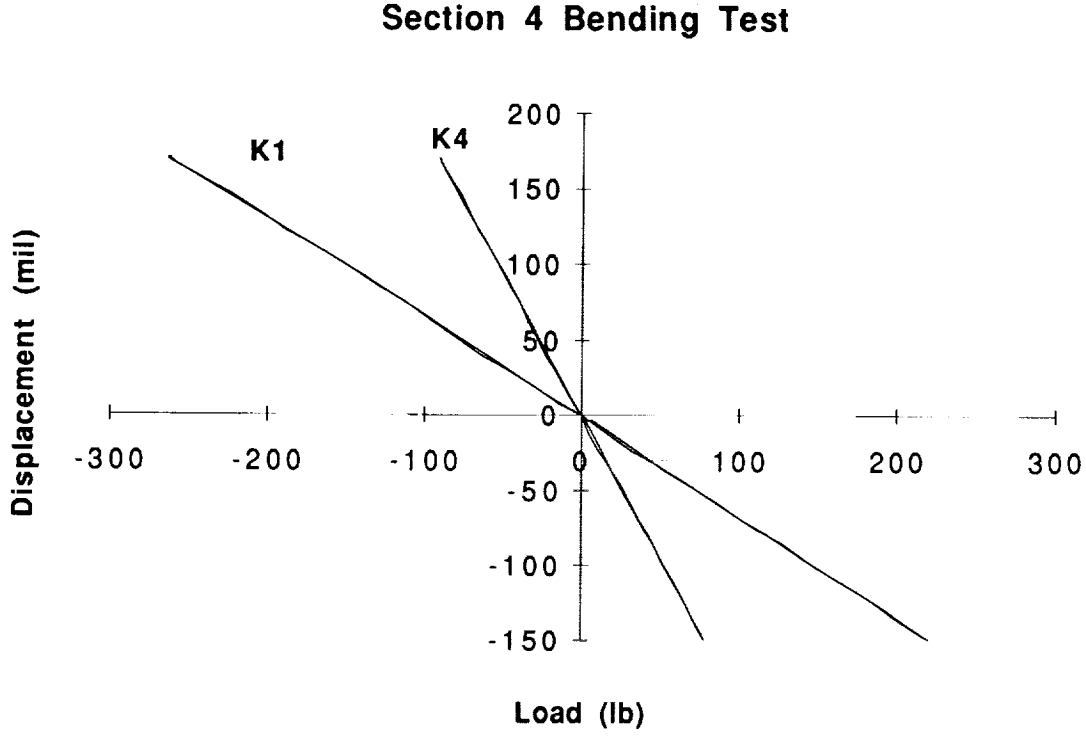

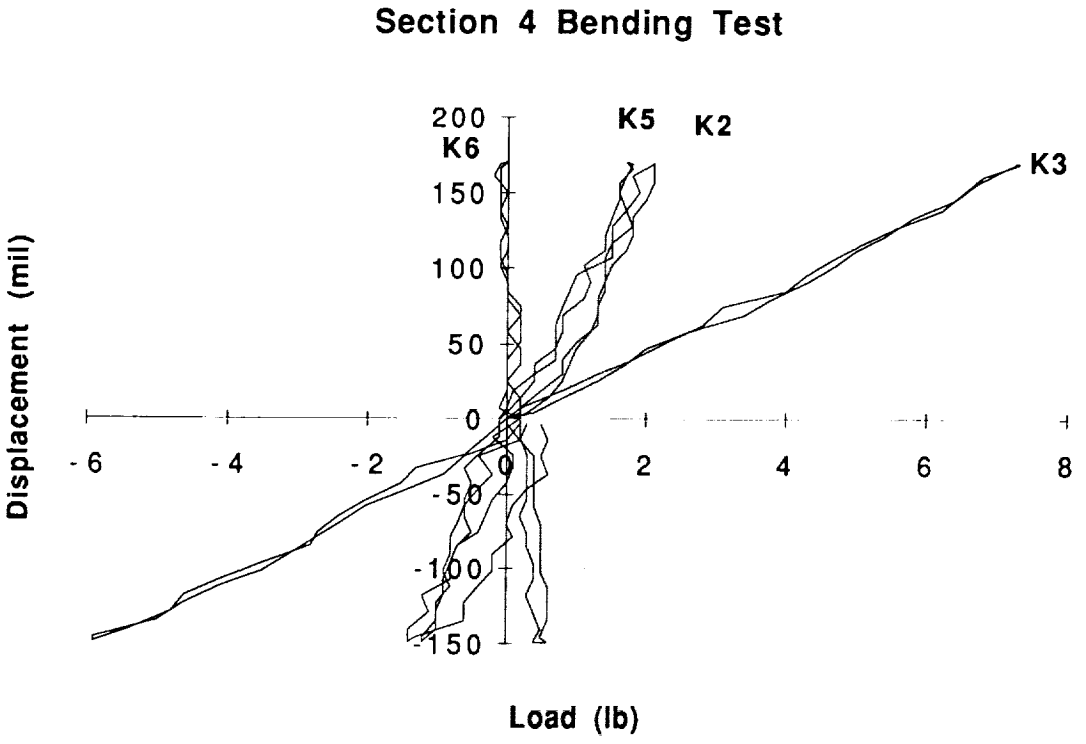

Figure 5-16 Section-4 Bending Test Results

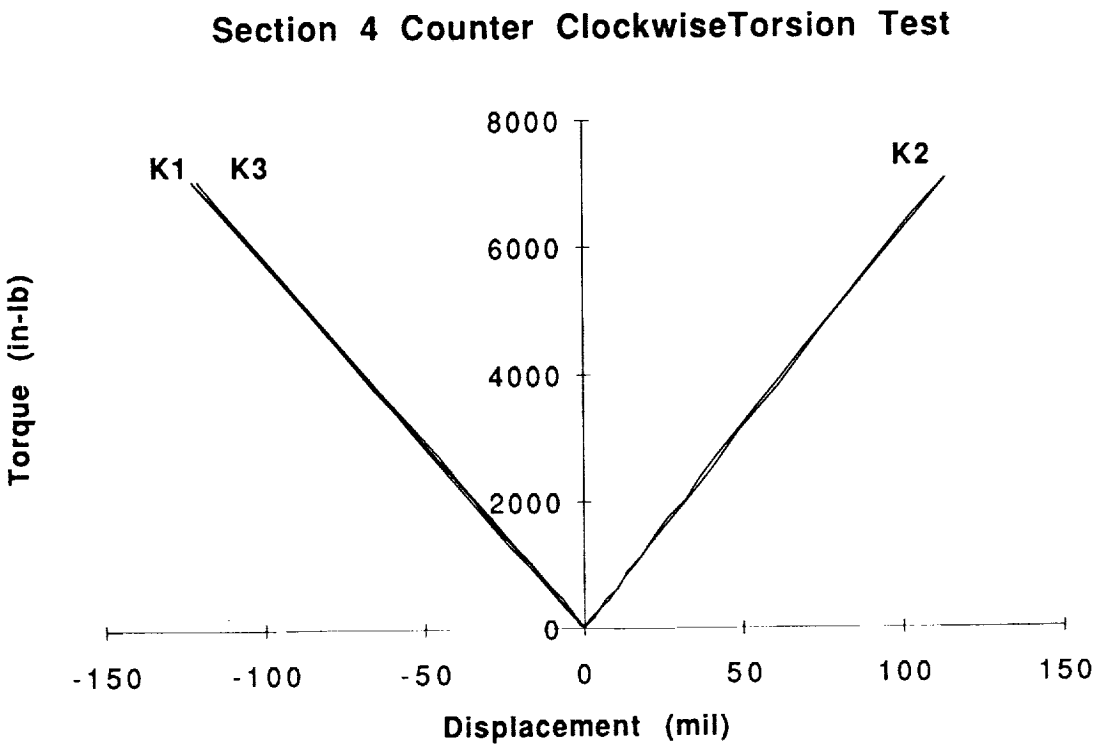

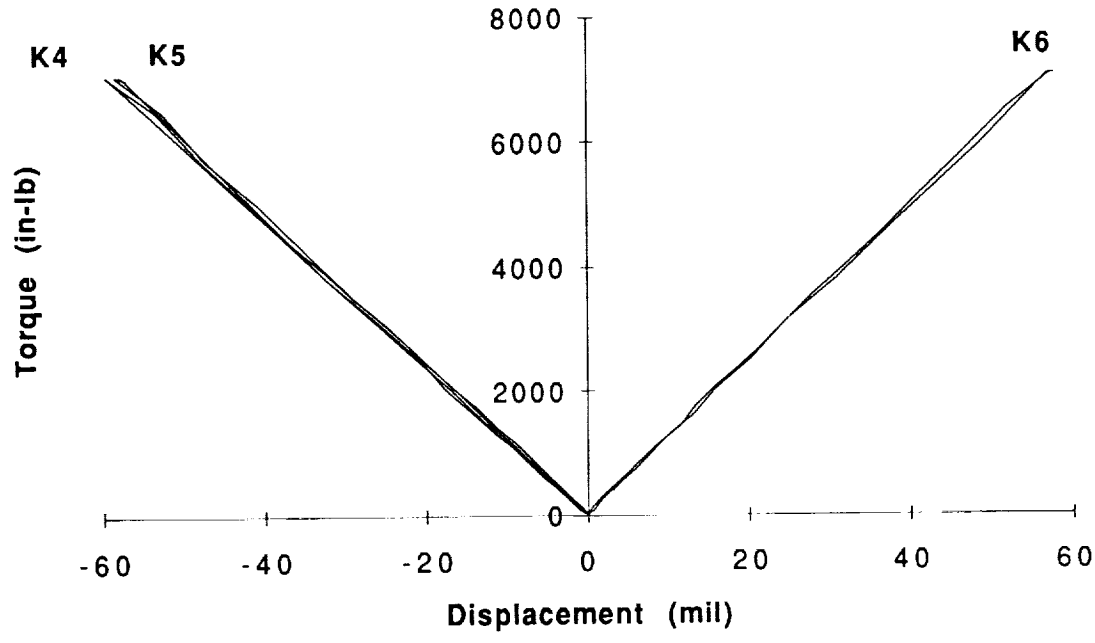

Figure 5-17 Section-4 CCW Torsion Test Results

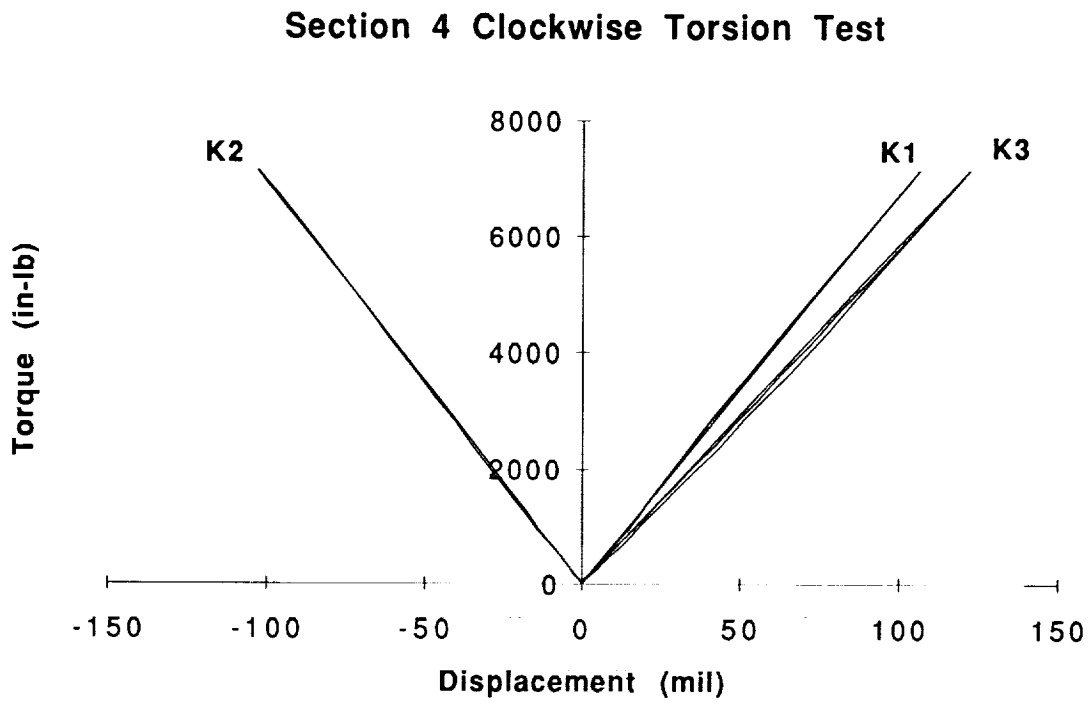

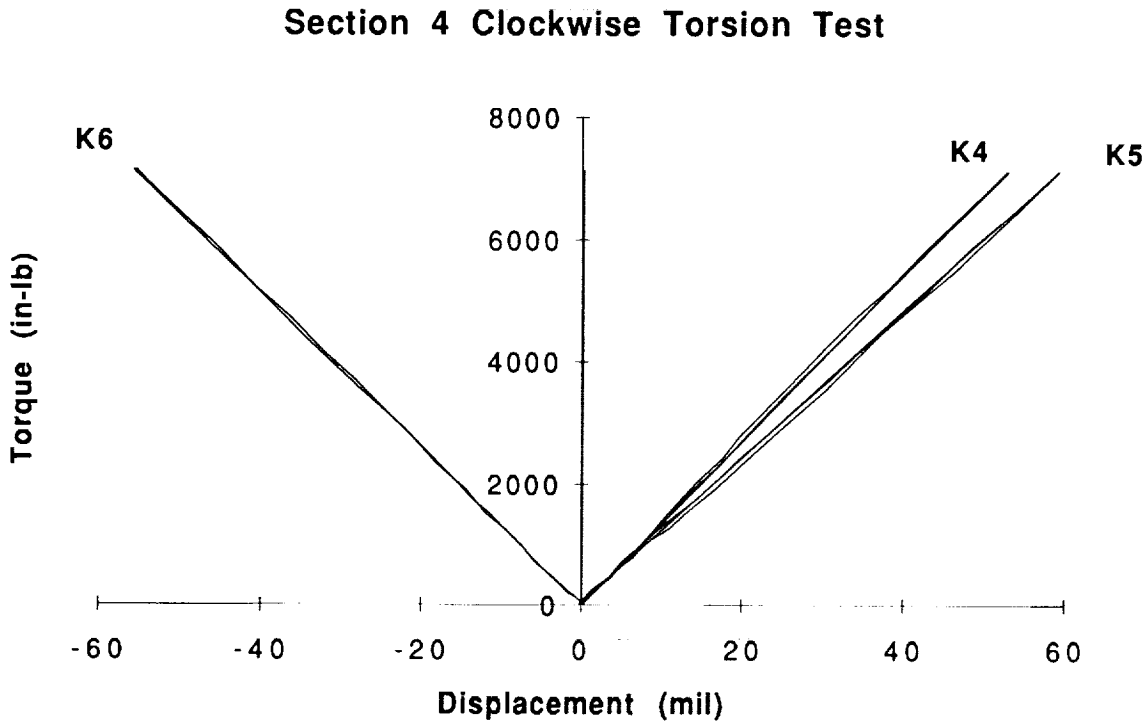

Figure 5-18 Section-4 CW Torsion Test Results

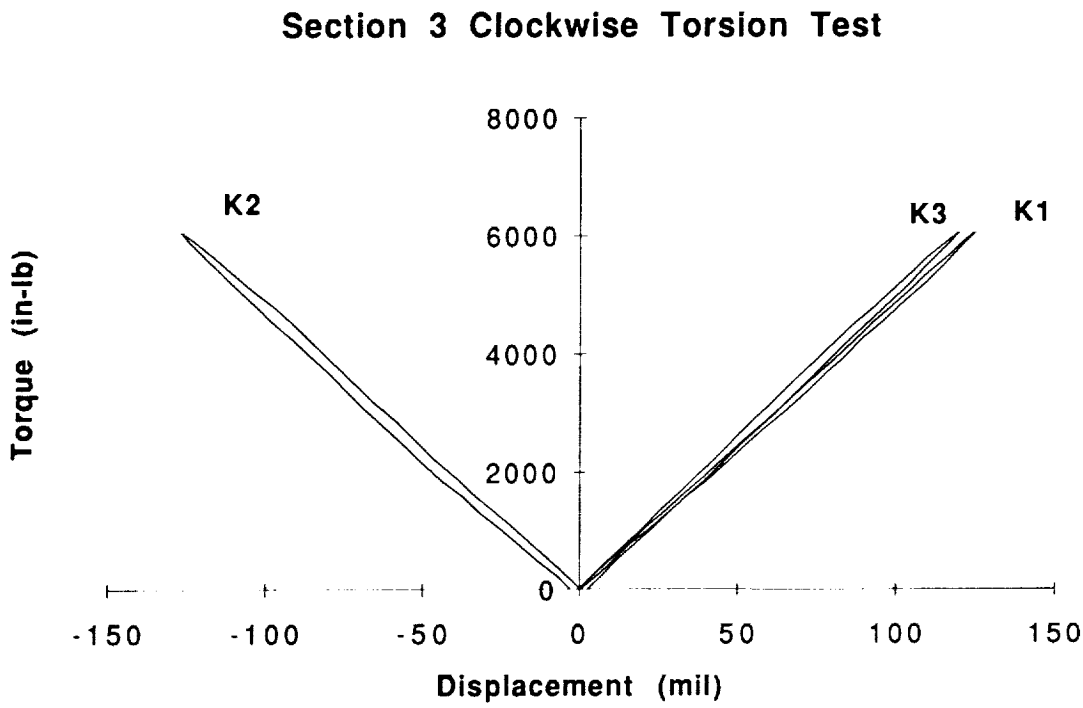

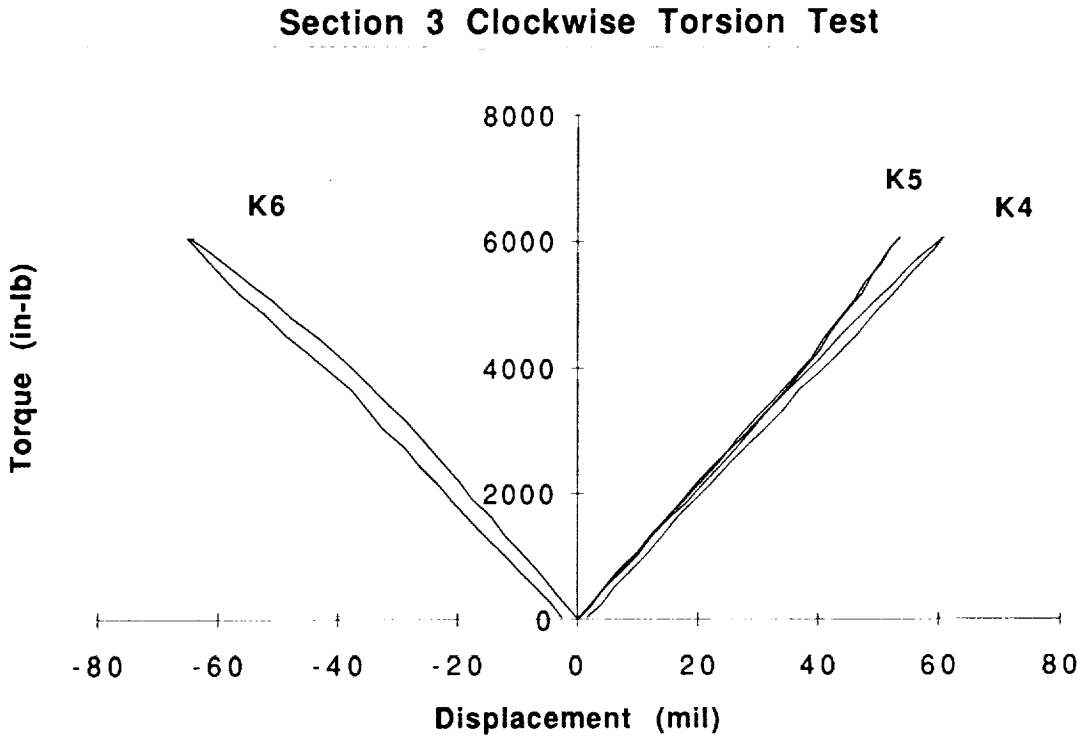

Figure 5-19 Section-3 CW Torsion Test Results

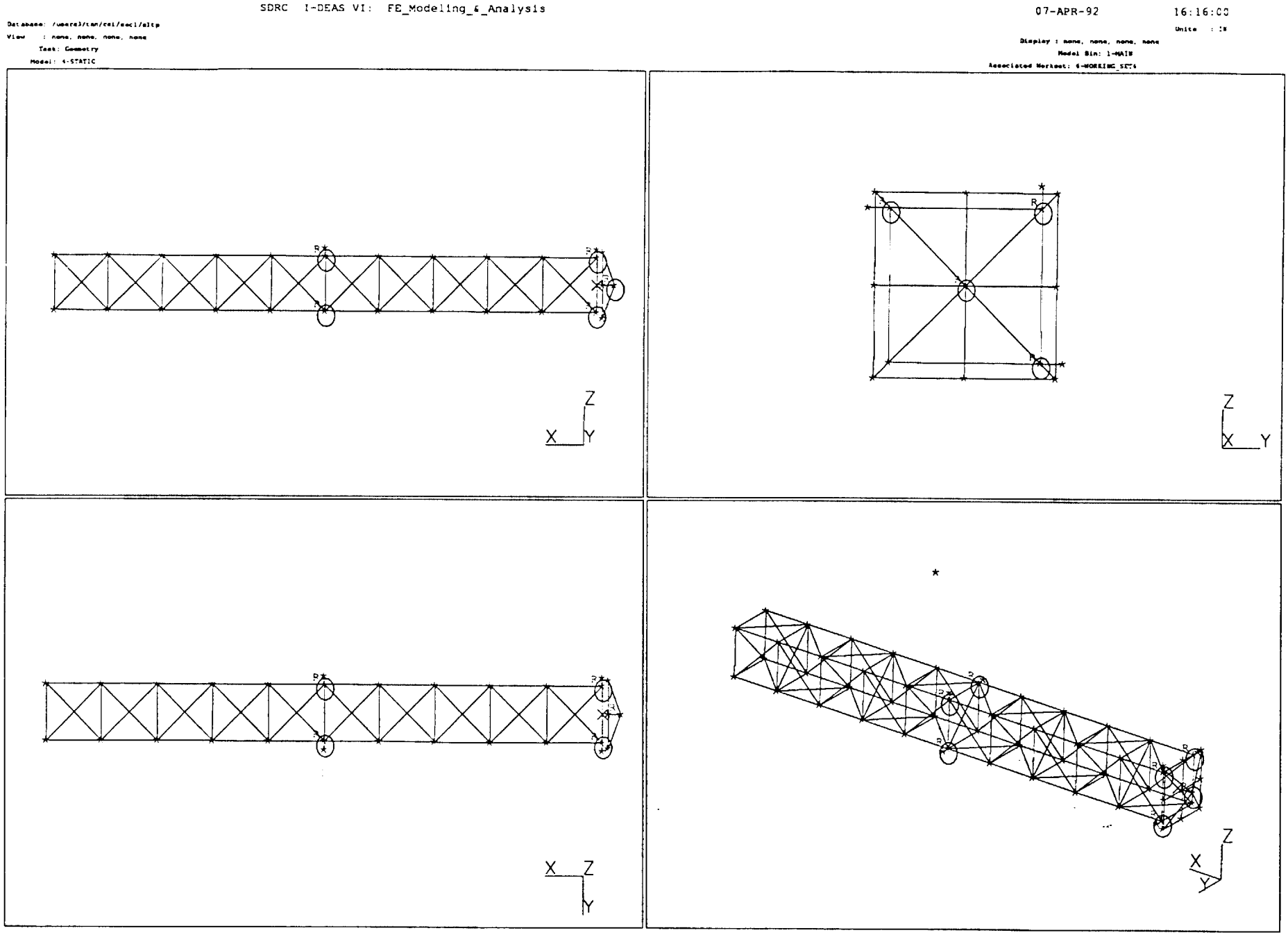

Figure 5-20 Ten Bay Truss Section Finite Element Model

displacements correspond to flexibility influence coefficients at the Kaman sensor locations.

As part of a "spot check" of the test data, Table 5-3 compares the flexibility influence coefficients predicted by the finite element model with those obtained from the test data for each Kaman sensor. The test data coefficients are obtained in an *approximate* sense by dividing the peak force into the peak deflection for each channel. Bending test data is not presented for K2, K3, K5, and K6 because no significant response was measured and the analytical model predicts zero response at these locations.

Overall, the bending test results show good agreement with the analytical predictions. The average displacement error is 5.7%, which would correspond to an average frequency error of 2.8% if one assumes all the error is in the stiffness matrix and not the mass matrix (frequency is proportional to the square root of stiffness). Therefore, the bending test errors are consistent with those presented in the previous section for the dynamic section tests (Section 4.0). Thus, the static section bending test results corroborate both the strut test results in Section 3.0 and the dynamic section test results in Section 4.0.

Overall, the counter-clockwise torsion test results also show good agreement with the analytical predictions, with an average displacement error of 7.61%. The average displacement error for the clockwise torsion tests is a larger 12.6%. The increase is primarily due to the bending behavior observed in the data for truss Sections -1, -2, and -4. It is strongly suspected that the torsional load application apparatus introduced some bending loads into these tests. The corresponding average frequency errors for the counter-clockwise and clockwise tests are 3.7% and 6.1%, respectively.

Since a model correlation effort was outside the scope of this effort, no further analyses were performed. Further, more rigorous model correlation efforts may be warranted, particularly with respect to an investigation of the clockwise torsion test anomaly. On the other hand, given the close agreement between the analytical predictions and the dynamic test results presented in Sections 4.0 and 6.0, further static test model correlation may be superfluous, and it may be more appropriate to concentrate on dynamic test model correlation activities.

Table 5-3 Spot Check of Section Static Test Results

Section 1

Kaman Sensor	Bending Updated FEM	Bending Test	Error (%)	Torsion Updated FEM	Torsion CW		Torsion CCW	
					Test	Error (%)	Test	Error (%)
K1	1.21E-03	1.24E-03	2.42%	1.74E-05	1.31E-05	-32.82%	1.58E-05	-10.13%
K2	-	-	-	1.74E-05	1.44E-05	-20.83%	1.59E-05	-9.43%
K3	-	-	-	1.74E-05	1.65E-05	-5.45%	1.62E-05	-7.41%
K4	4.07E-04	4.52E-04	9.96%	8.71E-06	6.89E-06	-26.44%	7.77E-06	-12.12%
K5	-	-	-	8.71E-06	8.16E-06	-6.76%	7.94E-06	-9.72%
K6	-	-	-	8.71E-06	7.34E-06	-18.69%	7.55E-06	-15.39%

Section 2

Kaman Sensor	Bending Updated FEM	Bending Test	Error (%)	Torsion Updated FEM	Torsion CW		Torsion CCW	
					Test	Error (%)	Test	Error (%)
K1	3.70E-03	3.81E-03	2.96%	1.68E-05	1.35E-05	-24.08%	1.60E-05	-5.00%
K2	-	-	-	1.68E-05	1.40E-05	-19.66%	1.58E-05	-6.06%
K3	-	-	-	1.68E-05	1.70E-05	1.00%	1.74E-05	3.45%
K4	1.18E-03	1.24E-03	4.45%	8.38E-06	7.38E-06	-13.55%	8.42E-06	0.48%
K5	-	-	-	8.38E-06	8.40E-06	0.19%	8.68E-06	3.46%
K6	-	-	-	8.38E-06	7.57E-06	-10.66%	8.00E-06	-4.75%

Section 3

Kaman Sensor	Bending Updated FEM	Bending Test	Error (%)	Torsion Updated FEM	Torsion CW		Torsion CCW	
					Test	Error (%)	Test	Error (%)
K1	2.17E-03	2.34E-03	7.37%	1.94E-05	2.06E-05	5.72%	1.99E-05	2.53%
K2	-	-	-	1.94E-05	2.05E-05	5.26%	2.10E-05	7.67%
K3	-	-	-	1.94E-05	2.04E-05	5.03%	2.07E-05	6.27%
K4	7.05E-04	7.98E-04	11.61%	9.68E-06	9.84E-06	1.64%	1.01E-05	4.24%
K5	-	-	-	9.68E-06	9.74E-06	0.63%	8.94E-06	-8.32%
K6	-	-	-	9.68E-06	9.16E-06	-5.66%	1.16E-05	16.52%

Section 4

Kaman Sensor	Bending Updated FEM	Bending Test	Error (%)	Torsion Updated FEM	Torsion CW		Torsion CCW	
					Test	Error (%)	Test	Error (%)
K1	1.51E-03	1.52E-03	0.79%	1.81E-05	1.49E-05	-21.49%	1.71E-05	-6.05%
K2	-	-	-	1.81E-05	1.45E-05	-25.00%	1.61E-05	-12.66%
K3	-	-	-	1.81E-05	1.71E-05	-5.91%	1.74E-05	-4.33%
K4	4.99E-04	5.32E-04	6.33%	9.07E-06	7.50E-06	-20.91%	8.35E-06	-8.55%
K5	-	-	-	9.07E-06	8.31E-06	-9.10%	8.43E-06	-7.64%
K6	-	-	-	9.07E-06	7.85E-06	-15.52%	8.21E-06	-10.42%

Note: Units are |in/lb| and |in/in-lb|

5.4 TRUSS SECTION STATIC TEST SUMMARY

In summary, the supplemental data provided by the static section bending tests and the counter-clockwise torsion tests corroborates the strut static test results and the dynamic section test results presented in Sections 3.0 and 4.0. The larger errors associated with the clockwise torsion tests for truss sections -1, -2, and -4 are attributed to the test setup itself and not the behavior of the truss.

6.0 ASSEMBLY DYNAMIC TESTS

6.1. INTRODUCTION

To verify the CEM testbed and to allow the dynamic model of this hardware to be confirmed and correlated, a modal test of the structure was performed by SDRC in the Space Structures Research Laboratory at NASA/LaRC. This section of the report presents the findings of the pretest analysis efforts, the description of the test article and approach used in the testing, and the results of the modal tests performed on the CEM structural assembly.

The pretest analysis efforts described in this section were used to develop the required set of measurement locations for the modal test. This resulted in two groupings of instrumentation which could be used independently or together in comparing the model predictions and the test results. The preliminary analysis was used to confirm that the reduced number of measurement locations could be used to adequately represent the dynamics of the entire structure so that correlation could be performed.

Following the pretest analysis, the modal test was performed. The modal test involved applying an excitation force to the test article while measuring responses at the locations indicated by the pretest efforts. This information was used to quantify the dynamic characteristics of the CEM test article. Several tests were performed using multiple excitation sources. Different excitation source types were investigated as well as different shaker combinations to determine if the structure was sensitive to variation in these parameters.

Pretest analysis predictions were used at the test site to make immediate comparisons as soon as the test results were available. This allowed for quick verification of the test data and an assessment of the model fidelity before testing was completed.

The following sections of the report present the details of the different phases of the pretest analysis and testing that were performed.

6.2. PRETEST ANALYSIS

This section discusses the development of the CEM test-analysis models (TAMs) using an updated pretest finite element model. Because the number of low frequency servo accelerometers was limited, two TAMs were developed. The first contained all the degrees of freedom required to accurately represent the CEM structure's first 27 modes. This TAM is described in Section 6.2.2. The second TAM, described in Section 6.2.3, was developed to determine locations at which the low frequency accelerometers should be placed.

6.2.1. CEM Finite Element Model

Both test-analysis models were derived from the CEM finite element model, using NASTRAN version 65, for all modal analyses. An overall view of the CEM finite element model is shown in Figure 6-1. The main truss is completely composed of uniform cross-section beam elements, with a concentrated mass element at each corner node. The cable suspension system is comprised of rod elements, with vertical springs at the top to represent the air springs between the suspension cables and "ground."

Table 6-1 shows the physical properties used in the CEM pretest analysis. The truss properties shown in the table correspond with those presented in Lockheed's Progress Review III, February 26, 1992. Data for the cable suspension system was supplied by NASA/LaRC.

Because the main purpose of this pretest analysis was to provide an accurate test-analysis model, the results presented in this section were calculated from a finite element model which included the mass of the modal survey accelerometers. The maximum target mode frequency discrepancy between FEM with and without the accelerometer mass was approximately 4.8%.

The modes for the CEM finite element and test-analysis models were calculated in two steps. First, a differential stiffness analysis was performed to determine structural preloading due to gravity. Using these results, the structural modes were then calculated. The first three columns of Table 6-2 describe the CEM finite element mode frequencies and shapes for the 27 modes below 35 Hz. Included in these modes are first truss torsion; first, second, and third main truss bending; and first bending for both towers. These FEM modes were used to develop the TAMs, as described in the following sections.

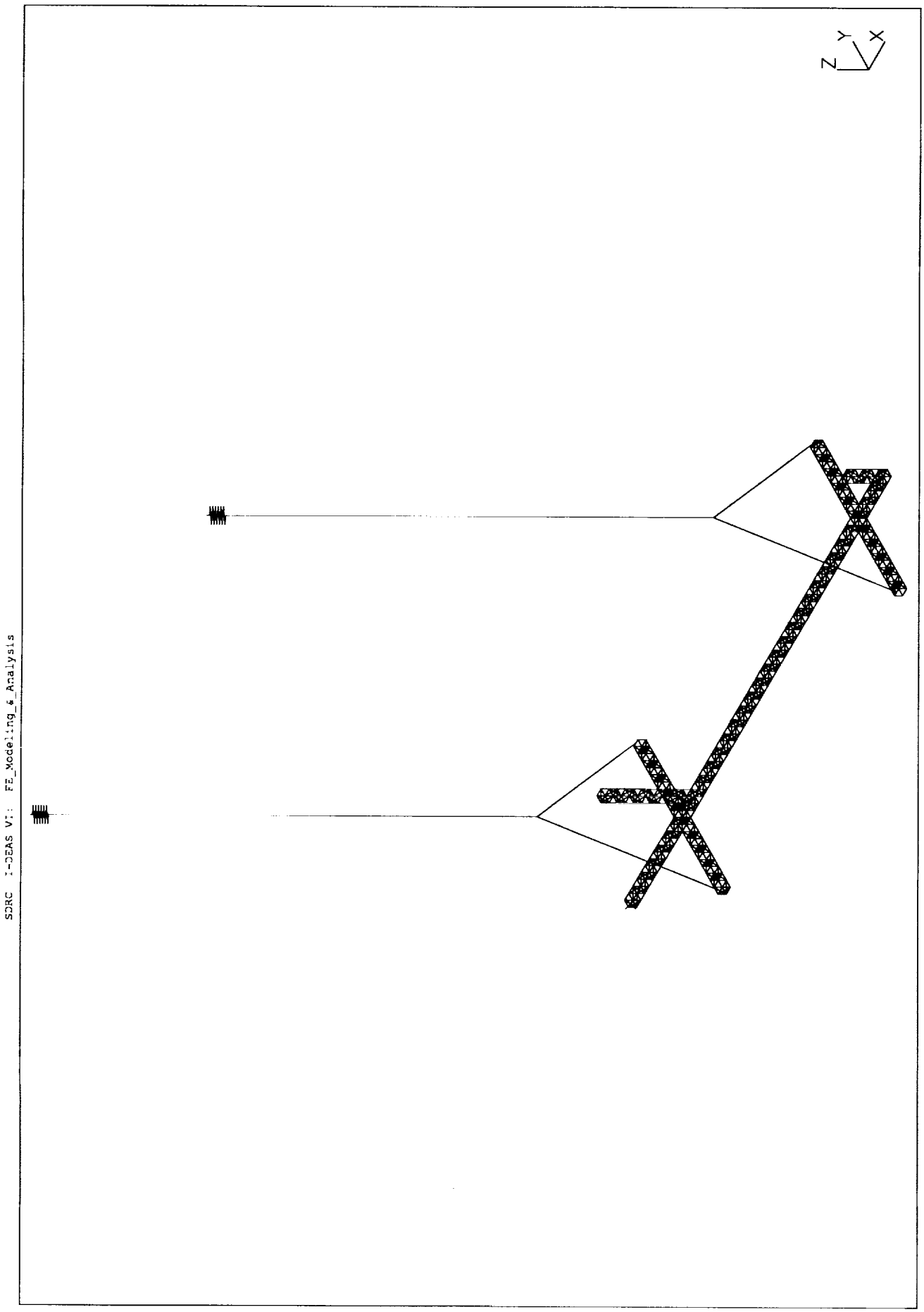

Figure 6-1. CEM Finite Element Model.

Table 6-1. Updated CEM Physical Properties Used In Pretest Analyses.

FEM Property ID	Property Description	C-S Area (in^2)	Area Moment of Inertia (in^4)	Torsional Constant (in^4)	Spring Constant (lb/in)
101	S1 Longeron	0.333	0.027789	0.055579	-
102	Batten	0.097	0.002314	0.004628	-
103	Diagonal	0.083	0.002442	0.004883	-
201	S2 Longeron	0.099	0.002736	0.005471	-
202	Batten	0.097	0.002314	0.004628	-
203	Diagonal	0.083	0.002442	0.004883	-
301	S3 Longeron	0.175	0.00629	0.01258	-
302	Batten	0.097	0.002314	0.004628	-
303	Diagonal	0.083	0.002442	0.004883	-
401	S4 Longeron	0.264	0.015703	0.031406	-
402	Batten	0.097	0.002314	0.004628	-
403	Diagonal	0.083	0.002442	0.004883	-
14	Cable Suspension Rods	0.0022	-	0.000052	-
2201	Suspension Spring	-	-	-	25.0
2202	Suspension Spring	-	-	-	25.0

Table 6-2. CEM Pretest Finite Element Model Versus 103 DOF Static TAM.

FEM Mode No.	Description	FEM Freq (Hz)	103 DOF TAM Mode No.	103 DOF TAM Freq (Hz)	103 DOF TAM Error (%)	103 DOF TAM Cross-Ortho
1	Cable Pendulum	0.112	1	0.112	0.0%	100
2	Cable Pendulum	0.112	2	0.112	0.0%	100
3	Cable Twist Pendulum	0.129	3	0.129	0.0%	100
4	Cable Axial	0.825	4	0.825	0.0%	100
5	Cable Junction Bending	0.959	5	0.959	0.0%	100
6	Cable Axial	0.963	6	0.963	0.0%	100
7	First Torsion	1.807	7	1.808	0.1%	100
8	First Main Truss Bending (y-dir)	3.125	8	3.126	0.0%	100
9	Cable Junction	3.460	9	3.460	0.0%	100
10	First Main Truss Bending (z-dir)	3.683	10	3.684	0.0%	100
11	Cable Junction	3.940	11	3.940	0.0%	100
12	In-phase Truss Appendage Torsion	6.122	12	6.132	0.2%	100
13	Laser Tower Bending	7.827	13	7.837	0.1%	100
14	Second Main Truss Bending (z-dir)	9.451	14	9.464	0.1%	100
15	Out-of-phase Truss Appendage Torsion	9.769	15	9.800	0.3%	100
16	Coupled Laser Tower/Truss End Bending	11.853	16	11.878	0.2%	100
17	Out-of-phase Truss Appendage Bending	12.141	17	12.208	0.6%	100
18	Coupled Tower/Appendage Bending	13.418	18	13.469	0.4%	100
19	Coupled Tower/Appendage Bending	13.572	19	13.622	0.4%	100
20	In-phase Truss Appendage Bending	14.113	20	14.173	0.4%	100
21	Coupled Tower/Appendage Bending	14.715	21	14.767	0.4%	100
22	Reflector Tower Bending	16.556	22	16.611	0.3%	100
23	Third Main Truss Bending (z-dir)	20.114	23	20.256	0.7%	100
24	Third Main Truss Bending (y-dir)	23.259	24	23.493	1.0%	100
25	Main Truss Cross-Section Warping	30.724	25	31.338	2.0%	100
26	Main Truss Cross-Section Warping	31.011	26	31.752	2.4%	100
27	Reflector Tower/Main Truss Bending	34.298	27	34.967	2.0%	100

6.2.2. 103-DOF Static Test-Analysis Model

To provide test accelerometer locations and a mass matrix for orthogonality and cross-orthogonality between test and analysis modes, a test-analysis model (TAM) was developed for the CEM structure. The CEM TAM is a model whose degrees of freedom correspond one for one with accelerometers to be used in the modal survey. A TAM is generated by reducing the mass and stiffness matrices of the full FEM to the DOF of the TAM. For the CEM analysis, the TAMs were generated using static (Guyan) reduction.

The goal of the CEM TAM was to accurately predict the 27 FEM mode shapes and frequencies below 35 Hz. Grid point modal kinetic energies and engineering judgment were used to choose an initial accelerometer set which was then modified to a final set. The final TAM included 103 DOF measured at 41 grid locations. A comparison of TAM and FEM dynamic results is shown in Table 6-2. As seen in this table, the 103-DOF TAM is very accurate, with a maximum frequency discrepancy of 2.4% and all cross-orthogonality terms of 100.

The 103-DOF TAM accelerometer locations are shown in Figure 6-2, while the corresponding NASTRAN ASET cards are shown in Table 6-3. The main truss bending modes were captured with a bi-axial accelerometer set at approximately every fifth truss bay. At approximately every tenth truss bay, an extra bi-axial accelerometer set was included to capture the truss torsional motion. Extra accelerometers were included on the CEM Section 1 truss appendage to characterize its bending and torsion.

The suspension truss appendages were involved in many of the overall structural modes, as well as their own bending modes. A pair of tri-axial accelerometers was used at each end of the four suspension truss appendages. These were sufficient to capture the first bending and any torsion in the suspension truss structure.

Laser tower motion was characterized with two tri-axial accelerometers on the tower's top bay and two additional bi-axial accelerometers at a midpoint station. The shorter reflector tower motion was captured with two tri-axial accelerometers on the tower's top truss bay. Both towers' first bending modes were among those targeted for measurement.

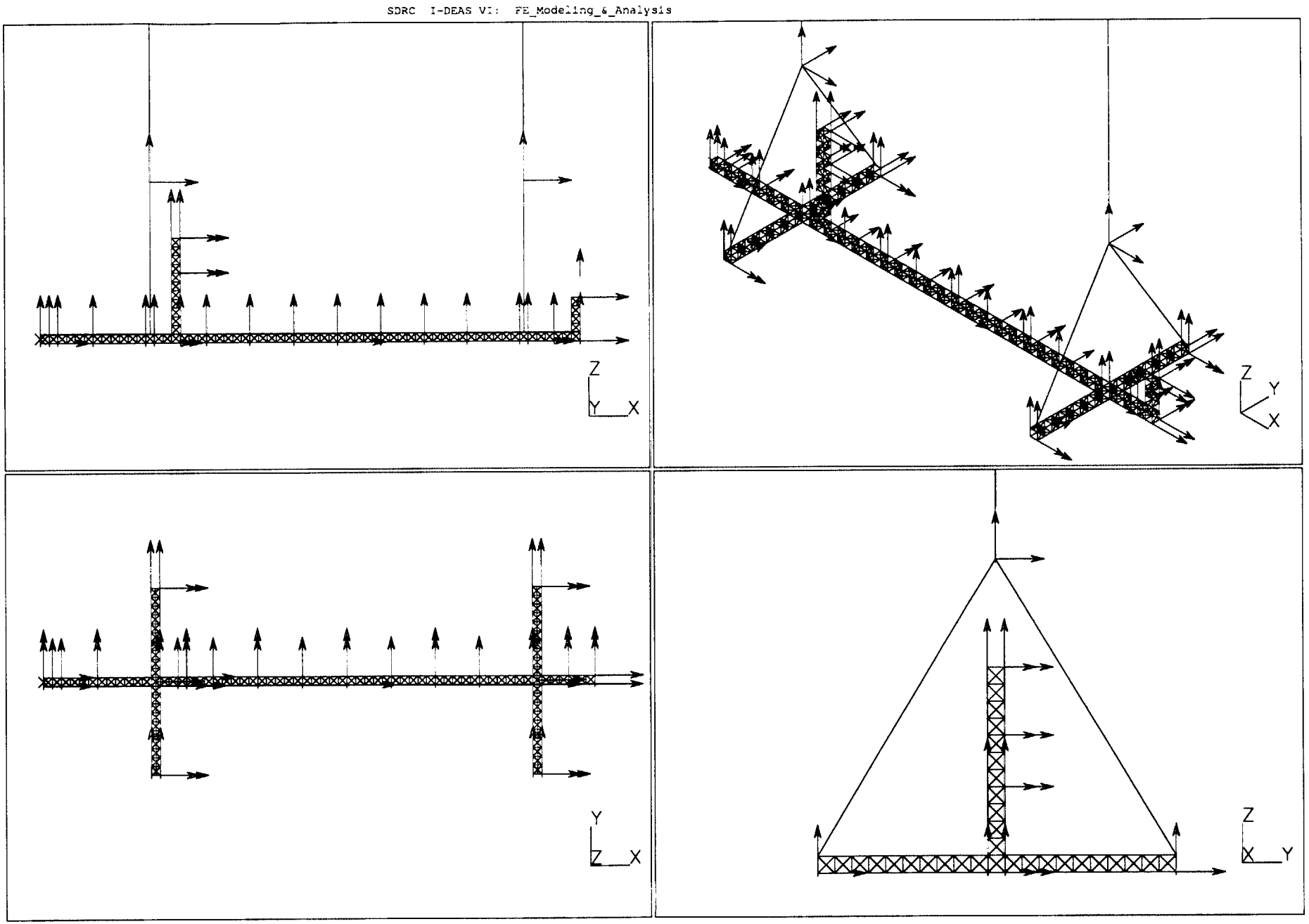

Figure 6-2. CEM Test Accelerometer Locations - 103 DOF TAM.

Table 6-3. 103 DOF TAM NASTRAN ASET Cards.

```
$ ------------------------------------------------
$   ASET1 CARDS FOR CSI TRUSS STRUCTURE (103 DOF TAM)
$ ------------------------------------------------
$
$  CABLE SUPPORT JUNCTION NODES
$  ----------------------------
ASET1    123      396      480
$
$  MAIN TRUSS STRUCTURE
$  --------------------
ASET1    123      3        4        251      252
ASET1    123      55       139      223
$
ASET1    23       7        11
$
ASET1    23       67       79       99       119      159      179      199
ASET1    23       56       100      140      180      224
ASET1    23       27       28       239      240
$
$  LASER TOWER
$  -----------
ASET1    123      310      312
ASET1    12       294      296
$
$  REFLECTOR TOWER
$  ---------------
ASET1    123      267      268
$
$  SUSPENSION TRUSS
$  ----------------
ASET1    123      387      388      391      392
ASET1    123      471      472      475      476
```

6.2.3. 41-DOF Static Test-Analysis Model

The 41-DOF TAM was developed in an attempt to predict the CEM mode shapes and frequencies using only about 40 accelerometers. The available modal survey equipment included approximately 40 high-precision, low frequency, servo accelerometers. To find optimal locations for the high-precision accelerometers, an analysis was performed to identify a subset of the 103-DOF TAM which would accurately predict most of the target modes.

The reduced 41-DOF TAM was developed using the same procedure described in Section 6.2.2. The final reduced TAM included 41 DOF at 19 grid locations. Table 6-4 shows a comparison between the CEM 41 DOF reduced TAM and the FEM. In the 41 DOF TAM, the maximum mode frequency discrepancy increases to 8.6%, while the minimum cross-orthogonality term is 94. The reduced TAM did not include any DOF on the cable suspension system, thus suspension cable modes are "invisible" to the reduced TAM. There were two reasons for not placing servo accelerometers on the suspension cables: (1) the cable modes were not as important as the test article flexible modes, and (2) the servo accelerometers are very massive relative to the cables. Thus, FEM modes 9 and 11 were not captured by this reduced TAM since they are suspension cable modes. Figure 6-3 shows the 41 reduced TAM measurement locations, while Table 6-5 shows the NASTRAN ASET card deck for the 41-DOF TAM.

6.3. TEST DESCRIPTION

This section of the report relates the performance of the modal testing on the CEM Phase 1 structure. The test article is described along with the instrumentation which was used to make the measurements. Also, the test approach is described including the methods used to evaluate the test data.

6.3.1. Test Article Description

The modal test was performed in the room 123 high bay at NASA/LaRC in Building 1293. The test article was the CEM Phase 1 testbed, which was suspended from the ceiling of the high bay with a low frequency suspension system consisting of low stiffness springs and steel cable support wires. These wire cables were of sufficient length to result in low frequency rigid body pendulum modes below 0.5 Hz. The suspension system was also designed to ensure that all rigid body modes were below 1.0 Hz. Figure 6–4 shows the configuration of the test article.

Table 6-4. CEM Pretest Finite Element Model Versus 41 DOF Static TAM.

FEM Mode No.	Description	FEM Freq (Hz)	41 DOF TAM Mode No.	41 DOF TAM Freq (Hz)	41 DOF TAM Error (%)	41 DOF TAM Cross-Ortho
1	Cable Pendulum	0.112	1	0.112	0.0%	100
2	Cable Pendulum	0.112	2	0.112	0.0%	100
3	Cable Twist Pendulum	0.129	3	0.129	0.0%	100
4	Cable Axial	0.825	4	0.825	0.0%	100
5	Cable Junction Bending	0.959	5	0.959	0.0%	100
6	Cable Axial	0.963	6	0.963	0.0%	100
7	First Torsion	1.807	7	1.809	0.1%	100
8	First Main Truss Bending (y-dir)	3.125	8	3.129	0.1%	100
9	Cable Junction	3.460	-			
10	First Main Truss Bending (z-dir)	3.683	9	3.686	0.1%	100
11	Cable Junction	3.940	-			
12	In-phase Truss Appendage Torsion	6.122	10	6.154	0.5%	100
13	Laser Tower Bending	7.827	11	7.894	0.9%	100
14	Second Main Truss Bending (z-dir)	9.451	12	9.503	0.6%	100
15	Out-of-phase Truss Appendage Torsion	9.769	13	9.895	1.3%	100
16	Coupled Laser Tower/Truss End Bending	11.853	14	11.941	0.7%	99
17	Out-of-phase Truss Appendage Bending	12.141	15	12.253	0.9%	99
18	Coupled Tower/Appendage Bending	13.418	16	13.644	1.7%	97
19	Coupled Tower/Appendage Bending	13.572	17	13.759	1.4%	98
20	In-phase Truss Appendage Bending	14.113	18	14.325	1.5%	97
21	Coupled Tower/Appendage Bending	14.715	19	14.945	1.6%	99
22	Reflector Tower Bending	16.556	20	16.770	1.3%	100
23	Third Main Truss Bending (z-dir)	20.114	21	20.725	3.0%	100
24	Third Main Truss Bending (y-dir)	23.259	22	23.868	2.6%	100
25	Main Truss Cross-Section Warping	30.724	23	32.162	4.7%	99
26	Main Truss Cross-Section Warping	31.011	24	33.678	8.6%	94
27	Reflector Tower/Main Truss Bending	34.298	25	36.550	6.6%	94

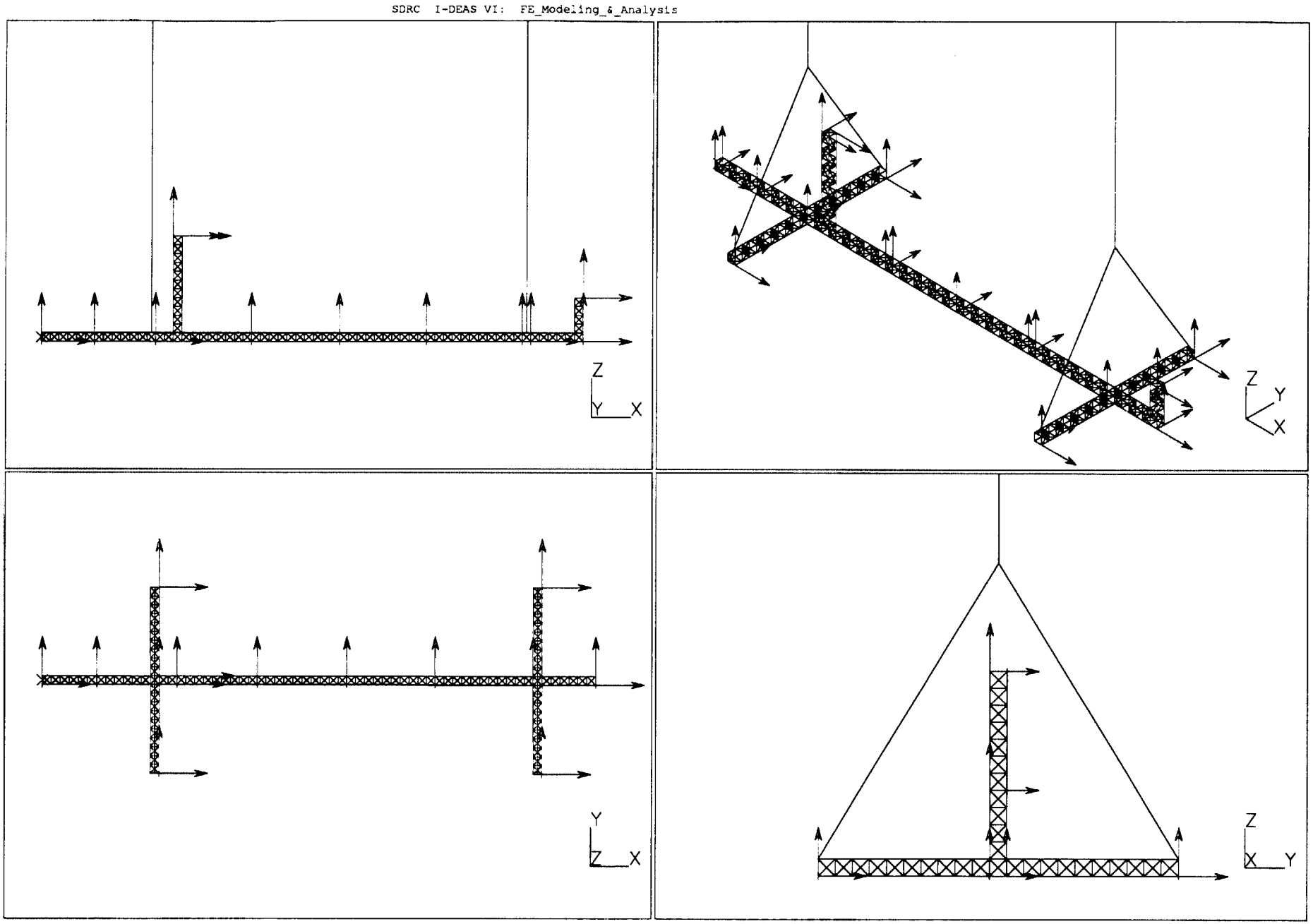

Figure 6-3. CEM Test Accelerometer Locations - 41 DOF TAM.

Table 6-5. 41 DOF TAM NASTRAN ASET Cards.

```
$ ------------------------------------------------
$   ASET1 CARDS FOR CSI TRUSS STRUCTURE (41 DOF TAM)
$ ------------------------------------------------
$
$  MAIN TRUSS STRUCTURE
$  --------------------
ASET1   123     3       251
ASET1   23      55      139     223
ASET1   3       4       252     100     180
ASET1   23      99      179     27
$
$  LASER TOWER
$  -----------
ASET1   123     310
ASET1   1       312
$
$  REFLECTOR TOWER
$  ---------------
ASET1   123     267
$
$  SUSPENSION TRUSS
$  ----------------
ASET1   123     387     391
ASET1   123     471     475
```

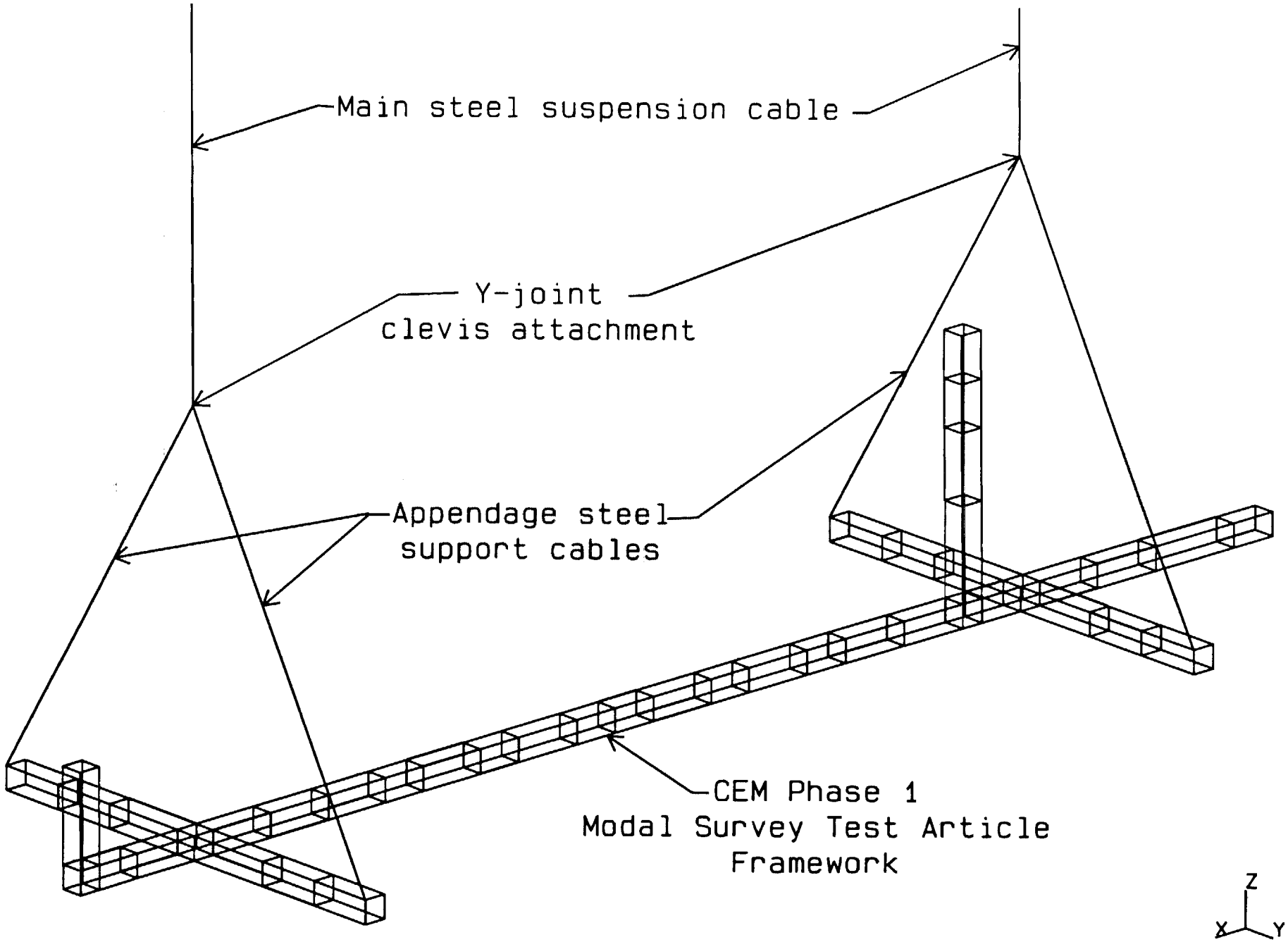

Figure 6-4. CEM Phase 1 Testbed Modal Survey Configuration.

6.3.2. Instrumentation

Two types of accelerometers were used to make the measurements on the test article. The pretest analysis defined specific measurement locations or degrees of freedom (DOF) where the accelerometers were to be installed. These locations were grouped in two sets to account for the different types of accelerometers used in the test. The first group of DOF were to be measured with servo accelerometers so that the low frequency modes (including the rigid body modes) could be accurately measured. These accelerometers were placed at 41 DOF so that the primary motion of the test article could be described. The selection of these locations was verified through the pretest analysis. The accelerometers used were Sundstrand Q-Flex servo accelerometers. These transducers, with mounting hardware, weigh about 80 grams, and since this was considered a substantial mass relative to the test article, the pretest analysis efforts included the mass of the accelerometers. The locations at which the 41 servo accelerometers were installed are shown in Figure 6–5. A listing of the measurement DOF is given in Table 6–6. In addition to the 41 DOF used in the TAM, servo accelerometers were installed at each of the driving points in the direction of the input, and two servos were installed at the suspension springs, one at each spring.

To provide further detail about the flexible modes of the CEM structure, another type of accelerometer was installed at an additional 62 DOF. These accelerometers were lightweight (3 gram) PCB Structcel transducers. These transducers are not capable of measuring very low frequency (less than 1 Hz) acceleration values like the servo accelerometers, but the light weight made them more appropriate for measuring the motion of lightweight components such as the suspension cables. These transducers were combined with the servo accelerometers to yield a total measurement set of 103 DOF. A pretest test-analysis model (TAM) was developed for the 41 DOF servo accelerometer measurements as well as for the combined set of 103 DOF. This allowed comparison of the two different pretest models in extracting the final test results. Figure 6–6 shows the DOF associated with the Structcel measurements. These are also listed in Table 6–6 with the servo accelerometer locations.

Excitation of the test article was performed using two different types of sources. The primary source was electrodynamic shakers. These were APS 10-inch stroke linear actuators. The shakers were attached to the test structure through a flexible stinger, or rod, which in turn connected to the CEM test article with a piezoelectric load cell. This load cell (PCB 208) was used to accurately measure the force applied during the test. Figure 6–7 shows the arrangement of the attachment of the shakers to the test article. The locations at which the shakers were attached are shown in Figure 6–8.

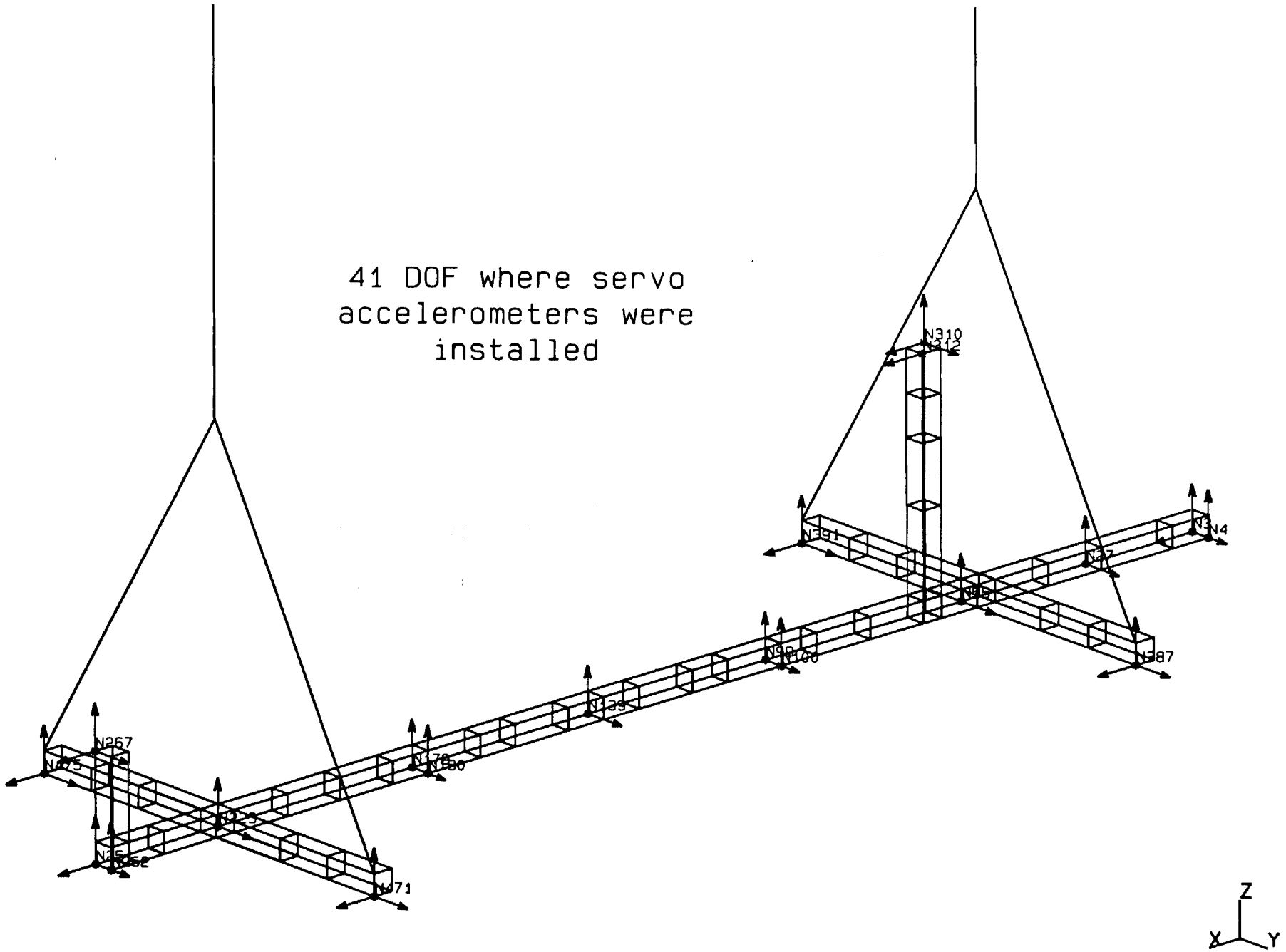

Figure 6-5. CEM Phase 1, 41 DOF TAM Instrumentation Locations.

Table 6-6. Accelerometer Installation Summary For CEM Modal Test.

Node Location FEM PT.	Direction	Accelerometer S/N	Accelerometer Type	Zonic TRUE Channel
268	x-	13633	Structcel	5
268	y+	13681	Structcel	6
268	z+	14743	Structcel	7
252	y+	13498	Structcel	8
252	x+	13507	Structcel	9
240	z+	13715	Structcel	10
240	y+	13890	Structcel	11
239	z+	14224	Structcel	12
239	y+	13503	Structcel	13
472	z+	13689	Structcel	14
472	x+	14746	Structcel	15
472	y+	14270	Structcel	16
480	z+	13574	Structcel	17
480	x+	13601	Structcel	18
480	y+	14152	Structcel	19
224	y+	13866	Structcel	20
224	z+	13602	Structcel	21
223	x-	13740	Structcel	22
476	x+	21844	Structcel	23
476	y+	13956	Structcel	24
476	z+	13481	Structcel	25
180	y+	21858	Structcel	26
199	y+	21641	Structcel	27
199	z+	13909	Structcel	28
159	y+	13537	Structcel	29
159	z+	21831	Structcel	30
140	y+	21762	Structcel	31
140	z+	14243	Structcel	32
139	x-	14151	Structcel	33
119	z+	13798	Structcel	34
119	y+	21857	Structcel	35
100	y+	13750	Structcel	36
79	y+	13566	Structcel	37
79	z+	13567	Structcel	38
396	x+	13869	Structcel	39
396	y+	13882	Structcel	40
396	z+	14234	Structcel	41
67	y+	13619	Structcel	42
67	z+	13652	Structcel	43
296	x+	21753	Structcel	44
294	y+	13564	Structcel	45
294	x+	13466	Structcel	46
312	z+	14049	Structcel	47
312	y+	13650	Structcel	48
296	y-	13591	Structcel	49
388	x+	13622	Structcel	50
388	y+	14233	Structcel	51
388	z+	13471	Structcel	52
56	y+	13634	Structcel	53
56	z+	13470	Structcel	54
55	x-	13700	Structcel	55
392	z+	14254	Structcel	56
392	y+	21816	Structcel	57
392	x+	13638	Structcel	58
4	y+	21812	Structcel	59
4	x+	21809	Structcel	60
7	z+	13852	Structcel	61
7	y+	13494	Structcel	62
11	y+	13878	Structcel	63
11	z+	14139	Structcel	64
28	z+	13769	Structcel	65
28	y+	21832	Structcel	66
3	Z+	1289	Servo	67
3	Y+	1321	Servo	68
3	X+	1318	Servo	69
4	Z+	559	Servo	70
27	Y+	1284	Servo	71
27	Z+	1272	Servo	72
387	y+	1215	Servo	73
387	z+	563	Servo	74
387	x+	1297	Servo	75
55	Z+	234	Servo	76
55	Y+	1296	Servo	77
391	X+	259	Servo	78
391	Y+	1324	Servo	79
391	Z+	1208	Servo	80
312	X+	1277	Servo	81
310	X+	1315	Servo	82
310	Y+	1317	Servo	83
310	Z-	1226	Servo	84
100	Z+	1271	Servo	85
99	Y+	257	Servo	86
99	Z+	240	Servo	87
139	Y+	1279	Servo	88
139	Z+	1281	Servo	89
180	Z+	569	Servo	90
179	Y+	1300	Servo	91
179	Z+	1330	Servo	92
223	Y+	241	Servo	93
223	Z+	249	Servo	94
471	X+	326	Servo	95
471	Y-	1334	Servo	96
471	Z+	572	Servo	97
475	X+	235	Servo	98
475	Y+	1635	Servo	99
475	Z+	245	Servo	100
251	X-	236	Servo	101
251	Y+	1531	Servo	102
251	Z-	1305	Servo	103
252	Z+	562	Servo	104
267	X-	566	Servo	105
267	Y+	333	Servo	106
267	Z+	567	Servo	107
1001	x+	252	Servo	108
1002	x+	233	Servo	109
1003	x+	242	Servo	110
1004	x+	238	Servo	111
1001	y+	1	shaker current	112
1002	y+	2	shaker current	113
1003	y+	3	shaker current	114
1004	y+	4	shaker current	115
481	Z-	1302	Servo	116
482	Z-	1331	Servo	117

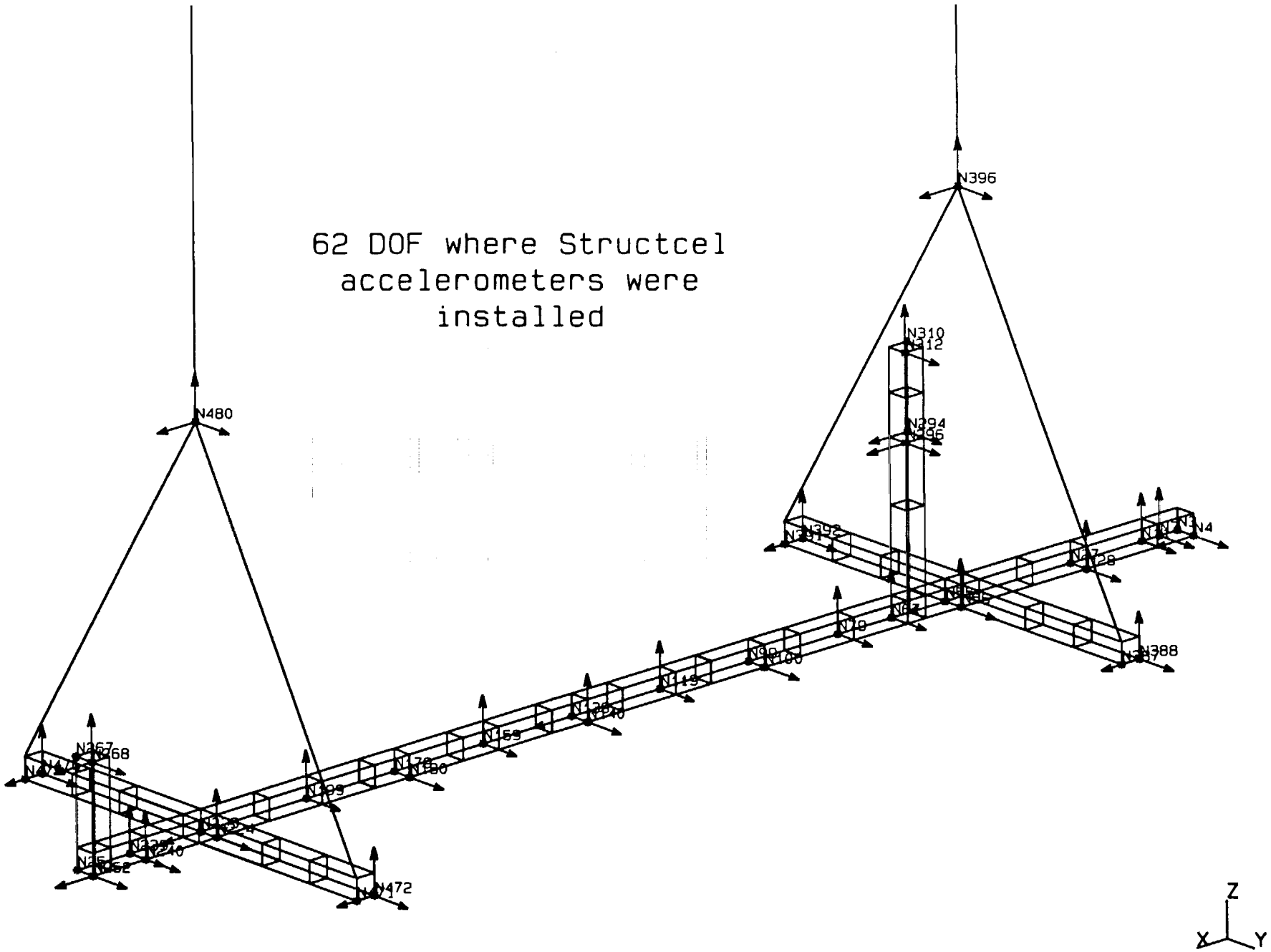

Figure 6-6. CEM Phase 1, Additional 62 DOF For Structcel Accelerometers. These Added To The 41 DOF Servo Locations Gave The Total 103 DOF.

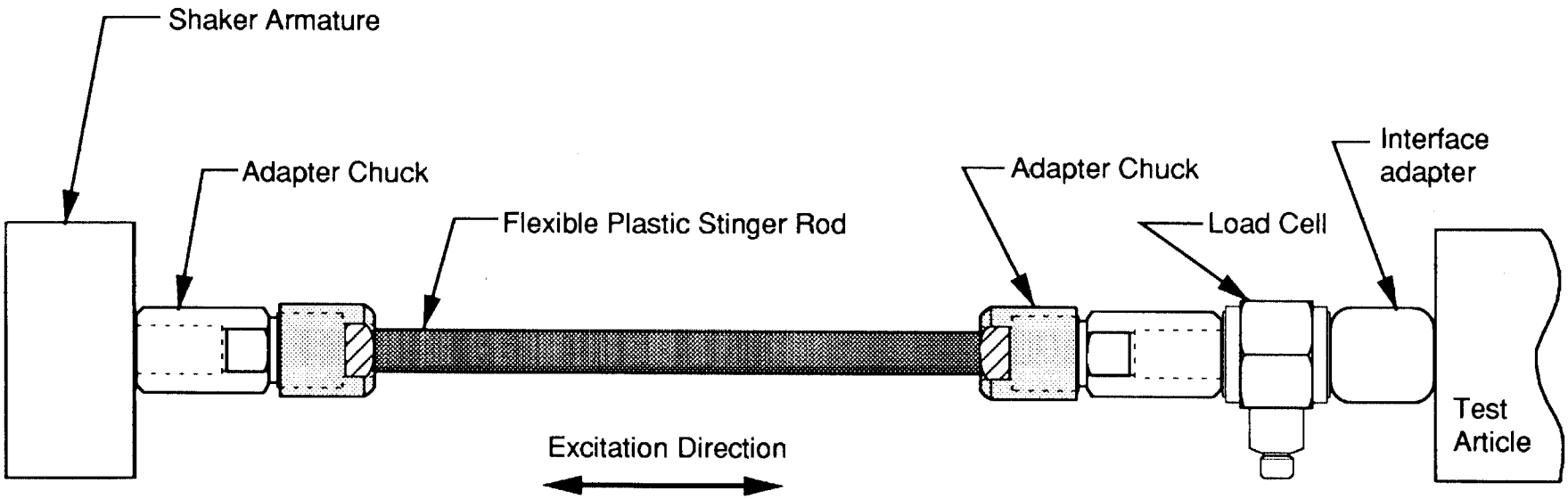

Figure 6-7. Attachment Between The Shakers And Test Article Was Made With A Stinger And Load Cell.

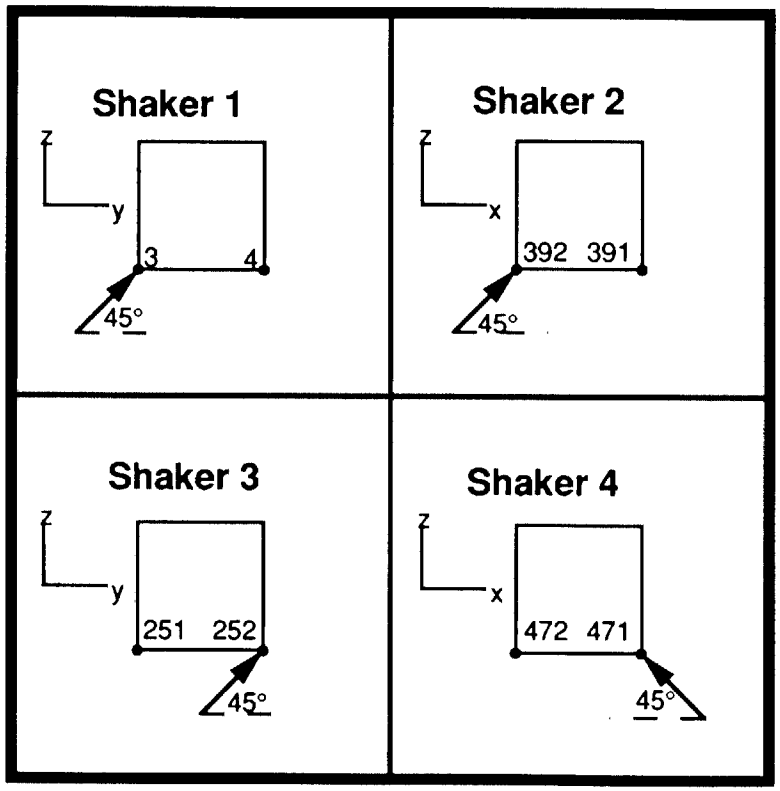

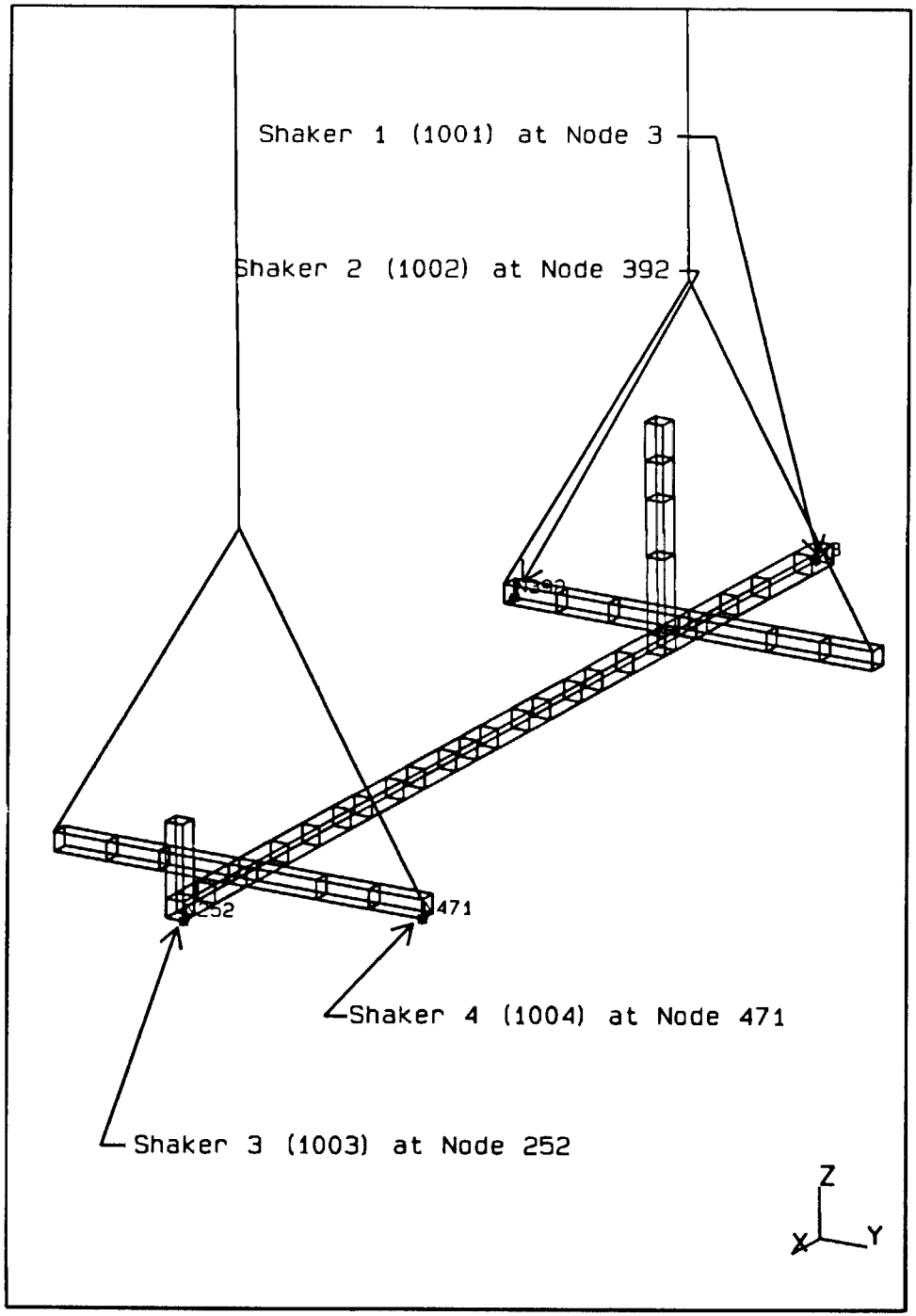

Figure 6-8. Shaker Attachment Locations Used In The CEM Modal Survey.

The second type of excitation source used during the test program was an instrumented impulse hammer with a foam-covered tip. This hammer also incorporated a piezoelectric load cell to measure the force applied to the structure. The hammer impulse was applied at two of the four locations used for the shaker excitation: locations 1001 and 1004. The tip of the hammer was covered with foam to lower the frequency content of the impulse to match the frequency range of interest in the test.

Signal conditioning for the instrumentation was provided as appropriate to the particular transducer type. The servo accelerometers were powered by six-channel amplifier banks developed by NASA/LaRC. The Structcel accelerometers were amplified by fifteen-channel PCB 433 differential power supplies. The load cells were powered by PCB 480D06 battery pack power supplies.

All measurement signals were routed to the data collection system, a Zonic System 7000 configured with a DEC VaxStation 3100 workstation. The Zonic was used to digitize all of the analog signals simultaneously for processing and provided the signal sources for the electrodynamic shakers.

Figure 6–9 shows the configuration of the data collection system used for the CEM Phase 1 modal test.

6.3.3. Test Performance

Multiple test runs were performed for the CEM Phase 1 modal survey. Each time a set of data was collected on the structure, it was assigned a run number. This was true even during preliminary testing where excitation force levels were being checked and instrumentation quality was being evaluated. A total of 22 test runs were performed between March 12, 1992, and March 19, 1992. In some cases, such as when there were obvious instrumentation problems, no data files were saved for particular runs. Once all of the instrumentation problems were solved, the test run data sets were stored.

Table 6–7 lists the test runs performed on the CEM Phase 1 test article. As can be seen, most testing was performed with a four-shaker excitation setup. Additional testing was performed with two shakers to determine the effects of the shaker attachments. In addition, single location, impact excitation was performed using a calibrated, instrumented hammer to apply the excitation force. Two separate locations (the same as were used for the two shaker excitation) were used as the points for this type of input.

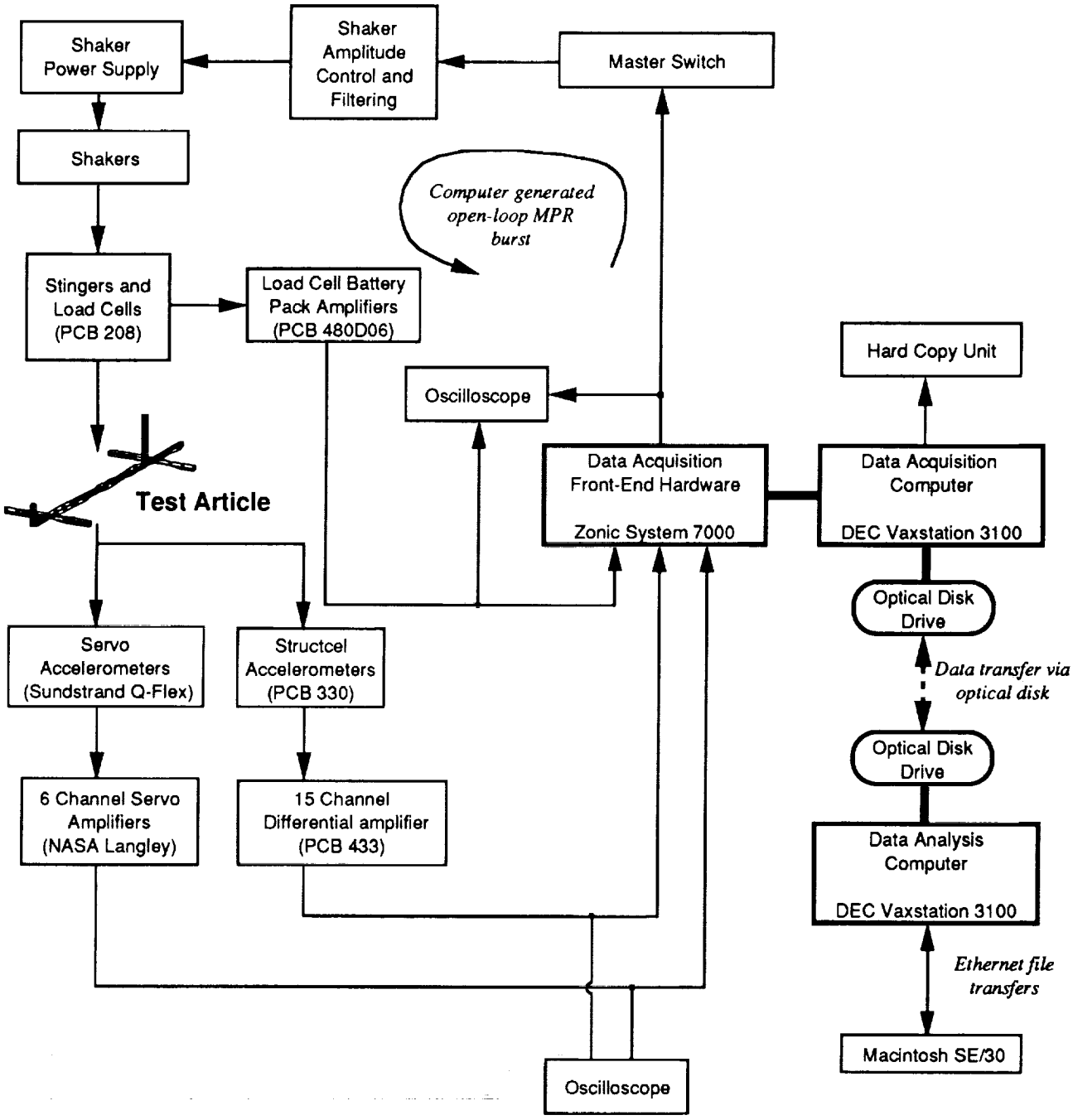

Figure 6-9. Data Acquisition System Configuration.

Table 6-7. CEM Phase 1 Modal Test Run Log.

Run No.	Run Date	Test Time	Test Type*	Exciter Coords	Force Level	Exc Dir/ Sym	Frequency Range	Notes	Function File Name
1	12-Mar	12:30	B	1001x,1002x,1003x,1004x	~2.2 lb pk	-	0.7-30 Hz	Prelim run	CSIB01.afu
2	12-Mar	16:45	B	1001x,1002x,1003x,1004x	~2.2 lb pk	-	0.7-30 Hz	First good data run (Sign errors & bad accels found later)	CSIB02.afu
3	12-Mar	-	B	1001x,1002x,1003x,1004x	~2.2 lb pk	-	0.7-30 Hz	Retry after working on accels (no file written)	no file
4	12-Mar	-	B	1001x,1002x,1003x,1004x	~2.2 lb pk	-	0.7-30 Hz	Retry after working on accels (no file written)	no file
5	13-Mar	17:30	B	1001x,1002x,1003x,1004x	~2 lb pk	-	0.7-30 Hz	Collected good set (found sign errors later) (30 sec on, 20 sec off)	CSIB05.afu
6	13-Mar	18:30	B	1001x,1002x,1003x,1004x	~2 lb pk	-	0.7-30 Hz	Sign Errors in reading into Zonic	CSIB06.afu
7	13-Mar	20:30	B	1001x,1002x,1003x,1004x	~2 lb pk	-	0.7-30 Hz	Fixed Zonic setup for sign errors, rerun 4 shaker burst	CSIB07.afu
8	14-Mar	18:00	B	1001x,1002x,1003x,1004x	~2 lb pk	-	0.7-30 Hz	Retry with thruput disk collection	CSIB08.afu
9	16-Mar	12:39	B	1001x,1002x,1003x,1004x	~2 lb pk	-	0.7-30 Hz	Retry after loosening shaker bands (same force level as run 8)	CSIB09.afu
10	16-Mar	14:20	B	1001x,1002x,1003x,1004x	~2.4 lb pk	-	0.7-30 Hz	Retry after loosening shaker bands (20% higher force level as run 9)	CSIB10.afu
11	16-Mar	17:30	B	1001x,1002x,1003x,1004x	~5 lb pk	-	0.7-30 Hz	Retry after loosening shaker bands (2.5 times higher force level as run 9	CSIB11.afu
12	17-Mar	11:30	B	1001y,1002y,1003y,1004y	~2.4 lb pk	-	0.7-30 Hz	Shaker in current mode (1.2 times higher force level as run 9) Current voltage level about 10 times lower than force (i.e. all FRF high by about a factor of 10)	CSIB12.afu
13	17-Mar	15:00	B	1001y,1002y,1003y,1004y	~5 lb pk	-	0.7-30 Hz	Shaker in current mode (2.5 times higher force level as run 9) Current voltage level about 10 times lower than force (i.e. all FRF high by about a factor of 10)	CSIB13.afu
14	17-Mar	19:30	B	1001y,1004y	~2.4 lb pk	-	0.7-30 Hz	Shaker in current mode (1.2 times higher force level as run 9)	CSIB14.afu
15	18-Mar	11:10	B	1001x,1004x	~2.4 lb pk	-	0.7-30 Hz	Shaker in voltage mode (1.2 times higher force level as run 9)	CSIB15.afu
16	18-Mar	13:50	B	1001x,1004x	~2.4 lb pk	-	0.7-30 Hz	Shaker in voltage mode (1.2 times higher force level as run 9) metal stin	CSIB16.afu
17	18-Mar	17:15	B	1001y,1004y	~2.4 lb pk	-	0.7-30 Hz	Shaker in current mode (1.2 times higher force level as run 9) metal stin	CSIB17.afu
18	18-Mar	17:15	B	1001x,1004x	~2.4 lb pk	-	0.7-30 Hz	Replay data from run#17 using load cells for reference	no file
19	19-Mar	10:00	I	1001x	-	-	0-32Hz	Impact data written with incorrect scaling due to Zonic program error	
20	19-Mar	11:55	I	1001x	-	-	0-32Hz	Impact excitation from thruput disk (USE VERSION #3 FOR PROCES: NOTE: first half of data written with correct scale factor for version #1 second half of data written with correct scale factor for version #2	CSII20.afu
21	19-Mar	15:30	I	1004x	-	-	0-32Hz	Impact excitation from thruput disk (ref was set as 1001X) NOTE: scaling is messed up on this data!!!	CSII21.afu
22	19-Mar	19:30	I	1004x	-	-	0-32Hz	Impact excitation from thruput disk Includes extra cable locations NOTE: there may have been a scale factor error in this data! (but it is consistent for all channels)	CSII22.afu

* D = Dwell; S = Sweep; B = Burst Random; R = Continuous Random; I = Impact

1001 = Node 3, Y-Z plane, 45° (+Y,+Z)
1002 = Node 392, X-Z plane, 45° (+X,+Z)
1003 = Node 252, Y-Z plane, 45° (+Y,+Z)
1004 = Node 471, X-Z plane, 45° (-X,+Z)

x - indicates shaker in voltage mode (or impact)
y - indicates shaker in current mode

The two excitation types (burst random using shakers and impact using the hammer) were selected due to the nature of the test article as well as the desired data quality. Each of these excitation types allowed the data to be collected without applying windows to the data which could result in distortion of the results. For example, in using a burst random excitation, a flat top window (or no window) could be used since the data was periodic (started at zero and ended at zero) within the sampling block of data. Other excitation types such as continuous random require application of some type of mathematical window to the time domain data to yield a periodic response. These windows result in distortion of the frequency domain data which can be exhibited as apparent increases in the structural damping. Continuous random excitation also can cause "structural leakage" effects which result in distorted FRF. This is caused by the response of the structure resulting from excitation started during one frame of data sampling but continuing into the next frame of data.

All of the data was collected simultaneously using the Zonic System 7000, for both burst random and impulse excitation. When the burst random waveform was being used as the excitation source, the command signal was generated by the data collection computer. All of the force signals and response signals were digitized and processed to yield frequency response functions (FRF) which could be used for data analysis. In some cases, the time domain histories of all of the channels were stored on a through-put disk which is part of the Zonic front-end. These histories could later be replayed to review the data as well as to generate the required FRF. The FRF could also be generated as the data was being collected, the typical method used for most of the data collection. Often, the stored results were both the FRF and the histories of the digitized data.

The data was collected using a block size of 4096 samples. The total sample time for each data sample was 50 seconds, or a sampling frequency of 81.92 samples/second. This was equivalent to a maximum frequency of 32 Hz. The time resolution was 0.01221 seconds/sample, and the frequency resolution was 0.02 Hz/spectral line. This gave good spectral resolution which could be used in evaluating closely spaced modes throughout the frequency range of interest. The 32 Hz upper frequency was selected based on the pretest analysis results and preliminary data collected in the test.

The computed FRF showed the relative magnitude and phase between each excitation input location and each response location on the structure. Multiple Input-Multiple Output (MIMO) calculation techniques were used for all of the multiple shaker burst random testing, whereas Single Input-Multiple Output (SIMO) was used when

employing the impulsive excitation input (References 5,6 and 7). These FRF were stored on the data collection computer disk and then transferred to an optical disk which was used as the transfer media to the data analysis computer.

An investigation was made during early testing to determine whether the excitation force level would affect the dynamic response of the test article. Moderate changes in force level were used to acquire sets of FRF which were then compared for similarity and data quality. No significant differences were observed in the data quality for minor changes in the force level. Initially, the force level was varied only about 10-20%. A level of approximately 2 pounds peak force (at each shaker) was selected for most of the early testing. This was established as the baseline force level since good signal levels were observed on the accelerometers without overloads and the data quality was very good. Later, the force level was increased by factors of 1.2 and 2.5 over the baseline level. These variations in force level did not result in significant changes in the FRF obtained.

Other excitation investigations were performed to study the effect of the shaker excitation mode used (voltage mode versus current mode) as well as to identify any effects of the shakers' being attached to the test article. Reducing the number of shakers to two from the original four and installing metal stingers between the shaker and the structure as compared to the plastic stingers allowed evaluation of the additional stiffness restraint being provided by the stinger attachment. The impact data was obtained to yield a definition of the test article in its unrestrained state for direct comparison to the data with shakers attached.

During the on-site evaluation of the test data, several mode shapes were defined from the test data which could not be uniquely separated from each other. There were multiple modes in narrow frequency ranges exhibiting the same general shape as determined by Modal Assurance Criteria (MAC) and orthogonality computations. These modes were apparent in the test data, but were not predicted in the pretest analysis. Therefore, an extra set of data was collected in which accelerometers were added to the upper cable supports to determine whether any phase changes could be observed for the cables in the regions where these multiple modes were present. This testing was performed using impact testing after lowering the test article to install the accelerometers and raising it back to its previous support level. The rationale for performing this test was that the analysis model did not adequately represent the cables in the suspension and visible cable motion could be seen during the test. In addition to the extra data collection performed, some spectra were generated from plucking the suspension cables and observing the responses.

6.3.4. Data Analysis

Data analysis was performed using SDRC I–DEAS™ test software installed on a DEC Vaxstation 3100. The data files (which contained all of the FRF obtained in the test runs) from the collection system were delivered on an optical disk and placed on the analysis machine. This data was then analyzed to extract all of the modal parameters from the measured FRF.

The data analysis involved a multiple-step process in which the quality of the data from a particular test run was reviewed and then used to extract modal parameters as required. Following the modal parameter extraction, the mode shape data from the test was expanded to allow direct comparison with the analysis results. In addition, other correlation steps were taken to compare the test and pretest analysis results.

Quality of the FRF data was determined by reviewing plots of selected FRF, evaluating the coherence and partial coherence obtained at each of the excitation locations, looking at the excitation input power spectra, and generating Mode Indicator Functions (MIF) and Multivariate Mode Indicator Functions (MMIF). This preliminary evaluation of the data quality was used in conjunction with observations made during the data collection to decide if a particular set of test run data was acceptable or not.

Once the quality of the FRF data was deemed acceptable, the next step was to extract preliminary mode shape information from the FRF so that proper functioning of all of the transducers could be verified. This step was performed by searching the MIF and MMIF for the frequencies of interest. Minima in the MIF and MMIF indicate resonances which exist in the test article. By searching for these minima, the resonant frequencies indicated by the test data were quickly identified. A shape extraction was then performed at these frequencies using a simple single-frequency parameter extraction method. These mode shapes were animated to determine where any transducer problems might exist. During the first six test runs, this approach identified several transducers which were either not functioning properly, or were not connected to the proper channel in the data collection system, or the polarity (sense) of the transducer was different than that which had been documented. In all of these cases, the transducers were replaced or corrected for subsequent test runs. Once all of the transducer problems had been corrected, subsequent testing results were used for further detailed data analysis.

Detailed modal parameter extraction followed the preliminary data evaluation process. During this part of the data analysis, more sophisticated parameter extraction methods were used such as direct parameter estimation [8] and polyreference[9]. Mode shapes as

well as modal frequency and damping were extracted for each of the resonant frequencies indicated in the test data. The MMIF was again used as a guide to locate the frequencies of interest. FRF were also used to define important frequencies. In particular, the driving point (excitation location) responses yielded clear indications of which modes were excited by specific shaker locations. This type of information was also evaluated from MIF computed from each of the individual references.

Once the mode shape information was extracted, steps were taken to make comparisons between the pretest analysis results and the test results. The first step of this process was to expand the test mode shapes from the measured DOF to a more descriptive representation which could be compared to the FEM. This expansion was performed using the constraint matrix extracted from the FEM during the TAM development. This matrix uses the measured DOF as independent DOF and the other display DOF as dependent DOF which are computed from the measurement set. Two sets of expansion matrices were developed: one for the 41-DOF servo accelerometer locations and the other for the 103-DOF full instrumentation set which included cable measurement locations. Figure 6–10 shows the abbreviated representation which is described by the 41-DOF servo measurements compared to the expanded set which is more representative of the actual hardware. Similarly, Figure 6–11 shows the 103-DOF representation compared to the expanded set.

Both sets of expansion matrices were used in the evaluation process since it was believed that the servo accelerometers were more reliable at the low frequency modes of the structure. In turn, the expansion using the 41-DOF would be more reliable at low frequencies. However, at higher frequencies, the cable motion becomes more important to the comparison to analysis, and the expansion using the 103-DOF set was felt to be more appropriate. MAC comparisons were made to show the difference between shapes expanded from the 41-DOF and the original shapes which included all 103-DOF. Final mode shape displays were all generated using the expanded shapes. Expansions were performed with the most appropriate matrix, either the 41-DOF or the 103-DOF.

A MAC matrix was developed as the next step to determine whether the test modes were independent of each other. Then a cross-MAC comparison was made to start matching the test modes with the pretest analysis modes. The mode pairs established from this comparison were then used for further mode shape comparisons.

After MAC comparisons were made, orthogonality and cross-orthogonality or cross-generalized mass (CGM) calculations were made to include the mass matrix weighting in the comparison process. The FEM mode shapes used in the cross-MAC

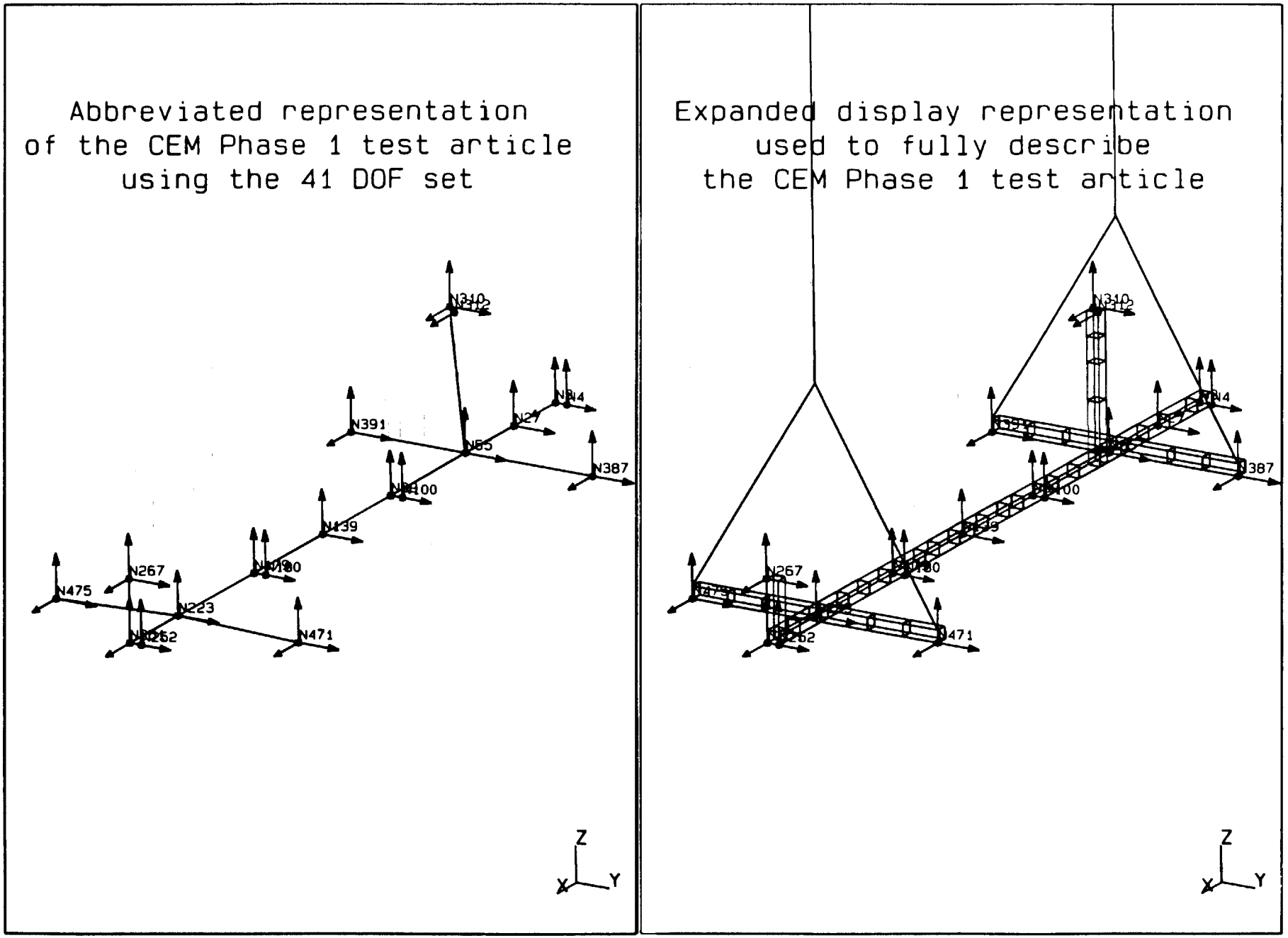

Figure 6-10. The 41 DOF Servo Measurements Limited Representation Was Expanded To A Full Display Representation.

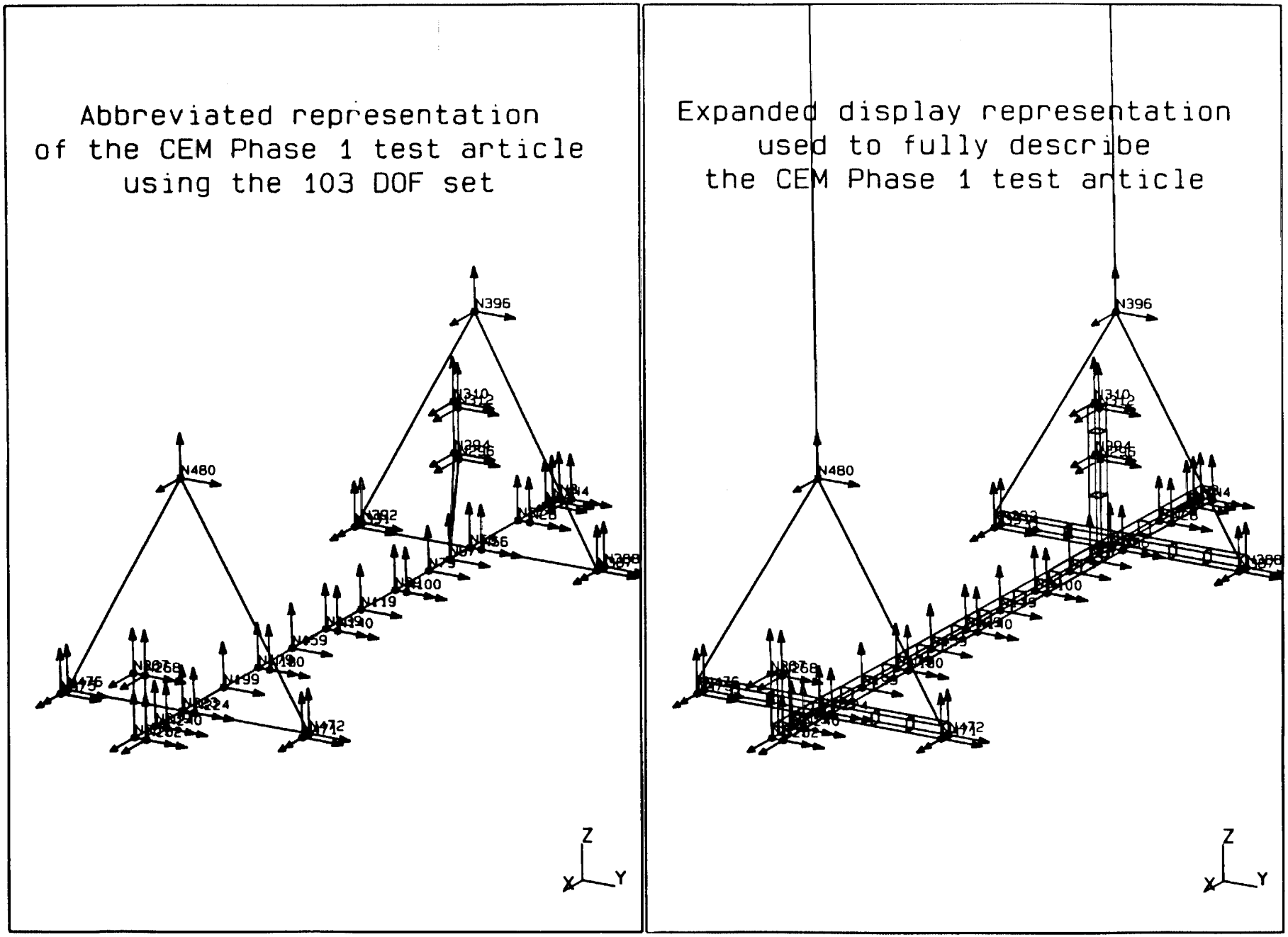

Figure 6-11. The 103 DOF Total Test Measurements Were Expanded To A More Descriptive Display With An Expansion Matrix From The Finite Element Model.

and cross-orthogonality calculations were the FEM modes partitioned to the measurement DOF. Those modes which showed good agreement to the pretest analysis were separated from the other shapes for the final comparisons. These comparisons showed differences in frequency as well as cross-MAC and CGM values between the test and analysis results.

Once the mode shape pairings were made between test and analysis, plots of the deformed shapes were made to show the similarity between the two shape sets. These plots were made showing the static deformed display over a dashed line display of the undeformed structure (see Figure 6–12). Split screen animation was also used to compare the mode shapes. Test mode shapes were compared to other test mode shapes during this process to determine if similar mode shapes showed any problems. Dominant response in the FRF, MMIF, and comparisons achieved using the cross-MAC and CGM were used to select the best mode shapes for the final set. These results were then tabulated for the final report.

6.4. MODAL TEST RESULTS

The modal survey of the CEM Phase 1 test article defined a significant number of modes in the frequency range of interest. Many of the modes identified involved substantial motion of the suspension system which could not be uniquely identified relative to the pretest model. However, the primary modes predicted by the pretest model were identified in the test and are presented in this section of the report. This section of the report also discusses the various excitation techniques employed in the test and how these affected the results. This part of the report also compares the pretest analysis results with those identified in the test. The mode shape appendix (Appendix H) contains the comparisons of the pretest modes and the test modes selected as mode pairs. Test modes not paired with pretest analysis modes are also presented in a separate appendix (Appendix I).

6.4.1. Summary of Test Results

A total of 67 modes were identified from the CEM Phase 1 modal survey in the frequency range of 0.7 to 32 Hz. Table 6–8 lists the summary of the frequencies and damping values identified from the test. Most of the modal information from the test was extracted from test run number 7 (see Table 6–7) which employed four shakers.

Comparisons based on MAC and orthogonality were used to determine whether a set of linearly independent modes had been extracted from the test data. Orthogonality

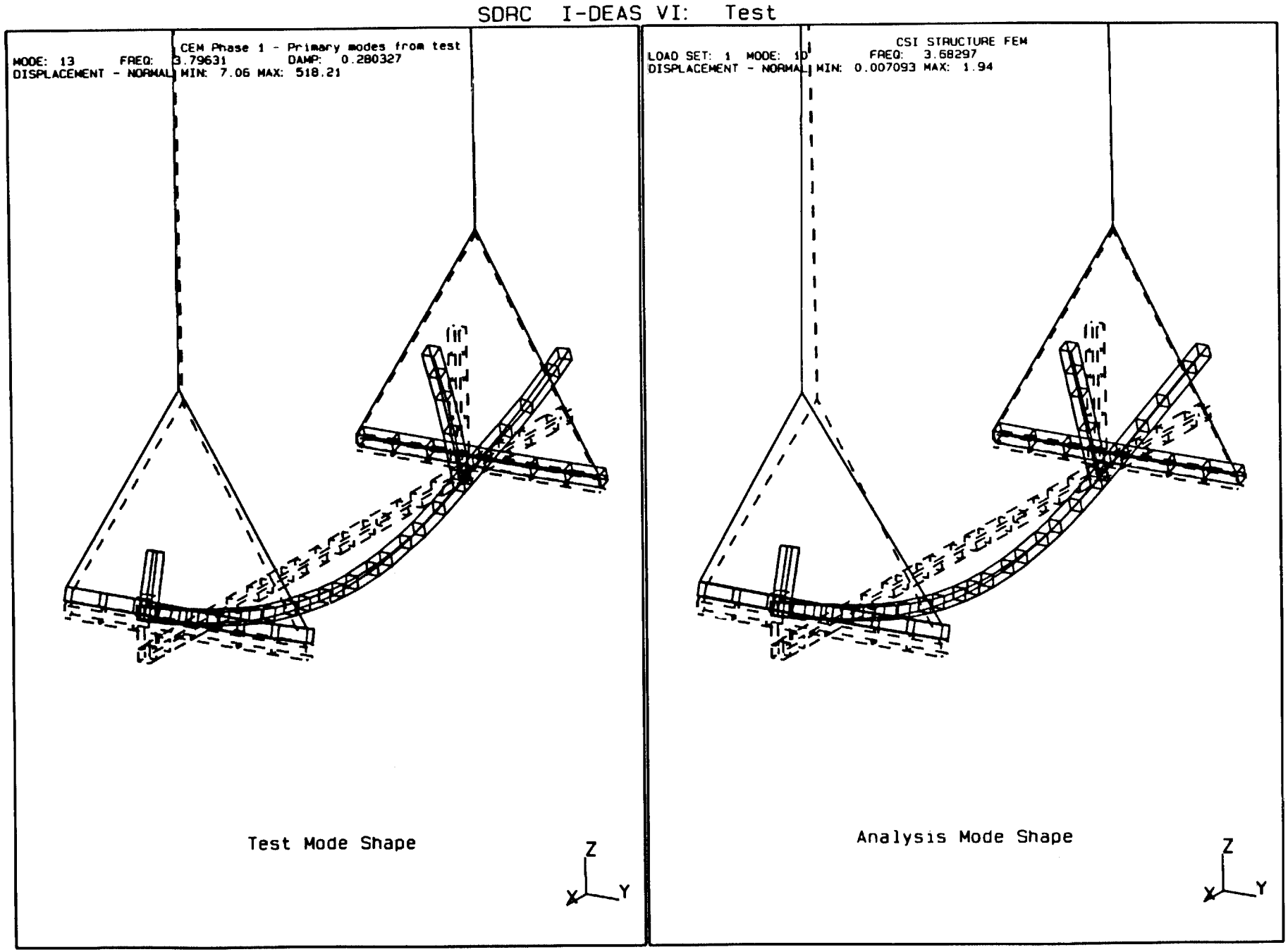

Figure 6-12. Expanded Mode Shapes From The Test Data Were Compared With The Pretest Analysis Mode Shapes.

Table 6-8. Summary Of Frequencies And Damping Values Identified In The CEM Phase 1 Modal Survey.

Test Mode No.	Test Frequency (Hz)	Equivalent Viscous Damping (%)	Test Mode No.	Test Frequency (Hz)	Equivalent Viscous Damping (%)
1	0.865	0.184	46	18.394	0.107
2	0.956	0.136	47	18.843	0.118
3	1.013	0.198	48	19.926	0.895
4	1.735	0.380	49	20.462	0.563
5	1.851	0.185	50	21.000	0.227
6	2.065	0.589	51	21.499	0.351
7	2.124	0.730	52	21.951	0.397
8	2.540	0.158	53	23.081	0.242
9	2.760	0.100	54	23.689	0.788
10	2.860	0.092	55	23.788	0.146
11	2.900	0.100	56	24.416	0.138
12	3.249	0.141	57	26.651	0.093
13	3.796	0.280	58	26.799	0.119
14	5.117	0.584	59	27.078	0.122
15	5.758	0.293	60	27.120	0.092
16	6.401	0.180	61	27.883	0.511
17	7.416	2.757	62	28.892	0.161
18	7.547	2.824	63	29.548	0.292
19	8.001	0.138	64	31.302	0.110
20	8.464	0.112	65	31.503	0.117
21	8.649	0.109	66	31.649	1.413
22	9.760	0.500	67	31.784	0.178
23	9.848	0.948			
24	9.916	0.835			
25	9.919	0.200			
26	9.975	1.206			
27	10.020	0.665			
28	10.122	0.139			
29	10.243	0.193			
30	10.311	0.623			
31	10.939	0.241			
32	11.142	0.218			
33	11.639	0.096			
34	12.310	0.445			
35	12.857	0.965			
36	13.656	0.199			
37	13.909	0.188			
38	14.508	0.164			
39	15.066	0.138			
40	15.508	0.048			
41	15.831	0.246			
42	17.027	0.196			
43	17.151	0.136			
44	17.571	0.041			
45	17.970	0.098			

computations were made with the 103-DOF mass matrix as the primary matrix of interest since there were many modes involving cable motion which could not be properly represented using the 41-DOF model. These comparisons showed that several of the mode shapes were very similar. Assuming that the modes were really unique, this would suggest that insufficient instrumentation was installed to capture all important mode shape information to prevent spatial aliasing.

Table 6–9 shows the MAC matrix which was obtained from the final set of test modes. Table 6–10 shows the orthogonality for the same set of modes. Review of the test data would indicate that adequate excitation of the modes took place, and sufficient care was taken in the mode shape extraction process to conclude that spatial aliasing takes place between a significant number of the modes in the test. This appears to be true even for the first flexible mode of the structure.

Two clearly distinct modes (test modes 4 and 5) at 1.73 Hz and 1.86 Hz were apparent in the FRF and resulting MIF and MMIF. Figure 6–13 shows these two frequencies in the driving point FRF for shaker location 4. However, when these modes were extracted, they were found to be almost identical in shape. A MAC value of 0.96 and orthogonality of 98 percent between these two modes indicated that they were very close to being the same mode, based on the mass matrix and the test measurement DOF.

Given the data quality and extraction techniques, it is concluded that insufficient measurements were made to yield a linearly independent set of modes. This is the same conclusion reached for some higher frequency modes as well. We believe that parts of the suspension system (not measured in the test) change their phase relationship in these modes. Since the FEM, pretest TAM, and test measurements did not provide enough data to identify this, spatial aliasing resulted.

6.4.2. Comparison of Test and Pretest Analysis Results

A total of twenty-four of the first thirty pretest analysis mode shapes were matched in the test. The six analysis modes not identified were the three lowest frequency rigid body modes and three of the upper frequency pretest modes believed to be outside the test frequency range of 32 Hz. The three highest frequency pretest modes were predicted to be above the test cutoff frequency of 32 Hz. One of these (a cable mode) was predicted to be above the 32 Hz limit, but was found in the test at a lower frequency.

Table 6-9. Modal Assurance Criteria Matrix Developed From All Test Modes.

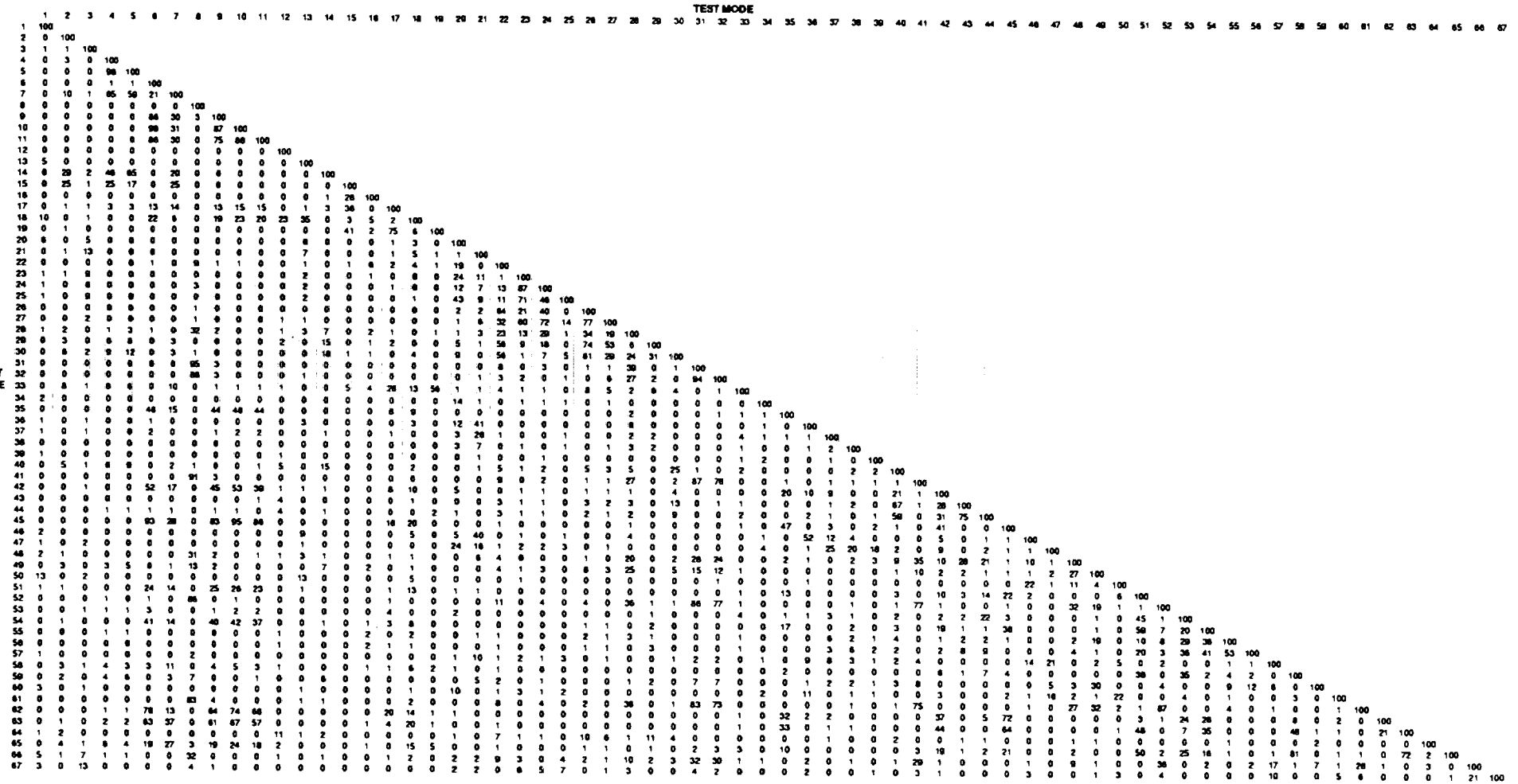

Table 6-10. Orthogonality Matrix Developed From All Test Modes Relative To The 103 DOF TAM Mass Matrix.

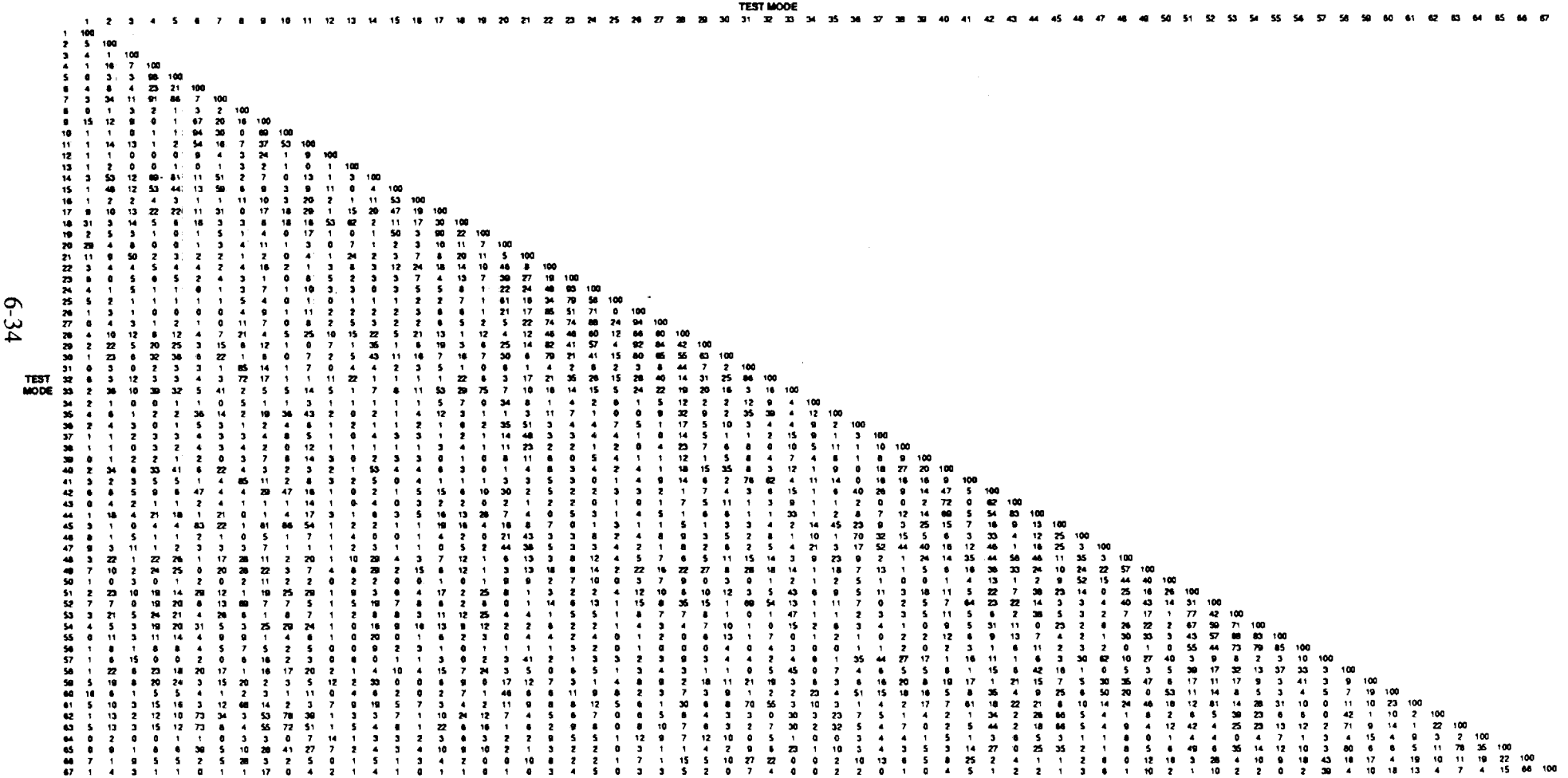

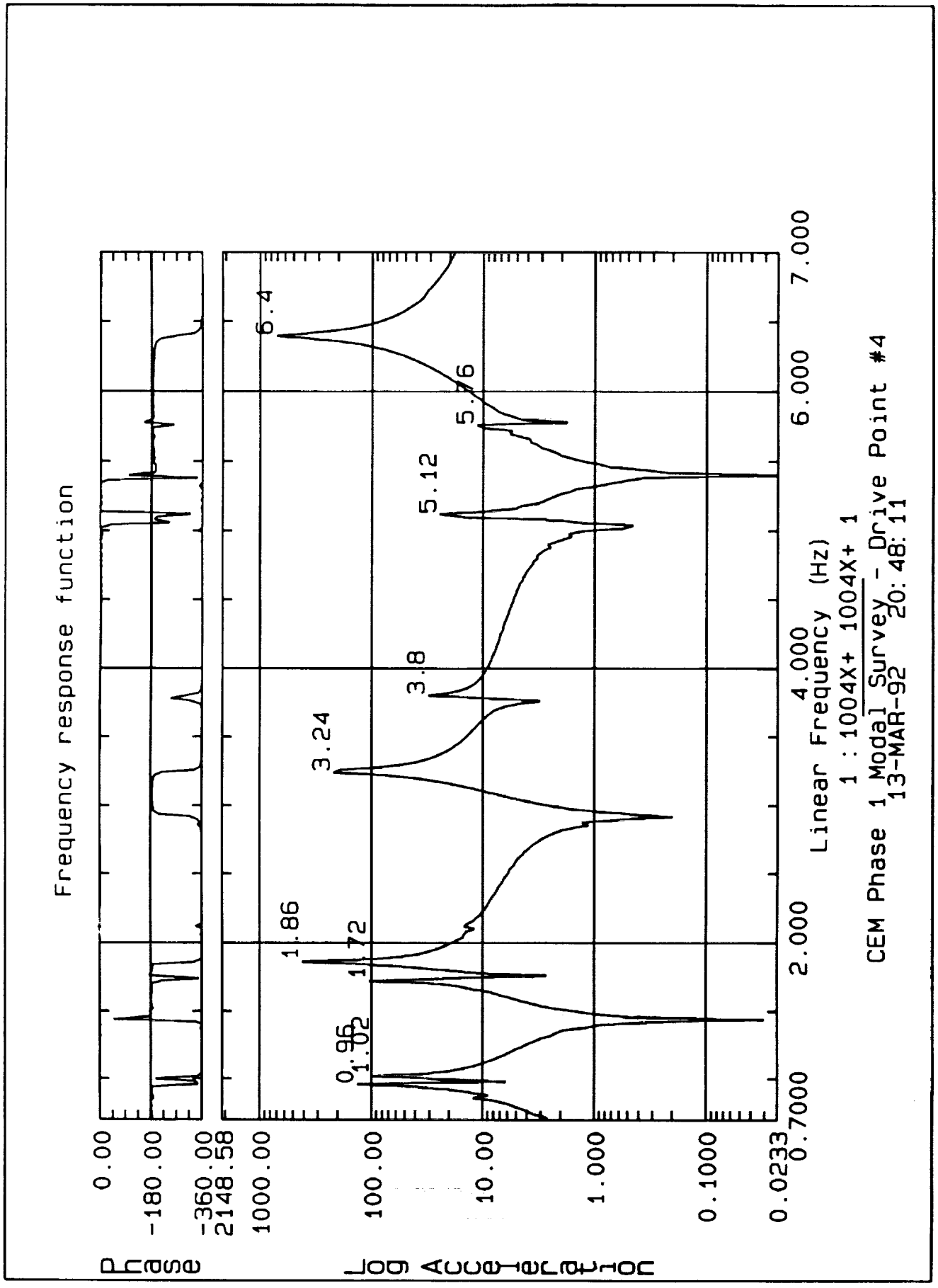

Figure 6-13. Driving Point FRF For Shaker 4 Indicated Two Distinct Natural Frequencies At 1.73 And 1.86 Hz. The Corresponding Modes Were Highly Coupled In MAC And Orthogonality Comparisons.

The three rigid body modes which were not determined from the test FRF are pendulum modes whose frequency is dependent on the suspension cable length. All of these modes were predicted to be below 0.13 Hz. Since these modes were so low in frequency, they could be easily excited and timed manually, and the shaker attachment could easily influence the frequency of these modes. Therefore, no attempt was made to excite the structure with frequency content low enough to characterize these modes.

The modes which were matched to the pretest analysis showed very good agreement. The largest frequency error between the test and analysis for significant structural modes was just over 5.5%. There were three modes dominated by suspension cable response which showed errors in excess of 30%. The cross-MAC values obtained from the matching modes were in excess of 80% except for two modes. When the mass matrix weighting was added to give CGM values, the results improved. All CGM values were in excess of 90% except for one mode which showed a 71% term. This was for a higher frequency mode and was dominated by cable motion. The combination of good frequency agreement and high CGM terms obtained between the test and analysis predictions showed very good correlation of the model without making any FEM changes. Table 6–11 lists the comparison results between the pretest and test data.

A total of 67 test modes were identified, but many of these modes did not appear to be unique. The first evaluation of the test modes was performed using MAC calculations. This was followed by cross-MAC comparisons between the test and analysis shapes to gain an initial determination of the mode pairing between the two sets of data. Next, the orthogonality of the test modes was computed using the 103 DOF TAM mass matrix.

Using the highest cross-MAC and cross-orthogonality terms as criteria, a table of shape correspondence was created. In cases where two test modes matched the analysis results, the highest CGM term was selected to build a list of the best comparisons between the test and analysis. The test modes selected through this process were identified as the primary modes which were then used to recompute the MAC and orthogonality tables. These are presented in Figures 6–14 and 6–15. The numerical listings corresponding to these figures are given in Tables 6–12 and 6–13. The largest off-diagonal terms which result in this abbreviated set of test modes are the result of coupling between modes dominated by suspension cable motion and the other modes. Since the largest frequency errors present are for the cable modes, and it is believed that the suspension cables are not modeled to accurately represent the test article, these off-diagonal terms are of no concern.

Table 6-11. CEM Phase 1 Modal Test Comparisons (Pretest versus Test).

Test Mode No.	Test Frequency (Hz)	Equivalent Viscous Damping (%)	Pretest Analysis Mode No.	Analysis Frequency (Hz)	% Frequency Difference	MAC Value	CGM Value
1	0.865	0.184	4	0.825	-4.624%	0.994	0.9978
2	0.956	0.136	5	0.959	0.314%	0.971	0.9740
3	1.013	0.198	6	0.963	-4.936%	0.943	0.9817
5	1.851	0.185	7	1.808	-2.323%	0.995	0.9973
8	2.540	0.158	9	3.460	36.220%	0.973	0.9223
10	2.860	0.092	11	3.940	37.762%	0.985	0.9838
12	3.249	0.141	8	3.125	-3.817%	0.997	0.9988
13	3.796	0.280	10	3.683	-2.977%	0.987	0.9981
16	6.401	0.180	12	6.122	-4.359%	0.996	0.9984
19	8.001	0.138	13	7.827	-2.175%	0.995	0.9975
25	9.919	0.200	14	9.451	-4.718%	0.966	0.9847
26	9.975	1.206	15	9.769	-2.065%	0.989	0.9960
34	12.310	0.445	16	11.853	-3.712%	0.990	0.9957
35	12.857	0.965	17	12.141	-5.569%	**0.475**	0.9037
36	13.656	0.199	18	13.418	-1.743%	0.914	0.9615
37	13.909	0.188	19	13.572	-2.423%	0.868	0.9299
38	14.508	0.164	20	14.113	-2.723%	0.812	0.9138
39	15.066	0.138	21	14.715	-2.330%	0.830	0.9092
43	17.151	0.136	22	16.556	-3.469%	0.996	0.9978
50	21.000	0.227	23	20.114	-4.219%	0.995	0.9976
56	24.416	0.138	24	23.258	-4.743%	0.940	0.9846
58	26.799	0.119	28	37.125	38.531%	**0.681**	0.7129
64	31.302	0.110	26	31.011	-0.930%	0.887	0.9482
67	31.784	0.178	25	30.724	-3.335%	0.928	0.9777

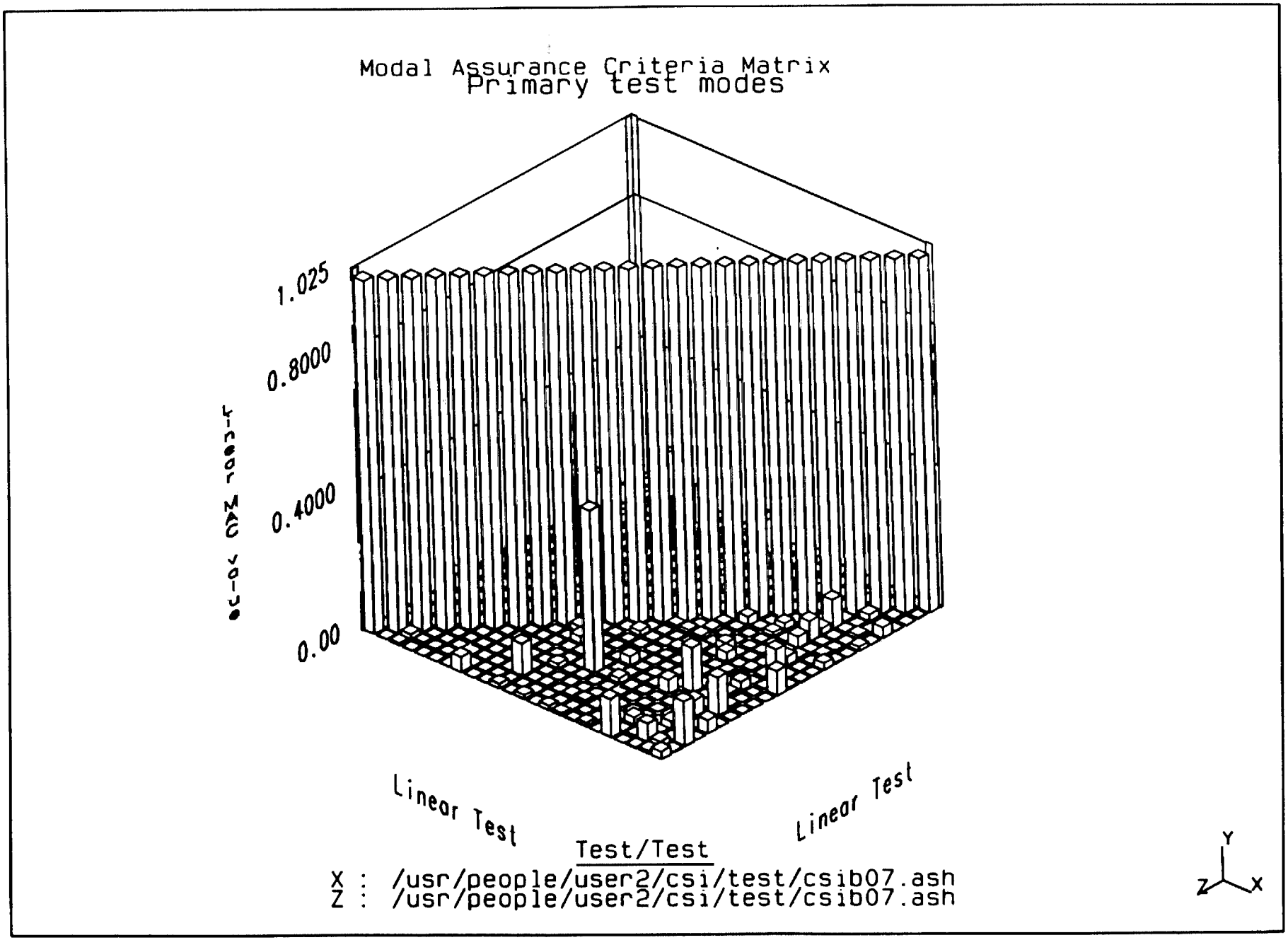

Figure 6-14. MAC Matrix Plot For Primary Modes Identified From The CEM Modal Test.

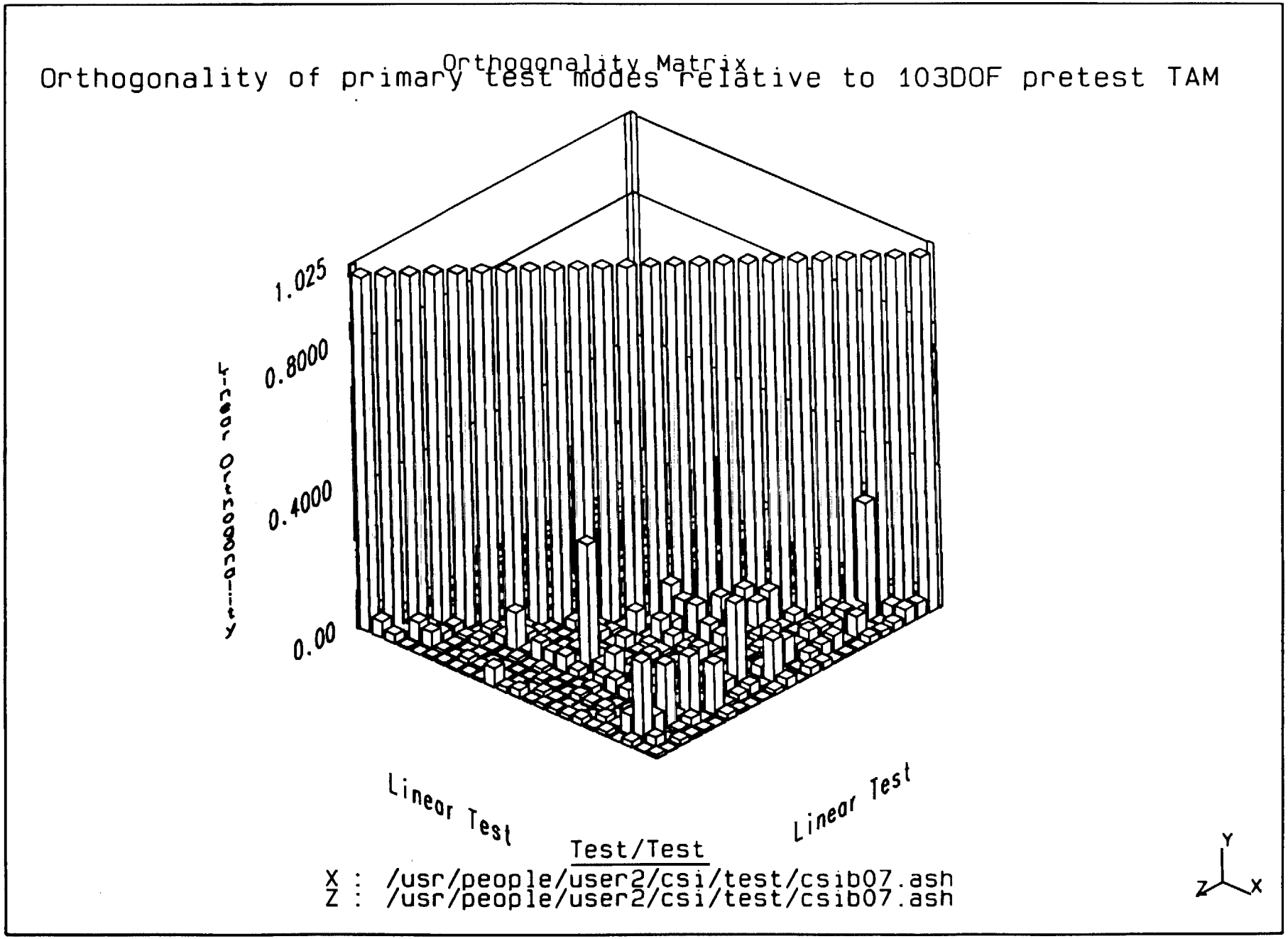

Figure 6-15. Orthogonality Matrix Plot For Primary Modes Identified From The CEM Modal Test.

Table 6-12. MAC Matrix For Primary Modes Identified From The CEM Modal Test.

TEST MODE	1	2	3	5	8	10	12	13	16	19	25	26	34	35	36	37	38	39	43	50	56	58	64	67
1	100																							
2	0	100																						
3	1	1	100																					
5	0	0	0	100																				
8	0	0	0	0	100																			
10	0	0	0	0	0	100																		
12	0	0	0	0	0	0	100																	
13	4	0	0	0	0	0	0	100																
16	0	0	0	0	0	0	0	0	100															
19	0	0	0	0	0	0	0	0	2	100														
25	1	0	9	0	0	0	0	2	0	0	100													
26	0	0	0	0	0	0	0	0	0	0	2	100												
34	1	0	0	0	0	0	0	0	0	0	1	0	100											
35	0	0	0	0	0	46	0	0	0	0	0	0	1	100										
36	1	0	1	0	0	0	0	3	0	0	0	0	1	0	100									
37	1	0	1	0	0	2	0	0	0	0	1	0	1	1	1	100								
38	0	0	0	0	0	0	0	0	0	0	1	1	0	0	1	2	100							
39	1	0	0	0	0	0	1	0	0	0	0	0	2	0	0	1	0	100						
43	0	0	0	0	0	0	4	0	0	0	0	3	0	0	0	1	2	0	100					
50	11	0	2	0	0	0	0	13	0	0	0	0	0	0	1	0	0	0	0	100				
56	0	0	0	0	0	0	1	0	2	0	0	1	0	0	0	3	6	2	8	0	100			
58	0	5	1	2	0	5	1	0	1	2	0	0	0	2	0	0	0	0	1	0	2	100		
64	1	2	0	0	0	0	11	1	0	0	0	10	0	0	0	1	0	0	1	0	0	0	100	
67	2	0	13	0	4	0	0	0	0	0	7	0	0	0	2	0	0	1	0	3	0	0	0	100

Table 6-13. Orthogonality Matrix For Primary Modes Identified From The CEM Modal Test Relative To The 103 DOF TAM Mass Matrix.

TEST MODE	TEST MODE																							
	1	2	3	5	8	10	12	13	16	19	25	26	34	35	36	37	38	39	43	50	56	58	64	67
1	100																							
2	5	100																						
3	2	1	100																					
5	0	6	3	100																				
8	0	4	2	3	100																			
10	1	1	0	1	0	100																		
12	1	0	0	2	3	1	100																	
13	0	2	1	1	3	1	1	100																
16	1	1	0	0	11	3	2	1	100															
19	1	1	0	1	1	0	1	0	3	100														
25	5	1	0	0	5	0	0	1	2	1	100													
26	0	2	1	0	7	0	0	2	4	2	12	100												
34	2	0	1	0	5	1	1	1	1	0	6	1	100											
35	1	1	1	1	2	**36**	2	0	4	1	0	2	12	100										
36	1	1	1	1	1	4	1	2	2	2	7	4	9	2	100									
37	1	0	2	2	3	8	1	0	3	1	4	3	9	1	3	100								
38	1	0	1	0	4	0	1	1	1	1	2	1	5	11	1	10	100							
39	2	0	1	0	3	6	3	0	3	0	4	1	4	8	1	8	9	100						
43	1	2	0	0	1	1	1	0	3	0	1	1	1	1	2	0	0	2	100					
50	1	1	3	0	2	2	0	2	0	1	0	0	1	2	5	1	0	0	1	100				
56	0	6	1	8	7	2	0	0	3	1	0	2	0	0	1	1	2	0	6	0	100			
58	2	**22**	5	**18**	1	**17**	2	1	4	**24**	1	1	0	7	4	6	5	5	6	5	**33**	100		
64	0	3	0	1	3	0	14	1	2	3	1	13	0	0	3	4	4	1	6	1	1	4	100	
67	1	0	2	1	1	0	2	1	0	0	1	1	0	2	2	0	1	0	2	2	2	4	4	100

The results of the test indicate that the suspension cables interact substantially with the test structure. The pretest model did not take into account the flexibility or motion of the suspension cables other than at the Y-joint where the cables join. As a result, the DOF indicated by the model could not include any flexible motion of the cables. This meant that the number of modes predicted in the pretest efforts was lower than those which occurred during the test. The test modes could still be matched with the analysis modes, but there were extra modes indicated in the test which were not present in the pretest predictions. To improve the comparison between the test and analysis results, the suspension system in the model needs to be updated to allow for the cable flexibility and modes.

The mode shape plots which show the matching test and analysis shapes are contained in Appendix H. The mode shape plots of all other test modes which were not matched with the analysis predictions are presented in Appendix I.

6.4.3. Comparison of Excitation Type and Stingers

Seven different excitation configurations were used during the modal test to evaluate shaker effects on the test article:

(1) Multi-input 4 shaker excitation, plastic stinger rod, voltage mode
(2) Multi-input 4 shaker excitation, plastic stinger rod, current mode
(3) Multi-input 2 shaker excitation, plastic stinger rod, voltage mode
(4) Multi-input 2 shaker excitation, plastic stinger rod, current mode
(5) Multi-input 2 shaker excitation, metal stinger rod, voltage mode
(6) Multi-input 2 shaker excitation, metal stinger rod, current mode
(7) Single-input calibrated hammer impulse excitation, no shaker connection

The two shaker modes, voltage and current, refer to the control method used to supply the electrical command signal to the shaker. In voltage mode, there is some back Electromotive Force (EMF) which is generated by the shaker motion. The current mode of operation can be used to eliminate this EMF. There have been previous indications that the shaker EMF can influence the FRF results, so these comparisons were made to evaluate this theory.

The different shaker modes were investigated to determine whether there was a measurable difference in the FRF data when no EMF was present. Different stinger types were investigated to determine if the stiffness of the stingers supplied any significant constraint to the motion of the test article. The impact testing was performed to give a baseline measurement of the structural response with no external restraints or added mass.

Comparisons of FRF were made to document the effects of the different shaker effects. If a change in the shaker caused a change in the structural behavior, then the FRF should exhibit that change. Most of these comparisons showed no change, although exceptions are discussed here.

The impact testing did not result in the same high quality data obtained in the shaker testing. This was exhibited by the poorer FRF data quality in the frequencies away from the resonances, partially due to the lower force levels used and some problems in the software implementation on the data collection system. Even so, a good comparison was made between the impact excitation and the other excitation types. Also, the FRF computation made during the current mode excitation was obtained by using the shaker drive current as the force applied to the structure rather than using the load cell which was attached to the test article. This is discussed further in the paragraphs which follow.

There was a measurable shift in the three measured rigid body modes when changes in the excitation type were tried. As expected, the frequencies were slightly higher when the shakers were attached to the test article. This reflected the slight stiffness increase contributed by the stingers. A slight frequency shift could be observed at some other higher frequencies, but in most cases, the shift, if any, was insignificant. The 1/8 inch diameter metal stinger provided more lateral stiffness than the 1/4 inch diameter plastic stinger. This yielded some higher frequencies, but most of the changes were minor. Figure 6–16 shows a comparison of FRF obtained using the two different stinger types.

There was virtually no difference between the two-shaker excitation and the four-shaker excitation for most of the frequency range. The driving point FRF from these two surveys overlay so that almost no difference could be seen. This indicated that there was little additional stiffening effect from the extra two shakers. However, there was a narrow frequency range in which some change was observed. In the frequency range between 9 and 15 Hz, changes in the response frequency and amplitude were observed. These effects can be seen in Figure 6–17. Outside that frequency range, differences between the two data sets were very small.

Some of the biggest differences in the FRF were observed when switching between current mode and voltage mode excitation. The FRF obtained using current mode excitation were noticeably noisier at frequencies below about 4 Hz. The force (current) spectrum was reviewed, and the force amplitude was lower at the low frequency range for the current mode excitation. All other data collection parameters were kept the

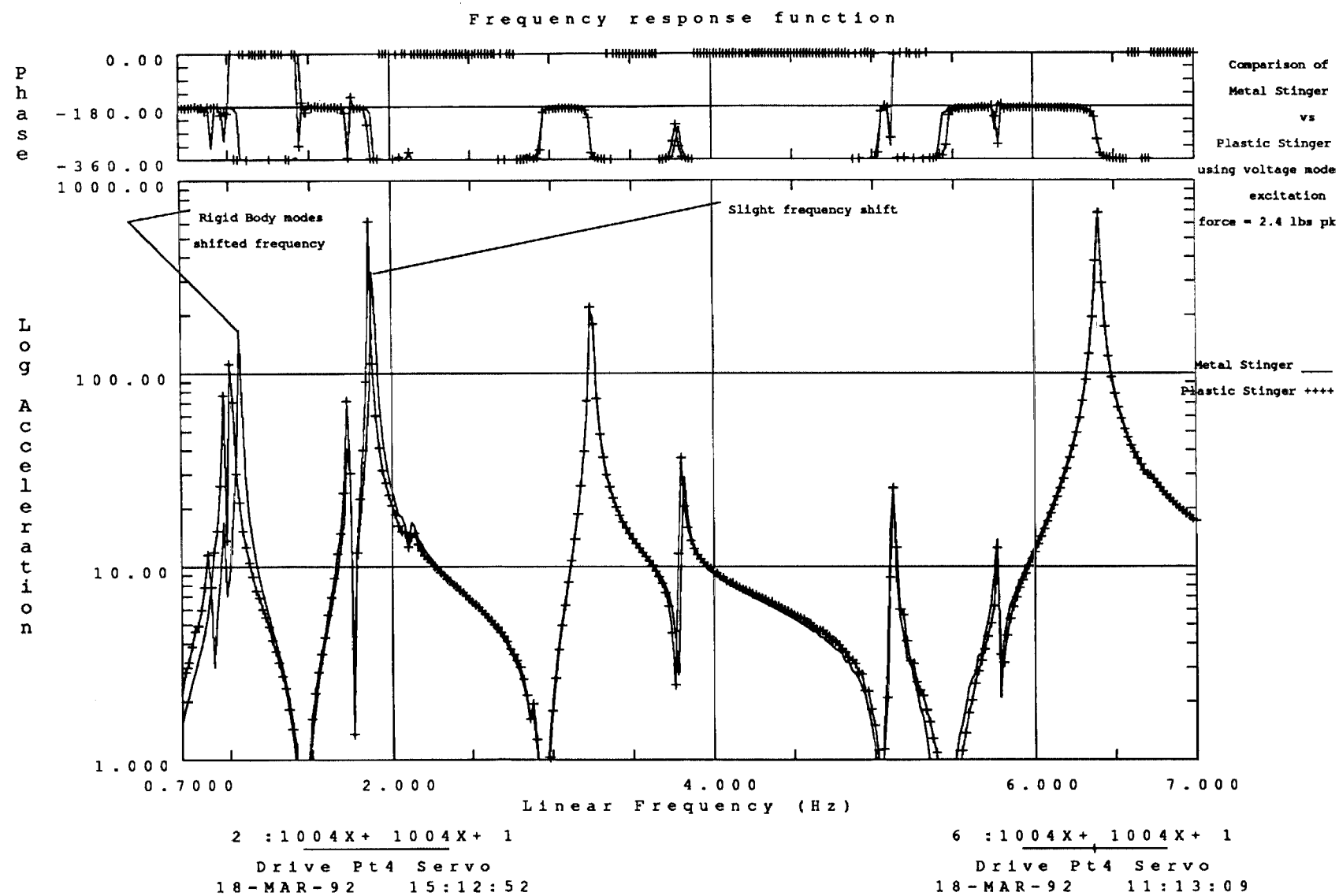

Figure 6-16. Comparison Of FRF Obtained From Plastic And Metal Stinger Rods Showed Some Slight Frequency Shifts.

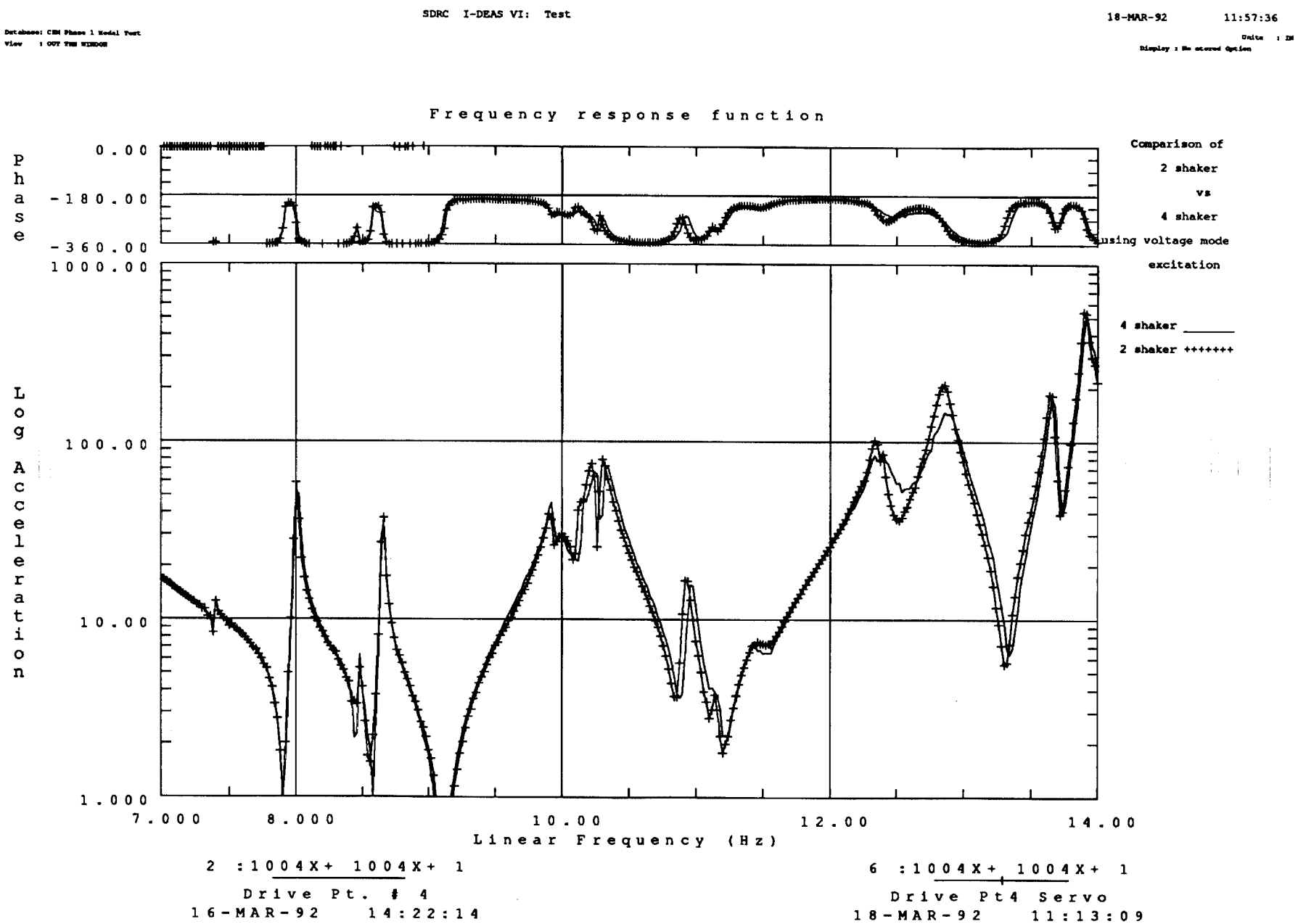

Figure 6-17. Some FRF Changes Were Observed In The 9-15 Hz Frequency Range When Switching From 4 Shakers To 2 Shakers.

same for these comparisons, so the shaker excitation type was the only variable. Figure 6–18 shows an example of the spectrum associated with the current mode excitation where the low frequency roll-off can be observed.

The current mode excitation also resulted in a frequency shift around 14.5 Hz which was not indicated during the voltage mode excitation when switching from four shakers to two shakers (Figure 6–19). Figure 6–20 shows the mode shape associated with this particular frequency. Direct comparison of FRF obtained using the two exciter modes showed measurable differences. The current mode resulted in lower frequencies than the voltage mode in general. Figure 6–21 shows a comparison of the FRF obtained with the two excitation modes. Since comparison between impact excitation and the voltage mode FRF showed results which were very comparable, it appears that the current mode excitation results in either an added mass effect not apparent in the voltage mode excitation or a computational difference in the generation of the FRF resulting from use of the current rather than the true force.

6.4.4. Excitation Force Level Comparisons

A limited number of force levels were used to collect data with the burst random input. These different force levels were only for the four-shaker excitation testing. The force levels used were approximately 2, 2.4, and 5 pounds peak force and were adjusted by controlling the excitation voltage going to the shaker. A full set of force level studies was performed using voltage mode shaker control while two force levels, 2.4 and 5 pounds, were studied for the current mode shaker control.

Only minor differences were seen when the excitation force level was changed as described. The conclusion was that the test article behaved in a very linear fashion within the range of excitation forces applied. No extremely large excitation force was applied during the modal test since that was not the objective of the test. This result was consistent with similar findings obtained during the dynamic section tests (Section 4.0).

6.4.5. Evaluation of Suspension Cable

Several modes identified during the test appeared to be the same—that is, they were not shown to be linearly independent. In some cases, these modes were clearly shown to be suspension cable modes. For example, modes 10 and 62 are both dominated by cable motion and since the instrumentation was limited to only the Y-joint where the cables intersect, the mode shapes for these well-separated frequencies could not be uniquely identified. The high MAC terms and orthogonality

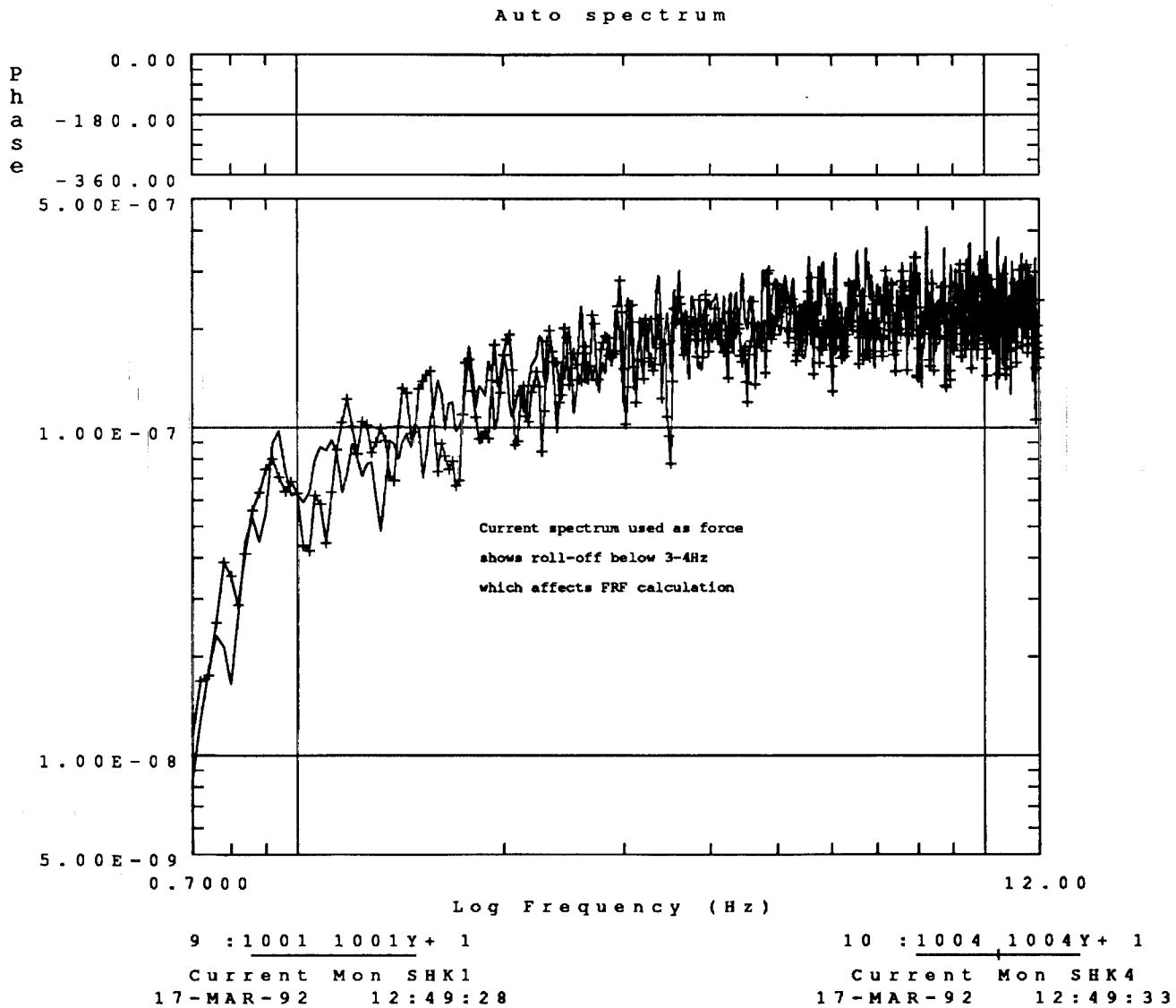

Figure 6-18. The Excitation Spectrum Associated With Current Mode Showed A Roll-Off Below 4 Hz.

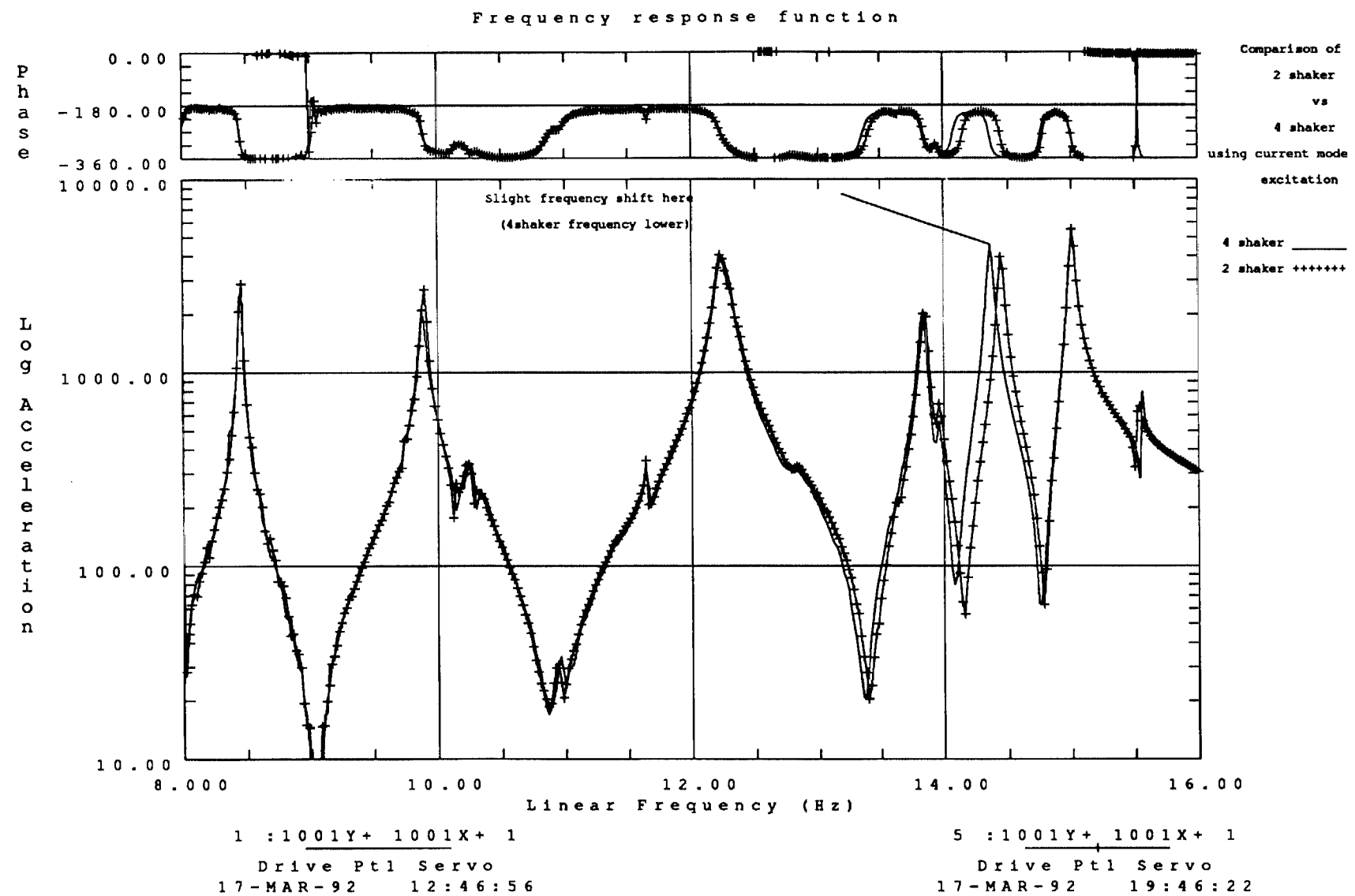

Figure 6-19. Frequency Shift Around 14.5 Hz Was Observed When Changing From 4 Shakers To 2 Shakers With Current Mode Only.

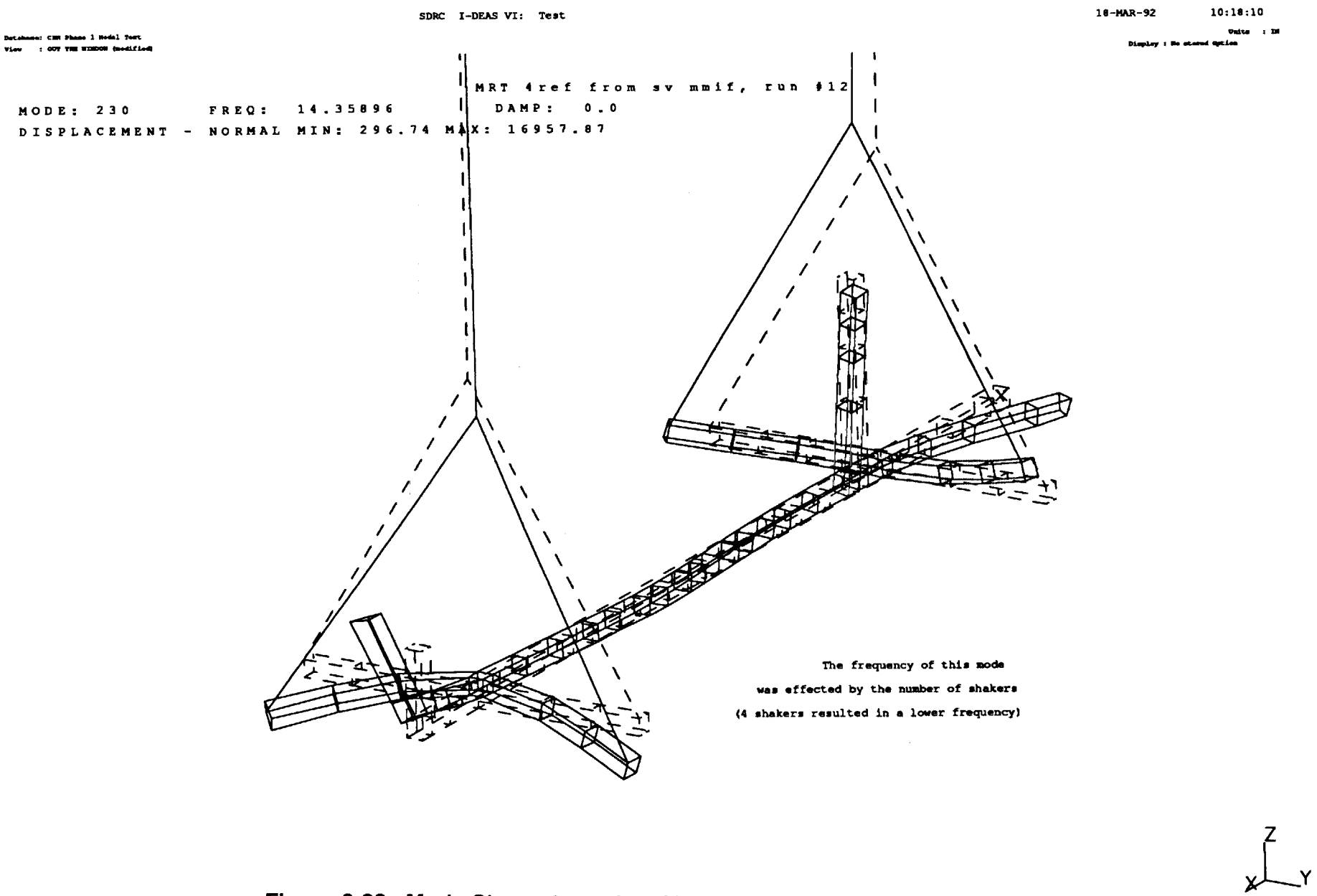

Figure 6-20. Mode Shape Associated With The Frequency Which Shifted With The Change From 4 To 2 Shakers (Current Mode Only).

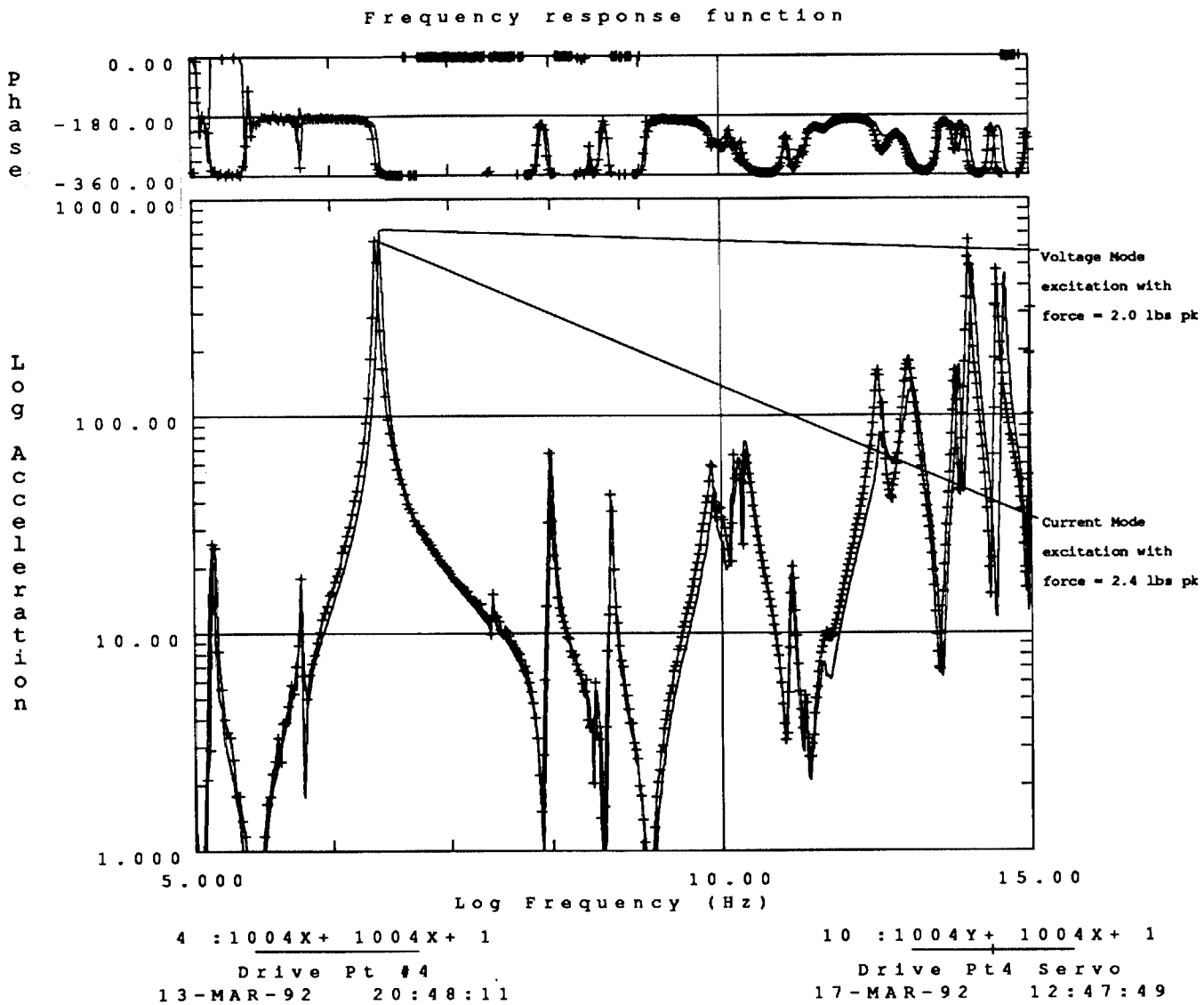

Figure 6-21. Comparison Of FRF Obtained With Two Different Modes Of Shaker Control - Voltage Mode And Current Mode.

off-diagonal terms obtained for some of the other test modes indicated that these shapes were not uniquely defined as well. Since 24 of the first 30 pretest analysis modes could be matched with selected test modes, the extra test modes were believed to be the result of the suspension system cables coupling with the test structure.

Based on this conclusion during the test, an extra set of accelerometers was installed on the main suspension cables at each end of the test article (see Figure 6–22). The accelerometers were installed using local displacement coordinate systems since they could not be accurately placed in the global system. The local coordinate system definition is shown in Figure 6–23. These transducers were added to determine whether the cable motion changed its phase relationship to the rest of the structure in any of the flexible modes. This data was collected near the end of the testing and was performed with impact excitation. The FRF obtained from this data were compared to see if the phase changed between the two locations, particularly in the first two flexible modes.

No change was observed for the first flexible mode pair, so it was concluded that this was not the area of the fundamental difference. No additional measurements could be made on the upper portion of the suspension near the spring, so it is still likely that part of the upper suspension system exhibits a phase reversal between the two modes. Further analysis modeling needs to be performed in order to give a better description of the suspension cable interactions with the CEM structure.

Some preliminary data was collected from the new transducers installed on the cables to see if some of the fundamental cable frequencies could be identified. A suspension cable was "plucked" manually and the response of the accelerometers was measured and Fourier transformed to yield the frequency content. Several averages were collected to smooth the response spectra. The largest dynamic responses were observed and plotted. The cable frequencies measured during this limited testing were in the 1.5 to 3 Hz frequency range just as those where some multiple modes were observed. However, no overall clear definition of the extra modes was found using this excitation type.

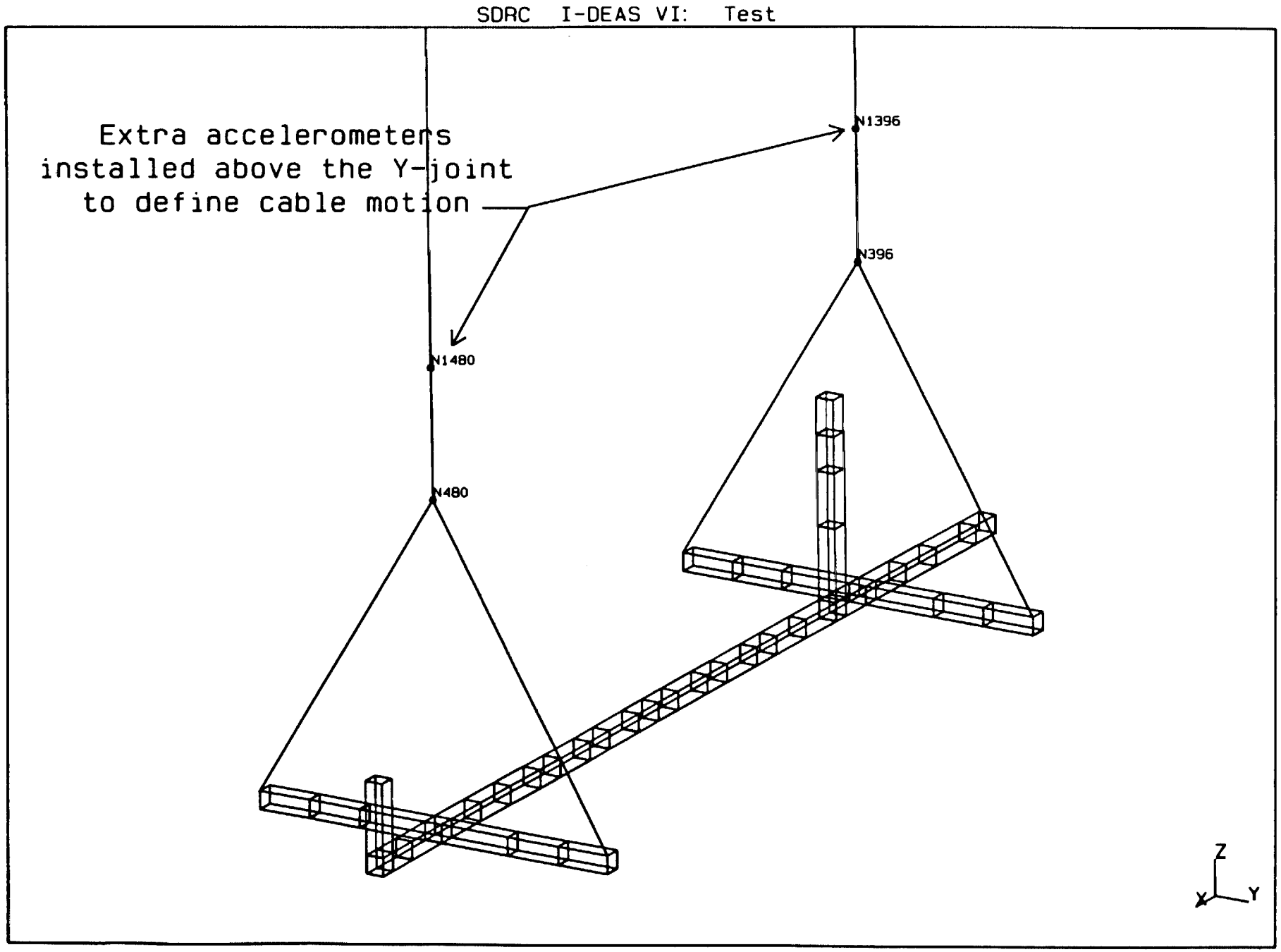

Figure 6-22. Additional Triaxial Accelerometers Were Installed On The Main Suspension Cable Approximately 6 Feet Above The Y-Joint.

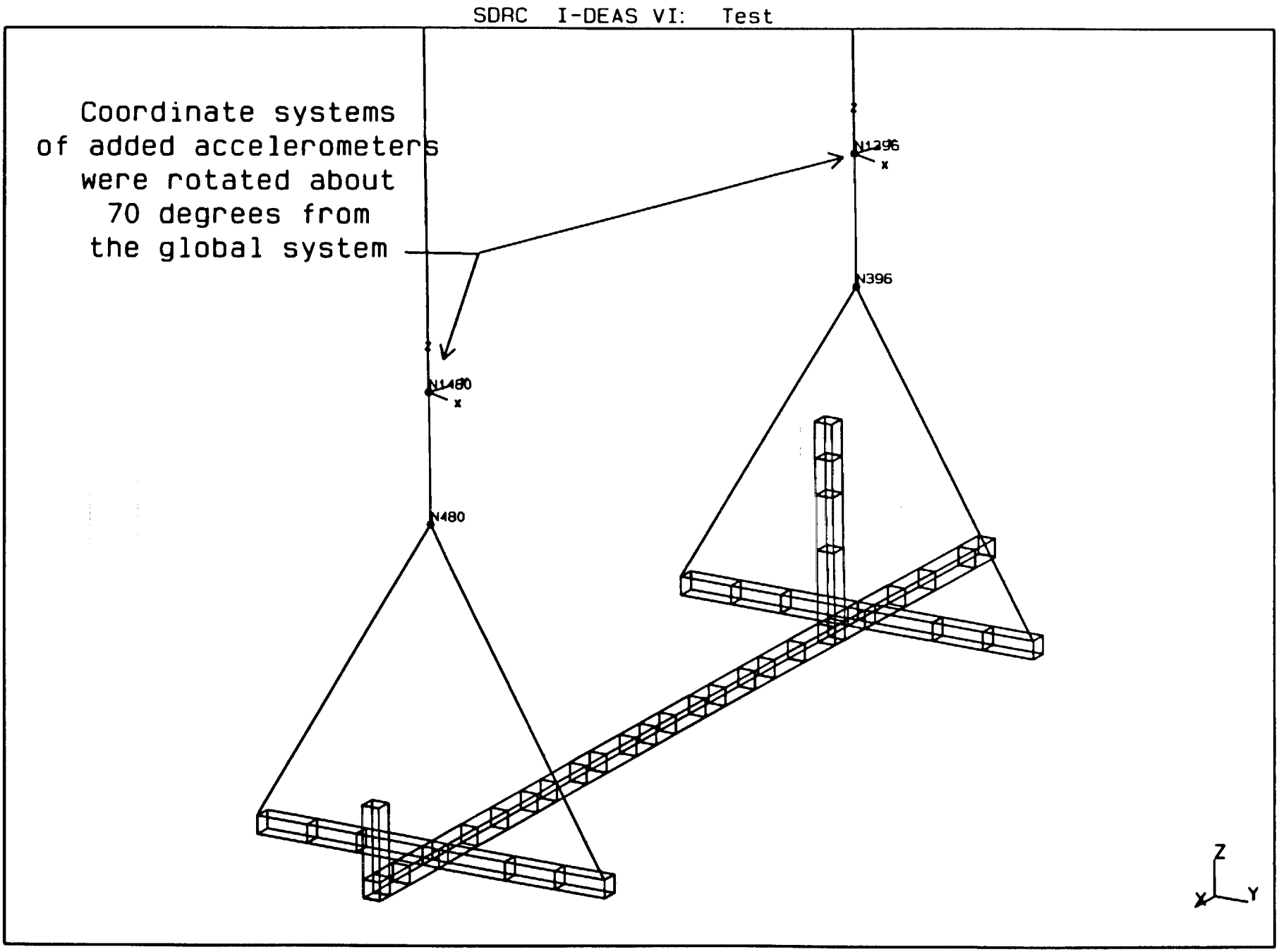

Figure 6-23. The Orientation Of The X And Y Axes For The Extra Cable Accelerometers Was Rotated Slightly From The Global Coordinate System.

6.5. ASSEMBLY DYNAMIC TEST SUMMARY

A very successful modal survey of the CEM Phase 1 test bed was completed in which excellent agreement was obtained between selected pretest analysis modes and the test results. Twenty-four of the primary modes below 32 Hz were matched with the model predictions. Frequency agreement was very good with all errors between test and analysis being less than 6 percent for all primary flexible modes. Natural frequencies of the suspension cable modes showed greater errors. The cross-generalized mass (CGM) values between test and analysis were also excellent with all of them 90 percent or higher except for one cable mode. The summary of all test and analysis comparisons is provided in section 6.4.2.

Substantially more modes, however, were identified in the test than in the pretest efforts. This is believed to be the result of the modeling approach used for the suspension system. The suspension system in the pretest model did not take into account the flexible modes which result from the tensioned cable. These modes tended to interact with the test structure during the test and yield a much larger number of modes. This also resulted in the disparity between the measured cable frequencies and the pretest predictions. If further improvement in the test-to-analysis correlation is desired, the suspension system in the model needs to be updated to allow for the cable flexibility and modes.

7.0 REFERENCES

1. Maghami, P.G., S.M. Joshi, J.E. Walz, and K.B. Elliott, "Integrated Design of the CSI Evolutionary Structure: A Verification of the Design Methodology", 5th NASA/DOD Controls-Structures Interaction Technology Conference, Lake Tahoe, Nevada, March 1992.

2. Belvin, W.K., K.B. Elliott, and L.G. Horta, "A Synopsis of Test Results and Knowledge Gained from the Phase 0 CSI Evolutionary Model", 5th NASA/DOD Controls-Structures Interaction Technology Conference, Lake Tahoe, Nevada, March 1992.

3. O'Callahan, J., "A Procedure for an Improved Reduced System (IRS) Model", 7th International Modal Analysis Conference, Las Vegas, Nevada, 1989.

4. Olsen, N., "Burst Random Excitation", Sound and Vibration, ,pp. 20-23, 1983.

5. Allemang, R., "Investigation of Some Multiple Input/Output Frequency Response Function Experimental Modal Analysis Techniques," Doctor of Philosophy Dissertation, Department of Mechanical and Industrial Engineering, University of Cincinnati, 1980.

6. Zimmerman, R., and D. Hunt, "Multiple-Input Excitation Using Burst Random for Modal Testing", Sound and Vibration, October 1985.

7. Hunt, D., H. Vold, E. Peterson, and R. Williams, "Optimal Selection of Excitation Methods for Enhanced Modal Testing," AIAA/ASME/ASCE/AHS 25th Structures, Structural Dynamics & Materials Conference, and AIAA Dynamics Specialists Conference, Palm Springs, California, May, 1984.

8. Leuridan, J.M., and J.A. Kundrat, "Advanced Matrix Methods for Experimental Modal Analysis - A Multi-Matrix Method for Direct Parameter Extraction," 1st International Modal Analysis Conference, Orlando, Florida, 1982.

9. Vold, H., J. Kundrat, G. T. Rocklin, and, Russell R., "A Multi-input Modal Estimation Algorithm for Mini-Computers," SAE Paper Number 820194, 1982.

APPENDIX A

STRUT DRAWINGS

REVISIONS				
REV	ZONE	DESCRIPTION	DATE	APPROVED
A		REVISED STRUT, ADDED TORQUES	91-11-26	NWG.MRE.RG
B		ADDED -1 THRU -6 TO PL	91-12-16	

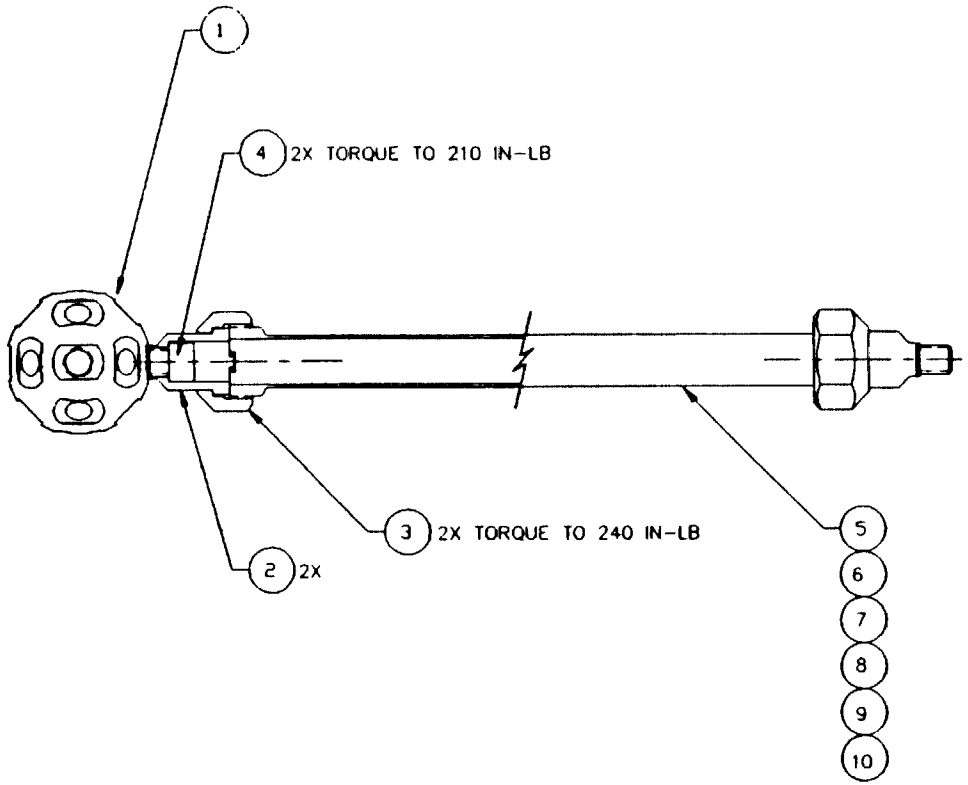

590-000 B

-6	-5	-4	-3	-2	-1	CAGE CODE	PART OR IDENTIFYING NO.	NOMENCLATURE OR DESCRIPTION	NOTE OR REMARK	FIND NO.
						QTY REQD		PARTS LIST		
1	-	-	-	-	-	-	590-024-6	STRUT	-	10
-	1	-	-	-	-	-	590-024-5	STRUT	-	9
-	-	1	-	-	-	-	590-024-4	STRUT	-	8
-	-	-	1	-	-	-	590-024-3	STRUT	-	7
-	-	-	-	1	-	-	590-024-2	STRUT	-	6
-	-	-	-	-	1	-	590-024-1	STRUT	-	5
2	2	2	2	2	2	-	590-014	SCREW, MODIFIED	-	4
2	2	2	2	2	2	-	590-013	NUT	-	3
2	2	2	2	2	2	-	590-012	STANDOFF	-	2
1	1	1	1	1	1	-	590-011	NODE	-	1

PART DASH NO	NEXT ASSY	USED ON
	APPLICATION	
CONTRACT NO.	-	

INTERPRET DWG PER DOD-STD-100
UNLESS OTHERWISE SPECIFIED DIMENSIONS ARE IN INCHES TOLERANCES ARE
ANGULAR ± 5'
DECIMAL X ± .1, .XX ± .03, .XXX ± .010
HOLES < Ø.500 +.003 -.000
SURFACE ROUGHNESS
BREAK CORNERS .005-.020
FILLET RADII .005-.020
DO NOT SCALE DRAWING

APPROVALS		DATE
DRAWN	M EVERMAN	91-10-21
CHECKED	R CRAWFORD	91-10-22
ENGR	M EVERMAN	91-10-22
MFG ENGR	R CRAWFORD	91-10-22
QA	N W GRANT	91-11-5
PROJ MGR	R GARZA	91-11-5
COMP	RFC	91-11-5

AEC-ABLE ENGINEERING COMPANY, INC GOLETA, CA

TITLE
CSI TRUSS
NODE-STRUT ASSY

SIZE	CAGE CODE	DWG NO	REV
C	55864	590-000	B
SCALE 1 / 1	WEIGHT -	SHEET 1 OF 1	

A-2
C-3

REV	ZONE	DESCRIPTION	DATE	APPR.
A		ADDED -2 CONFIGURATION	91-11-8	WMR, MRE, RG
B		ADDED .375 SLOT DIM	91-11-26	WMR, MRE, RG
C	A4	ADDED SPEC TO NOTE 1.		

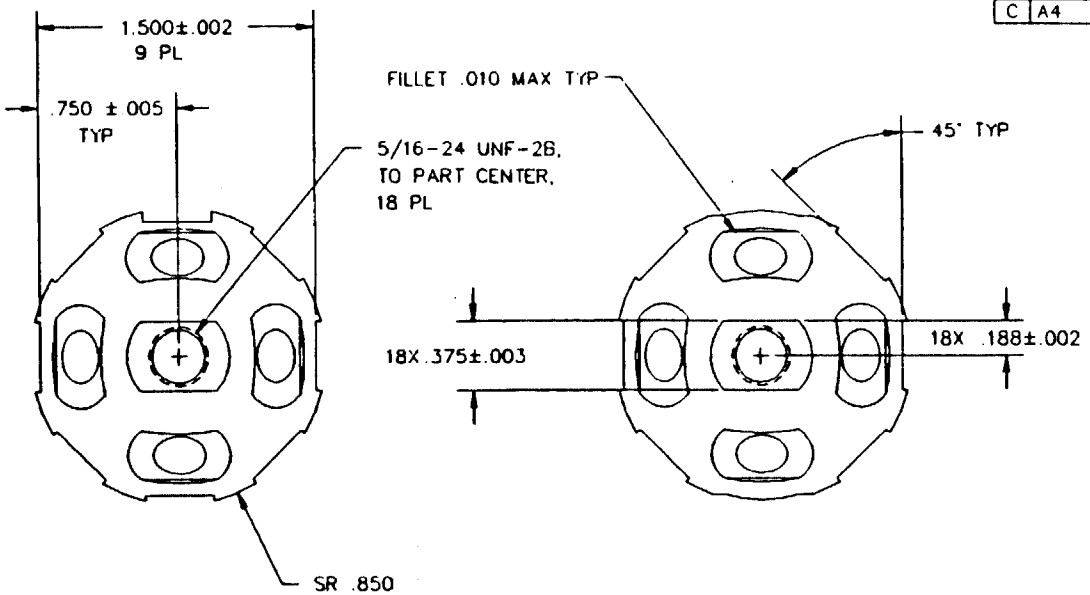

THIS VIEW REFERENCE ONLY

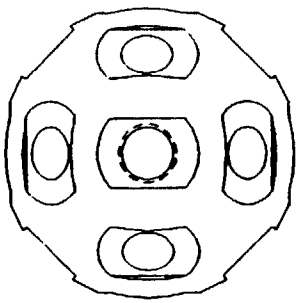

590-011 | C

NOTES:

1. MATERIAL: 7075-T6 PER QQ-A-225/9E.
2. ANGULAR TOLERANCE AND IMPLIED PERPENDICULAR OR PARALLEL SURFACES ±0°10'.
3. BRIGHT DIP AND ANODIZE GOLD PER MIL-A-8625, TYPE II, CLASS 2, .0002 MAX BUILDUP.
4. MATERIAL: 316 SST.

QTY REQD	CAGE CODE	PART OR IDENTIFYING NO.	NOMENCLATURE OR DESCRIPTION	NOTE OR REMARK	FIND NO.
PARTS LIST					
1	–	590-0011-2	NODE	4	2
1	–	590-011-1	NODE	1	1

PART DASH NO	NEXT ASSY	USED ON
-2	590F002	
APPLICATION		

CONTRACT NO. –

INTERPRET DRG PER DOD-STD-100
UNLESS OTHERWISE SPECIFIED DIMENSIONS ARE IN INCHES
TOLERANCES ARE:
ANGULAR ±–°
DECIMAL .X ± 1
.XX ± 03
.XXX ± 010
HOLES < Ø.500 +.005 −.000
SURFACE ROUGHNESS 125 (2)
BREAK CORNERS .005-.020
FILLET RADII .005-.020
DO NOT SCALE DRAWING

APPROVALS		DATE
DRAWN	M EVERMAN	91-10-10
CHECKED	R F C	91-10-28
ENGR	M R E	91-10-28
MFG ENGR	R F C	91-10-28
QA	N W GRANT	91-10-28
PROJ MGR	R GARZA	91-10-28
COMP	R F C	91-10-28

AFC-ABLE ENGINEERING COMPANY, INC GOLETA, CA

TITLE: NODE

SIZE	CAGE CODE	DWG NO	REV
C	55864	590-011	C

SCALE 2/1 | WEIGHT .159 LB | SHEET 1 OF 1

A-3

4 3 2 1

REVISIONS				
REV	ZONE	DESCRIPTION	DATE	APPROVED
A		ADDED DATUMS B AND C, WITH ASSOCIATED TOL CALLOUTS	91-11-26	WMR, MRE, RG
B	B1 A4	(1) RELOCATED DATUM "D" (2) ADDED SPEC TO NOTE 1		

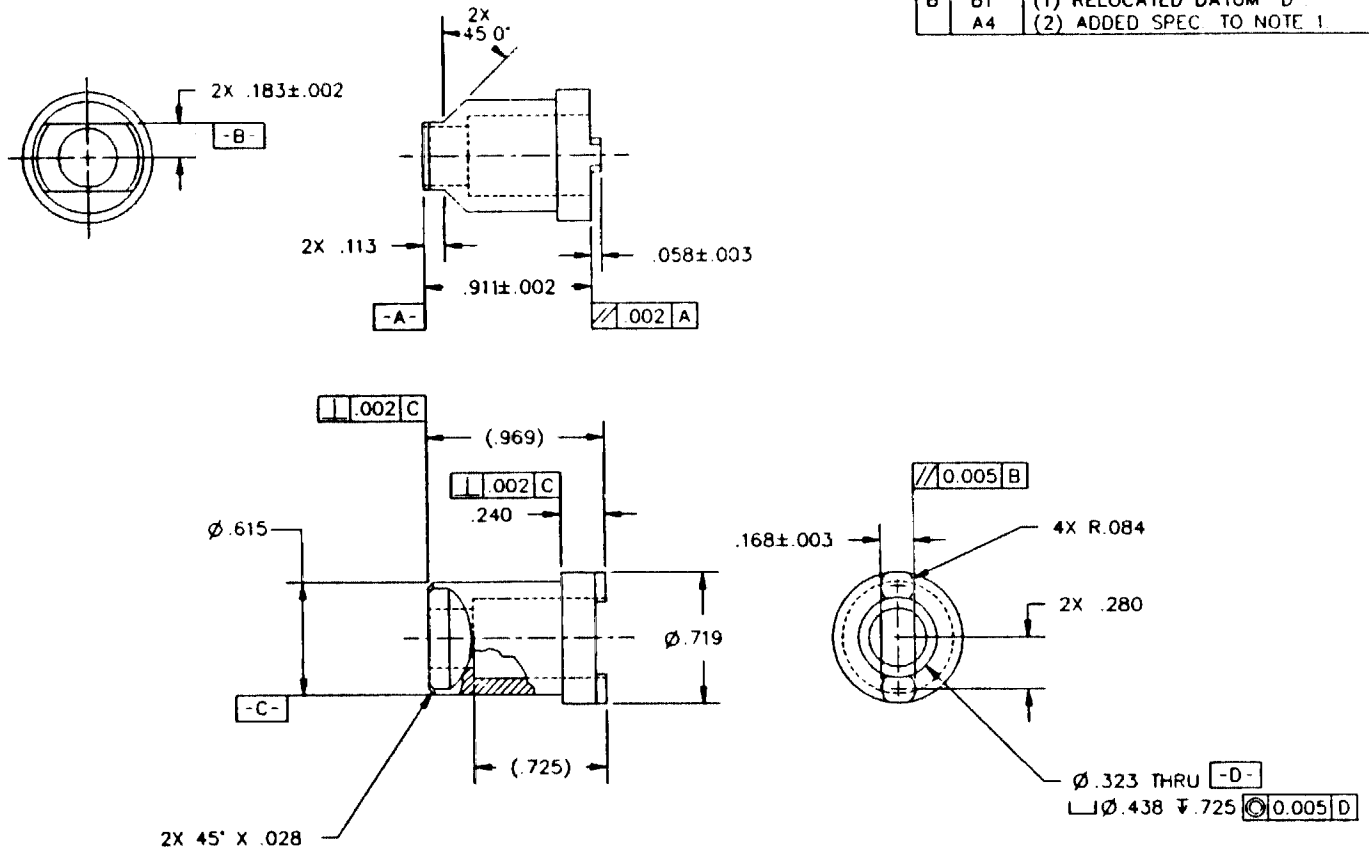

590-012 B

NOTES:

1. MATERIAL: 303 SS ASTM A582, CONDITION A.

2. .010 FILLET R MAX.
   DECIMAL TOL: .XX ±.01
   .XXX ±.005

3. TUMBLE DE-BURR.

PART DASH NO	NEXT ASSY	USED ON
	APPLICATION	

CONTRACT NO –

QTY REQD	CAGE CODE	PART OR IDENTIFYING NO.	NOMENCLATURE OR DESCRIPTION	NOTE OR REMARK	FIND NO.
			PARTS LIST		

INTERPRET DRG PER DOD-STD-100
UNLESS OTHERWISE SPECIFIED DIMENSIONS ARE IN INCHES
TOLERANCES ARE:
ANGULAR ± 5'
DECIMAL X ± 1
.XX ± .01
.XXX ± .005
HOLES < Ø.500 +.005 -.000
SURFACE ROUGHNESS 63 (2)
BREAK CORNERS .005 - .020
FILLET RADII .005 - .020
DO NOT SCALE DRAWING

APPROVALS		DATE
DRAWN	V EDWARDS	91-10-01
CHECKED	MRE	91-10-26
ENGR APPD	MRE	91-10-26
MFG APPD	RFC	91-10-26
QA	N W GRANT	91-10-26
PROJ APPD	R GARZA	91-10-26
COMP	RFC	91-10-26

AEC-ABLE ENGINEERING COMPANY, INC GOLETA, CA

TITLE: STANDOFF

SIZE	CAGE CODE	DWG NO	REV
C	55864	590-012	B

SCALE 2/1 WEIGHT .043 LB SHEET 1 OF 1

A-4

4 3 2 1

D C B A

REV	ZONE	DESCRIPTION	DATE	APPROVED
A		630 WAS 625	91-11-27	NWG, MRE, RG
B		NOTE 1 WAS 2024-T3511 STOCK		

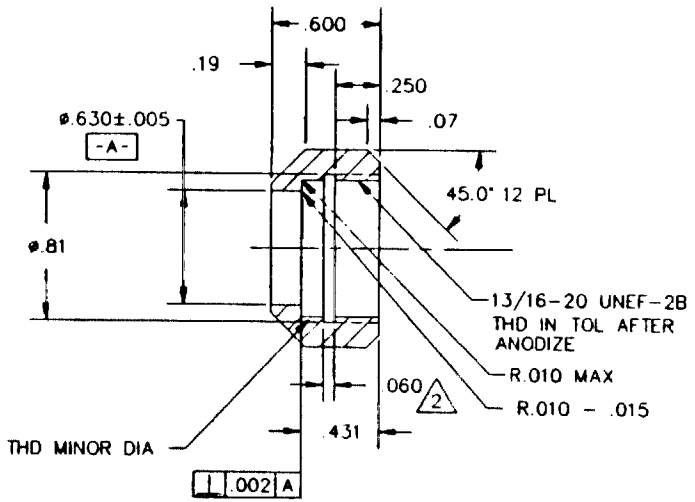

SECTION A-A

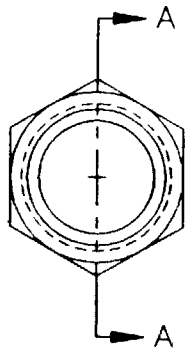

590-013 B

NOTES:

1. MATERIAL: 2024-T351 15/16 HEX STOCK, PER AMS 4120.
2. THD RELIEF MAY BE .031 FULL RADIUS.
3. TUMBLE DE-BURR.
4. BRIGHT DIP AND ANODIZE GOLD PER MIL-A-8625, TYPE II, CLASS 2, .0002 MAX BUILDUP.

QTY REQD	CAGE CODE	PART OR IDENTIFYING NO.	NOMENCLATURE OR DESCRIPTION	NOTE OR REMARK	FIND NO.
		PARTS LIST			

INTERPRET DWG PER DOD-STD-100
UNLESS OTHERWISE SPECIFIED
DIMENSIONS ARE IN INCHES
TOLERANCES ARE:
ANGULAR ± 5°
DECIMAL X ± 1
XX ± 03
XXX ± 010
HOLES < ø.500 +.005 -.001
SURFACE ROUGHNESS
BREAK CORNERS .005-.020
FILLET RADII .005-.020
DO NOT SCALE DRAWING

APPROVALS		DATE
DRAWN	V EDWARDS	91-10-01
CHECKED	M R E	91-10-28
ENGR	M R E	91-10-28
MFG APPR	R F C	91-10-28
QA	N W GRANT	91-10-28
PROJ MGR	R GARZA	91-10-28
COMP	R F C	91-10-28

AEC-ABLE ENGINEERING COMPANY, INC GOLETA, CA

TITLE: NUT

PART DASH NO.	NEXT ASSY	USED ON
	APPLICATION	

CONTRACT NO. —

SIZE	CAGE CODE	DWG NO.	REV
C	55864	590-013	B

SCALE 2/1 WEIGHT 017 LB SHEET 1 OF 1

A-5

4 3 2 1

D C B A

REVISIONS				
REV	ZONE	DESCRIPTION	DATE	APPROVED
A		THD CALLOUT IS NOW REF	91-12-2	WMR, MRE, RG
B		ADDED DATUM "A" AND CONCENTRICITY TOLERANCE		

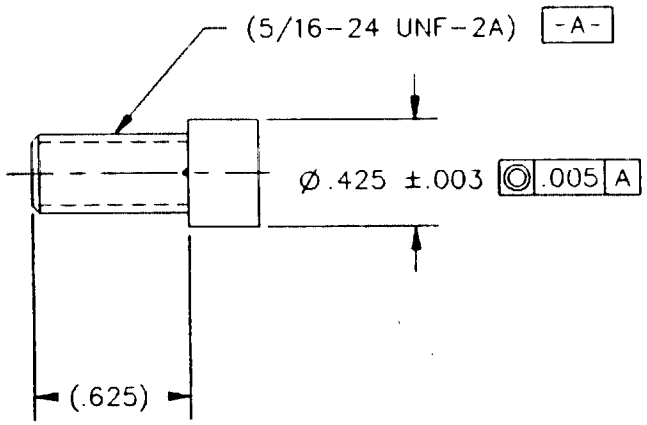

NOTES:

1. MATERIAL: 5/16-24 X 5/8 LG. ALLOY BOLT PER NAS 1351-5-10.

QTY REQD	CAGE CODE	PART OR IDENTIFYING NO.	NOMENCLATURE OR DESCRIPTION	NOTE OR REMARK	FIND NO.
PARTS LIST					

PART DASH NO.	NEXT ASSY	USED ON
	APPLICATION	
CONTRACT NO.	–	

INTERPRET DWG PER DOD-STD-100
UNLESS OTHERWISE SPECIFIED DIMENSIONS ARE IN INCHES
TOLERANCES ARE
ANGULAR ± 5°
DECIMAL X ± .1
.XX ± .03
.XXX ± .010
HOLES < Ø.500 +.005 −.001
SURFACE ROUGHNESS 63
BREAK CORNERS .005-.020
FILLET RADII .005-.020
DO NOT SCALE DRAWING

APPROVALS		DATE
DRAWN	V.EDWARDS	91-10-02
CHECKER	MRE	91-10-28
ENGR	MRE	91-10-28
TECH DIR	RFC	91-10-28
QA	N.W.GRANT	91-10-28
PROJ MGR	R.GARZA	91-10-28
CORP	RFC	91-10-28

AEC-ABLE ENGINEERING COMPANY, INC GOLETA, CA

TITLE: SCREW, MODIFIED

SIZE	CAGE CODE	DWG NO.	REV
B	55864	590-014	B

SCALE 2/1 WEIGHT 019 LB SHEET 1 OF 1

590-014 B

ABLE-AUTOCAD 91-05-23

A-6

REV	ZONE	DESCRIPTION	DATE	APPROVED
A		094 WAS 093	91-11-26	WMR, MRE, RG.
B	C4	(1) ADDED DATUM "A"		
	D1	(2) RELOCATED PARALLELISM CALLOUT & ADDED REFERENCE "A"		
	A4	(3) ADDED SPEC TO NOTE 1		

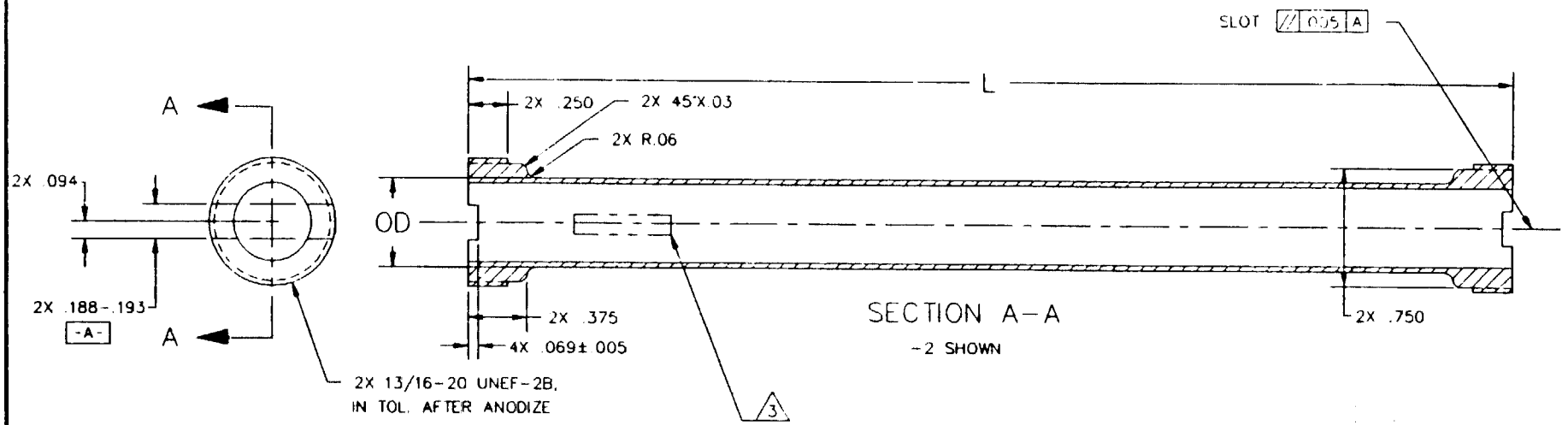

DASH NO.	OD ±.002	L ± 004	TUBE AREA (REF)
-1	STOCK(.875)	6.678	.491
-2	.587	6.678	.074
-3	.661	6.678	.147
-4	.787	6.678	.290
-5	.576	6.678	.064
-6	.579	10.820	.067

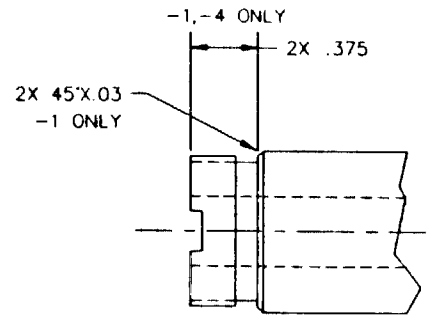

DETAIL, -1 AND -4

590-024 B

NOTES:

1. MATERIAL: 6061-T6 TUBING, .875 OD x .250 WALL (-1 ONLY). ALL OTHERS: 2024-T3 TUBING, .875 OD x .188 WALL, PER WW-T-700/3.
2. BRIGHT DIP AND ANODIZE GOLD PER MIL-A-8625, TYPE II, CLASS 2.
3. FOR EACH STRUT, RECORD ACTUAL LENGTH, WEIGHT AND TUBE OD IN THE QA CSI LOGBOOK UNDER THE NEXT UNIQUE 5-DIGIT SERIAL NUMBER. STAMP SERIAL NUMBER WITH WHITE EPOXY INK IN INDICATED AREA WITH 09-15 HIGH LETTERS.

CAGE CODE	PART OR IDENTIFYING NO.	NOMENCLATURE OR DESCRIPTION	NOTE OR REMARK	FIND NO.
QTY REQD		PARTS LIST		

PART DASH NO	NEXT ASSY	USED ON
CONTRACT NO	APPLICATION	

INTERPRET DWG PER DOD-STD-100
UNLESS OTHERWISE SPECIFIED DIMENSIONS ARE IN INCHES
TOLERANCES ARE:
ANGULAR ± 5°
DECIMAL X ± 1, XX ± 03, XXX ± 010
HOLES < Ø 500 : ⁺⁰⁰⁸₋₀₀₀
SURFACE ROUGHNESS 63
BREAK CORNERS .005-.020
FILLET RADII .005-.020
DO NOT SCALE DRAWING

	APPROVALS	DATE
DRAWN	M EVERMAN	91-11-14
CHECKED	R GARZA	91-11-21
ENGR	MRE	91-11-21
MFG	R F CRAWFORD	91-11-21
QA	N W GRANT	91-11-21
ENGR APPR	R GARZA	91-11-21
COMP	R F CRAWFORD	91-11-21

AFC-ABLE ENGINEERING COMPANY, INC GOLETA, CA

TITLE: STRUT

SIZE	CAGE CODE	DWG NO.	REV
C	55864	590-024	B

SCALE 2/1 WEIGHT — SHEET 1 OF 1

A-7

4 3 2 1

APPENDIX B

STRUT IDENTIFICATION NUMBERS FOR TRUSS TEST SECTIONS

STRUTS I.D. TRUSS SECTION NO. 1

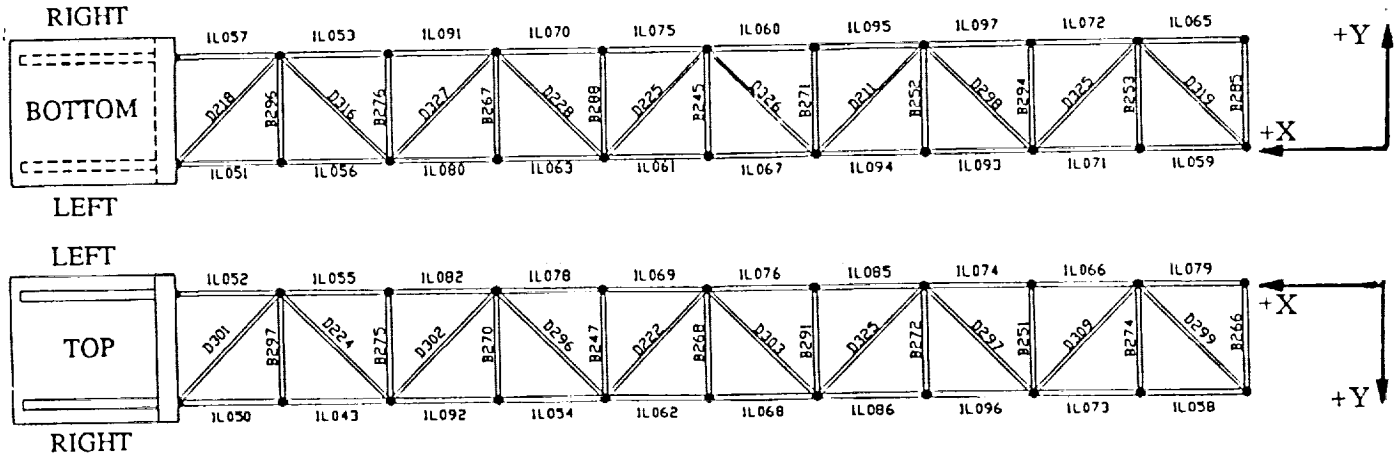

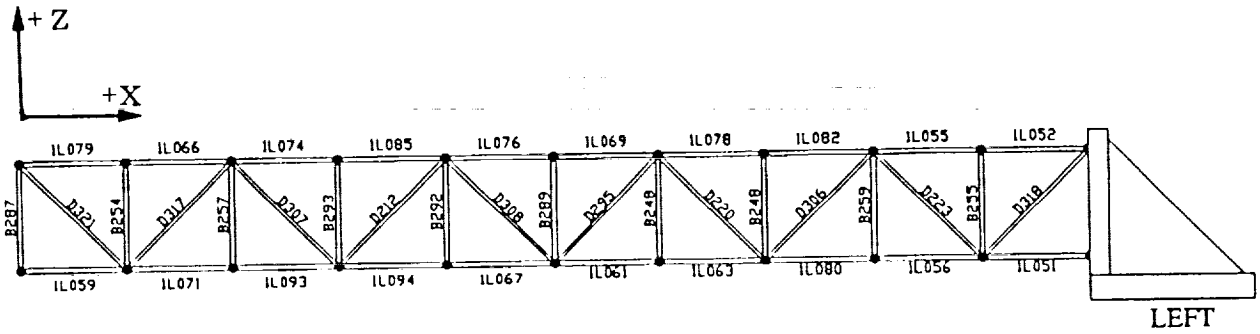

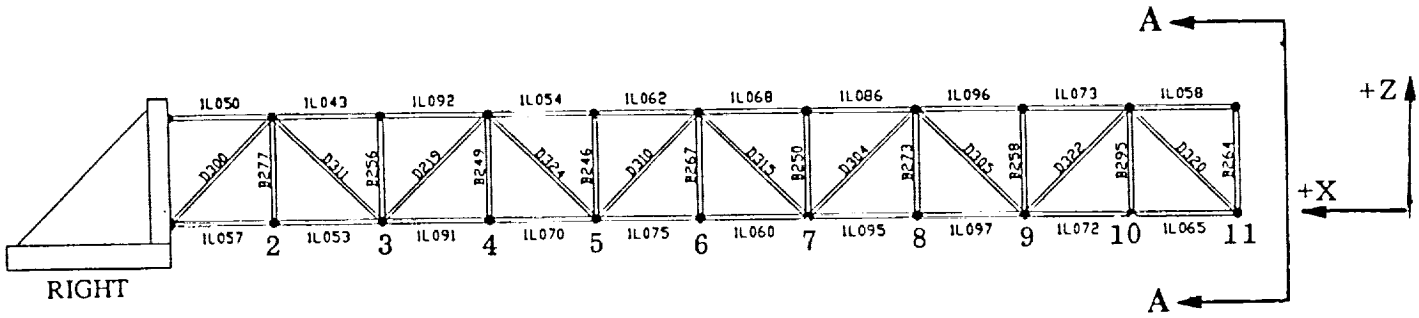

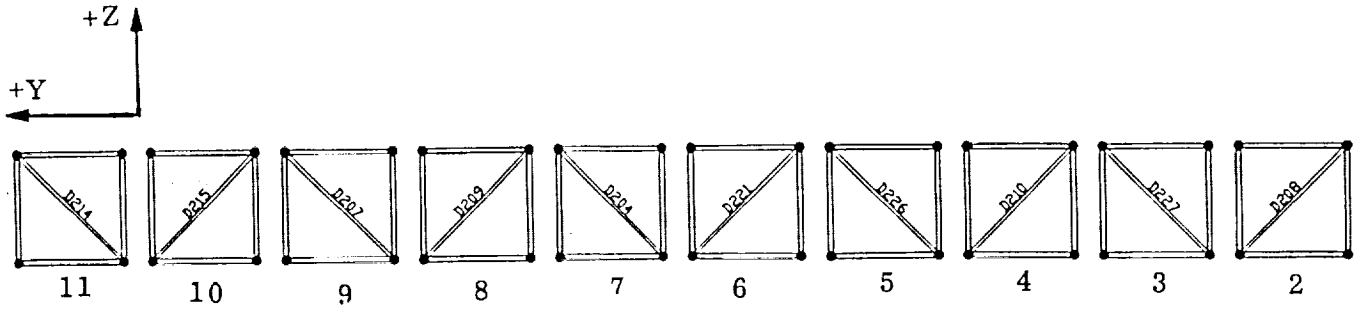

VIEW A-A
(BATTEN PLANES)

STRUTS I.D. TRUSS SECTION NO. 2

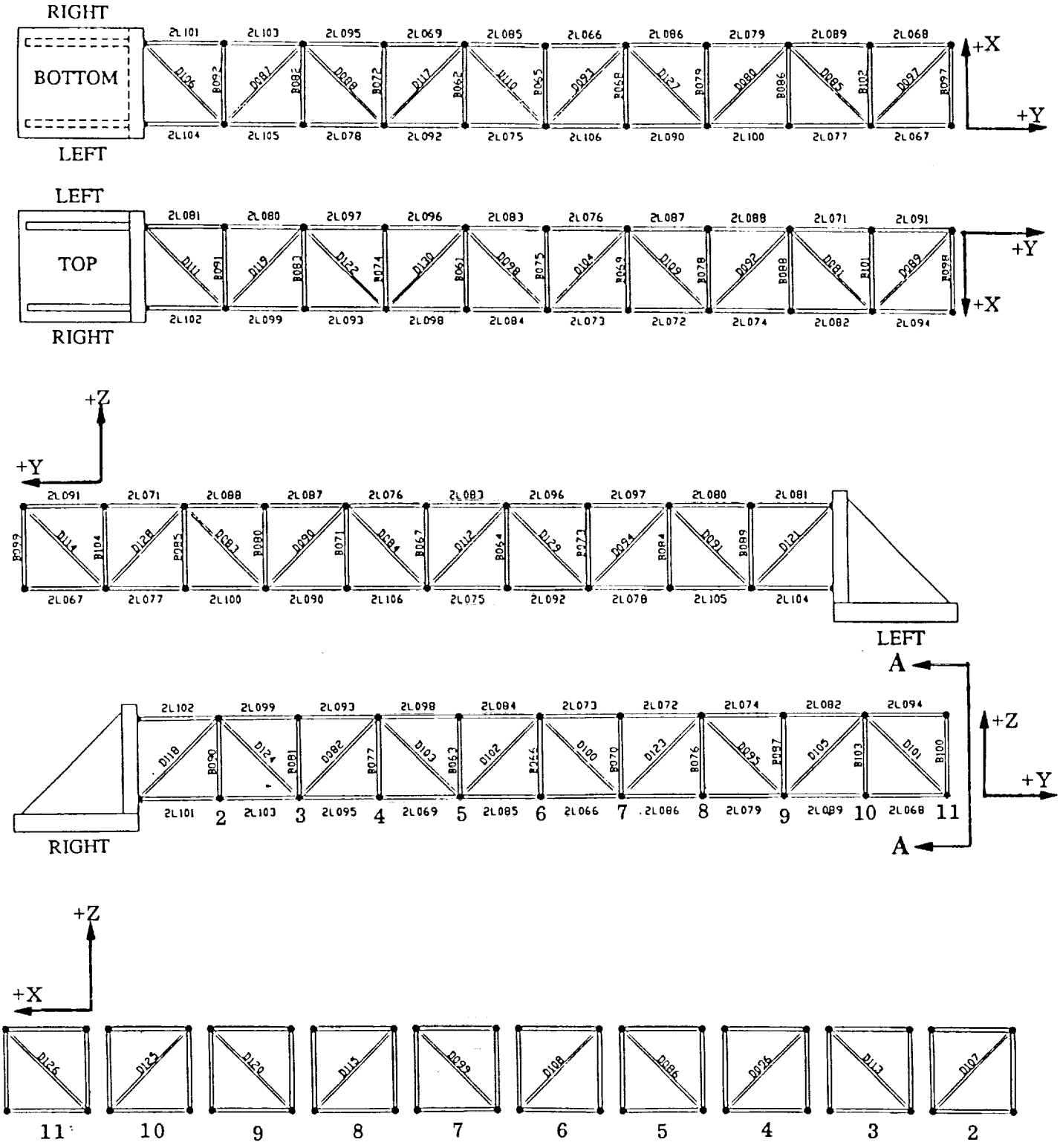

VIEW A-A
(BATTEN PLANES)

STRUTS I.D. TRUSS SECTION NO. 3

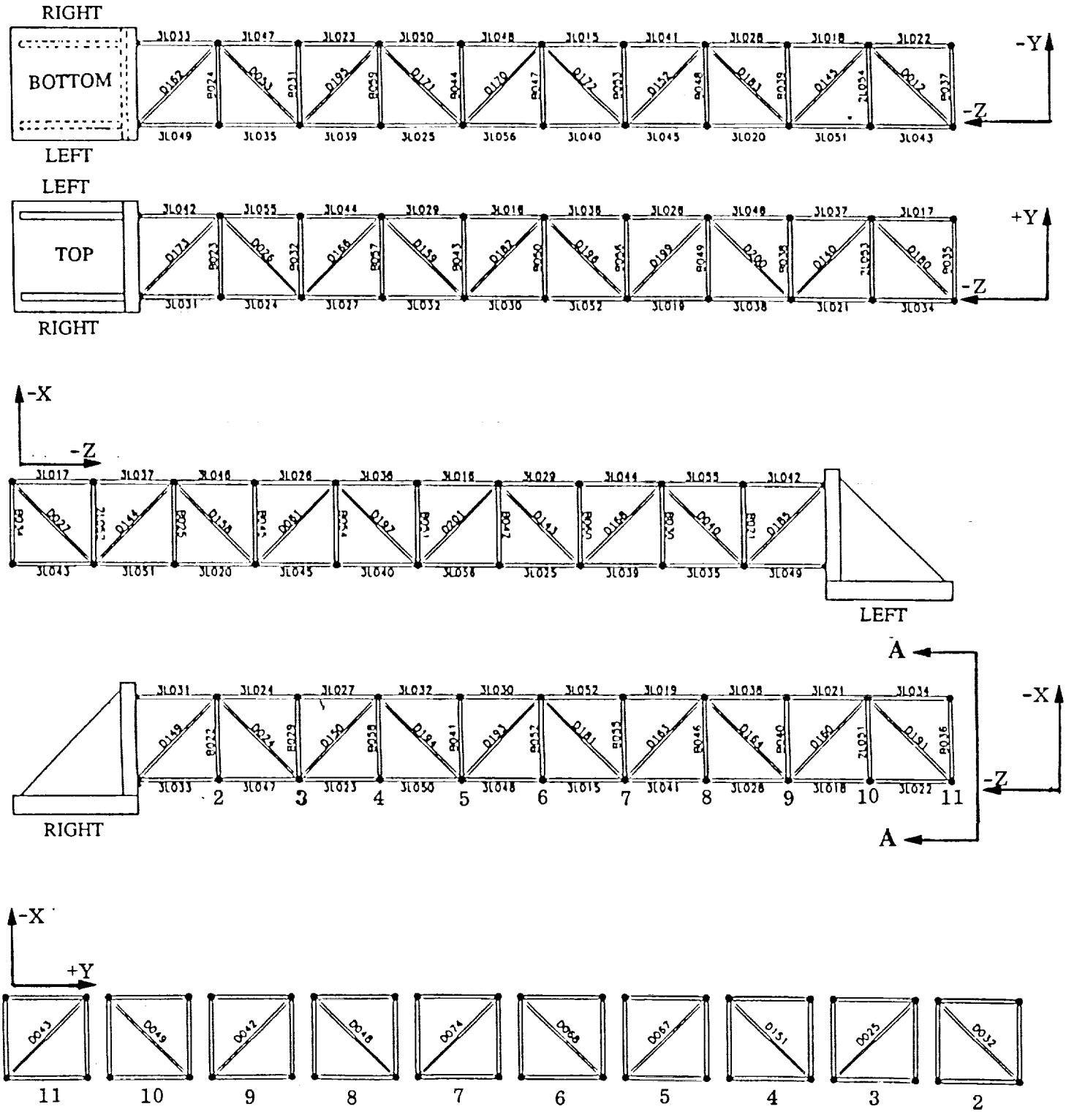

VIEW A-A
(BATTEN PLANES)

STRUTS I.D. TRUSS SECTION NO. 4

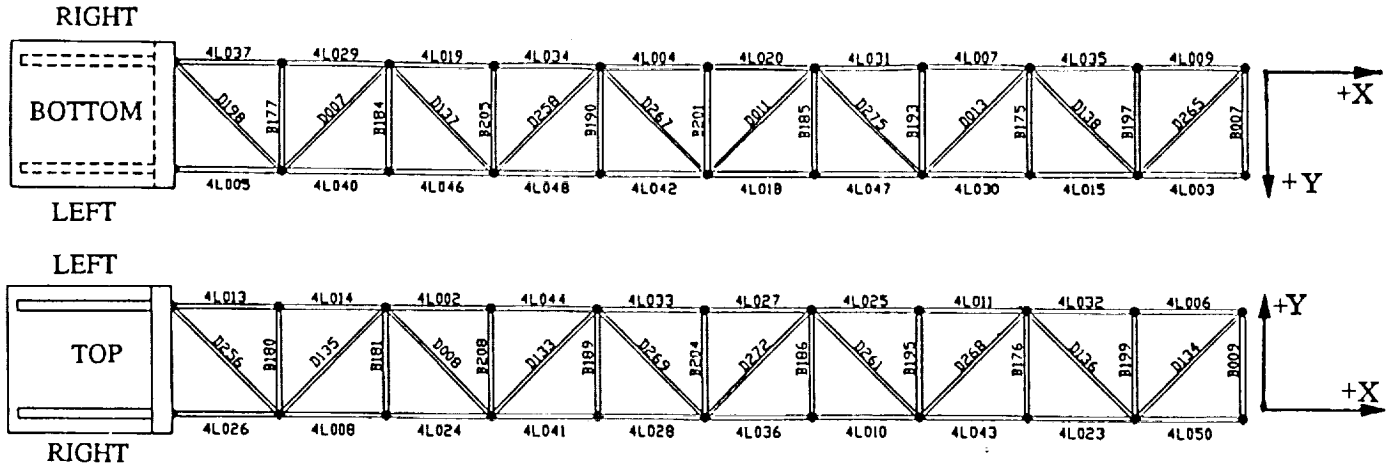

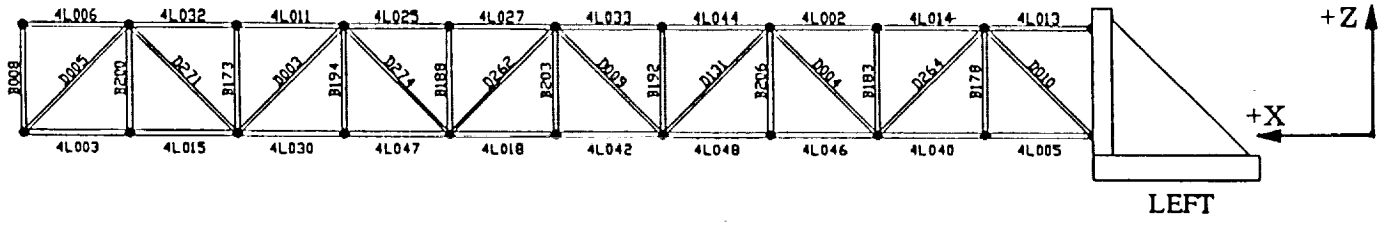

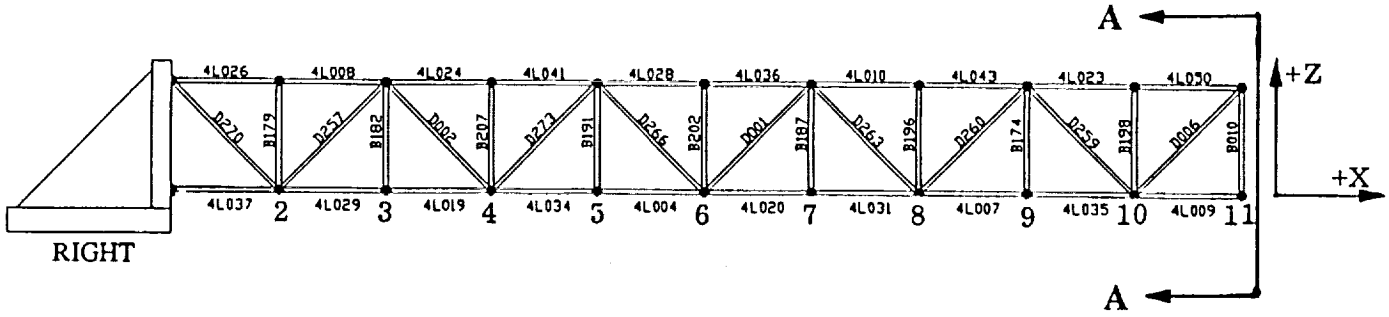

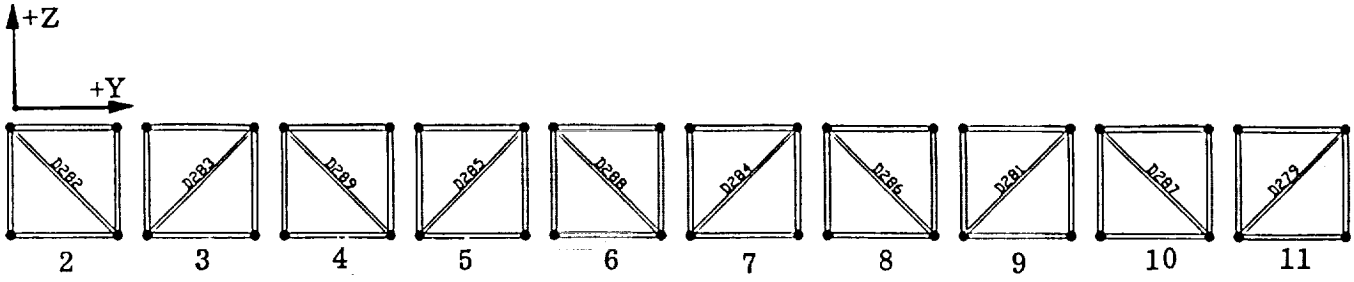

VIEW A-A
(BATTEN PLANES)

APPENDIX C

TEST AND ANALYSIS RESULTS FOR TRUSS SECTION NO. 1 DYNAMIC TESTS

Table C-1 Test Log of Modal Tests of Section 1 - Free-Free Tests

Test No.	Type of Excitation	Frequency Range	Comments
1a	Continuous Random	0 - 200 Hz	Free-Free test setup, with Section 1 test item supported at four points with seperate bungee cords. Dual shaker setup, with one shaker at each end supported by seperate bungee cords. Shaker at test point no. 2 oriented to apply loading in the horizontal plane with a skew angle of 45 degrees relative to the longitudinal and lateral axes. Shaker at test point no. 21 oriented to apply loading in the vertical plane with a skew angle of 45 degrees relative to vertical and lateral axes.
1b	Continuous Random	0 - 400 Hz	Same test configuration as test no. 1a.
1c	Continuous Random	0 - 800 Hz	Same test configuration as test no. 1a.
1d	Continuous Random	109.25 Hz - 121.75 Hz	Same test configuration as test no. 1a. Zoom for 1st torsional mode.
1e	Continuous Random	128.75 Hz - 141.25 Hz	Same test configuration as test no. 1a. Zoom for 1st set of bending modes.
1f	Continuous Random	217.25 Hz - 229.75 Hz	Same test configuration as test no. 1a. Zoom for 2nd torsional mode.
1g	Continuous Random	244.75 Hz - 257.25 Hz	Same test configuration as test no. 1a. Zoom for 2nd set of bending modes.
1h	Continuous Random	300.00 Hz - 500.00 Hz	Same test configuration as test no. 1a. Zoom for higher order bending modes and 1st axial mode.
1i	Continuous Random	481.75 Hz - 494.25 Hz	Same test configuration as test no. 1a. Zoom for 1st axial mode.

Table C-1 Test Log of Modal Tests of Section 1 - Cantilevered Tests

Test No.	Type of Excitation	Frequency Range	Comments
1j	Continuous Random	0 - 200 Hz	Cantilevered test setup, with Section 1 test item affixed at one end to the test fixture which had been previously bolted to the laboratory concrete floor. Single shaker setup, with the shaker supported by a bungee cord. Shaker at test point no. 21, oriented to apply loading in the horizontal plane with a skew angle of 45 degrees relative to the longitudinal and lateral axes.
1k	Continuous Random	0 - 400 Hz	Same test configuration as test no. 1j.
1l	Continuous Random	18.25 Hz - 30.75 Hz	Same test configuration as test no. 1j. Zoom for 1st set of bending modes.
1m	Continuous Random	52.75 Hz - 65.25 Hz	Same test configuration as test no. 1j. Zoom for 1st torsional mode.
1n	Continuous Random	101.25 Hz - 113.75 Hz	Same test configuration as test no. 1j. Zoom for 2nd set of bending modes.
1o	Continuous Random	166.75 Hz - 179.25 Hz	Same test configuration as test no. 1j. Zoom for 2nd torsional mode.
1p	Continuous Random	210.75 Hz - 223.25 Hz	Same test configuration as test no. 1j. Zoom for higher order modes.
1q	Continuous Random	225.75 Hz - 238.25 Hz	Same test configuration as test no. 1j. Zoom for 1st axial mode.

Table C-2 Modal Testing Parameters Summary - Section 1 Free-Free Modes

Mode No.	Nat Freq (Hz)	Excitation Method	Frequency Span (Hz)	No. Avg	Test No.	Type of Window	% Overlap	Sample Length(Sec)	Frequency Resolution (Hz)	No. of Freq Lines	Function Universal File Name ( ).unv
1	115.0	Continuous Random	109.25 - 121.75	30	1d	Hanning	50	32	0.03125	400	s1fffu109
2	134.7	Continuous Random	128.75 - 141.25	30	1e	Hanning	0	32	0.03125	400	s1fffu129
3	135.2	Continuous Random	128.75 - 141.25	30	1e	Hanning	0	32	0.03125	400	s1fffu129
4	223.1	Continuous Random	217.25 - 229.75	30	1f	Hanning	50	32	0.03125	400	s1fffu217
5	250.5	Continuous Random	244.75 - 257.25	30	1g	Hanning	0	32	0.03125	400	s1fffu244
6	251.1	Continuous Random	244.75 - 257.25	30	1g	Hanning	0	32	0.03125	400	s1fffu244
7	488.2	Continuous Random	481.75 - 494.25	30	1i	Hanning	50	32	0.03125	400	s1fffu482

Table C-2 Modal Testing Parameters Summary - Section 1 Cantilever Modes

Mode No.	Nat Freq (Hz)	Excitation Method	Frequency Span (Hz)	No. Avg	Test No.	Type of Window	% Overlap	Sample Length(Sec)	Frequency Resolution (Hz)	No. of Freq Lines	Function Universal File Name ( ).unv
1	24.2	Continuous Random	18.25 - 30.75	30	1l	Hanning	0	32	0.03125	400	s1cafu18
2	25.2	Continuous Random	18.25 - 30.75	30	1l	Hanning	0	32	0.03125	400	s1cafu18
3	59.0	Continuous Random	52.75 - 65.25	30	1m	Hanning	0	32	0.03125	400	s1cafu53
4	107.1	Continuous Random	101.25 - 113.75	30	1n	Hanning	0	32	0.03125	400	s1cafu101
5	107.9	Continuous Random	101.25 - 113.75	30	1n	Hanning	0	32	0.03125	400	s1cafu101
6	173.0	Continuous Random	166.75 - 179.25	30	1o	Hanning	0	32	0.03125	400	s1cafu167
7	234.0	Continuous Random	225.75 - 238.25	30	1q	Hanning	0	32	0.03125	400	s1cafu226

Table C-3 Modal Data Analysis Parameters Summary - Section 1 Free-Free Modes

Mode No.	Nat Freq (Hz)	Curve-Fit Technique	Frequency Range (Hz)	No. of Resp Pts	Matrix Size	No. of Roots	Reference Points	Shape/Parameter File Name ( ).unv	Model Universal File Name ( ).unv
1	115.0	Polyref	109.25 - 121.75	44	16	2	2y+, 21z-	s1ffmodes	s1fftestpt
2	134.7	Polyref	128.75 - 141.25	44	16	4	2y+, 21z-	s1ffmodes	s1fftestpt
3	135.2	Polyref	128.75 - 141.25	44	16	4	2y+, 21z-	s1ffmodes	s1fftestpt
4	223.1	Polyref	217.25 - 229.75	44	16	6	2y+, 21z-	s1ffmodes	s1fftestpt
5	250.5	Polyref	244.75 - 257.25	44	16	6	2y+, 21z-	s1ffmodes	s1fftestpt
6	251.1	Polyref	244.75 - 257.25	44	16	6	2y+, 21z-	s1ffmodes	s1fftestpt
7	488.2	Polyref	481.75 - 494.25	44	16	8	2y+, 21z-	s1ffmodes	s1fftestpt

Table C-3 Modal Data Analysis Parameters Summary - Section 1 Cantilever Modes

Mode No.	Nat Freq (Hz)	Curve-Fit Technique	Frequency Range (Hz)	No. of Resp Pts	Matrix Size	No. of Roots	Reference Point	Shape/Parameter File Name ( ).unv	Model Universal File Name ( ).unv
1	24.2	Polyref	18.25 - 30.75	45	16	5	21x+	s1camodes	s1catestpt
2	25.2	Polyref	18.25 - 30.75	45	16	5	21x+	s1camodes	s1catestpt
3	59.0	Polyref	52.75 - 65.25	45	16	2	21x+	s1camodes	s1catestpt
4	107.1	Polyref	101.25 - 113.75	45	16	6	21x+	s1camodes	s1catestpt
5	107.9	Polyref	101.25 - 113.75	45	16	6	21x+	s1camodes	s1catestpt
6	173.0	Polyref	166.75 - 179.25	45	16	2	21x+	s1camodes	s1catestpt
7	234.0	Polyref	225.75 - 238.25	45	16	6	21x+	s1camodes	s1catestpt

O U T P U T F R O M G R I D P O I N T W E I G H T G E N E R A T O R

REFERENCE POINT = 0

M O

```
*  1.291826E-01  6.830474E-18  1.585646E-18 -7.433561E-17  3.669689E-04  4.733898E-04 *
*  6.830474E-18  1.291826E-01  6.146071E-17 -3.669689E-04 -2.746880E-15  6.462786E+00 *
*  1.585646E-18  6.147426E-17  1.291826E-01 -4.733898E-04 -6.462786E+00  2.818641E-15 *
* -7.367154E-17 -3.669689E-04 -4.733898E-04  5.485237E+00  4.733898E-02 -3.669689E-02 *
*  3.669689E-04 -2.770191E-15 -6.462786E+00  4.733898E-02  4.431185E+02  1.078682E-01 *
*  4.733898E-04  6.462786E+00  2.835934E-15 -3.669689E-02  1.078682E-01  4.431975E+02 *
```

S

```
*  1.000000E+00  0.000000E+00  0.000000E+00 *
*  0.000000E+00  1.000000E+00  0.000000E+00 *
*  0.000000E+00  0.000000E+00  1.000000E+00 *
```

DIRECTION MASS AXIS SYSTEM (S)	MASS	X-C.G.	Y-C.G.	Z-C.G.
X	1.291826E-01	-5.754307E-16	-3.664503E-03	2.840700E-03
Y	1.291826E-01	5.002832E+01	-2.126356E-14	2.840700E-03
Z	1.291826E-01	5.002832E+01	-3.664503E-03	2.181905E-14

I(S)

```
*  5.485234E+00 -2.365609E-02  1.833805E-02 *
* -2.365609E-02  1.197962E+02 -1.078669E-01 *
*  1.833805E-02 -1.078669E-01  1.198752E+02 *
```

I(Q)

```
*  5.485226E+00                             *
*                1.197208E+02               *
*                             1.199505E+02  *
```

Q

```
*  1.000000E+00  2.616939E-04  0.000000E+00 *
* -2.145158E-04  8.197201E-01  5.727643E-01 *
*  1.498889E-04 -5.727643E-01  8.197201E-01 *
```

Section-1 Truss Updated FEM Mass Properties (Cantilevered and Free-Free) With Sensor Mass Included

GRAVITY

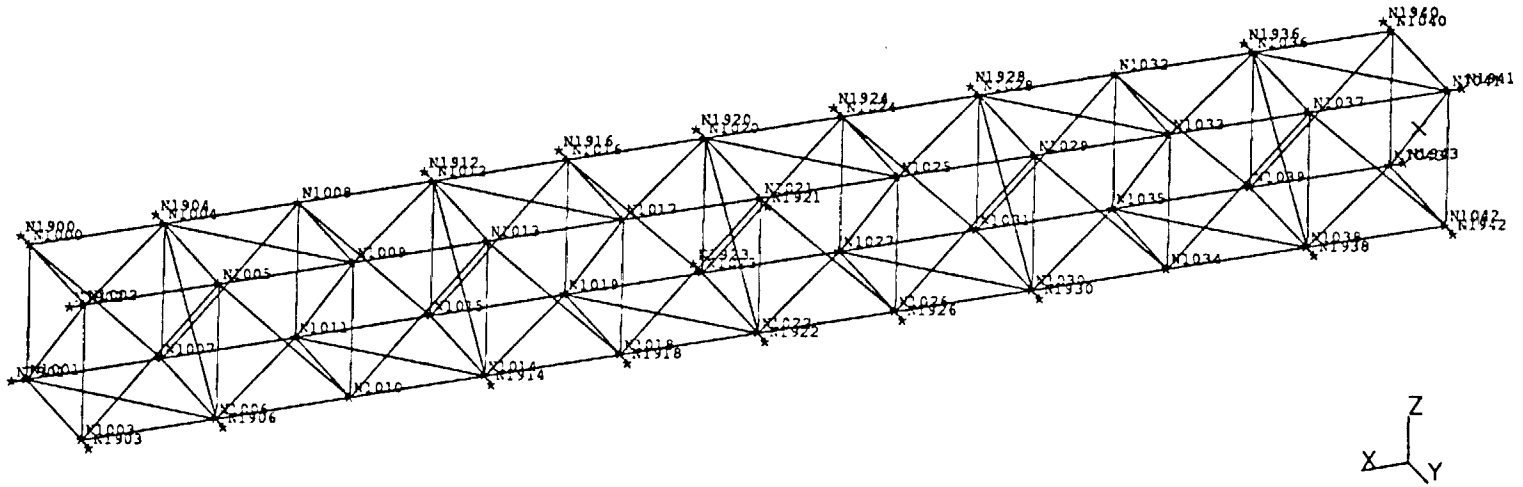

CANTILEVERED END

SDRC I-DEAS V1: FE Modeling & Analysis 18-MAR-92 14:21:07

Database: /umere3/tan/cal/sscl/alt@ Units : IN
View : none, none, none, none Display : none, none, none, none
Task: Post Processing Model Dir: 1-MAIN
Model: 2-10_BAY Associated Workset: 2-MORRING_SET2

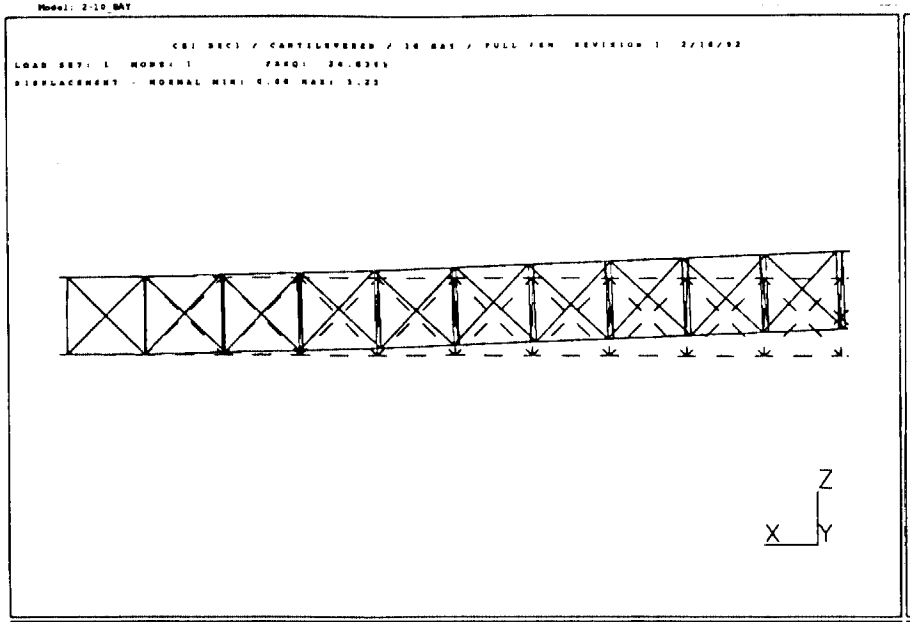

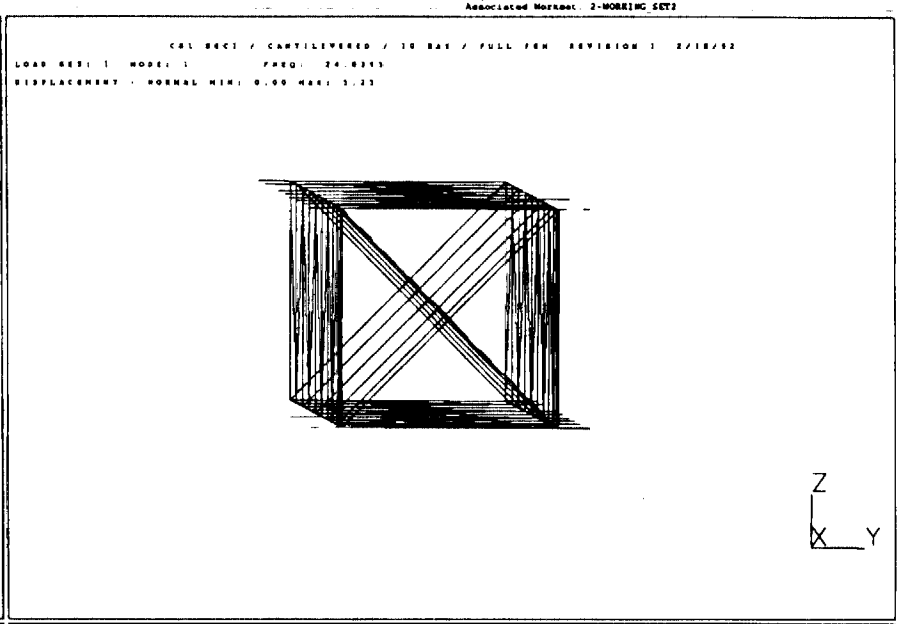

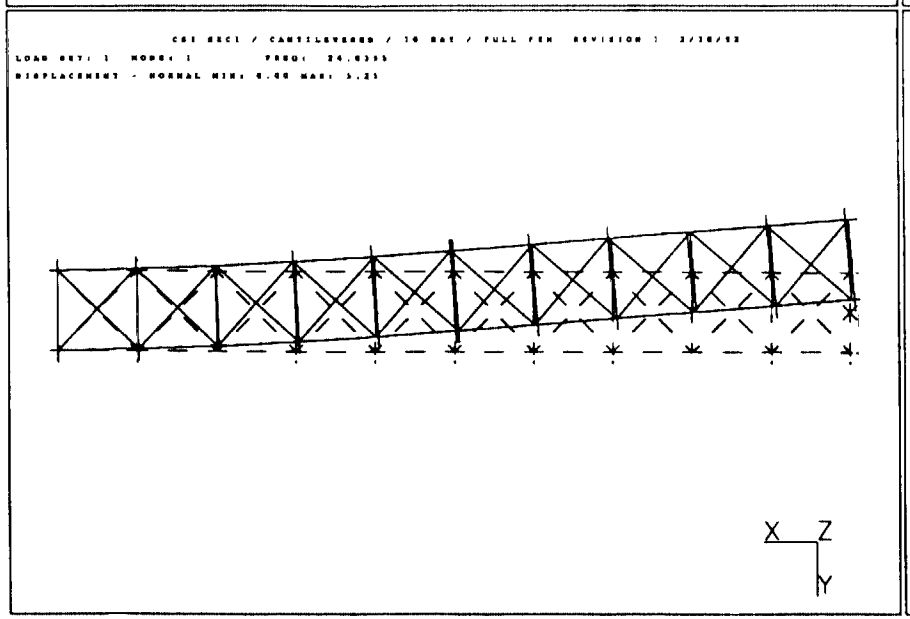

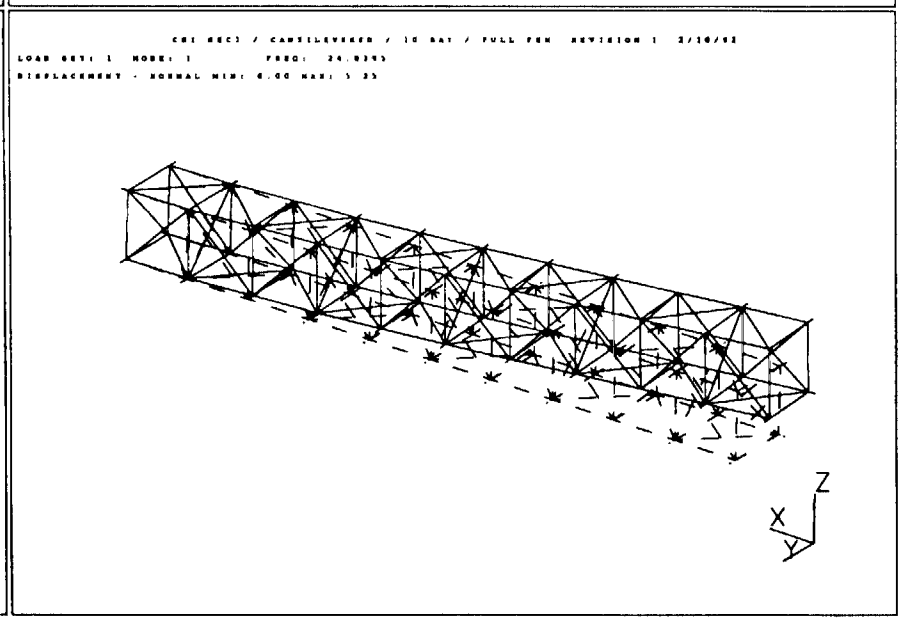

SDRC I-DEAS V1: FE_Modeling_&_Analysis 18-MAR-92 14:20:54

Database: /umarel/tan/cei/eeci/eltp
View : none, none, none, none
Task: Post Processing
Model: 2-10_BAY

Units : IN
Display : none, none, none, none
Model Blk: 1-MAIN
Associated Workset: 2-WORKING_SET2

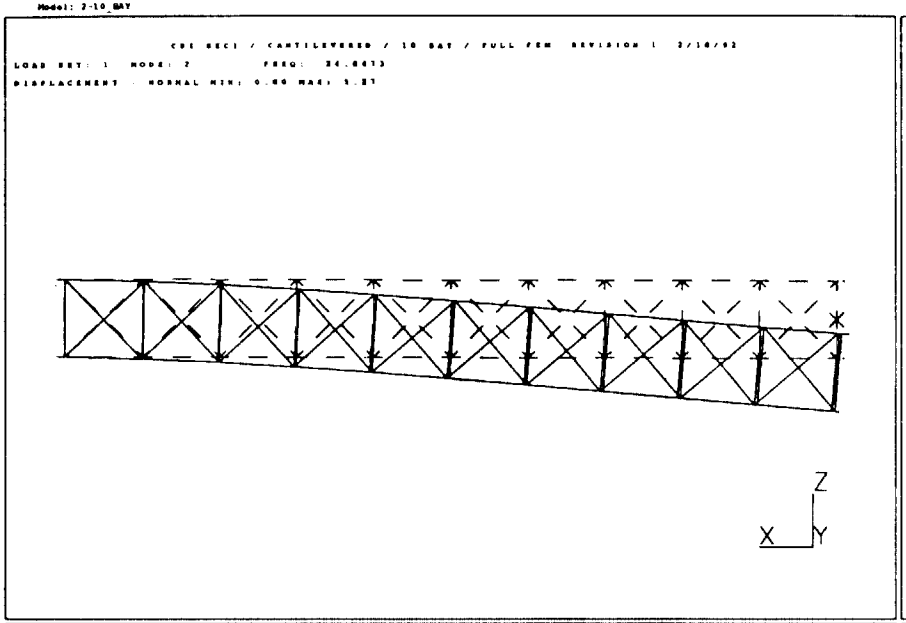

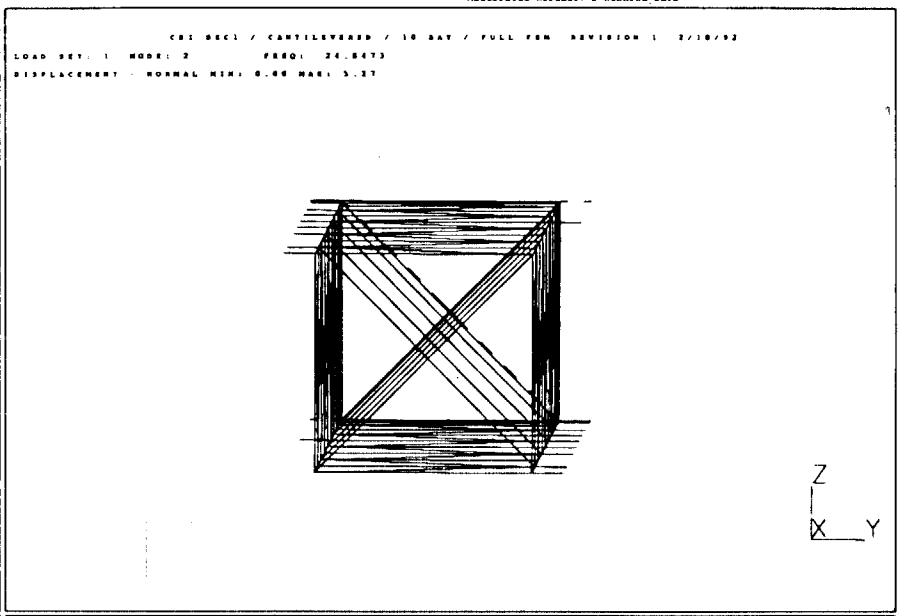

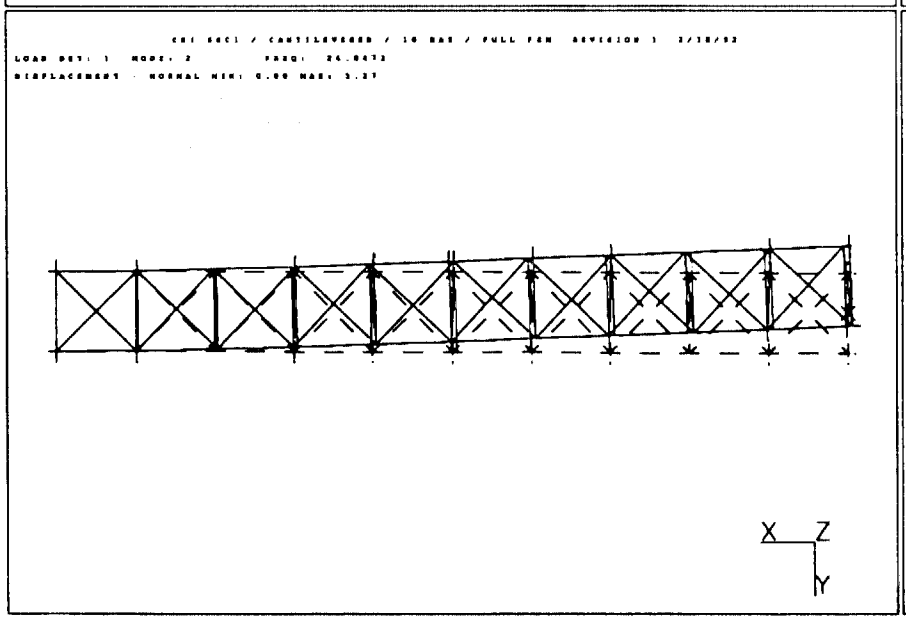

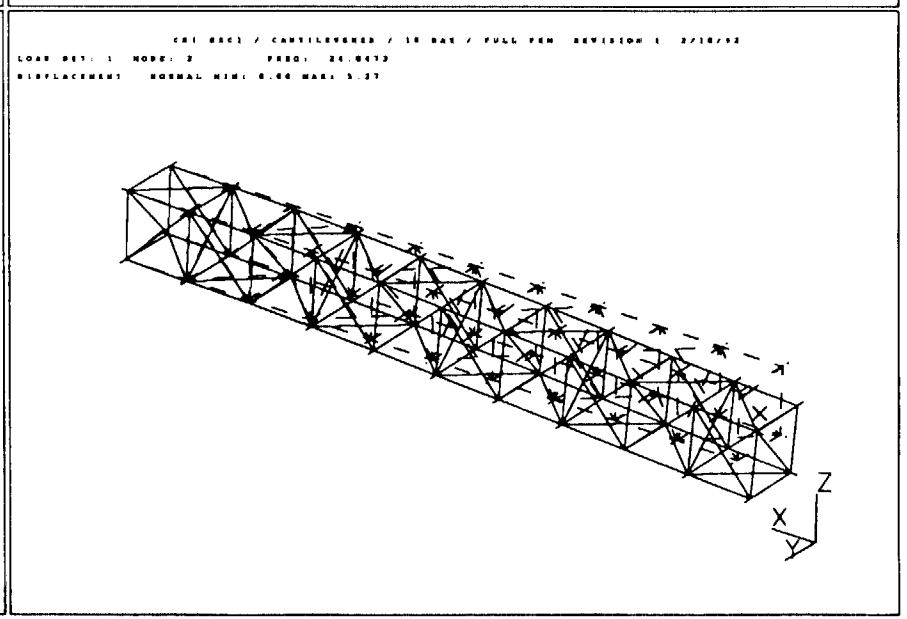

SDRC I-DEAS VI: FE_Modeling_&_Analysis

18-MAR-92 14:21:23

Database: /ubora3/tan/cai/asc1/oltp
View : none, none, none, none
Task: Post Processing
Model: 2-10_BAY

Units : IN
Display : none, none, none, none
Model Bin: 1-MAIN
Associated Workset: 2-WORKING SET2

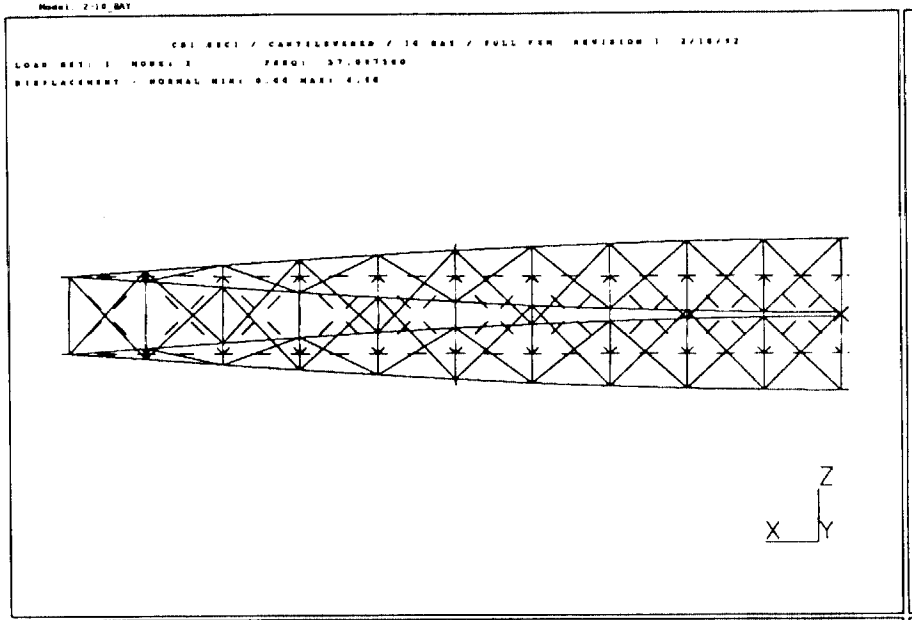

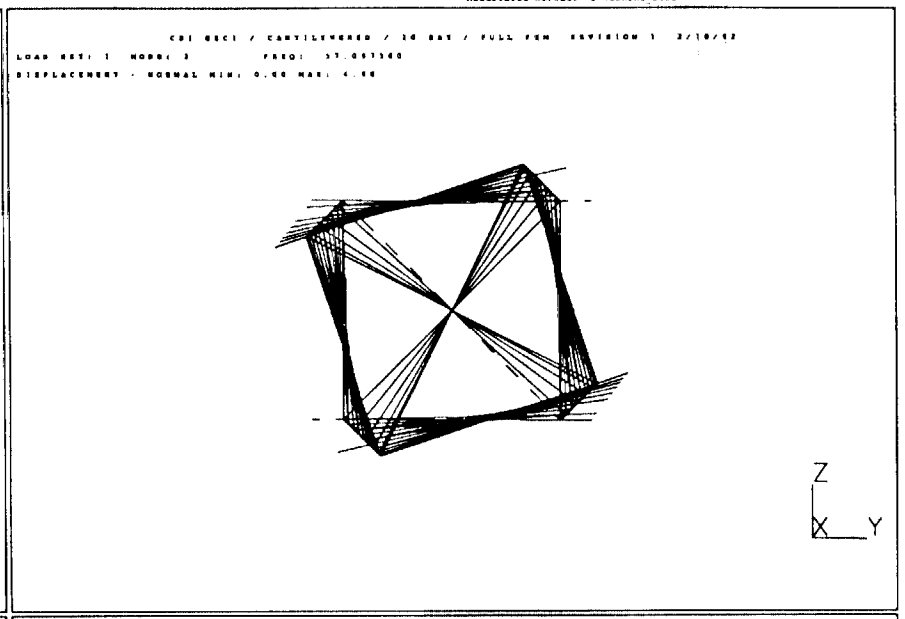

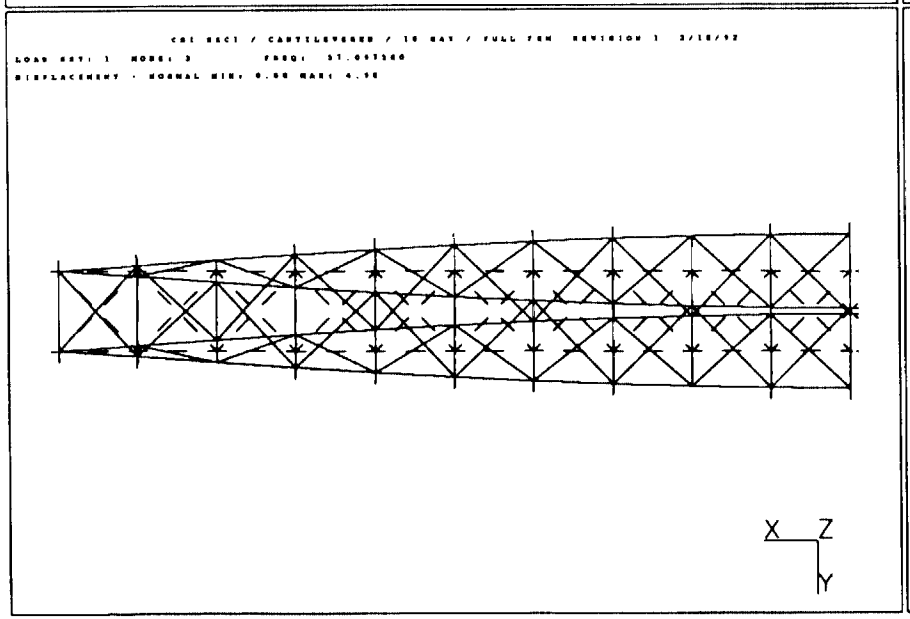

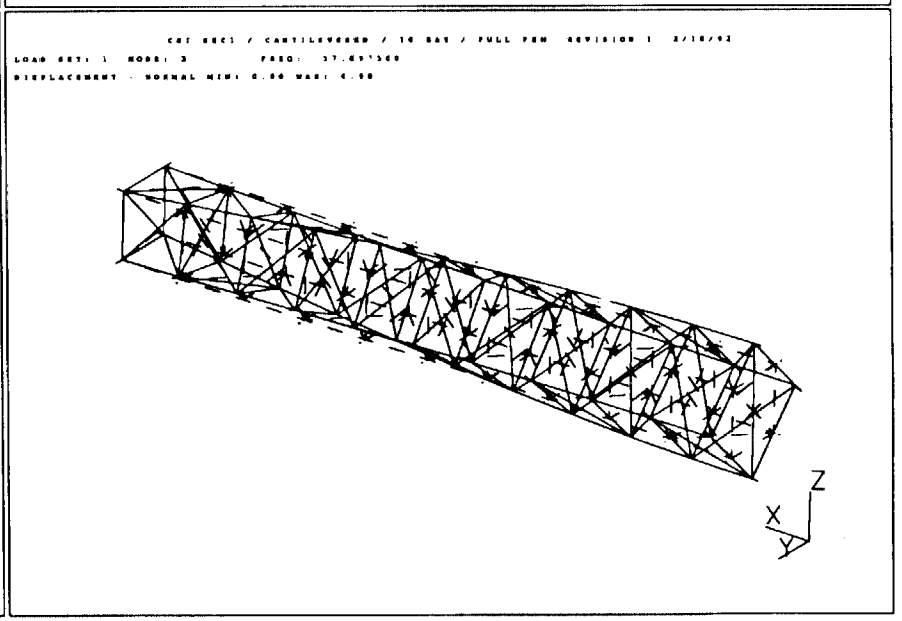

SDRC I-DEAS VI: FE_Modeling_&_Analysis 18-MAR-92 14:21:47

Database: /umeral/tan/cal/sec1/d1tp
View : none, none, none, none
Task: Post Processing
Model: 2-10_BAY

Units : IN
Display : none, none, none, none
Model Bin: 1-MAIN
Associated Workset: 2-MORRING_SET2

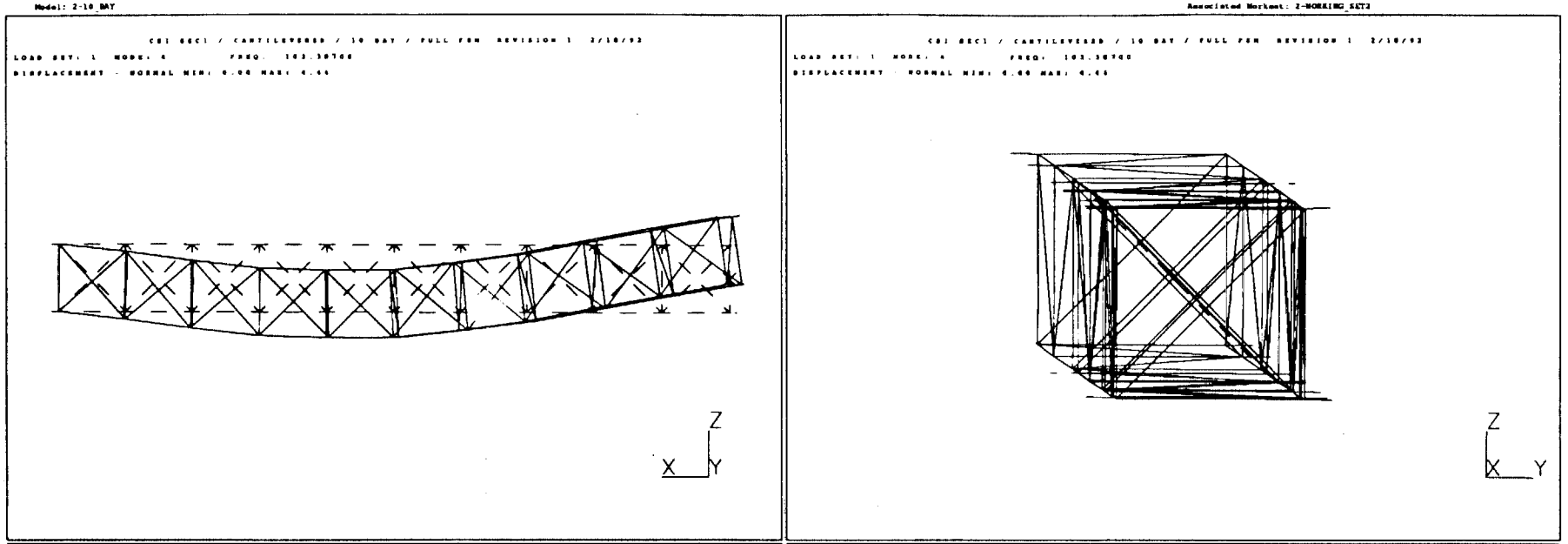

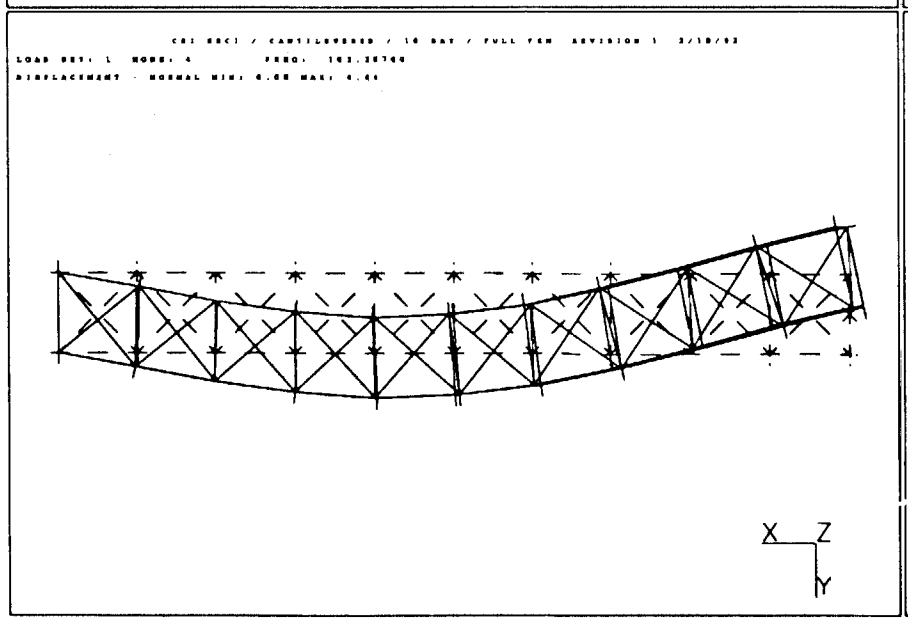

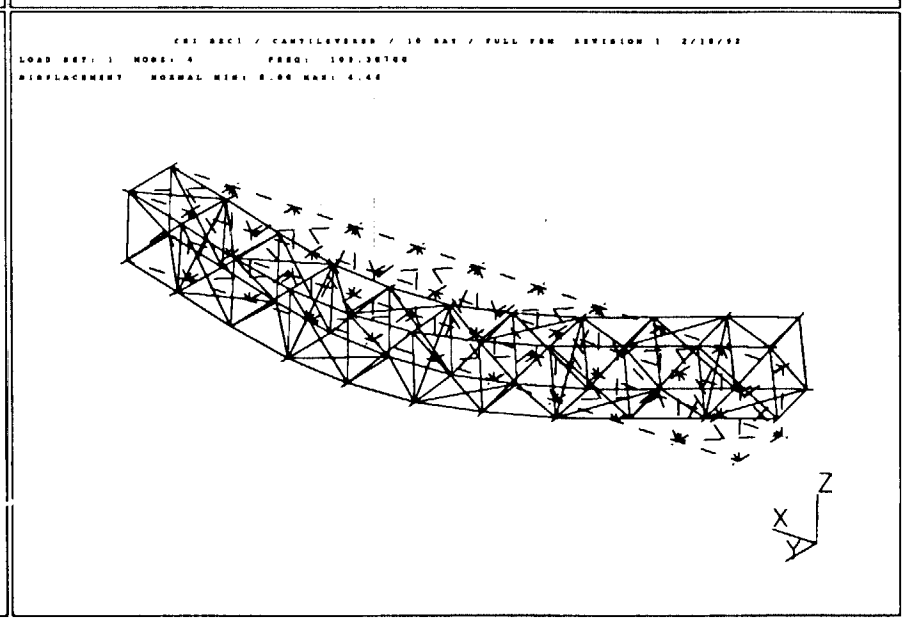

SDRC I-DEAS VI: FE_Modeling_&_Analysis 18-MAR-92 14:22:07

Database: /users3/tan/col/accl/oltp
View : none, none, none, none
Task: Post Processing
Model: 2-18_BAY

Units : IN
Display : none, none, none, none
Model Bin: 1-MAIN
Associated Workset: 2-MODELING_SET2

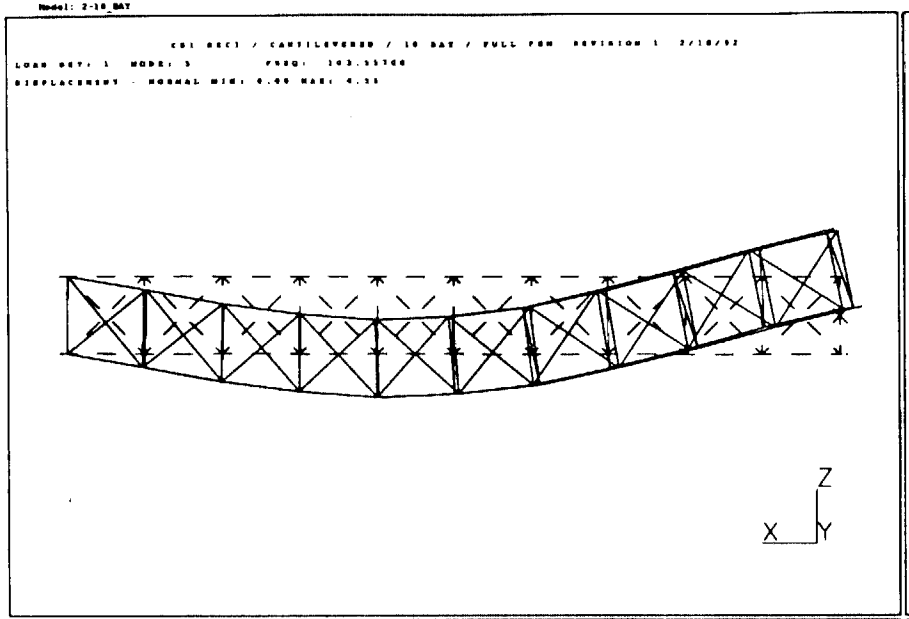

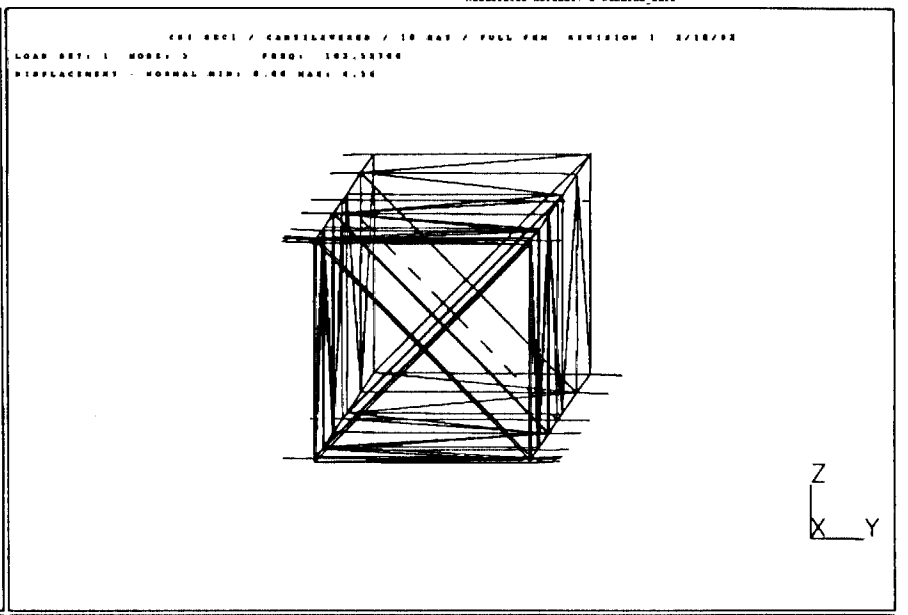

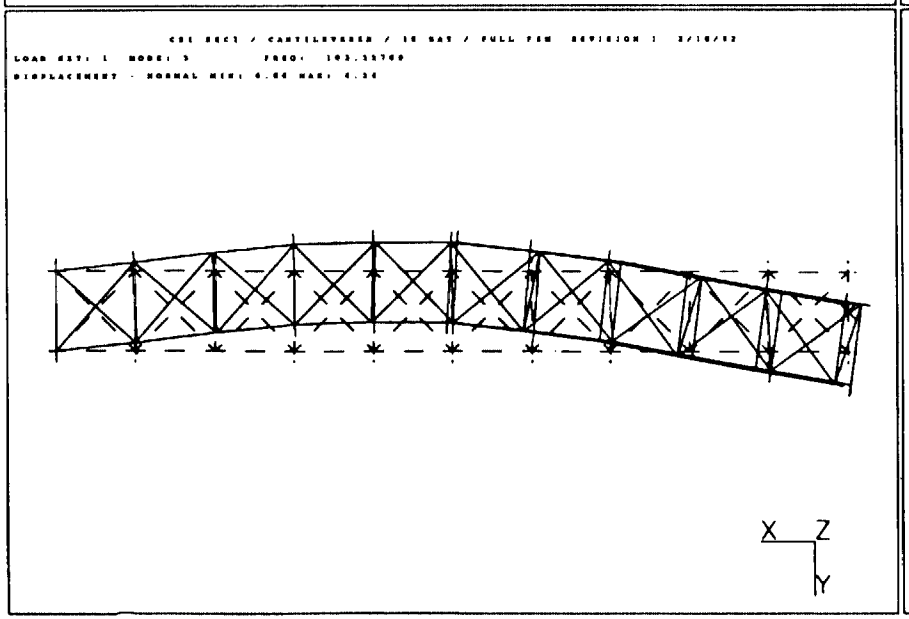

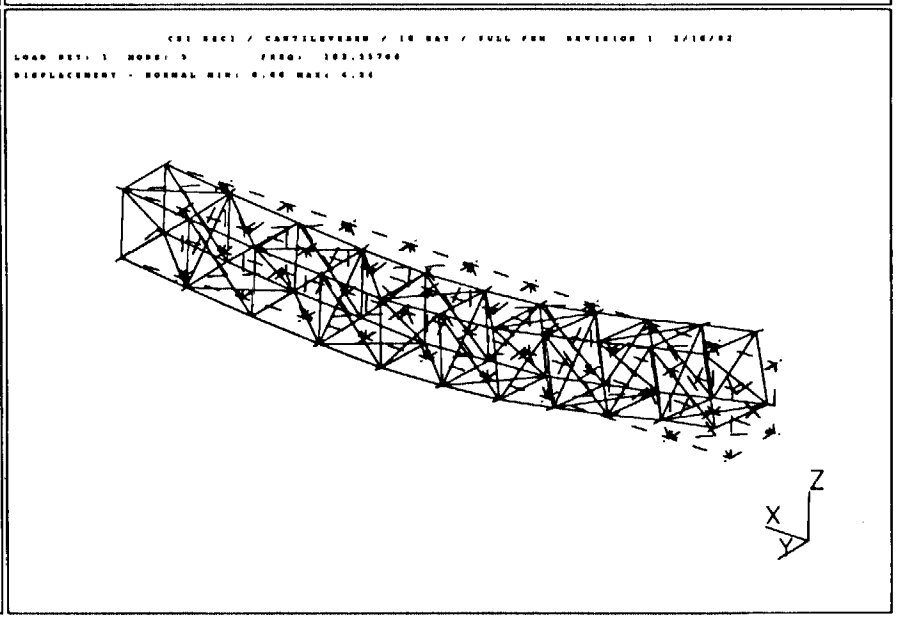

Database: /users3/tan/cai/eacl/altp
View : none, none, none, none
Task: Post Processing
Model: 2-10_BAY

Units : IN
Display : none, none, none, none
Model Bin: 1-MAIN
Associated Workset: 2-MOBRING_SET2

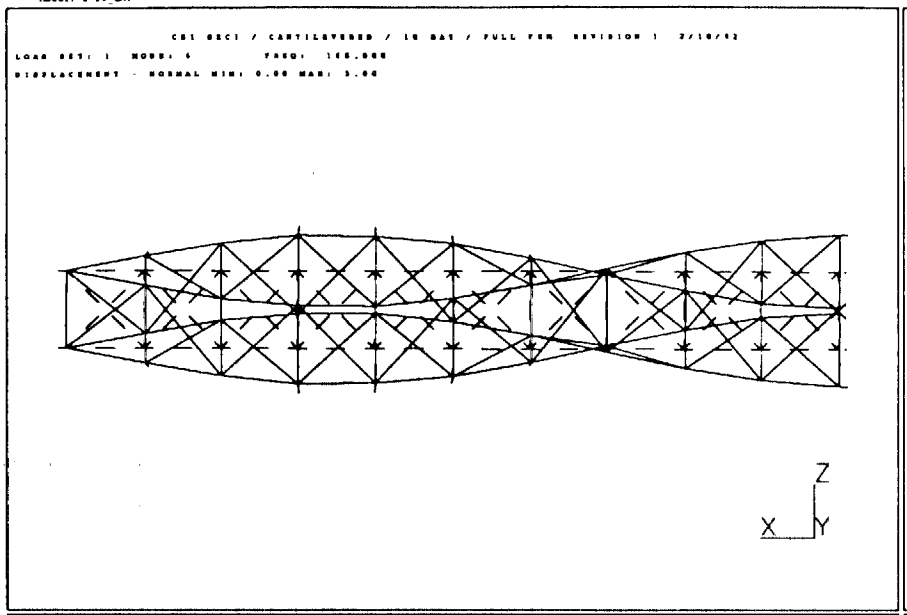

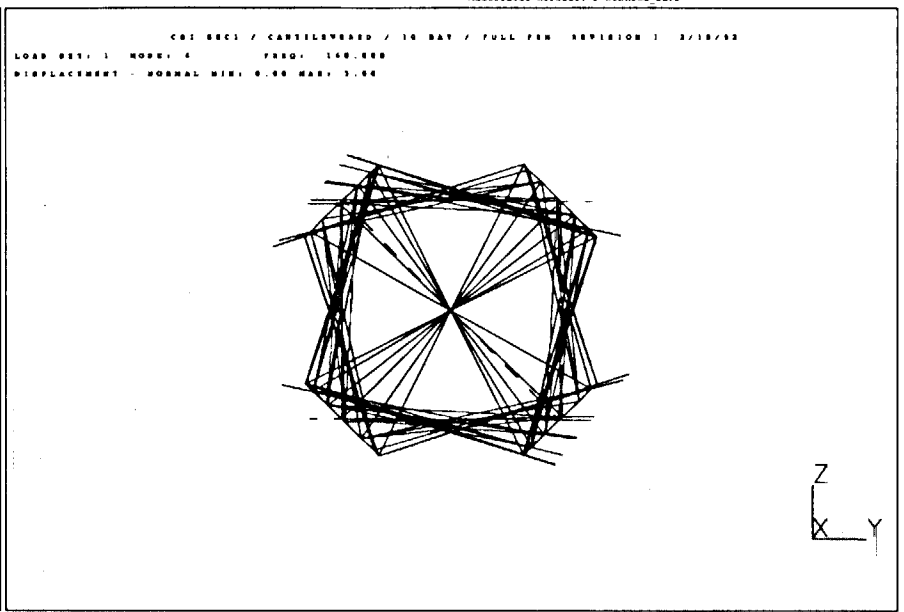

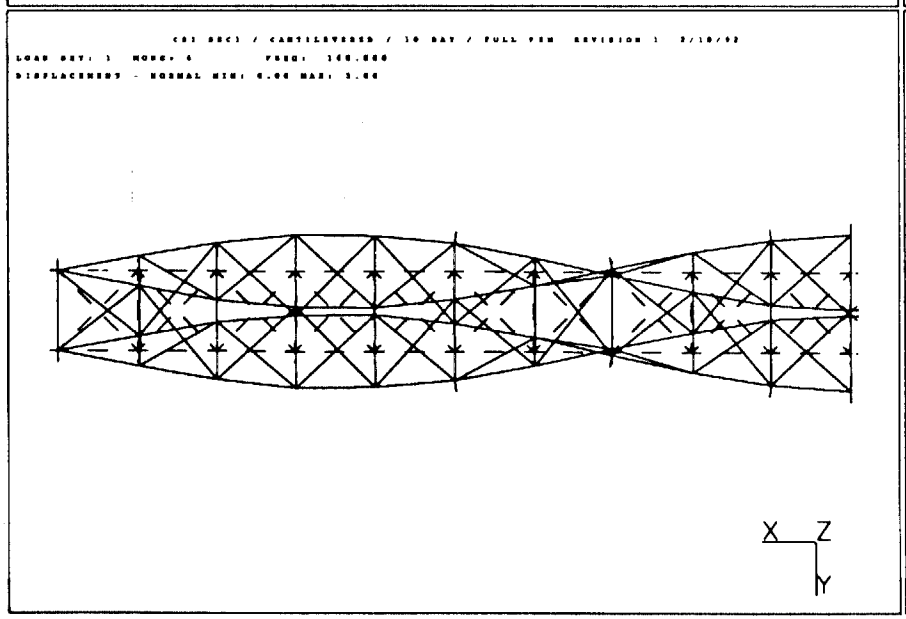

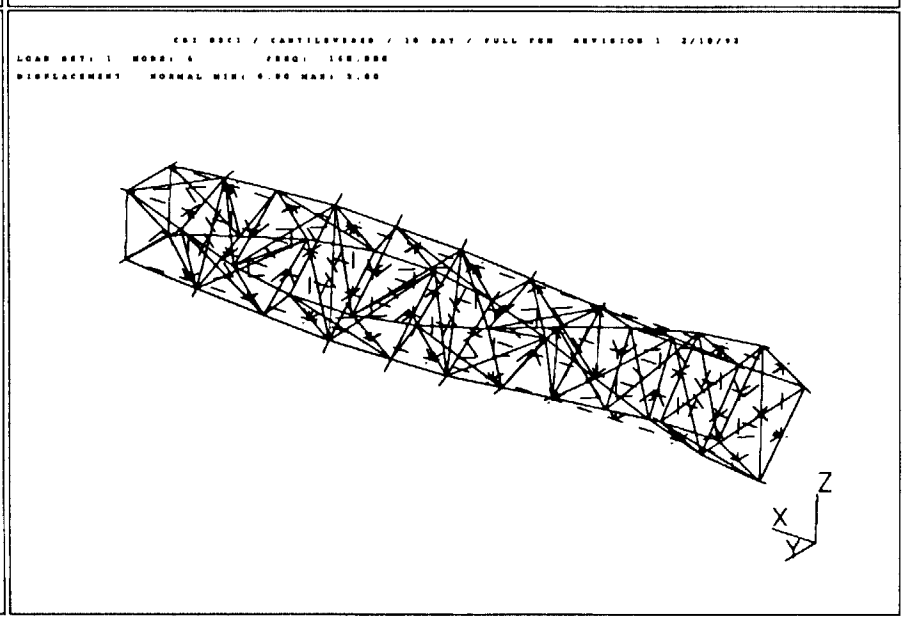

SDRC I-DEAS VI: FE_Modeling_&_Analysis 18-MAR-92 14:22:58

Database: /smore3/tam/coi/secl/altp
View : none, none, none, none
Task: Post Processing
Model: 2-10_BAY
Units : In
Display : none, none, none, none
Model Bin: 1-MAIN
Associated Workset: 2-WORKING_SET2

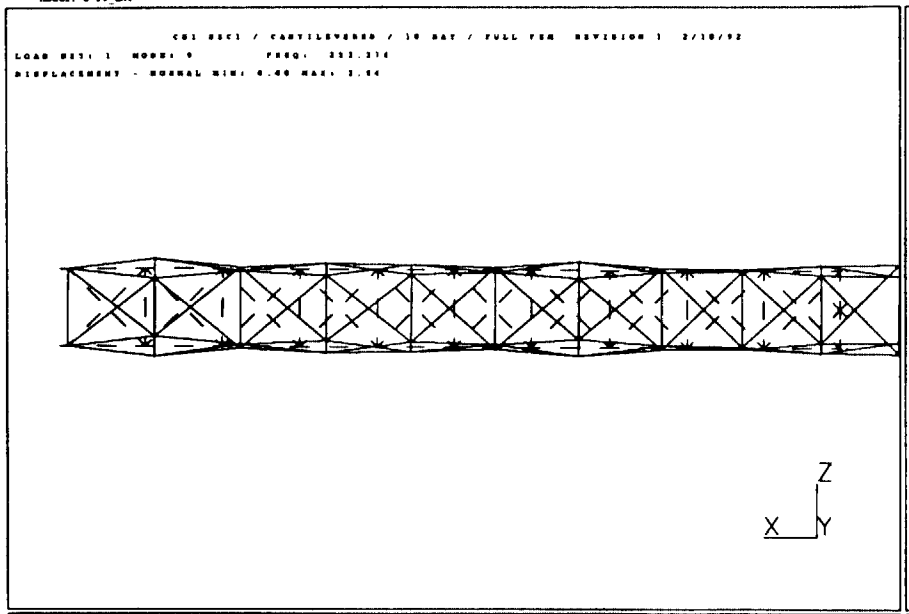

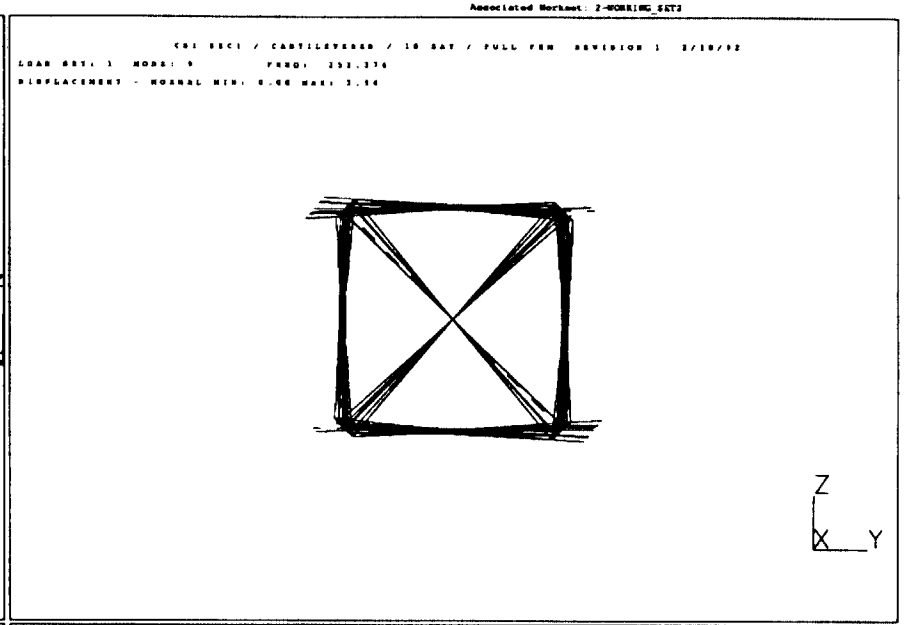

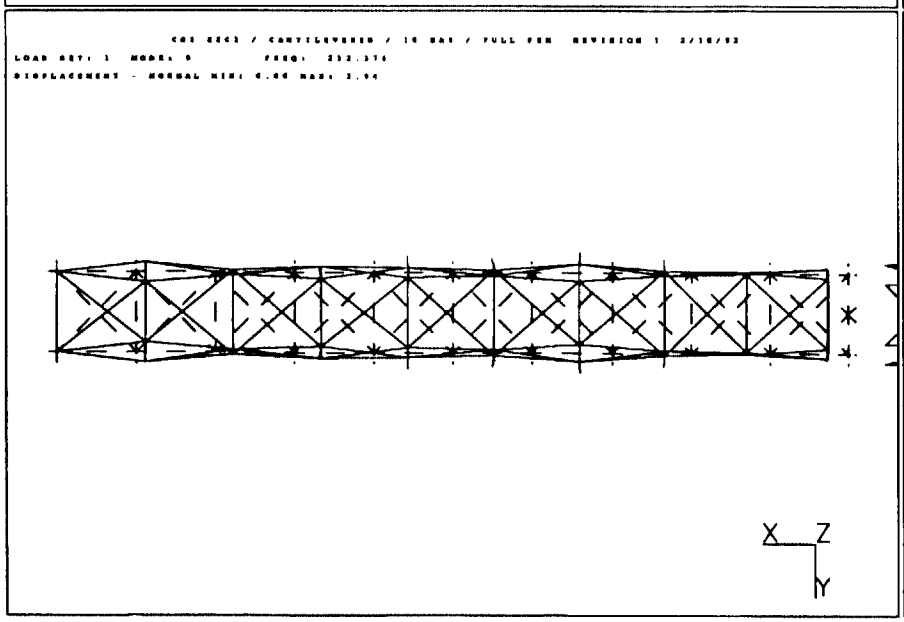

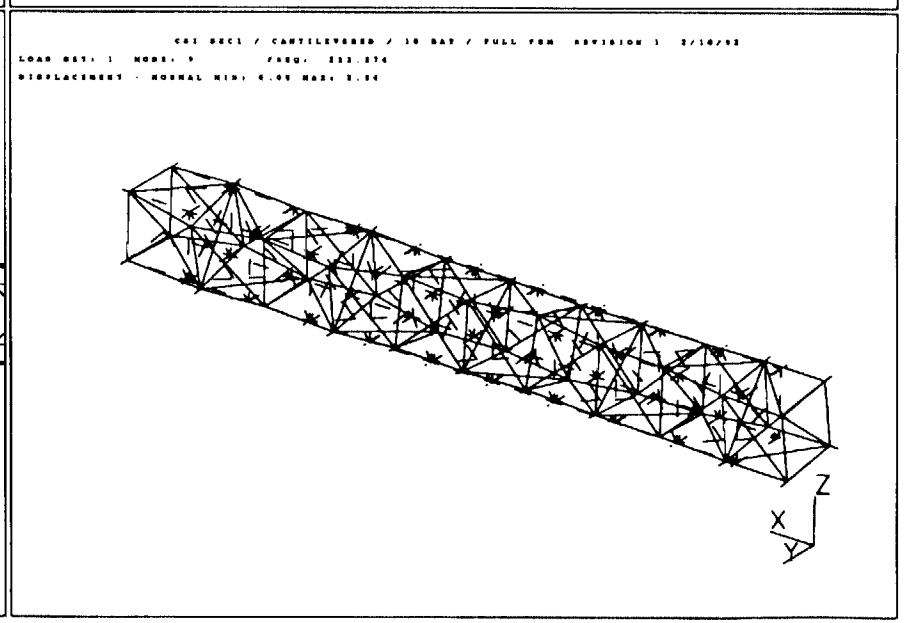

SDRC I-DEAS VI: FE_Modeling_&_Analysis 18-MAR-92 14:10:45

Database: /users3/tan/sal/sacl/mltp
View : none, none, none, none
Task: Post Processing
Model: 2-16_BAY

Units : IN
Display : none, none, none, none
Model Bin: 1-MAIN
Associated Mortset. 2-MORBMC_SET2

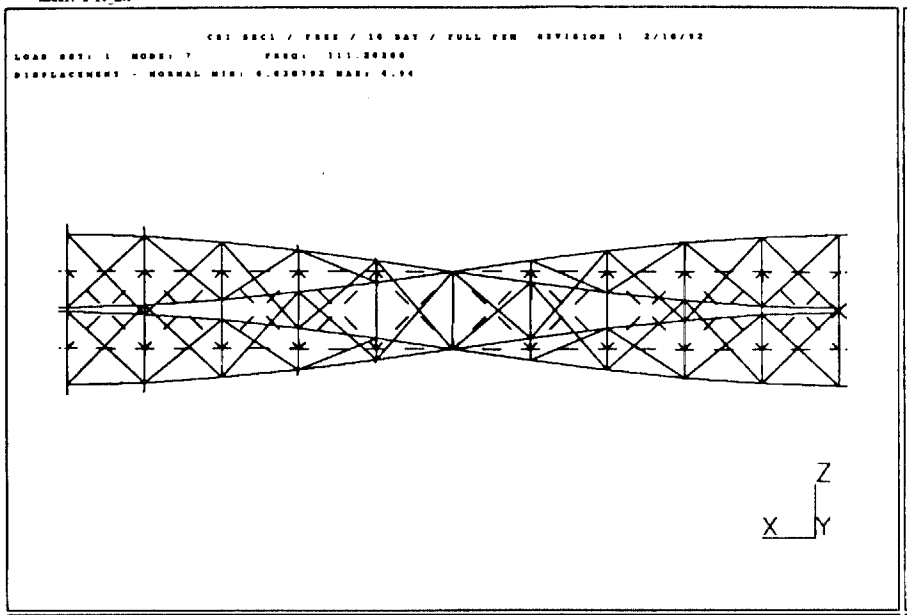

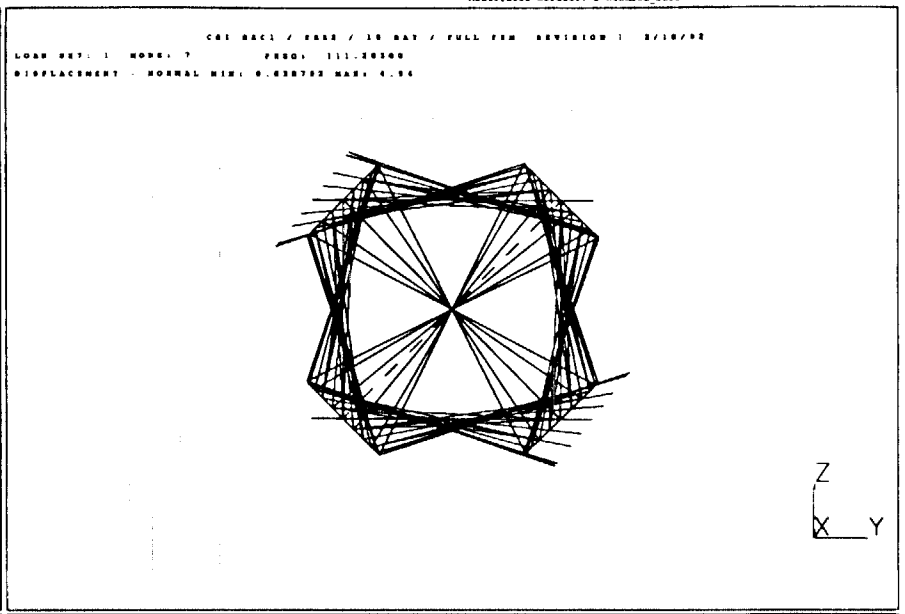

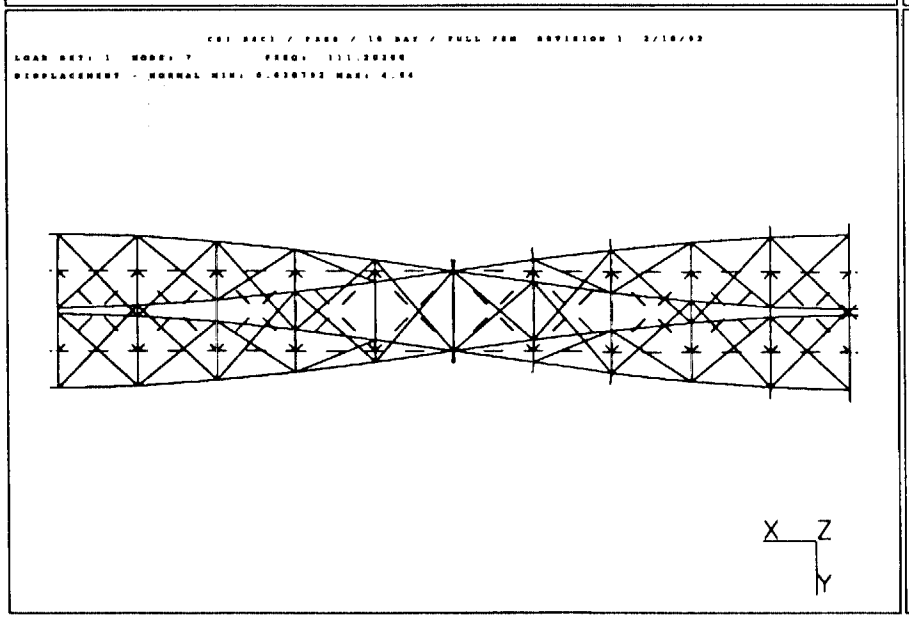

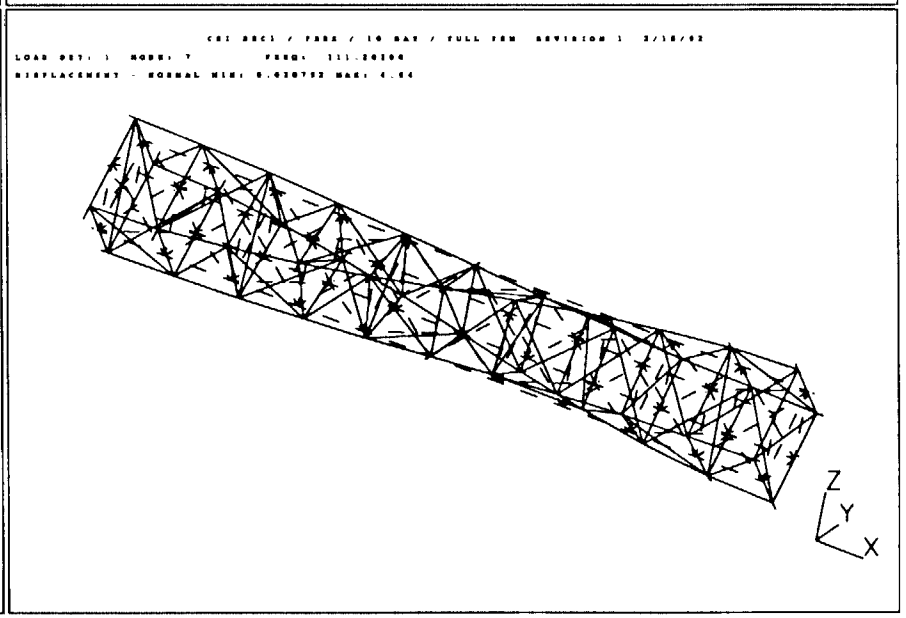

C-17

ORIGINAL PAGE IS
OF POOR QUALITY

SDRC I-DEAS VI: FE_Modeling_&_Analysis 18-MAR-92 14:11:26

Database: /users3/tan/cal/eecl/altp
View : none, none, none, none
Task: Post Processing
Model: 2-10_BAY
Units : IN
Display : none, none, none, none
Model Bin: 1-MAIN
Associated Workset: 2-MORRIS SET2

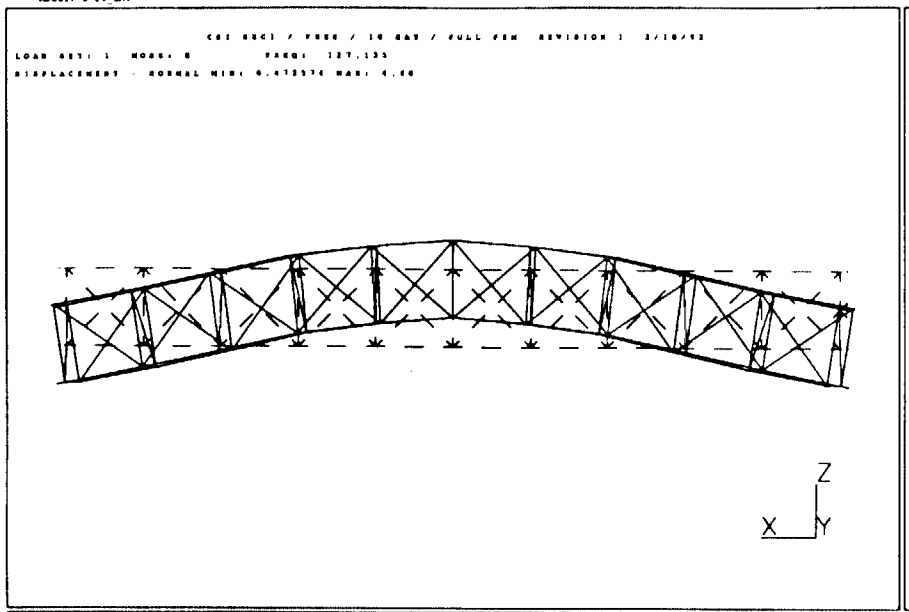

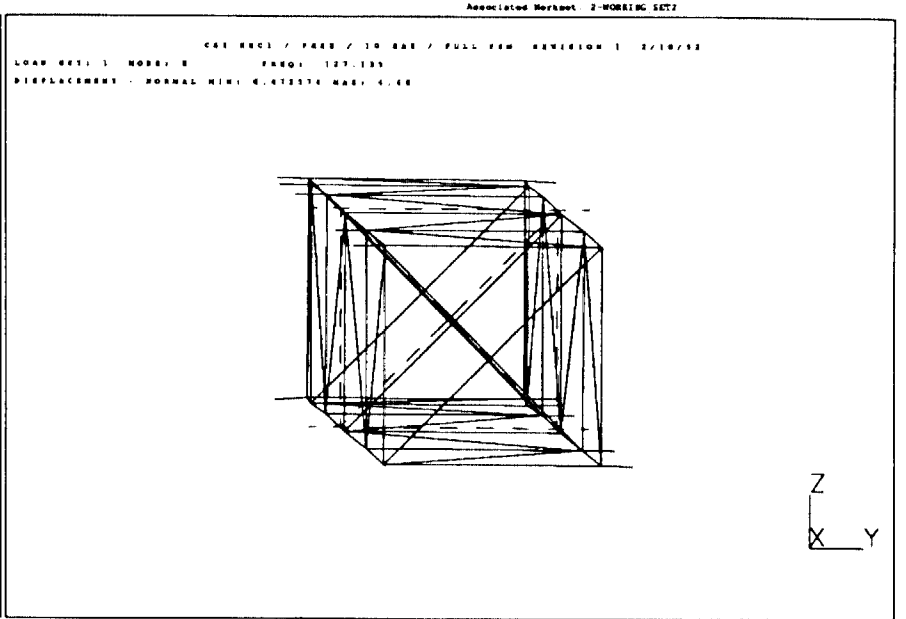

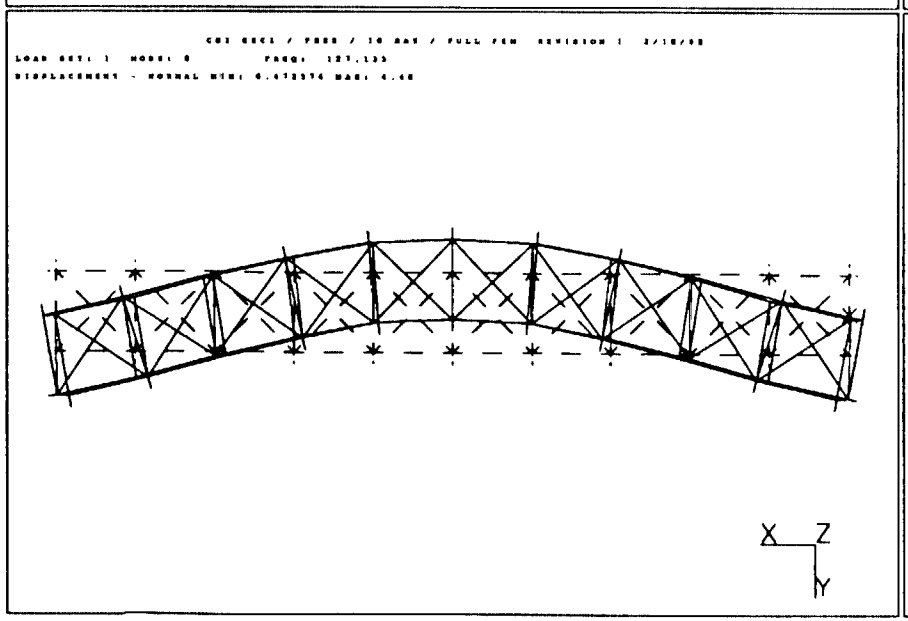

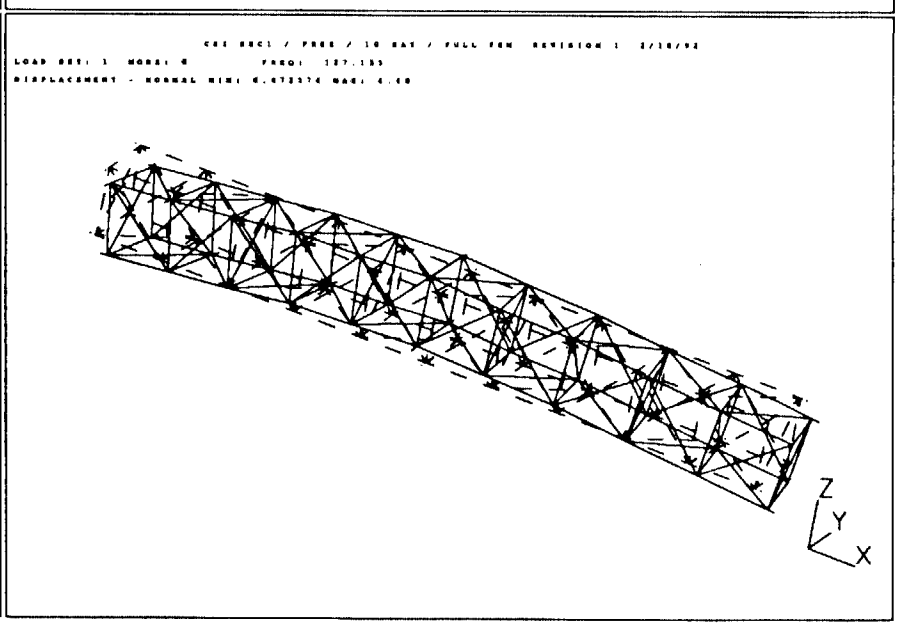

SDRC I-DEAS VI: FE_Modeling_&_Analysis

18-MAR-92 14:13:42

Units : IN

Database: /umore3/tam/cel/eeml/mltp
View : none, none, none, none
Task: Post Processing
Model: 2-10_BAY

Display : none, none, none, none
Model Dis: 1-MAIN
Associated Workset: 2-WORKING SET2

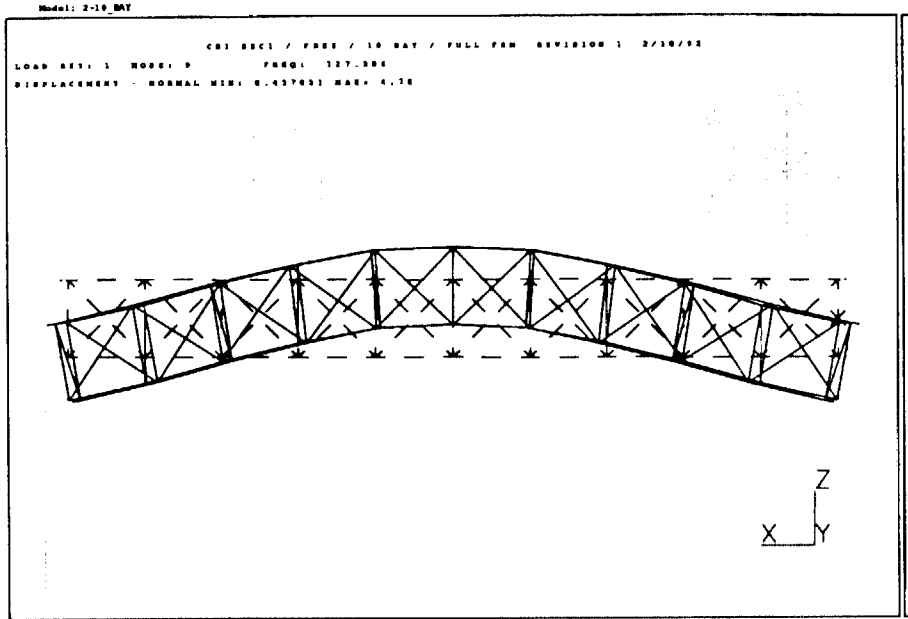

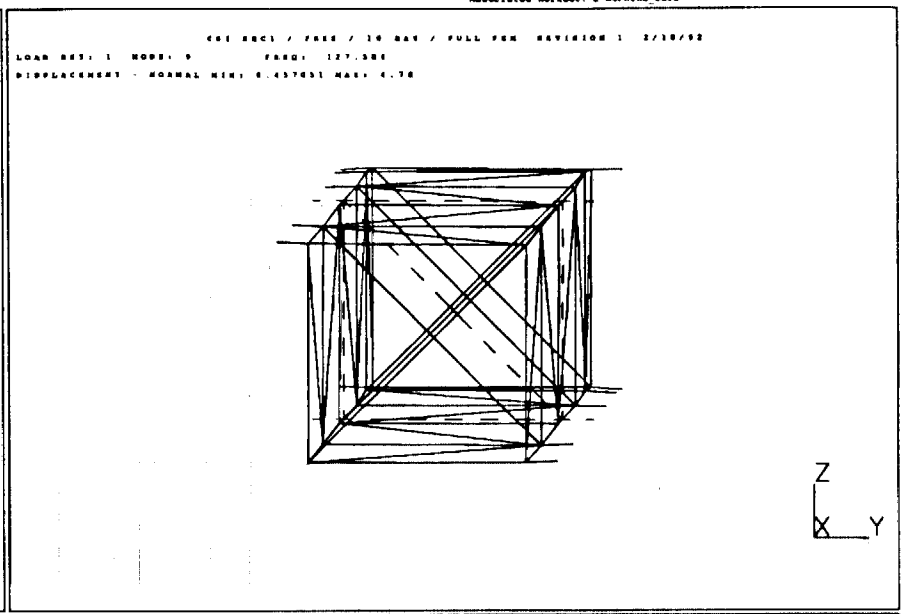

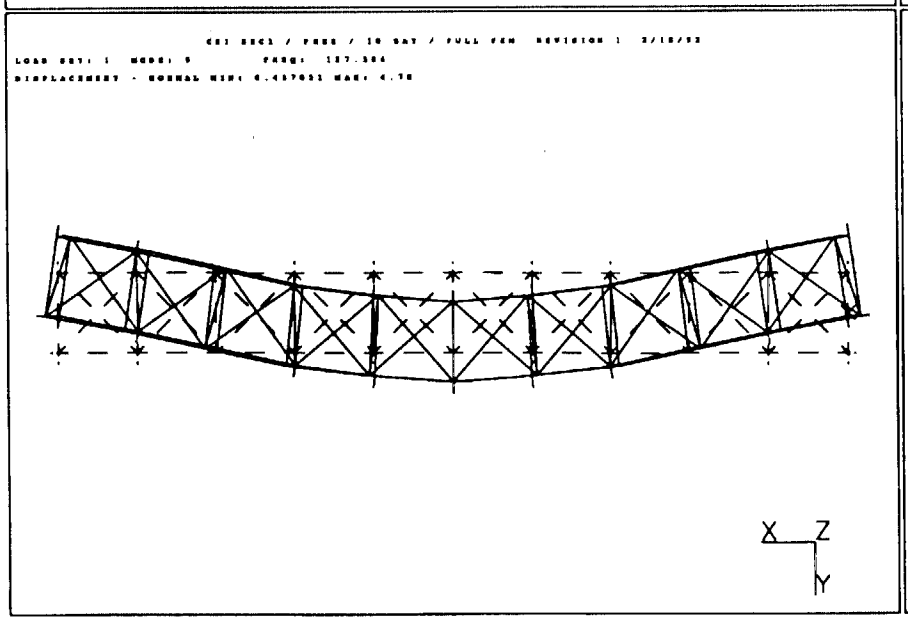

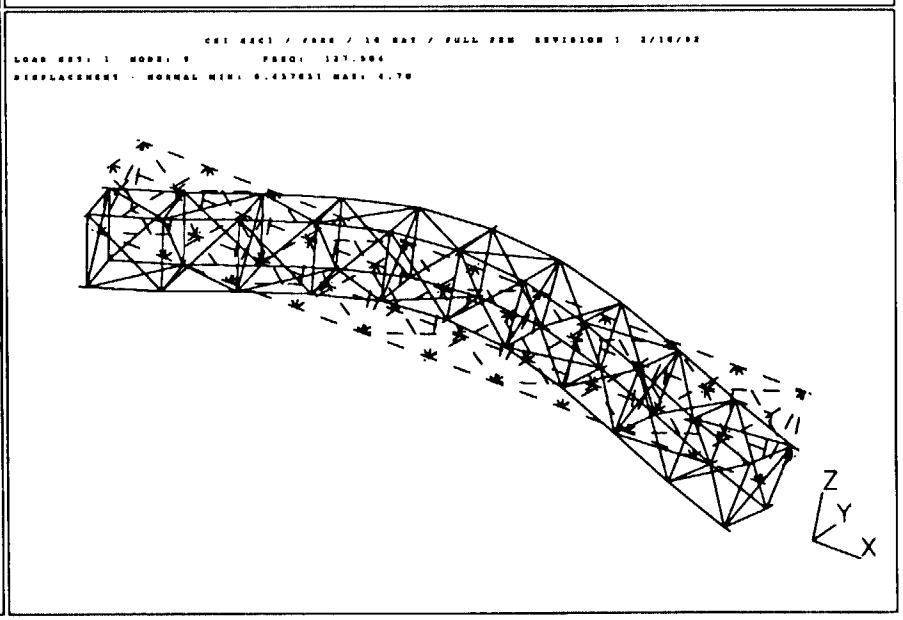

SDRC I-DEAS VI: FE_Modeling_&_Analysis

18-MAR-92 14:14:21

Database: /users3/tan/csi/sec1/eltp
View : none, none, none, none
Task: Post Processing
Model: 2-10_BAT

Units : IN
Display : none, none, none, none
Model Bin: 1-MAIN
Associated Workset: 2-WORKING_SET2

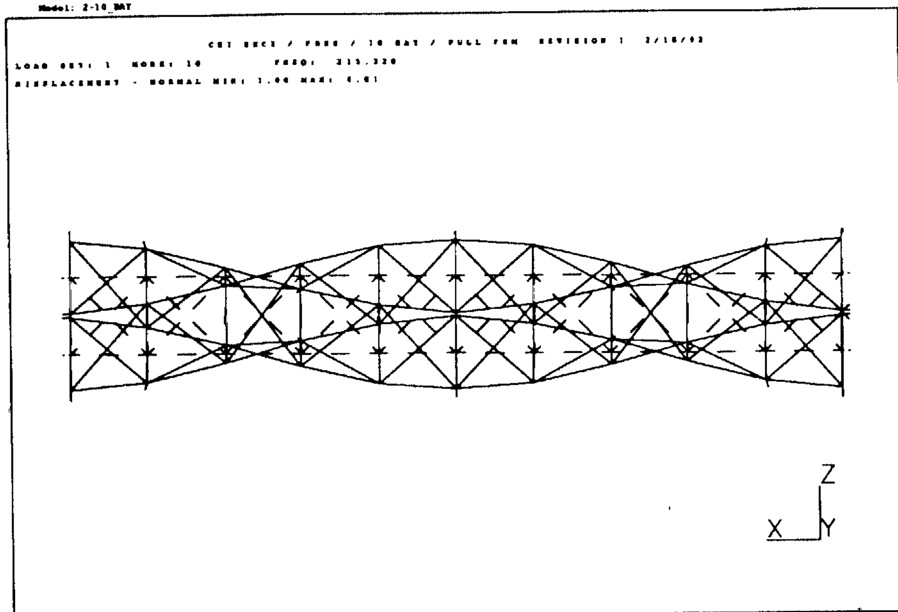

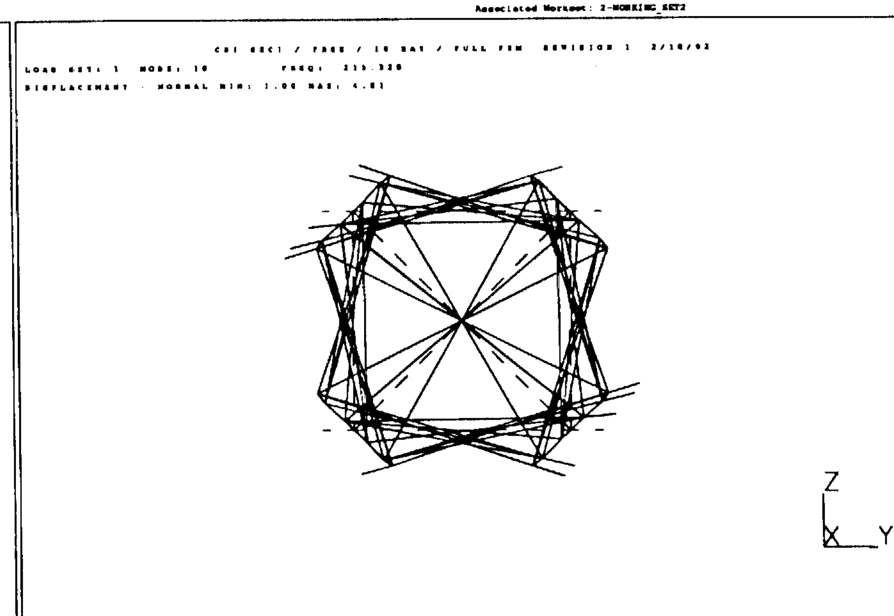

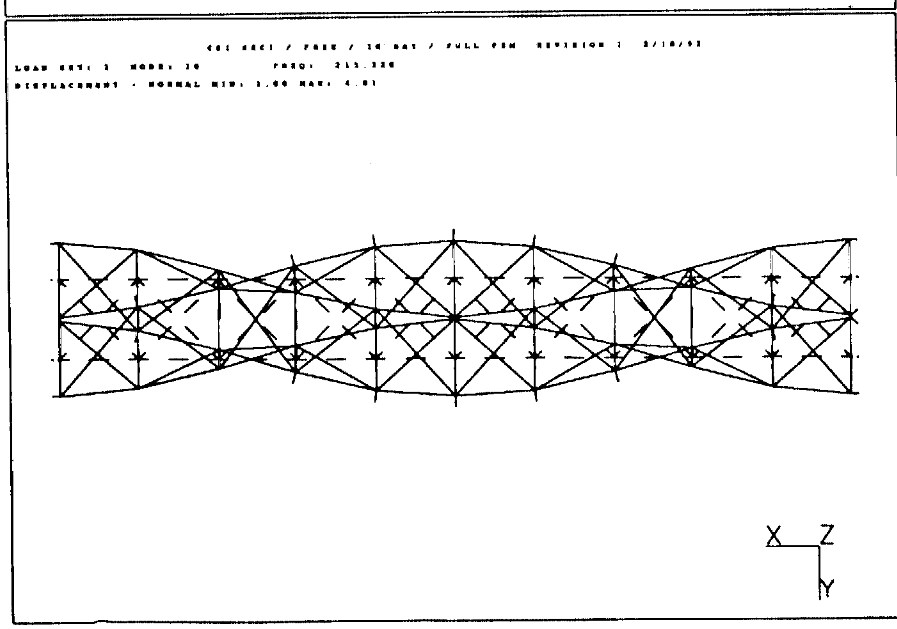

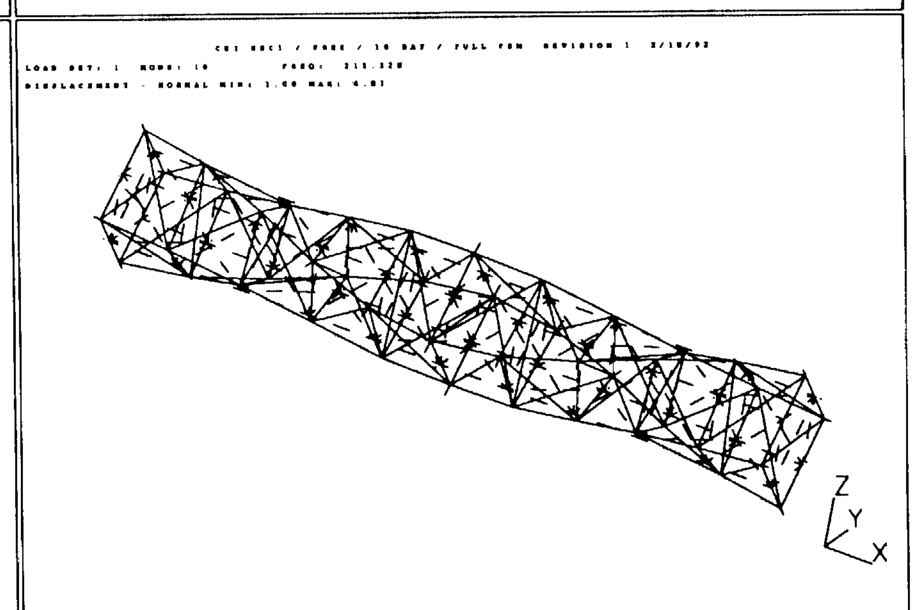

SDRC I-DEAS VI: FE_Modeling_& Analysis

18-MAR-92 14:14:56

Database: /umare3/tan/col/escl/mltp
View : none, none, none, none
Task: Post Processing
Model: 2-10_BAY

Units : IN
Display : none, none, none, none
Model Bin: 1-MAIN
Associated Workset: 2-WORKING_SET2

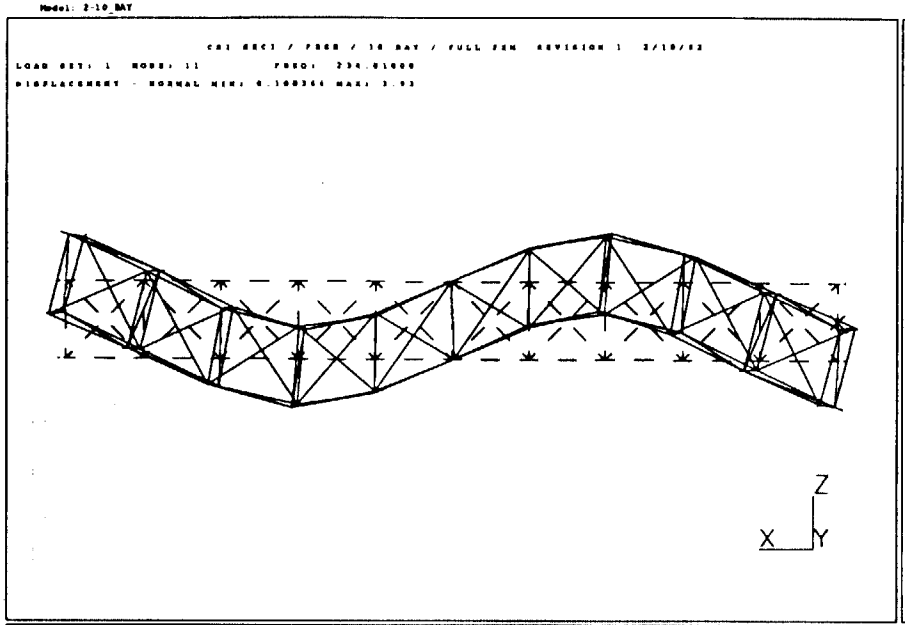

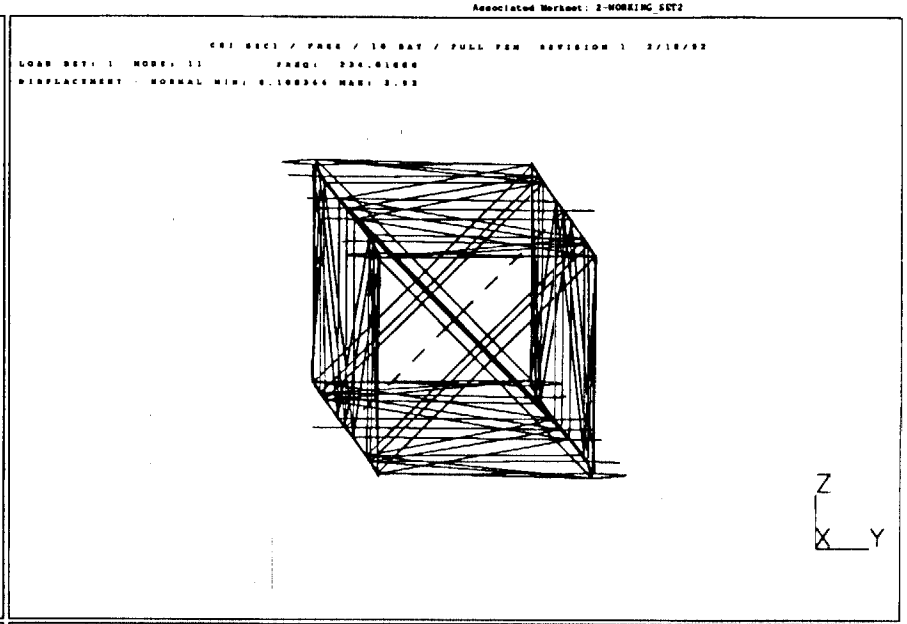

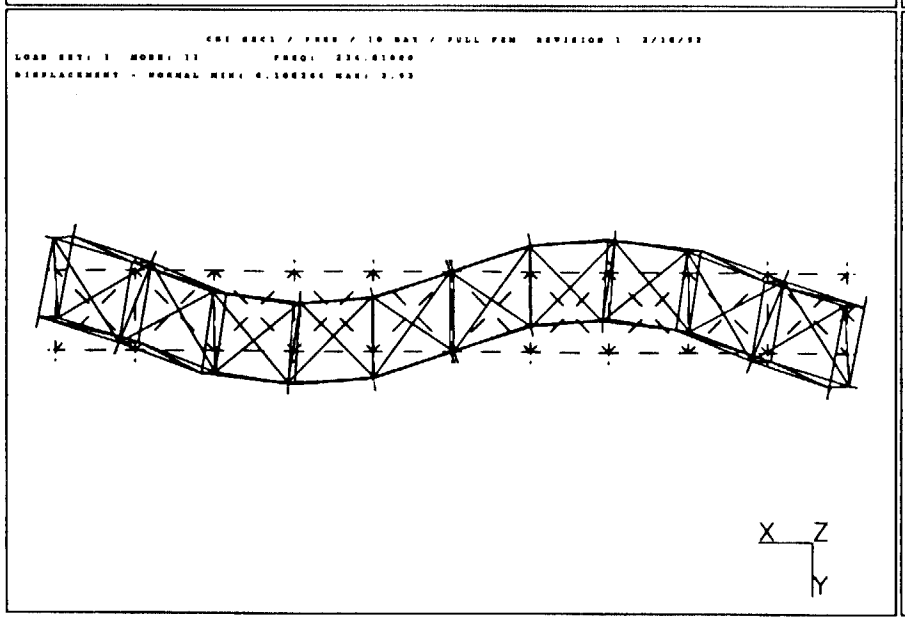

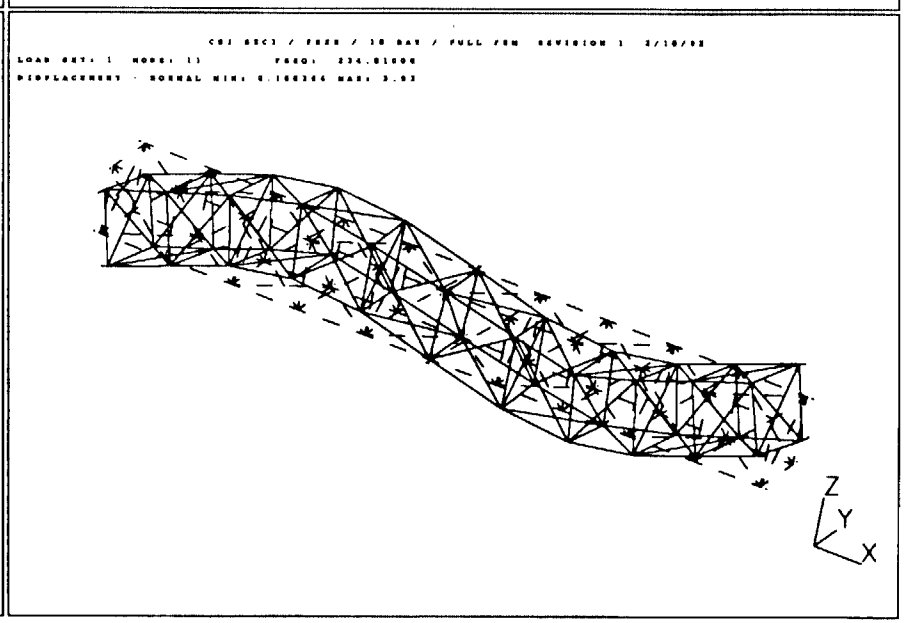

SDRC I-DEAS VI: FE_Modeling_&_Analysis 18-MAR-92 14:15:09

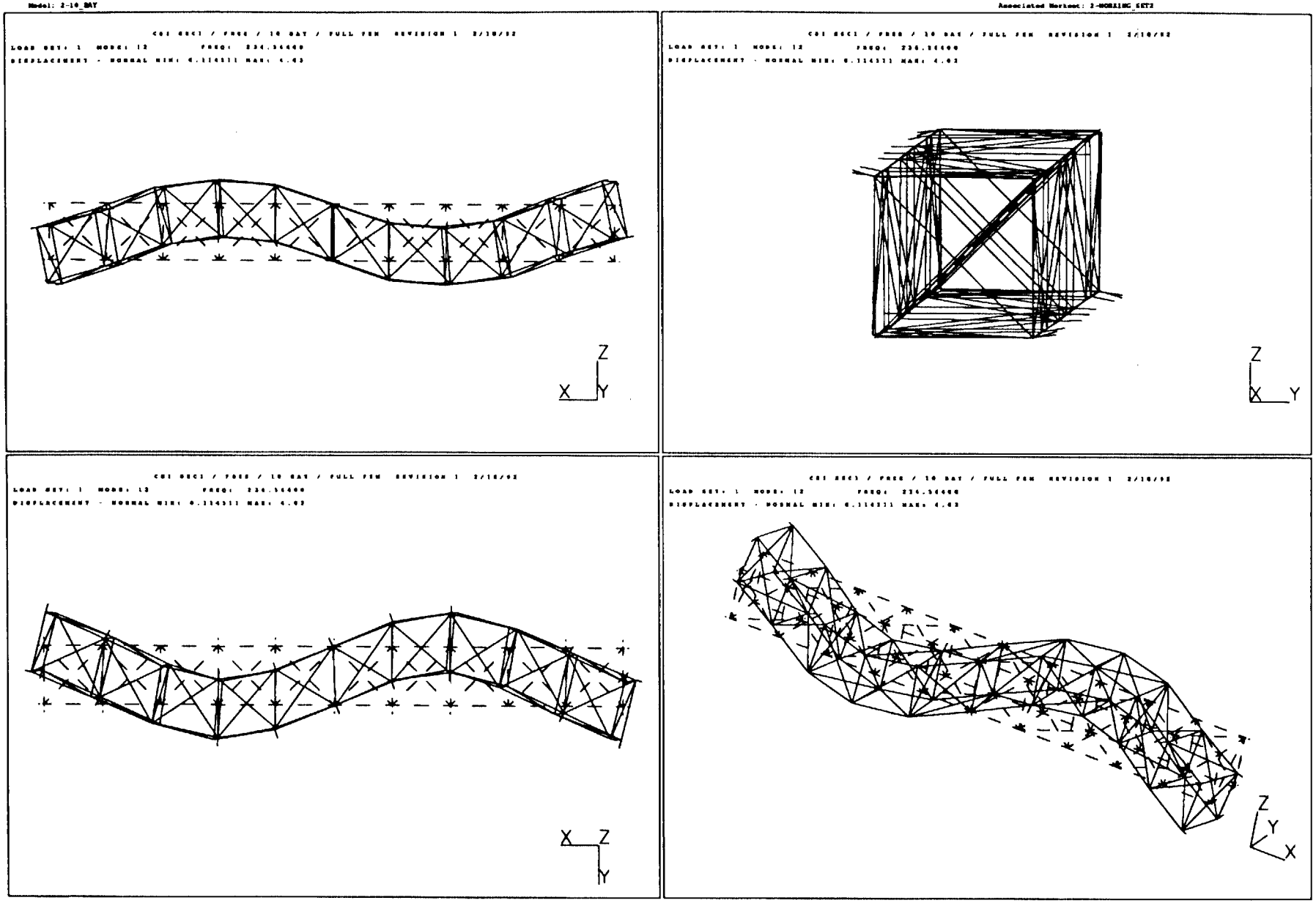

SDRC I-DEAS VI: FE_Modeling_&_Analysis

18-MAR-92 14:15:29

Database: /umeral/tan/cel/secl/dltp
View : none, none, none, none
Task: Post Processing
Model: 2-10_BAY

Units : IN
Display : none, none, none, none
Model Bin: 1-MAIN
Associated Workset: 2-MORRING_6CT2

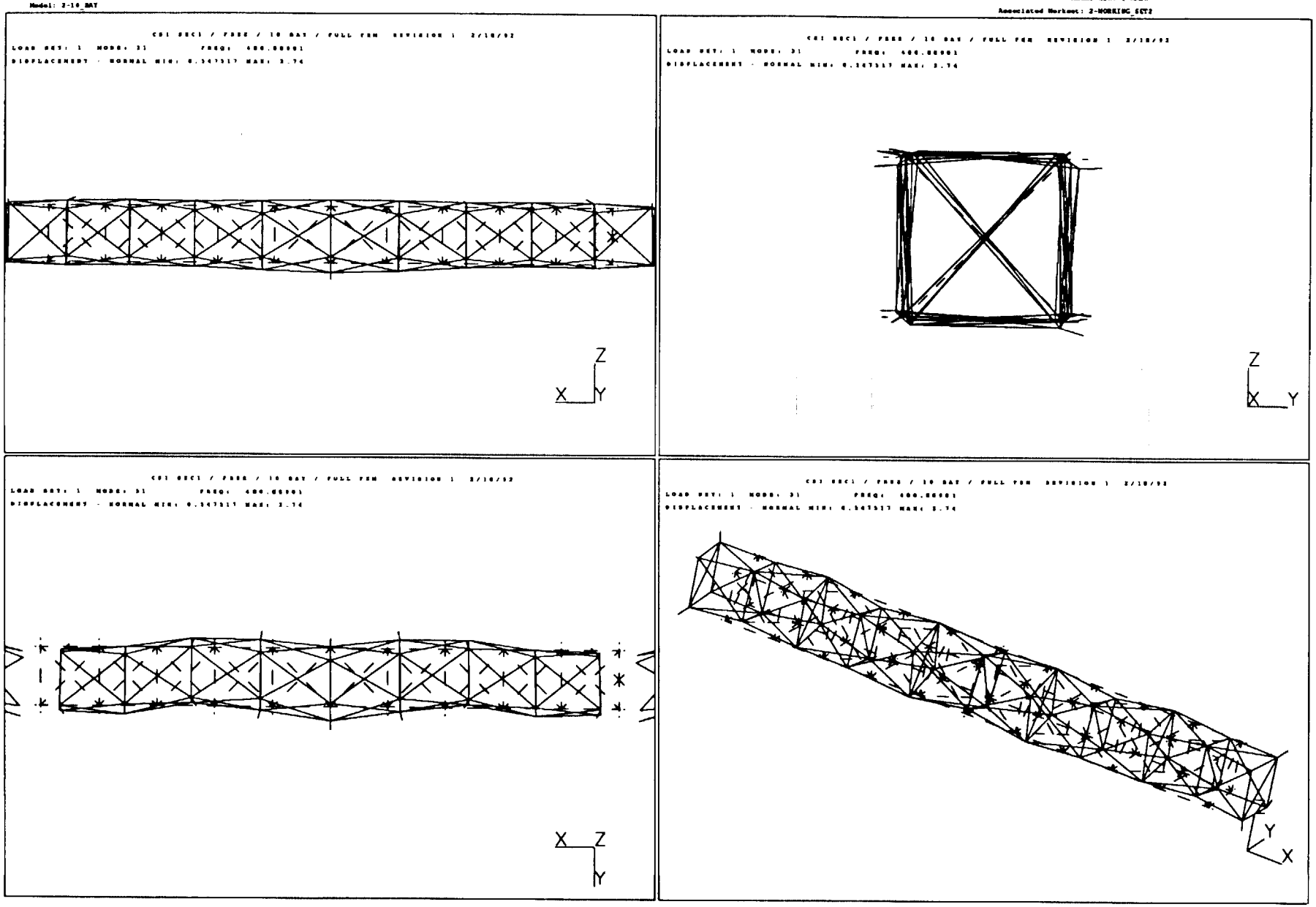

C-23

ORIGINAL PAGE IS
OF POOR QUALITY

APPENDIX D

TEST AND ANALYSIS RESULTS FOR TRUSS SECTION NO. 2 DYNAMIC TESTS

Table D-1 Test Log of Modal Tests of Section 2 - Cantilevered Tests

Test No.	Type of Excitation	Frequency Range	Comments
2a	Continuous Random	0 - 400 Hz	Cantilevered test setup, with Section 2 test item affixed at one end to the test fixture which had been previously bolted to the laboratory concrete floor. Single shaker setup, with the shaker supported by a bungee cord. Shaker at test point no. 22, oriented to apply loading in the horizontal plane with a skew angle of 45 degrees relative to the longitudinal and lateral axes.
2b	Continuous Random	0 - 50 Hz	Same test configuration as test no. 2a.
2c	Continuous Random	0 - 100 Hz	Same test configuration as test no. 2a.
2d	Continuous Random	0 - 200 Hz	Same test configuration as test no. 2a.
2e	Continuous Random	9.75 Hz - 22.25 Hz	Same test configuration as test no. 2a. Zoom for 1st set of bending modes.

Table D-1 Test Log of Modal Tests of Section 2 - Free-Free Tests

Test No.	Type of Excitation	Frequency Range	Comments
2f	Continuous Random	0 - 200 Hz	Free-Free test setup, with Section 2 test item supported at four points with seperate bungee cords. Dual shaker setup, with one shaker at each end supported by seperate bungee cords. Shaker at test point no. 2 oriented to apply loading in the horizontal plane with a skew angle of 45 degrees relative to the longitudinal and lateral axes. Shaker at test point no. 22 oriented to apply loading in the horizontal plane with a skew angle of 45 degrees relative to horizontal and lateral axes.
2g	Continuous Random	0 - 400 Hz	Same test configuration as test no. 2f.
2h	Continuous Random	83.75 Hz - 96.25 Hz	Same test configuration as test no. 2f. Zoom for 1st set of bending modes.
2h	Continuous Random	299.75 Hz - 311.25 Hz	Same test configuration as test no. 2f. Zoom for higher order modes.
2i	Continuous Random	193.75 Hz - 206.25 Hz	Same test configuration as test no. 2f. Zoom for 2nd set of bending modes.
2j	Continuous Random	83.75 Hz - 96.25 Hz	Same test configuration as test no. 2f with the exception of the shaker being moved from test point no. 22 to test point no. 21. Shaker re-oriented to apply loading in the vertical plane with a skew angle of 45 degrees relative to vertical and lateral axes. Purpose of shaker movement was to get better data quality for the 1st set of bending modes.
2k	Continuous Random	86.875 Hz - 93.125 Hz	Moved shaker back to original test configuration, same as test no. 2f. Zoom for 1st set of bending modes.
2l	Continuous Random	88.437 Hz - 91.562 Hz	Same test configuration as test no. 2k. Zoom for 1st set of bending modes.
2m	Continuous Random	119.75 Hz - 132.25 Hz	Same test configuration as test no. 2f. Zoom for 1st torsion mode.
2n	Continuous Random	237.75 Hz - 250.25 Hz	Same test configuration as test no. 2f. Zoom for 2nd torsion mode.

Table D-1 Test Log of Modal Tests of Section 2 - Free-Free Tests of Suspension Modes

Test No.	Type of Excitation	Frequency Range	Comments
2o	Hammer Impact	0 - 12.5 Hz	Free-Free test setup, with Section 2 test item supported at four points with seperate bungee cords. Both shakers disconnected. Hammer taps applied in the lateral direction on upper non-instrumented node ball at batten frame no 6.
2p	Hammer Impact	0 - 12.5 Hz	Same test configuration as 2o. Hammer taps applied in the vertical direction on the node ball with accelerometer test point no. 1.
2q	Hammer Impact	0 - 12.5 Hz	Same test configuration as 2o. Hammer taps applied in the lateral direction on the node ball with accelerometer test point no. 1.
2r	Free Decay	0 - 12.5 Hz	Same test configuration as 2o. Free decay time history recorded after test item was pulled out in the axial direction and released.
2s	Free Decay	0 - 12.5 Hz	Same test configuration as 2o. Free decay time history recorded after test item was pulled out in the lateral direction and released.
2t	Free Decay	0 - 12.5 Hz	Same test configuration as 2o. Free decay time history recorded after test item was pulled out in the vertical direction and released.

Table D-2 Modal Testing Parameters Summary - Section 2 Cantilever Modes

Mode No.	Nat Freq (Hz)	Excitation Method	Frequency Span (Hz)	No. Avg	Test No.	Type of Window	% Overlap	Sample Length(Sec)	Frequency Resolution (Hz)	No. of Freq Lines	Function Universal File Name ( ).unv
1	16.0	Continuous Random	9.75 - 22.25	30	2e	Hanning	50	64	0.015625	800	s2cafu1022
2	16.4	Continuous Random	9.75 - 22.25	30	2e	Hanning	50	64	0.015625	800	s2cafu1022
3	65.2	Continuous Random	0 - 100	30	2c	Hanning	0	8	0.125	800	s2cafu0100
4	80.8	Continuous Random	0 - 100	30	2c	Hanning	0	8	0.125	800	s2cafu0100
5	84.6	Continuous Random	0 - 100	30	2c	Hanning	0	8	0.125	800	s2cafu0100
6	157.9	Continuous Random	0 - 200	30	2d	Hanning	0	4	0.25	800	s2cafu0200
7	190.2	Continuous Random	0 - 200	30	2d	Hanning	0	4	0.25	800	s2cafu0200

Table D-2 Modal Testing Parameters Summary - Section 2 Free-Free Modes

Mode No.	Nat Freq (Hz)	Excitation Method	Frequency Span (Hz)	No. Avg	Test No.	Type of Window	% Overlap	Sample Length(Sec)	Frequency Resolution (Hz)	No. of Freq Lines	Function Universal File Name ( ).unv
1	89.9	Continuous Random	83.75 - 96.25	30	2j	Hanning	0	32	0.03125	400	s2fffu84
2	90.0	Continuous Random	83.75 - 96.25	30	2j	Hanning	0	32	0.03125	400	s2fffu84
3	126.5	Continuous Random	119.75 - 132.25	30	2m	Hanning	50	32	0.03125	400	s2fffu120
4	198.8	Continuous Random	193.75 - 206.25	30	2i	Hanning	0	32	0.03125	400	s2fffu194
5	199.5	Continuous Random	193.75 - 206.25	30	2i	Hanning	0	32	0.03125	400	s2fffu194
6	243.9	Continuous Random	237.75 - 250.25	30	2n	Hanning	50	32	0.03125	400	s2fffu238
7	307.7	Continuous Random	298.75 - 311.25	30	2h	Hanning	0	32	0.03125	400	s2fffu299

Table D-2 Modal Testing Parameters Summary - Section 2 Rigid Body Free-Free Modes

Mode No.	Nat Freq (Hz)	Excitation Method	Frequency Span (Hz)	No. Avg	Test No.	Type of Window	% Overlap	Sample Length(Sec)	Frequency Resolution (Hz)	No. of Freq Lines
1	0.31	Free Decay	0 - 12.5	7	2r	Exponent.	0	32	0.03125	400
2	0.34	Free Decay	0 - 12.5	7	2s	Exponent.	0	32	0.03125	400
3	0.39	Hammer Tap	0 - 12.5	7	2o	Exponent.	0	32	0.03125	400
4	0.88	Free Decay	0 - 12.5	7	2t	Exponent.	0	32	0.03125	400
5	0.91	Hammer Tap	0 - 12.5	7	2p	Exponent.	0	32	0.03125	400
6	1.51	Hammer Tap	0 - 12.5	7	2q	Exponent.	0	32	0.03125	400

Table D-3 Modal Data Analysis Parameters Summary - Section 2 Cantilever Modes

Mode No.	Nat Freq (Hz)	Curve-Fit Technique	Frequency Range (Hz)	No. of Resp Pts	Matrix Size	No. of Roots	Reference Point	Shape/Parameter File Name ( ).unv	Model Universal File Name ( ).unv
1	16.0	Polyref	9.75 - 22.25	45	16	7	22x+	s2canmodes	s2catestpt
2	16.4	Polyref	9.75 - 22.25	45	16	7	22x+	s2canmodes	s2catestpt
3	65.2	Polyref	60.0 - 100.0	45	16	5	22x+	s2canmodes	s2catestpt
4	80.8	Polyref	60.0 - 100.0	45	16	5	22x+	s2canmodes	s2catestpt
5	84.6	Polyref	60.0 - 100.0	45	16	5	22x+	s2canmodes	s2catestpt
6	157.9	Polyref	150.0 - 200.0	45	16	8	22x+	s2canmodes	s2catestpt
7	190.2	Polyref	150.0 - 200.0	45	16	8	22x+	s2canmodes	s2catestpt

Table D-3 Modal Data Analysis Parameters Summary - Section 2 Free-Free Modes

Mode No.	Nat Freq (Hz)	Curve-Fit Technique	Frequency Range (Hz)	No. of Resp Pts	Matrix Size	No. of Roots	Reference Points	Shape/Parameter File Name ( ).unv	Model Universal File Name ( ).unv
1	89.9	Polyref	89.0 - 91.0	44	16	12	2y+, 21z-	s2ffmodes	s2fftestpt
2	90.0	Polyref	89.0 - 91.0	44	16	12	2y+, 21z-	s2ffmodes	s2fftestpt
3	126.5	Polyref	124.0 - 128.0	44	16	6	2y+, 22y-	s2ffmodes	s2fftestpt
4	198.8	Polyref	197.0 - 201.0	44	16	14	2y+, 22y-	s2ffmodes	s2fftestpt
5	199.5	Polyref	197.0 - 201.0	44	16	14	2y+, 22y-	s2ffmodes	s2fftestpt
6	243.9	Polyref	240.0- 248.0	44	16	6	2y+, 22y-	s2ffmodes	s2fftestpt
7	307.7	Polyref	300.0 - 309.0	44	16	10	2y+, 22y-	s2ffmodes	s2fftestpt

Table D-3 Modal Data Analysis Parameters Summary - Section 2 Rigid Body Free-Free Modes

Mode No.	Nat Freq (Hz)	Curve-Fit Technique	Frequency Range (Hz)	No. of Resp Pts	Matrix Size	No. of Roots	Reference Points
1	0.31	Peak Evaluation	0 - 12.5	44	—	—	—
2	0.34	Peak Evaluation	0 - 12.5	44	—	—	—
3	0.39	Polyref	0 - 2.0	44	16	16	1x-
4	0.88	Peak Evaluation	0 - 12.5	44	—	—	—
5	0.91	Polyref	0.1875 - 1.3125	44	16	9	1z-
6	1.51	Polyref	0 - 2.5	44	16	10	11x-

O U T P U T F R O M G R I D P O I N T W E I G H T G E N E R A T O R

REFERENCE POINT = 0

M O

```
*  1.038898E-01 -5.963112E-18 -1.067939E-17 -1.074851E-15  3.669689E-04 -5.710272E+00 *
* -5.963112E-18  1.038898E-01 -3.550762E-18 -3.669689E-04  4.204536E-16  1.298576E+01 *
* -1.067939E-17 -3.442342E-18  1.038898E-01  5.710272E+00 -1.298576E+01  6.578668E-16 *
* -1.068644E-15 -3.669689E-04  5.710272E+00  4.119483E+02 -7.137816E+02  6.200154E-02 *
*  3.669689E-04  4.462847E-16 -1.298576E+01 -7.137816E+02  1.627381E+03 -1.834844E-03 *
* -5.710272E+00  1.298576E+01  6.464013E-16  6.200154E-02 -1.834844E-03  2.035188E+03 *
```

S

```
*  1.000000E+00  0.000000E+00  0.000000E+00 *
*  0.000000E+00  1.000000E+00  0.000000E+00 *
*  0.000000E+00  0.000000E+00  1.000000E+00 *
```

MASS AXIS SYSTEM (S) DIRECTION	MASS	X-C.G.	Y-C.G.	Z-C.G.
X	1.038898E-01	-1.034606E-14	5.496468E+01	3.532288E-03
Y	1.038898E-01	1.249954E+02	4.047110E-15	3.532288E-03
Z	1.038898E-01	1.249954E+02	5.496468E+01	6.332349E-15

I(S)

```
*  9.808510E+01  2.365277E-02 -1.078710E-01 *
*  2.365277E-02  4.220762E+00 -1.833548E-02 *
* -1.078710E-01 -1.833548E-02  9.816410E+01 *
```

I(Q)

```
*  9.800973E+01                            *
*                4.220752E+00              *
*                             9.823948E+01 *
```

Q

```
*  8.197182E-01  2.522135E-04  5.727669E-01 *
* -3.187002E-04  9.999999E-01  1.576706E-05 *
* -5.727669E-01 -1.954655E-04  8.197183E-01 *
```

Section-2 Truss Updated FEM Mass Properties (Cantilevered and Free-Free) With Sensor Mass Included

SDRC I-DEAS V: FE_Modeling_&_Analysis 29-JAN-92 10:56:54

Database: emi
View : No stored View
Task: Post Processing
Model: 2-10_BAY

Units : IN
Display : No stored Option
Model Dim: 1-MAIN
Associated Workset: 2-MODELING_SET2

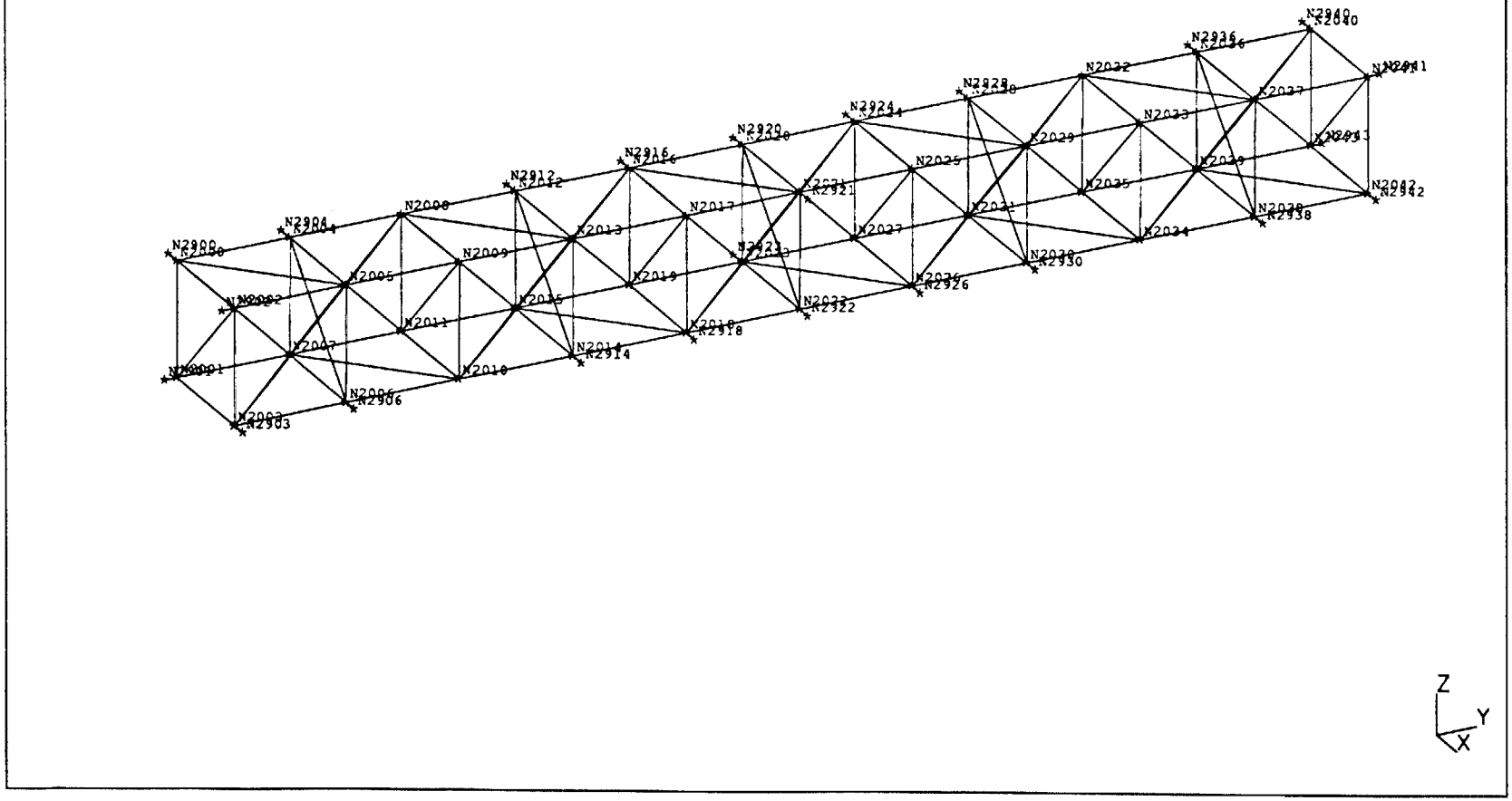

SDRC I-DEAS VI: FE_Modeling_&_Analysis 19-MAR-92 10:43:47

Database: cei
View : none, none, none, none
Task: Post Processing
Model: 2-10_BAY

Units : IN
Display : none, none, none, none
Model Bin: 1-MAIN
Associated Workset: 2-MODELING_SET2

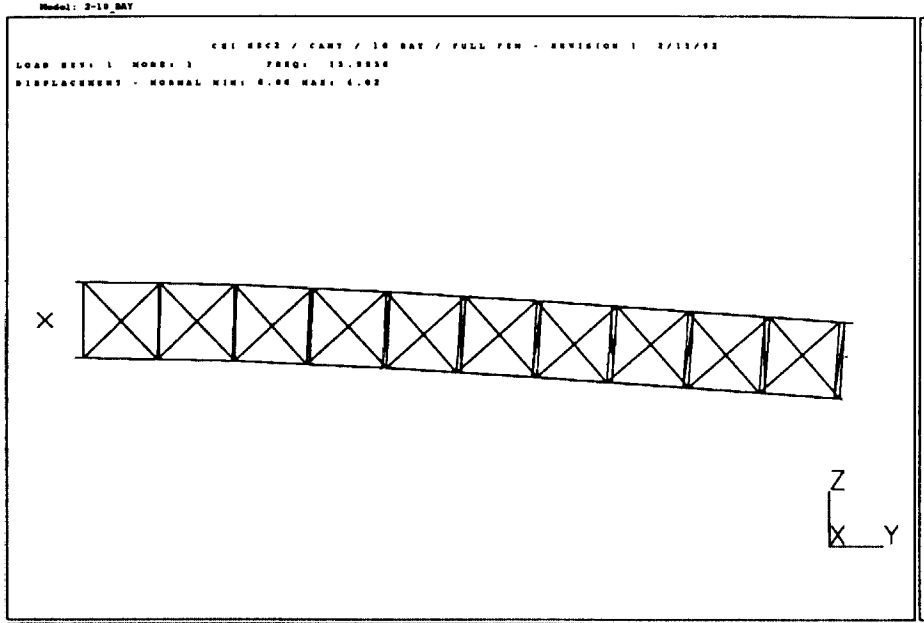

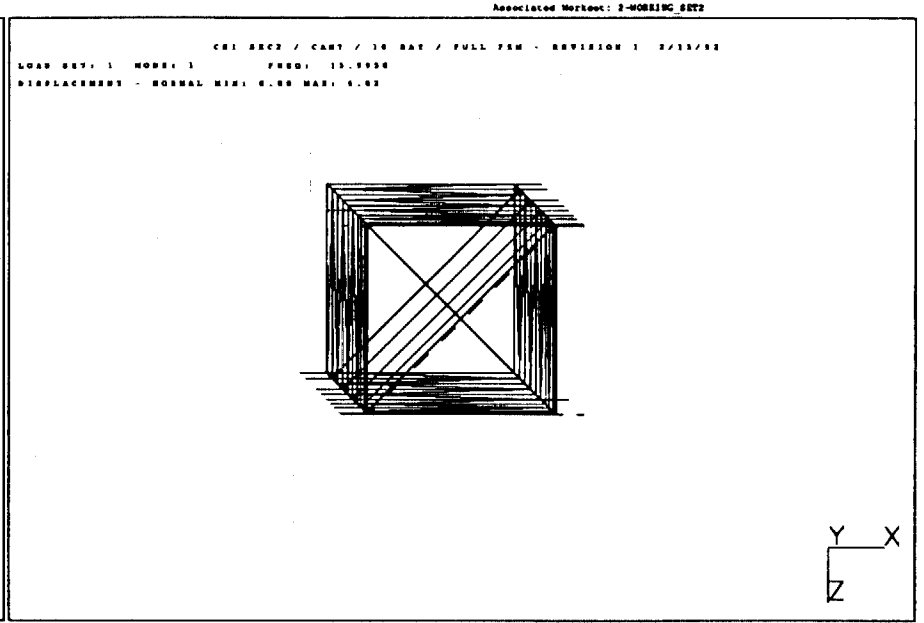

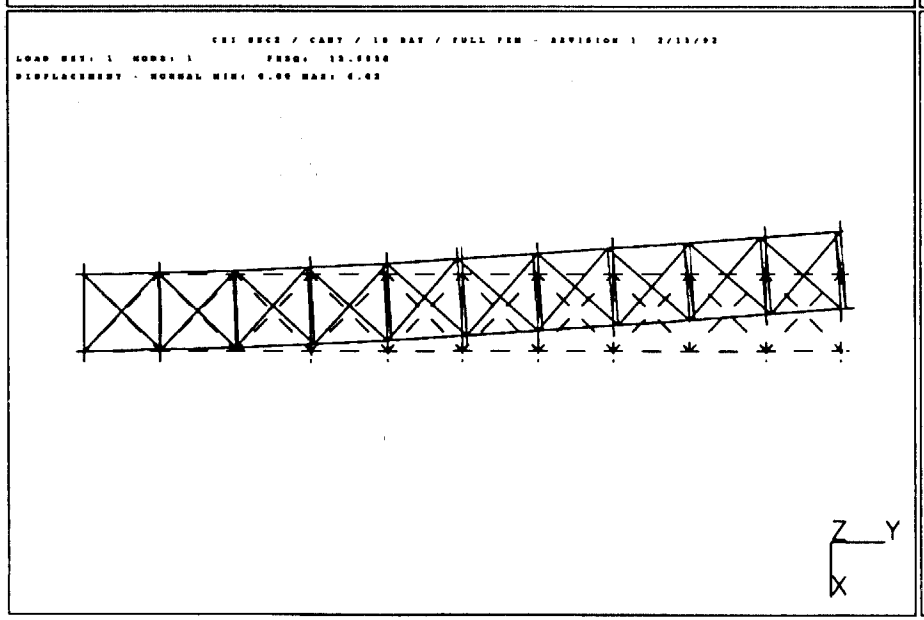

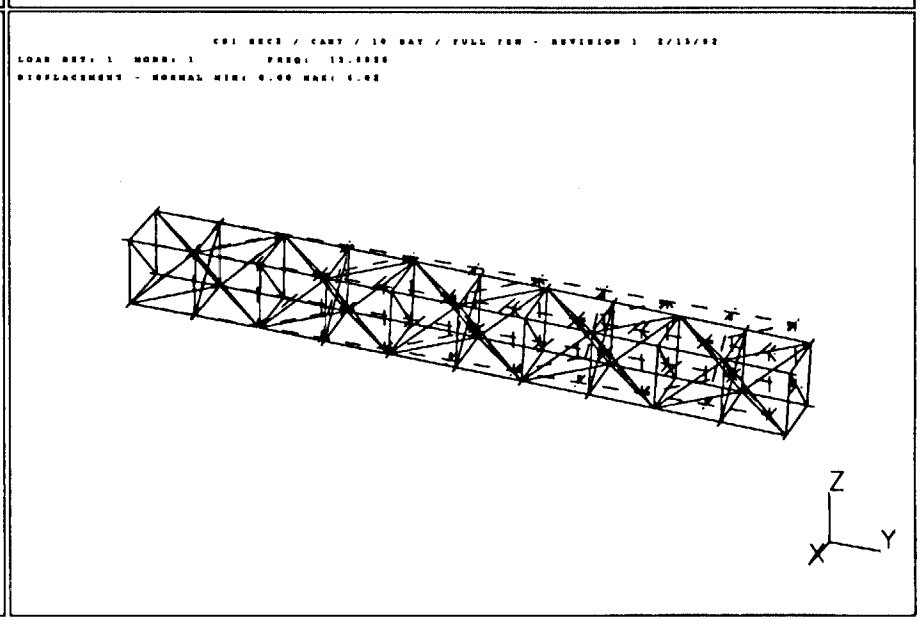

SDRC I-DEAS VI: FE_Modeling_&_Analysis 19-MAR-92 10:45:48

Database: col
View : none, none, none, none
Task: Post Processing
Model: 2-10_BAY

Units : IN
Display : none, none, none, none
Model Bin: 1-MAIN
Associated Workset: 2-MODELING_SET2

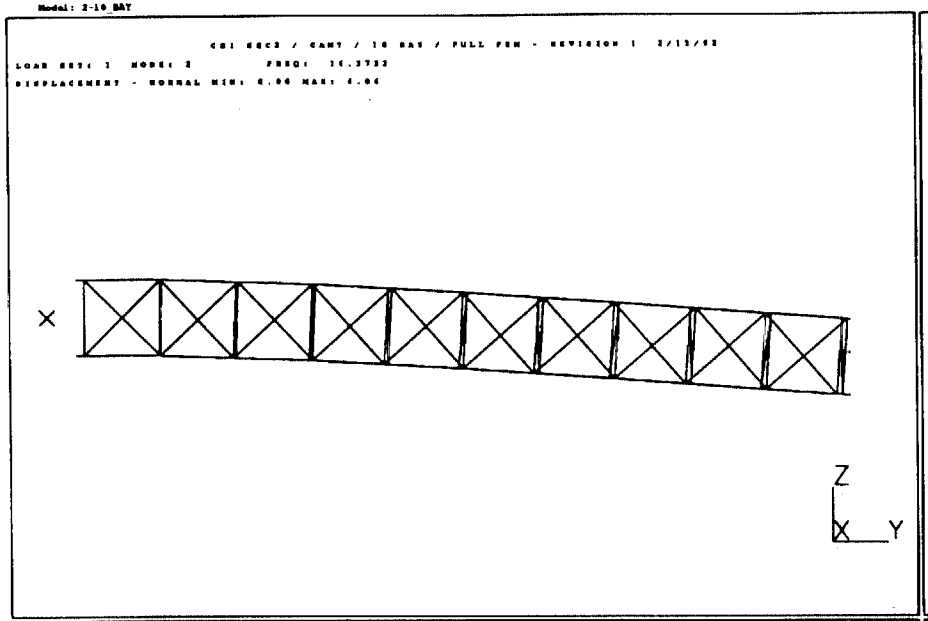

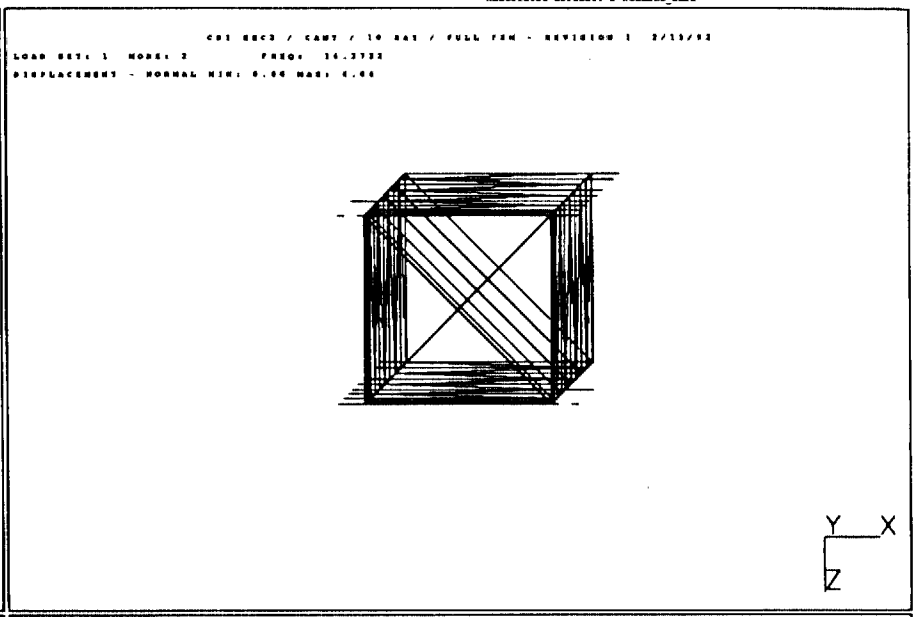

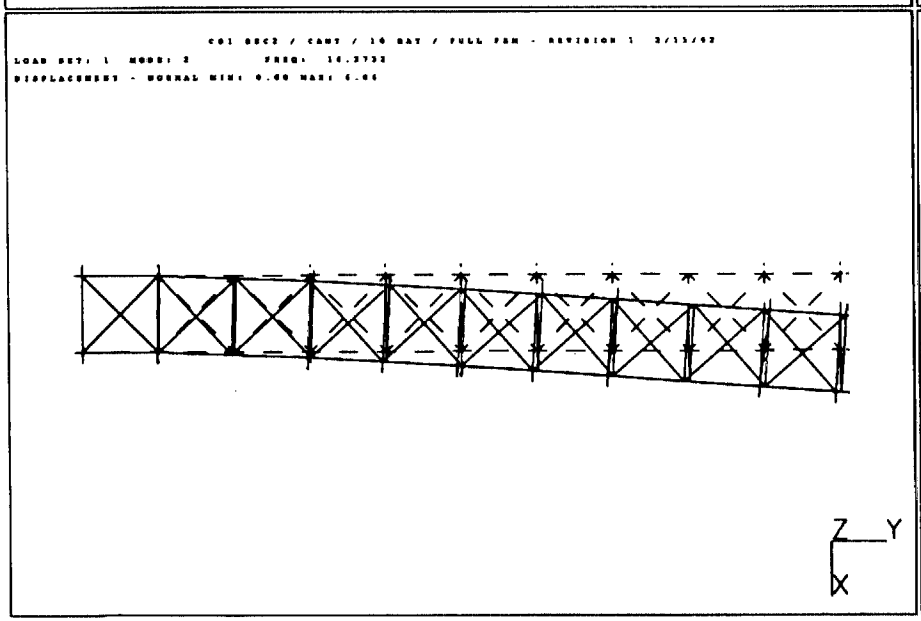

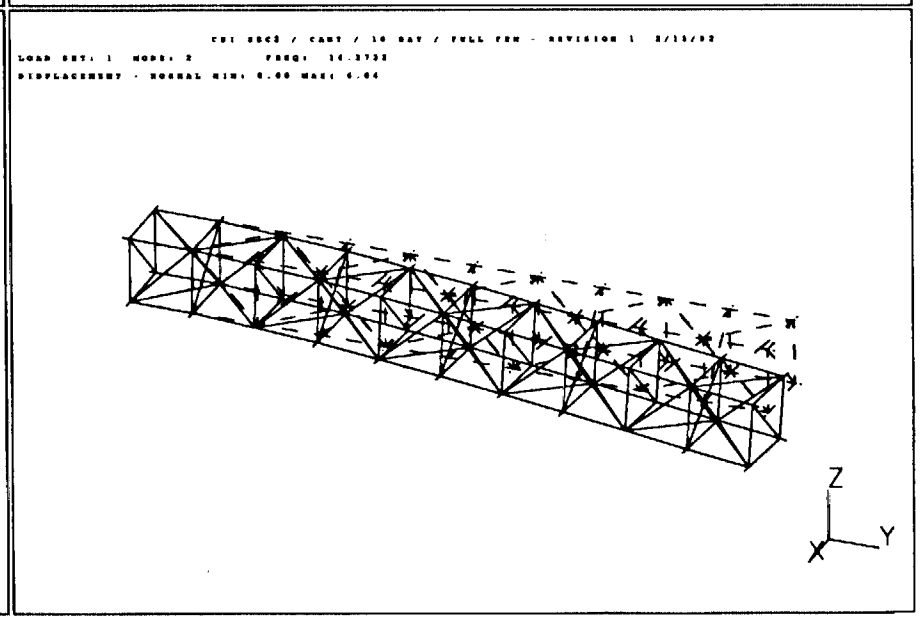

SDRC I-DEAS VI: FE_Modeling_&_Analysis

19-MAR-92 10:46:06

Database: coi
View : none, none, none, none
Task: Post Processing
Model: 2-10_BAY

Units : IN
Display : none, none, none, none
Model Bin: 1-MAIN
Associated Workset: 2-MORLING_SET2

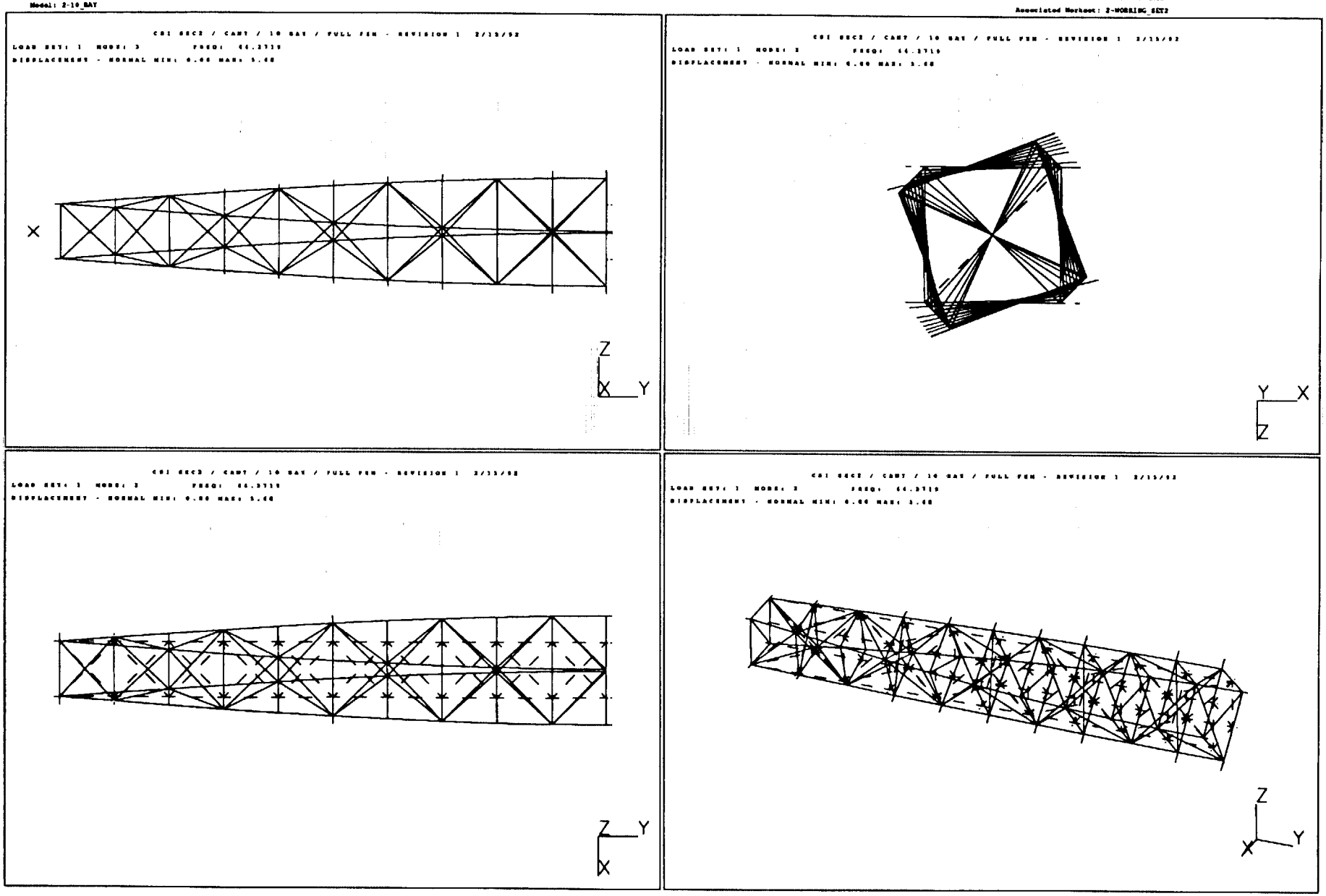

SDRC I-DEAS VI: FE_Modeling_&_Analysis

19-MAR-92 10:46:21

Database: cai
View : none, none, none, none
Task: Post Processing
Model: 2-10_BAY

Units : IN
Display : none, none, none, none
Model Bin: 1-MAIN
Associated Workset: 2-WORKING_SET2

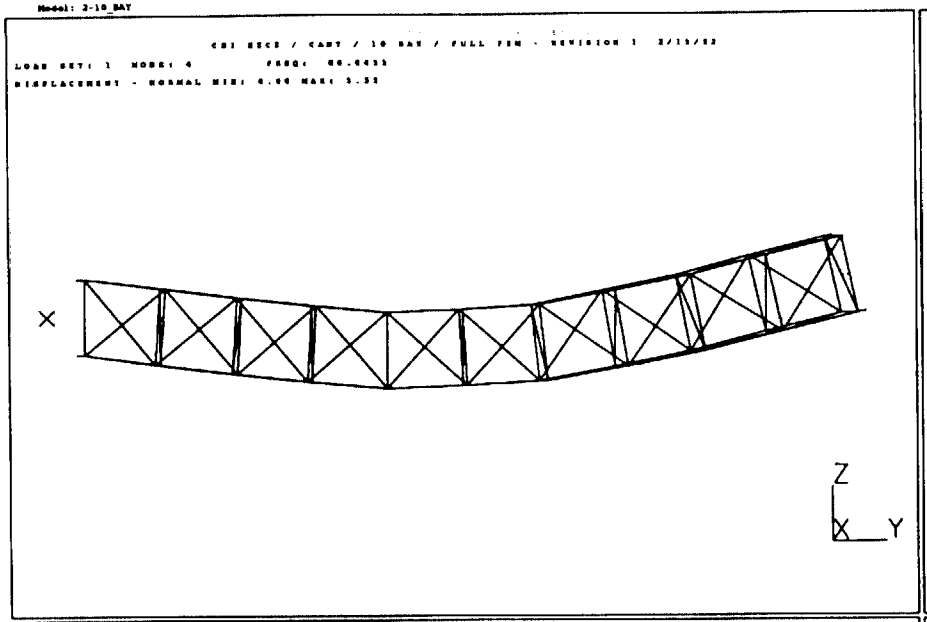

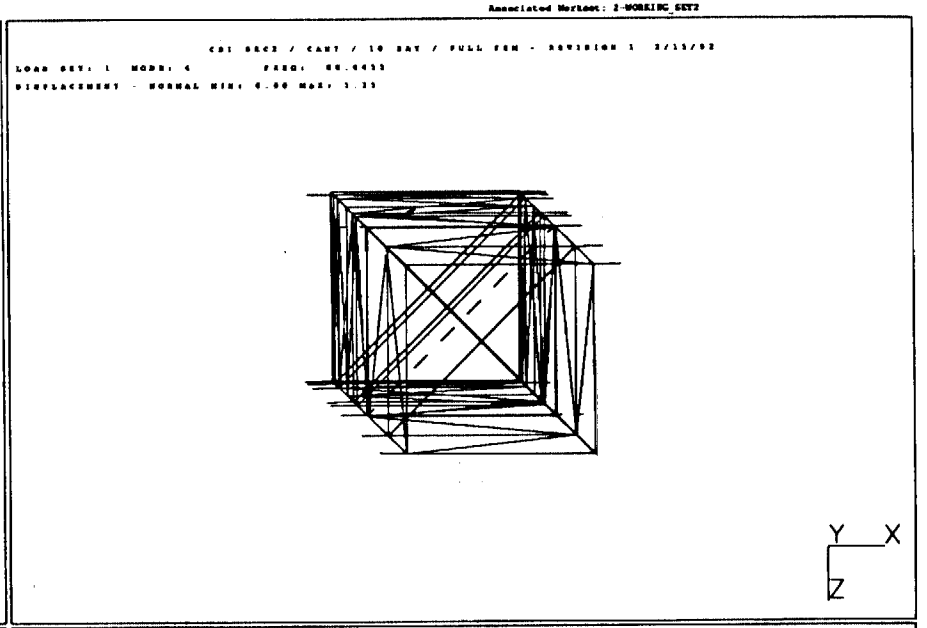

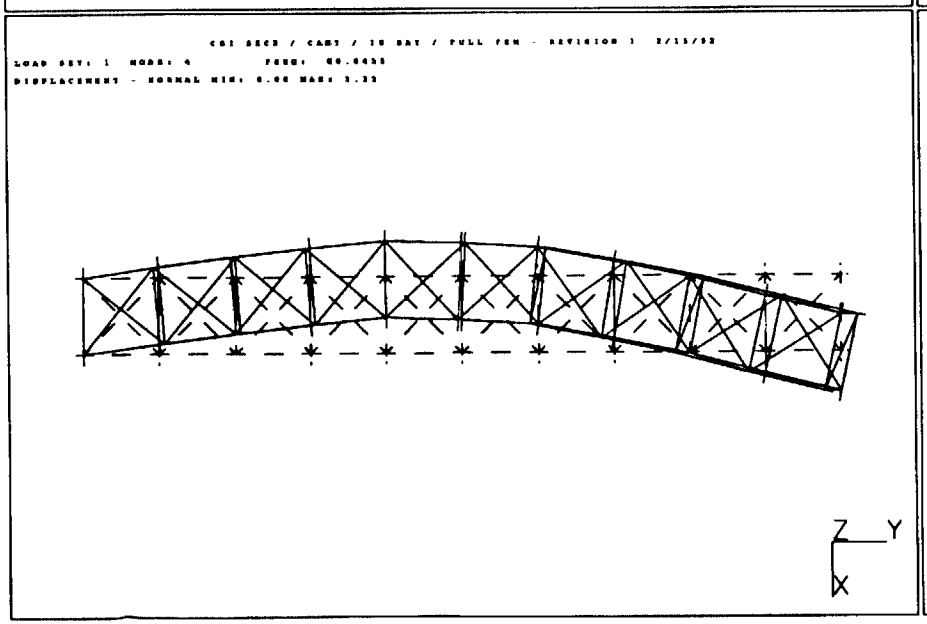

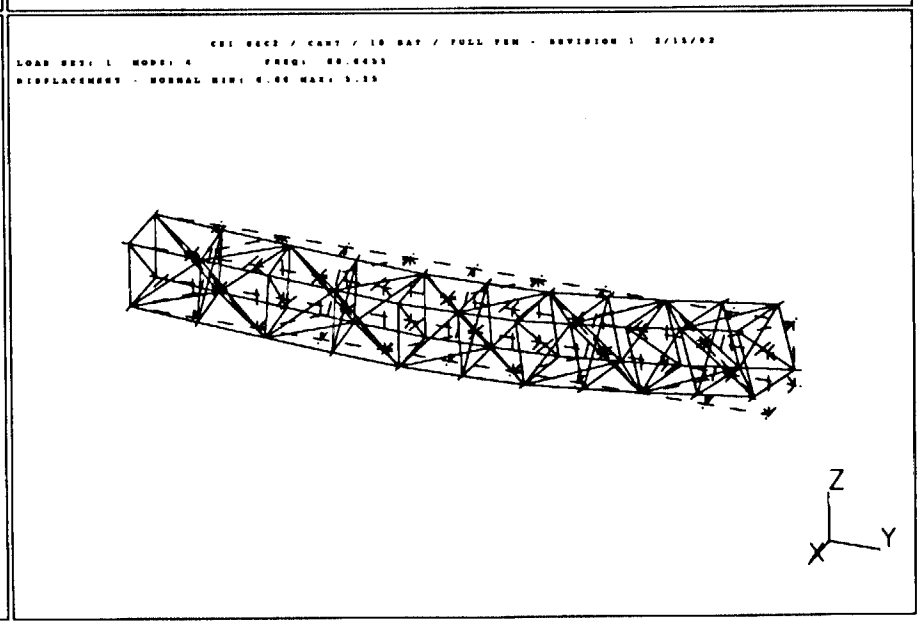

SDRC I-DEAS VI: FE_Modeling_&_Analysis

19-MAR-92 10:47:08

Database: cal
View : none, none, none, none
Task: Post Processing
Model: 2-10_BAY

Units : IN
Display : none, none, none, none
Model Dir: 1-MAIN
Associated Workset: 2-WORKING_SET2

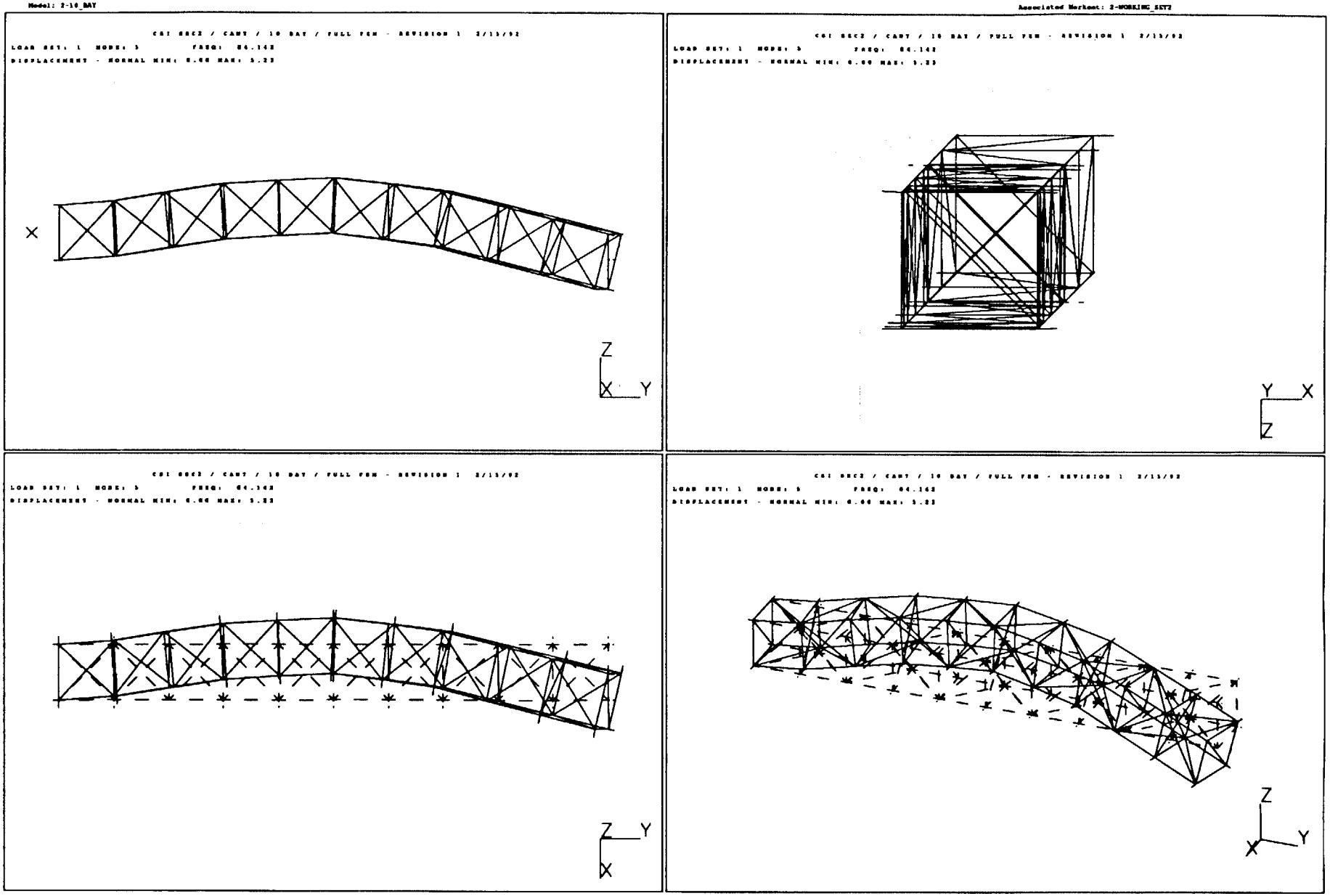

SDRC I-DEAS VI: FE_Modeling_&_Analysis

19-MAR-92 10:47:47

Database: cei
View : none, none, none, none
Task: Post Processing
Model: 2-10_BAY

Units : IN
Display : none, none, none, none
Model Dir: 1-MAIN
Associated Workset: 2-MORRING_SET2

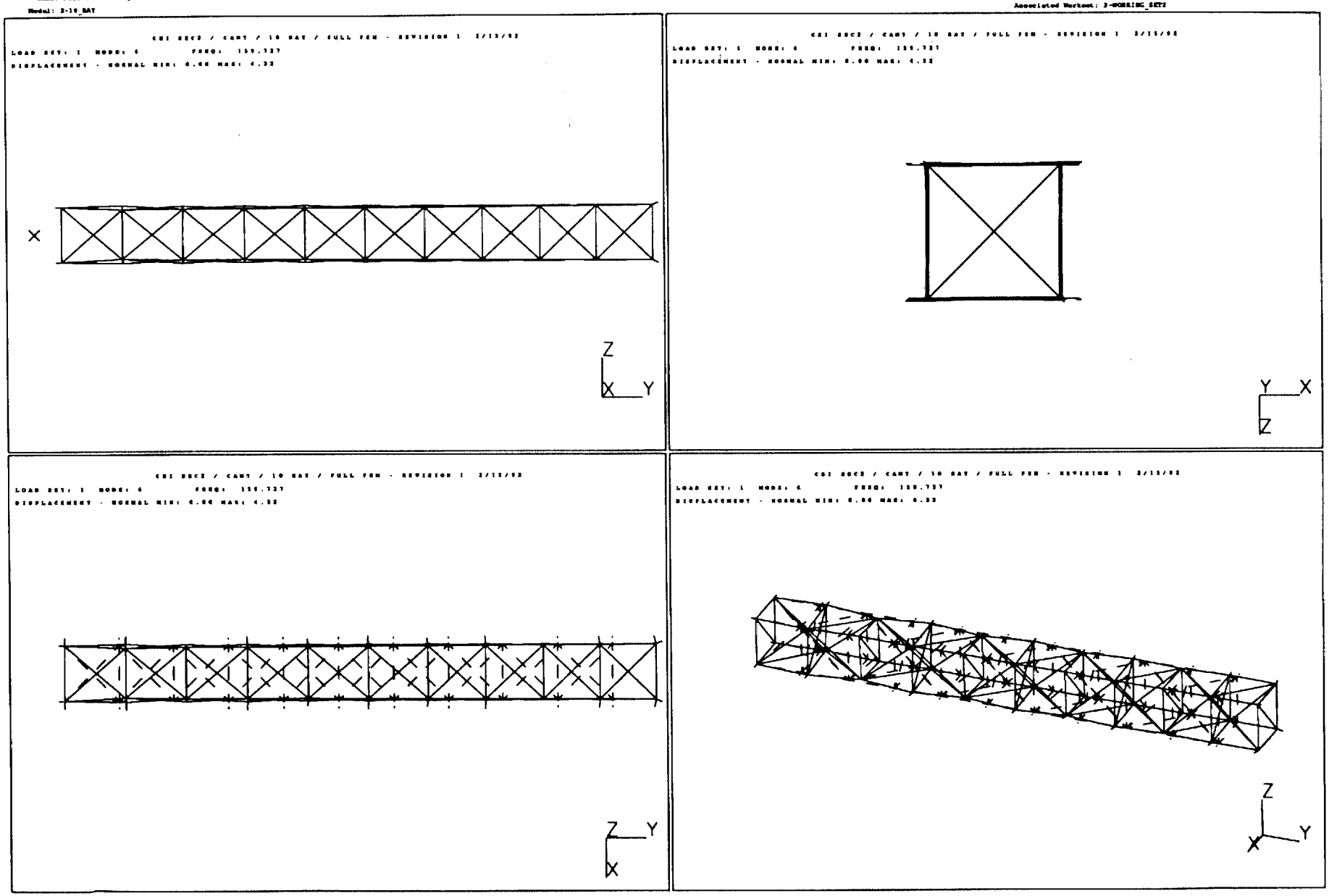

Database: cai
View : none, none, none, none
Task: Post Processing
Model: 2-10_BAY

Units : IN
Display : none, none, none, none
Model Blk: 1-MAIN
Associated Workset: 2-MODELING_SET2

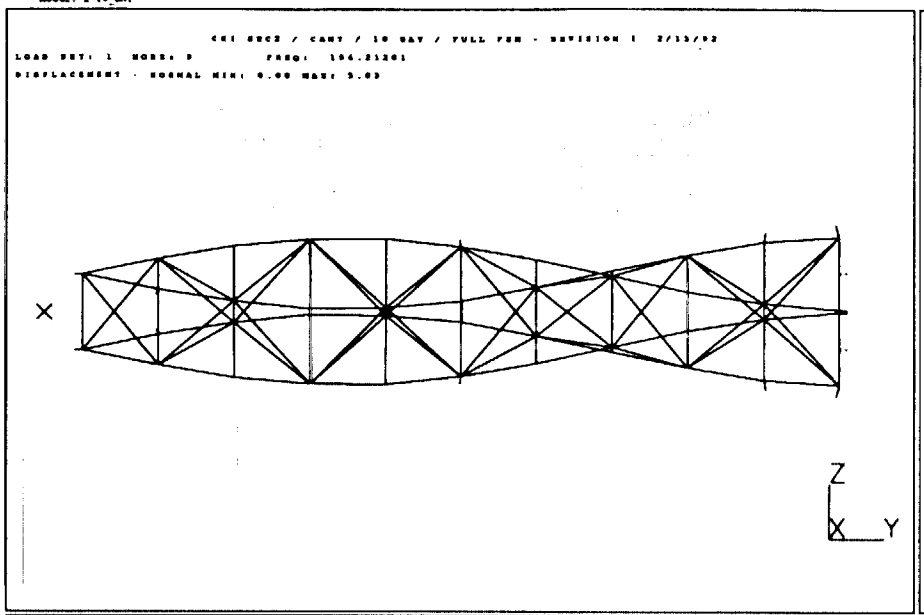

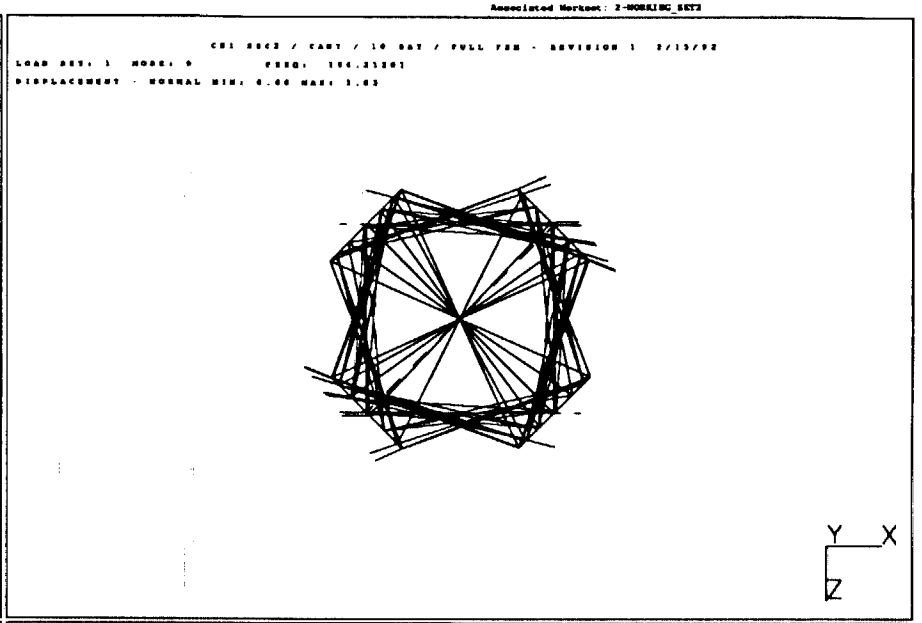

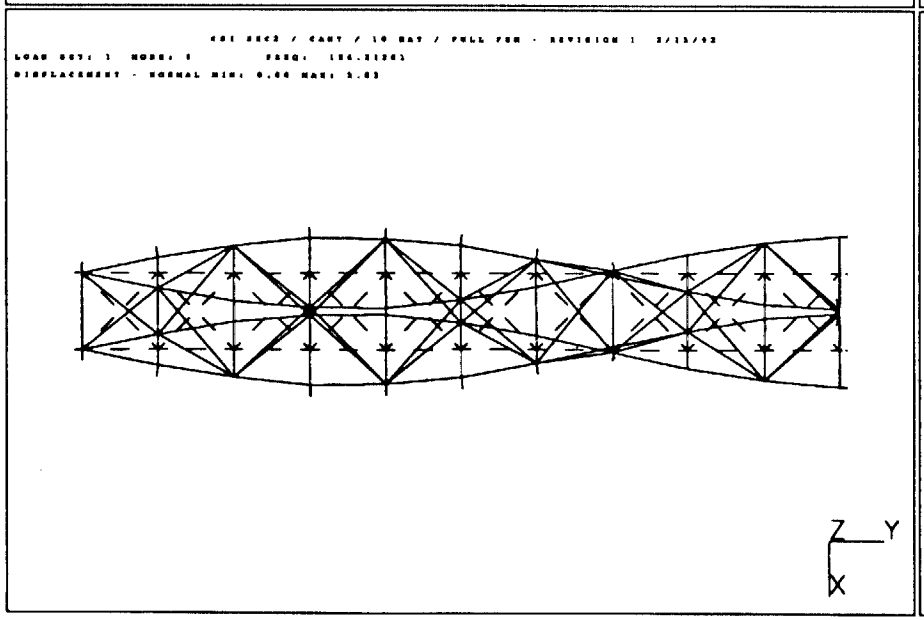

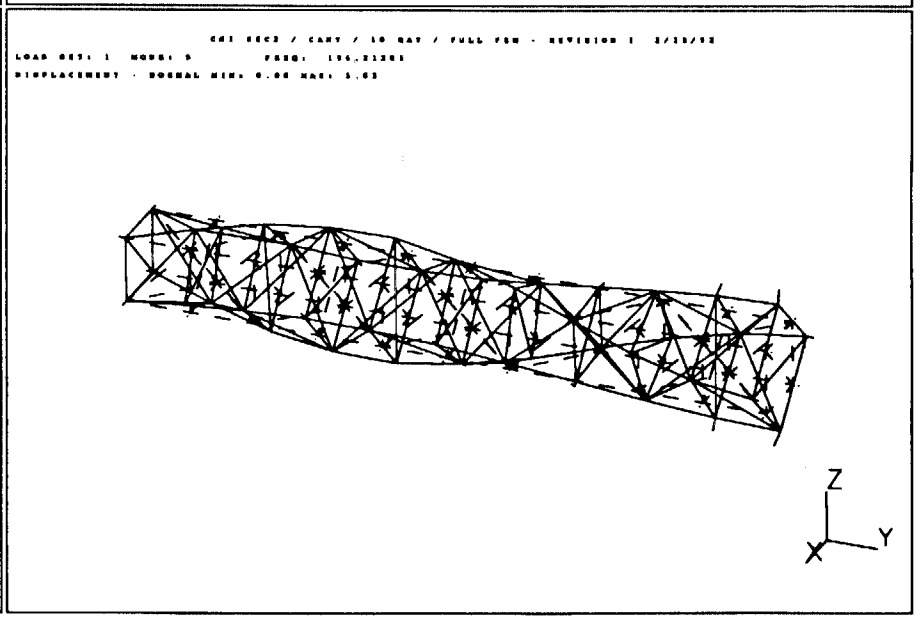

SDRC I-DEAS VI: FE_Modeling_&_Analysis

19-MAR-92 10:38:28

Database: cei
View : none, none, none, none
Task: Post Processing
Model: 2-10 BAY

Units : IN
Display : none, none, none, none
Model Bin: 1-MAIN
Associated Workset: 2-MODELING_SET2

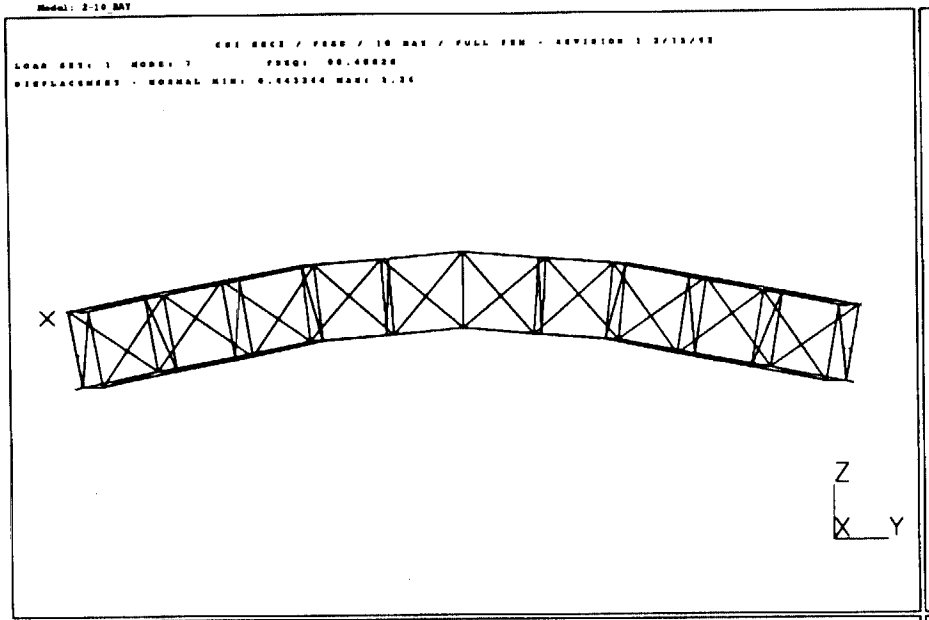

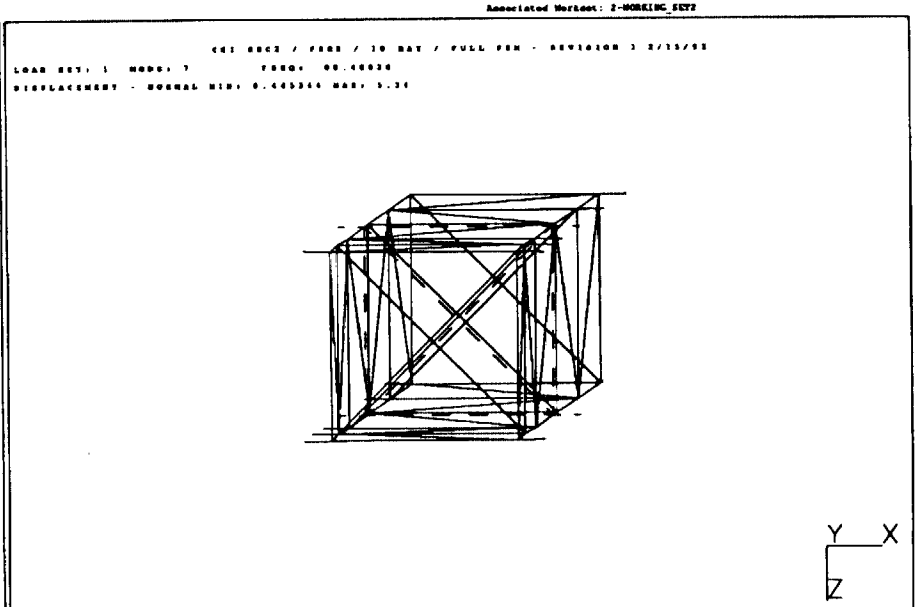

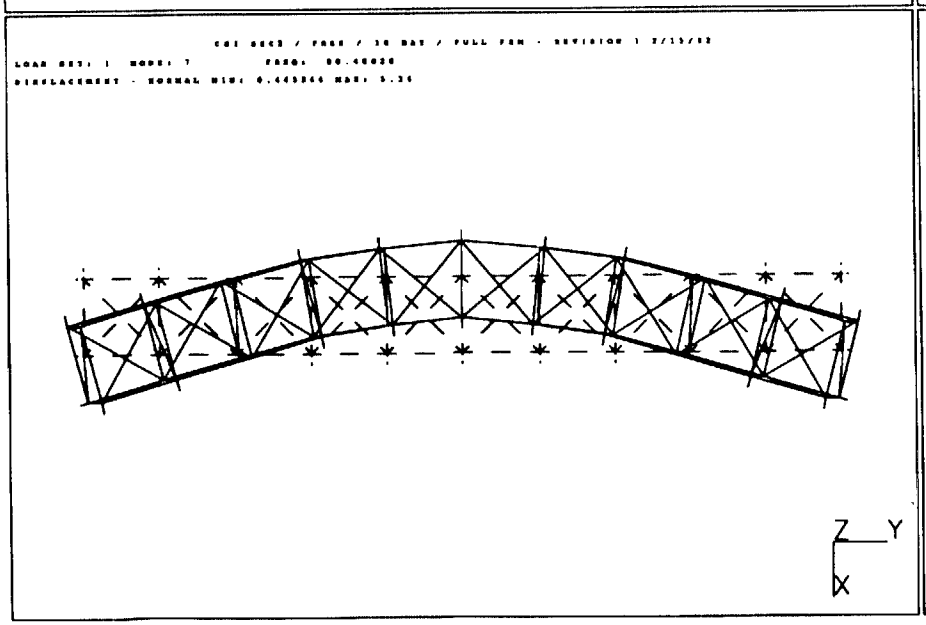

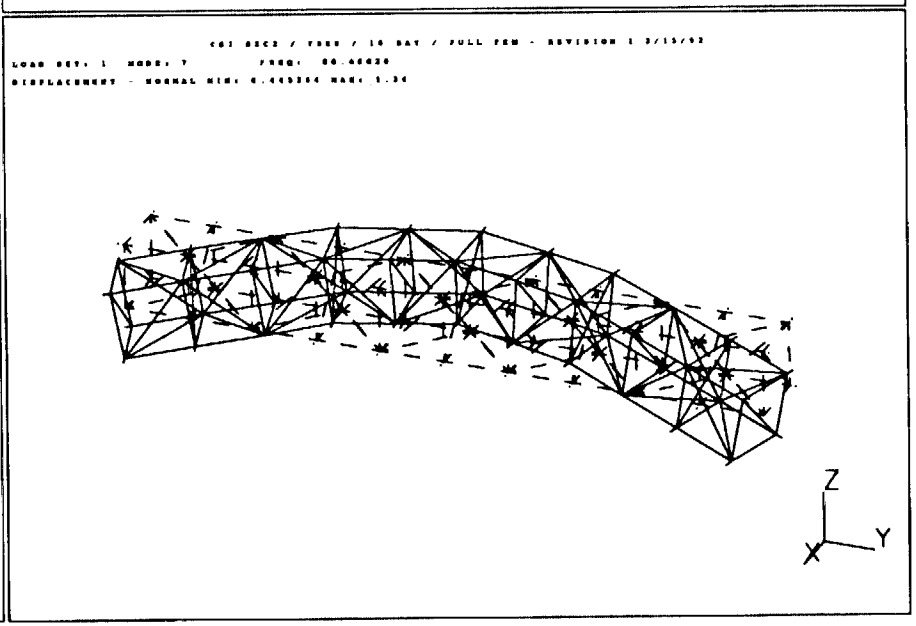

SDRC I-DEAS V1: FE_Modeling_&_Analysis 19-MAR-92 10:39:07

Database: cai
View : none, none, none, none
Task: Post Processing
Model: 2-10_BAY
Units : IN
Display : none, none, none, none
Model Bin: 1-MAIN
Associated Workset: 2-WORKING_SET2

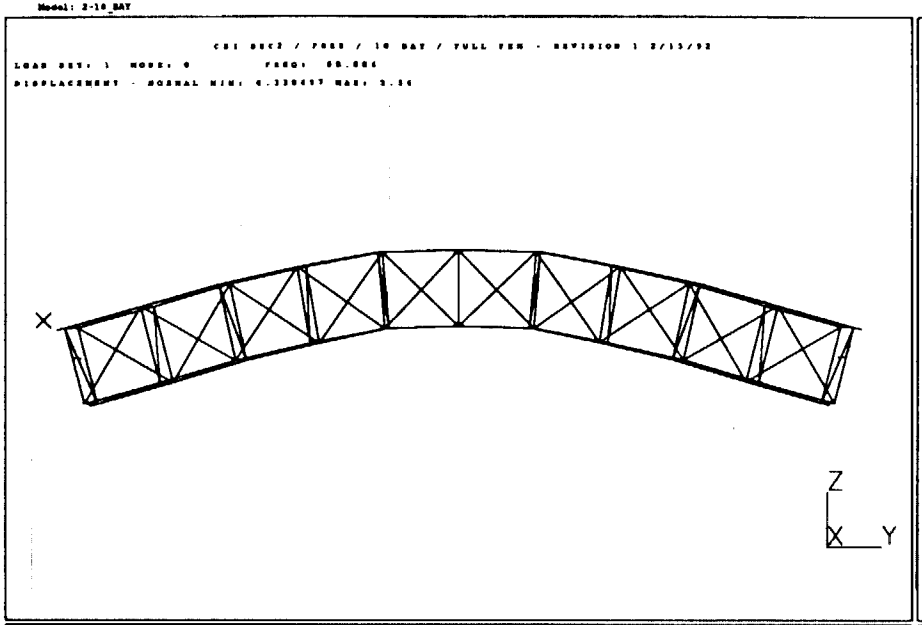

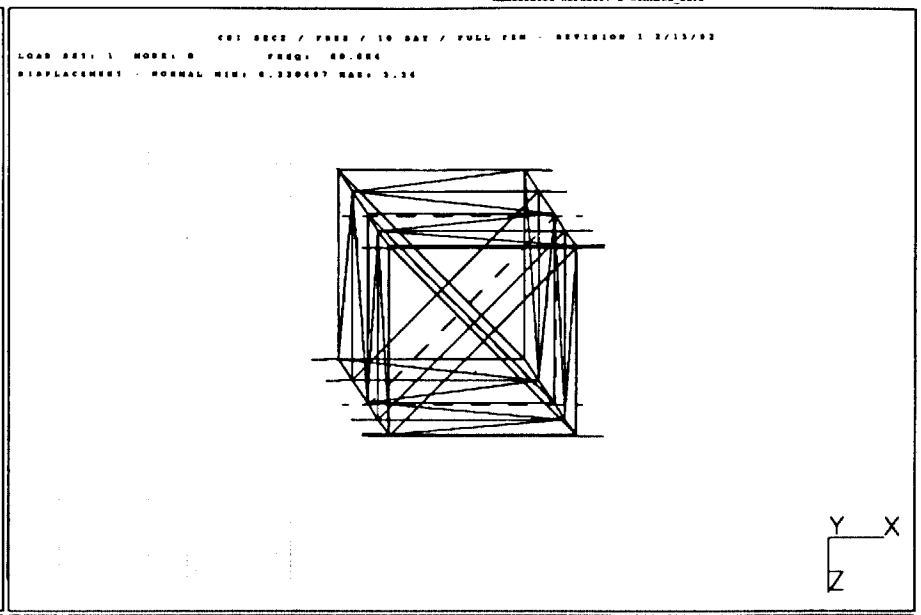

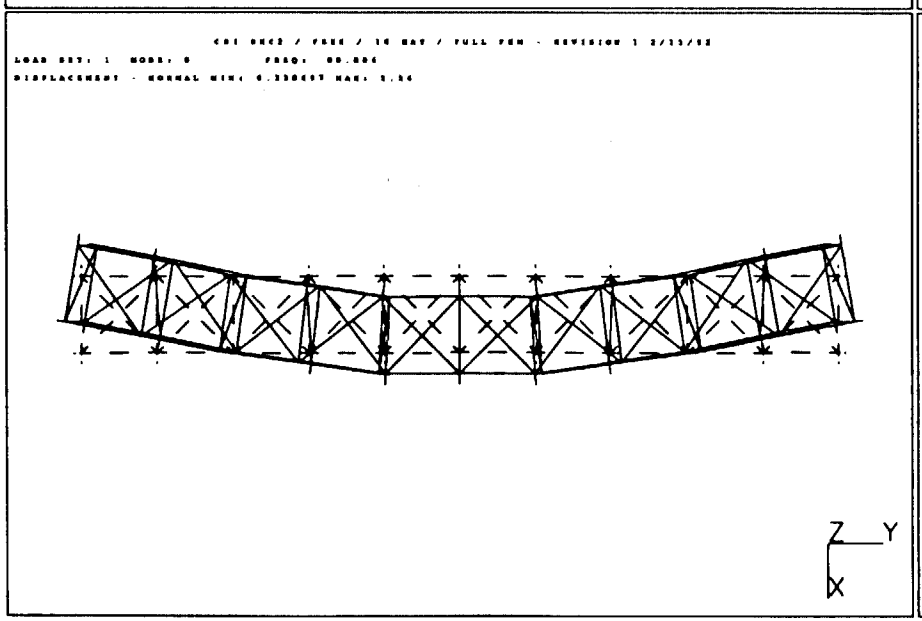

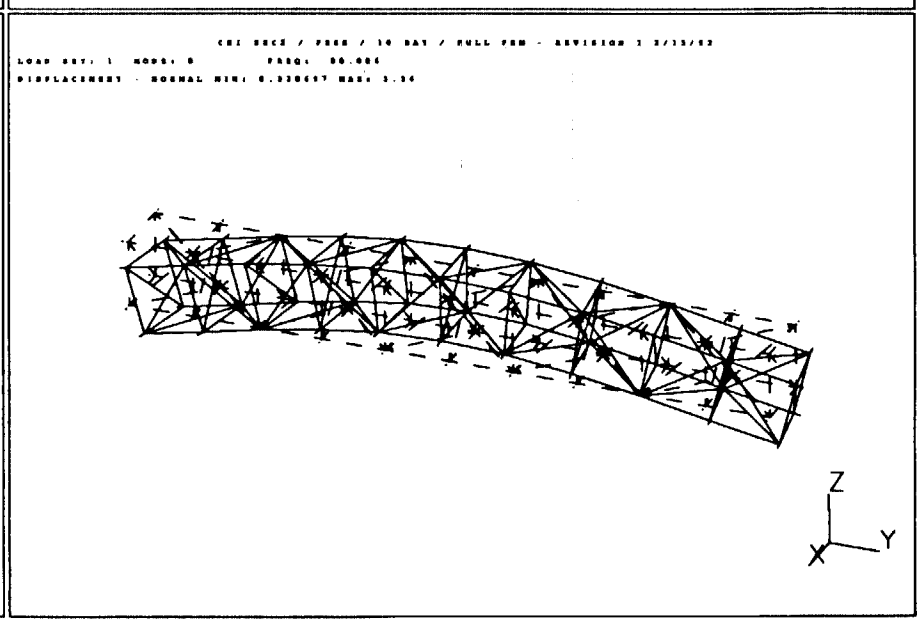

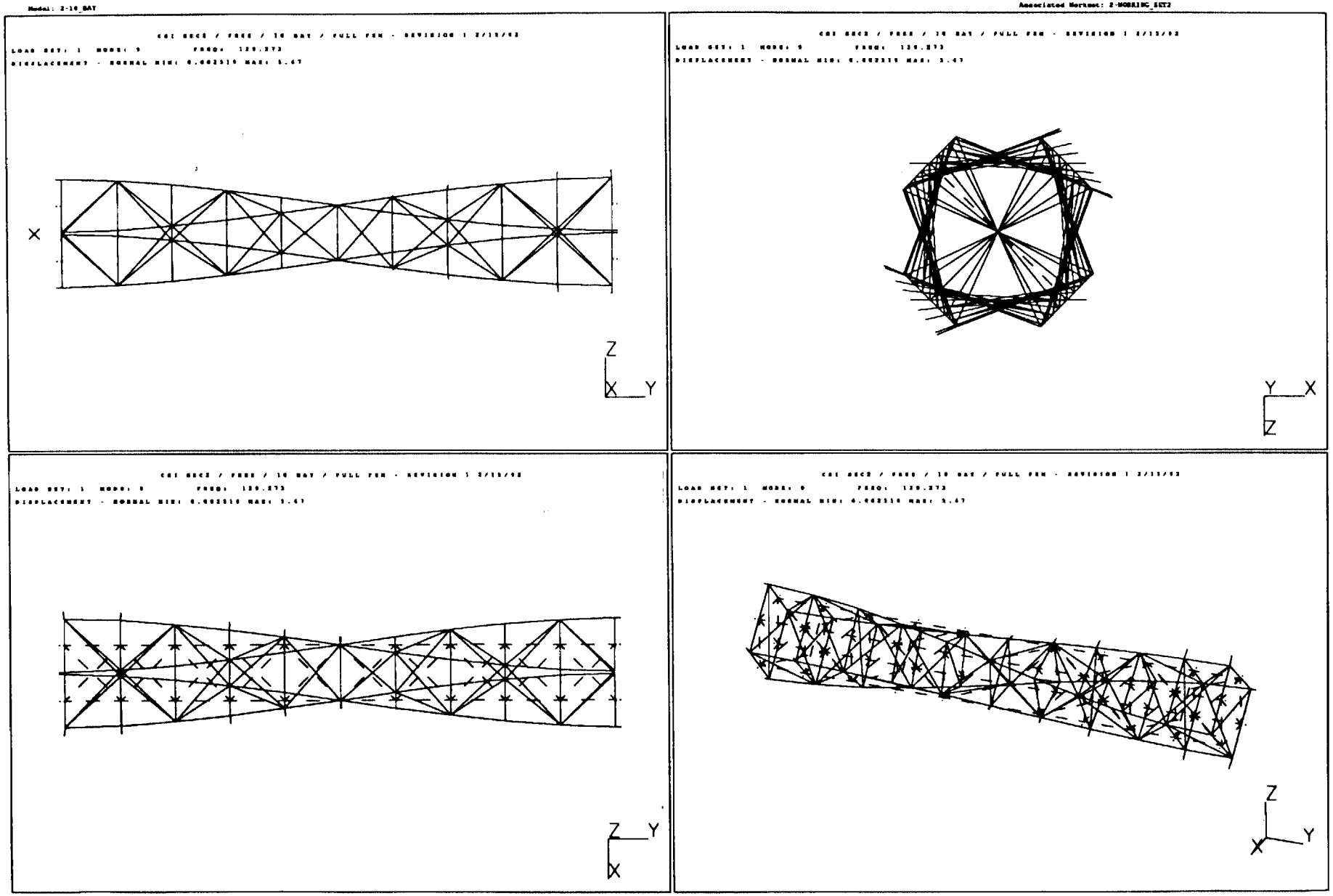

SDRC I-DEAS VI: FE_Modeling_&_Analysis

19-MAR-92 10:40:08

Database: col
View : none, none, none, none
Task: Post Processing
Model: 2-10_BAY

Units : IN
Display : none, none, none, none
Model Dir: 1-MAIN
Associated Workset: 2-WORKING_SET2

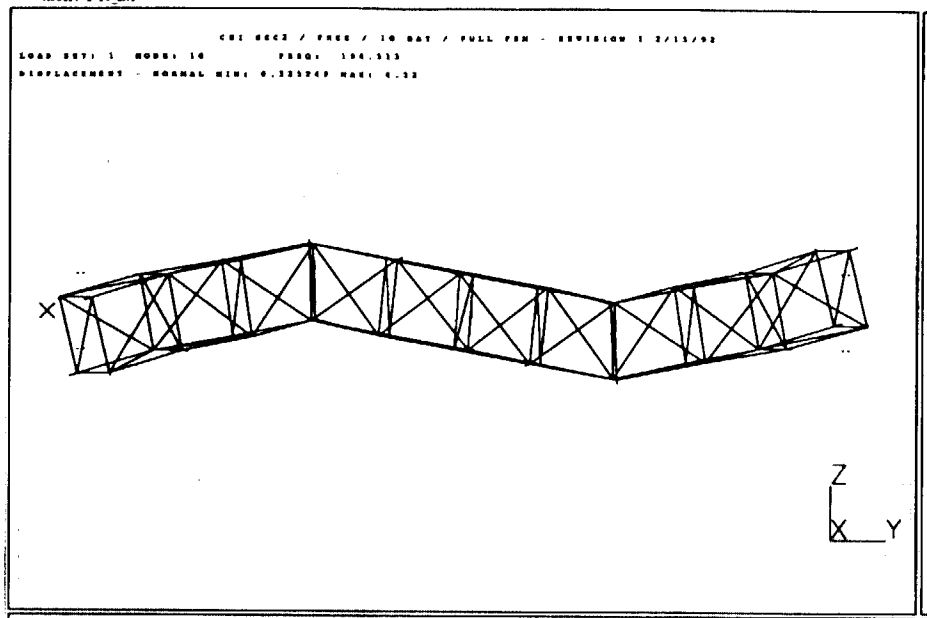

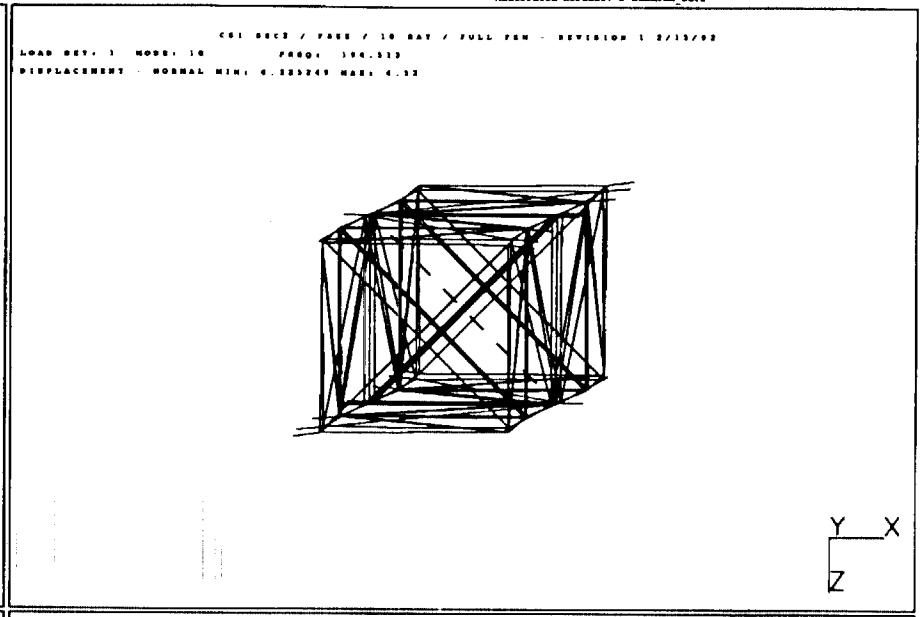

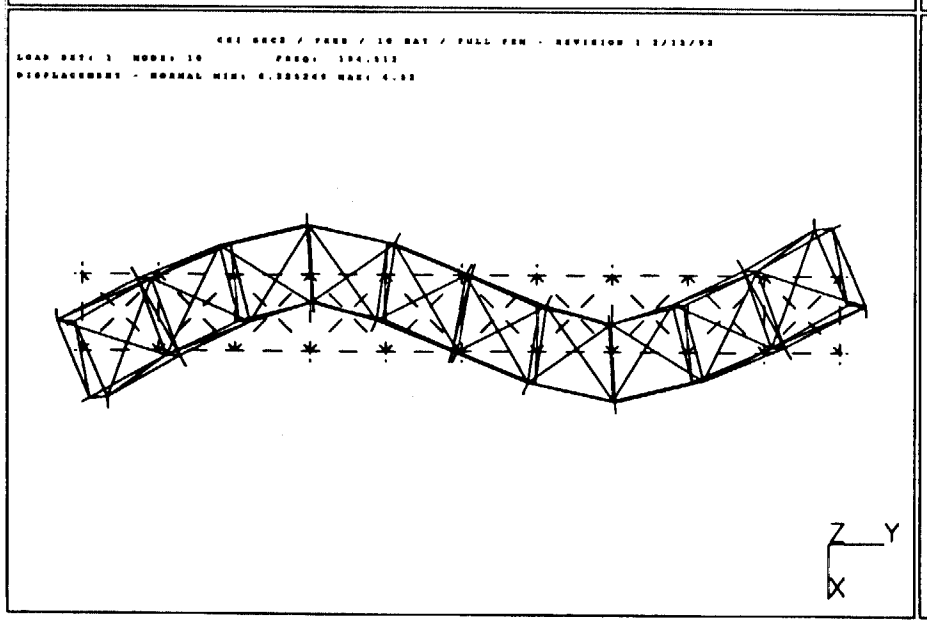

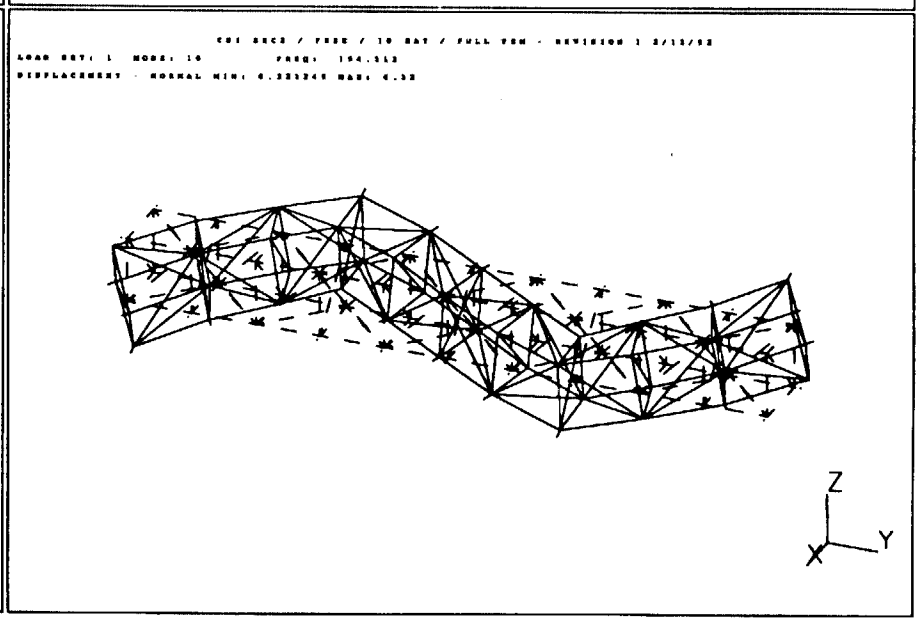

Database: osi
View : none, none, none, none
Task: Post Processing
Model: 2-10_BAY

Units : IN
Display : none, none, none, none
Model Dir: I-MAIN
Associated Workset: 2-MORRING_SET2

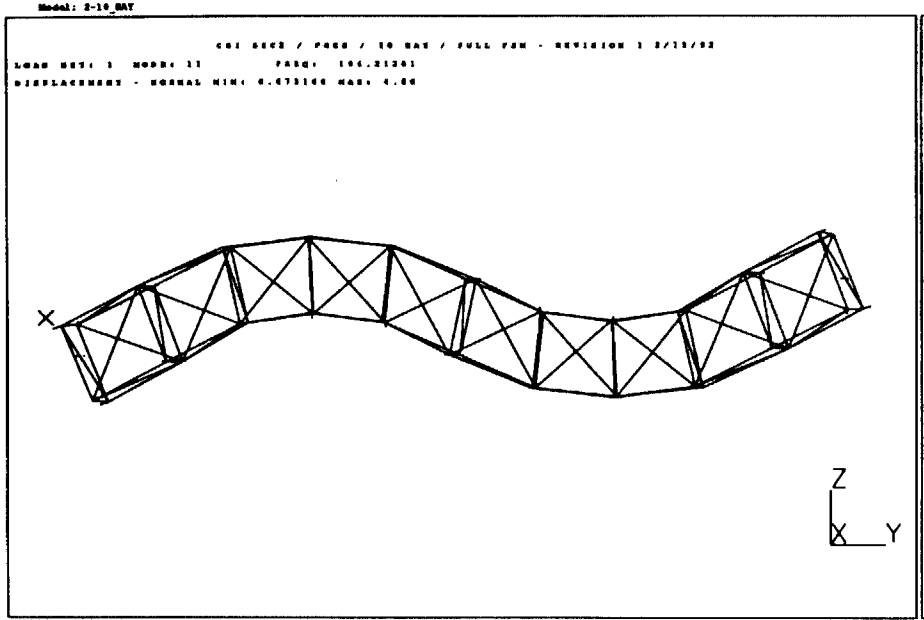

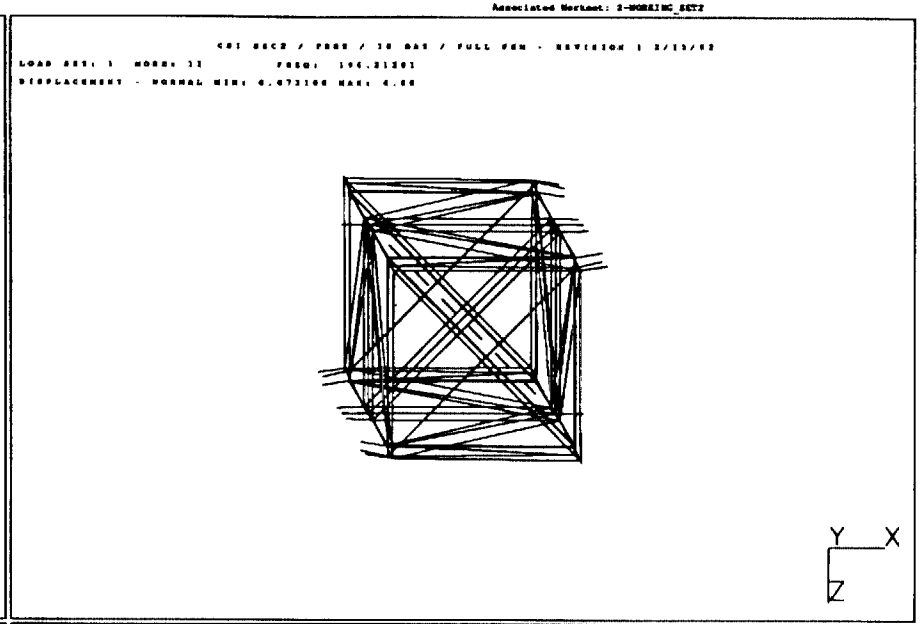

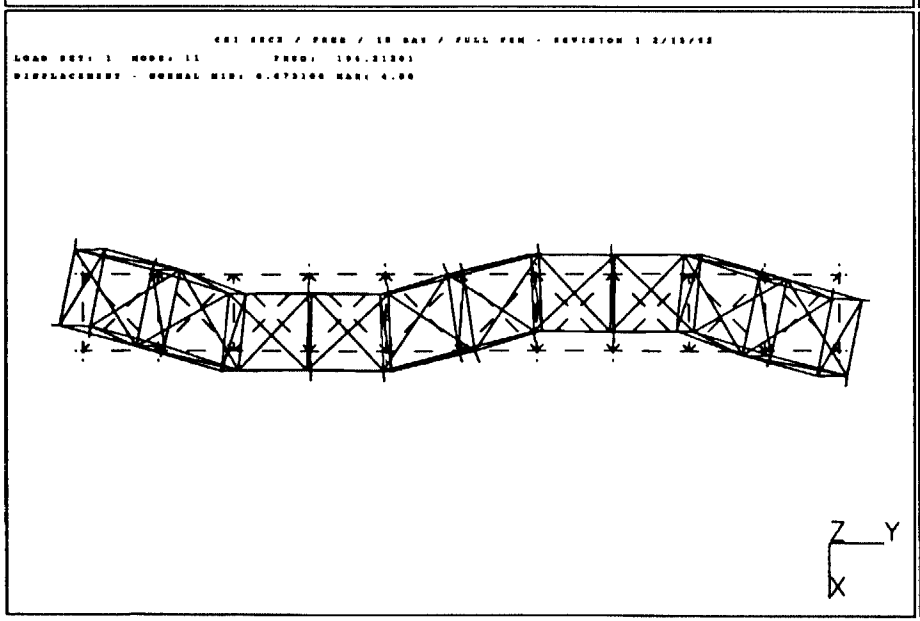

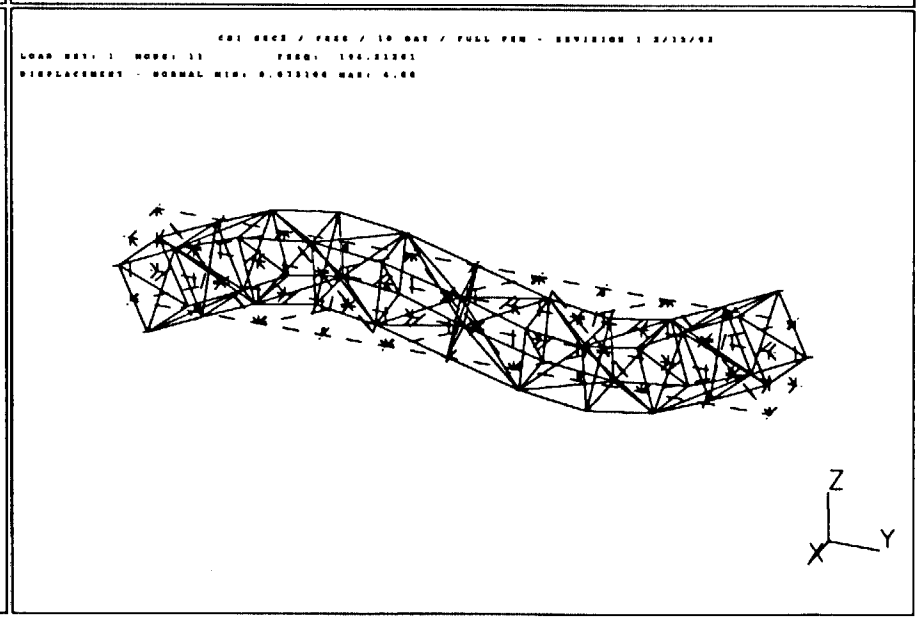

SDRC I-DEAS VI: FE_Modeling_&_Analysis

19-MAR-92 10:41:07

Database: col
View : none, none, none, none
Task: Post Processing
Model: 2-10_BAY

Units : IN
Display : none, none, none, none
Model Bin: 1-MAIN
Associated Workset: 2-WORKING_SET2

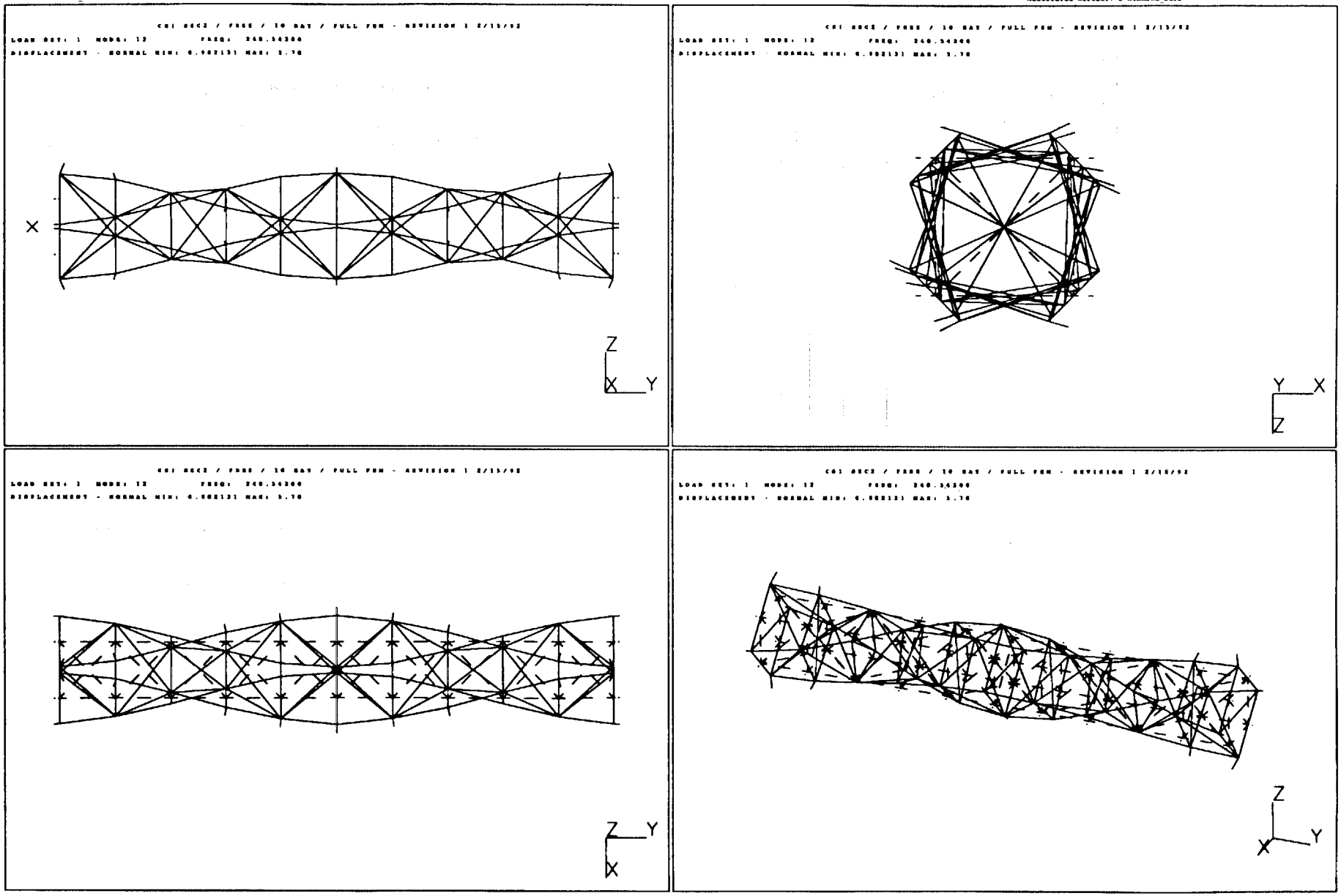

Database: csi
View : none, none, none, none
Task: Post Processing
Model: 2-10_BAY

Units : IN
Display : none, none, none, none
Model Bin: 1-MAIN
Associated Workset: 2-WORKING_SET2

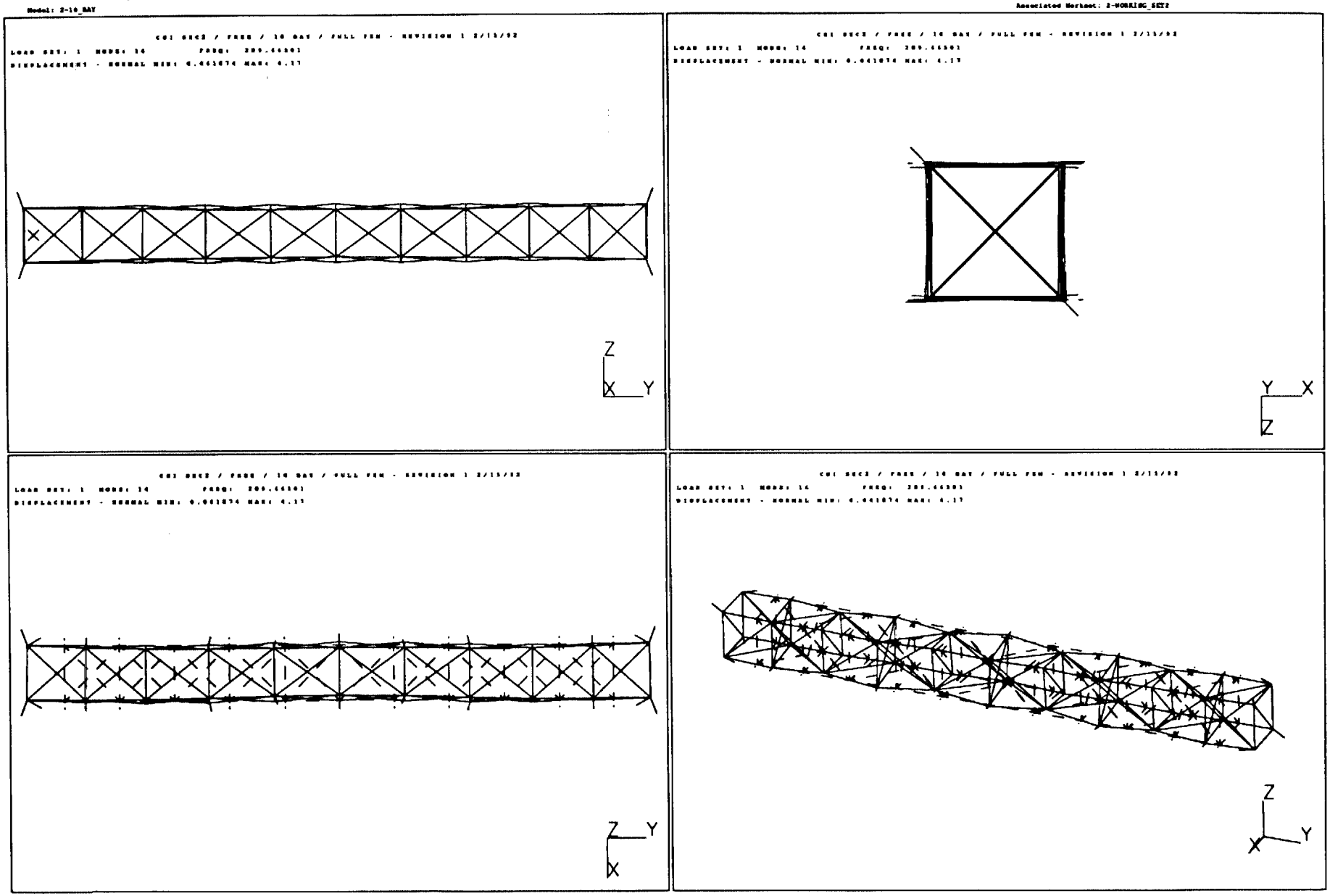

APPENDIX E

TEST AND ANALYSIS RESULTS FOR TRUSS SECTION NO. 3 DYNAMIC TESTS

Table E-1 Test Log of Modal Tests of Section 3 - Cantilevered Tests

Test No.	Type of Excitation	Frequency Range	Comments
3a	Continuous Random	0 - 200 Hz	Cantilevered test setup, with Section 3 test item affixed at one end to the test fixture which had been previously bolted to the laboratory concrete floor. Single shaker setup, with the shaker supported by a bungee cord. Shaker at test point no. 21, oriented to apply loading in the horizontal plane with a skew angle of 45 degrees relative to the longitudinal and lateral axes.
3b	Continuous Random	0 - 400 Hz	Same test configuration as test no. 3a.
3c	Continuous Random	14.75 Hz - 27.25 Hz	Same test configuration as test no. 3a. Zoom for 1st set of bending modes.
3d	Continuous Random	55.75 Hz - 68.25 Hz	Same test configuration as test no. 3a. Zoom for 1st torsional mode.
3e	Continuous Random	90.75 Hz - 103.25 Hz	Same test configuration as test no. 3a. Zoom for 2nd set of bending modes.
3f	Continuous Random	172.75 Hz - 185.25 Hz	Same test configuration as test no. 3a. Zoom for 2nd torsional mode.
3g	Continuous Random	185 Hz - 235 Hz	Same test configuration as test no. 3a. Zoom for higher order modes.
3h	Continuous Random	225.75 Hz - 238.25 Hz	Same test configuration as test no. 3a. Zoom for 1st axial mode.

Table E-1 Test Log of Modal Tests of Section 3 - Free-Free Tests

Test No.	Type of Excitation	Frequency Range	Comments
3i	Continuous Random	0 - 200 Hz	Free-Free test setup, with Section 3 test item supported at four points with seperate bungee cords. Dual shaker setup, with one shaker at each end supported by seperate bungee cords. Shaker at test point no. 2 oriented to apply loading in the horizontal plane with a skew angle of 45 degrees relative to the longitudinal and lateral axes. Shaker at test point no. 21 oriented to apply loading in the vertical plane with a skew angle of 45 degrees relative to vertical and lateral axes.
3j	Continuous Random	0 - 400 Hz	Same test configuration as test no. 3i.
3k	Continuous Random	109.875 Hz - 116.125 Hz	Same test configuration as test no. 3i. Zoom for 1st set of bending modes.
3l	Continuous Random	116.75 Hz - 129.25 Hz	Same test configuration as test no. 3i. Zoom for 1st torsional mode.
3m	Continuous Random	225.75 Hz - 238.25 Hz	Same test configuration as test no. 3i. Zoom for 2nd set of bending modes and 2nd torsional mode.
3n	Continuous Random	375.75 Hz - 388.25 Hz	Same test configuration as test no. 3i. Zoom for 1st axial mode.
3o	Continuous Random	112.219 Hz - 113.78 Hz	Same test configuration as test no. 3i. Zoom for 1st set of bending modes.
3p	Continuous Random	109.875 Hz - 116.125 Hz	Same test configuration as test no. 3i with the exception of moving the shaker at test point no. 21 from the vertical plane to the horizontal plane. The skew angle was 45 degrees relative to the longitudinal and lateral axes.
3q	Continuous Random	225.75 Hz - 238.25 Hz	Same test configuration as 3p. Check for linearity. Nominal input force levels. Zoom for 2nd set of bending modes and 2nd torsional mode.
3r	Continuous Random	225.75 Hz - 238.25 Hz	Same test configuration as 3p. Check for linearity. Twice nominal input force levels. Zoom for 2nd set of bending modes and 2nd torsional mode.
3s	Continuous Random	225.75 Hz - 238.25 Hz	Same configuration as 3p. Check for linearity. 20% of nominal input force levels. Zoom for 2nd set of bending modes and 2nd torsional mode.

Table E-2 Modal Testing Parameters Summary - Section 3 Cantilever Modes

Mode No.	Nat Freq (Hz)	Excitation Method	Frequency Span (Hz)	No. Avg	Test No.	Type of Window	% Overlap	Sample Length(Sec)	Frequency Resolution (Hz)	No. of Freq Lines	Function Universal File Name ( ).unv
1	20.4	Continuous Random	14.75 - 27.25	30	3c	Hanning	0	32	0.03125	400	s3cafu14
2	20.7	Continuous Random	14.75 - 27.75	30	3c	Hanning	0	32	0.03125	400	s3cafu14
3	61.3	Continuous Random	55.75 - 68.25	30	3d	Hanning	0	32	0.03125	400	s3cafu56
4	97.6	Continuous Random	90.75 - 103.25	30	3e	Hanning	0	32	0.03125	400	s3cafu91
5	97.9	Continuous Random	90.75 - 103.25	30	3e	Hanning	0	32	0.03125	400	s3cafu91
6	179.4	Continuous Random	172.75 - 185.25	30	3f	Hanning	0	32	0.03125	400	s3cafu173
7	190.6	Continuous Random	185.0 - 235.0	30	3g	Hanning	0	16	0.0625	800	s3cafu185

Table E-2 Modal Testing Parameters Summary - Section 3 Free-Free Modes

Mode No.	Nat Freq (Hz)	Excitation Method	Frequency Span (Hz)	No. Avg	Test No.	Type of Window	% Overlap	Sample Length(Sec)	Frequency Resolution (Hz)	No. of Freq Lines	Function Universal File Name ( ).unv
1	113.03	Continuous Random	109.875 - 116.125	30	3p	Hanning	75	128	0.0078125	800	s3fffu110
2	113.08	Continuous Random	109.875 - 116.125	30	3p	Hanning	75	128	0.0078125	800	s3fffu110
3	119.5	Continuous Random	116.75 - 129.25	30	3l	Hanning	0	32	0.03125	400	s3fffu117
4	230.1	Continuous Random	225.75 - 238.25	30	3m	Hanning	0	32	0.03125	400	s3fffu226
5	232.8	Continuous Random	225.75 - 238.25	30	3m	Hanning	0	32	0.03125	400	s3fffu226
6	234.5	Continuous Random	225.75 - 238.25	30	3m	Hanning	0	32	0.03125	400	s3fffu226
7	382.4	Continuous Random	375.75 - 388.25	30	3n	Hanning	0	32	0.03125	400	s3fffu376

Table E-3 Modal Data Analysis Parameters Summary - Section 3 Cantilever Modes

Mode No.	Nat Freq (Hz)	Curve-Fit Technique	Frequency Range (Hz)	No. of Resp Pts	Matrix Size	No. of Roots	Reference Point	Shape/Parameter File Name ( ).unv	Model Universal File Name ( ).unv
1	20.4	Polyref	14.75 - 27.25	45	16	4	21z-	s3camodes	s3catestpt
2	20.7	Polyref	14.75 - 27.25	45	16	4	21z-	s3camodes	s3catestpt
3	61.3	Polyref	55.75 - 68.25	45	16	2	21z-	s3camodes	s3catestpt
4	97.6	Polyref	90.75 - 103.25	45	16	4	21z-	s3camodes	s3catestpt
5	97.9	Polyref	90.75 - 103.25	45	16	4	21z-	s3camodes	s3catestpt
6	179.4	Polyref	172.75 - 185.25	45	16	4	21z-	s3camodes	s3catestpt
7	190.6	Polyref	185.0 - 235.0	45	16	8	21z-	s3camodes	s3catestpt

Table E-3 Modal Data Analysis Parameters Summary - Section 3 Free-Free Modes

Mode No.	Nat Freq (Hz)	Curve-Fit Technique	Frequency Range (Hz)	No. of Resp Pts	Matrix Size	No. of Roots	Reference Points	Shape/Parameter File Name ( ).unv	Model Universal File Name ( ).unv
1	113.03	Polyref	109.875 - 116.125	44	16	8	2y+, 21y+	s3ffmodes	s3fftestpt
2	113.08	Polyref	109.875 - 116.125	44	16	8	2y+, 21y+	s3ffmodes	s3fftestpt
3	119.5	Polyref	116.75 - 129.25	44	16	8	2y+, 21y+	s3ffmodes	s3fftestpt
4	230.1	Polyref	225.75 - 238.25	44	16	10	2y+, 21y+	s3ffmodes	s3fftestpt
5	232.8	Polyref	225.75 - 238.25	44	16	10	2y+, 21y+	s3ffmodes	s3fftestpt
6	234.5	Polyref	225.75 - 238.25	44	16	10	2y+, 21y+	s3ffmodes	s3fftestpt
7	382.4	Polyref	375.75 - 388.25	44	16	8	2y+, 21y+	s3ffmodes	s3fftestpt

OUTPUT FROM GRID POINT WEIGHT GENERATOR

REFERENCE POINT = 0

M O

1.088719E-01	1.233280E-17	-1.179070E-17	-8.410428E-16	8.161721E+00	-4.733898E-04
1.233280E-17	1.088719E-01	-3.455894E-17	-8.161721E+00	6.184994E-15	1.687477E+01
-1.179070E-17	-3.455894E-17	1.088719E-01	4.733898E-04	-1.687477E+01	-5.349914E-15
-8.380612E-16	-8.161721E+00	4.733898E-04	7.142946E+02	4.507147E-02	-1.265058E+03
8.161721E+00	6.265631E-15	-1.687477E+01	4.507147E-02	3.329749E+03	-1.183475E-02
-4.733898E-04	1.687477E+01	-5.311127E-15	-1.265058E+03	-1.183475E-02	2.620003E+03

S

1.000000E+00	0.000000E+00	0.000000E+00
0.000000E+00	1.000000E+00	0.000000E+00
0.000000E+00	0.000000E+00	1.000000E+00

DIRECTION MASS AXIS SYSTEM (S)	MASS	X-C.G.	Y-C.G.	Z-C.G.
X	1.088719E-01	-7.725069E-15	4.348137E-03	7.496629E+01
Y	1.088719E-01	1.549966E+02	5.680984E-14	7.496629E+01
Z	1.088719E-01	1.549966E+02	4.348137E-03	-4.913954E-14

I(S)

1.024406E+02	-1.184453E-01	1.833607E-02
-1.184453E-01	1.023616E+02	-2.365354E-02
1.833607E-02	-2.365354E-02	4.469700E+00

I(Q)

1.022763E+02		
	1.025260E+02	
		4.469690E+00

Q

5.846461E-01	8.112884E-01	1.787890E-04
-8.112884E-01	5.846462E-01	-2.480978E-04
-3.058072E-04	0.000000E+00	1.000000E+00

Section-3 Truss Updated FEM Mass Properties (Cantilevered and Free-Free) With Sensor Mass Included

SDRC I-DEAS V: FE_Modeling_&_Analysis 29-JAN-92 11:14:27

Database: cai
View : No stored View
Task: Post Processing
Model: 1-10-BAY

Units : IN
Display : No stored Option
Model Dir: 1-MAIN
Associated Workset: 2-WORKING SET2

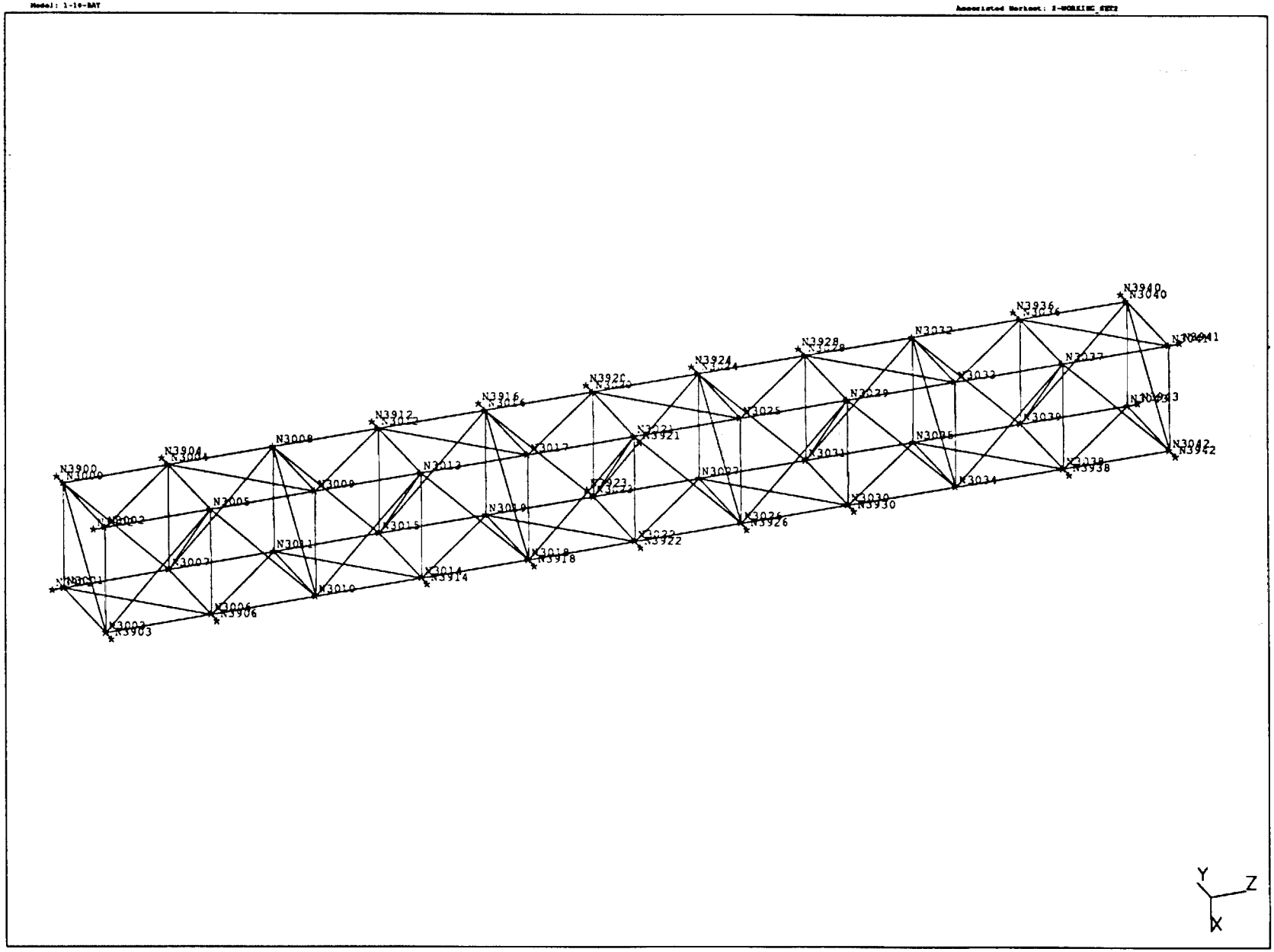

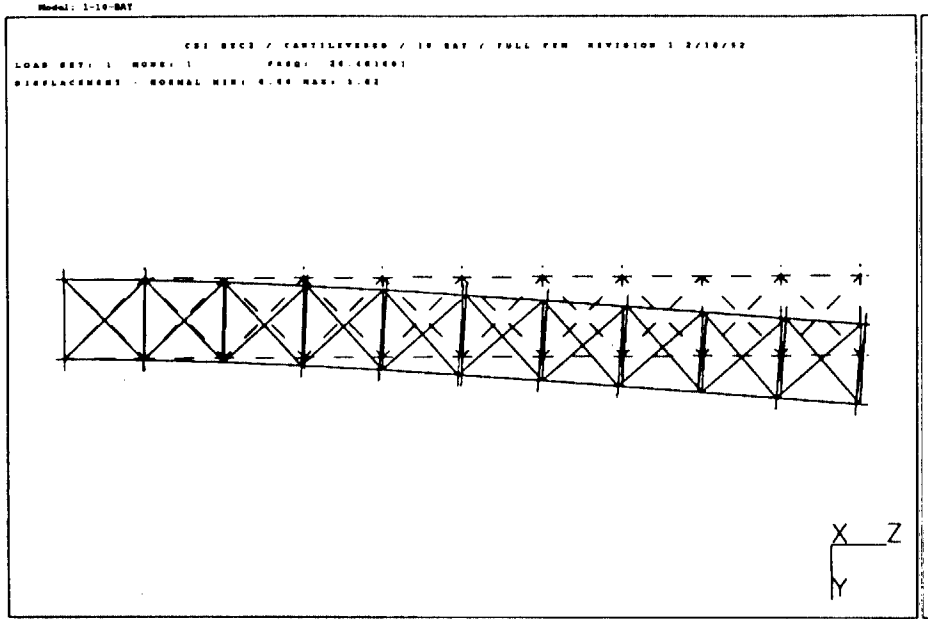
CSI DEC3 / CANTILEVERED / 10 BAY / FULL FEM REVISION 1 2/10/92
LOAD SET: 1 MODE: 1 FREQ: 26.481661
DISPLACEMENT - NORMAL MIN: 0.00 MAX: 1.02
X
Z
Y

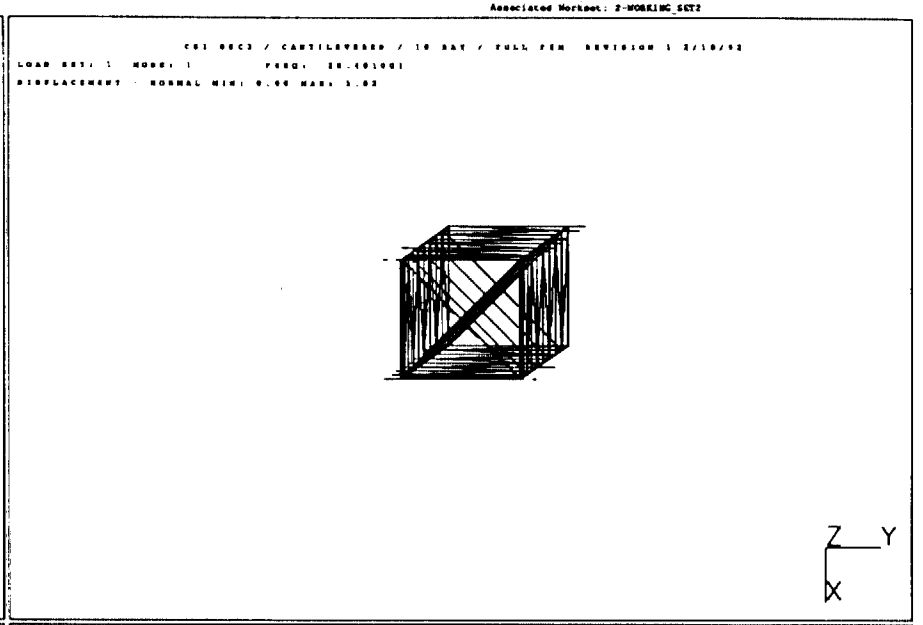
CSI DEC3 / CANTILEVERED / 10 BAY / FULL FEM REVISION 1 2/10/92
LOAD SET: 1 MODE: 1 FREQ: 26.481661
DISPLACEMENT - NORMAL MIN: 0.00 MAX: 1.02
Z
Y
X

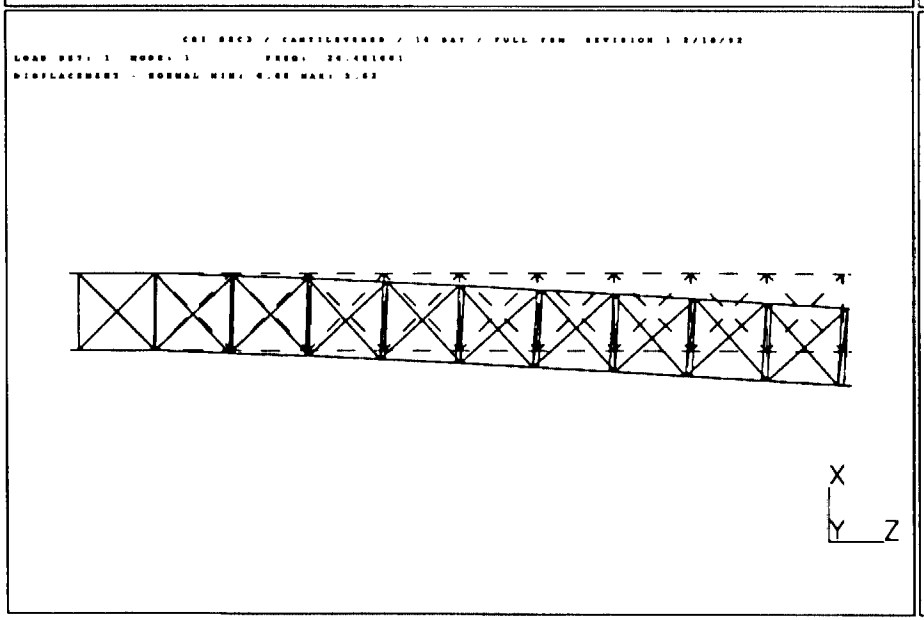
CSI DEC3 / CANTILEVERED / 10 BAY / FULL FEM REVISION 1 2/10/92
LOAD SET: 1 MODE: 1 FREQ: 26.481661
DISPLACEMENT - NORMAL MIN: 0.00 MAX: 1.02
X
Y
Z

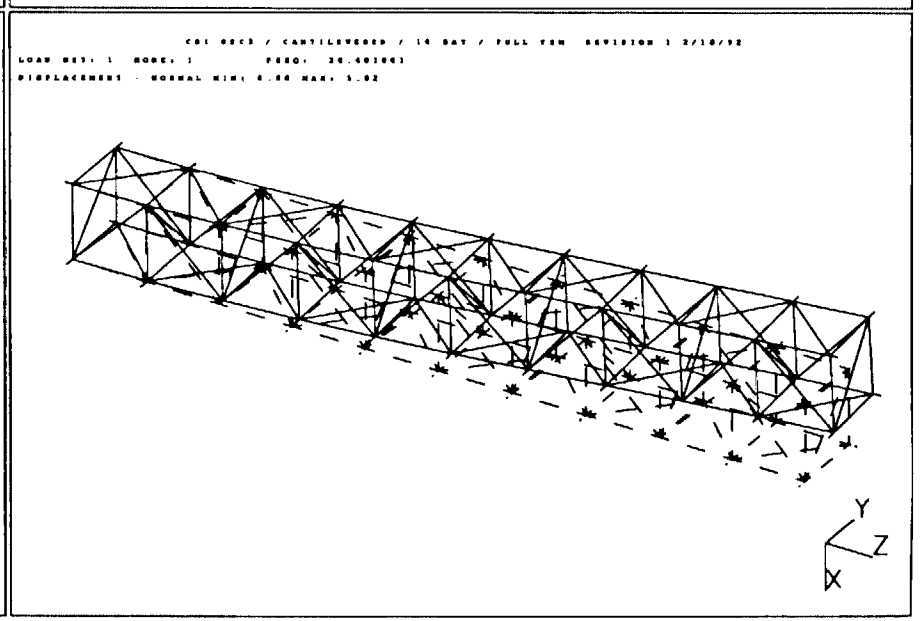
CSI DEC3 / CANTILEVERED / 10 BAY / FULL FEM REVISION 1 2/10/92
LOAD SET: 1 MODE: 1 FREQ: 26.481661
DISPLACEMENT - NORMAL MIN: 0.00 MAX: 1.02
Y
Z
X

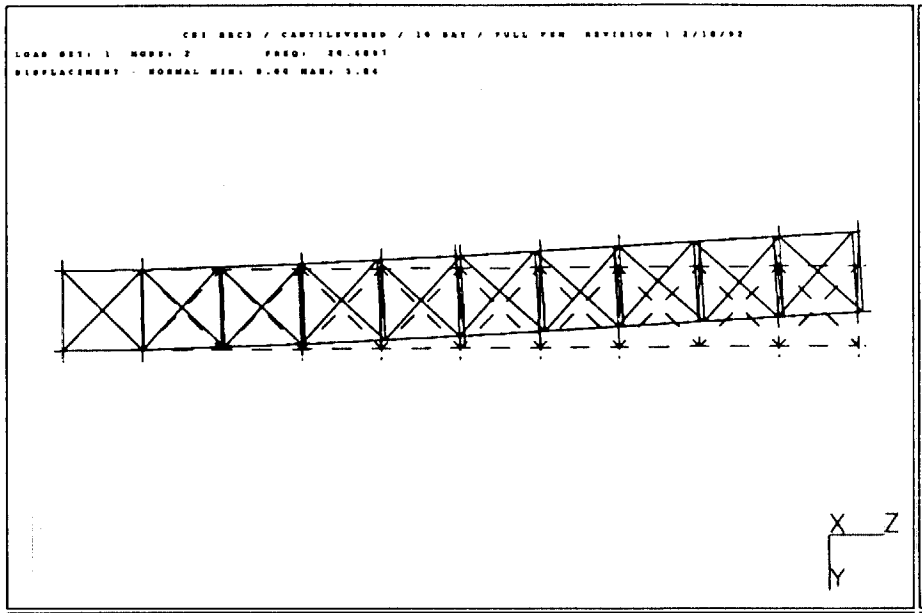
CSI SEC3 / CANTILEVERED / 10 BAY / FULL FEM REVISION 1 2/10/92
LOAD SET: 1 MODE: 2 FREQ: 26.4857
DISPLACEMENT - NORMAL MIN: 0.00 MAX: 1.00
X
Z
Y

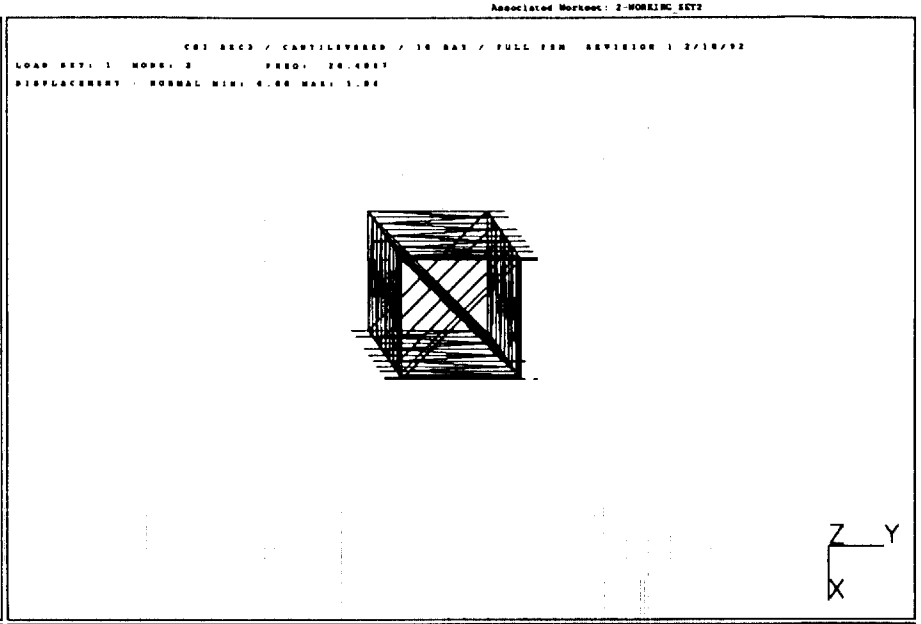
CSI SEC3 / CANTILEVERED / 10 BAY / FULL FEM REVISION 1 2/10/92
LOAD SET: 1 MODE: 2 FREQ: 26.4857
DISPLACEMENT - NORMAL MIN: 0.00 MAX: 1.00
Z
Y
X

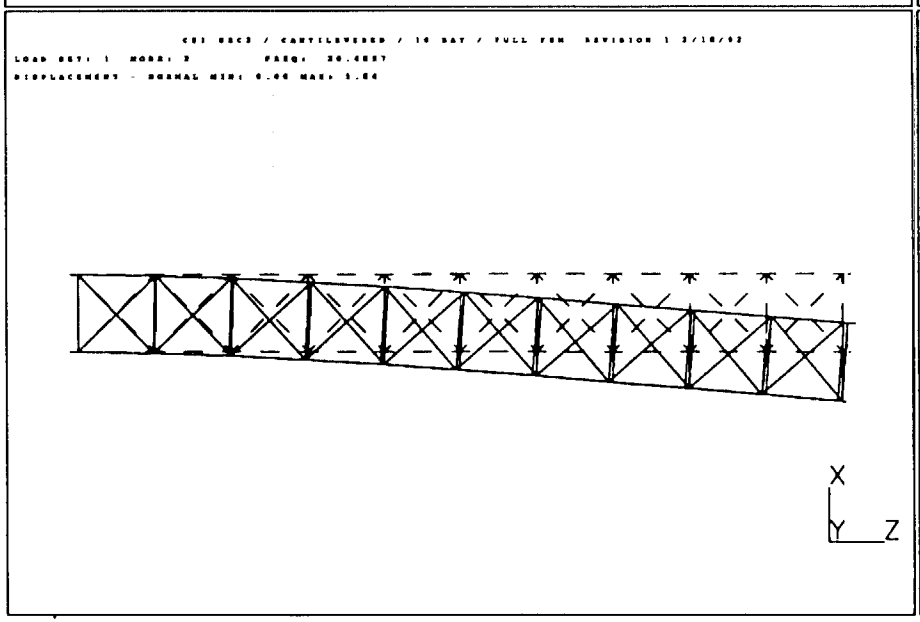
CSI SEC3 / CANTILEVERED / 10 BAY / FULL FEM REVISION 1 2/10/92
LOAD SET: 1 MODE: 2 FREQ: 26.4857
DISPLACEMENT - NORMAL MIN: 0.00 MAX: 1.00
X
Y
Z

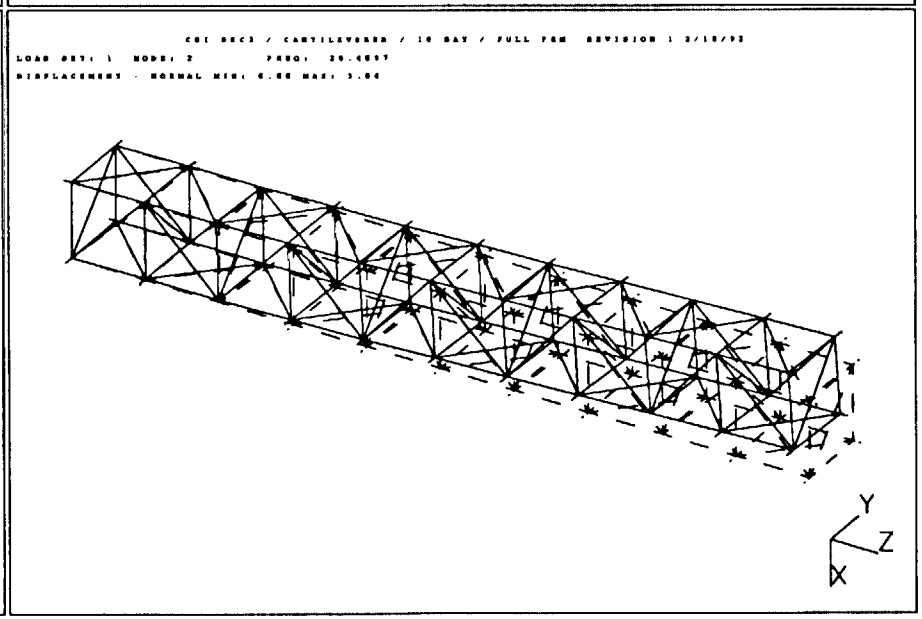
CSI SEC3 / CANTILEVERED / 10 BAY / FULL FEM REVISION 1 2/10/92
LOAD SET: 1 MODE: 2 FREQ: 26.4857
DISPLACEMENT - NORMAL MIN: 0.00 MAX: 1.00
Y
Z
X

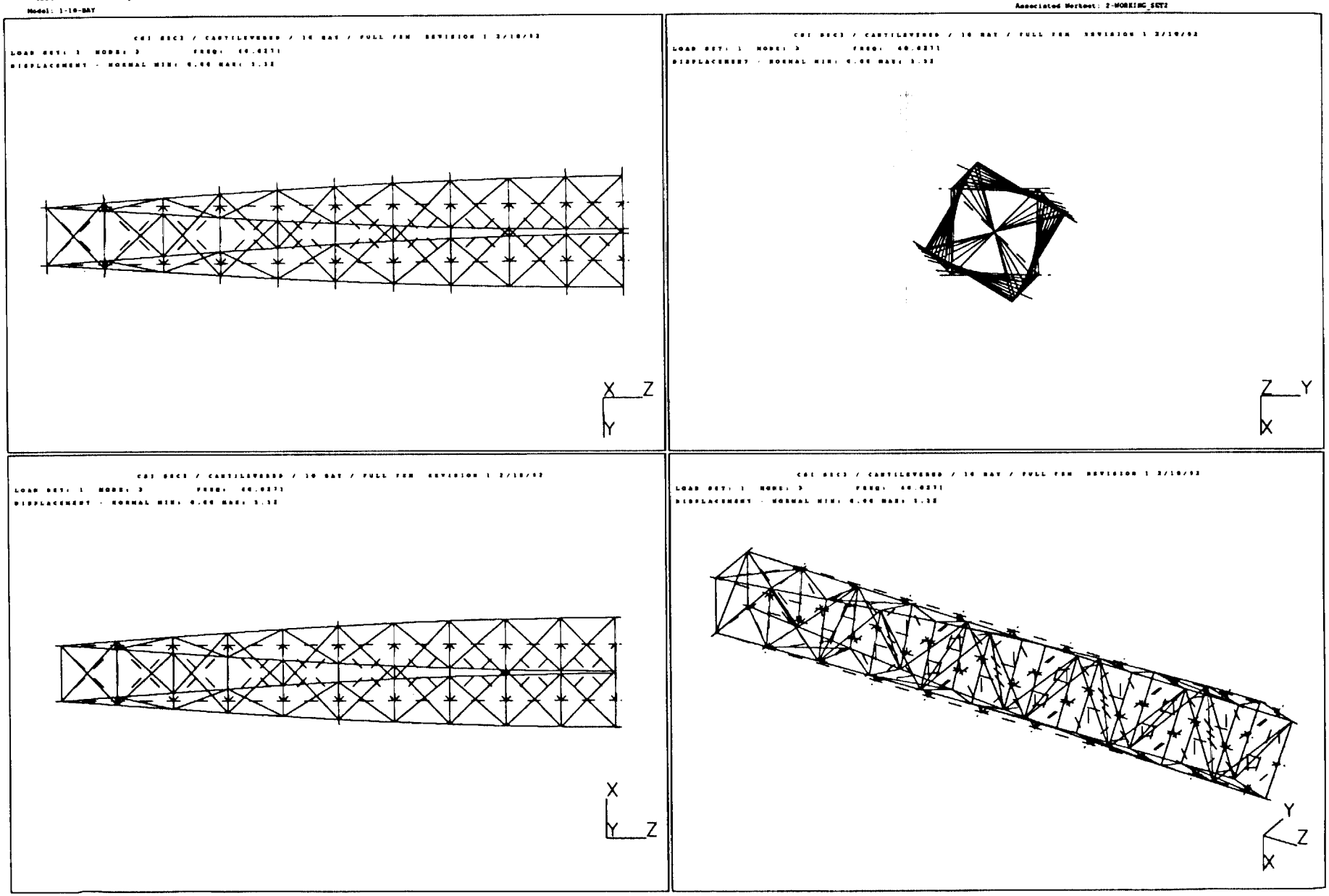
CEI EEC3 / CANTILEVERED / 16 BAY / FULL FEM REVISION 1 3/10/92
LOAD SET: 1 MODE: 3 FREQ: 46.6271
DISPLACEMENT - NORMAL MIN: 0.00 MAX: 3.32
X Z Y
CEI EEC3 / CANTILEVERED / 16 BAY / FULL FEM REVISION 1 3/10/92
LOAD SET: 1 MODE: 3 FREQ: 46.6271
DISPLACEMENT - NORMAL MIN: 0.00 MAX: 3.32
Z Y X
CEI EEC3 / CANTILEVERED / 16 BAY / FULL FEM REVISION 1 3/10/92
LOAD SET: 1 MODE: 3 FREQ: 46.6271
DISPLACEMENT - NORMAL MIN: 0.00 MAX: 3.32
X Y Z
CEI EEC3 / CANTILEVERED / 16 BAY / FULL FEM REVISION 1 3/10/92
LOAD SET: 1 MODE: 3 FREQ: 46.6271
DISPLACEMENT - NORMAL MIN: 0.00 MAX: 3.32
Y Z X

SDRC I-DEAS V1: FE_Modeling_&_Analysis 19-MAR-92 11:00:35

Database: cai
View : none, none, none, none
Task: Post Processing
Model: 1-10-BAY
Units : in
Display : none, none, none, none
Model Bin: 1-MAIN
Associated Workset: 2-WORKING_SET2

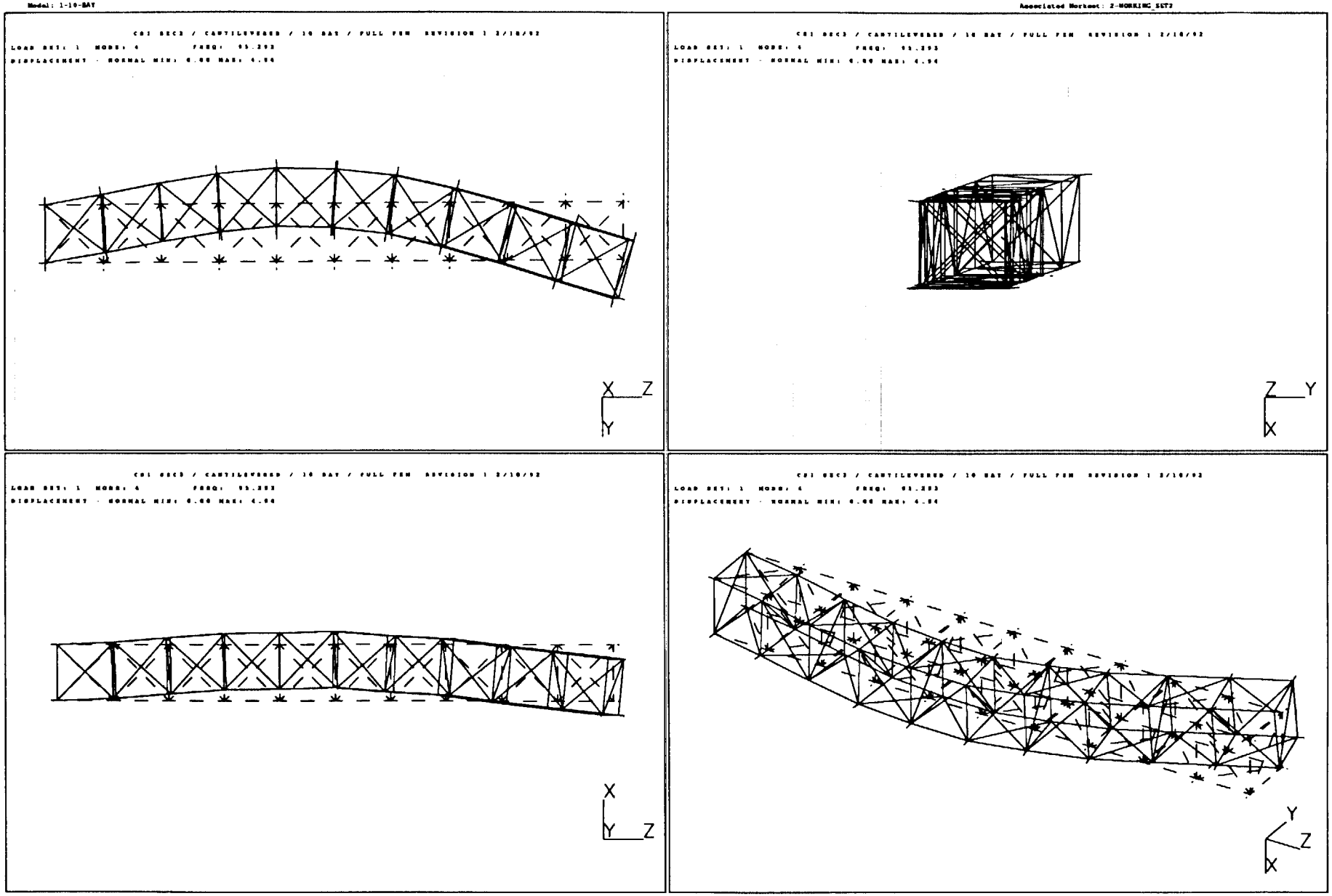

SDRC I-DEAS VI: FE_Modeling_&_Analysis

19-MAR-92 11:00:50

Database: cmi
View : none, none, none, none
Task: Post Processing
Model: 1-10-BAY

Units : IN
Display : none, none, none, none
Model Bin: 1-MAIN
Associated Workset: 2-MODELING_SET2

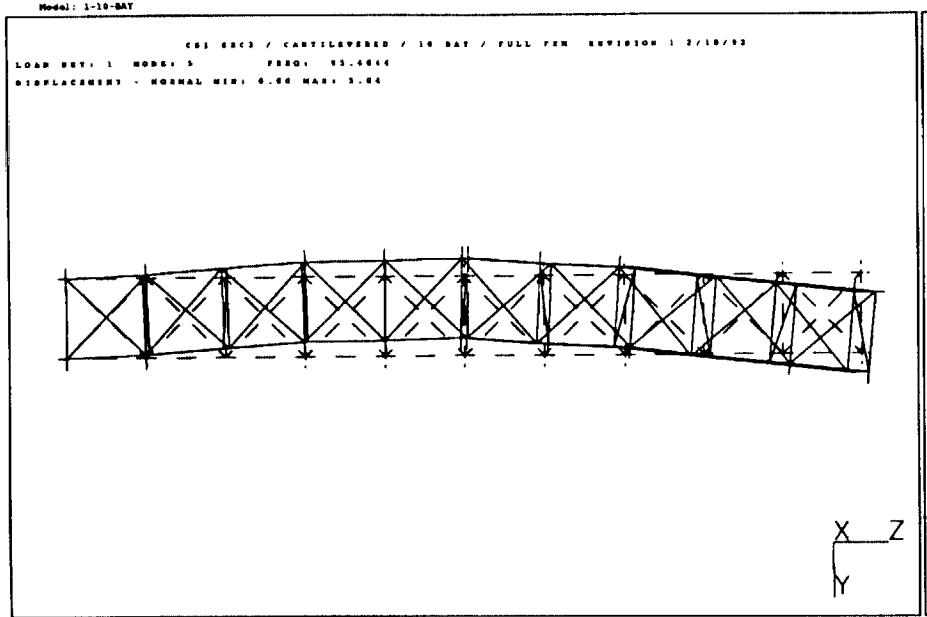

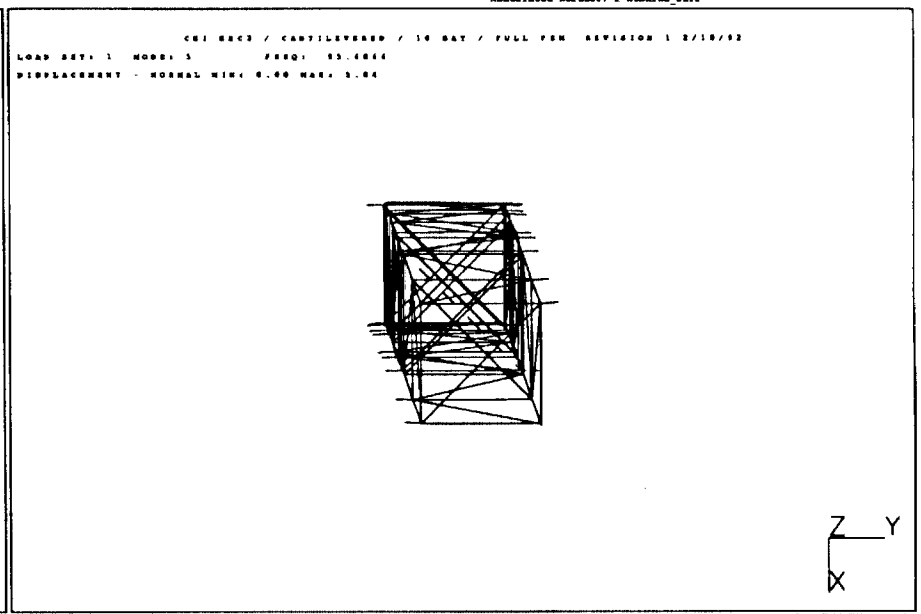

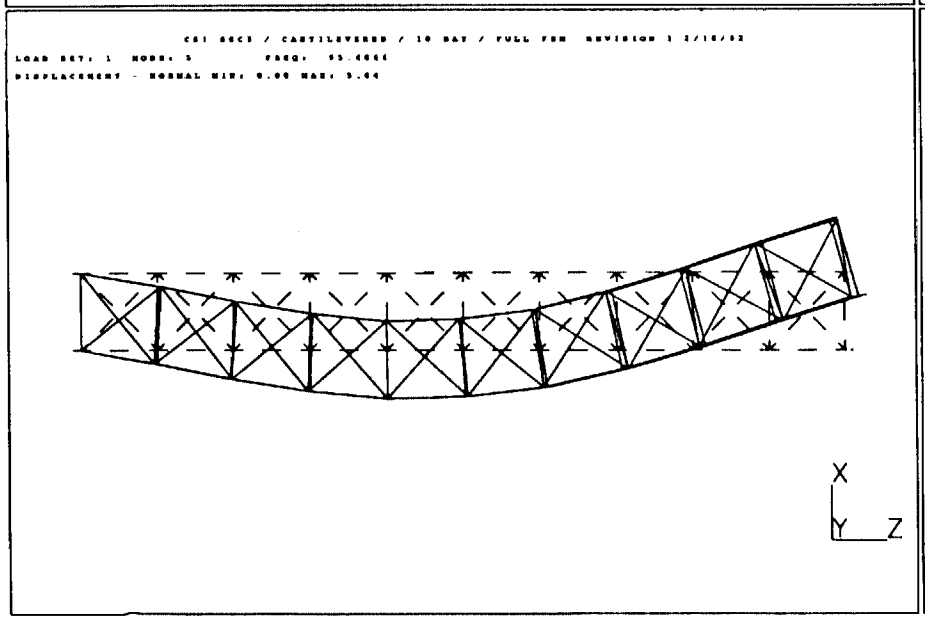

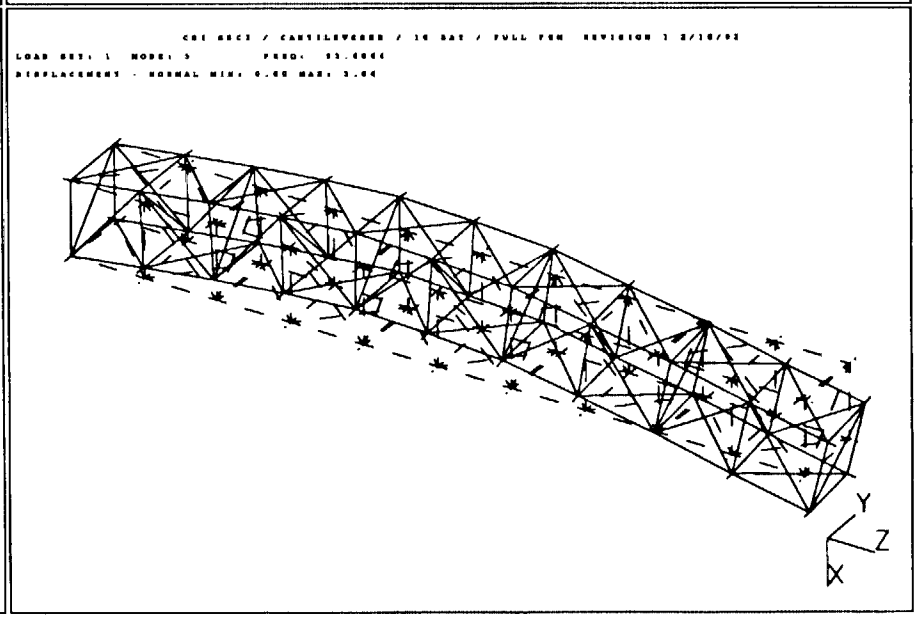

SDRC I-DEAS VI: FE_Modeling_&_Analysis

19-MAR-92 11:07:07

Database: cai
View : none, none, none, none
Task: Post Processing
Model: 1-10-BAY

Units : IN
Display : none, none, none, none
Model Bin: 1-MAIN
Associated Workset: 2-MODKING_SET2

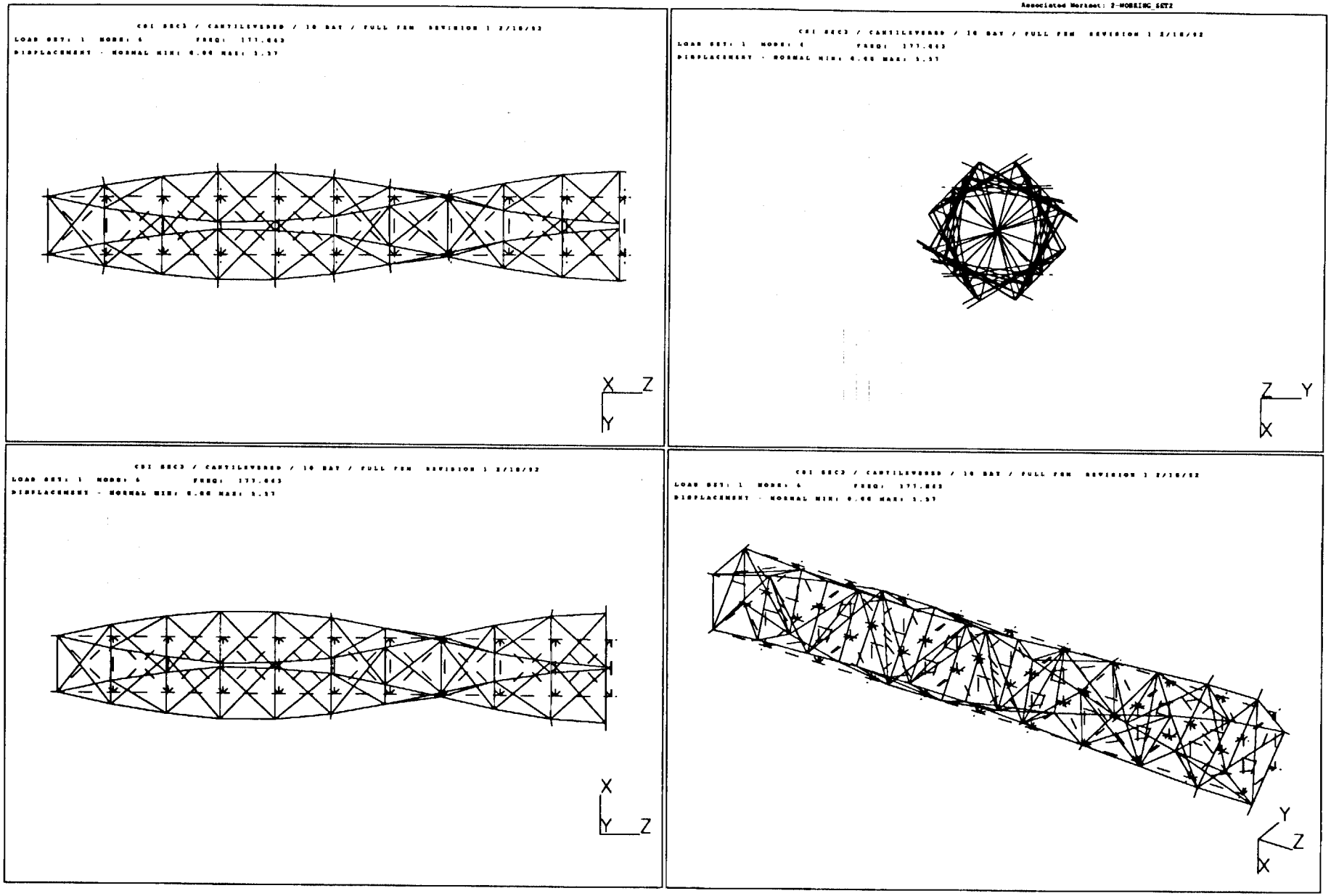

SDRC I-DEAS VI: FE_Modeling_&_Analysis

19-MAR-92 11:01:21

Database: cmi
View : none, none, none, none
Task: Post Processing
Model: 1-16-BAY

Units : IN
Display : none, none, none, none
Model Bin: 1-MAIN
Associated Workset: 2-MORRING_SET2

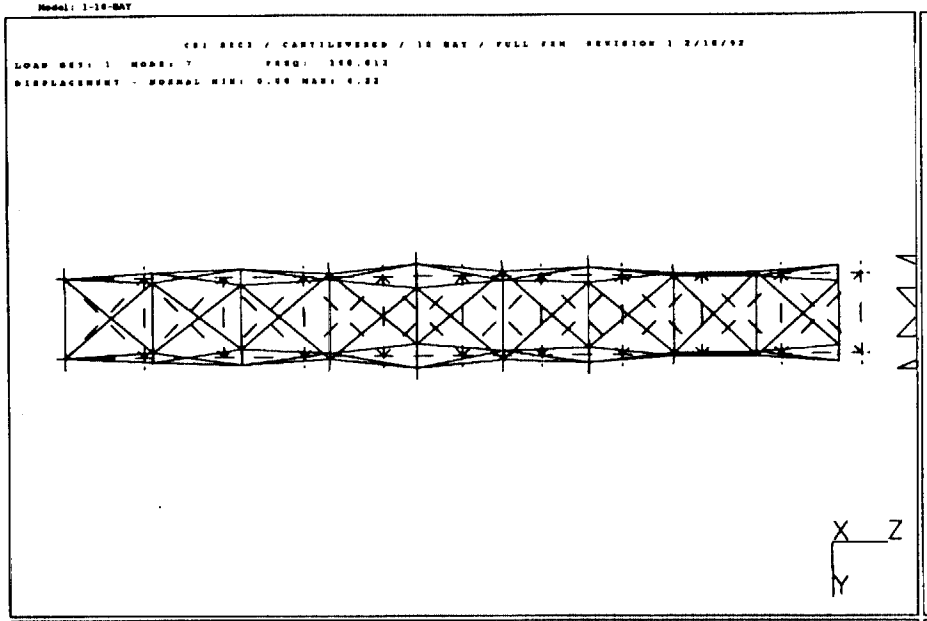

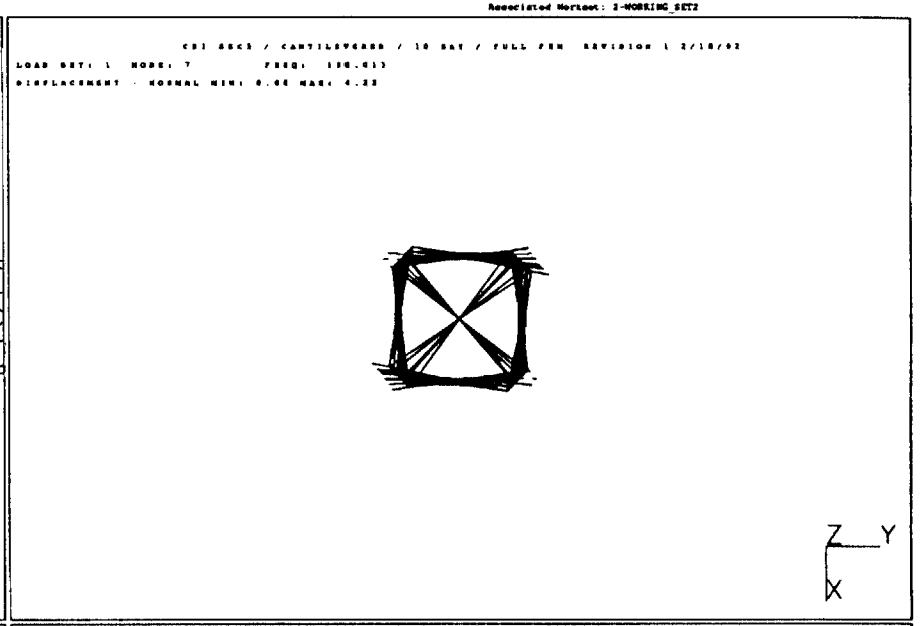

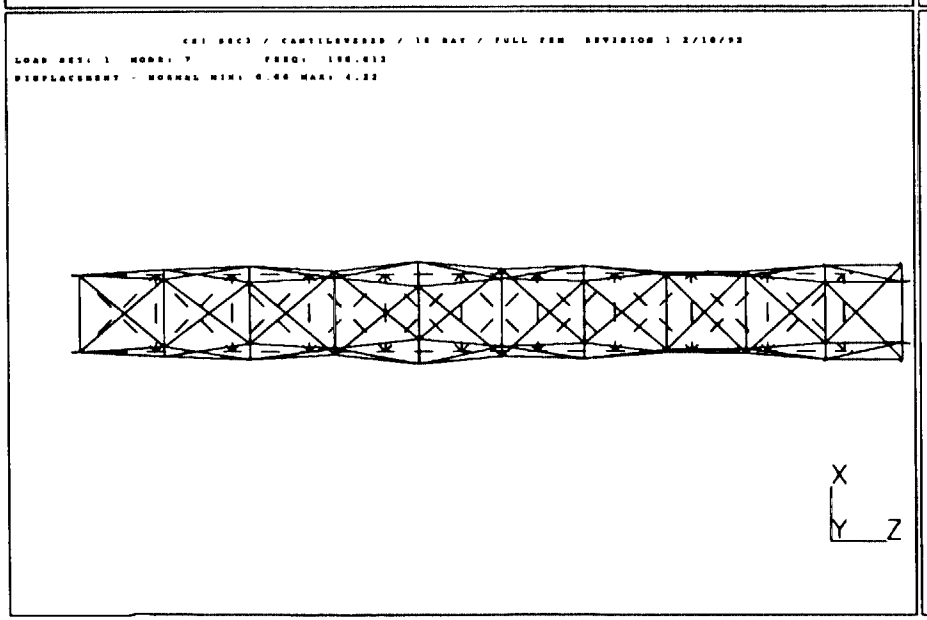

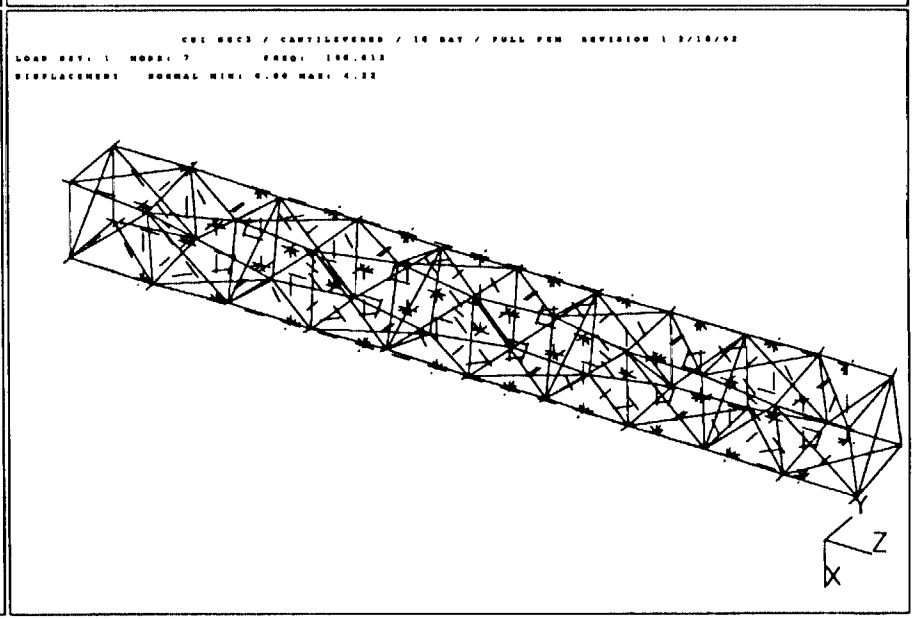

SDRC I-DEAS VI: FE_Modeling_&_Analysis

19-MAR-92 11:02:14

Database: csi
View : none, none, none, none
Task: Post Processing
Model: 1-10-BAY

Units : IN
Display : none, none, none, none
Model Bin: 1-MAIN
Associated Workset: 2-WORKING_SET2

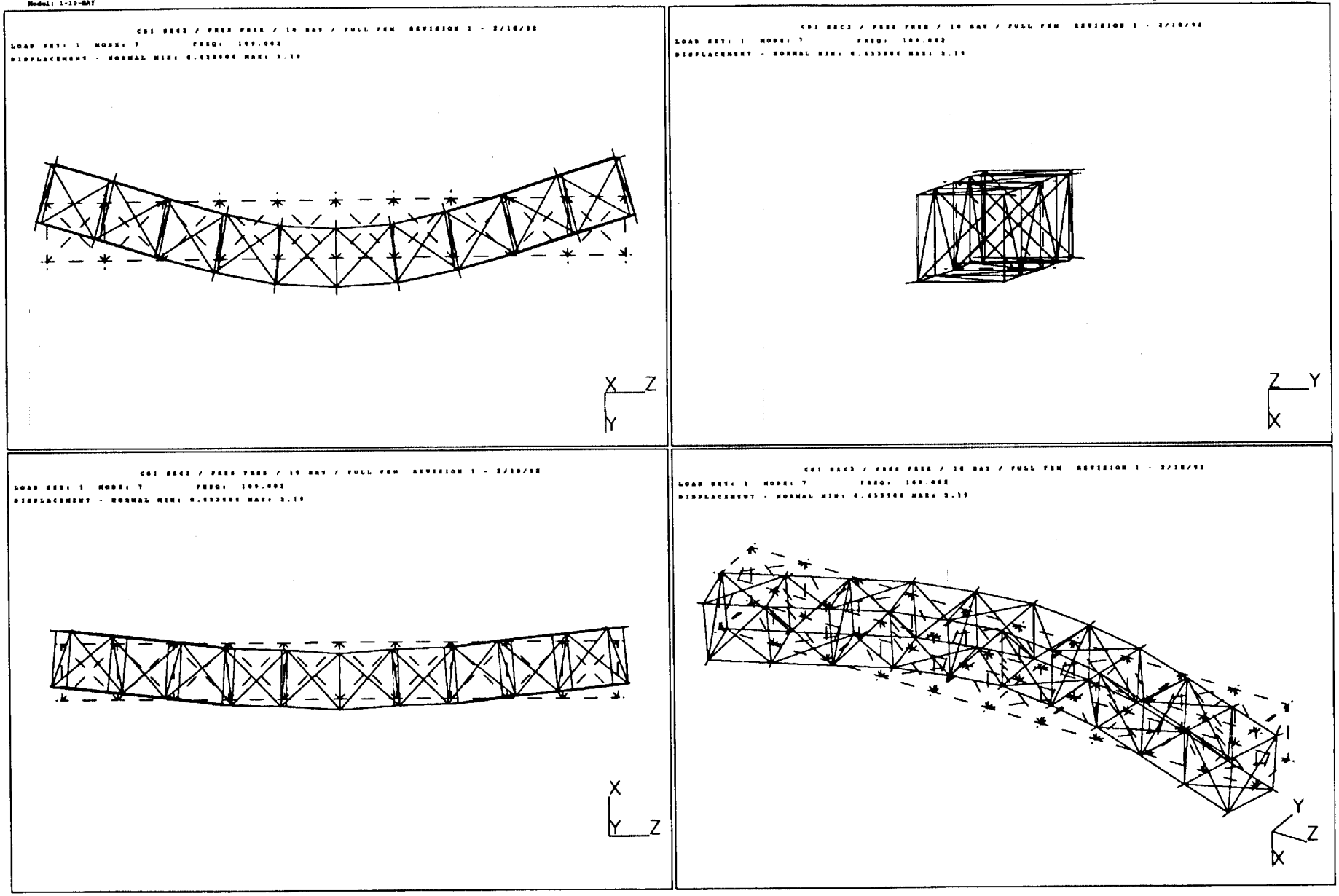

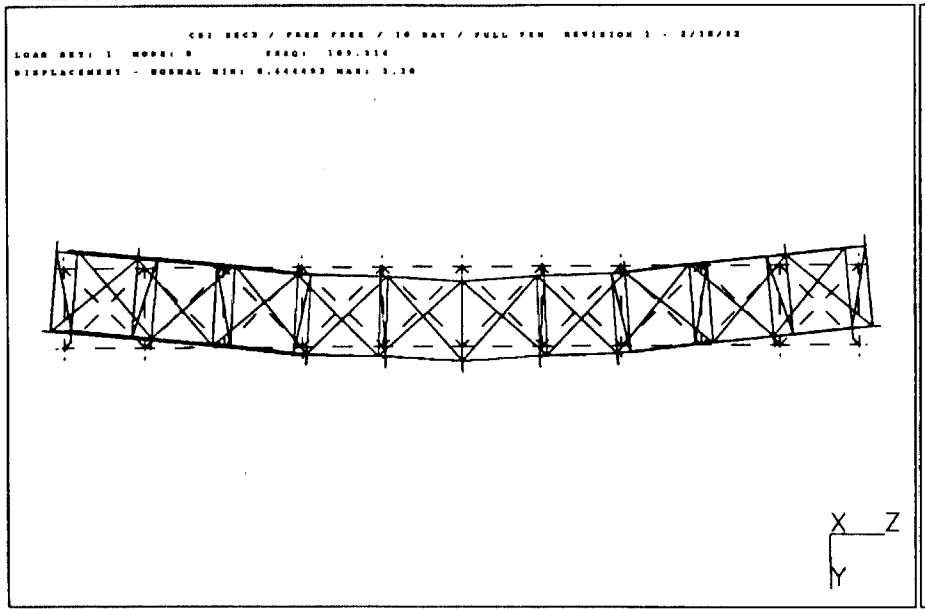
CBI BSC3 / FREE FREE / 10 BAY / FULL FEM REVISION 1 - 2/10/92
LOAD SET: 1 MODE: 8 FREQ: 109.314
DISPLACEMENT - NORMAL MIN: 0.644493 MAX: 3.36
X
Z
Y

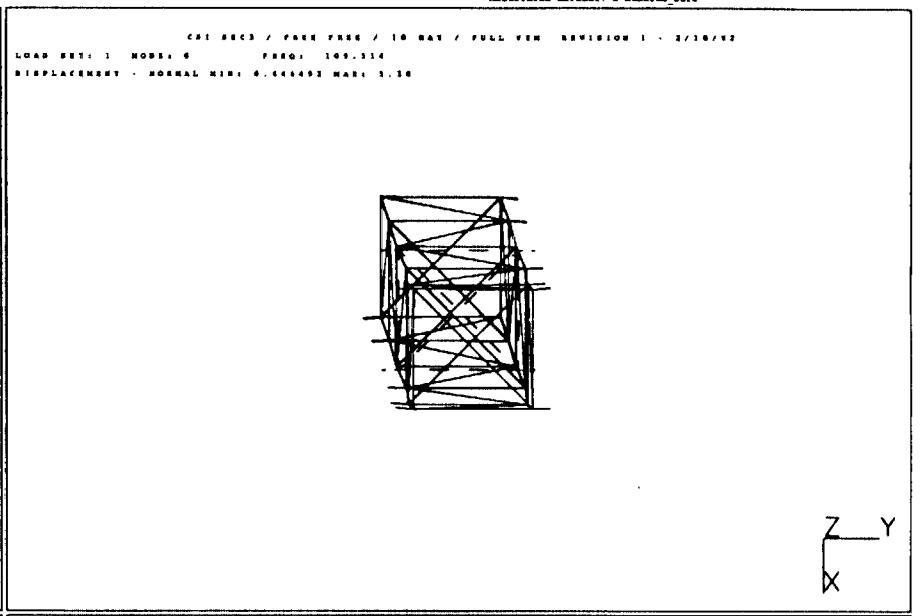
CBI BSC3 / FREE FREE / 10 BAY / FULL FEM REVISION 1 - 2/10/92
LOAD SET: 1 MODE: 6 FREQ: 109.314
DISPLACEMENT - NORMAL MIN: 0.644493 MAX: 3.36
Z
Y
X

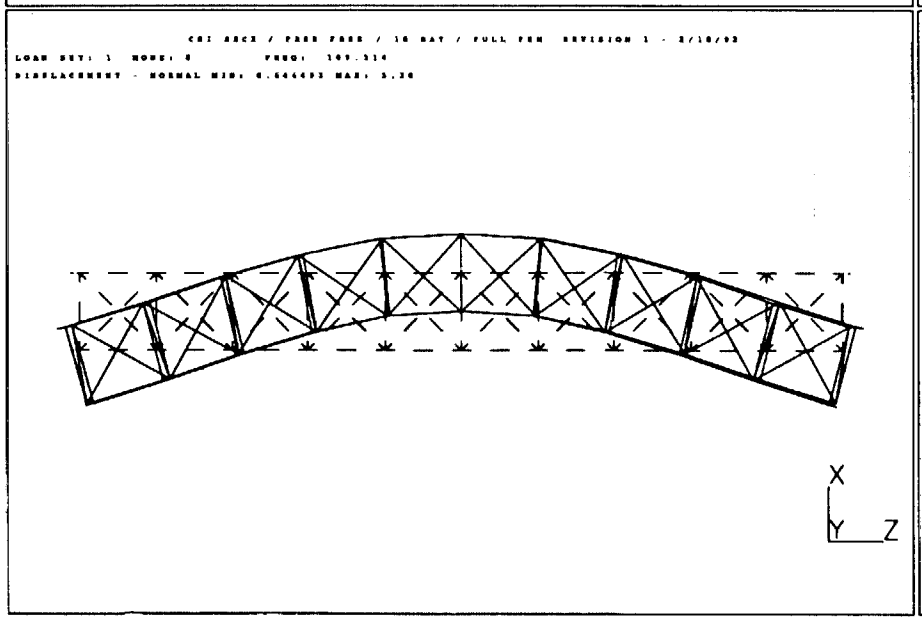
CBI BSC3 / FREE FREE / 10 BAY / FULL FEM REVISION 1 - 2/10/92
LOAD SET: 1 MODE: 8 FREQ: 109.314
DISPLACEMENT - NORMAL MIN: 0.644493 MAX: 3.36
X
Y
Z

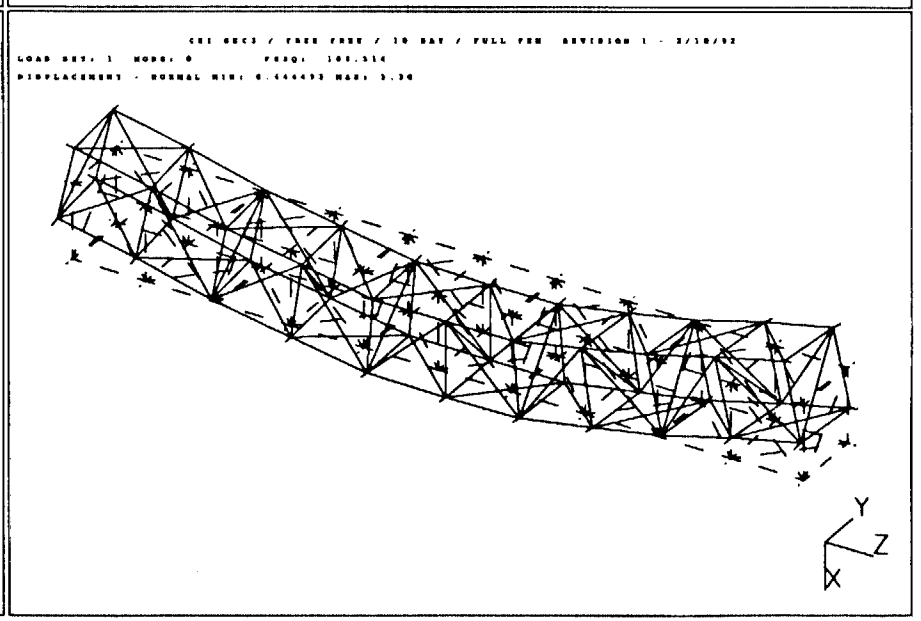
CBI BSC3 / FREE FREE / 10 BAY / FULL FEM REVISION 1 - 2/10/92
LOAD SET: 1 MODE: 6 FREQ: 109.314
DISPLACEMENT - NORMAL MIN: 0.644493 MAX: 3.36
Y
Z
X

SDRC I-DEAS VI: FE_Modeling_&_Analysis 19-MAR-92 11:03:00

Database: csi
View : none, none, none, none
Task: Post Processing
Model: 1-10-BAY
Units : IN
Display : none, none, none, none
Model Bin: 1-MAIN
Associated Workset: 2-MODELING_SET2

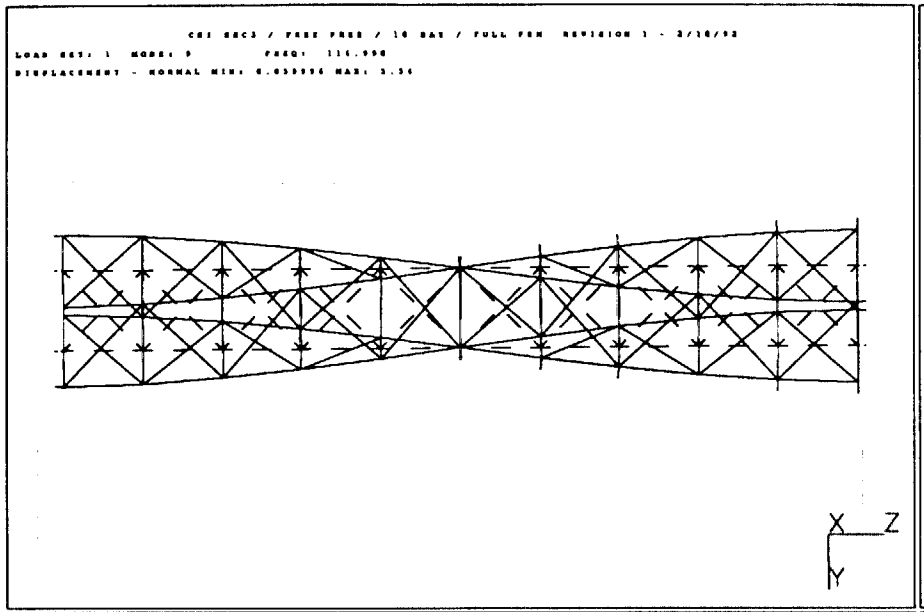

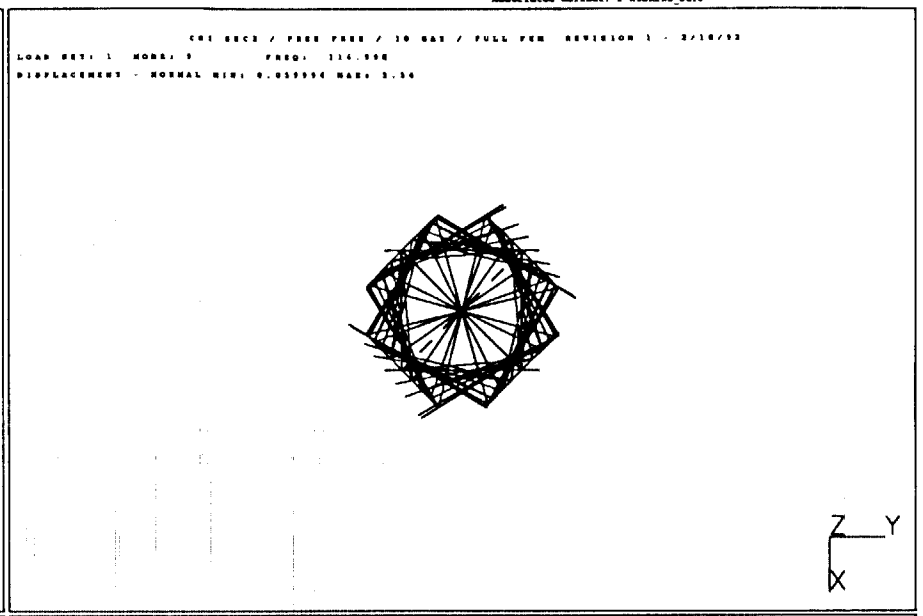

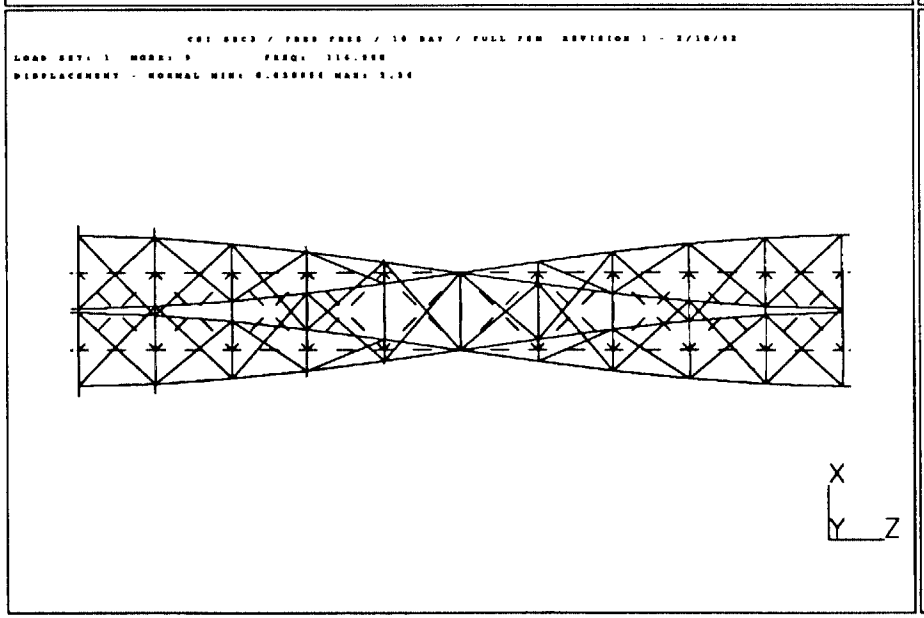

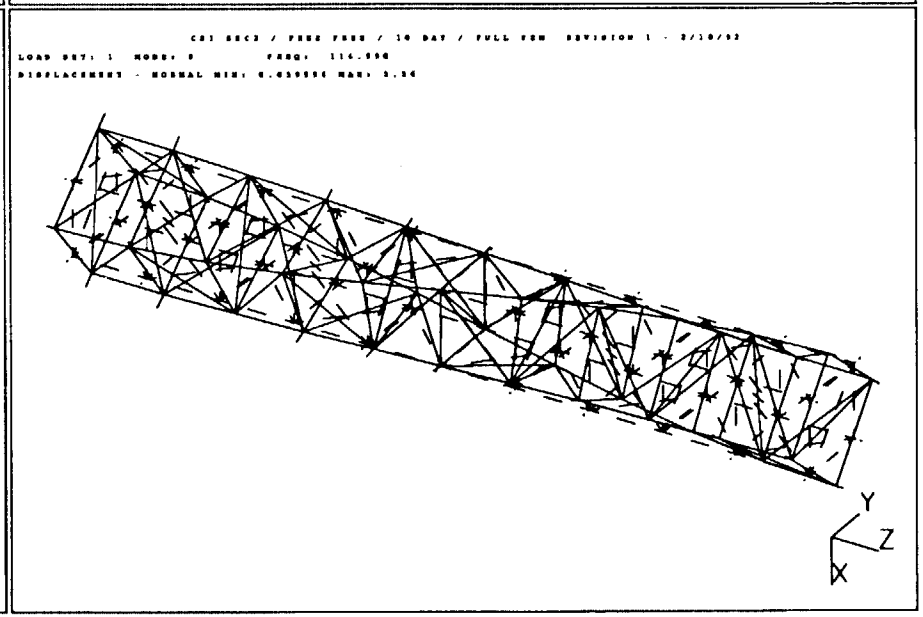

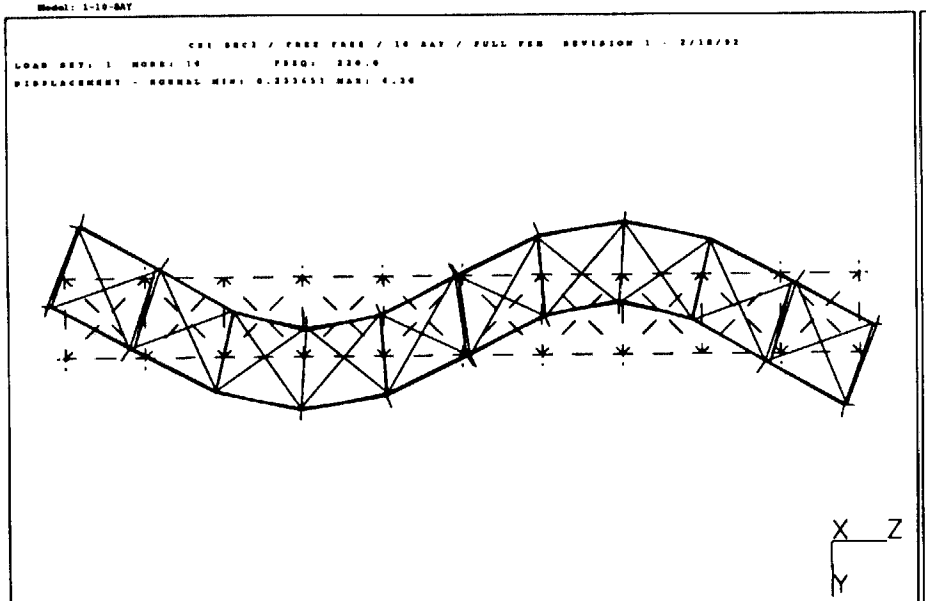
CAI SEC3 / FREE FREE / 10 BAY / FULL FEM REVISION 1 - 2/10/92
LOAD SET: 1 MODE: 10 FREQ: 220.6
DISPLACEMENT - NORMAL MIN: 0.233651 MAX: 4.36
X
Z
Y

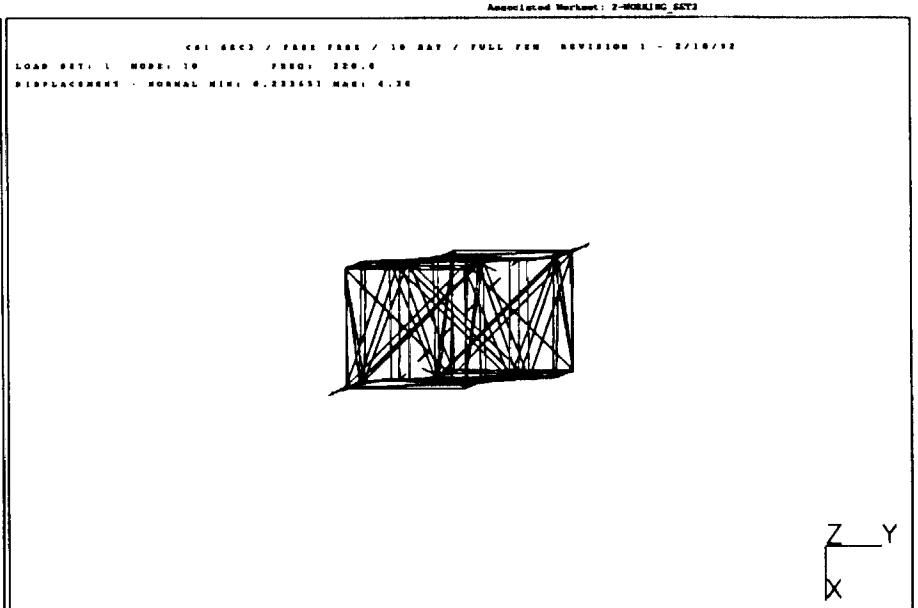
CAI SEC3 / FREE FREE / 10 BAY / FULL FEM REVISION 1 - 2/10/92
LOAD SET: 1 MODE: 10 FREQ: 220.6
DISPLACEMENT - NORMAL MIN: 0.233651 MAX: 4.36
Z
Y
X

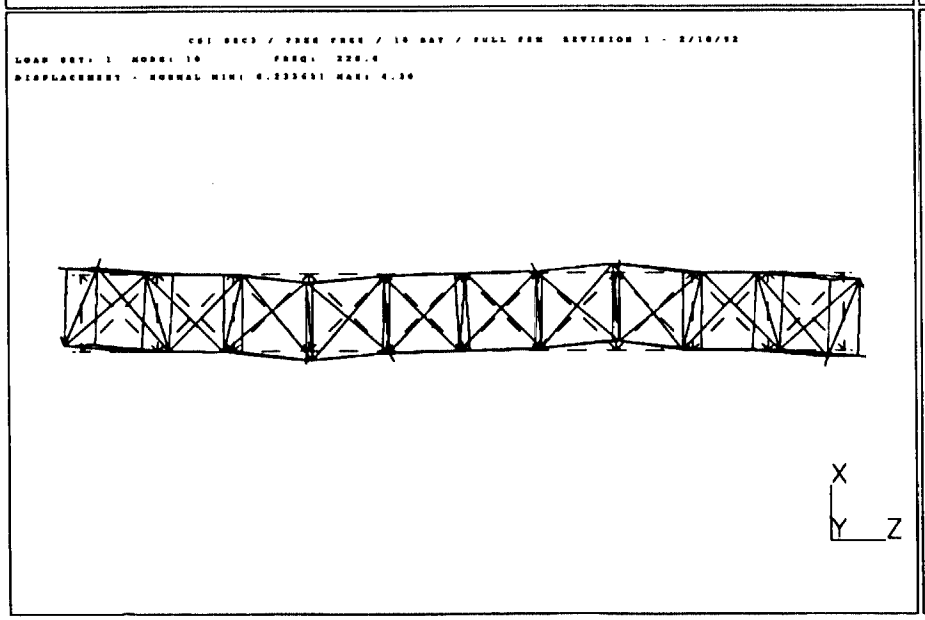
CAI SEC3 / FREE FREE / 10 BAY / FULL FEM REVISION 1 - 2/10/92
LOAD SET: 1 MODE: 10 FREQ: 220.6
DISPLACEMENT - NORMAL MIN: 0.233651 MAX: 4.36
X
Y
Z

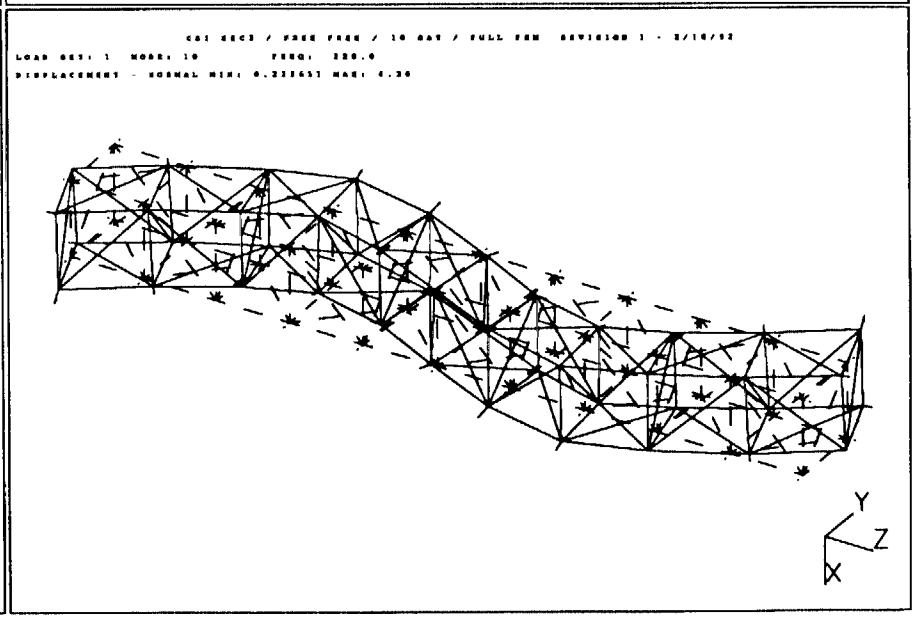
CAI SEC3 / FREE FREE / 10 BAY / FULL FEM REVISION 1 - 2/10/92
LOAD SET: 1 MODE: 10 FREQ: 220.6
DISPLACEMENT - NORMAL MIN: 0.233651 MAX: 4.36
Y
Z
X

Database: cel
View : none, none, none, none
Task: Post Processing
Model: 1-10-BAY

Units : IN
Display : none, none, none, none
Model Dir: I-MAIN
Associated Workset: Z-MODELING_SET2

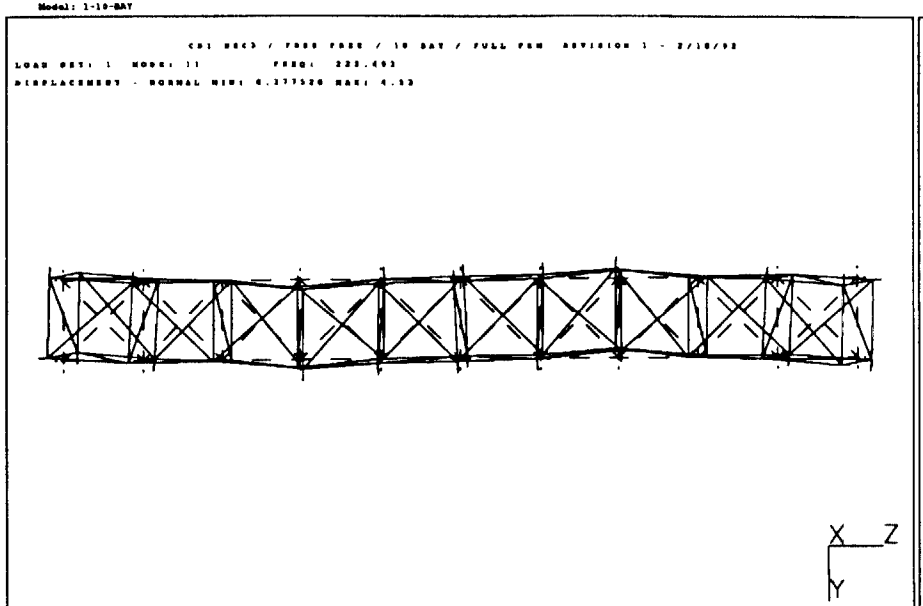

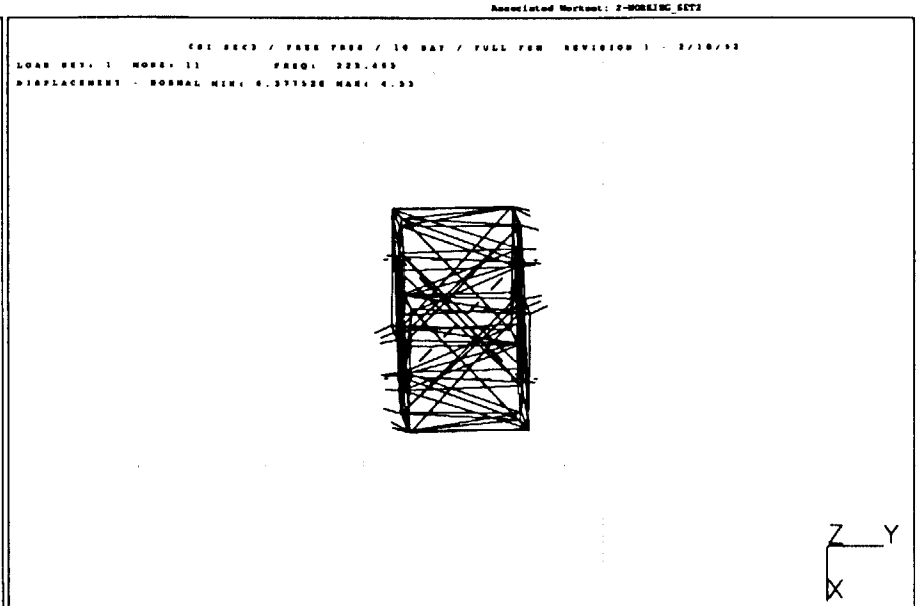

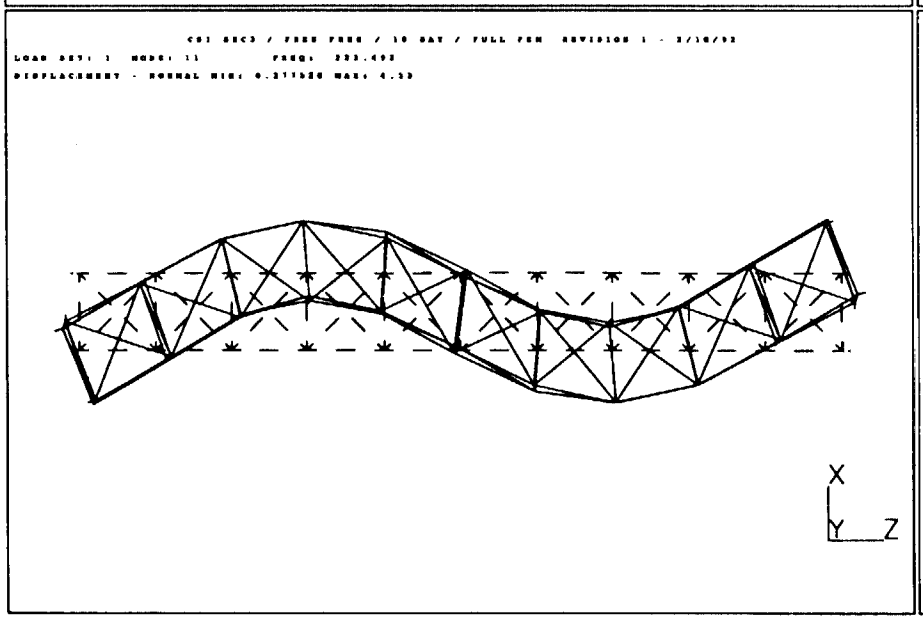

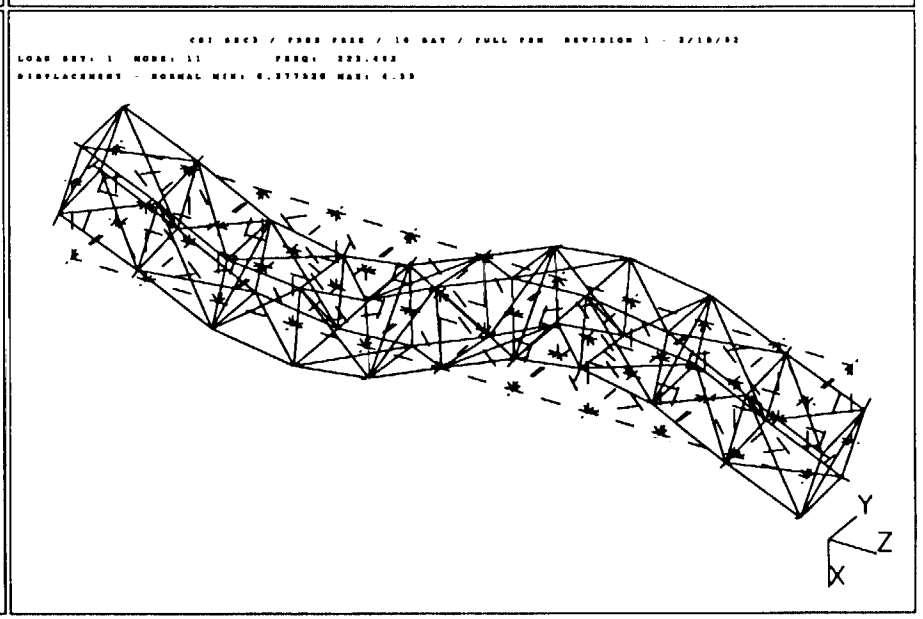

SDRC I-DEAS VI: FE_Modeling_&_Analysis 19-MAR-92 11:04:08

Database: col
View : none, none, none, none
Task: Post Processing
Model: 1-16-BAY

Units : IN
Display : none, none, none, none
Model Bin: 1-MAIN
Associated Workset: 2-MODELING_SET2

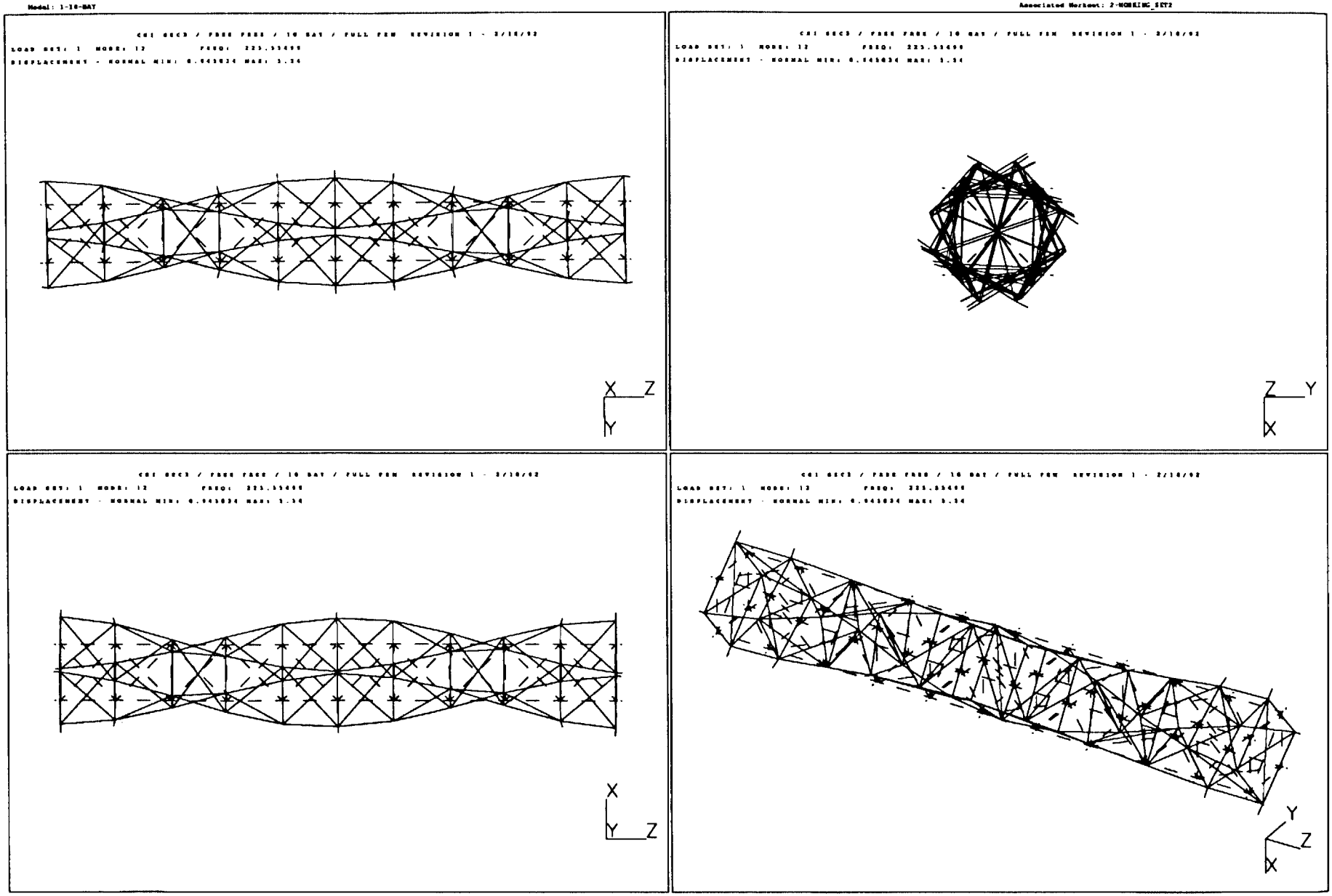

SDRC I-DEAS VI: FE_Modeling_&_Analysis 19-MAR-92 11:04:55

Database: col
View : none, none, none, none
Task: Post Processing
Model: 1-10-BAY

Units : IN
Display : none, none, none, none
Model Bin: 1-MAIN
Associated Workset: 2-WORKING_SET2

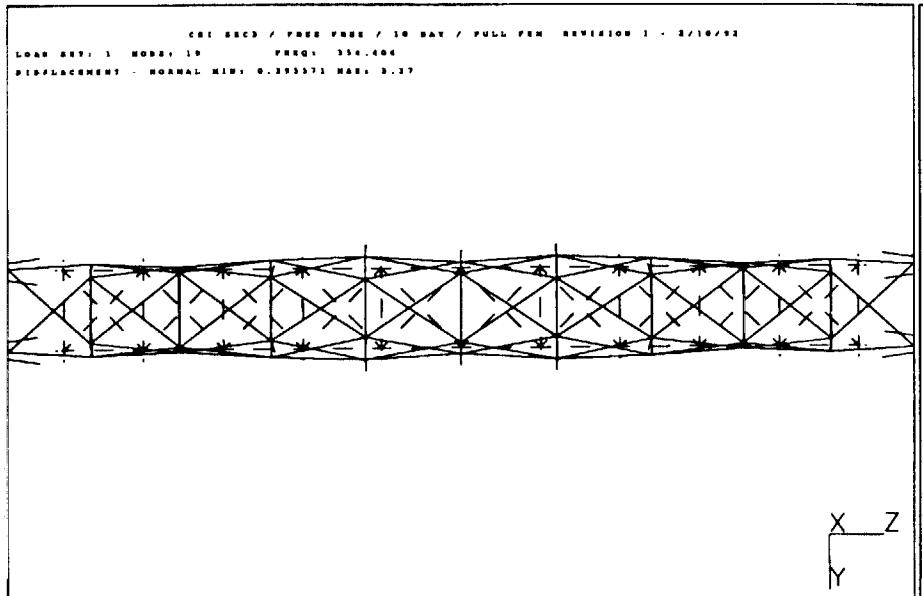

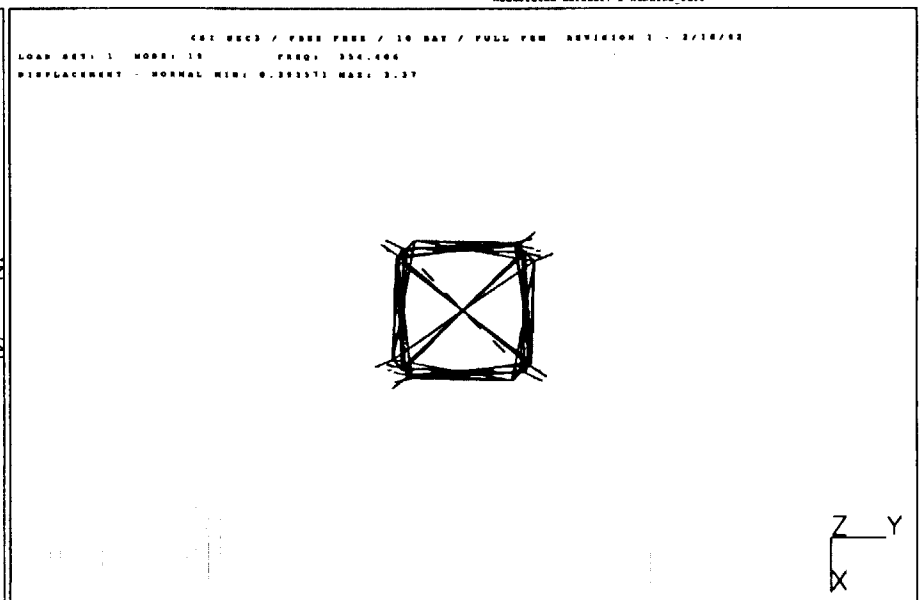

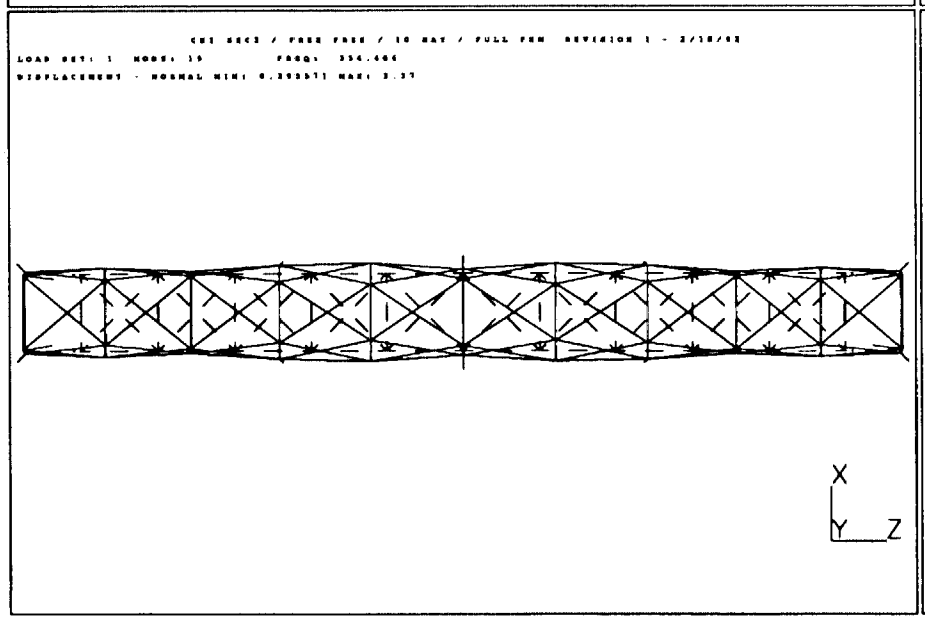

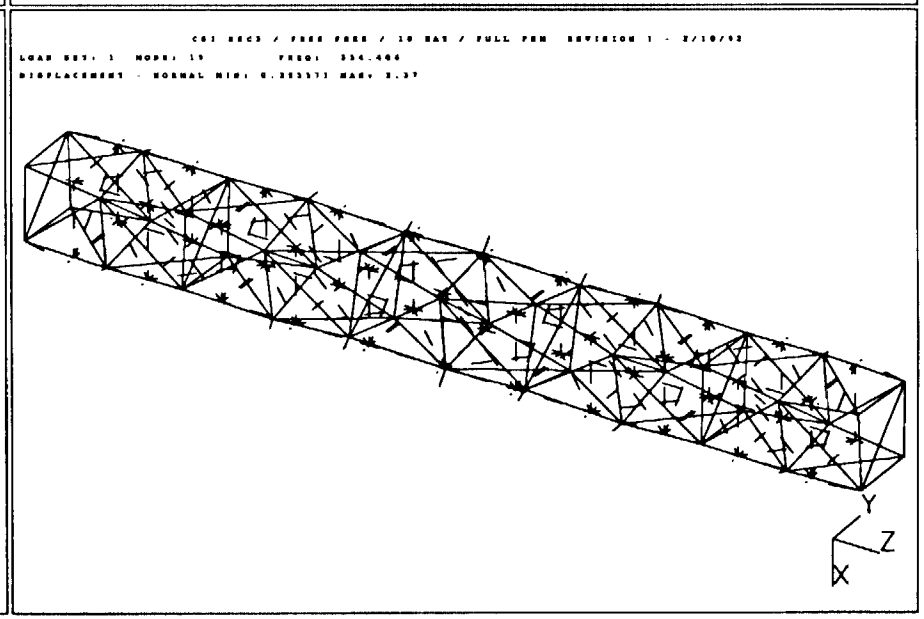

APPENDIX F

TEST AND ANALYSIS RESULTS FOR TRUSS SECTION NO. 4 DYNAMIC TESTS

Table F-1 Test Log of Modal Tests of Section 4 - Cantilevered Tests

Test No.	Type of Excitation	Frequency Range	Comments
4a	Continuous Random	0 - 200 Hz	Cantilevered test setup, with Section 4 test item affixed at one end to the test fixture which had been previously bolted to the laboratory concrete floor. Single shaker setup, with the shaker supported by a bungee cord. Shaker at test point no. 21, oriented to apply loading in the horizontal plane with a skew angle of 45 degrees relative to the longitudinal and lateral axes.
4b	Continuous Random	0 - 400 Hz	Same test configuration as test no. 4a.
4c	Continuous Random	16.75 Hz - 29.25 Hz	Same test configuration as test no. 4a. Zoom for 1st set of bending modes.
4d	Continuous Random	54.25 Hz - 66.75 Hz	Same test configuration as test no. 4a. Zoom for 1st torsional mode.
4e	Continuous Random	99.75 Hz - 112.25 Hz	Same test configuration as test no. 4a. Zoom for 2nd set of bending modes.
4f	Continuous Random	171.75 Hz - 184.25 Hz	Same test configuration as test no. 4a. Zoom for 2nd torsional mode.
4g	Continuous Random	209.75 Hz - 222.25 Hz	Same test configuration as test no. 4a. Zoom for 1st axial mode.

Table F-1 Test Log of Modal Tests of Section 4 - Free-Free Tests

Test No.	Type of Excitation	Frequency Range	Comments
4h	Continuous Random	0 - 200 Hz	Free-Free test setup, with Section 4 test item supported at four points with seperate bungee cords. Dual shaker setup, with one shaker at each end supported by seperate bungee cords. Shaker at test point no. 2 oriented to apply loading in the horizontal plane with a skew angle of 45 degrees relative to the longitudinal and lateral axes. Shaker at test point no. 21 oriented to apply loading in the vertical plane with a skew angle of 45 degrees relative to vertical and lateral axes.
4i	Continuous Random	0 - 400 Hz	Same test configuration as test no. 4h.
4j	Continuous Random	0 - 800 Hz	Same test configuration as test no. 4h.
4k	Continuous Random	111.75 Hz - 124.25 Hz	Same test configuration as test no. 4h. Zoom for 1st torsional mode.
4l	Continuous Random	122.75 Hz - 135.25 Hz	Same test configuration as test no. 4h. Zoom for 1st set of bending modes.
4m	Continuous Random	221.75 Hz - 234.25 Hz	Same test configuration as test no. 4h. Zoom for 2nd torsional mode.
4n	Continuous Random	243.75 Hz - 256.25 Hz	Same test configuration as test no. 4h. Zoom for 2nd set of bending modes.
4o	Continuous Random	420.00 Hz - 445.00 Hz	Same test configuration as test no. 4h. Zoom for higher order modes.
4p	Continuous Random	320.00 Hz - 370.00 Hz	Same test configuration as test no. 4h. Zoom for higher order modes.
4q	Continuous Random	446.75 Hz - 459.25 Hz	Same test configuration as test no. 4h. Zoom for 1st axial mode.

Table F-2 Modal Testing Parameters Summary - Section 4 Cantilever Modes

Mode No.	Nat Freq (Hz)	Excitation Method	Frequency Span (Hz)	No. Avg	Test No.	Type of Window	% Overlap	Sample Length(Sec)	Frequency Resolution (Hz)	No. of Freq Lines	Function Universal File Name ( ).unv
1	23.4	Continuous Random	16.75 - 29.25	30	4c	Hanning	0	32	0.03125	400	s4cafu16
2	23.9	Continuous Random	16.75 - 29.25	30	4c	Hanning	0	32	0.03125	400	s4cafu16
3	60.7	Continuous Random	54.25 - 66.75	30	4d	Hanning	0	32	0.03125	400	s4cafu54
4	105.5	Continuous Random	99.75 - 112.25	30	4e	Hanning	0	32	0.03125	400	s4cafu100
5	105.9	Continuous Random	99.75 - 112.25	30	4e	Hanning	0	32	0.03125	400	s4cafu100
6	177.8	Continuous Random	171.75 - 184.25	30	4f	Hanning	0	32	0.03125	400	s4cafu172
7	216.3	Continuous Random	209.75 - 222.25	30	4g	Hanning	0	32	0.03125	400	s4cafu210

Table F-2 Modal Testing Parameters Summary - Section 4 Free-Free Modes

Mode No.	Nat Freq (Hz)	Excitation Method	Frequency Span (Hz)	No. Avg	Test No.	Type of Window	% Overlap	Sample Length(Sec)	Frequency Resolution (Hz)	No. of Freq Lines	Function Universal File Name ( ).unv
1	118.0	Continuous Random	111.75 - 124.25	30	4k	Hanning	0	32	0.03125	400	s4fffu112
2	128.3	Continuous Random	122.75 - 135.25	30	4l	Hanning	0	32	0.03125	400	s4fffu123
3	129.0	Continuous Random	122.75 - 135.25	30	4l	Hanning	0	32	0.03125	400	s4fffu123
4	228.6	Continuous Random	221.75 - 234.25	30	4m	Hanning	0	32	0.03125	400	s4fffu222
5	247.9	Continuous Random	243.75 - 256.25	30	4n	Hanning	0	32	0.03125	400	s4fffu244
6	249.5	Continuous Random	243.75 - 256.25	30	4n	Hanning	0	32	0.03125	400	s4fffu244
7	453.5	Continuous Random	446.75 - 459.25	30	4q	Hanning	0	32	0.03125	400	s4fffu447

Table F-3 Modal Data Analysis Parameters Summary - Section 4 Cantilever Modes

Mode No.	Nat Freq (Hz)	Curve-Fit Technique	Frequency Range (Hz)	No. of Resp Pts	Matrix Size	No. of Roots	Reference Point	Shape/Parameter File Name ( ).unv	Model Universal File Name ( ).unv
1	23.4	Polyref	16.75 - 29.25	45	16	4	21y-	s4camodes	s4catestpt
2	23.9	Polyref	16.75 - 29.25	45	16	4	21y-	s4camodes	s4catestpt
3	60.7	Polyref	54.25 - 66.75	45	16	3	21y-	s4camodes	s4catestpt
4	105.5	Polyref	99.75 - 112.25	45	16	3	21y-	s4camodes	s4catestpt
5	105.9	Polyref	99.75 - 112.25	45	16	3	21y-	s4camodes	s4catestpt
6	177.8	Polyref	171.75 - 184.25	45	16	8	21y-	s4camodes	s4catestpt
7	216.3	Polyref	209.75 - 222.25	45	16	7	21y-	s4camodes	s4catestpt

Table F-3 Modal Data Analysis Parameters Summary - Section 4 Free-Free Modes

Mode No.	Nat Freq (Hz)	Curve-Fit Technique	Frequency Range (Hz)	No. of Resp Pts	Matrix Size	No. of Roots	Reference Points	Shape/Parameter File Name ( ).unv	Model Universal File Name ( ).unv
1	118.0	Polyref	111.75 - 124.25	44	16	12	2y+, 21z-	s4ffmodes	s4fftestpt
2	128.3	Polyref	122.75 - 135.25	44	16	12	2y+, 21z-	s4ffmodes	s4fftestpt
3	129.0	Polyref	122.75 - 135.25	44	16	12	2y+, 21z-	s4ffmodes	s4fftestpt
4	228.6	Polyref	221.75 - 234.25	44	16	6	2y+, 21z-	s4ffmodes	s4fftestpt
5	247.9	Polyref	243.75 - 256.25	44	16	16	2y+, 21z-	s4ffmodes	s4fftestpt
6	249.5	Polyref	243.75 - 256.25	44	16	16	2y+, 21z-	s4ffmodes	s4fftestpt
7	453.5	Polyref	446.75 - 459.25	44	16	12	2y+, 21z-	s4ffmodes	s4fftestpt

O U T P U T F R O M G R I D P O I N T W E I G H T G E N E R A T O R

REFERENCE POINT = 0

M O

```
*  1.173694E-01 -9.893345E-18 -1.406752E-17 -2.374403E-17  3.669689E-04 -4.733898E-04 *
* -9.893345E-18  1.173694E-01  6.633962E-17 -3.669689E-04 -1.702379E-14  3.168606E+01 *
* -1.406752E-17  6.628541E-17  1.173694E-01  4.733898E-04 -3.168606E+01  1.698481E-14 *
* -2.207707E-17 -3.669689E-04  4.733898E-04  4.894577E+00 -1.041458E-01 -8.073315E-02 *
*  3.669689E-04 -1.692136E-14 -3.168606E+01 -1.041458E-01  8.663900E+03 -1.184469E-01 *
* -4.733898E-04  3.168606E+01  1.685228E-14 -8.073315E-02 -1.184469E-01  8.663979E+03 *
```

S

```
*  1.000000E+00  0.000000E+00  0.000000E+00 *
*  0.000000E+00  1.000000E+00  0.000000E+00 *
*  0.000000E+00  0.000000E+00  1.000000E+00 *
```

DIRECTION MASS AXIS SYSTEM (S)	MASS	X-C.G.	Y-C.G.	Z-C.G.
X	1.173694E-01	-2.023018E-16	4.033334E-03	3.126616E-03
Y	1.173694E-01	2.699687E+02	-1.450446E-13	3.126616E-03
Z	1.173694E-01	2.699687E+02	4.033334E-03	1.447125E-13

I(S)

```
*  4.894574E+00 -2.365469E-02 -1.833697E-02 *
* -2.365469E-02  1.096553E+02  1.184454E-01 *
* -1.833697E-02  1.184454E-01  1.097343E+02 *
```

I(Q)

```
*  4.894565E+00                            *
*                1.098197E+02              *
*                             1.095700E+02 *
```

Q

```
*  1.000000E+00  0.000000E+00  2.857540E-04 *
* -2.318289E-04  5.846462E-01  8.112883E-01 *
* -1.670650E-04 -8.112884E-01  5.846462E-01 *
```

Section-4 Truss Updated FEM Mass Properties (Cantilevered and Free-Free) With Sensor Mass Included

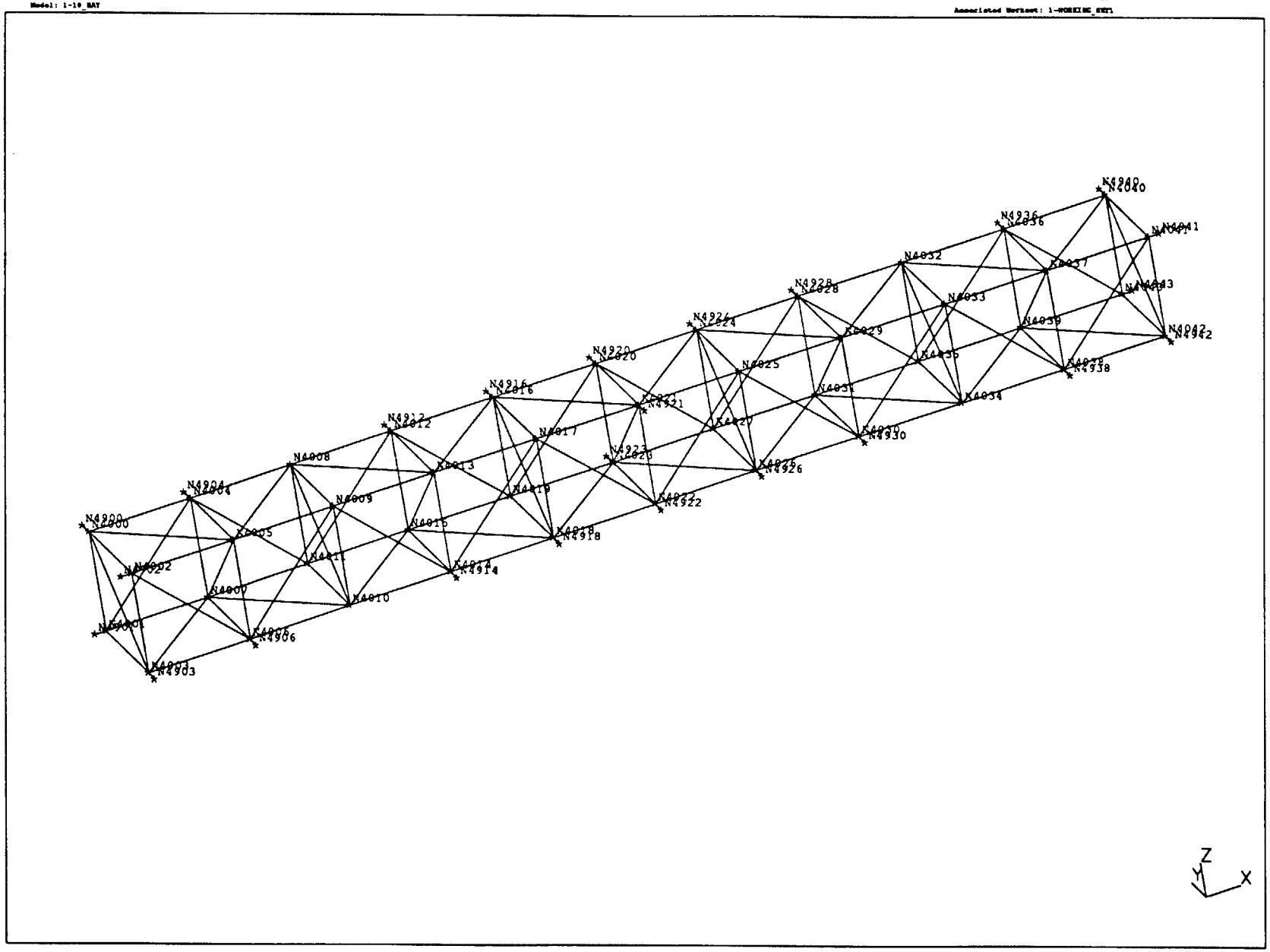
SDRC I-DEAS V: FE_Modeling_&_Analysis
31-JAN-92 16:47:08
Database: osi
View : No stored View
Task: Mesh Creation
Model: 1-10_BAY
Units : IN
Display : No stored Option
Model Dis: 1-SBIS
Associated Workset: 1-WORKING_SET1
N4900
N4901
N4902
N4903
N4904
N4905
N4906
N4907
N4908
N4909
N4910
N4911
N4912
N4913
N4914
N4915
N4916
N4917
N4918
N4919
N4920
N4921
N4922
N4923
N4924
N4925
N4926
N4927
N4928
N4929
N4930
N4931
N4932
N4933
N4934
N4935
N4936
N4937
N4938
N4939
N4940
N4941
N4942
N4943
Z
Y
X

SDRC I-DEAS VI: FE_Modeling_&_Analysis

19-MAR-92 11:14:38

Database: col
View : none, none, none, none
Task: Post Processing
Model: 1-10_BAY

Units : IN
Display : none, none, none, none
Model Bin: 1-MAIN
Associated Workset: 1-MOBILNG_SET1

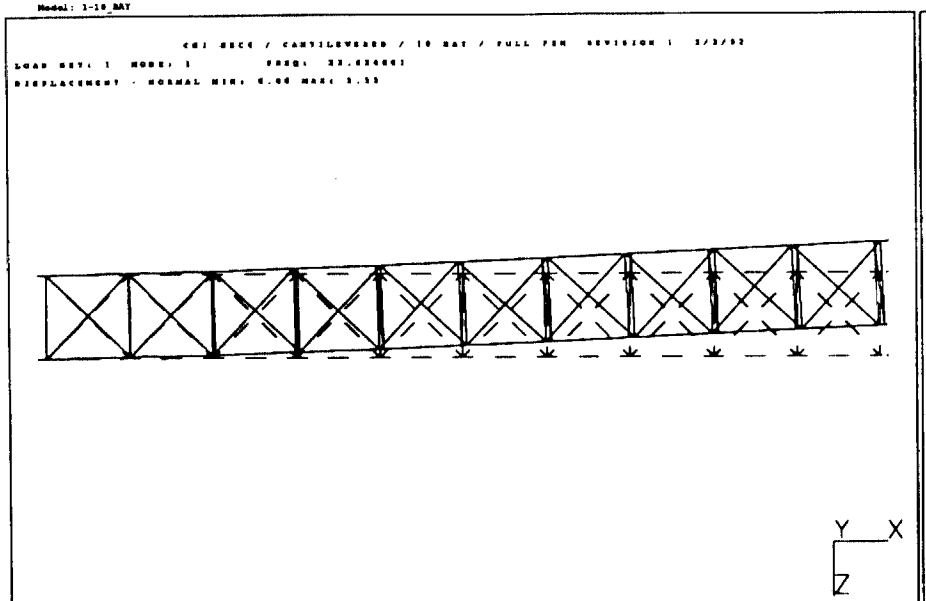

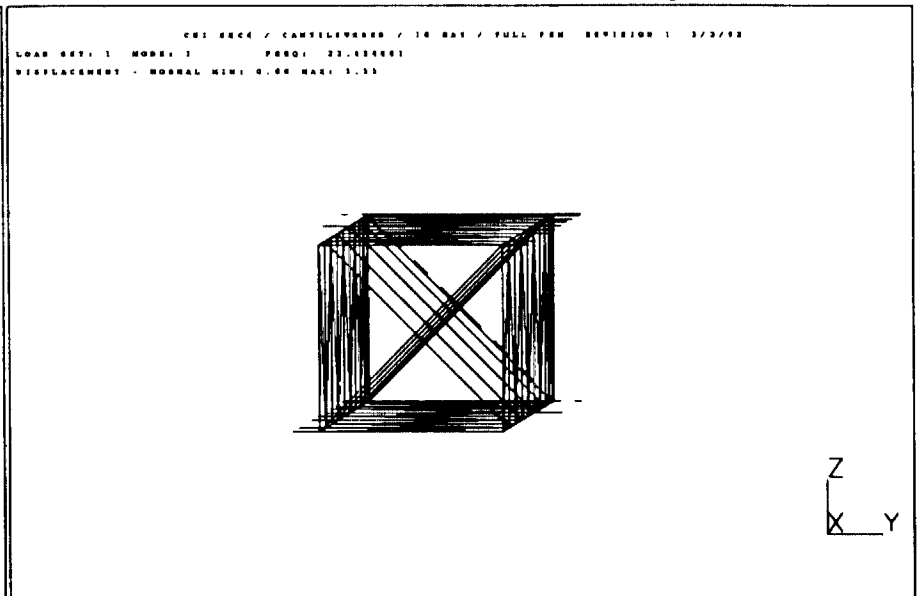

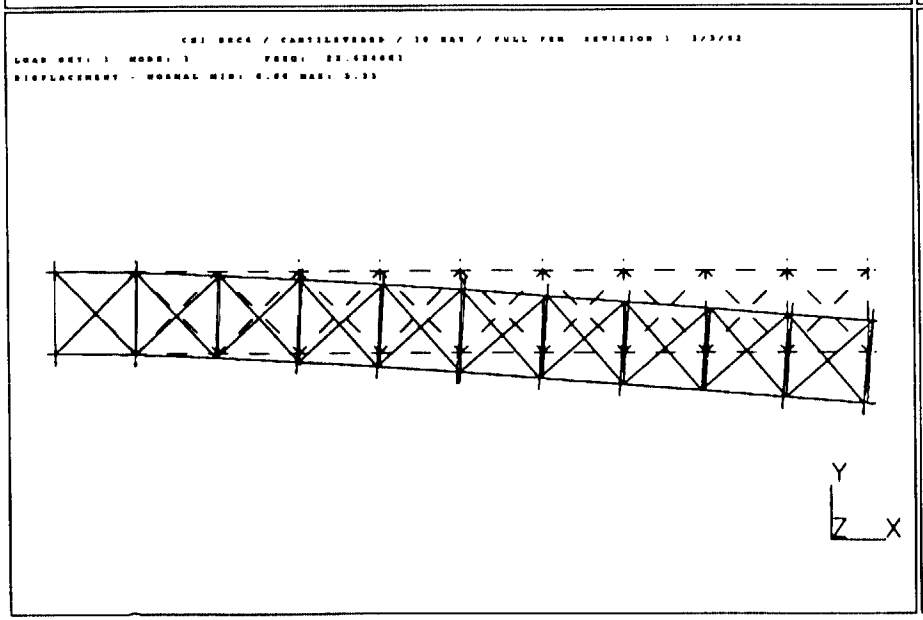

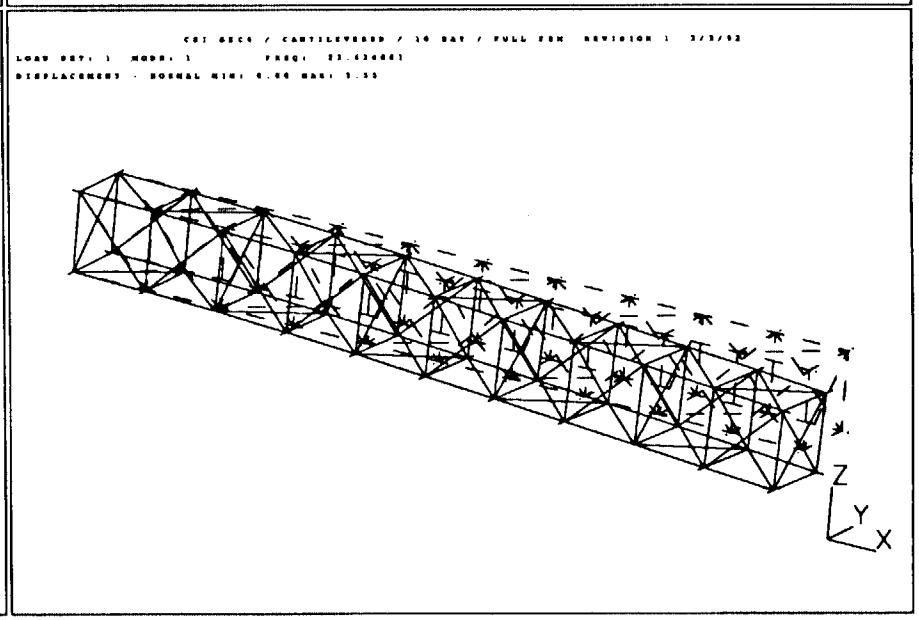

SDRC I-DEAS VI: FE_Modeling_&_Analysis 19-MAR-92 11:14:57

Database: cai
View : none, none, none, none
Task: Post Processing
Model: 1-10_BAY

Units : IN
Display : none, none, none, none
Model Bin: 1-MAIN
Associated Workset: 1-MOBEING_SET1

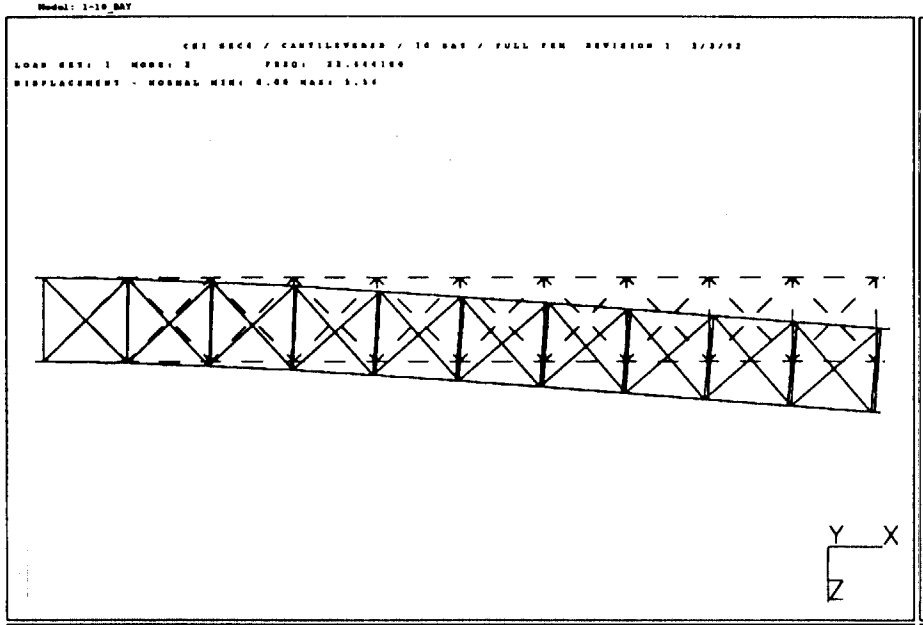

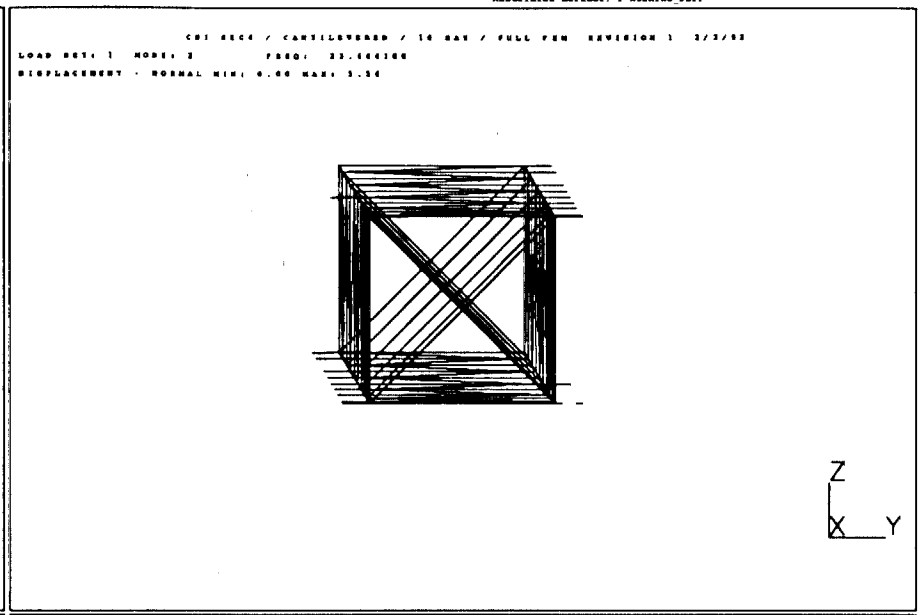

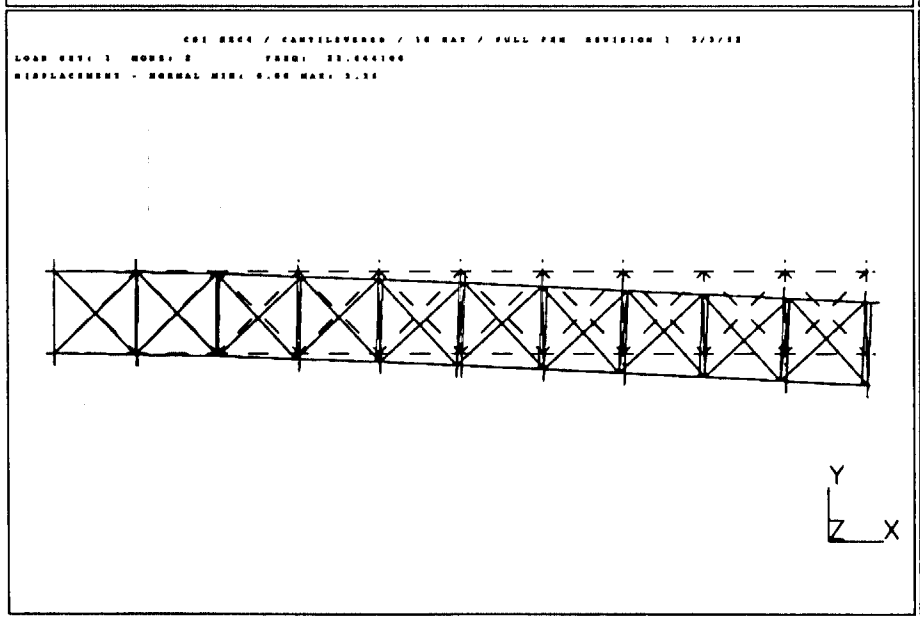

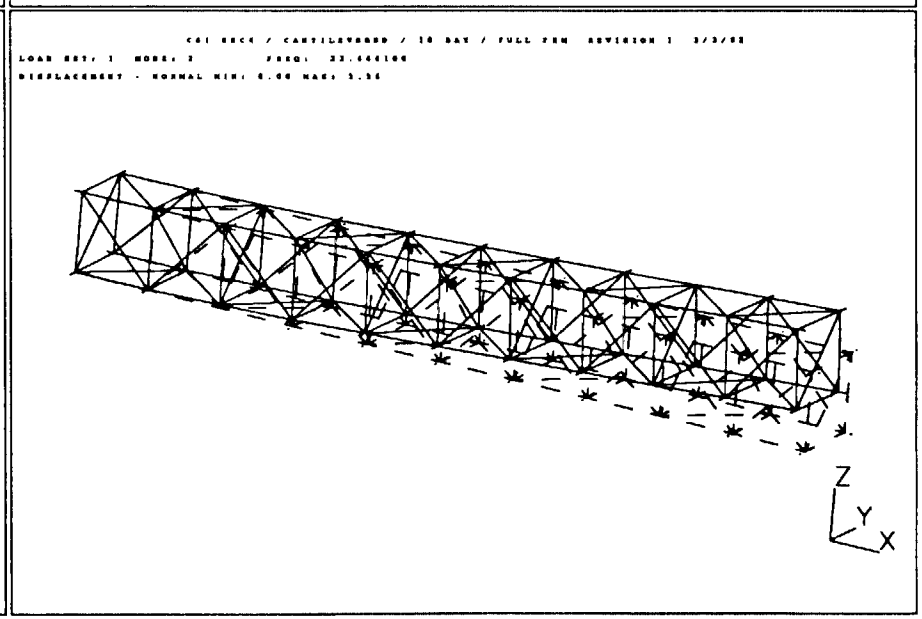

SDRC I-DEAS VI: FE_Modeling_&_Analysis 19-MAR-92 11:16:07

Database: cel
View : none, none, none, none
Task: Post Processing
Model: 1-10_BAY
Units : IN
Display : none, none, none, none
Model Dir: 1-MAIN
Associated Workset: 1-MODELNG_SET1

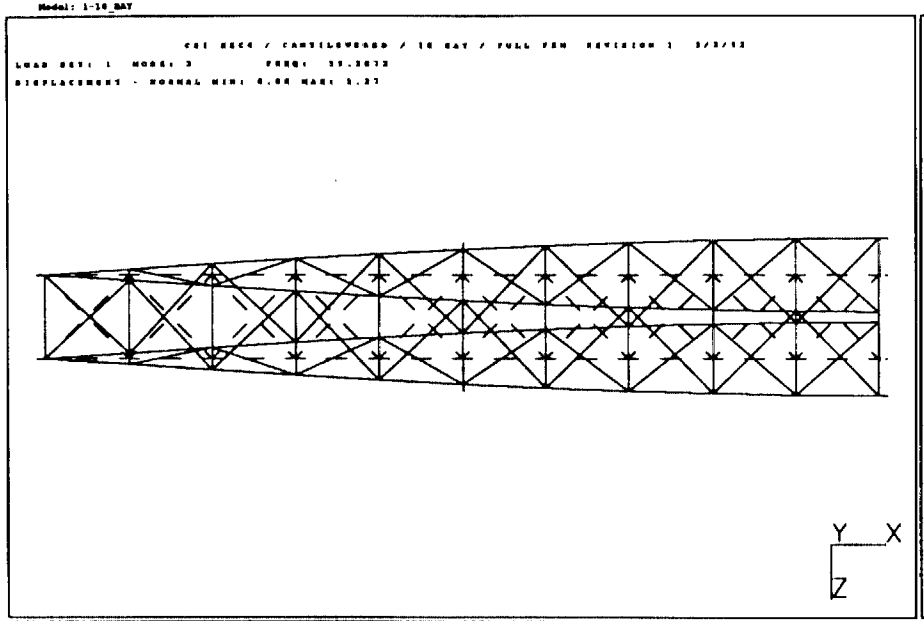

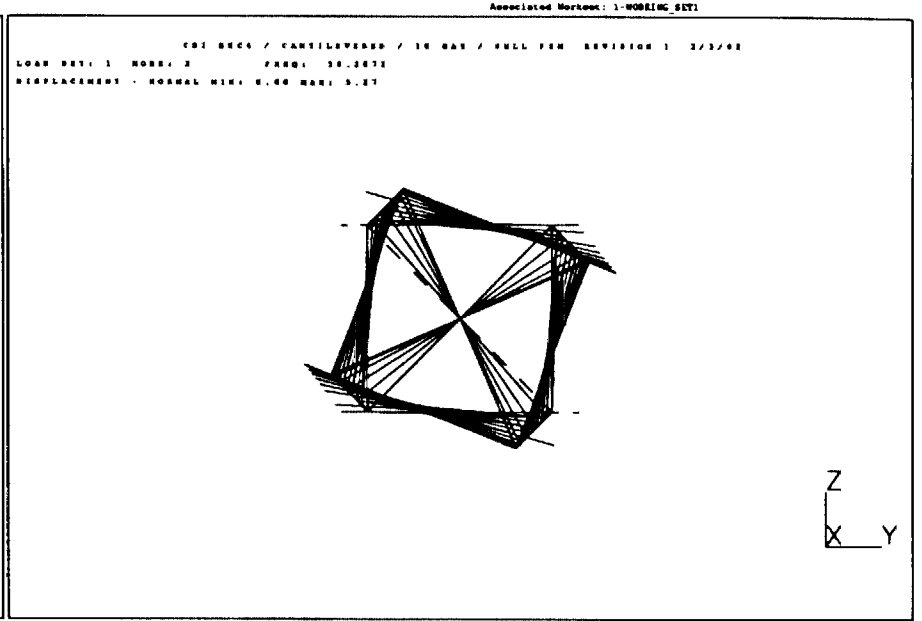

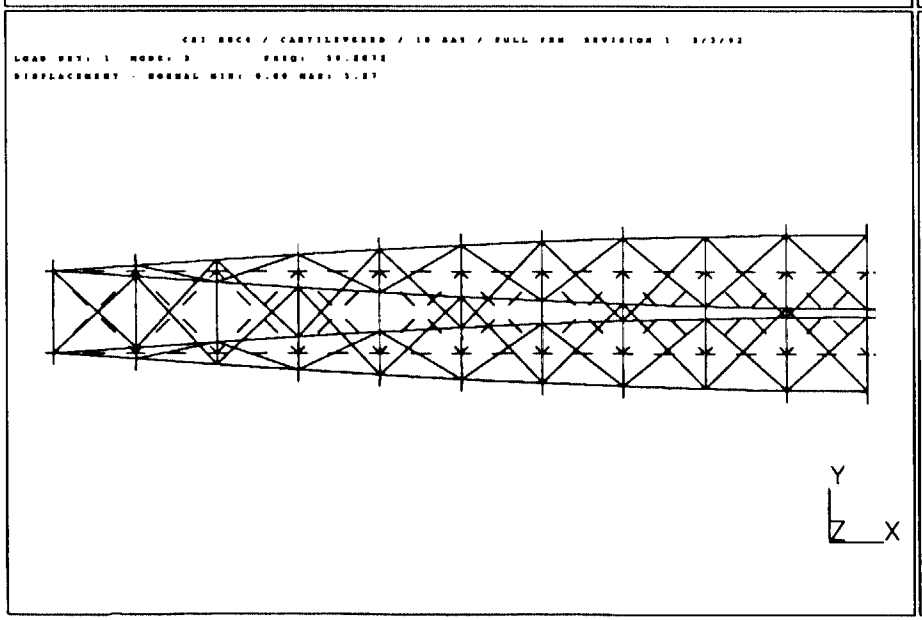

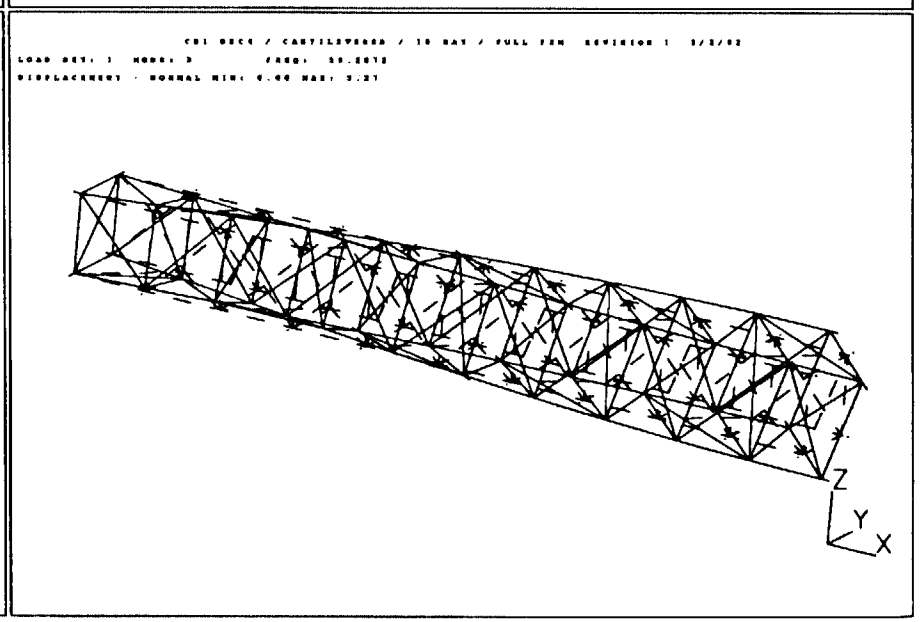

SDRC I-DEAS VI: FE_Modeling_&_Analysis

19-MAR-92 11:15:37

Database: cei
View : none, none, none, none
Task: Post Processing
Model: 1-10_BAY

Units : IN
Display : none, none, none, none
Model Bin: 1-MAIN
Associated Workset: 1-MORRISC_SET1

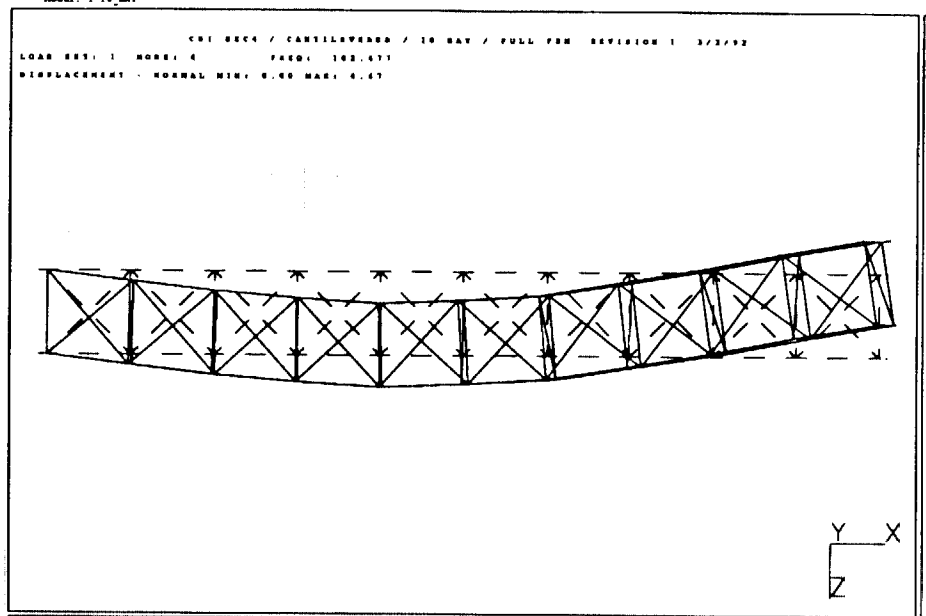

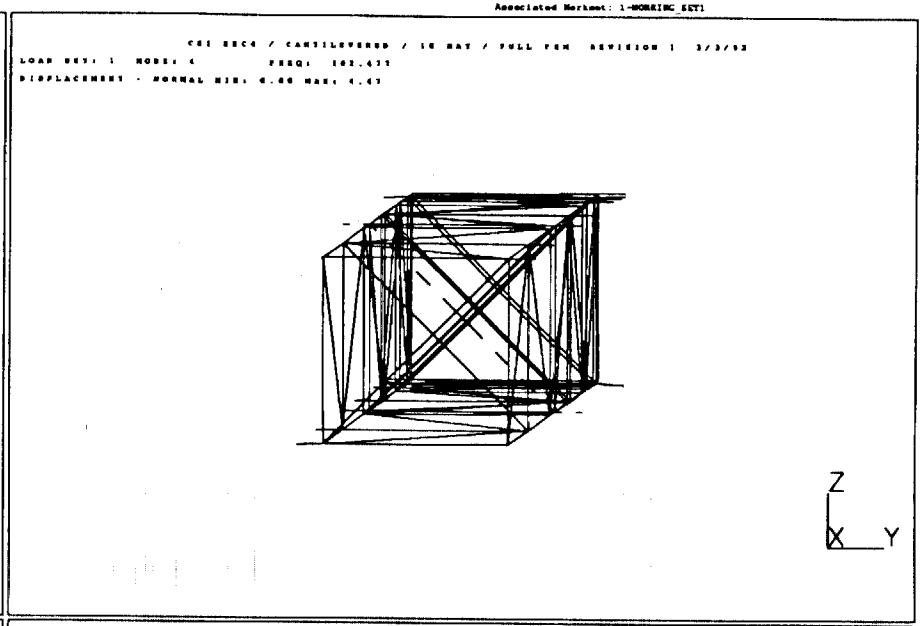

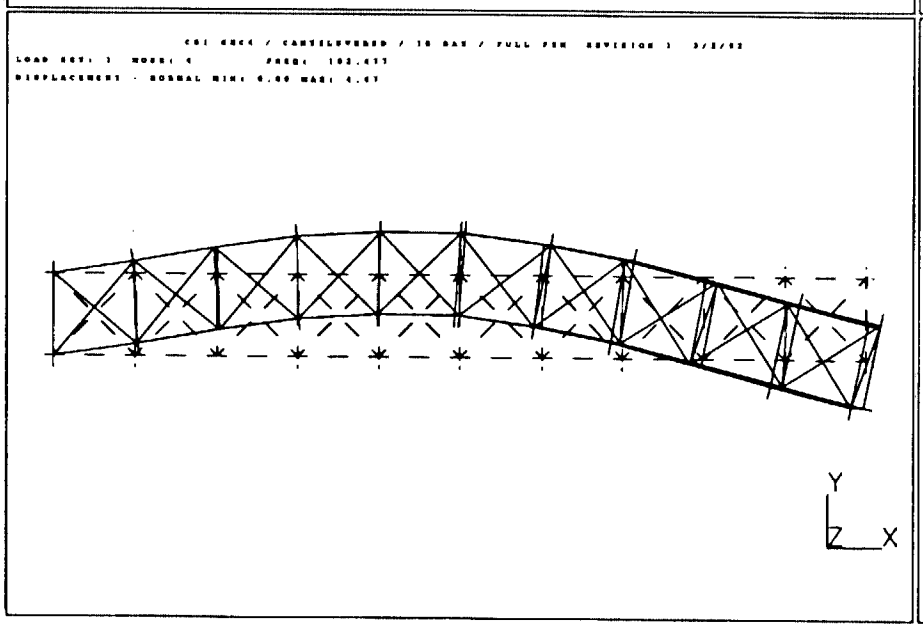

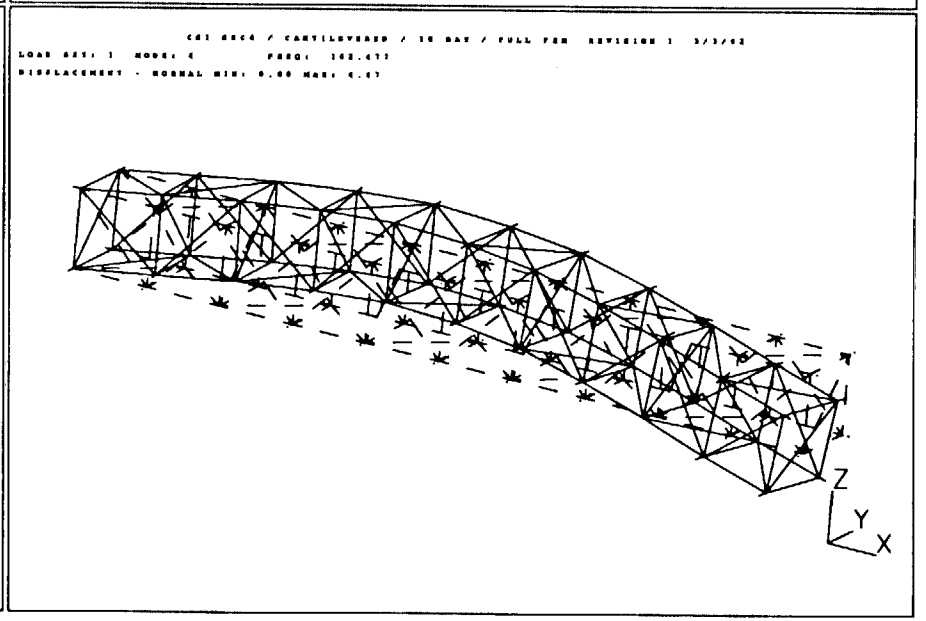

SDRC I-DEAS VI: FE_Modeling_&_Analysis

19-MAR-92 11:16:24

Database: cmi
View : none, none, none, none
Task: Post Processing
Model: 1-10_BAY

Units : IN
Display : none, none, none, none
Model Bin: 1-MAIN
Associated Workset: 1-MODELING_SET1

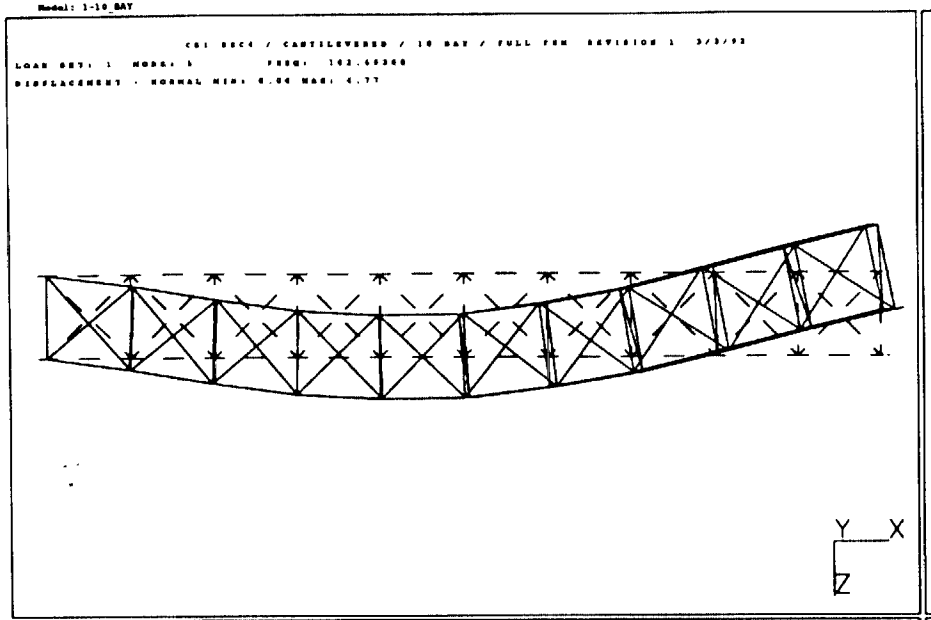

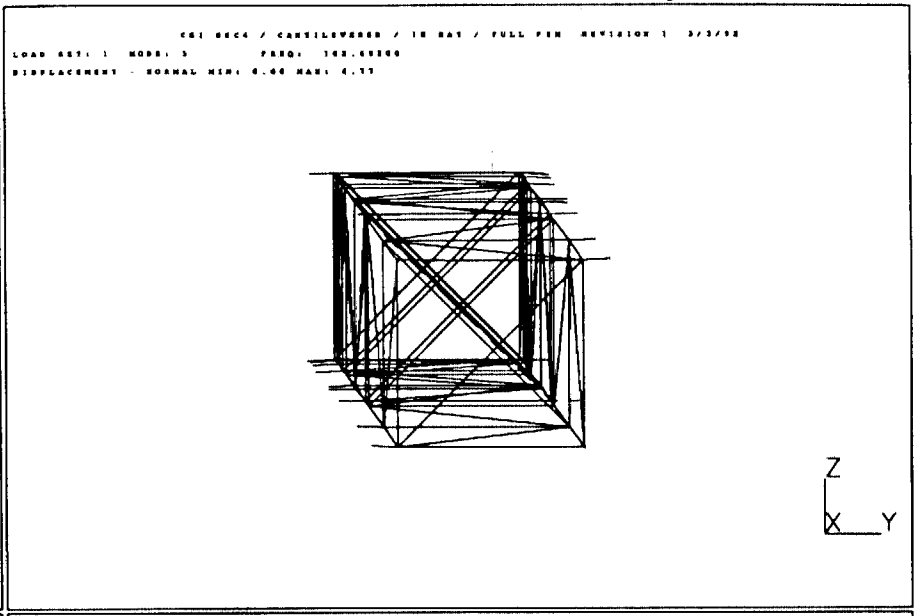

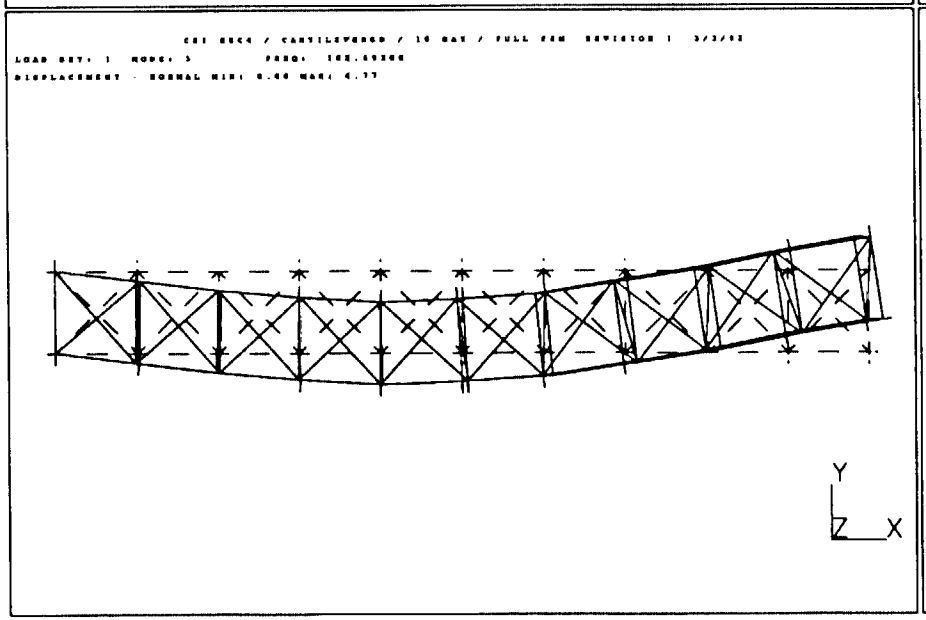

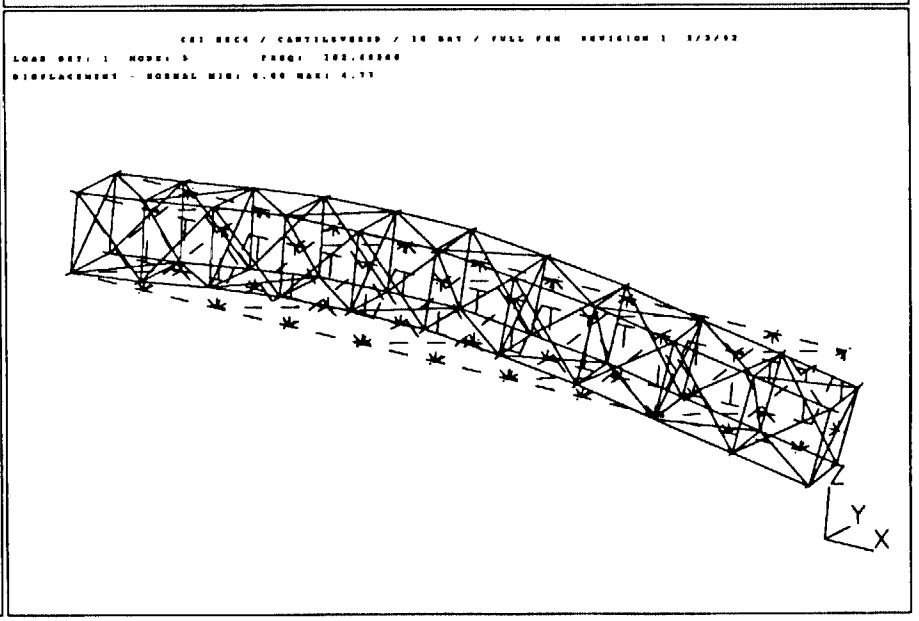

C-4

ORIGINAL PAGE IS
OF POOR QUALITY

SDRC I-DEAS VI: FE_Modeling_&_Analysis

19-MAR-92 11:16:53

Database: col
View : none, none, none, none
Task: Post Processing
Model: 1-16_BAY

Units : IN
Display : none, none, none, none
Model Bin: 1-MAIN
Associated Workset: 1-WORKING_SET1

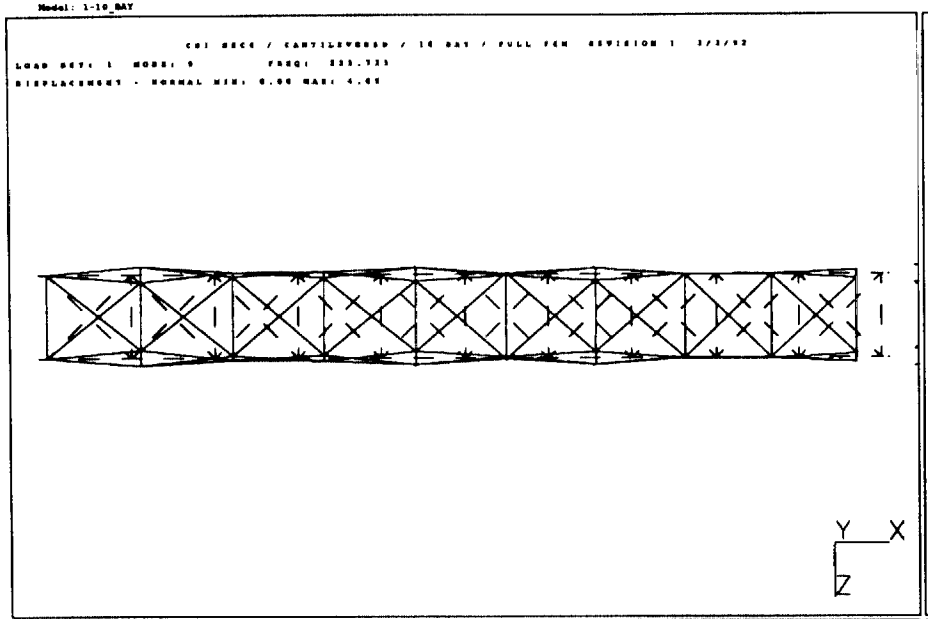

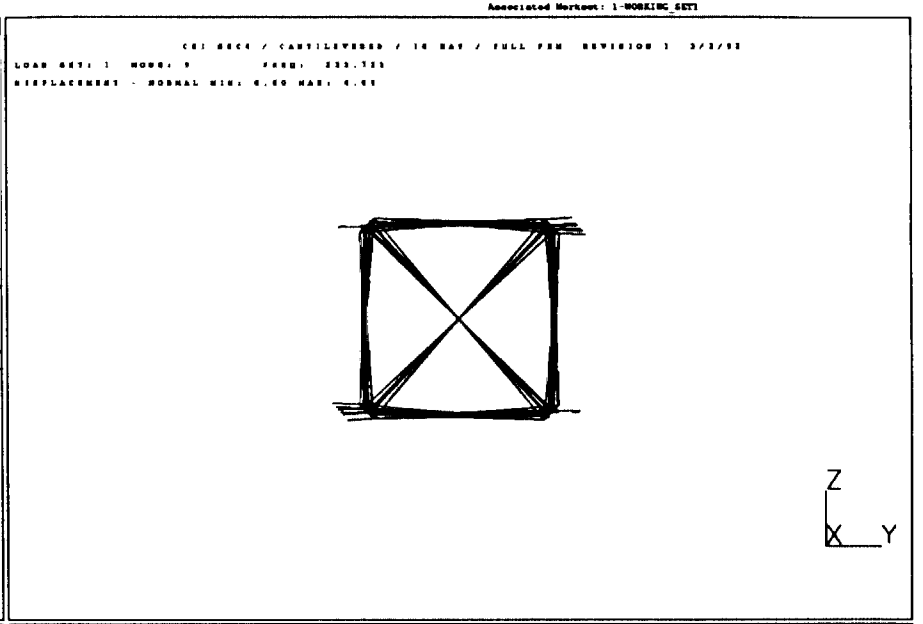

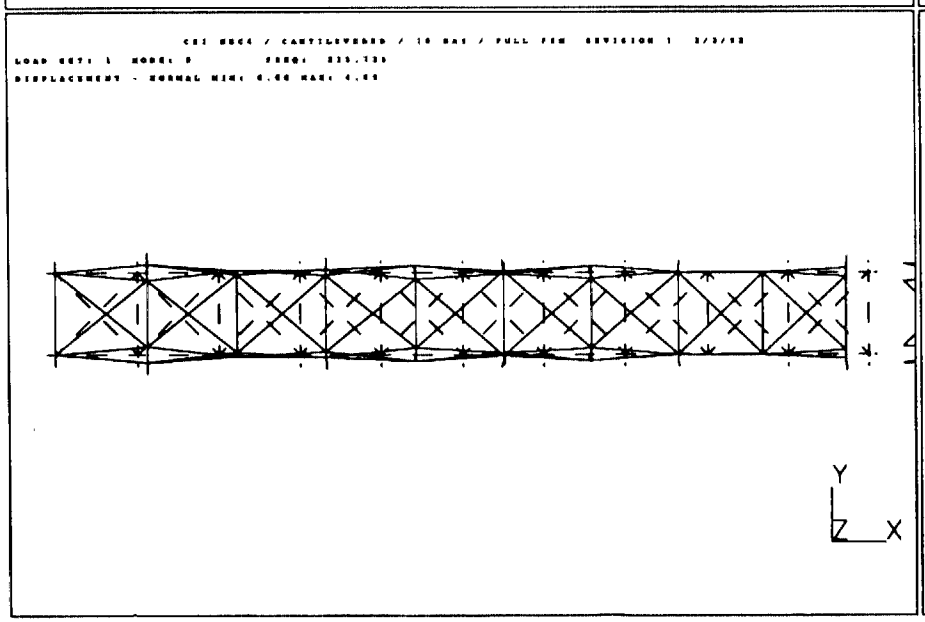

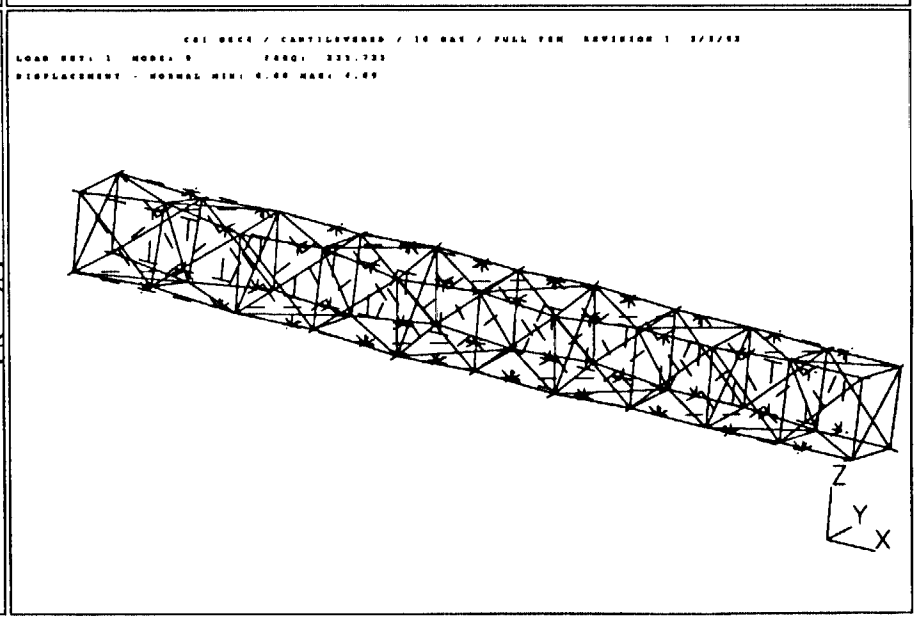

SDRC I-DEAS VI: FE_Modeling_&_Analysis 19-MAR-92 11:18:52

Database: col
View : none, none, none, none
Task: Post Processing
Model: 1-10_BAY

Units : IN
Display : none, none, none, none
Model Bin: 1-MAIN
Associated Workset: 1-WORKING_SET1

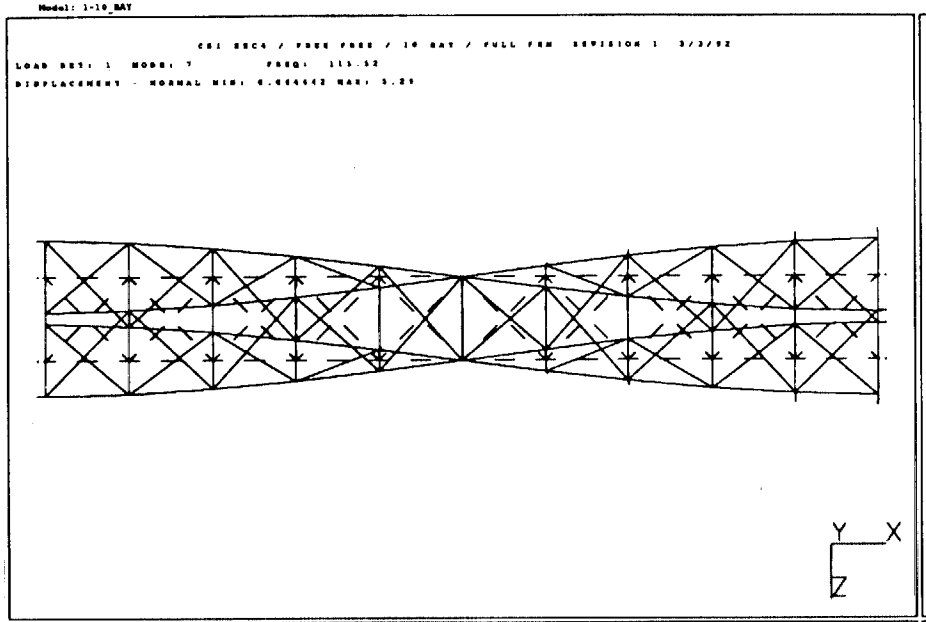

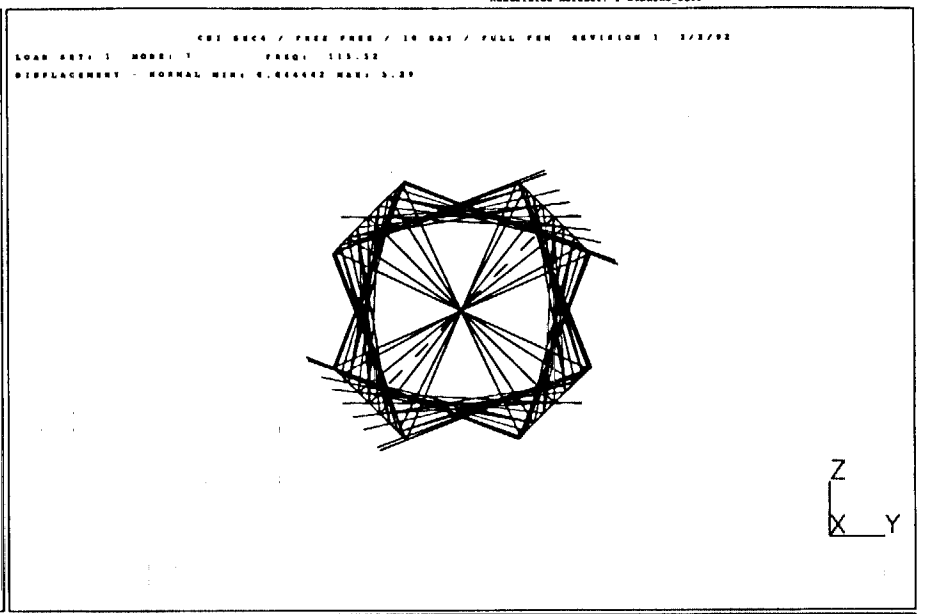

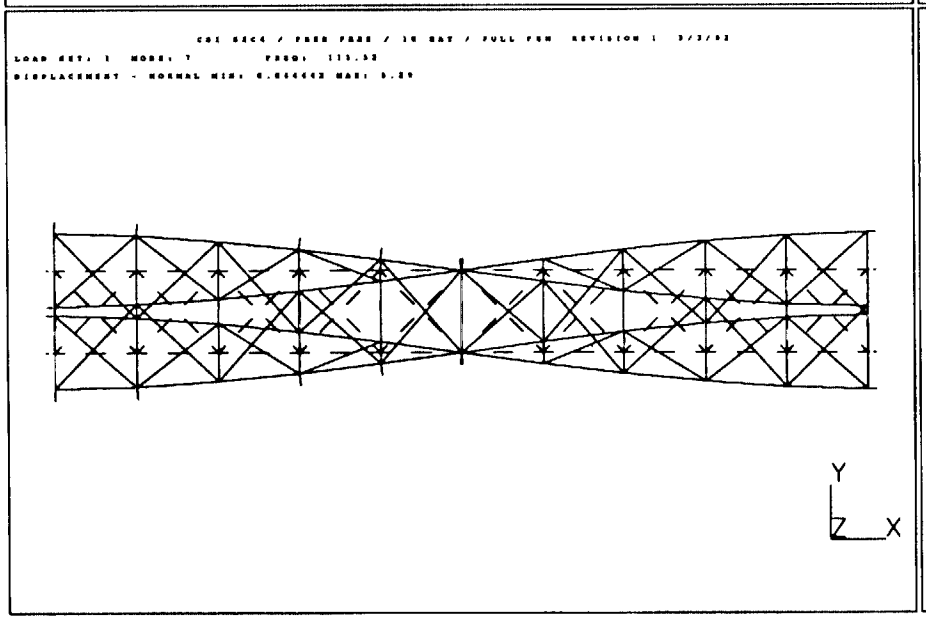

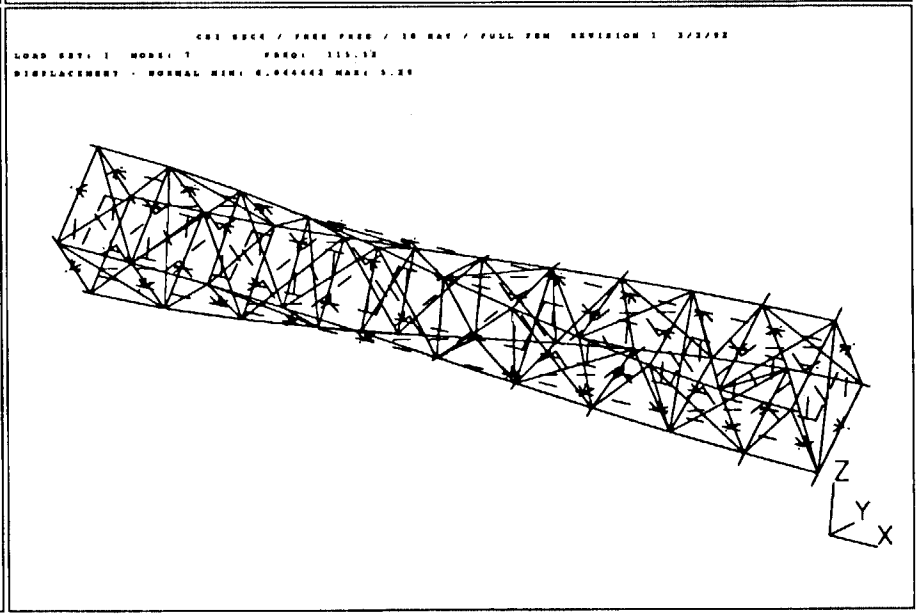

Database: cei
View : none, none, none, none
Task: Post Processing
Model: 1-10_BAY

Units : IN
Display : none, none, none, none
Model Bin: 1-MAIN
Associated Workset: 1-MOORING_SET1

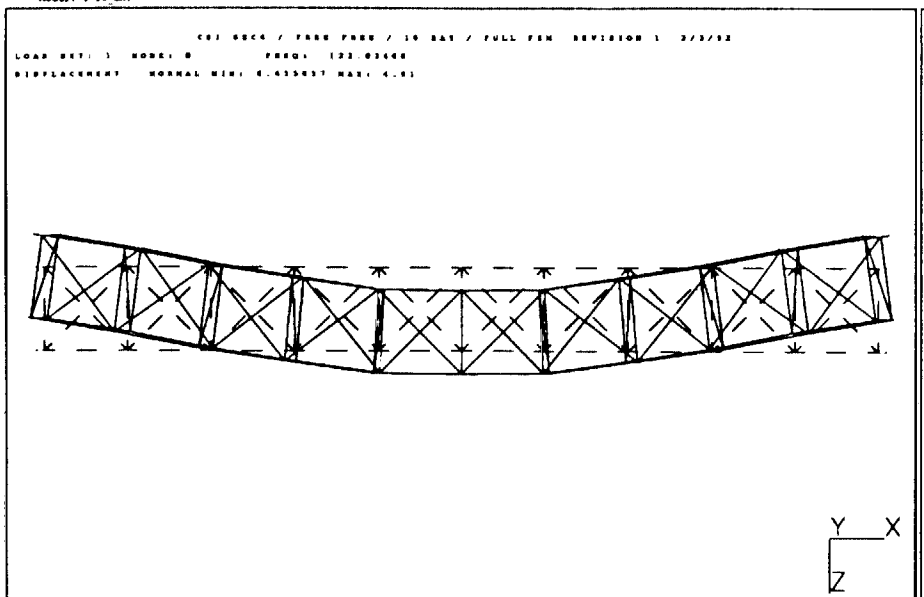

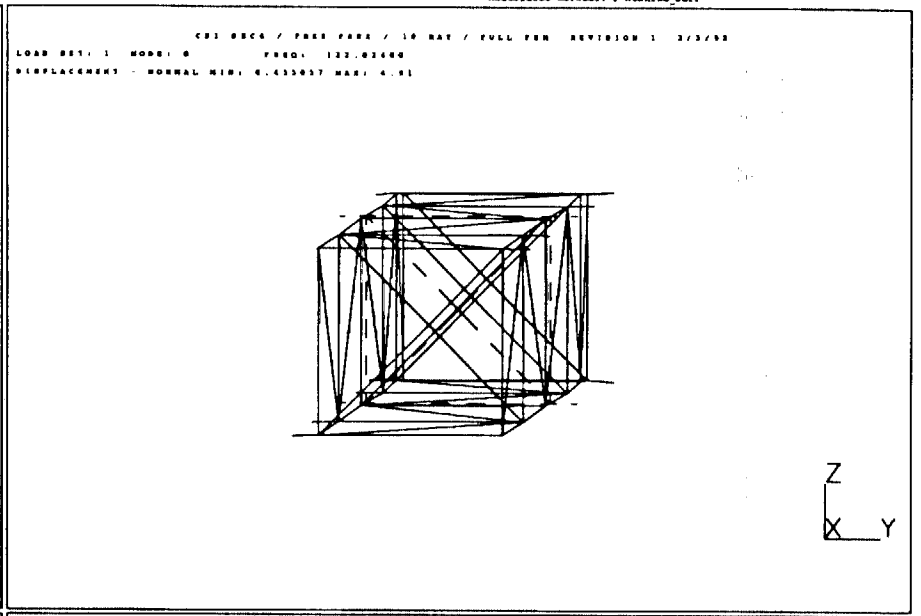

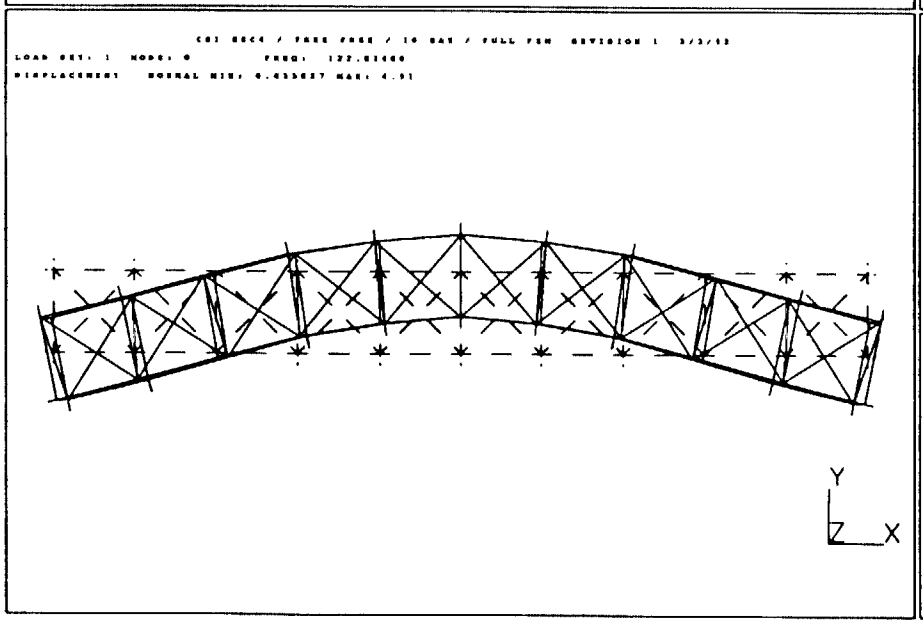

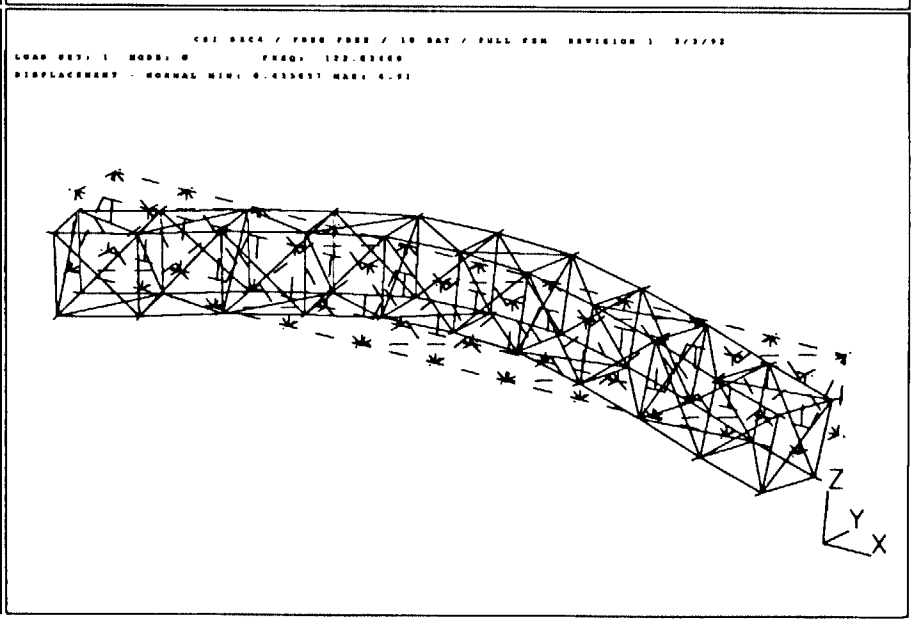

SDRC I-DEAS VI: FE_Modeling_&_Analysis 19-MAR-92 11:19:24

Database: col
View : none, none, none, none
Task: Post Processing
Model: 1-10_BAY

Units : IN
Display : none, none, none, none
Model Bin: 1-MAIN
Associated Workset: 1-MODELING_SET1

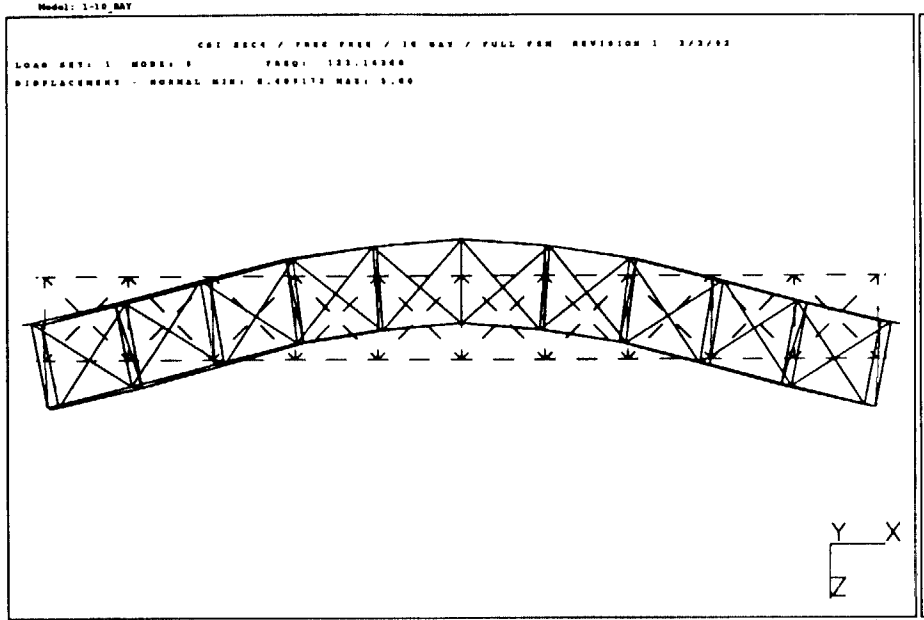

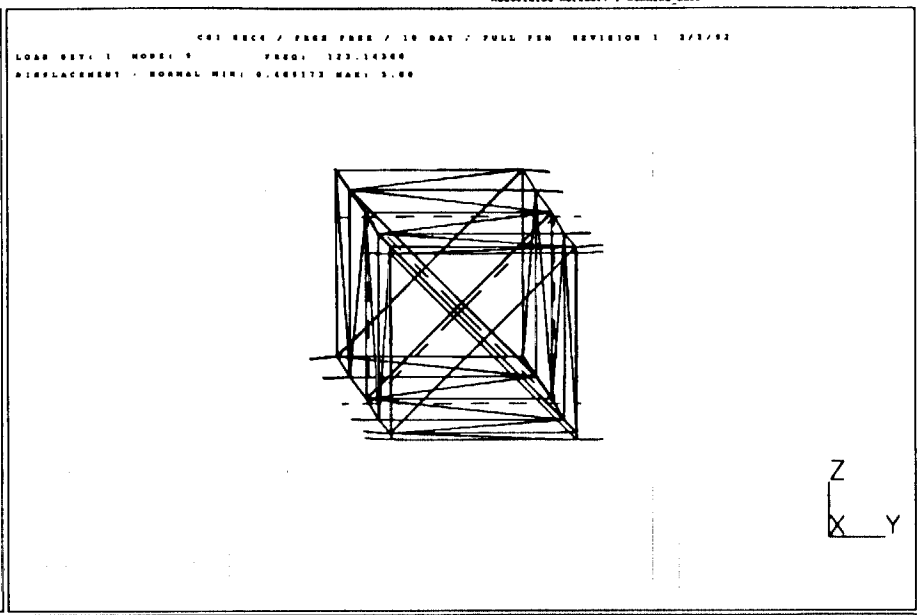

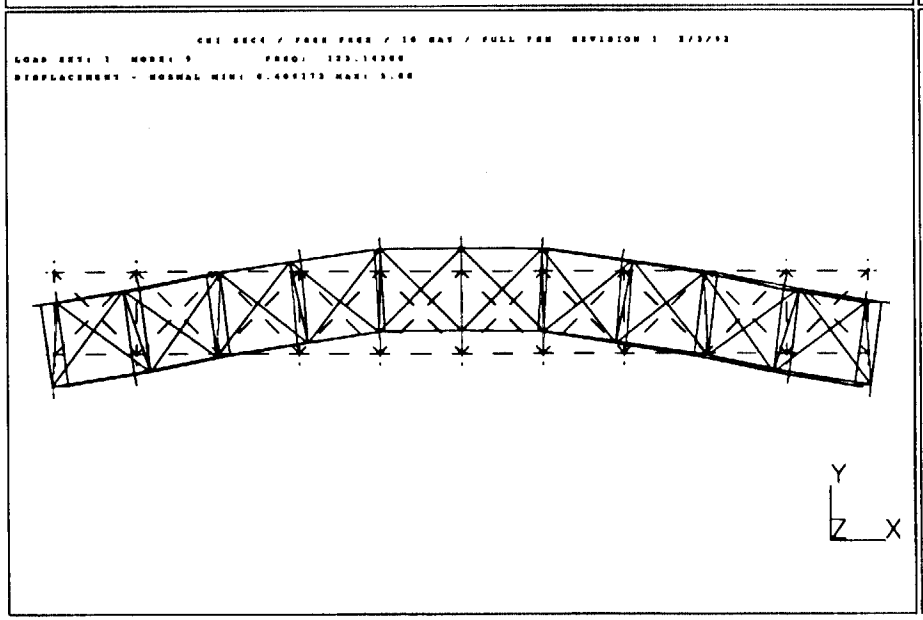

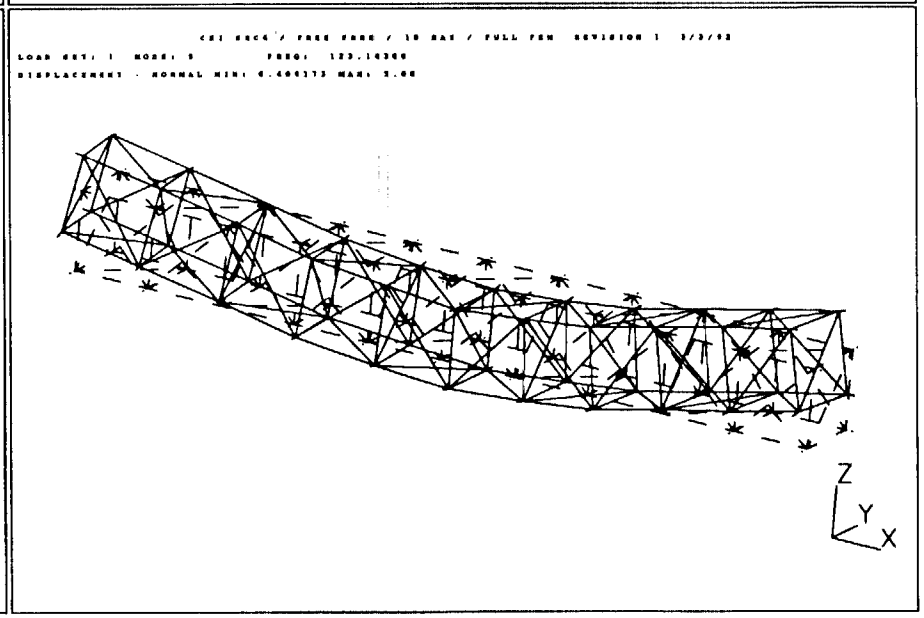

SDRC I-DEAS VI: FE_Modeling_&_Analysis 19-MAR-92 11:19:39

Database: cel
View : none, none, none, none
Task: Post Processing
Model: 1-10_BAY
Units : IN
Display : none, none, none, none
Model Bin: 1-MAIN
Associated Workset: 1-MOORING_SET1

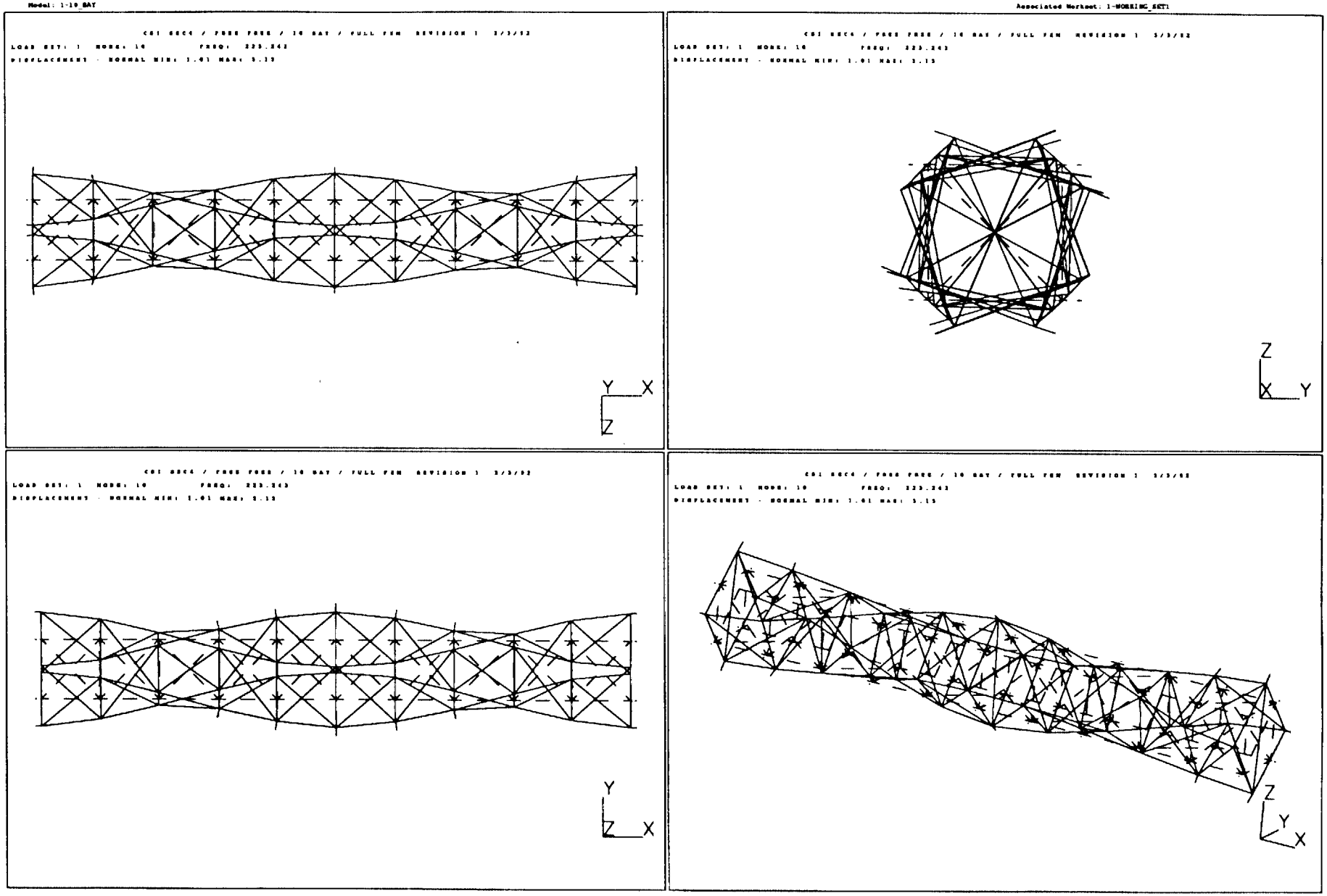

SDRC I-DEAS VI: FE_Modeling_&_Analysis 19-MAR-92 11:19:54

Database: cai
View : none, none, none, none
Task: Post Processing
Model: 1-10_BAY
Units : IN
Display : none, none, none, none
Model Bin: 1-MAIN
Associated Workset: 1-MODBING_SET1

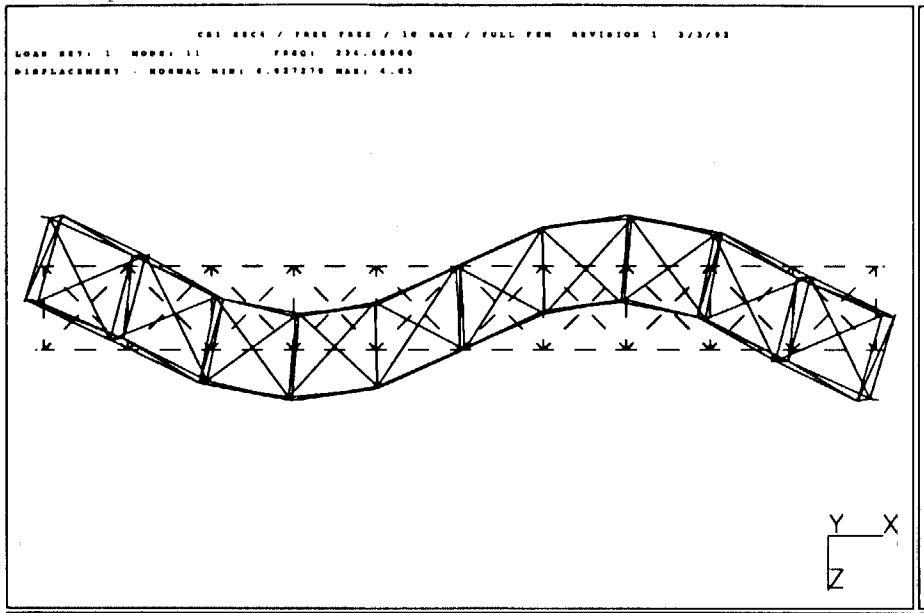

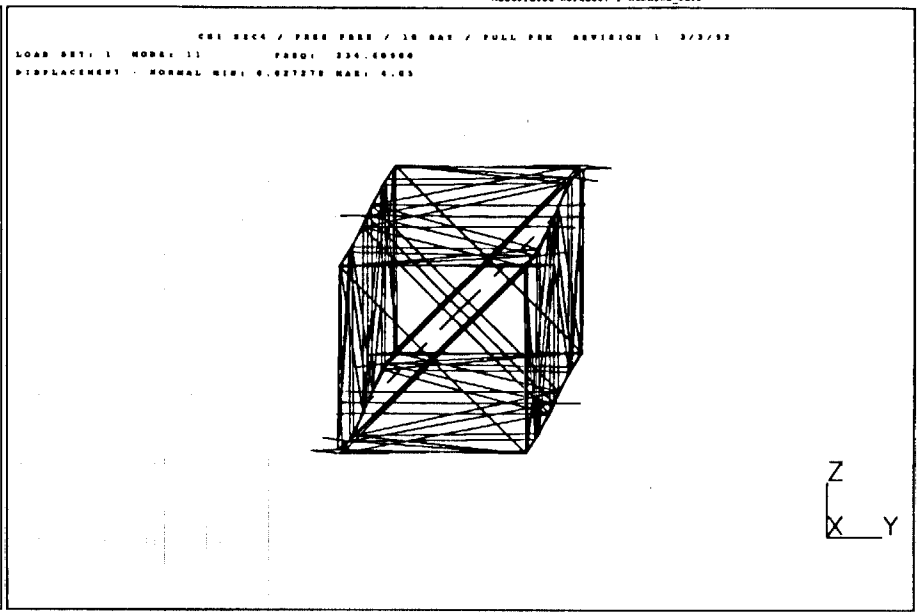

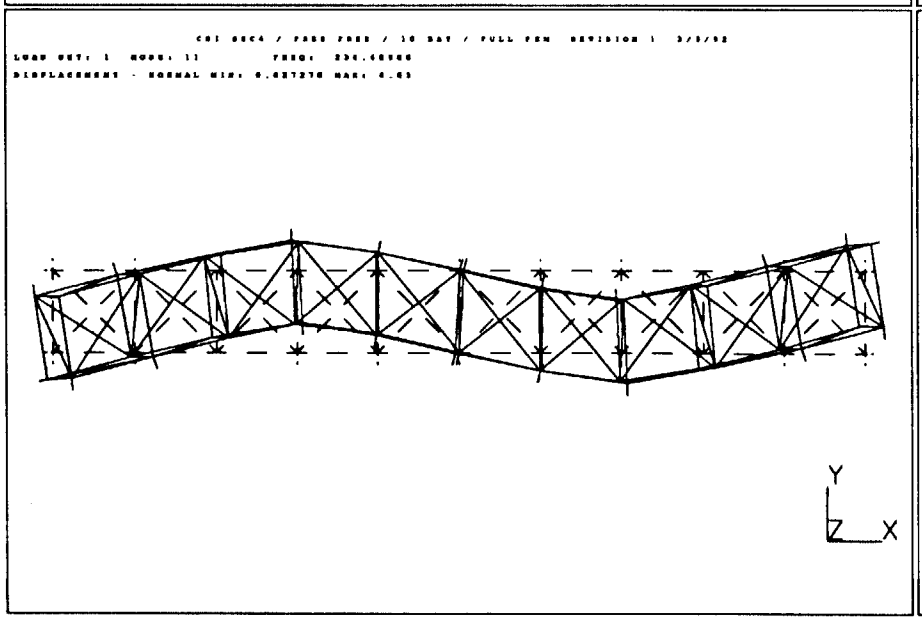

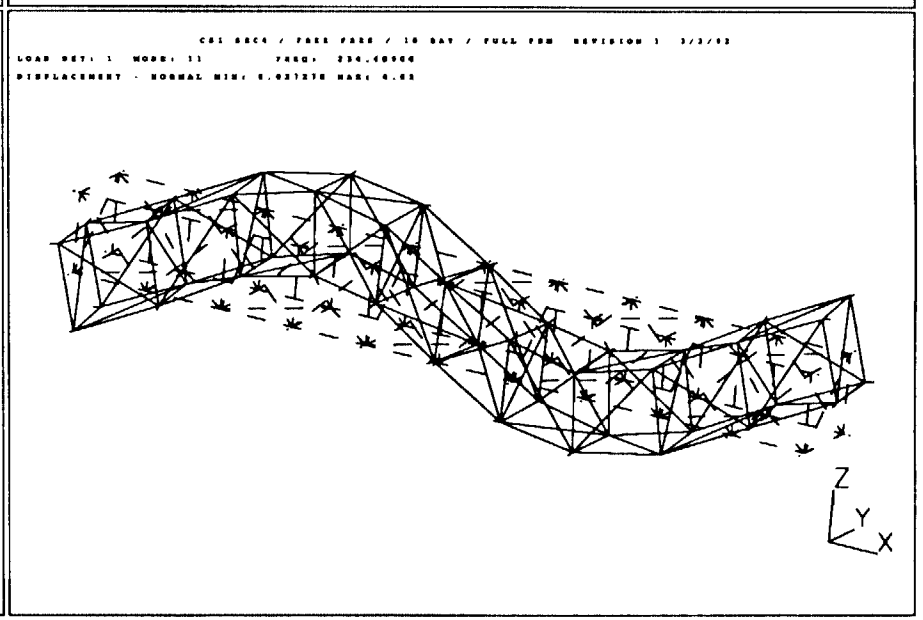

SDRC I-DEAS VI: FE_Modeling_&_Analysis 19-MAR-92 11:21:11

Database: csi
View : none, none, none, none
Task: Post Processing
Model: 1-16_BAY

Units : IN

Display : none, none, none, none
Model Sln: 1-MAIN
Associated Workset: 1-MODELING_SET1

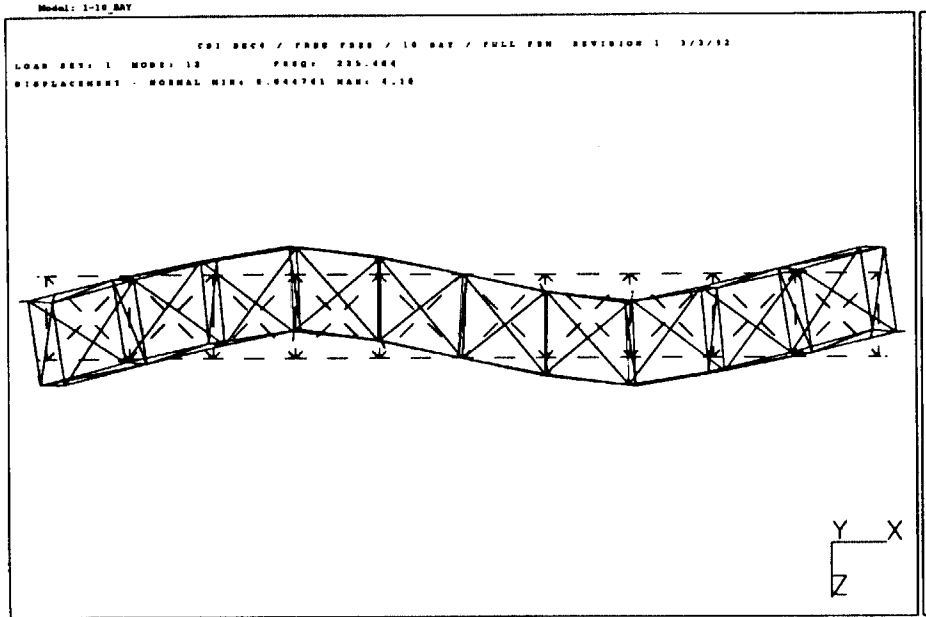

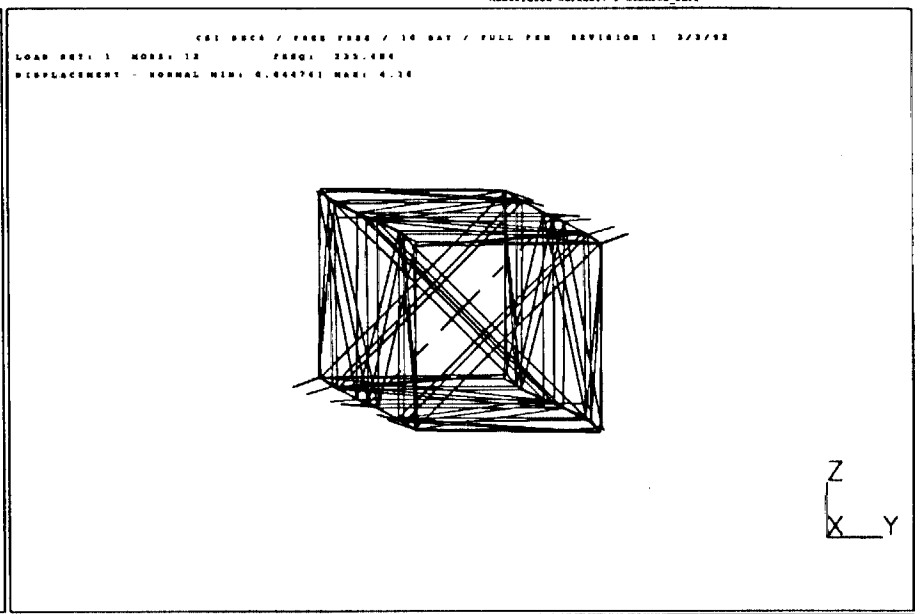

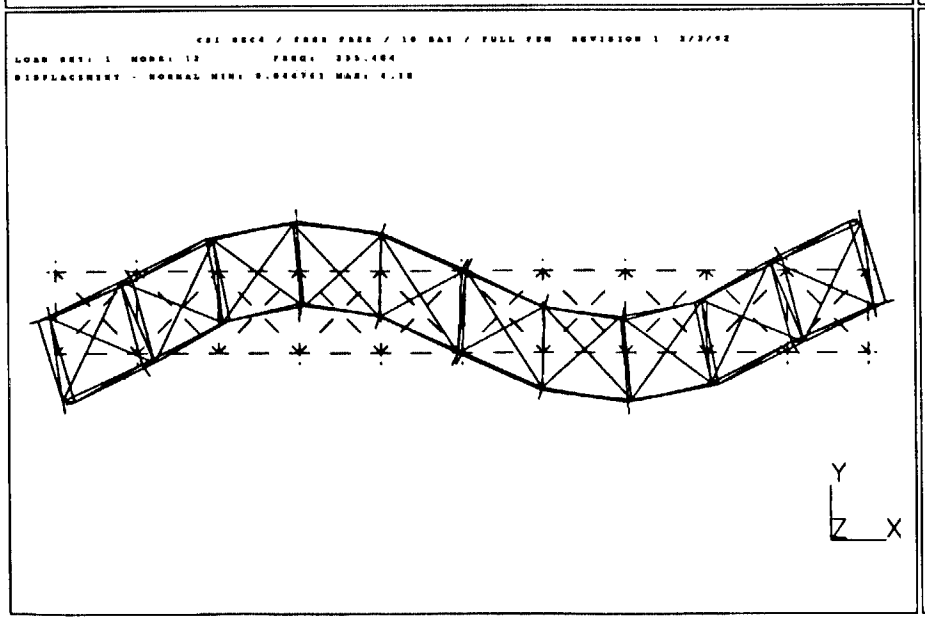

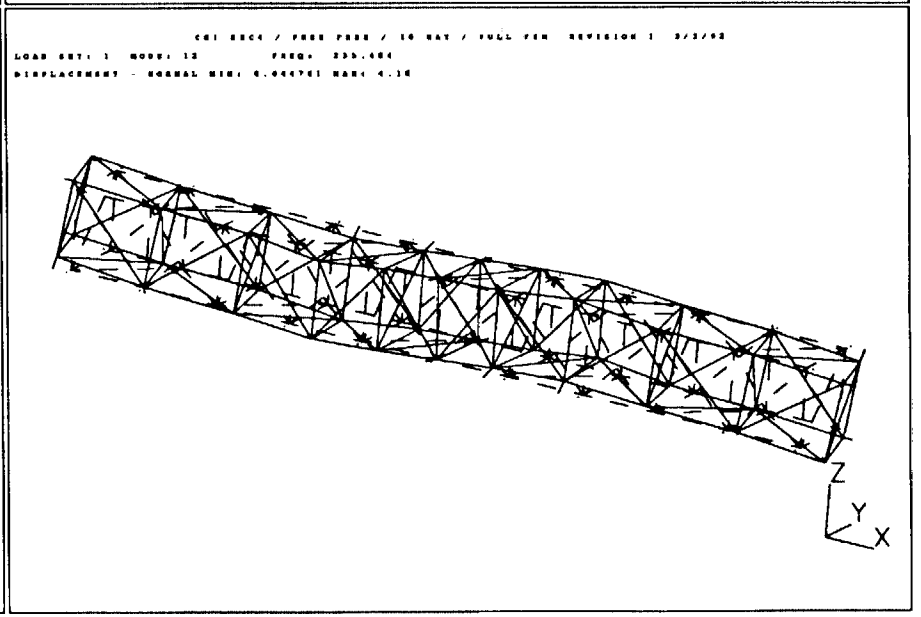

SDRC I-DEAS VI: FE_Modeling_6_Analysis 19-MAR-92 11:20:48

Database: cel
View : none, none, none, none
Task: Post Processing
Model: 1-10_BAY

Units : IN
Display : none, none, none, none
Model Bin: 1-MAIN
Associated Workset: 1-WORKING_SET1

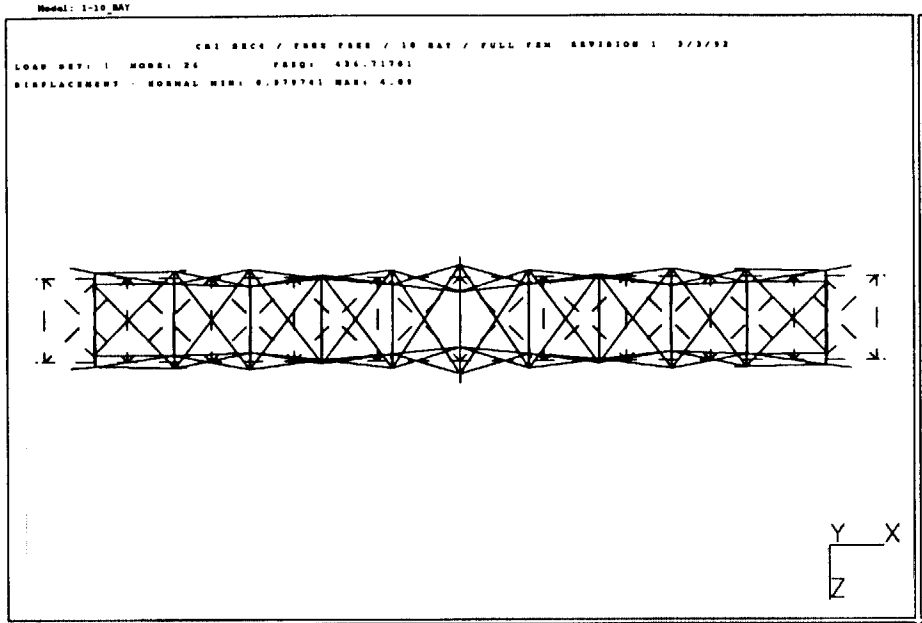

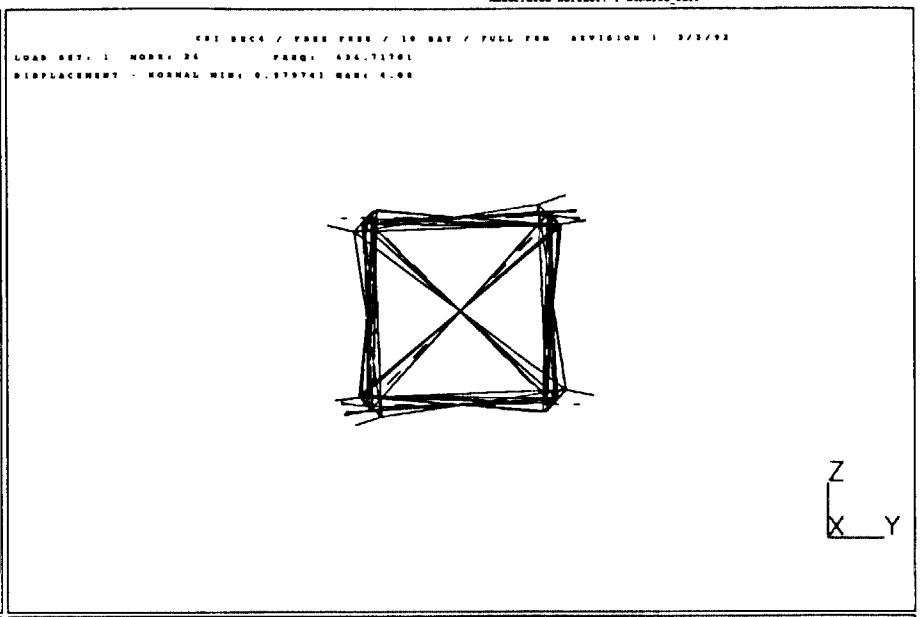

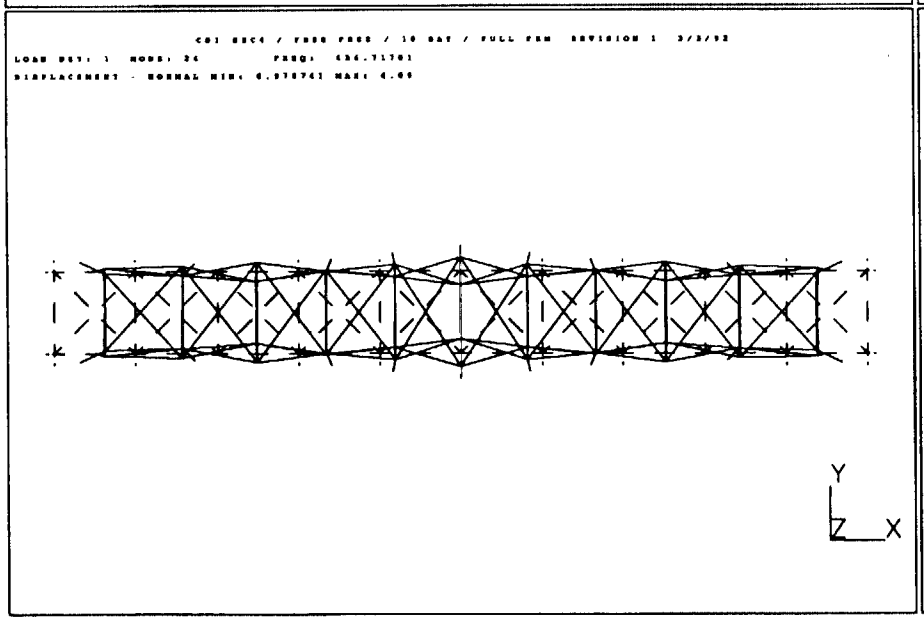

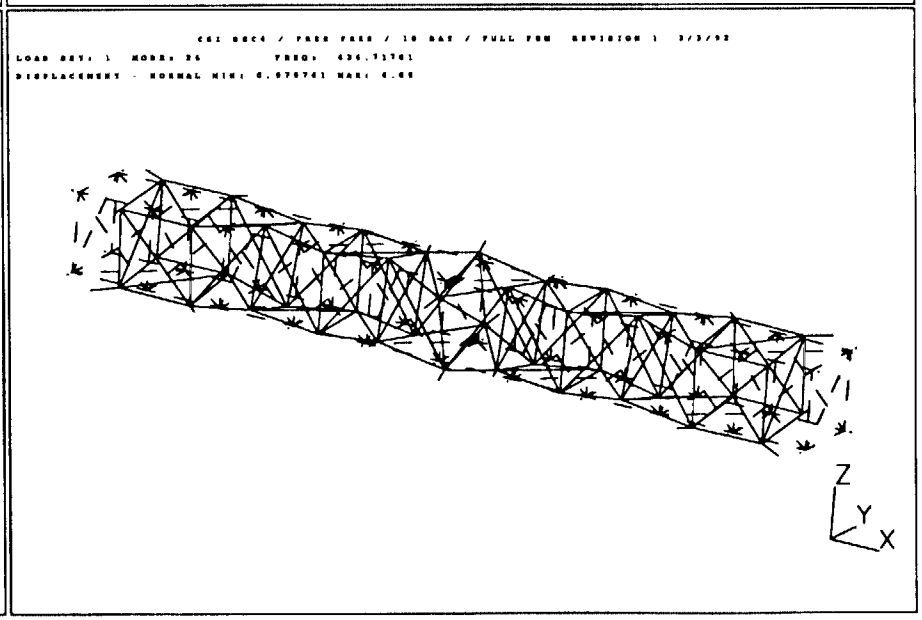

APPENDIX G

TEST DATA FOR STATIC TRUSS SECTION TESTS

Section 1 Bending Test

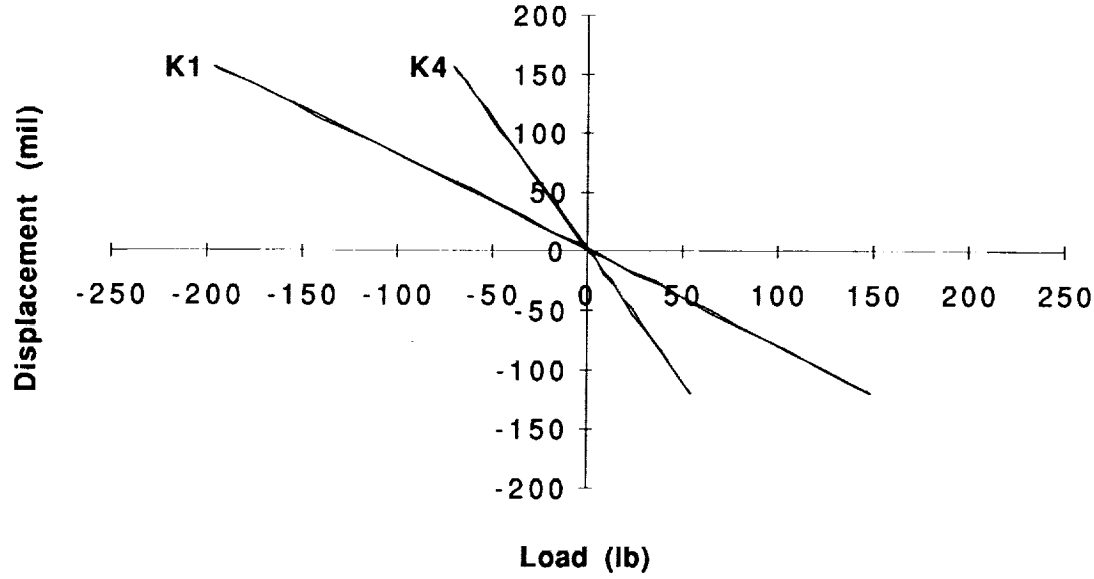

Section 1 Bending Test

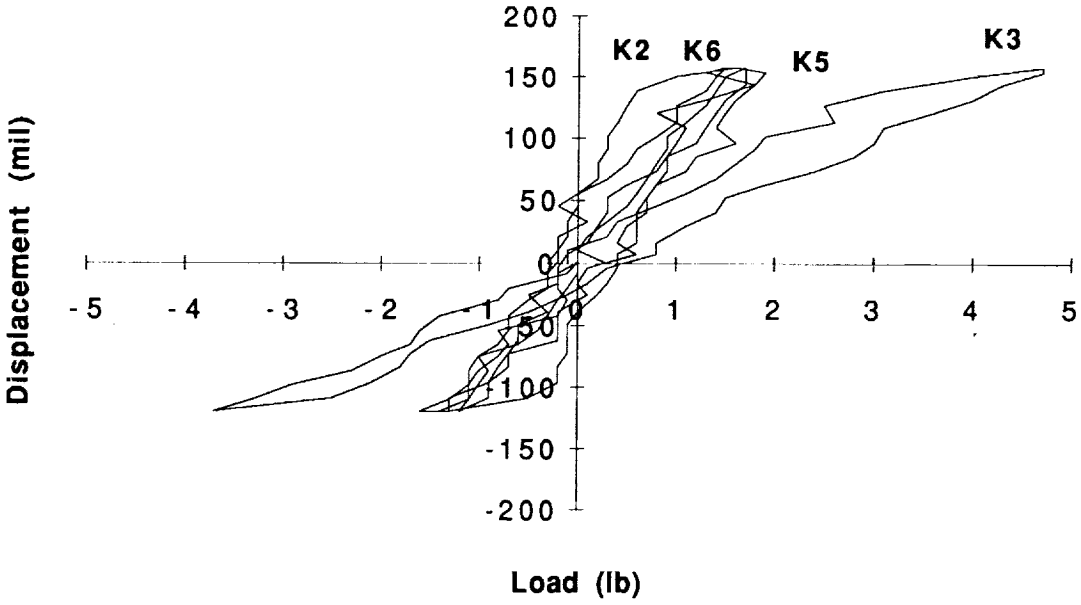

Section 1 Clockwise Torsion Test

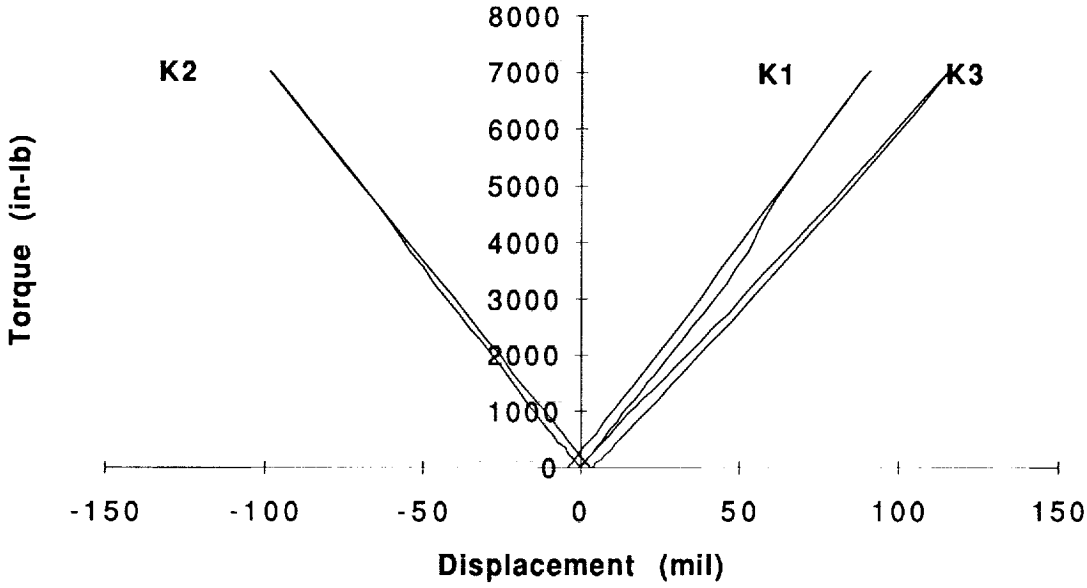

Section 1 Clockwise Torsion Test

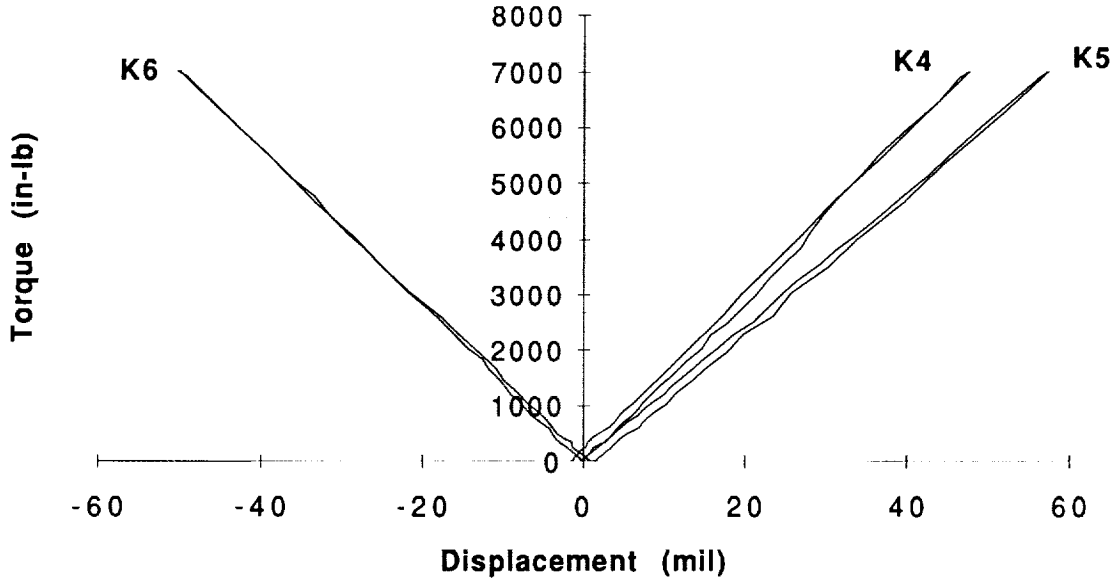

Section 1 Counter Clockwise Torsion Test

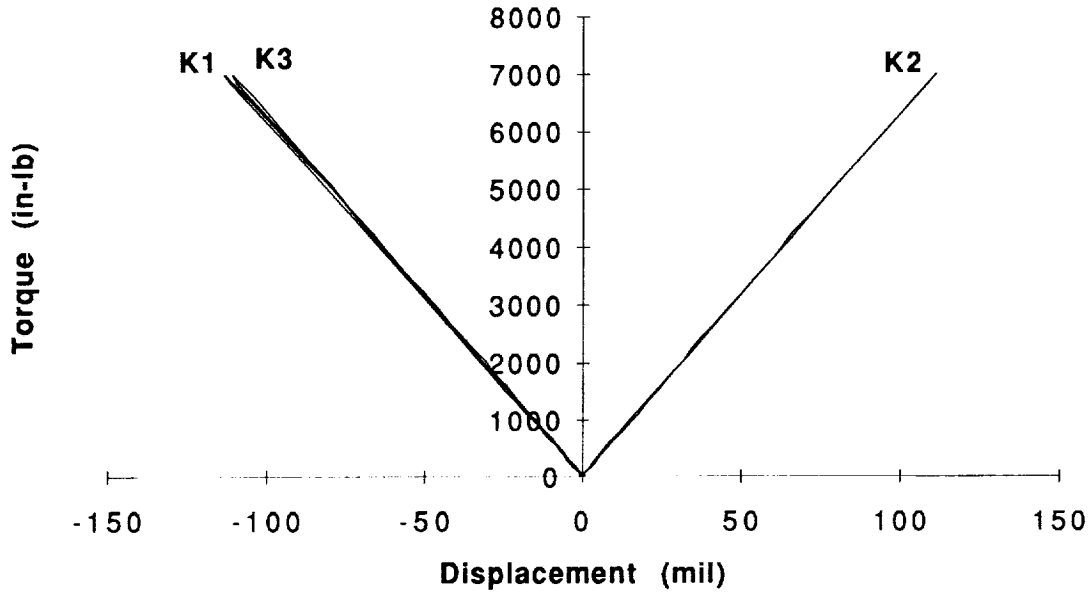

Section 1 Counter Clockwise Torsion Test

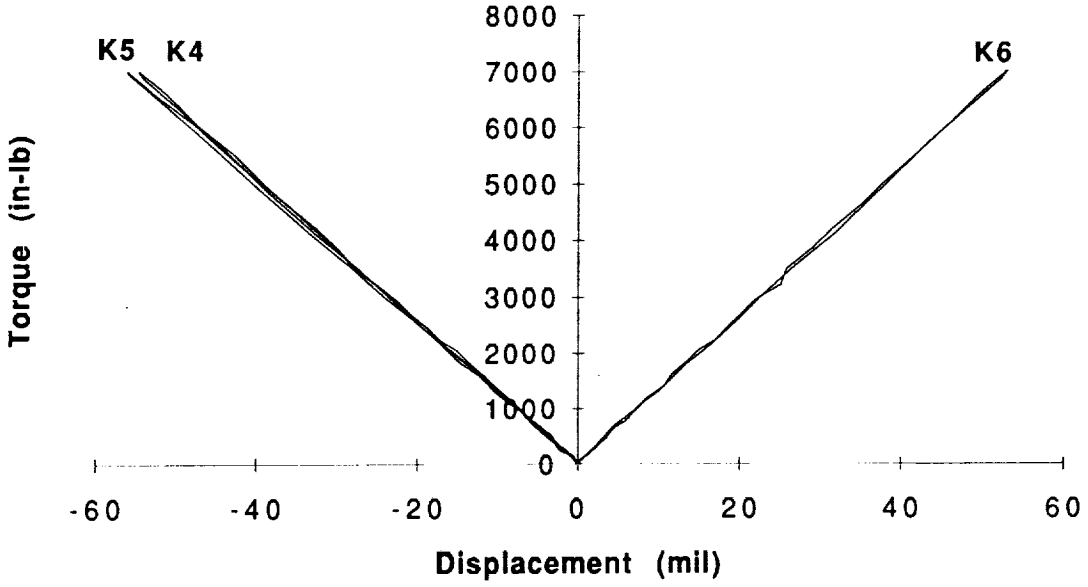

Section 2 Bending Test

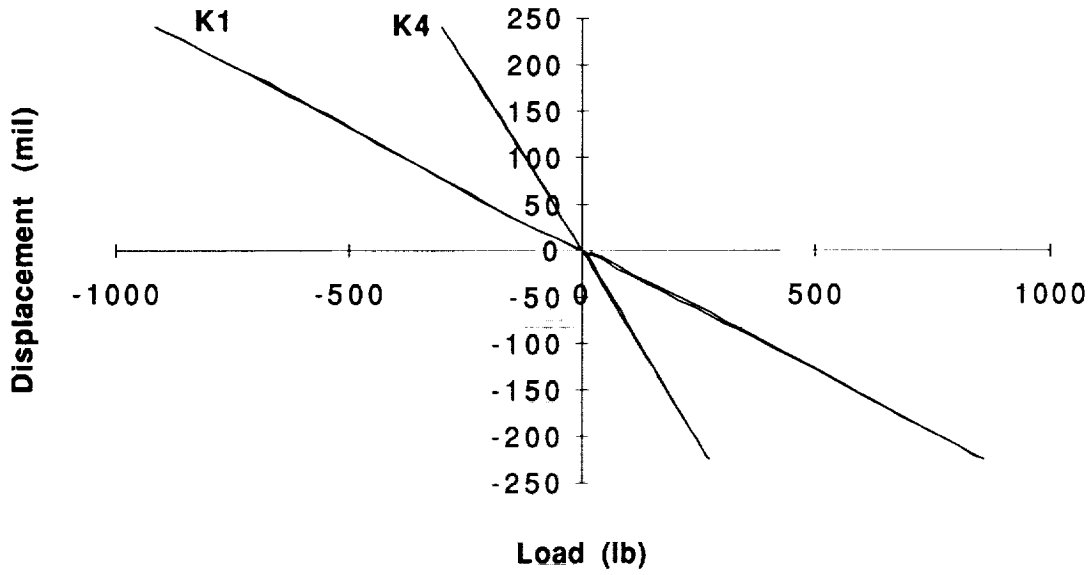

Section 2 Bending Test

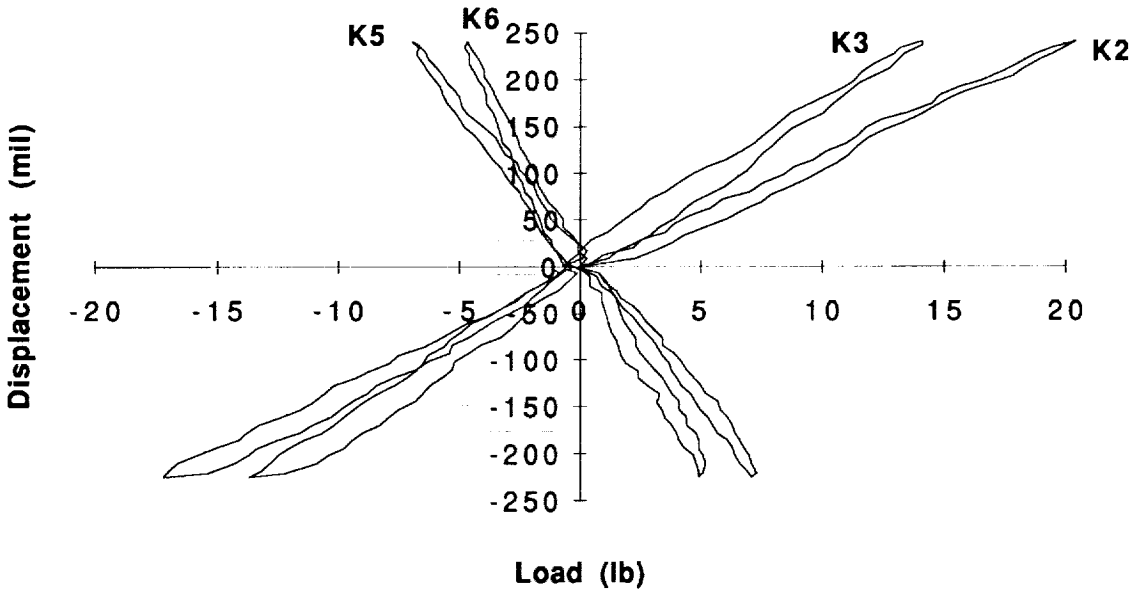

Section 2 Clockwise Torsion Test

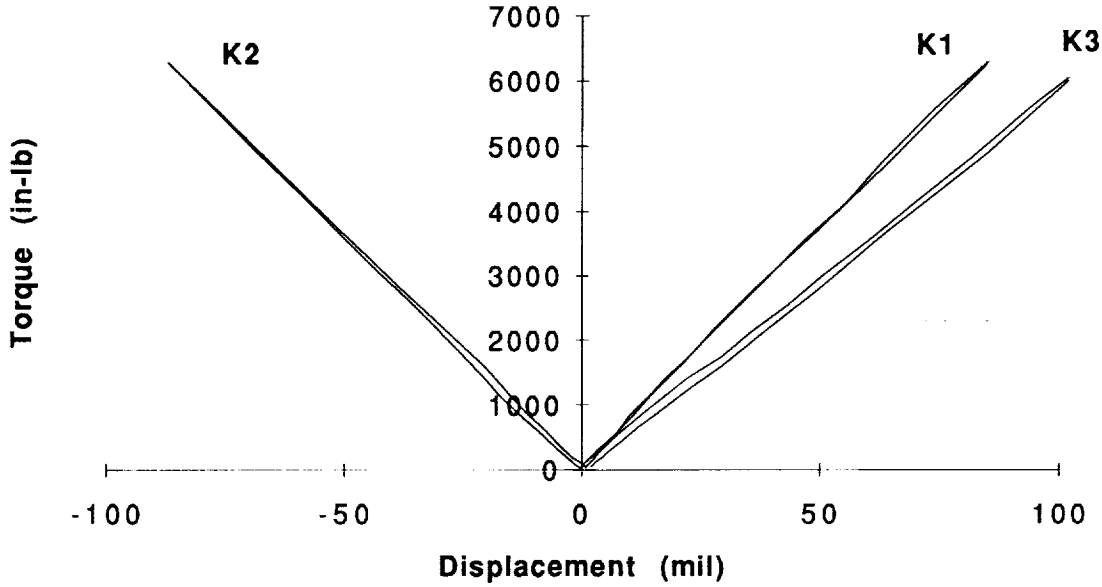

Section 2 Clockwise Torsion Test

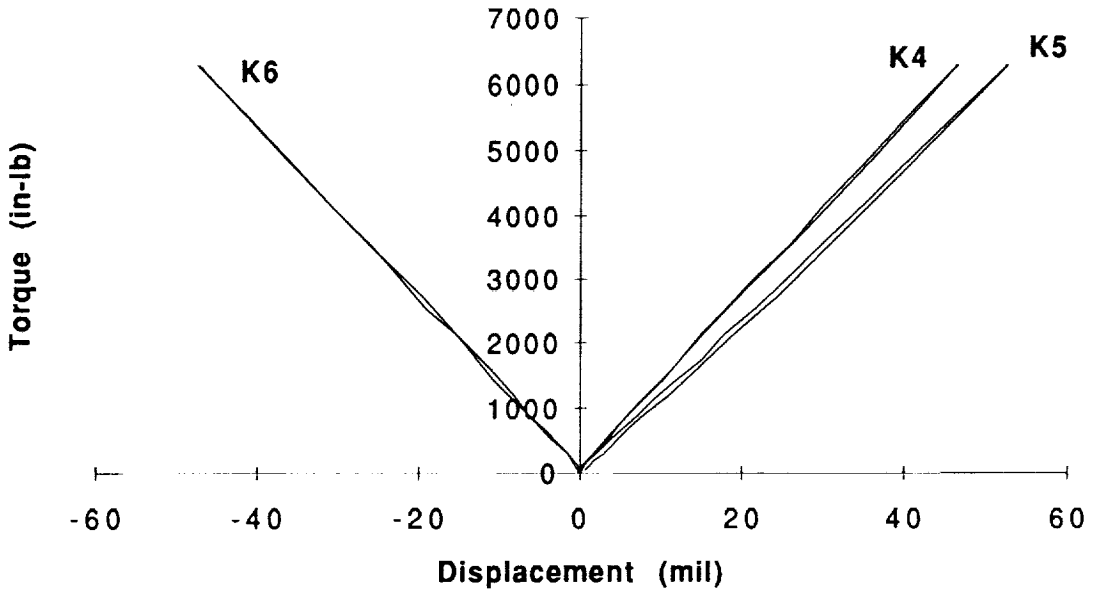

Section 2 Counter Clockwise Torsion Test

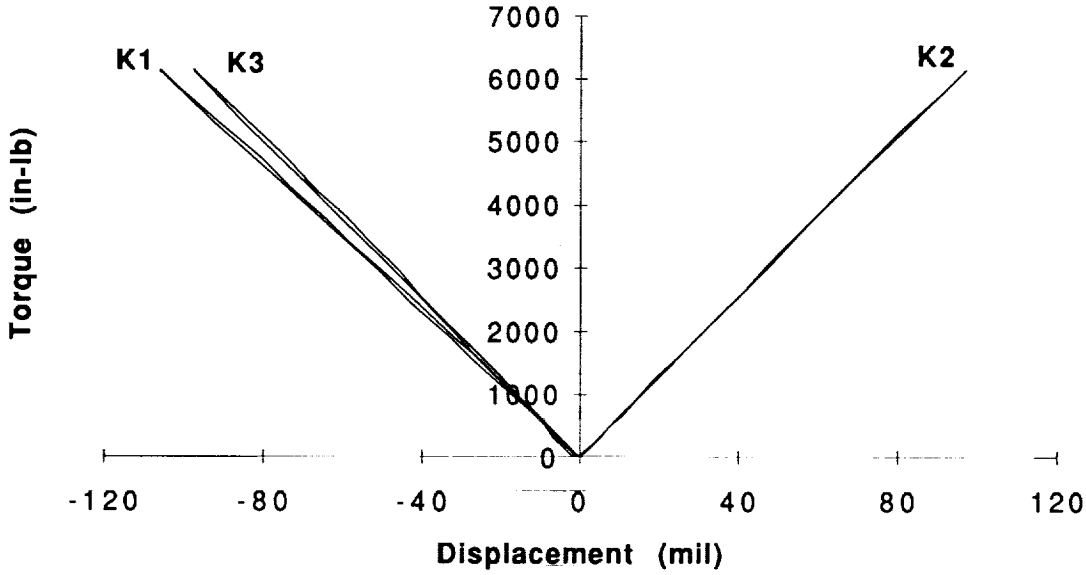

Section 2 Counter Clockwise Torsion Test

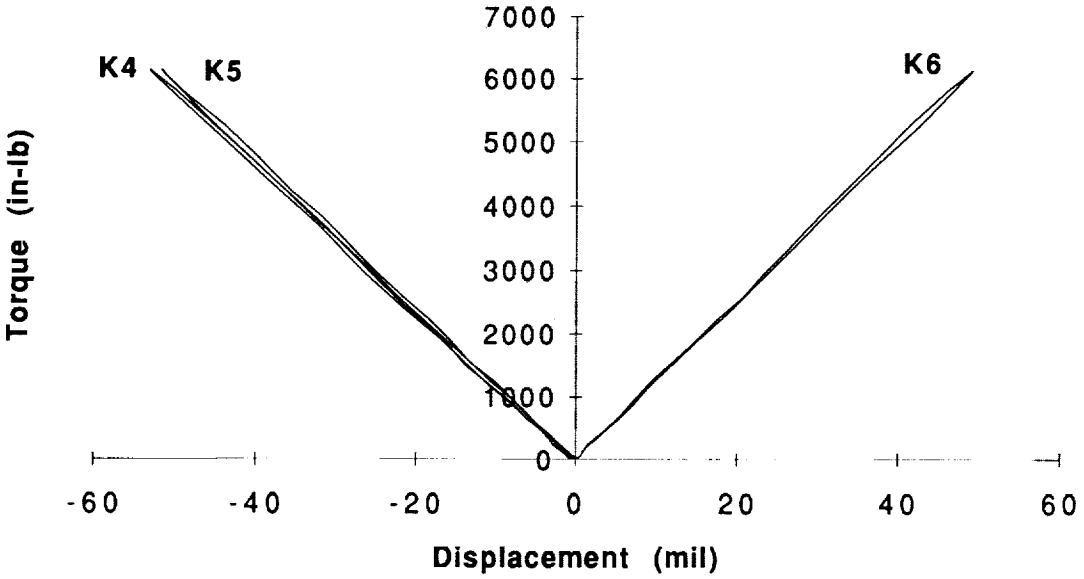

Section 3 Bending Test

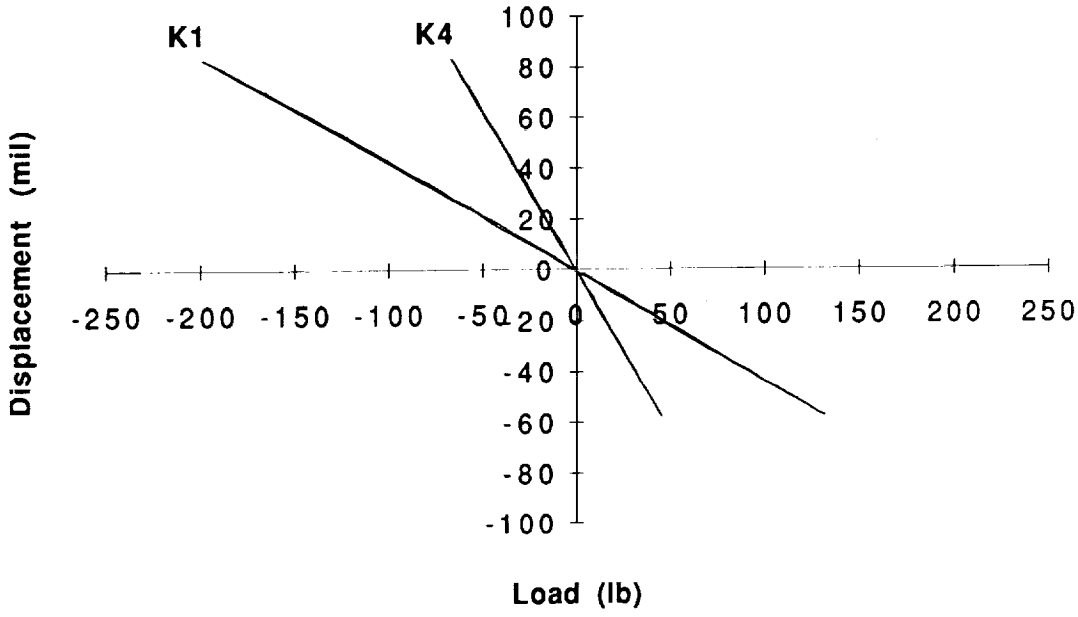

Section 3 Bending Test

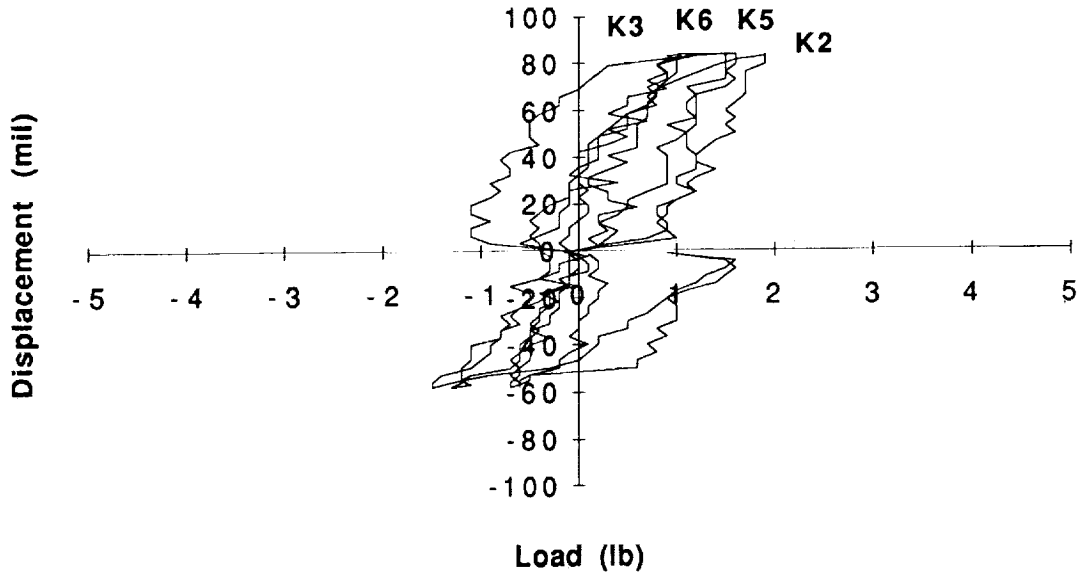

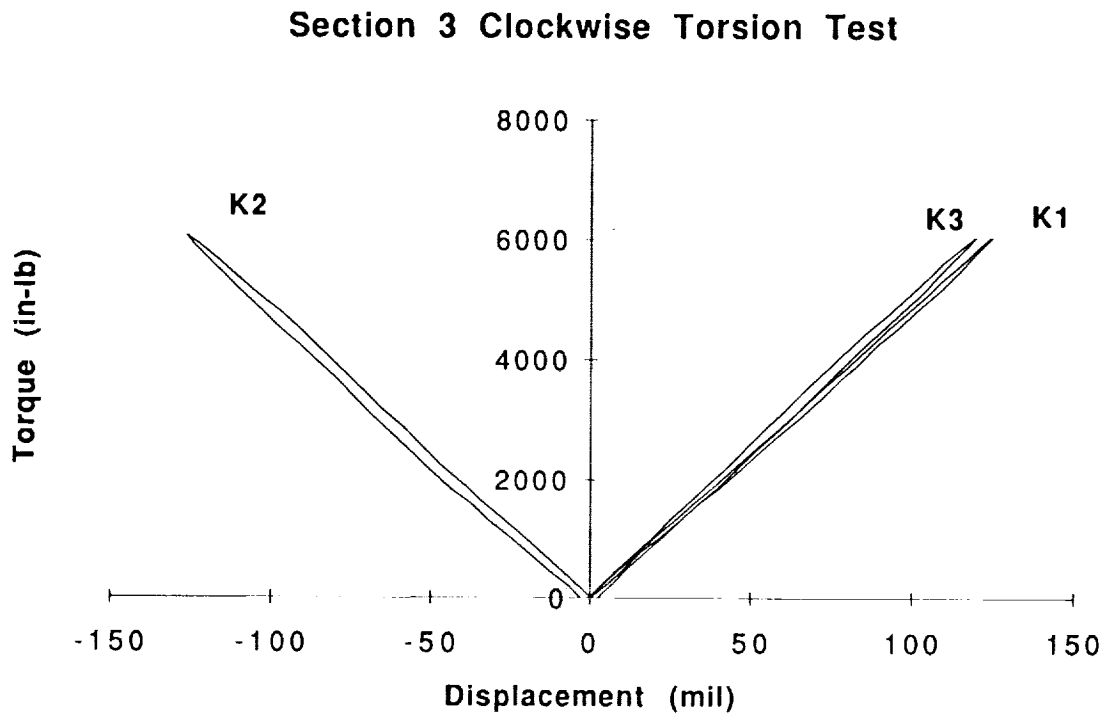

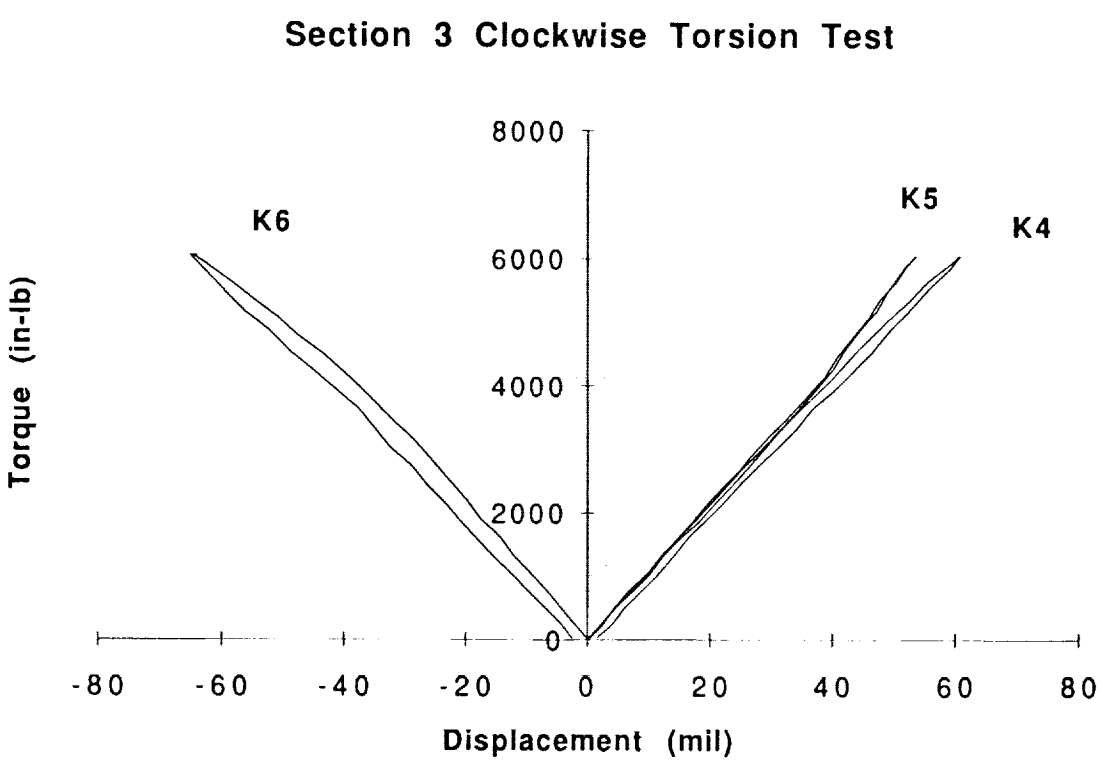

Figure 5-19 Section-3 CW Torsion Test Results

Section 3 Counter Clockwise Torsion Test

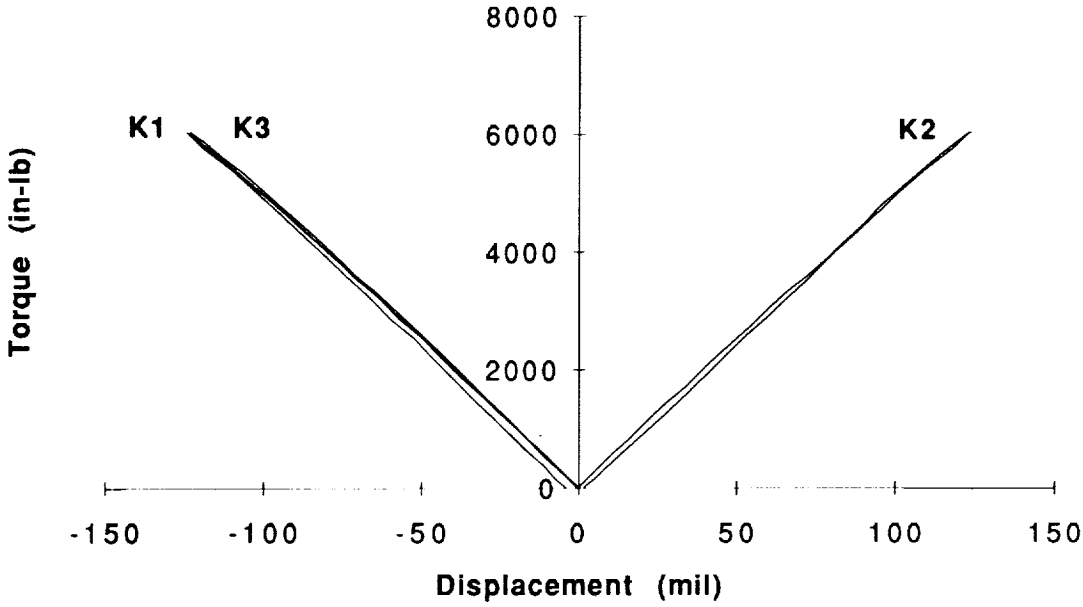

Section 3 Counter Clockwise Torsion Test

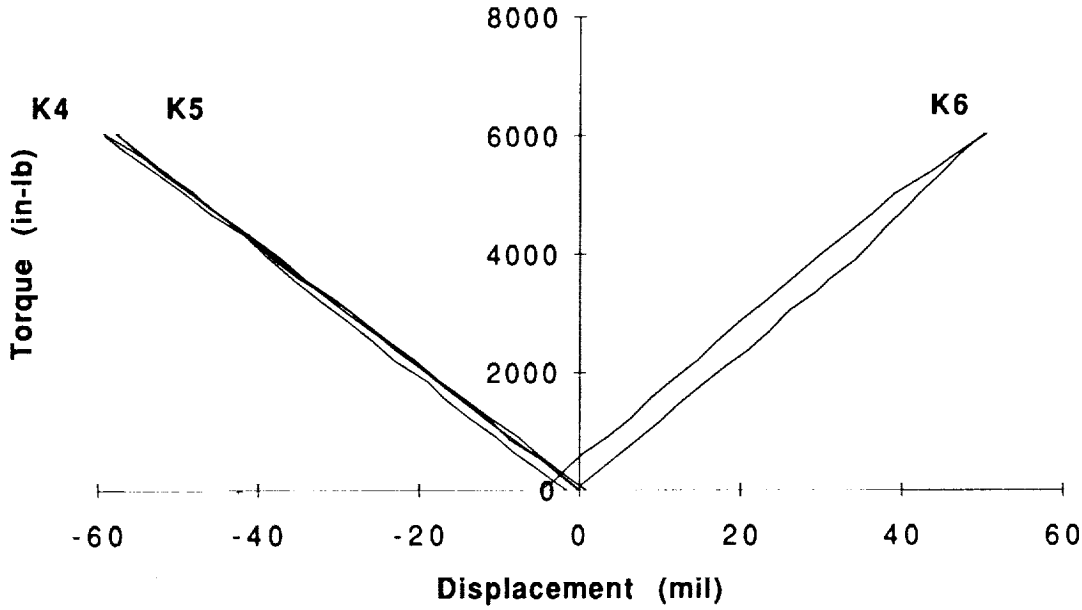

APPENDIX H

MATCHING TEST AND ANALYSIS MODE SHAPE PLOTS FOR ASSEMBLY DYNAMIC TESTS

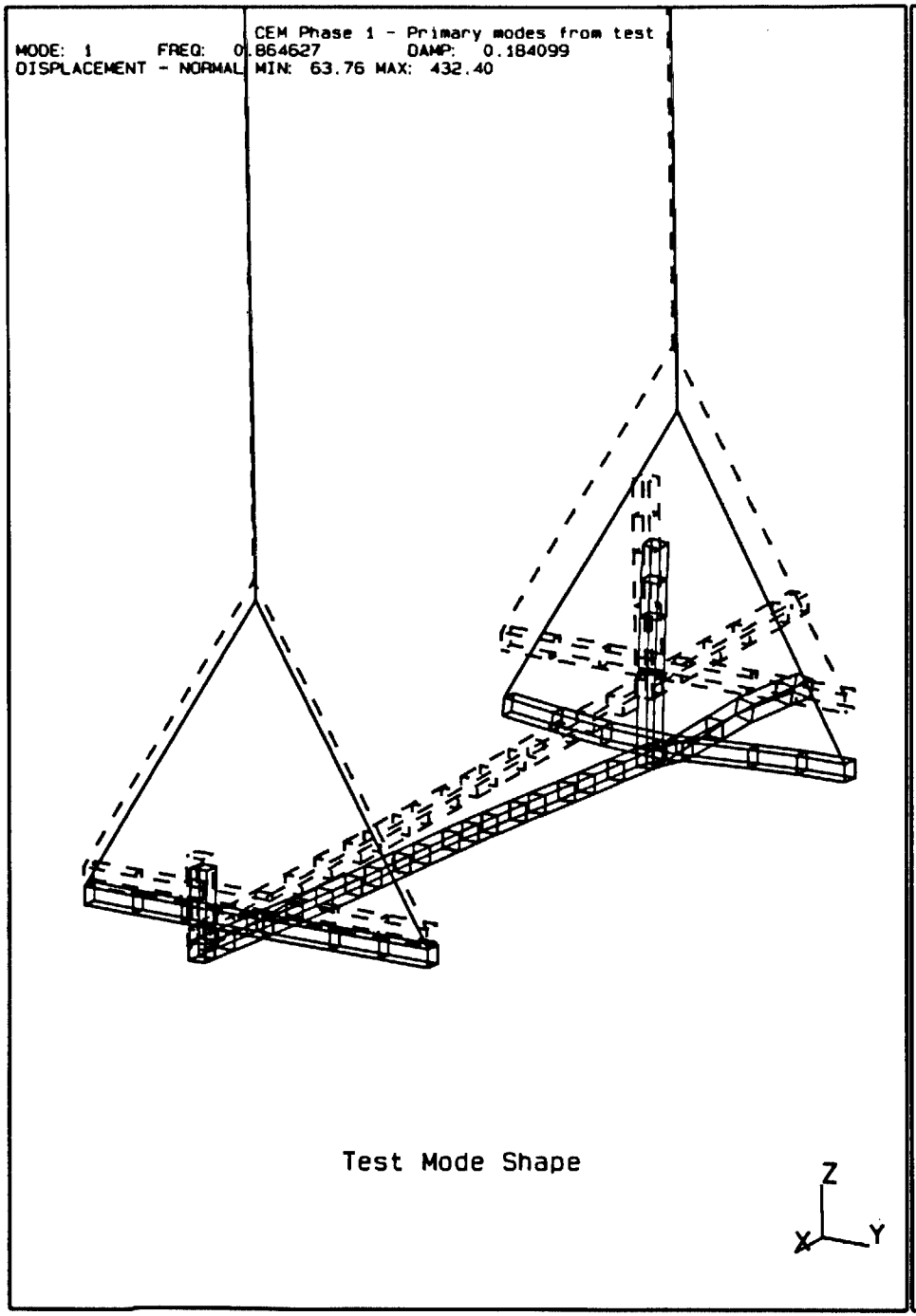

Test Mode Shape

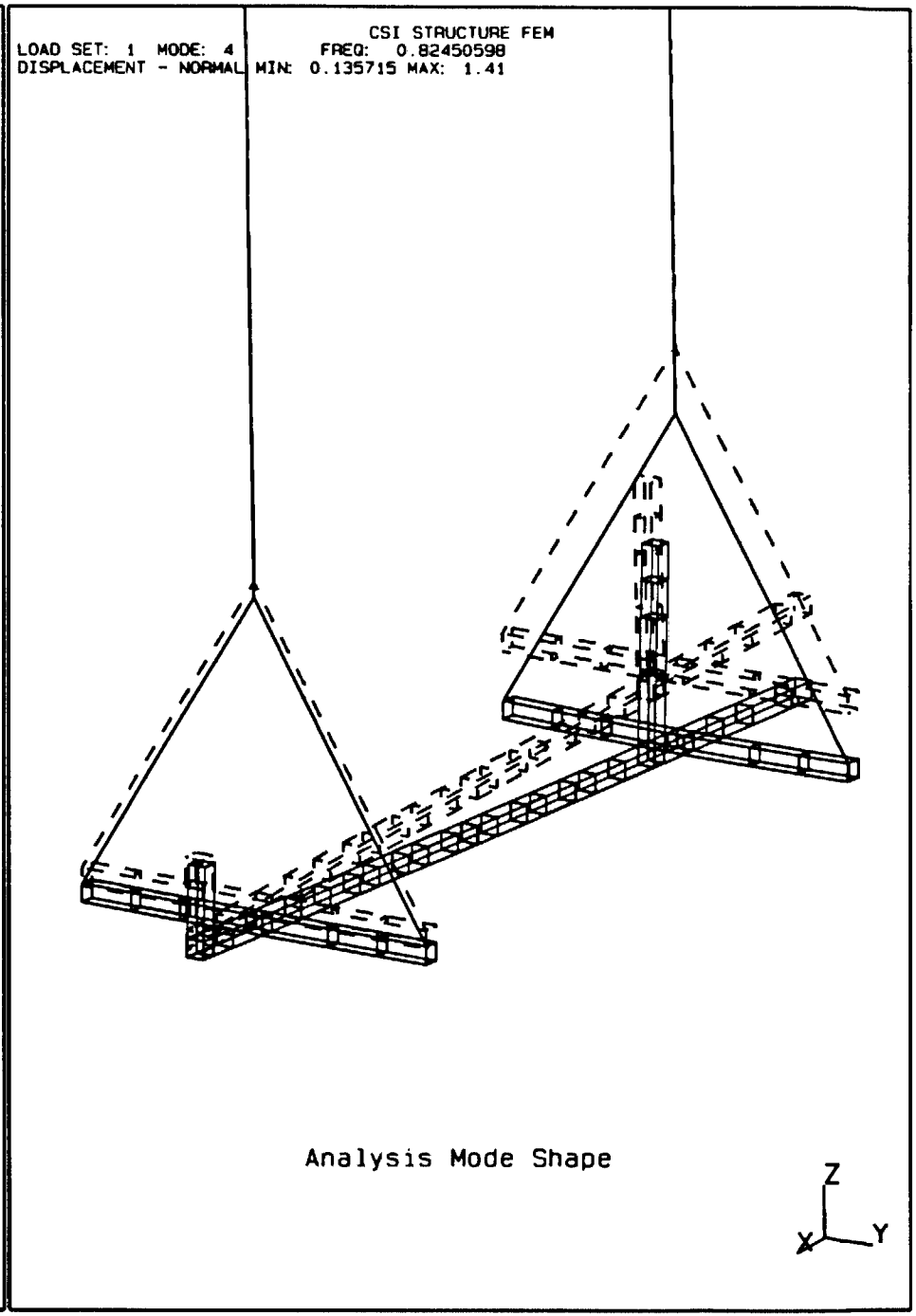

Analysis Mode Shape

SDRC I-DEAS VI: Test

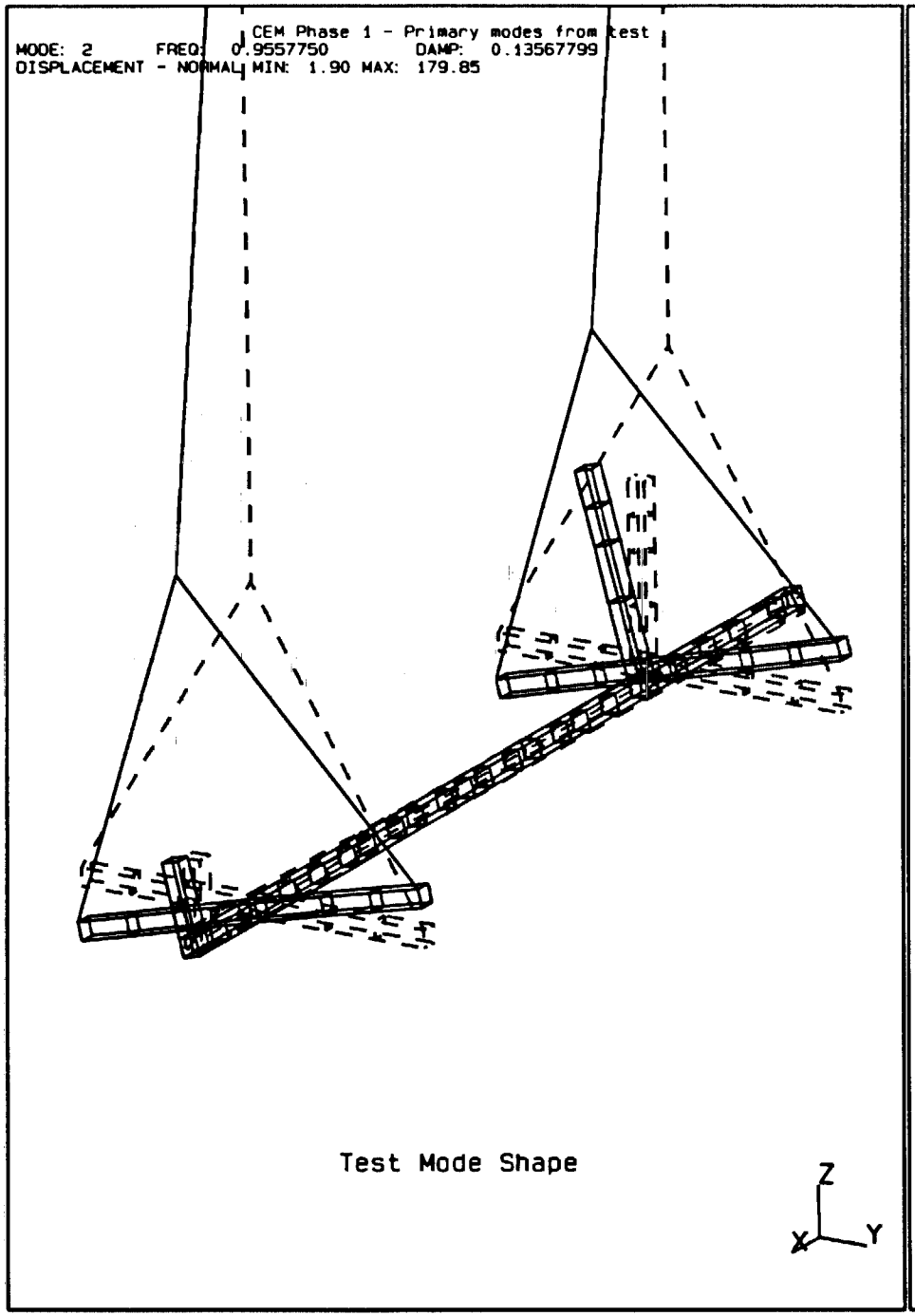

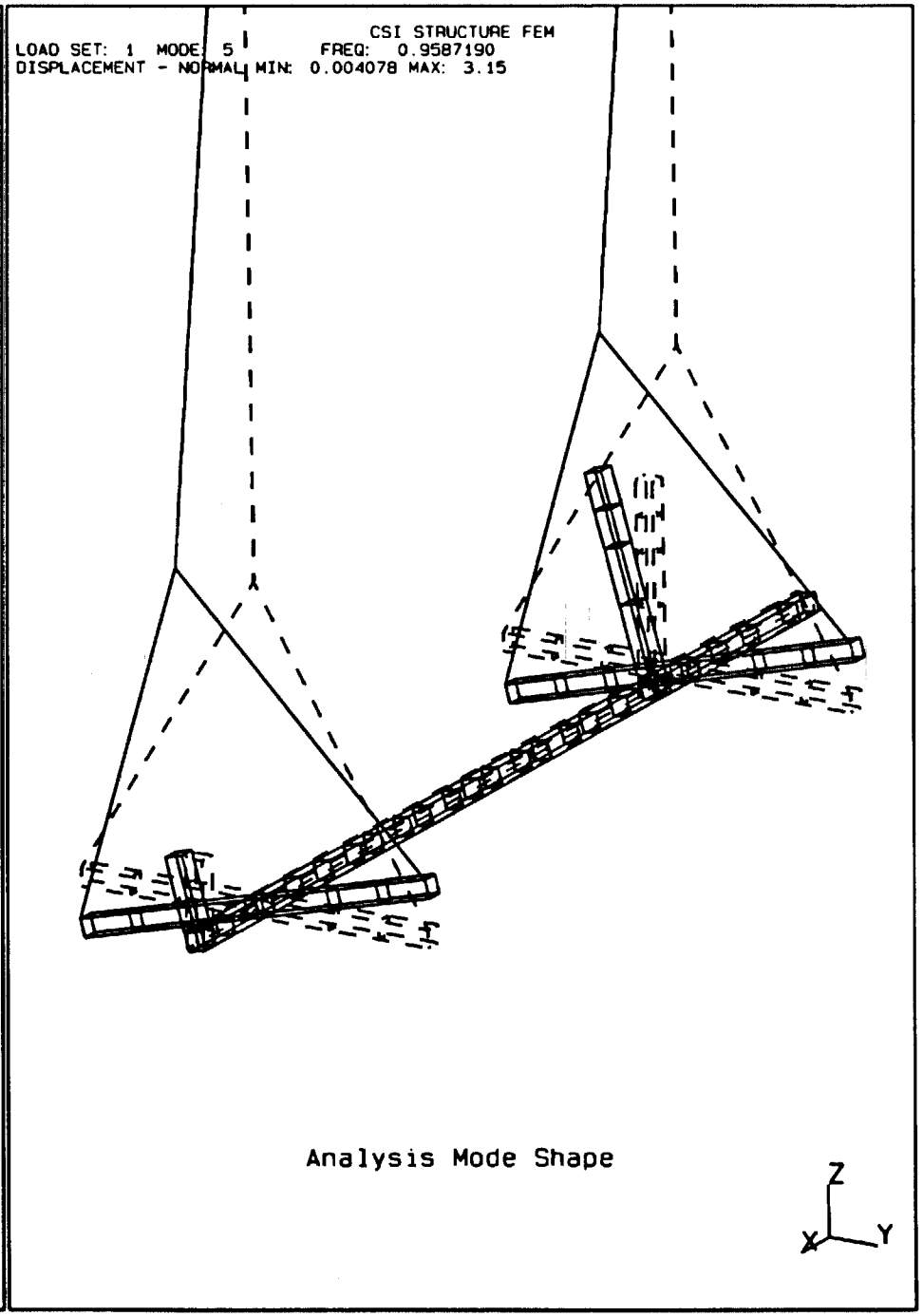

SDRC I-DEAS VI: Test

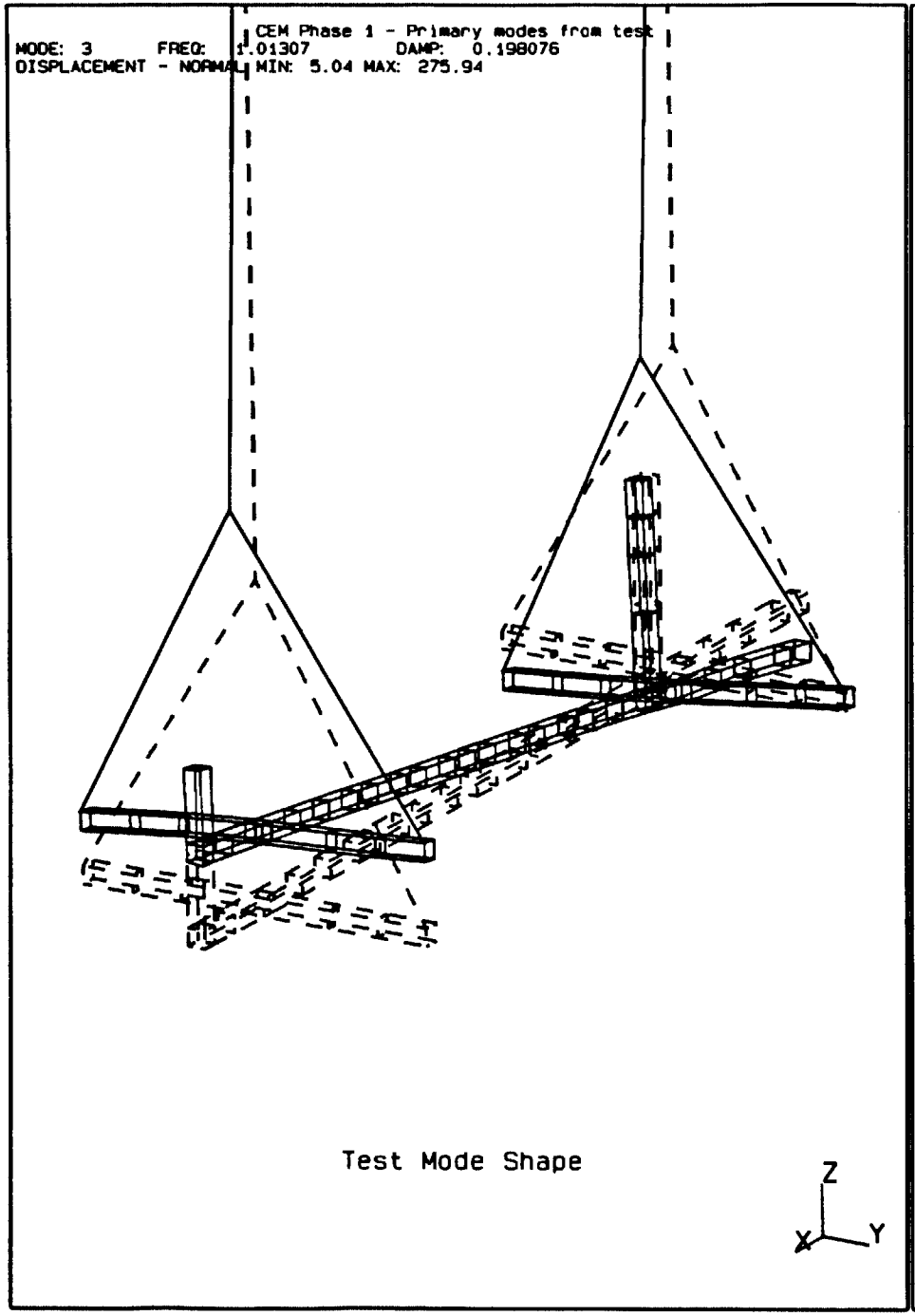

Test Mode Shape

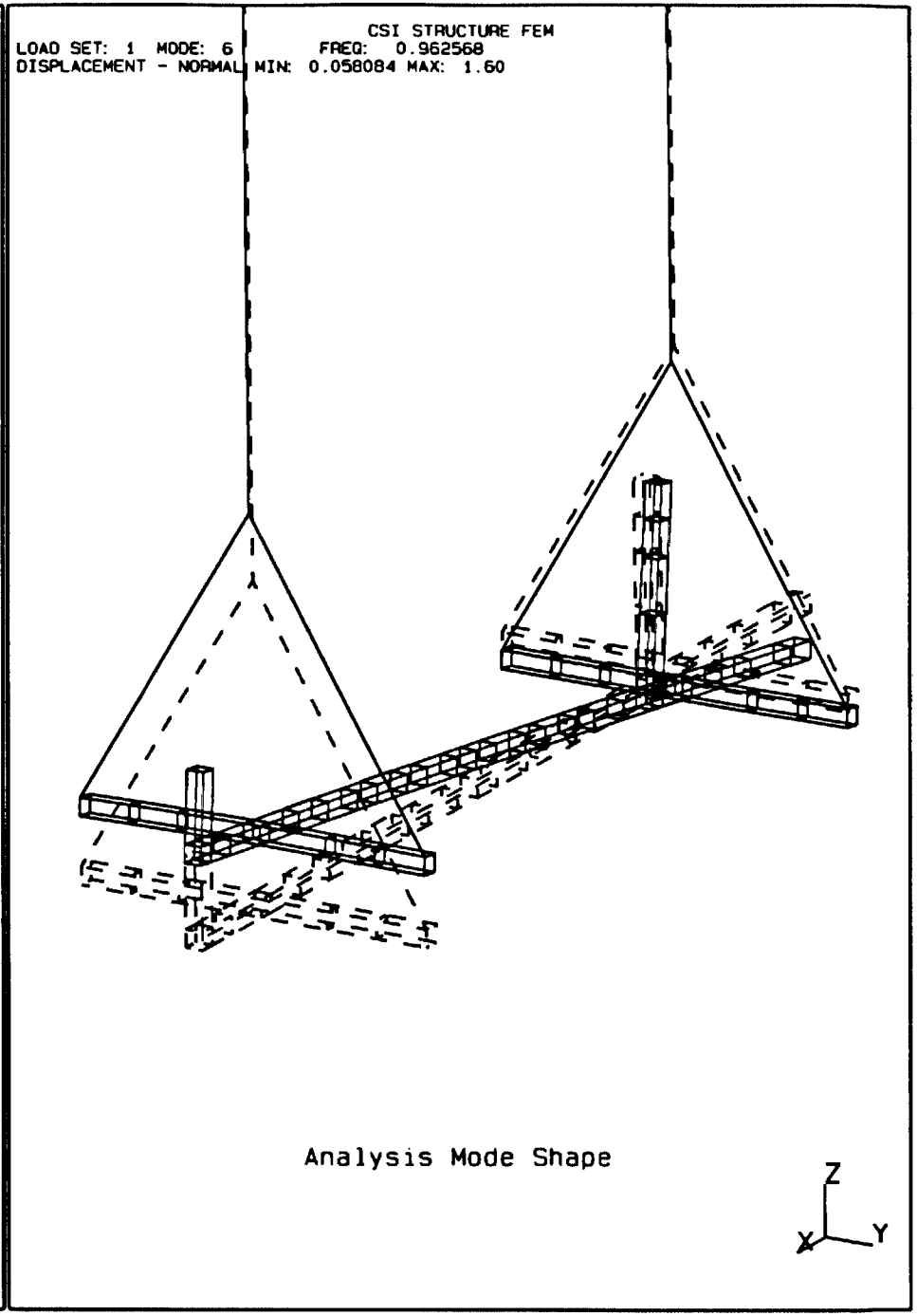

Analysis Mode Shape

SDRC I-DEAS VI: Test

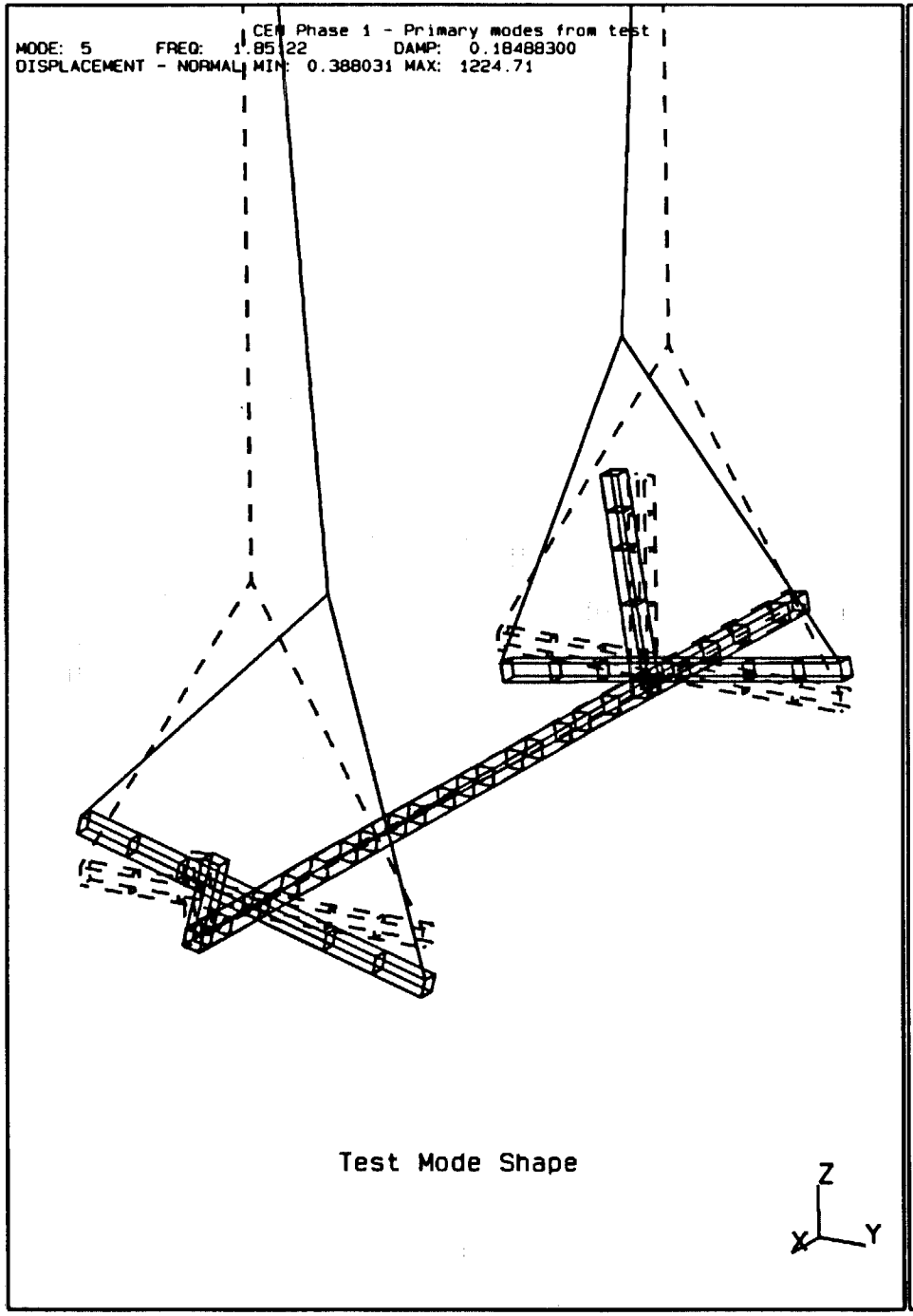

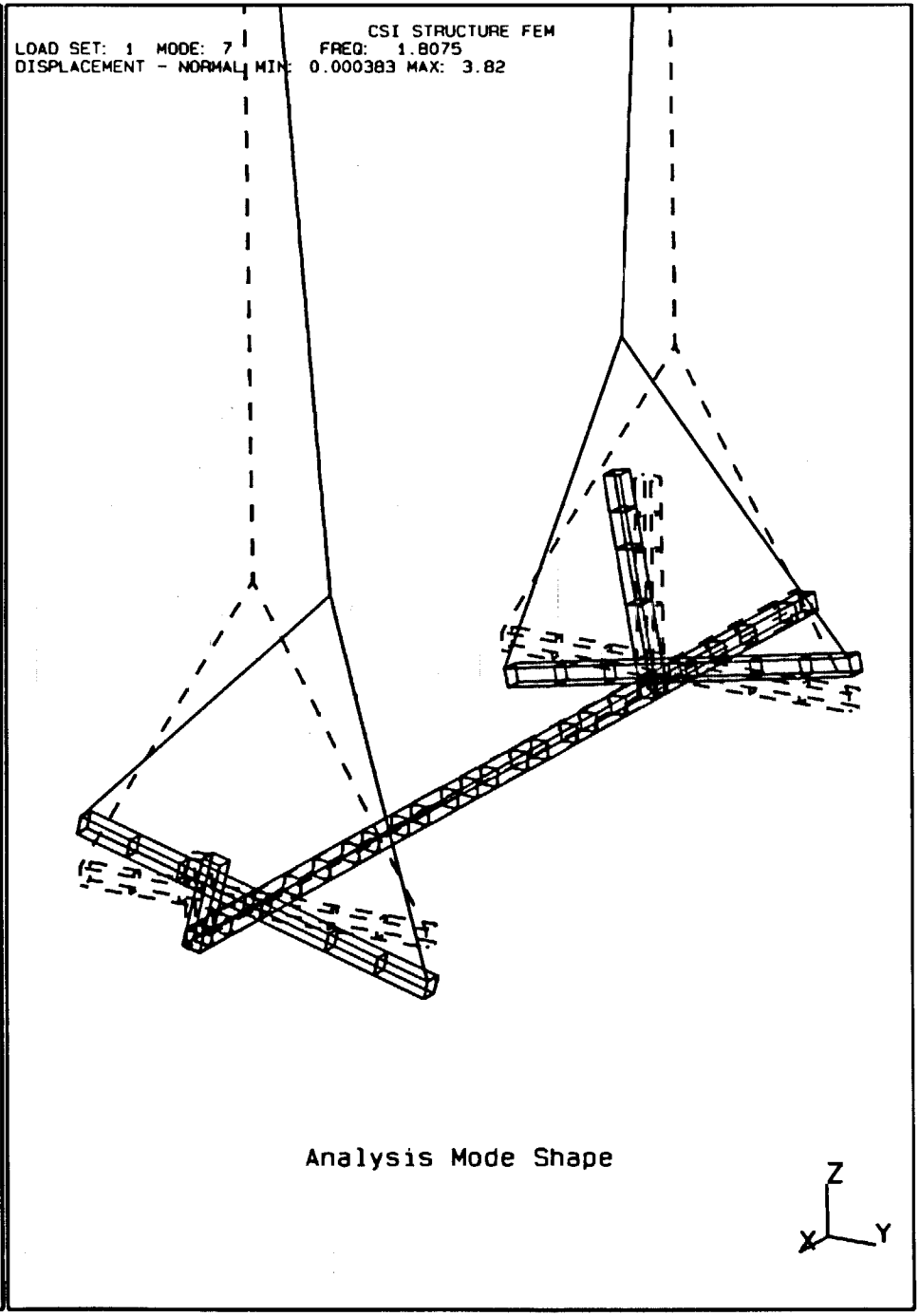

SDRC I-DEAS VI: Test

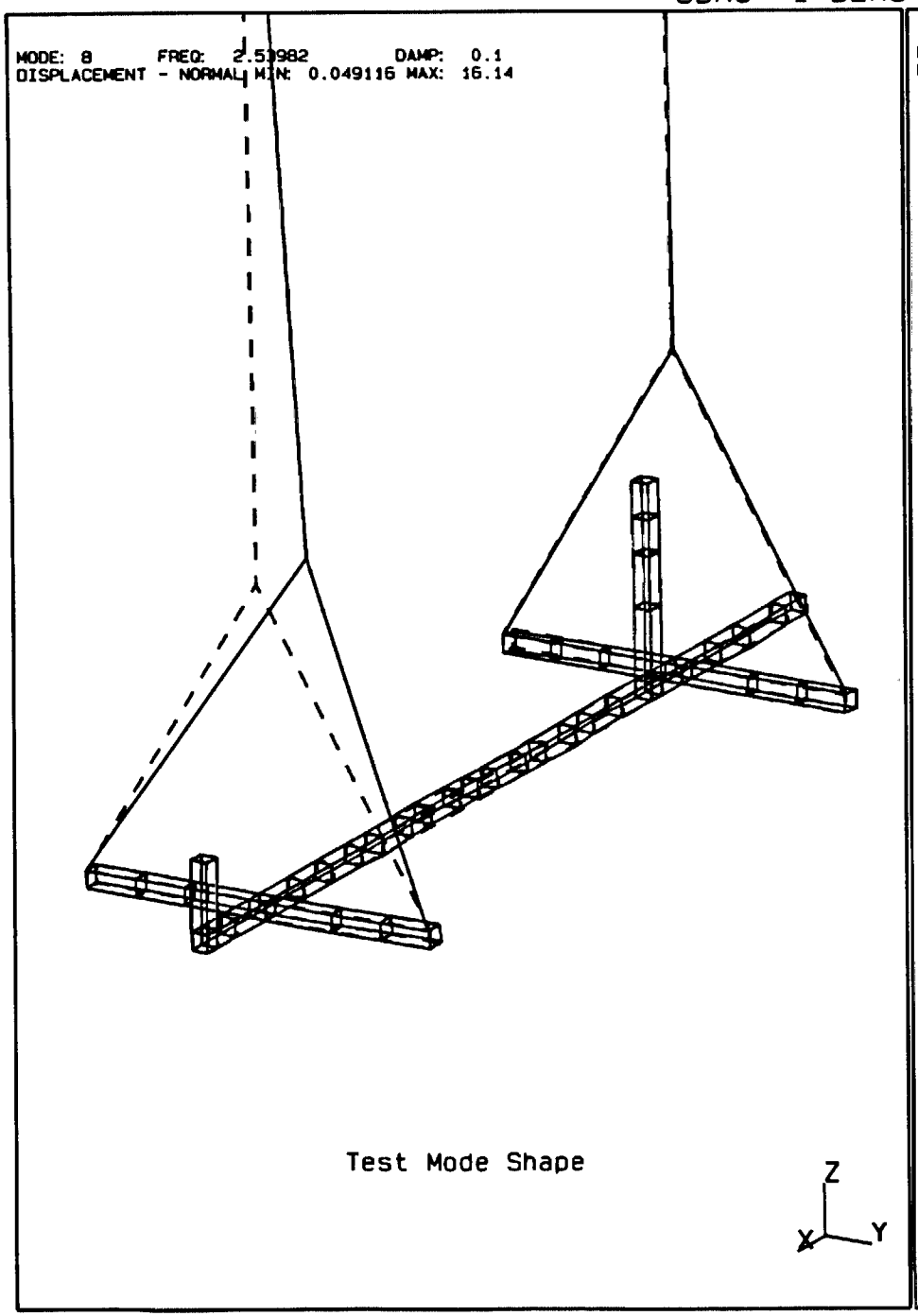

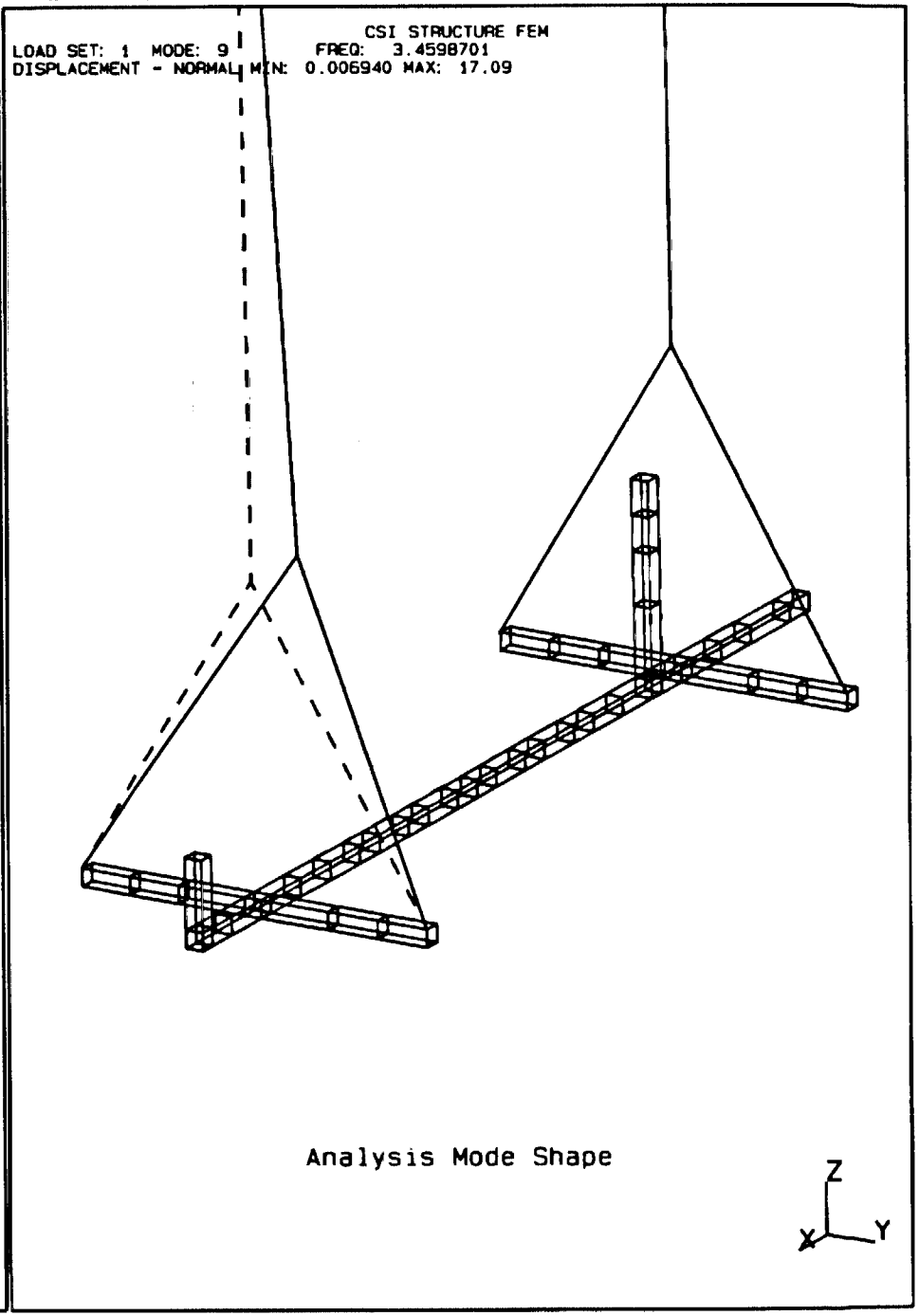

SDRC I-DEAS VI: Test

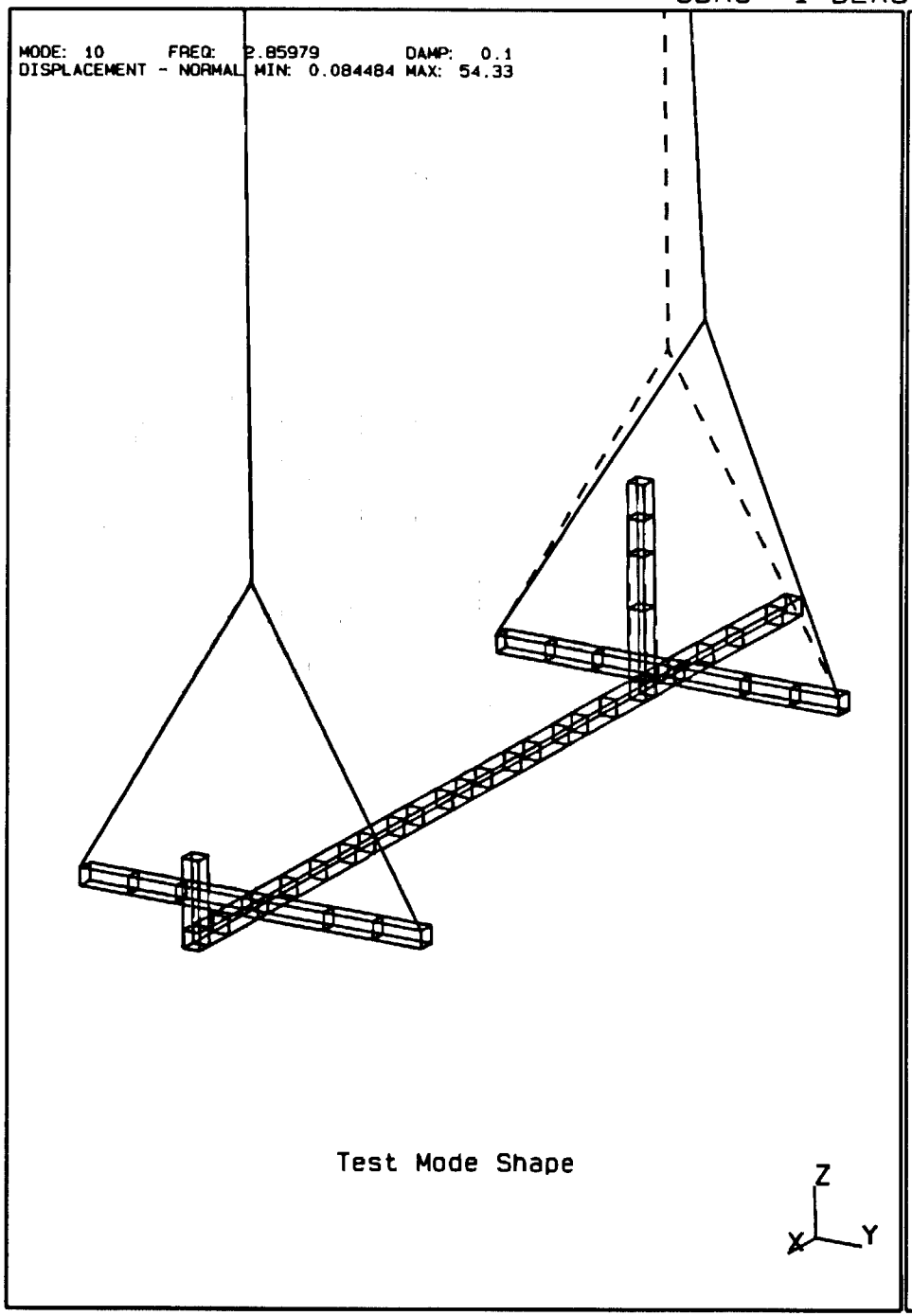

Test Mode Shape

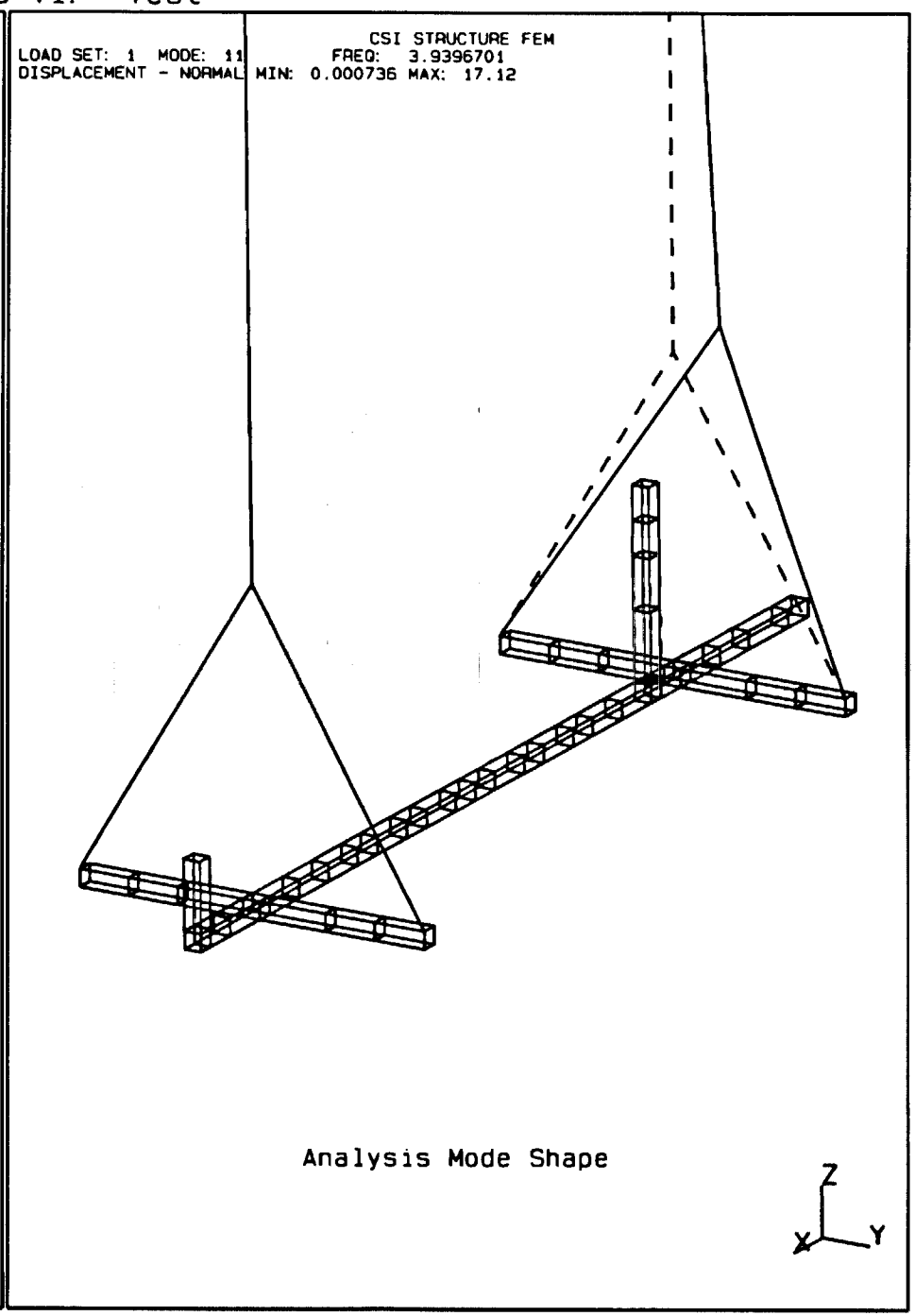

Analysis Mode Shape

SDRC I-DEAS VI: Test

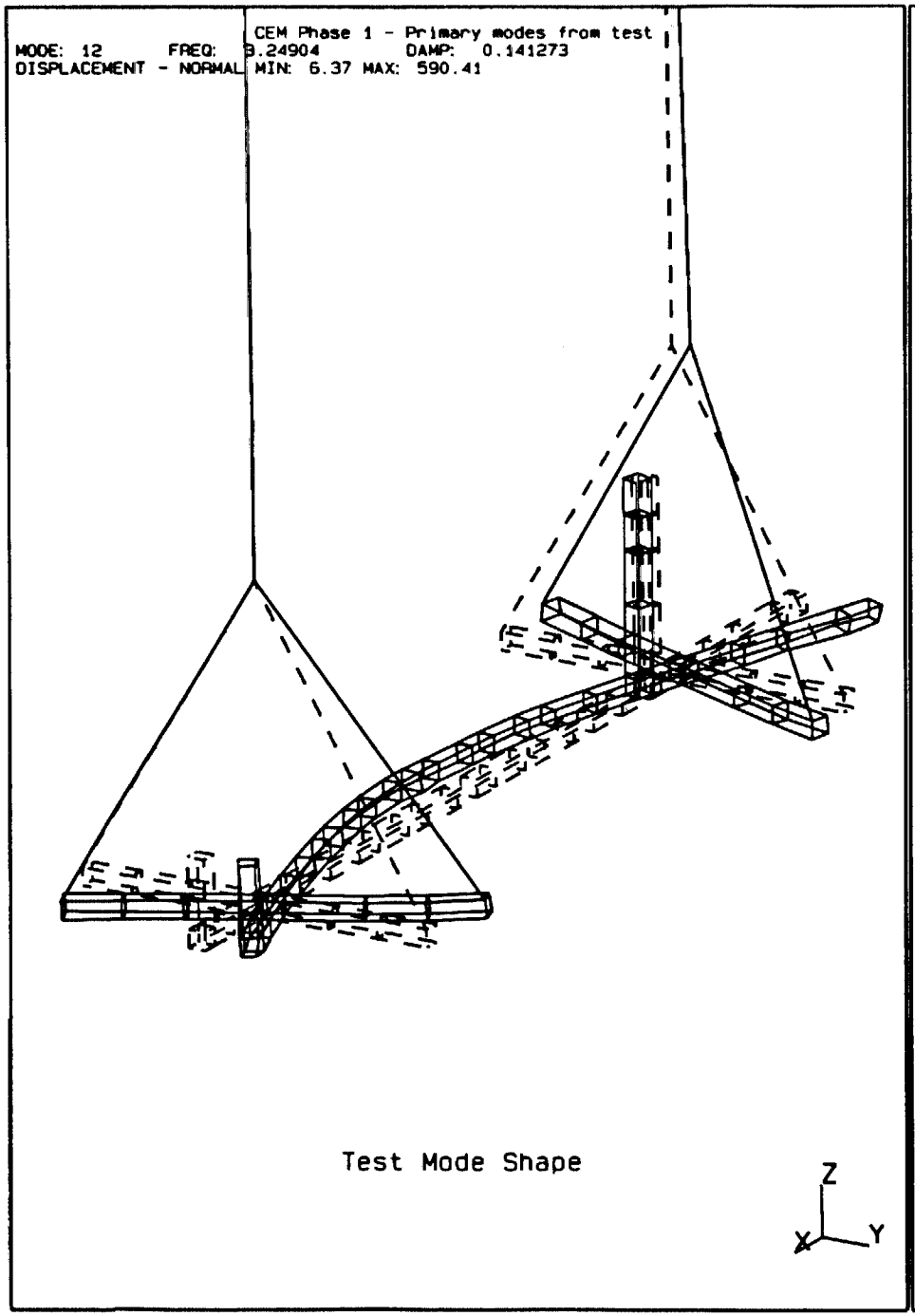

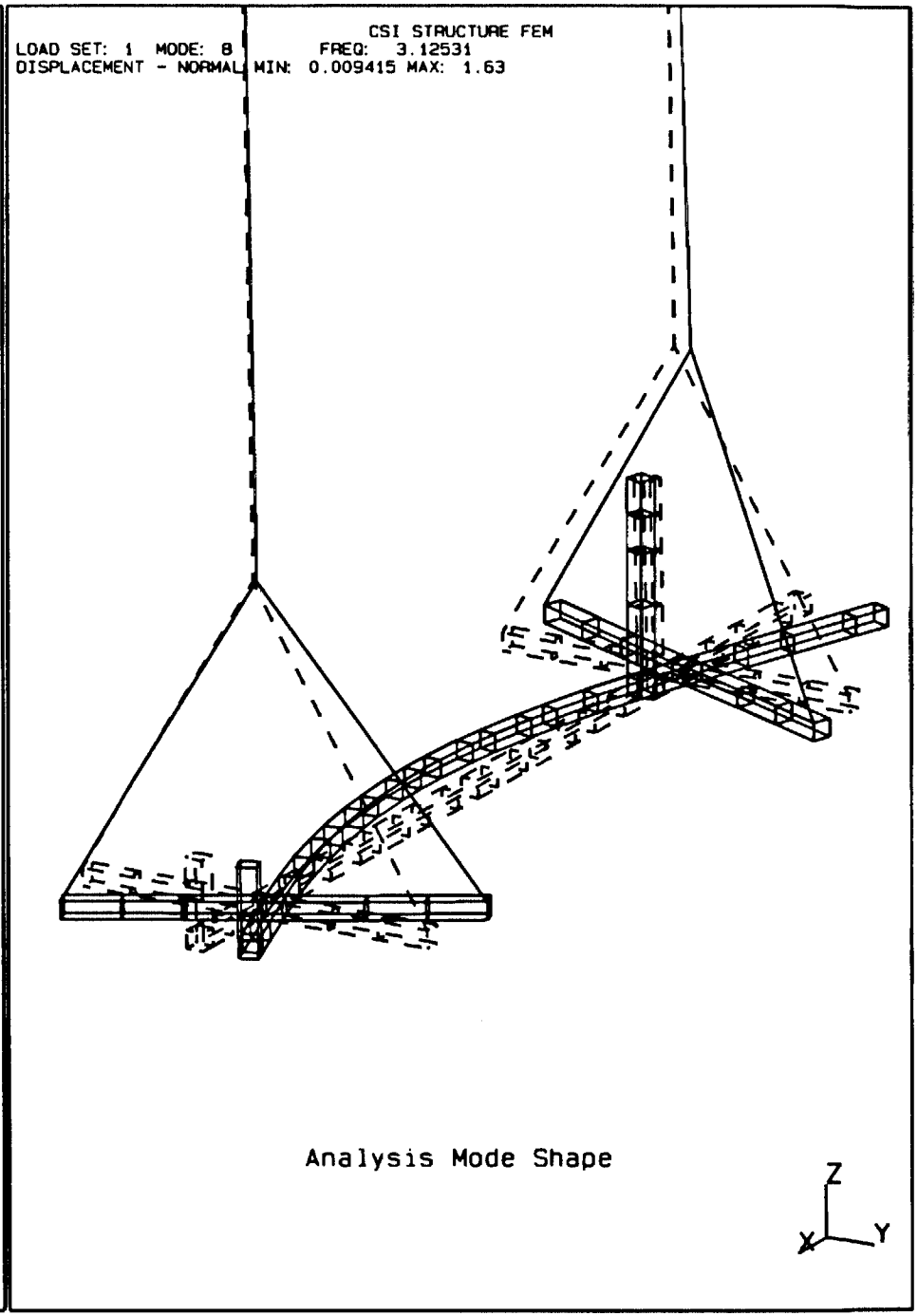

SDRC I-DEAS VI: Test

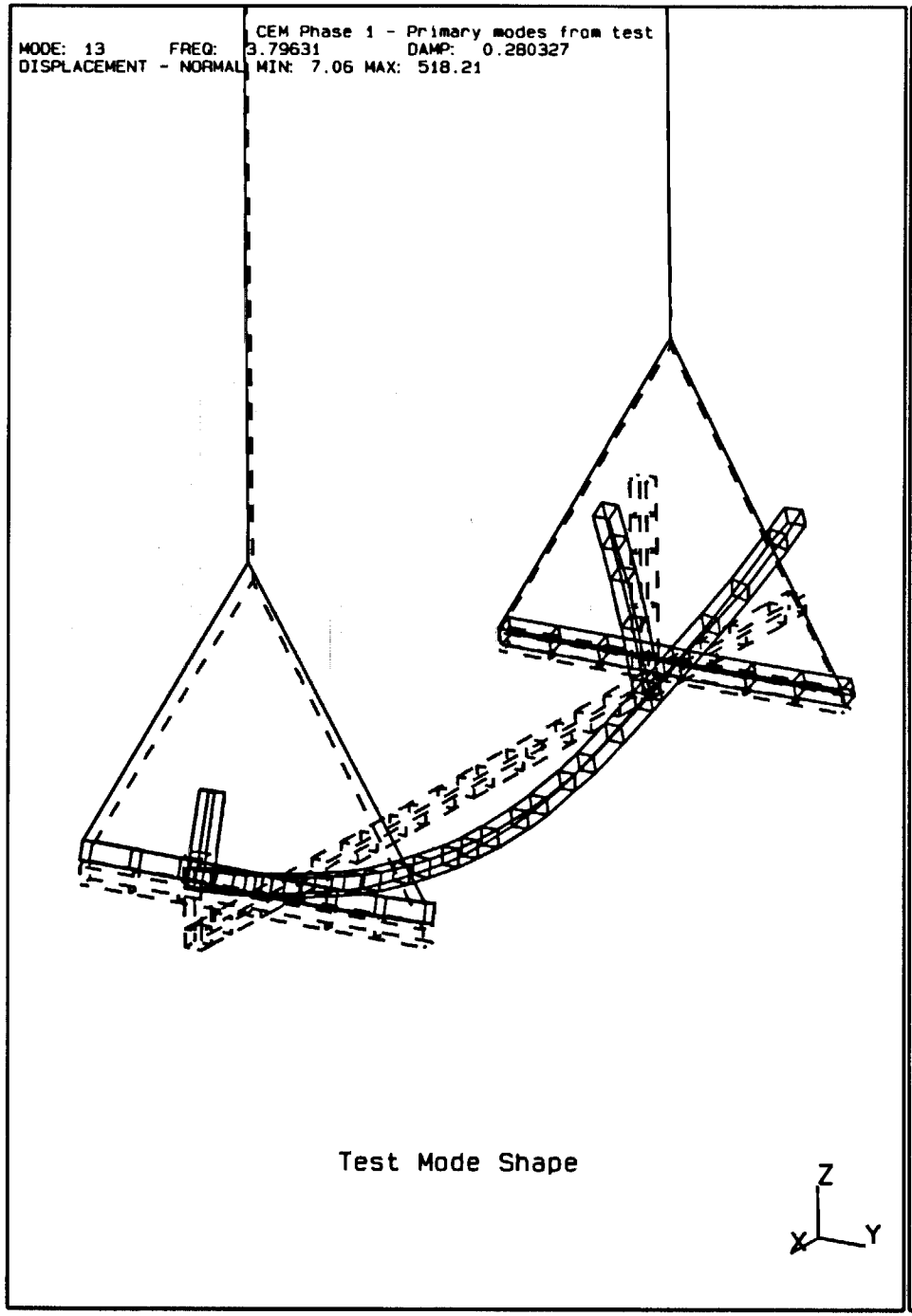

Test Mode Shape

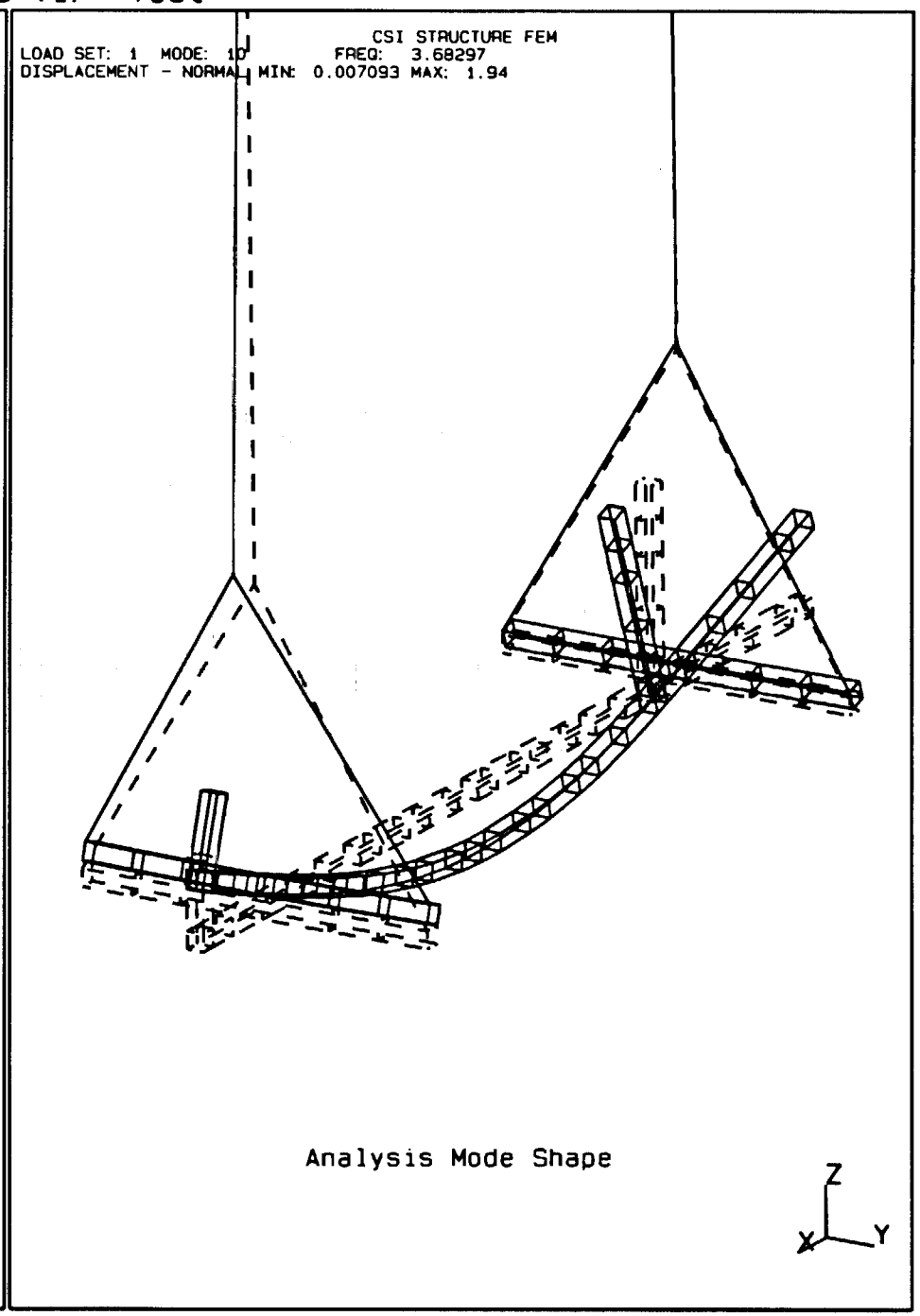

Analysis Mode Shape

SDRC I-DEAS VI: Test

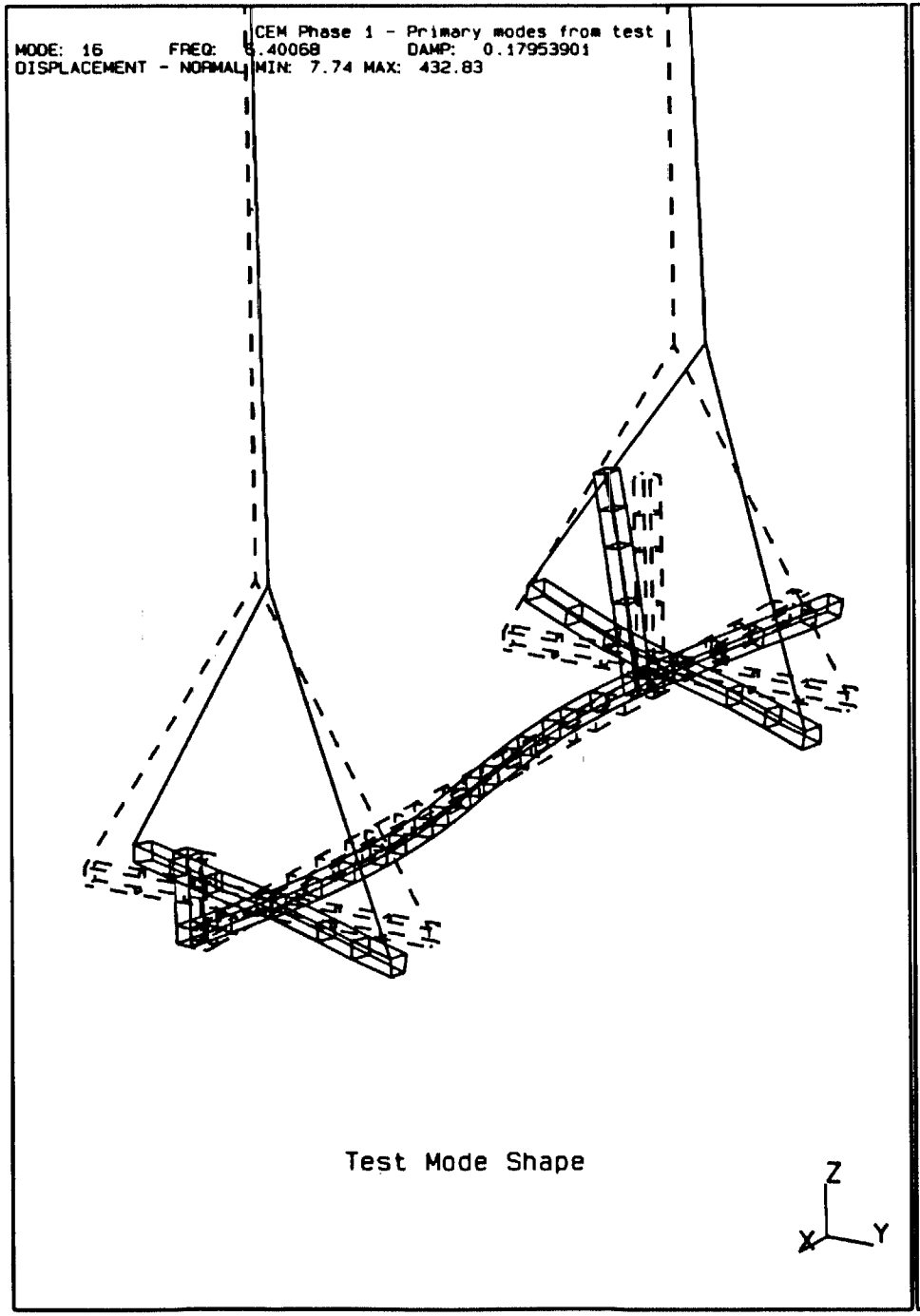

Test Mode Shape

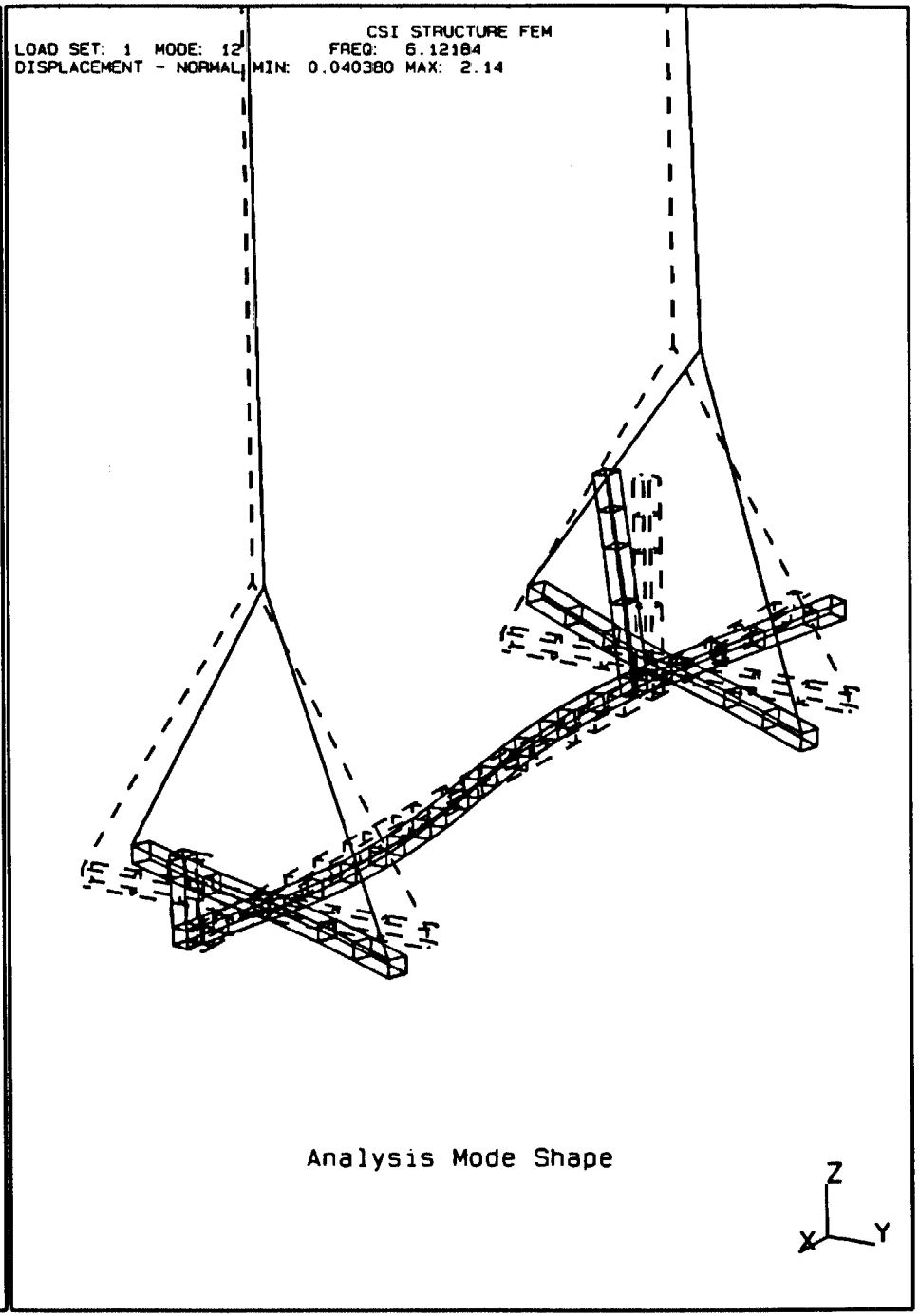

Analysis Mode Shape

SDRC I-DEAS VI: Test

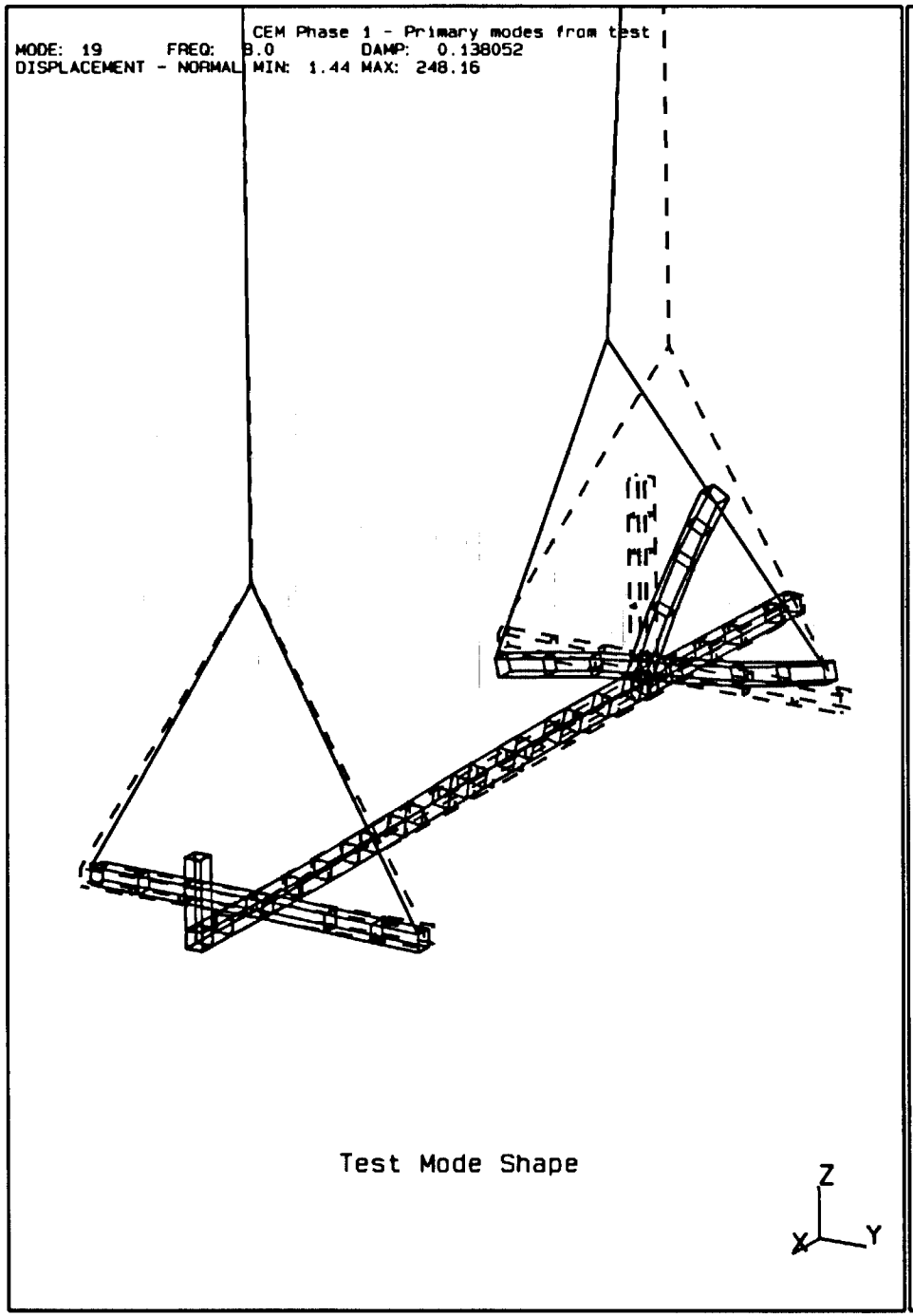

Test Mode Shape

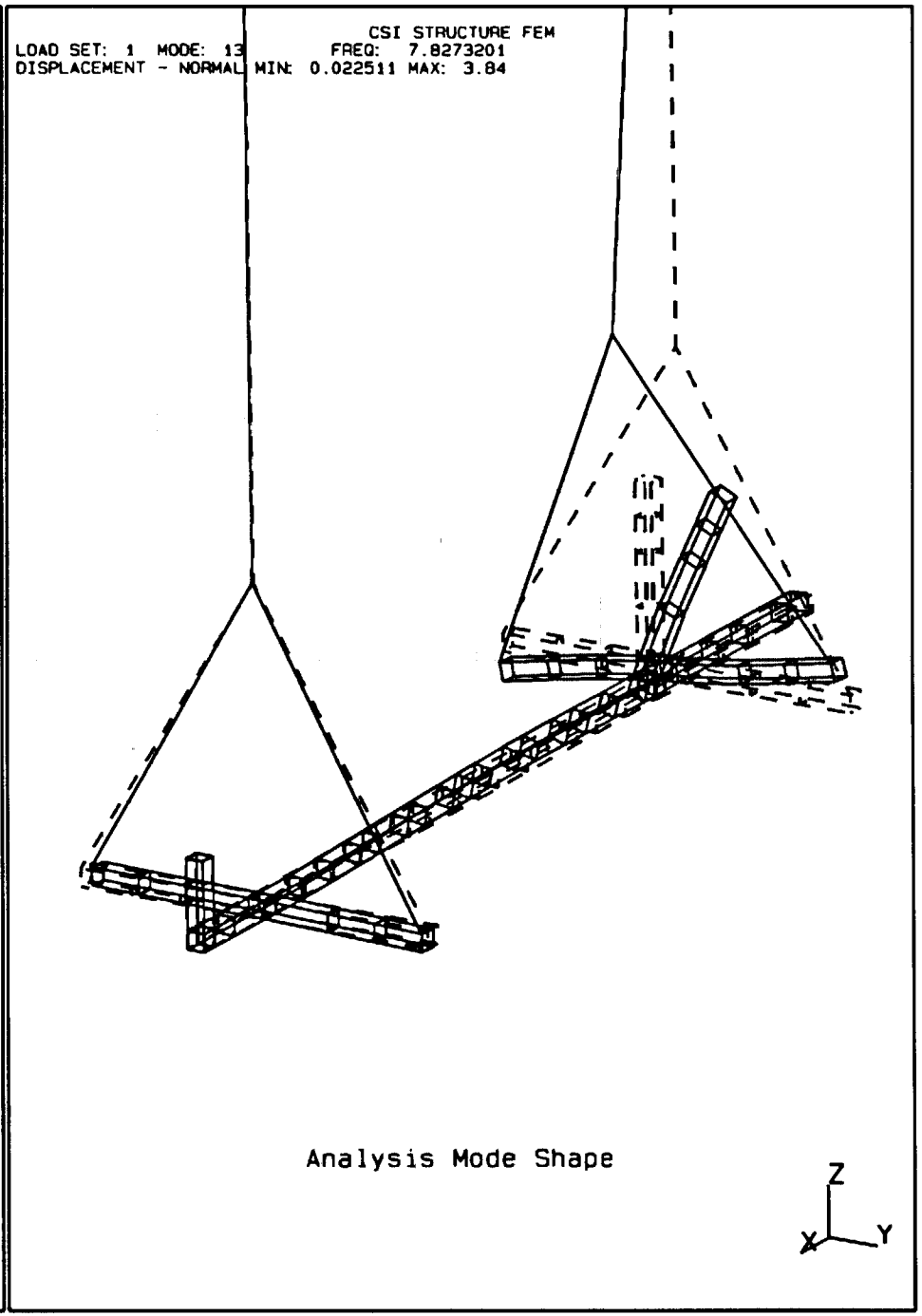

Analysis Mode Shape

SDRC I-DEAS VI: Test

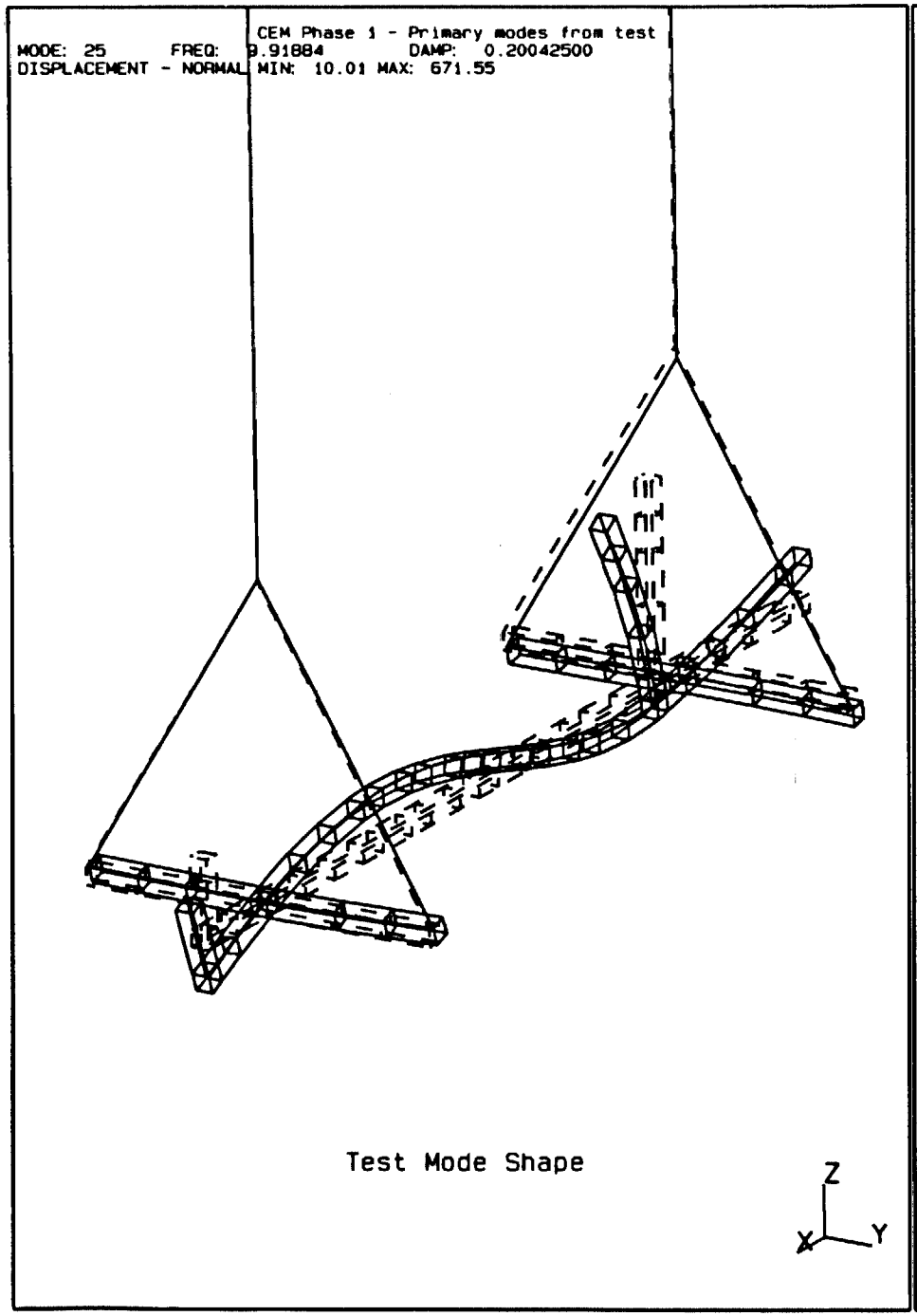

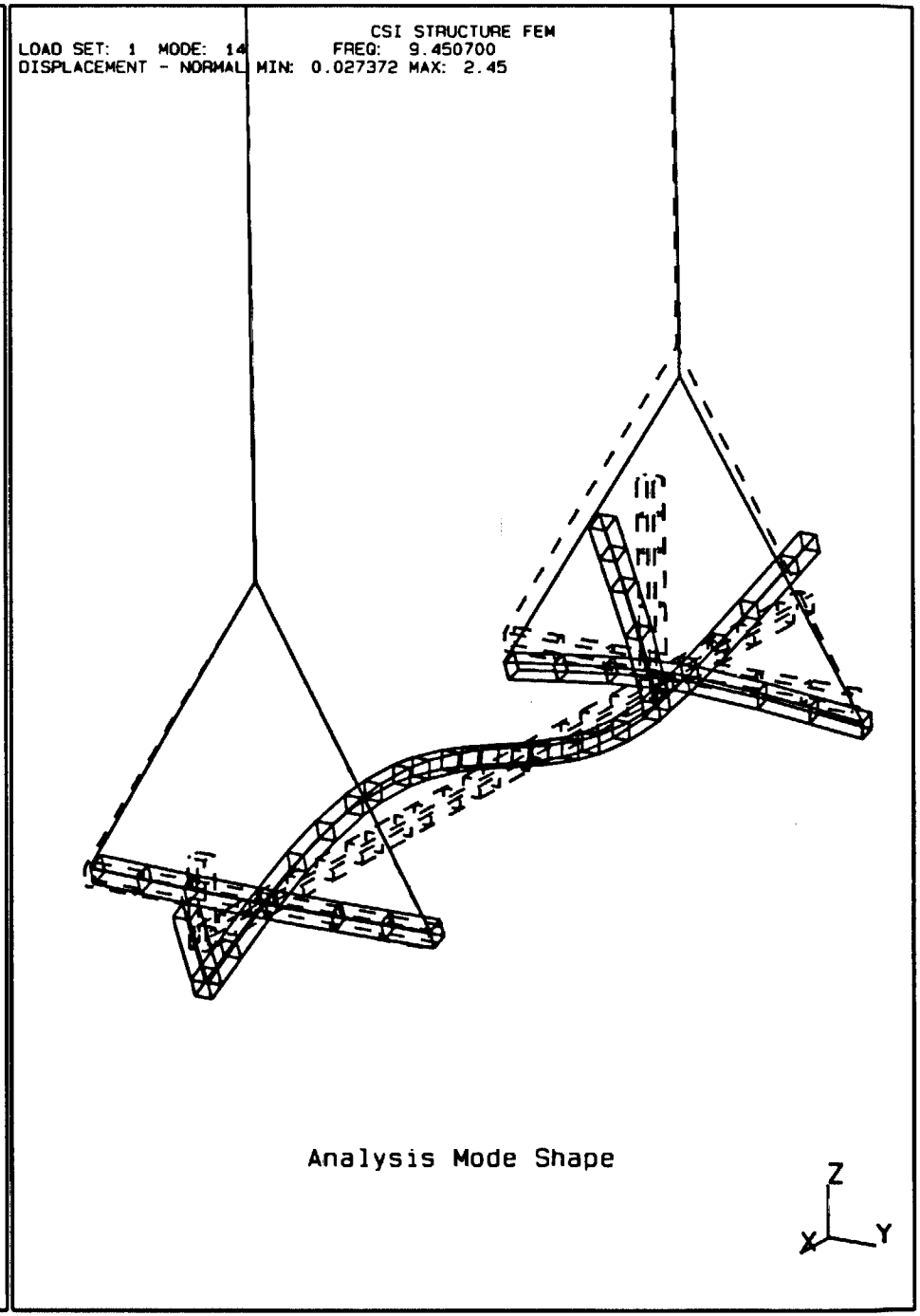

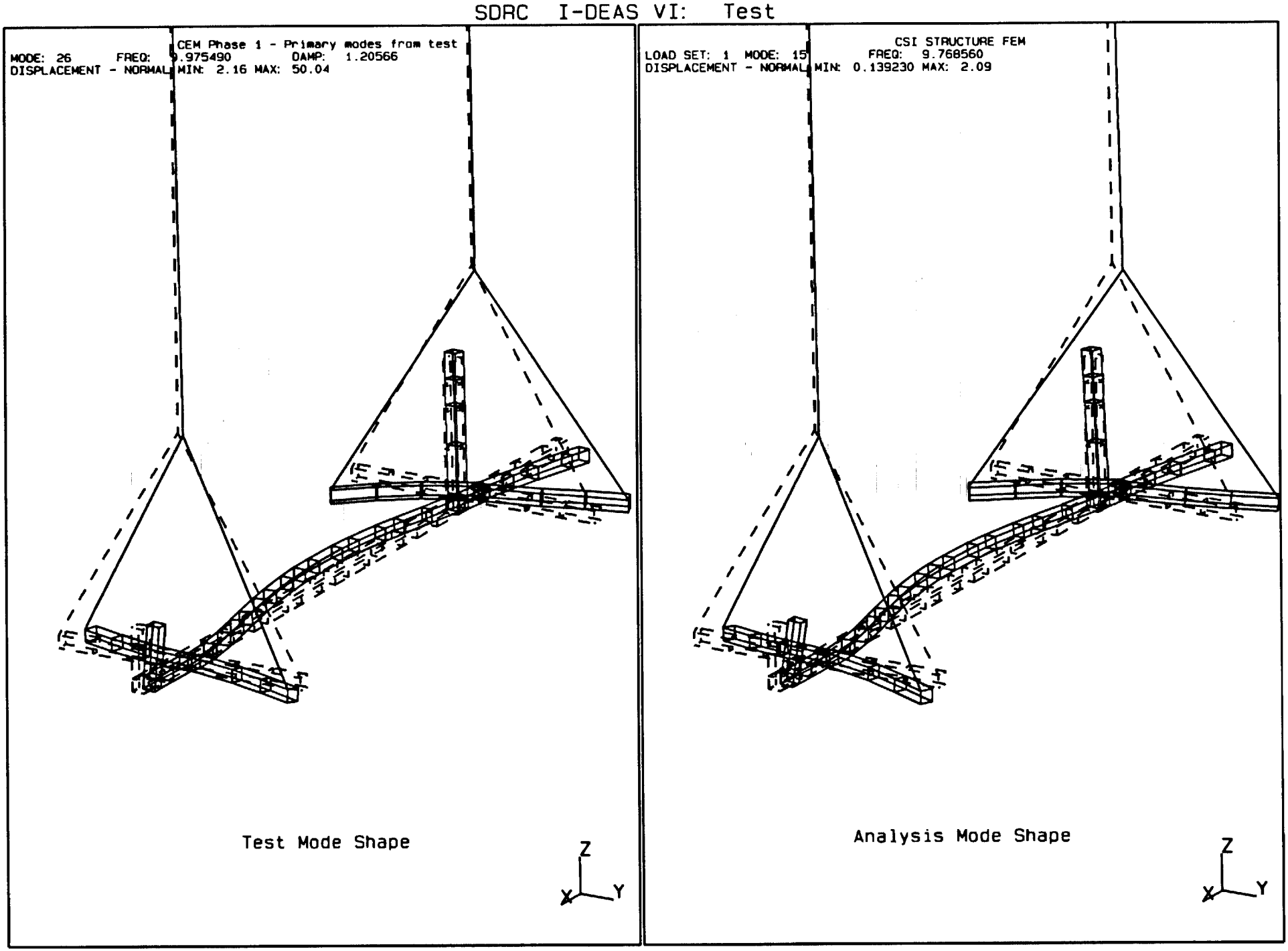
SDRC I-DEAS VI: Test
CEM Phase 1 - Primary modes from test
MODE: 26 FREQ: 9.975490 DAMP: 1.20566
DISPLACEMENT - NORMAL MIN: 2.16 MAX: 50.04
Test Mode Shape
Z
X
Y
CSI STRUCTURE FEM
LOAD SET: 1 MODE: 15 FREQ: 9.768560
DISPLACEMENT - NORMAL MIN: 0.139230 MAX: 2.09
Analysis Mode Shape
Z
X
Y

SDRC I-DEAS VI: Test

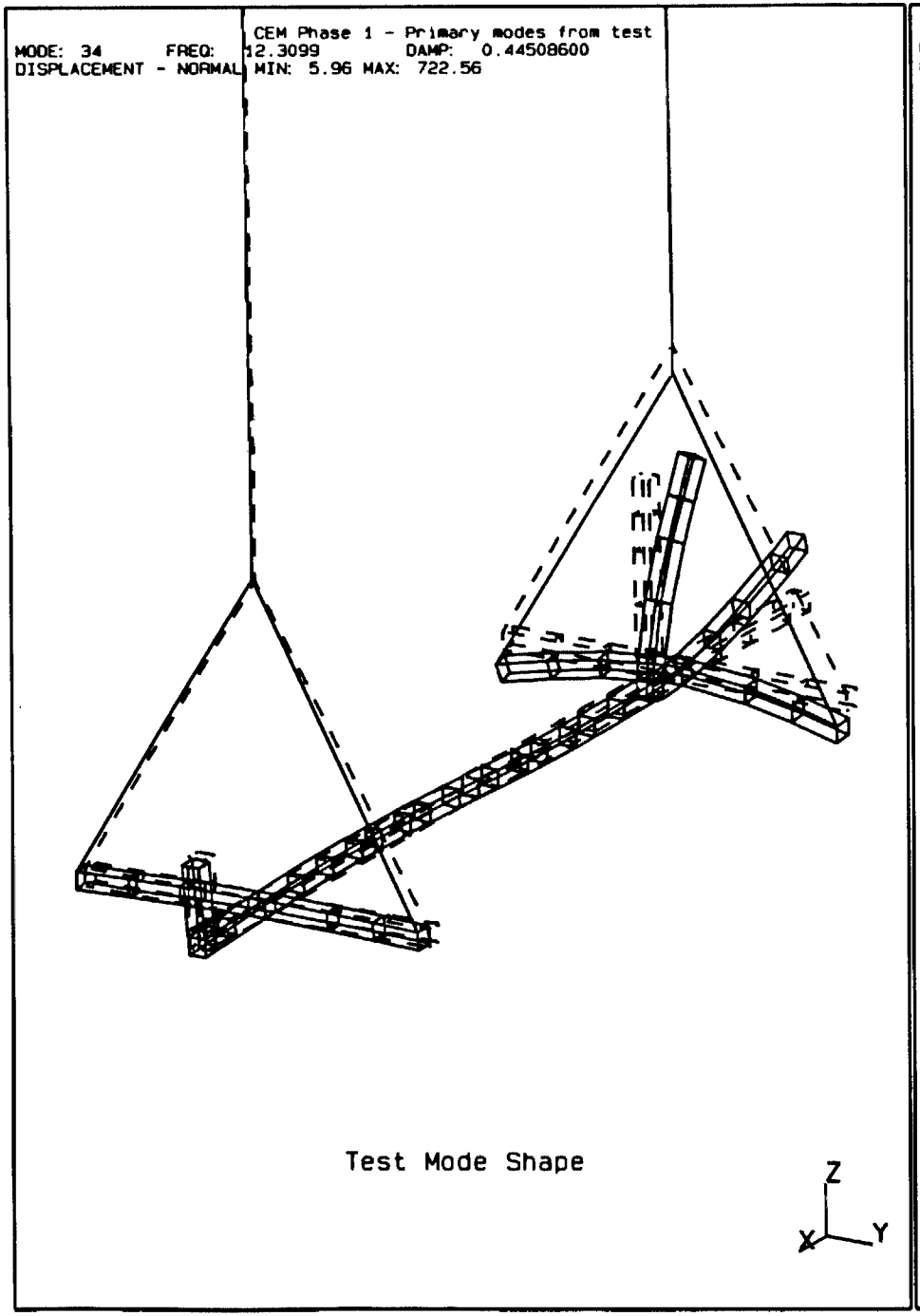

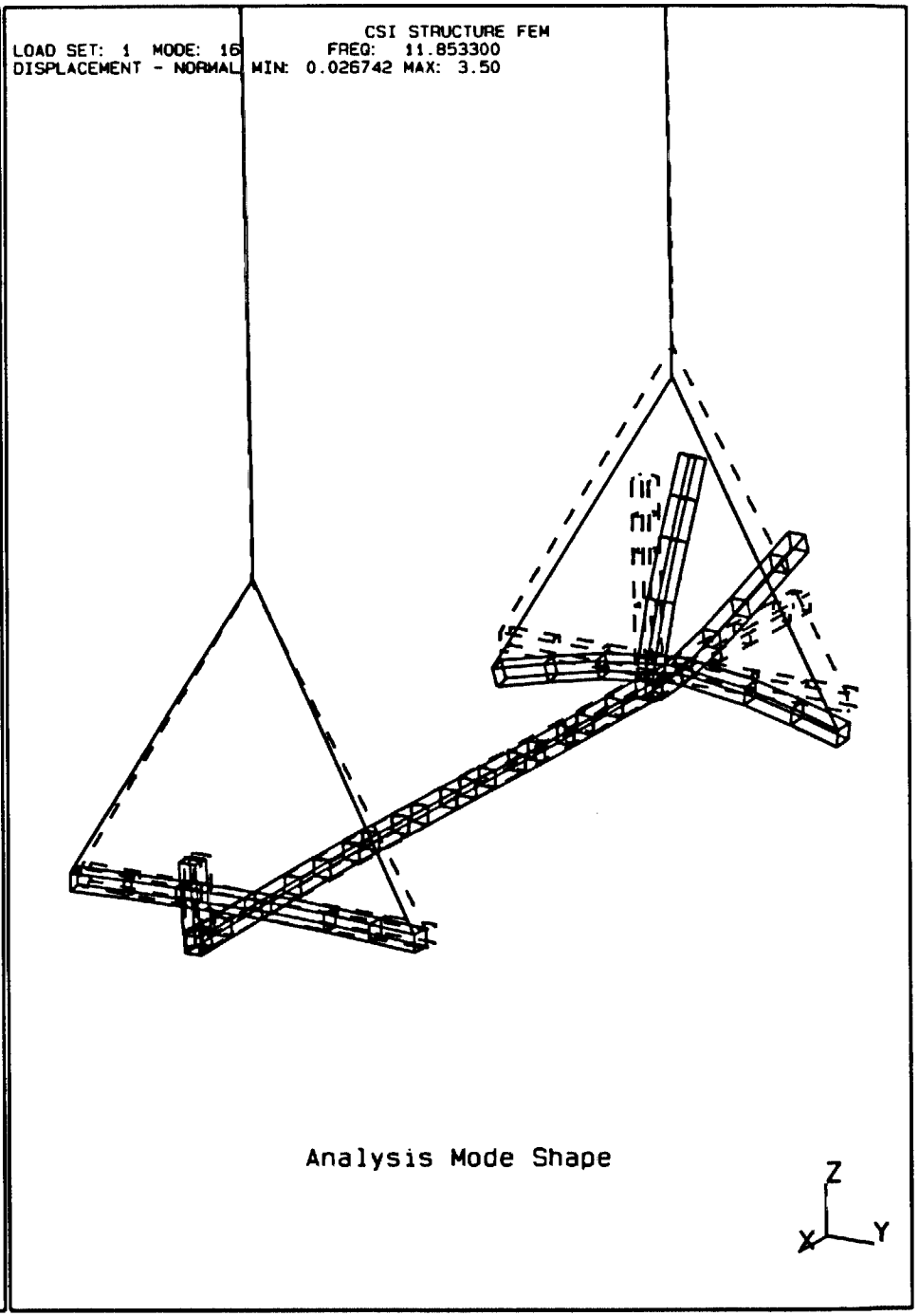

SDRC I-DEAS VI: Test

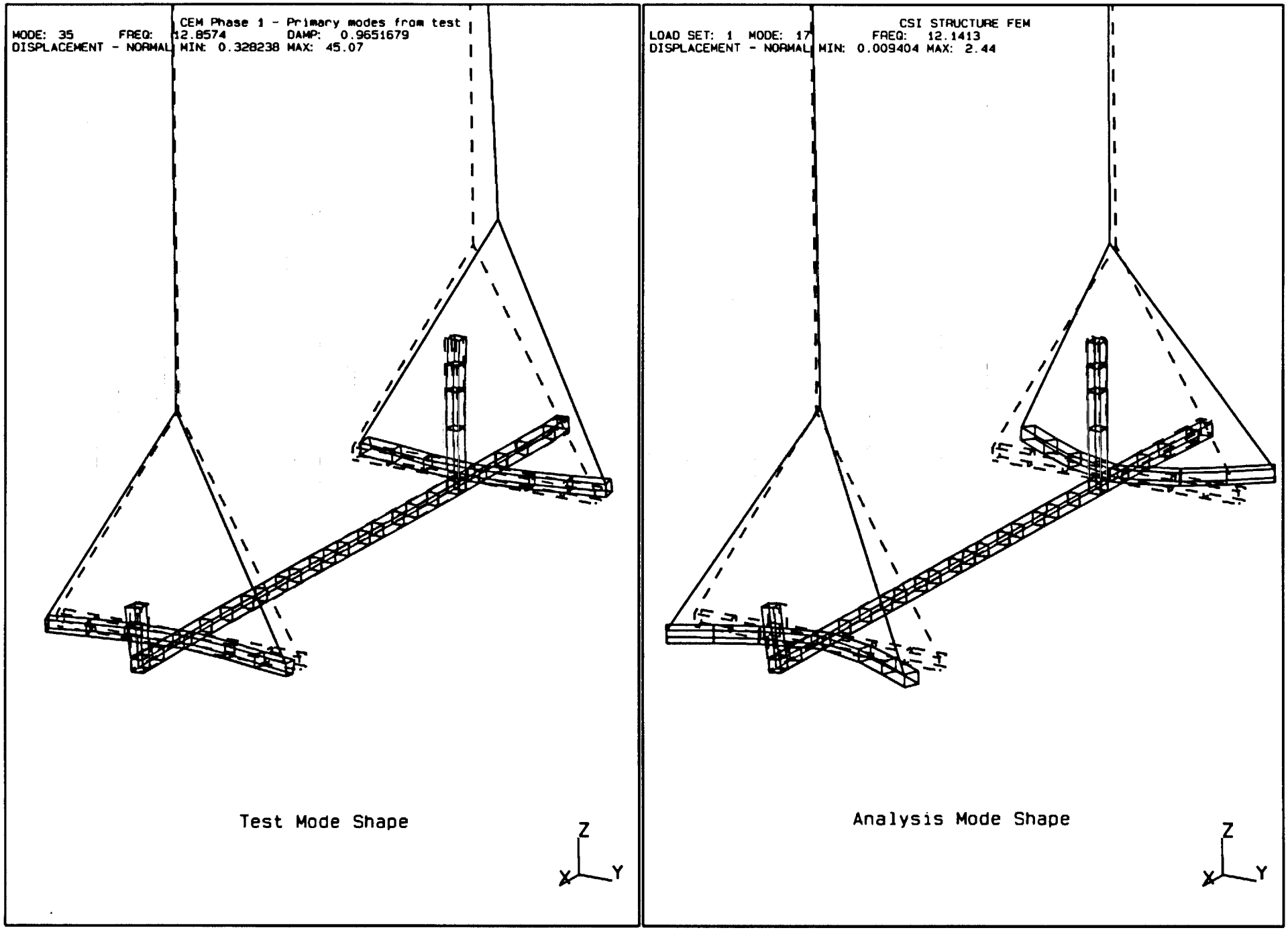

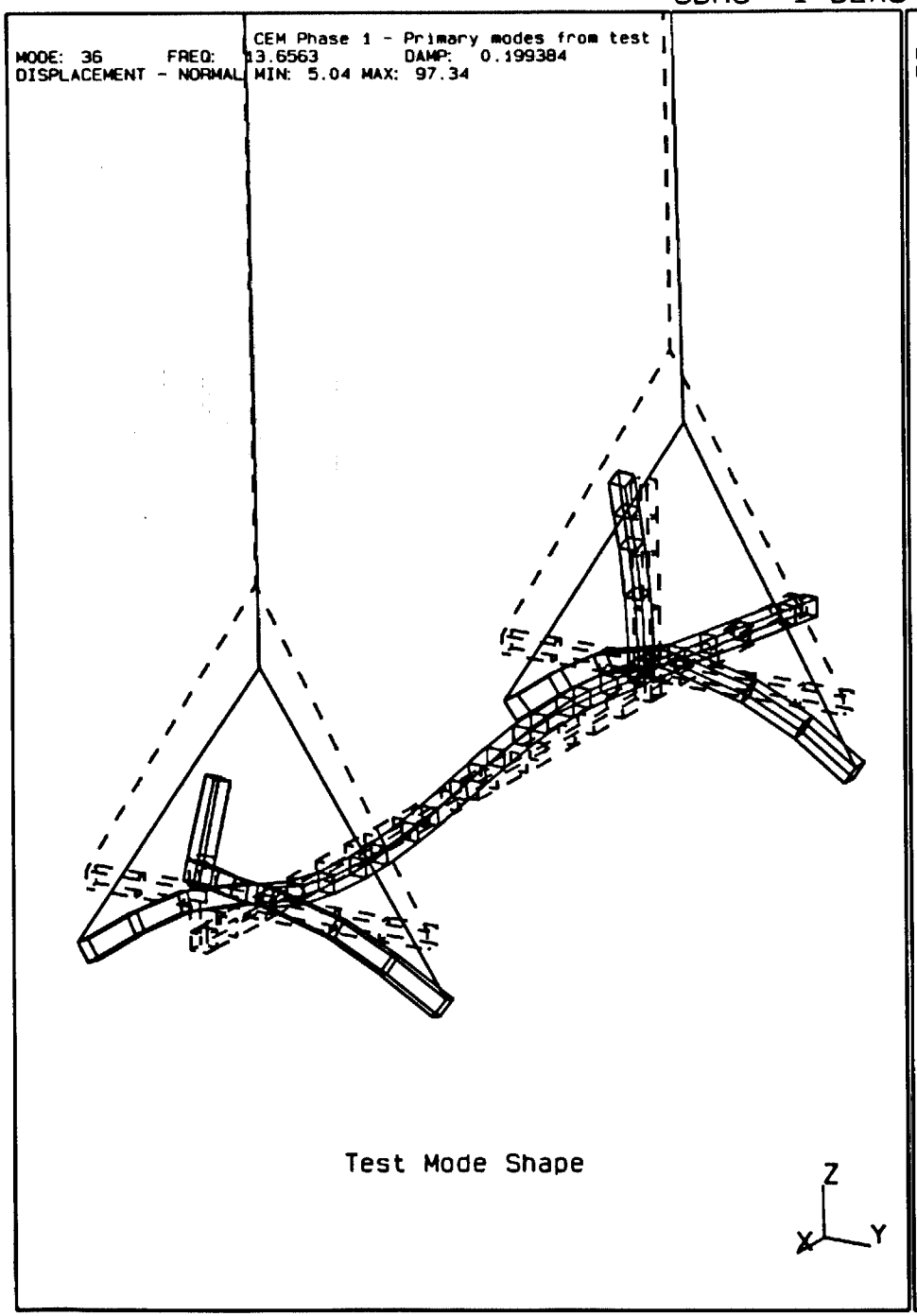
MODE: 36 FREQ: 13.6563 DAMP: 0.199384
DISPLACEMENT - NORMAL MIN: 5.04 MAX: 97.34
CEM Phase 1 - Primary modes from test
Test Mode Shape
Z
X
Y

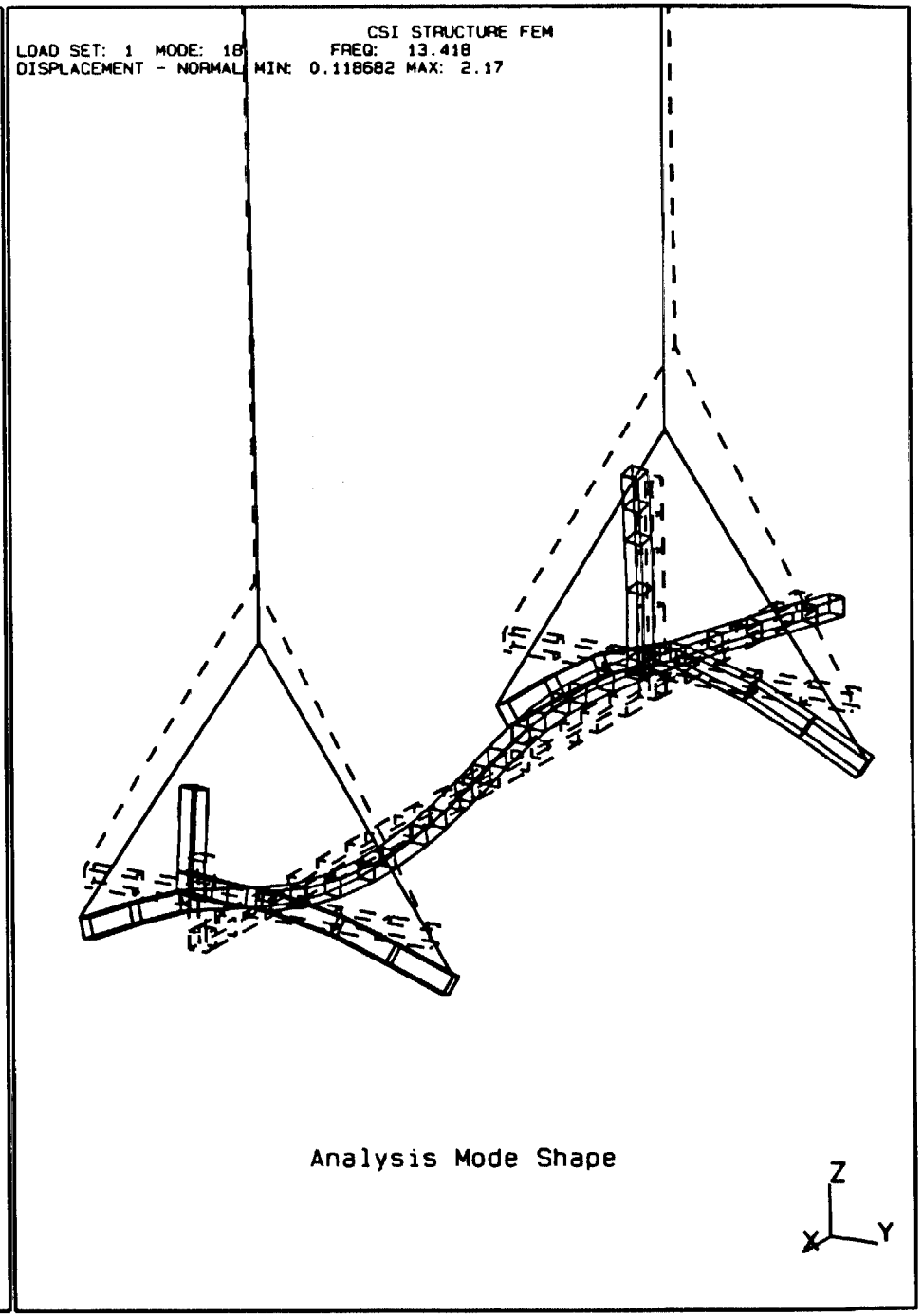
LOAD SET: 1 MODE: 18 FREQ: 13.418
DISPLACEMENT - NORMAL MIN: 0.118682 MAX: 2.17
CSI STRUCTURE FEM
Analysis Mode Shape
Z
X
Y

SDRC I-DEAS VI: Test

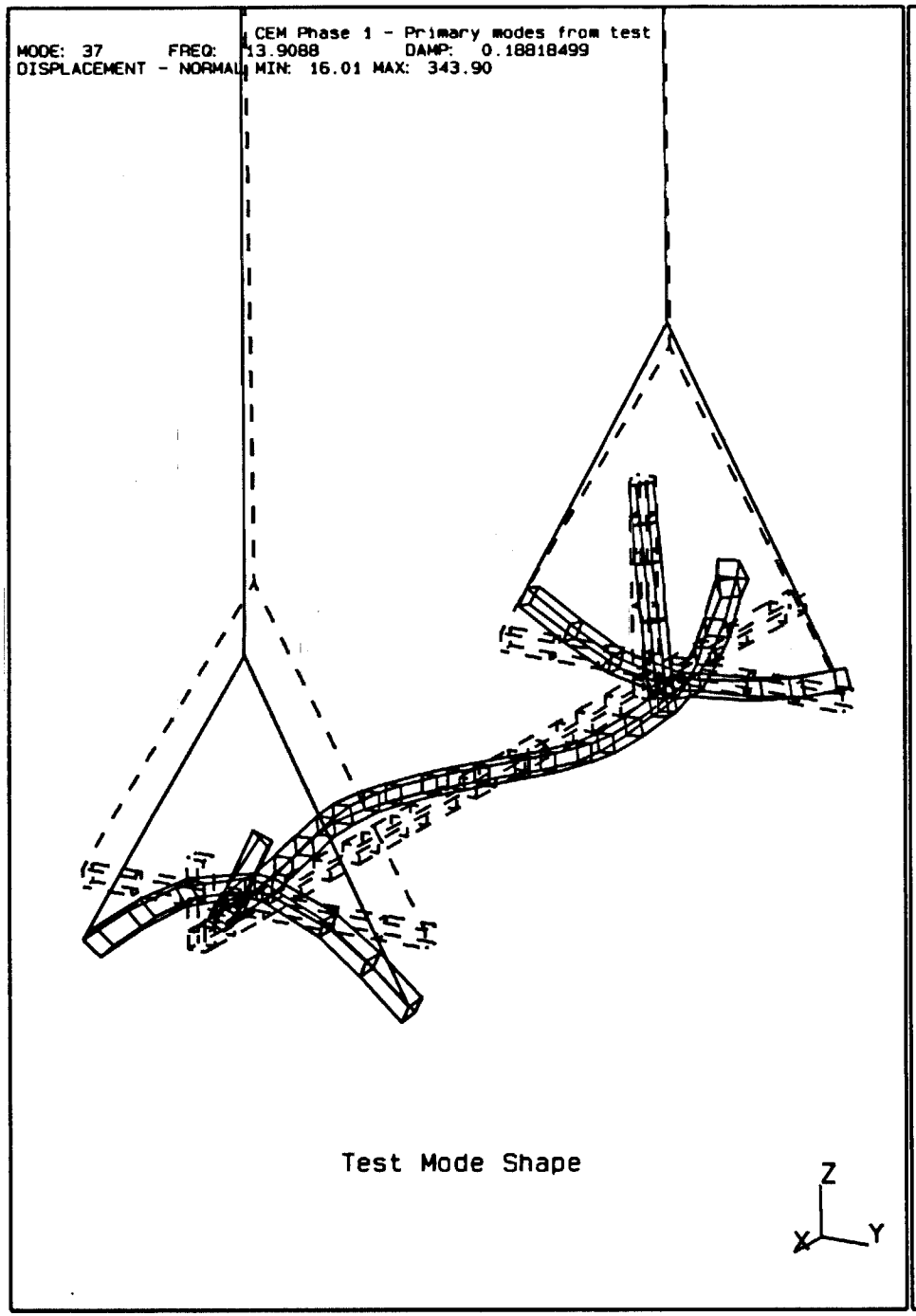

Test Mode Shape

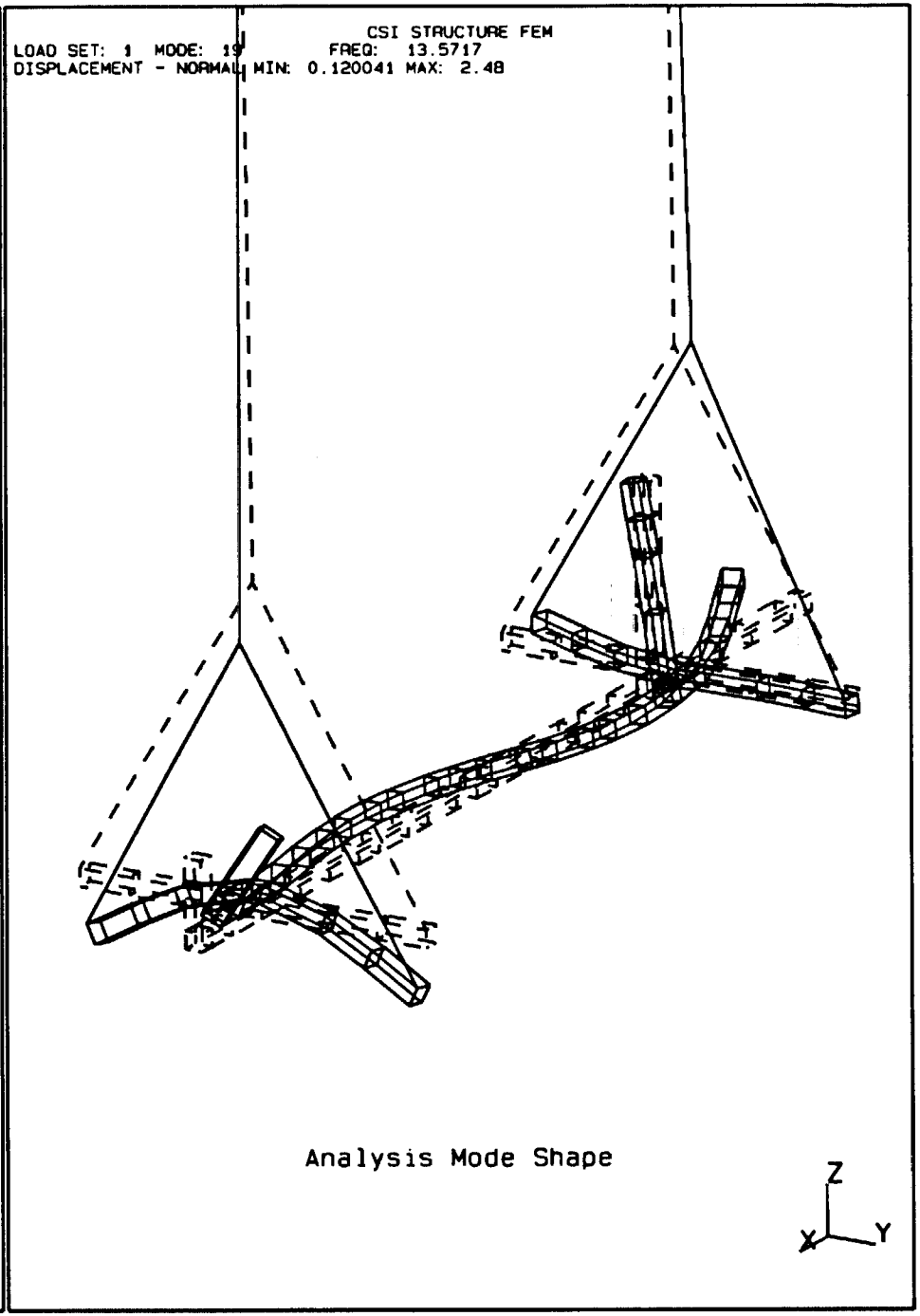

Analysis Mode Shape

SDRC I-DEAS VI: Test

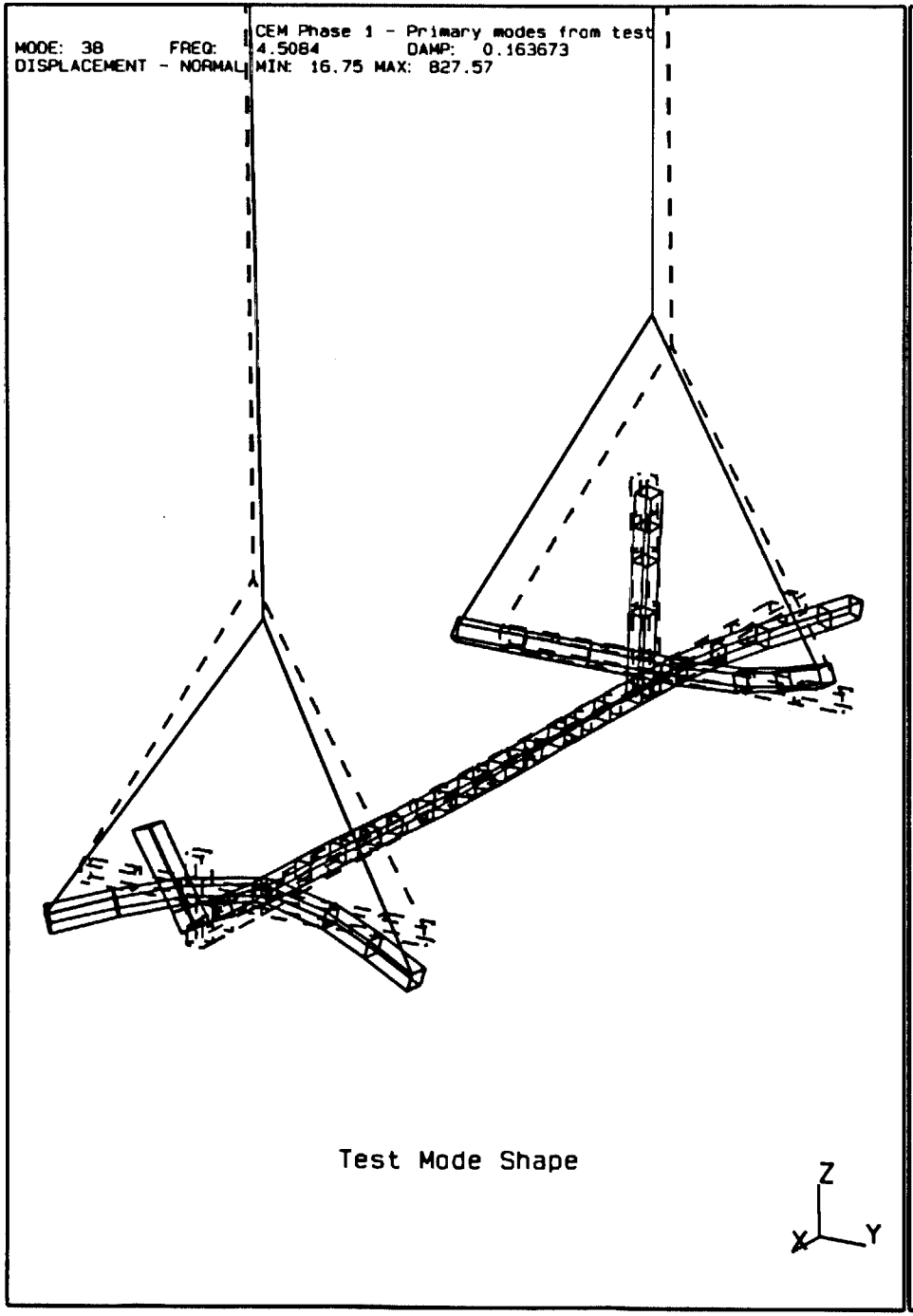

Test Mode Shape

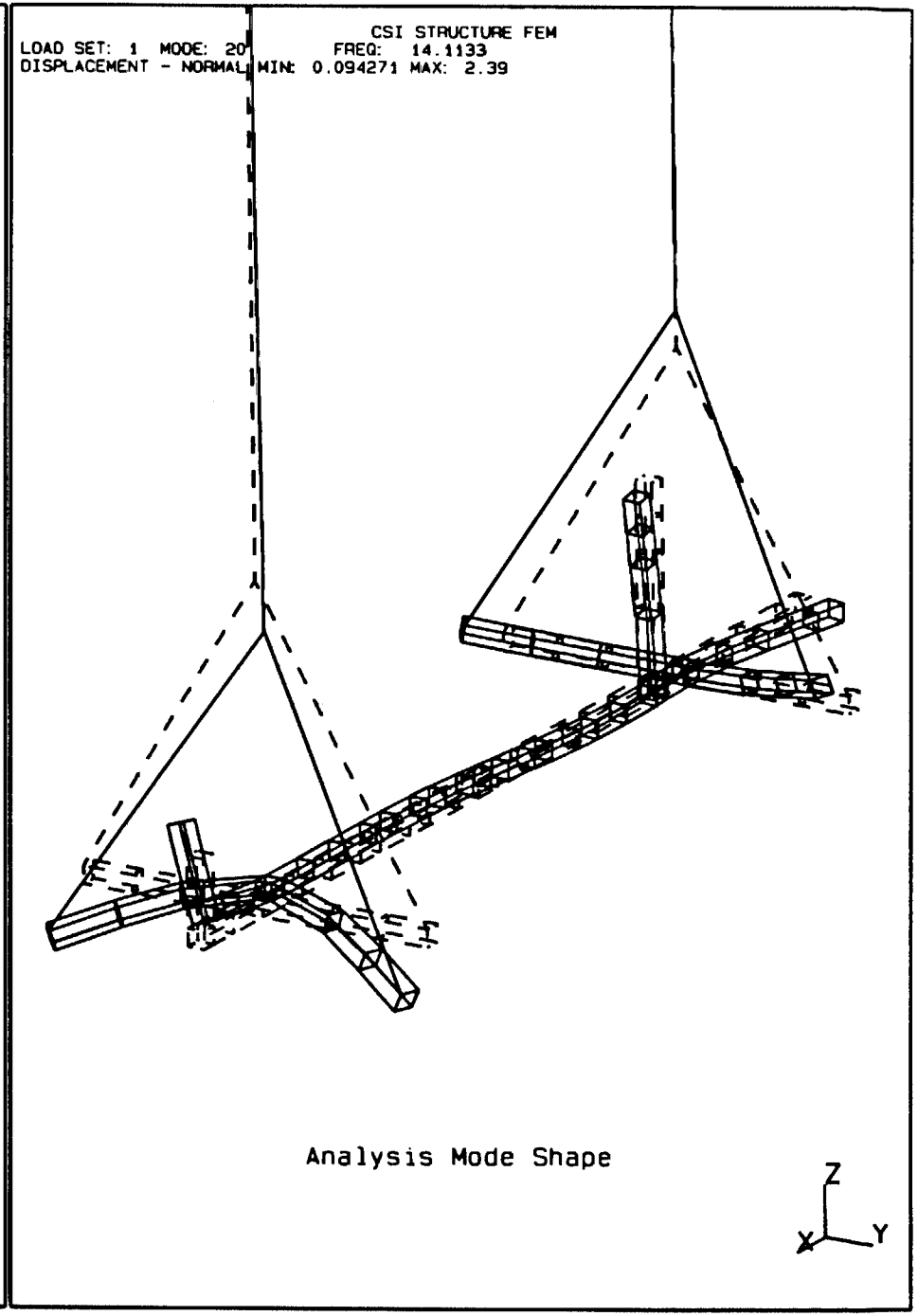

Analysis Mode Shape

SDRC I-DEAS VI: Test

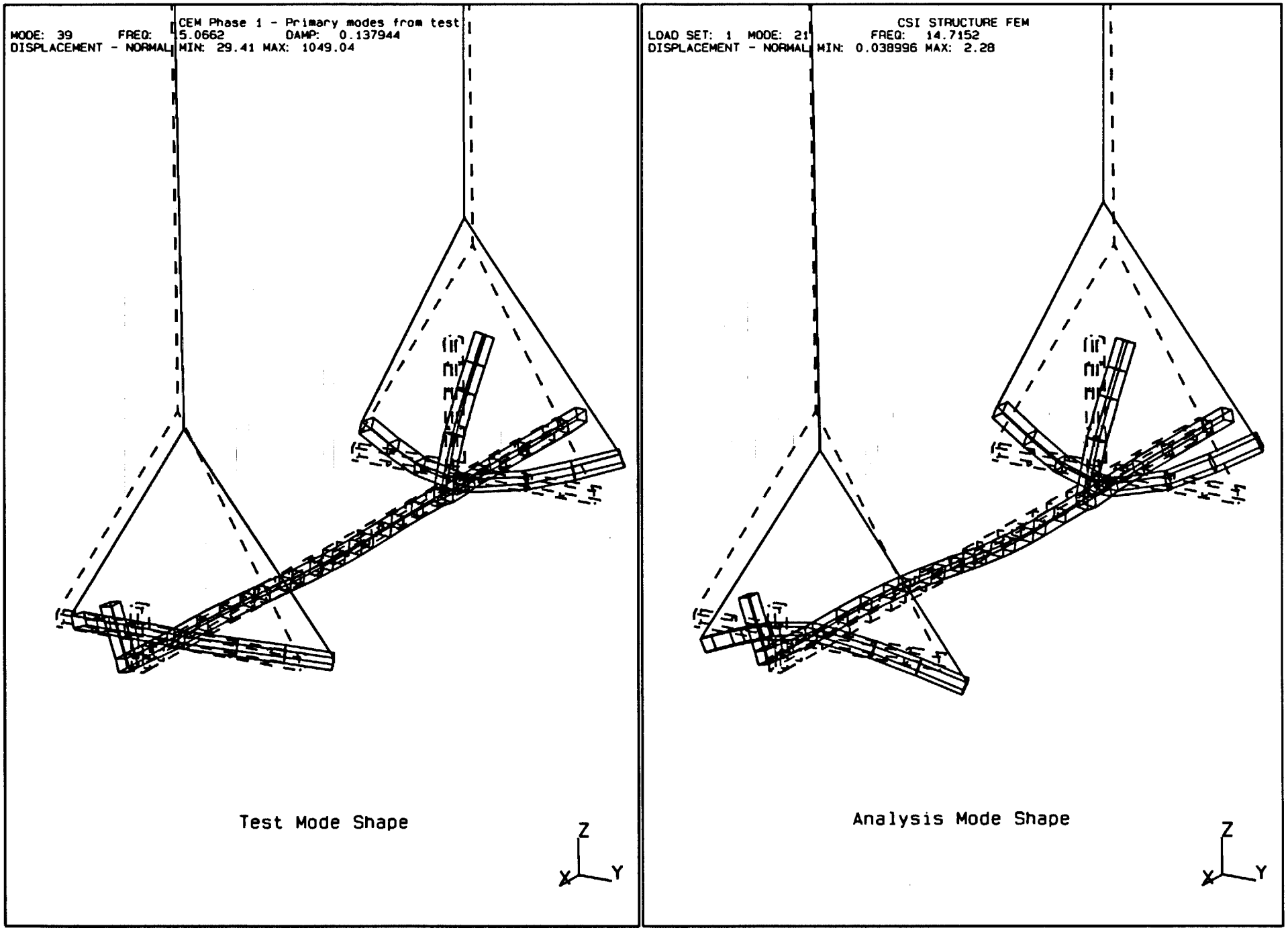

SDRC I-DEAS VI: Test

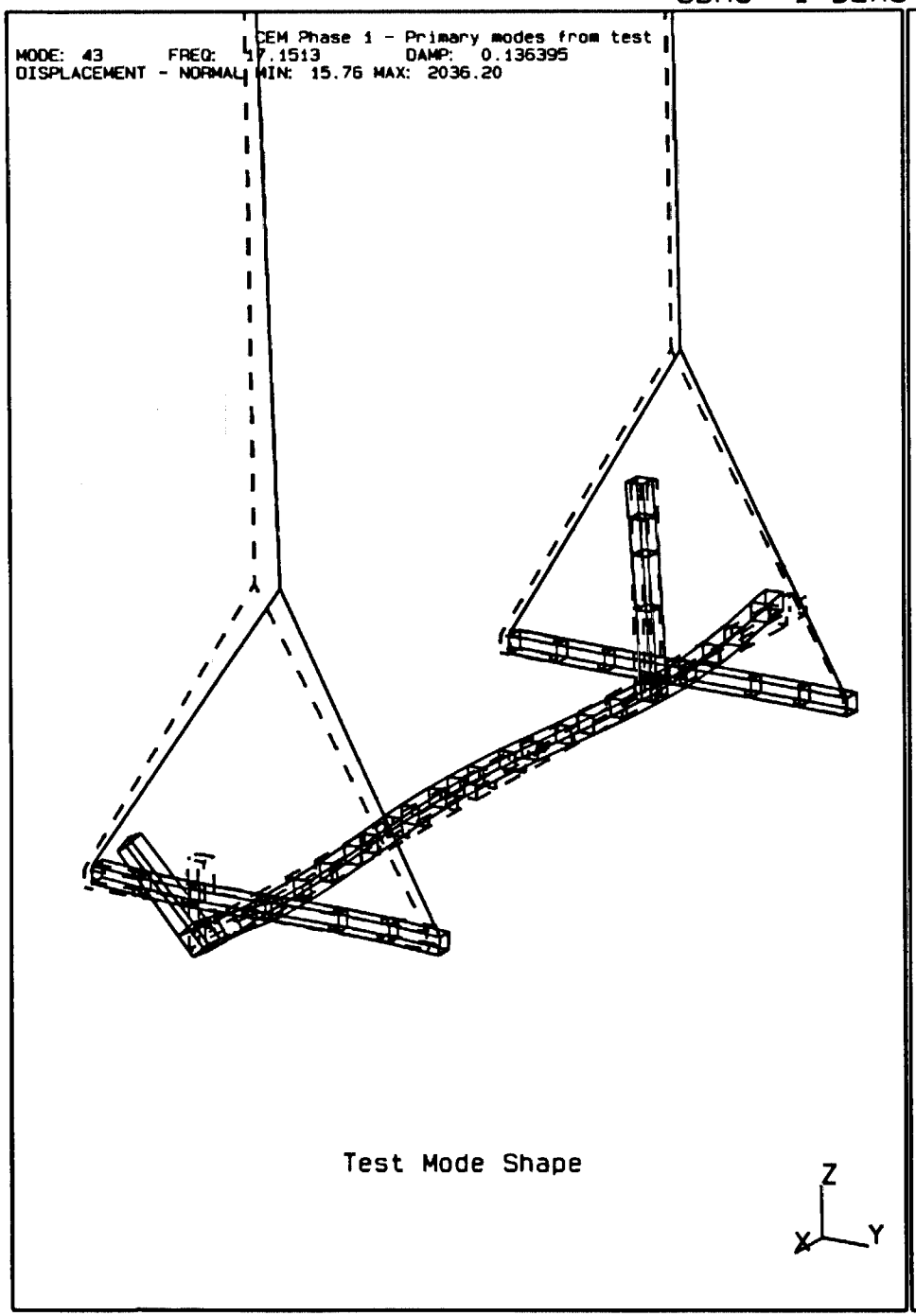

Test Mode Shape

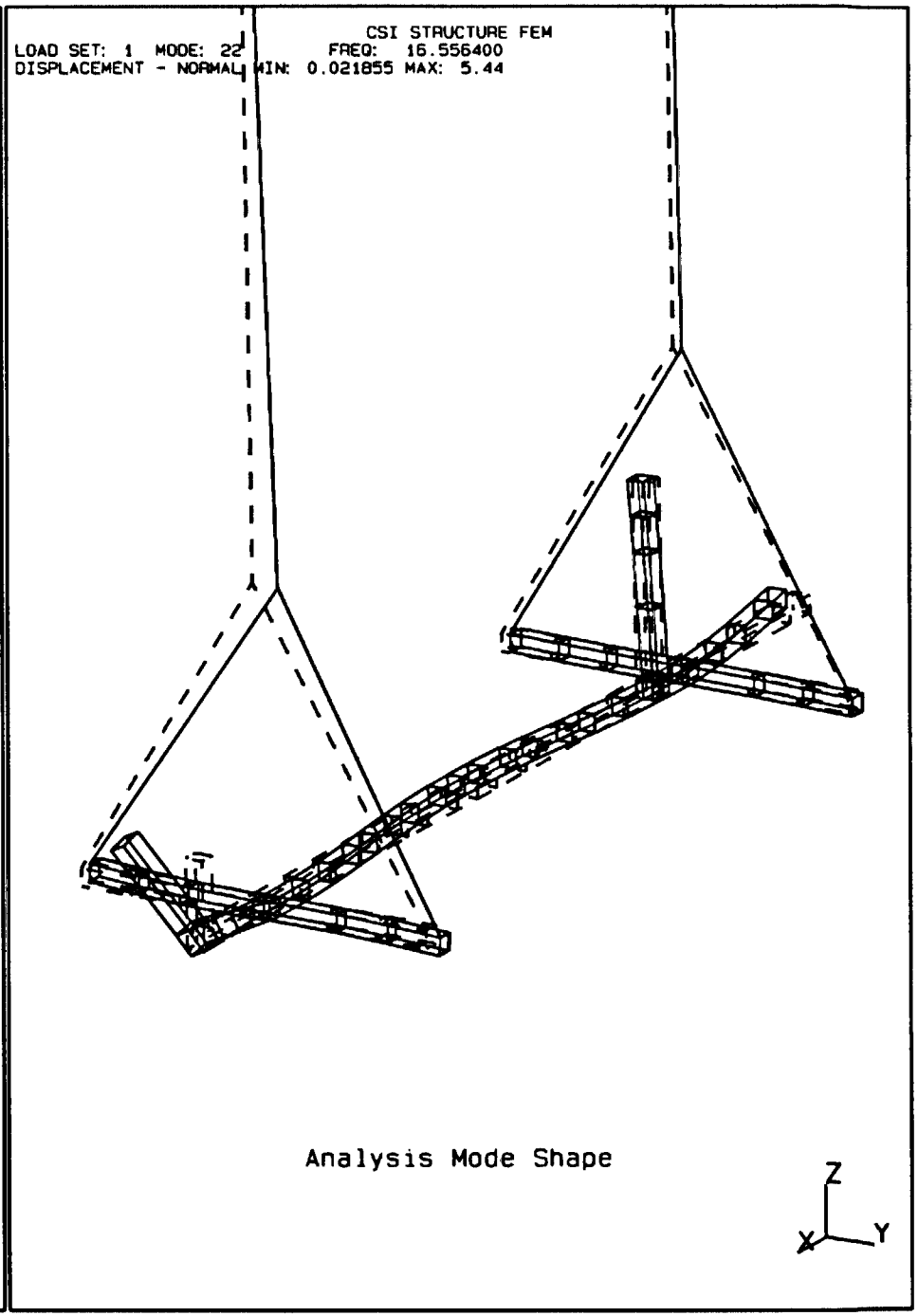

Analysis Mode Shape

SDRC I-DEAS VI: Test

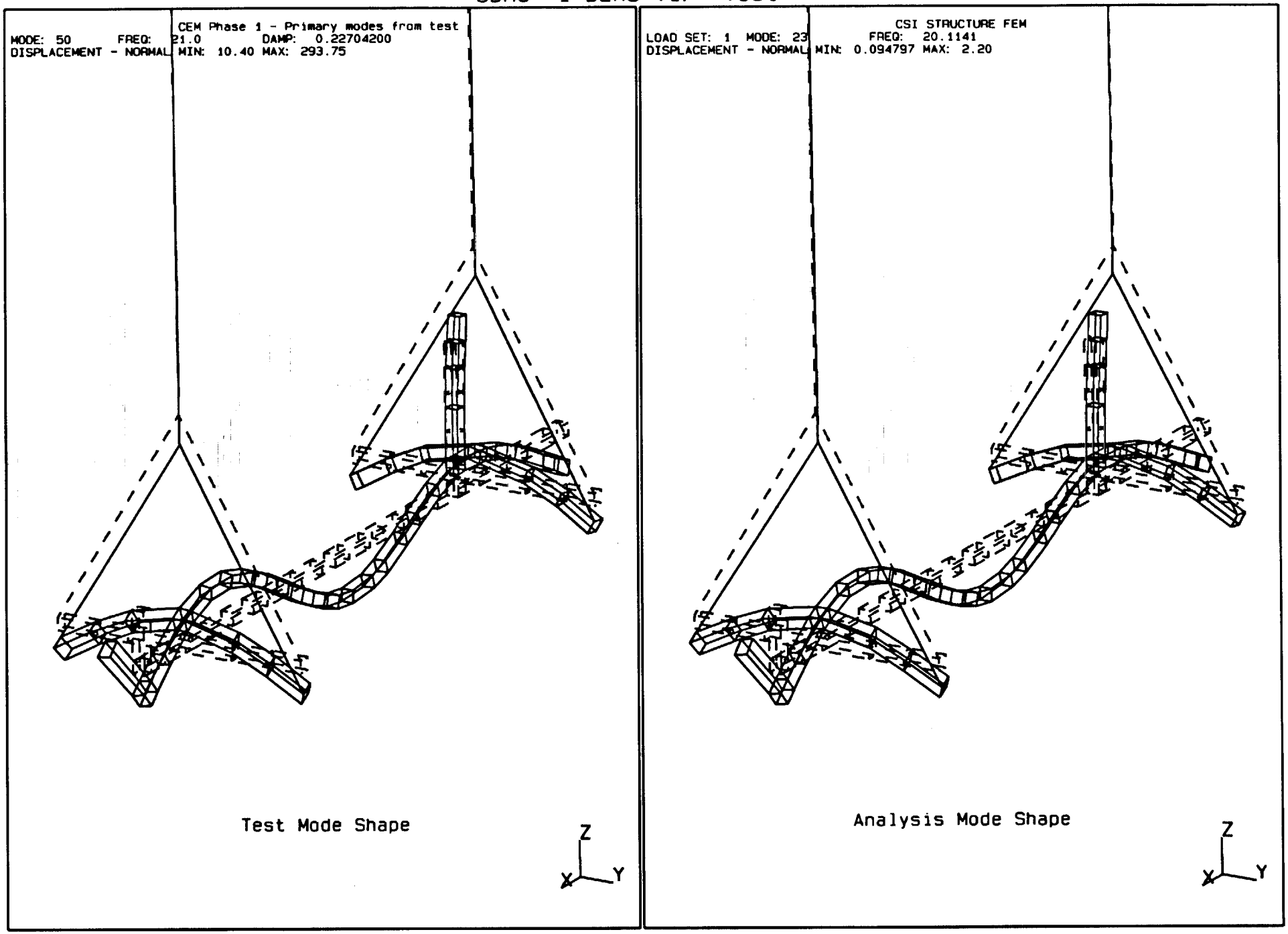

SDRC I-DEAS VI: Test

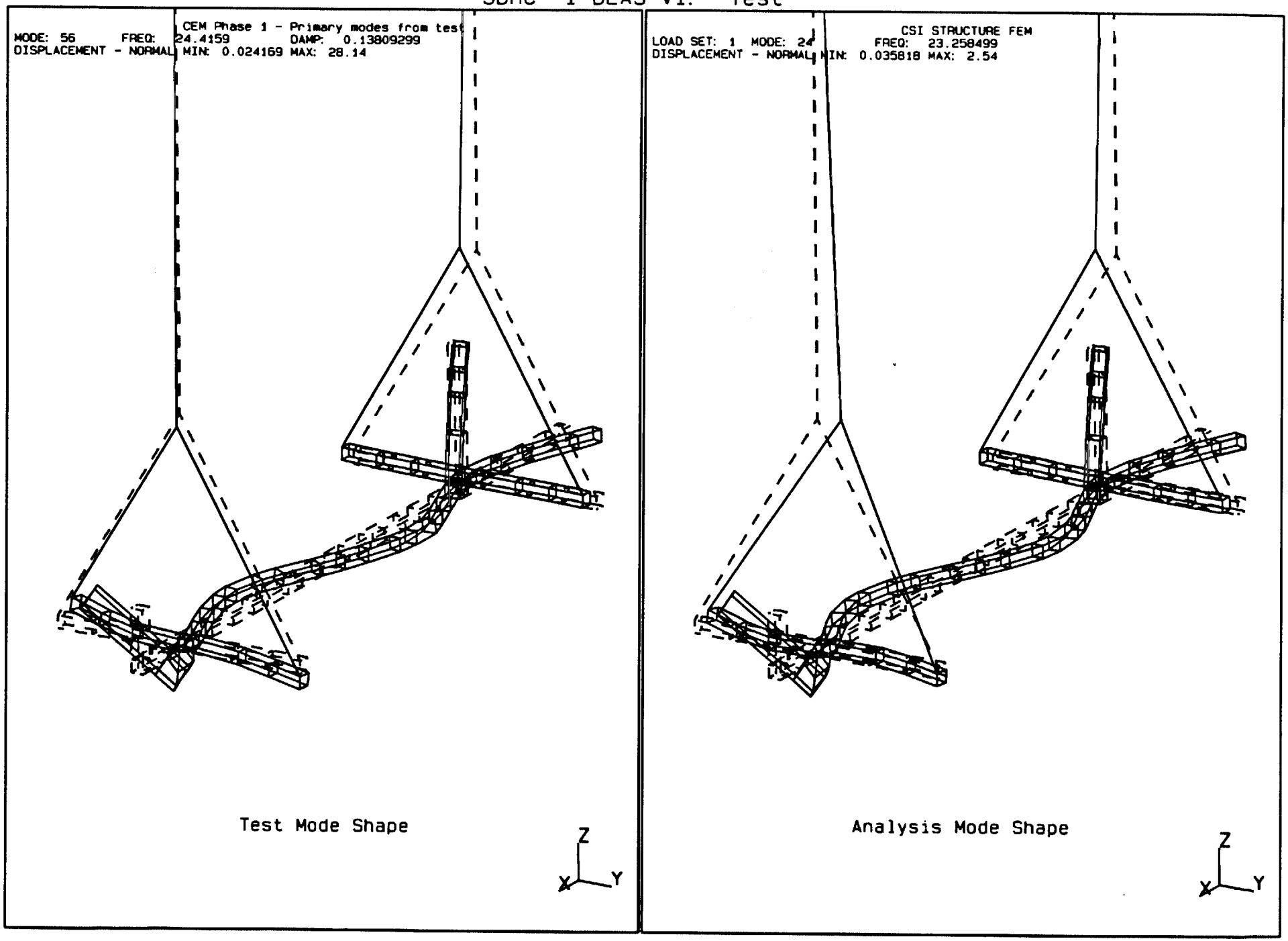

SDRC I-DEAS VI: Test

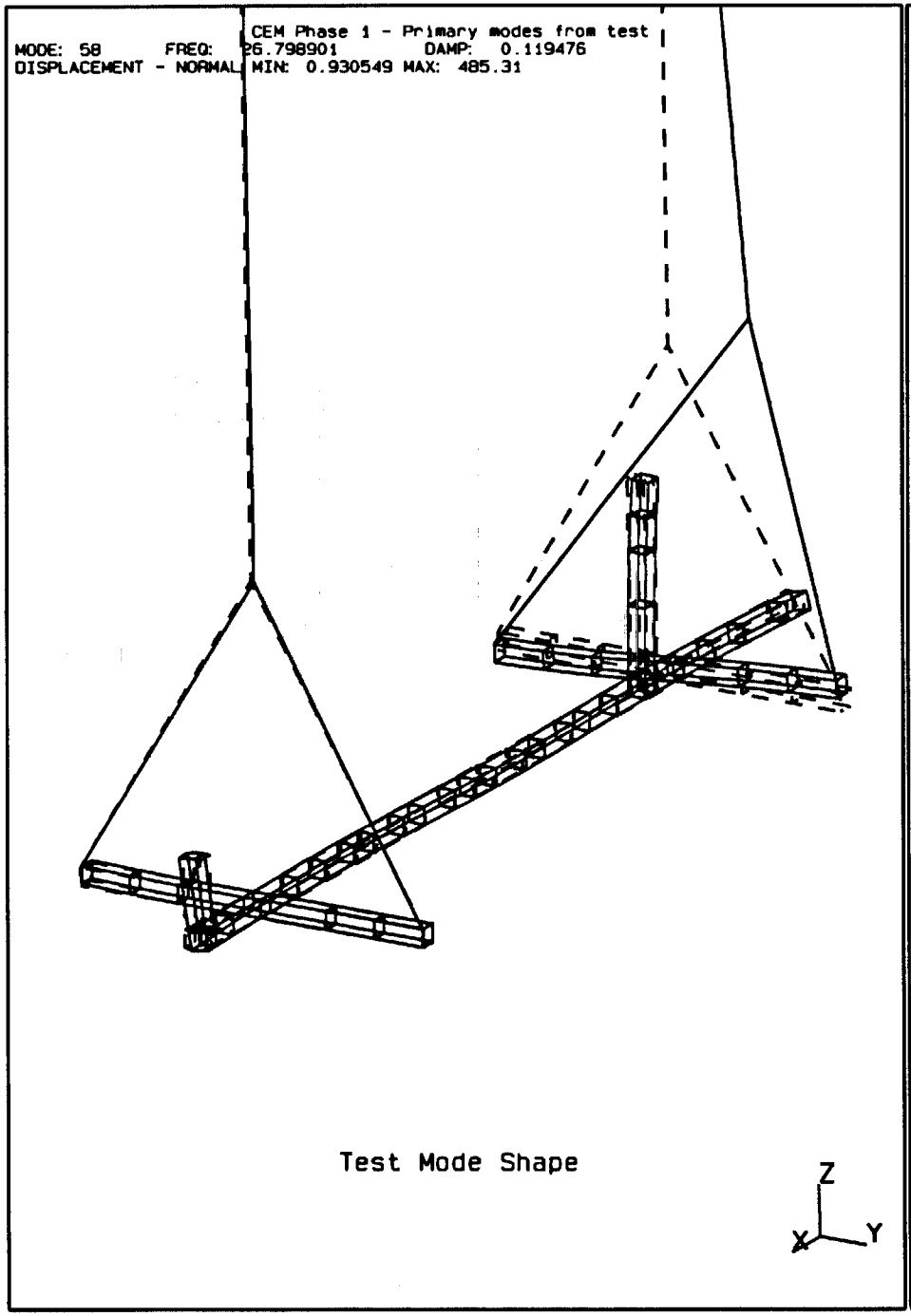

Test Mode Shape

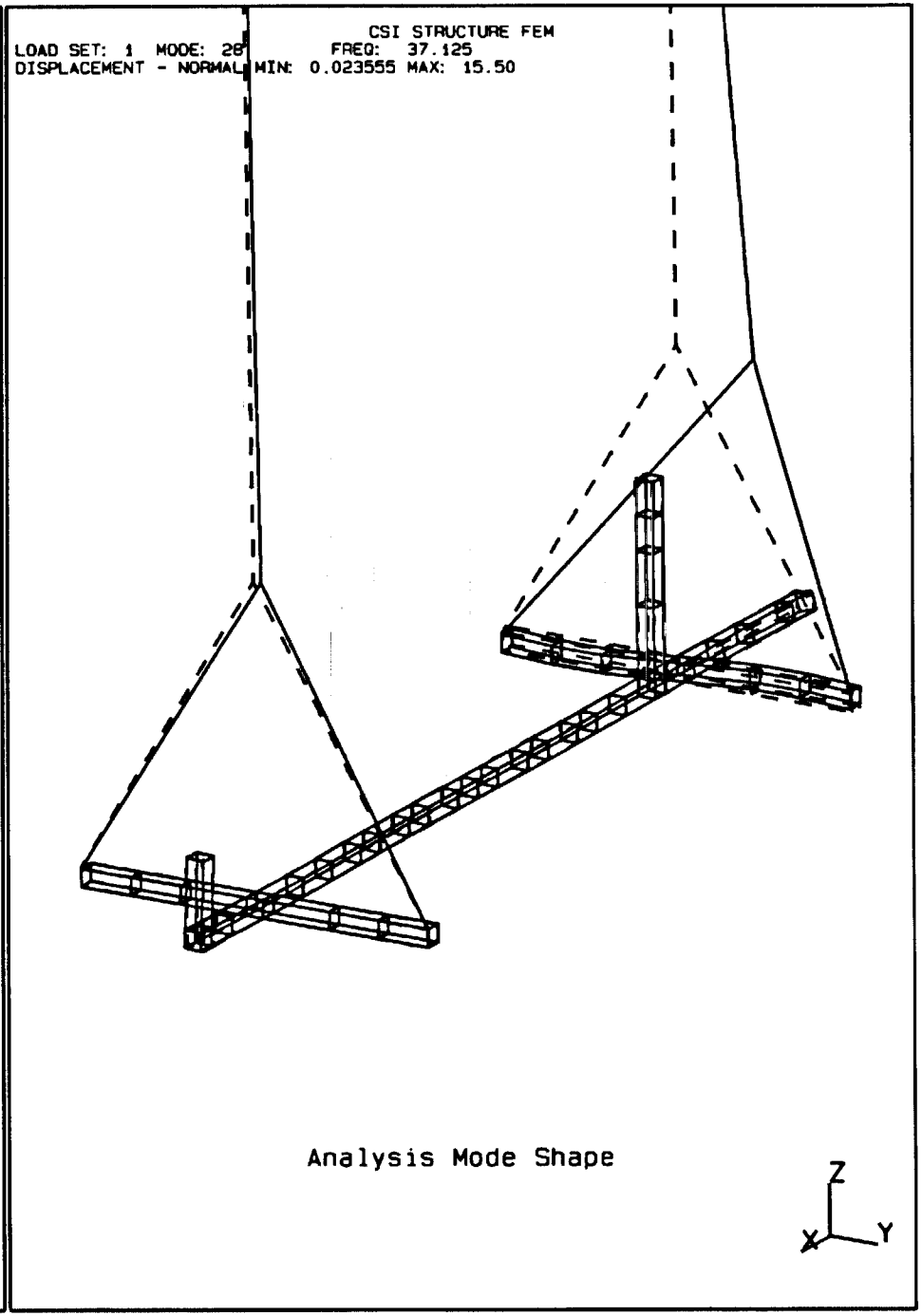

Analysis Mode Shape

SDRC I-DEAS VI: Test

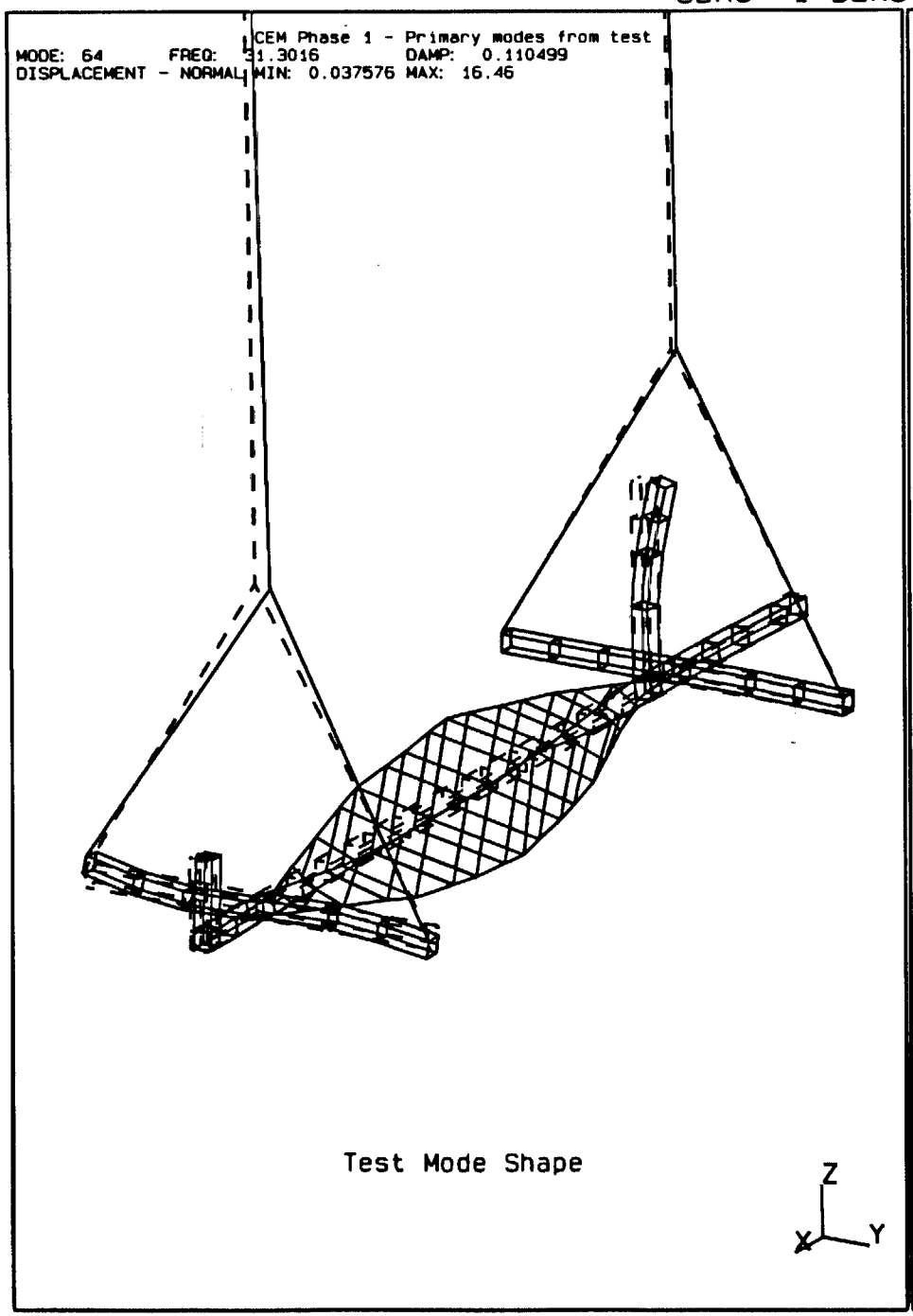

Test Mode Shape

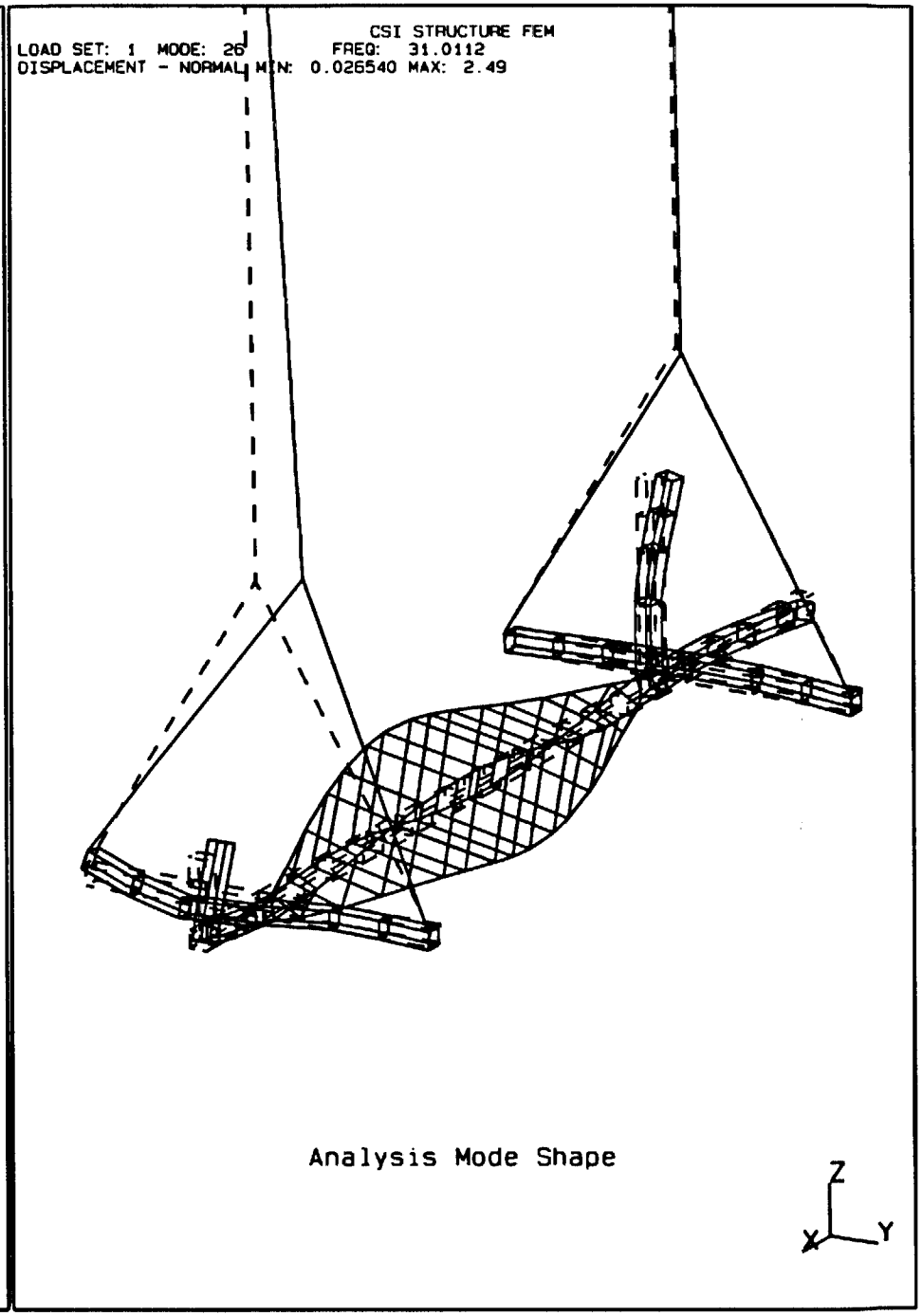

Analysis Mode Shape

SDRC I-DEAS VI: Test

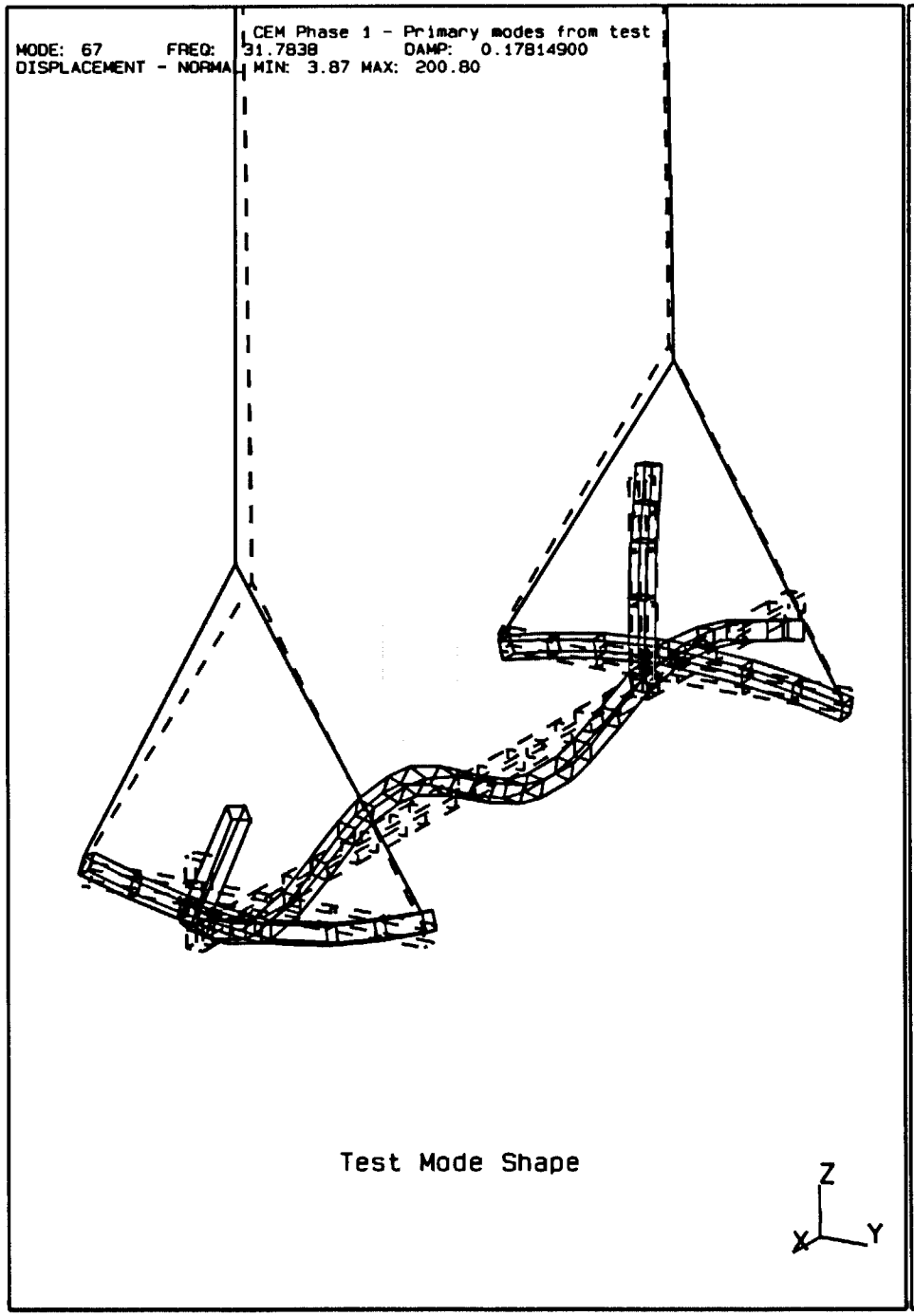

Test Mode Shape

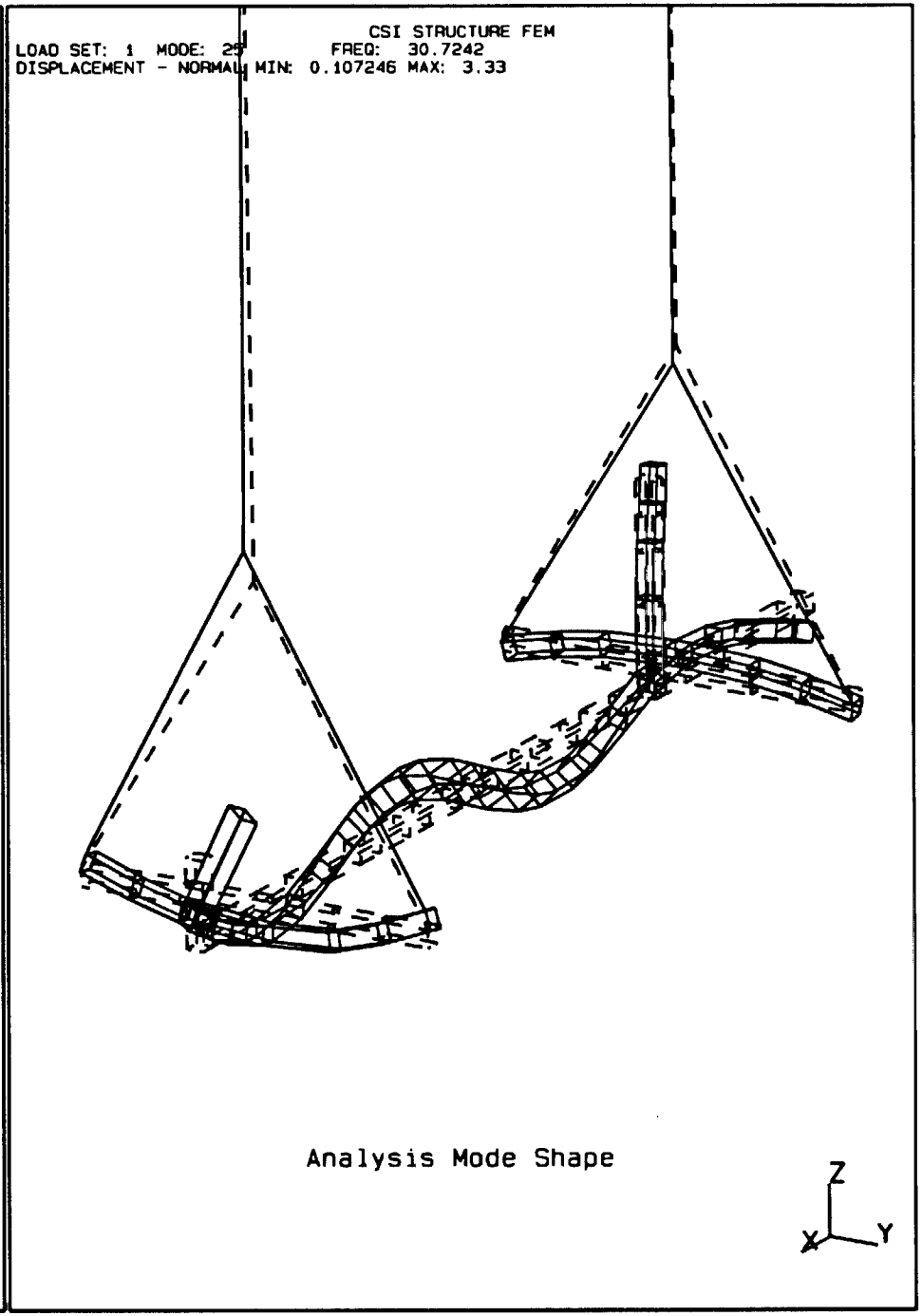

Analysis Mode Shape

APPENDIX I

ASSEMBLY DYNAMIC TEST MODE SHAPE PLOTS NOT MATCHED WITH ANALYTICAL PREDICTIONS

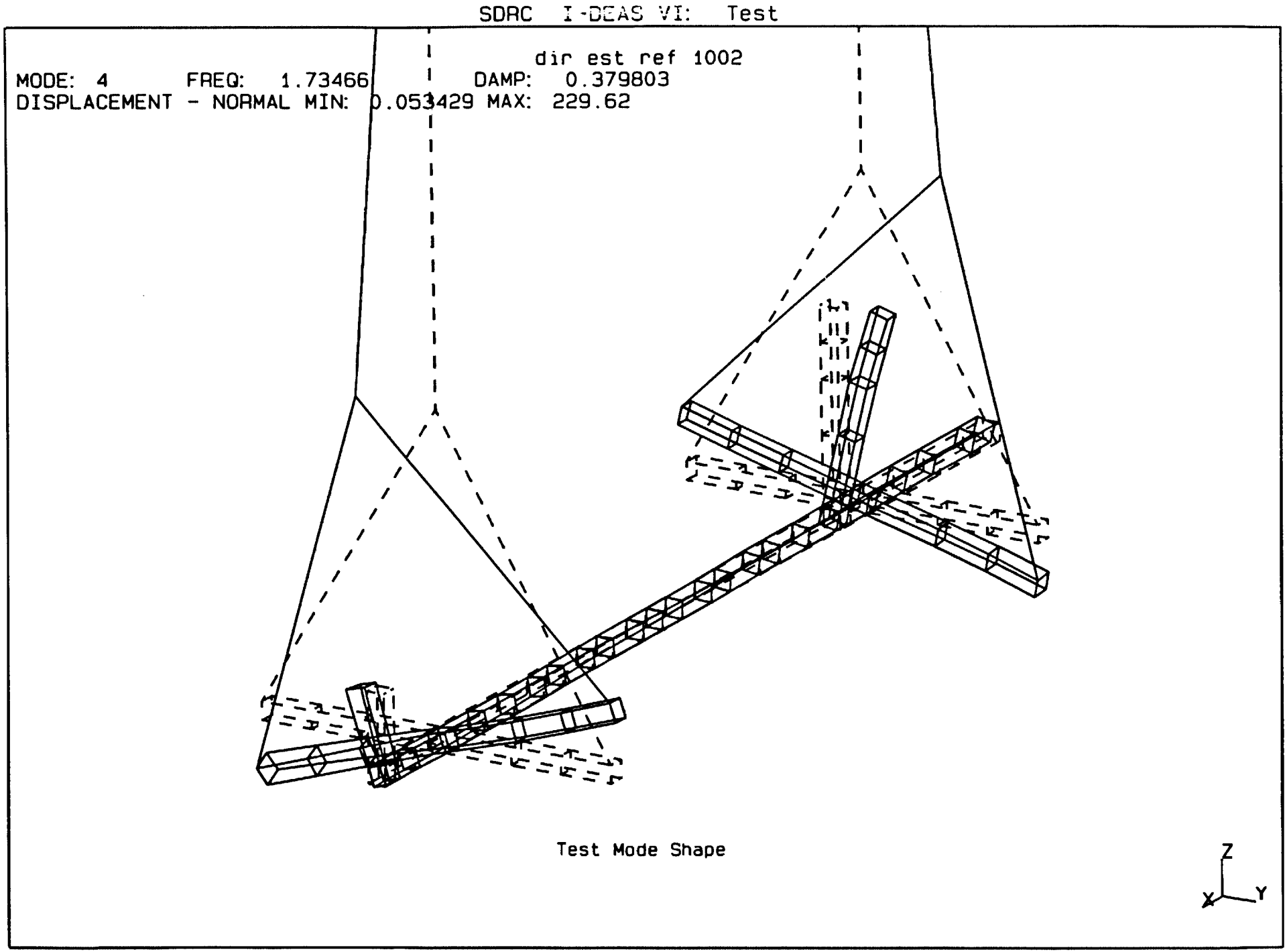
SDRC I-DEAS VI: Test
dir est ref 1002
MODE: 4 FREQ: 1.73466 DAMP: 0.379803
DISPLACEMENT - NORMAL MIN: 0.053429 MAX: 229.62
Test Mode Shape
Z
X
Y

SDRC I-DEAS VI: Test

dir est ref 1002x -

MODE: 6 FREQ: 2.0653400 DAMP: 0.58933902

DISPLACEMENT - NORMAL MIN: 0.094319 MAX: 37.15

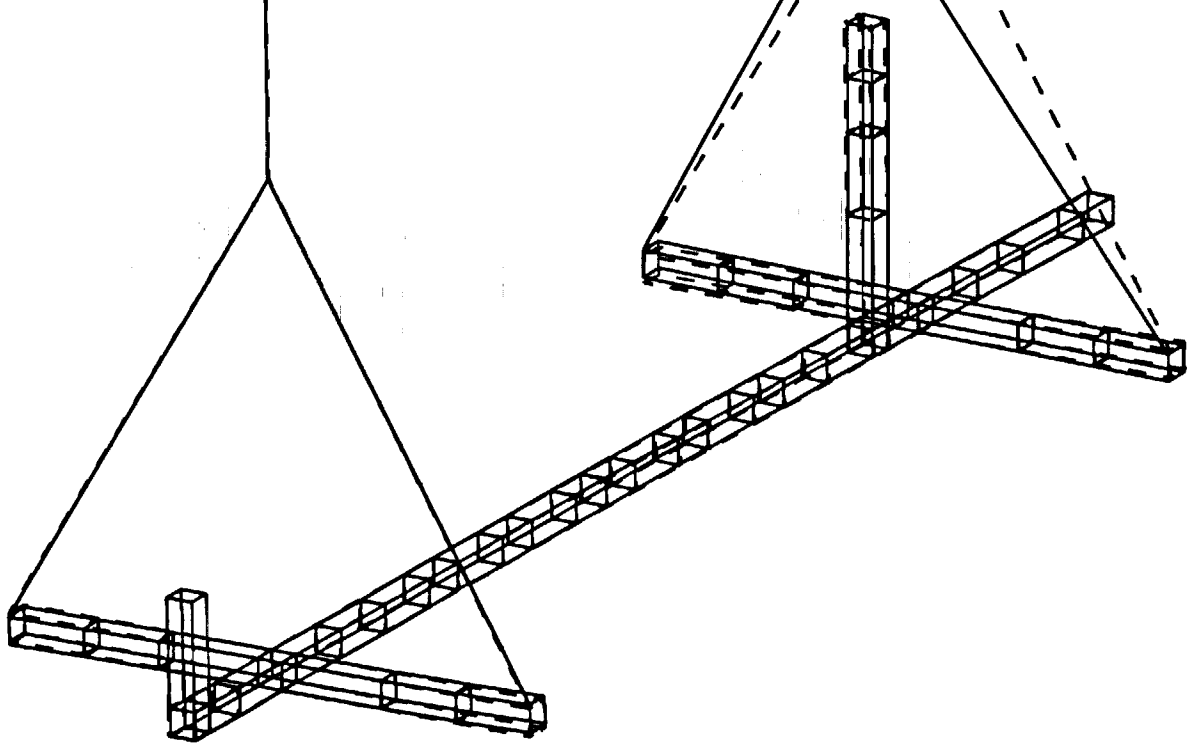

Test Mode Shape

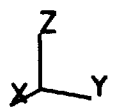

SDRC I-DEAS VI: Test

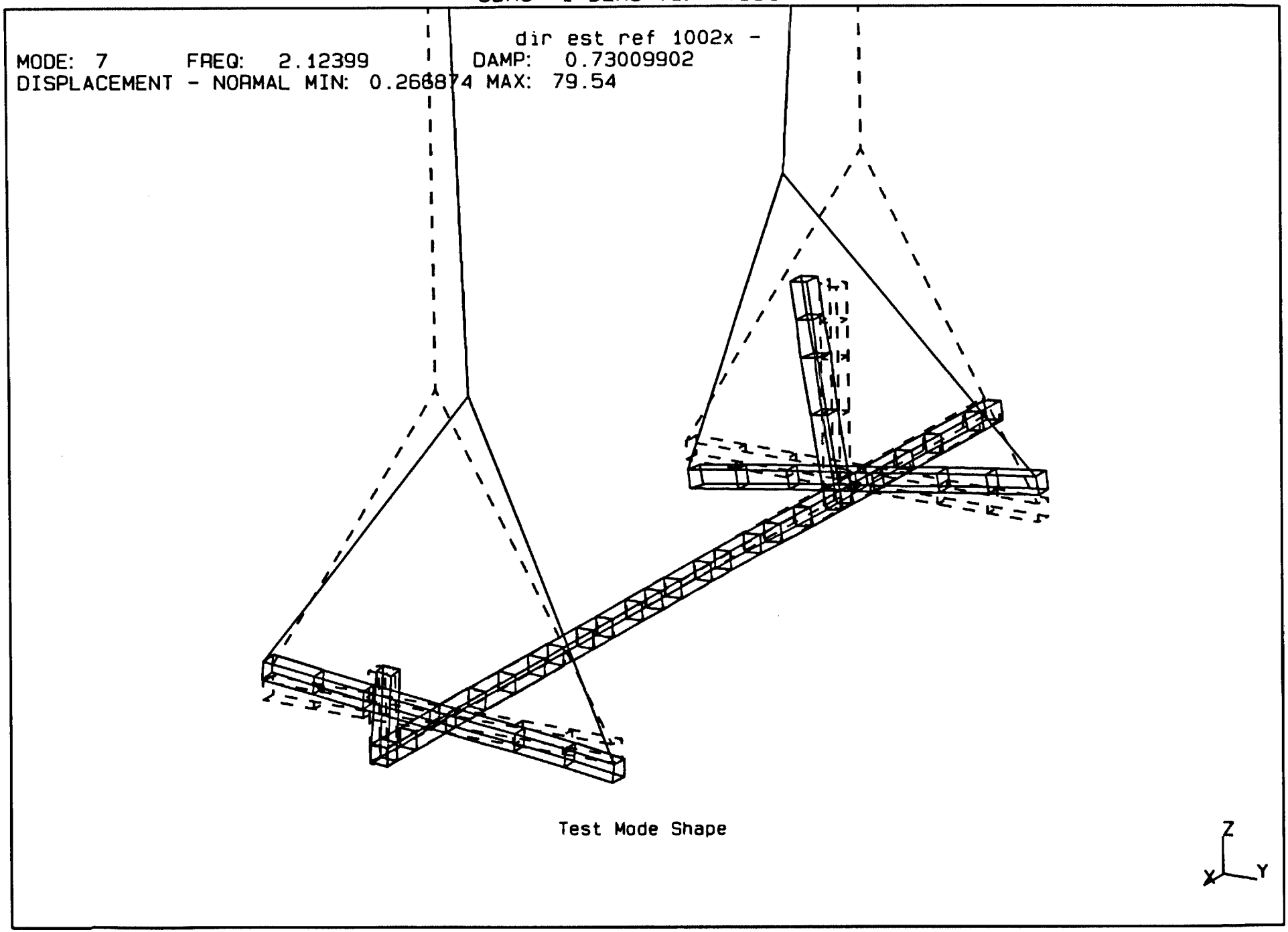

Test Mode Shape

SDRC I-DEAS VI: Test

MODE: 9 FREQ: 2.7598000 DAMP: 0.1
DISPLACEMENT - NORMAL MIN: 0.002970 MAX: 8.42

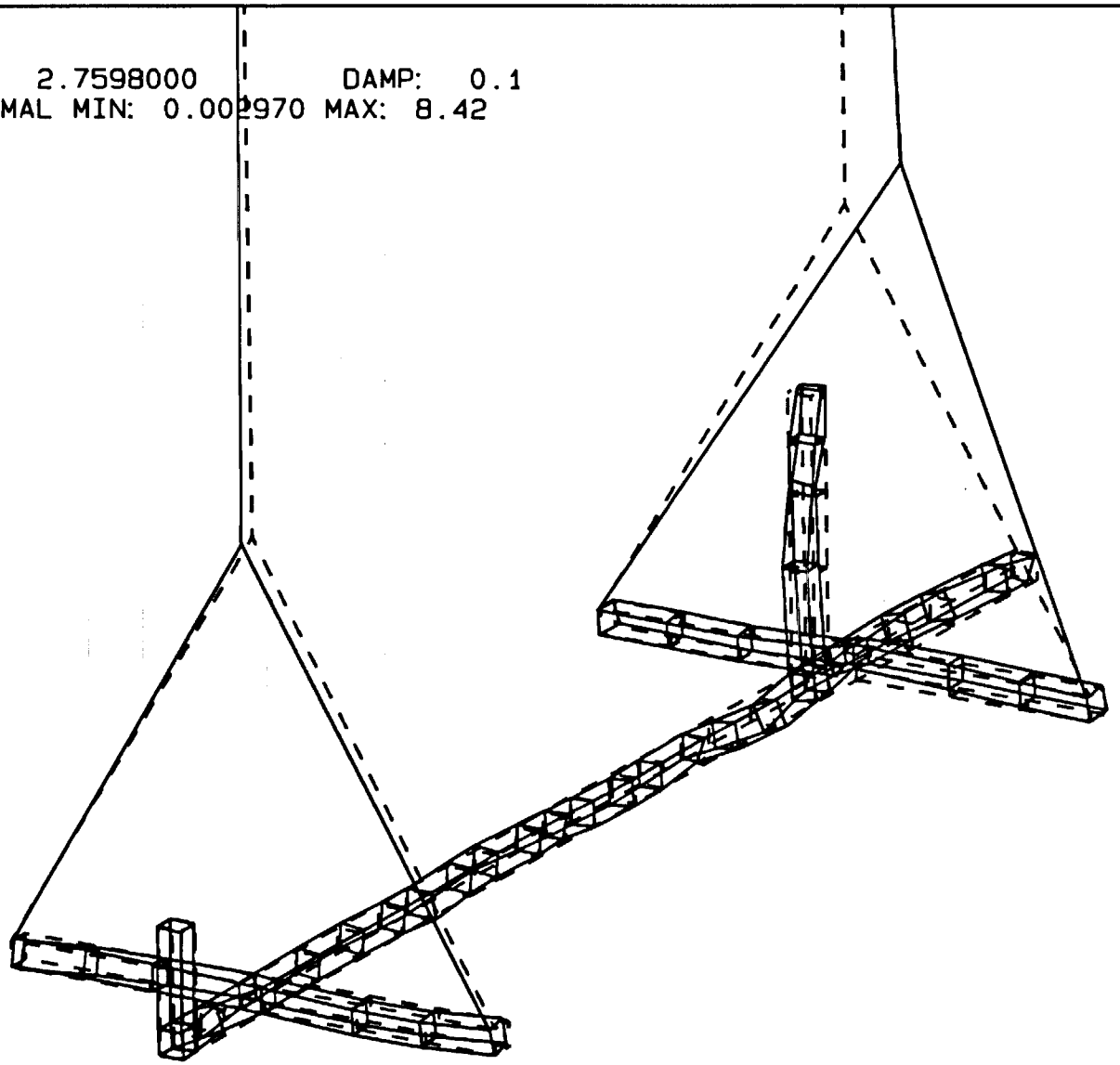

Test Mode Shape

SDRC I-DEAS VI: Test

MODE: 11 FREQ: 2.89979 DAMP: 0.1
DISPLACEMENT - NORMAL MIN: 0.043892 MAX: 9.94

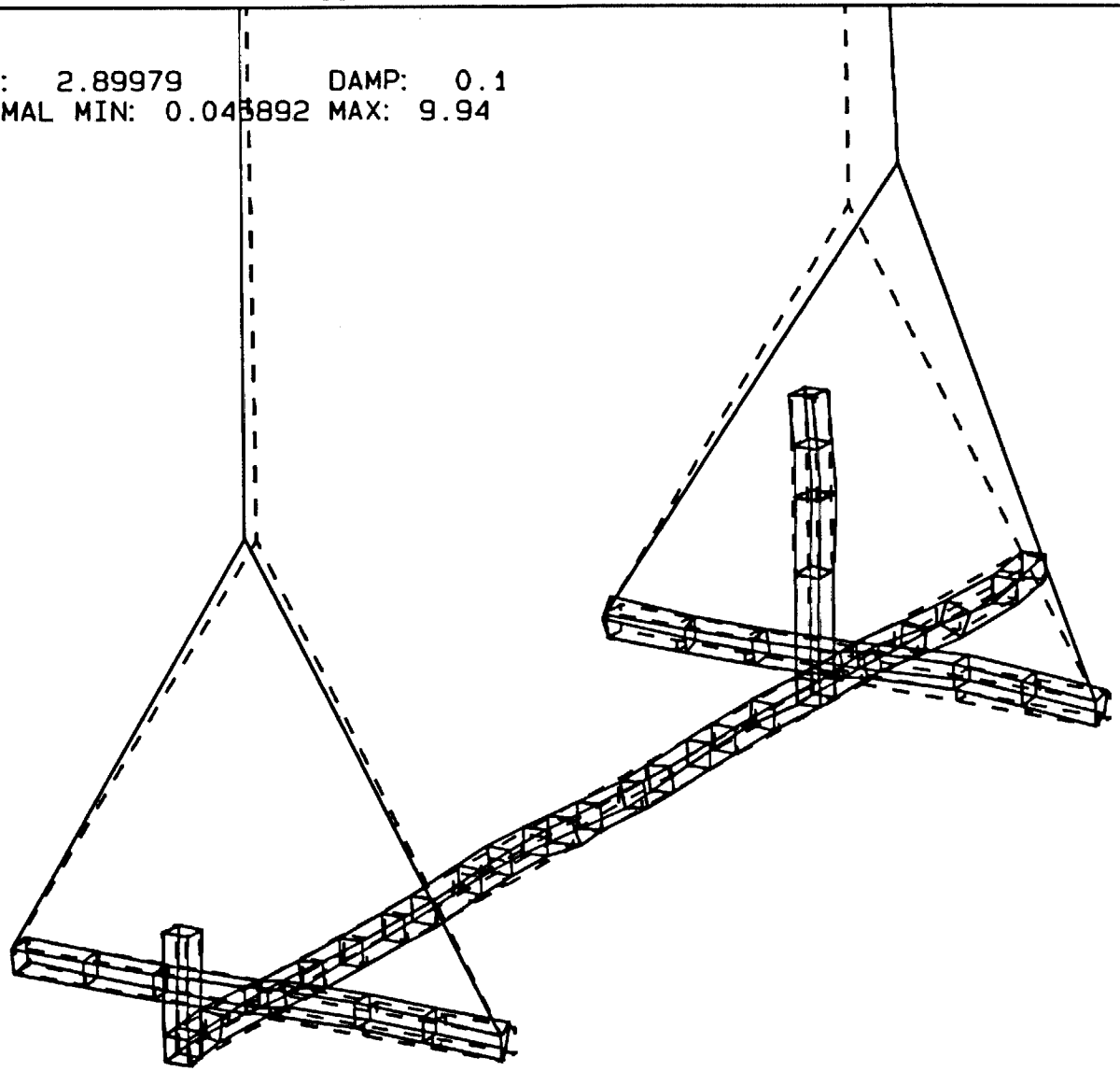

Test Mode Shape

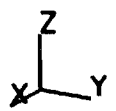

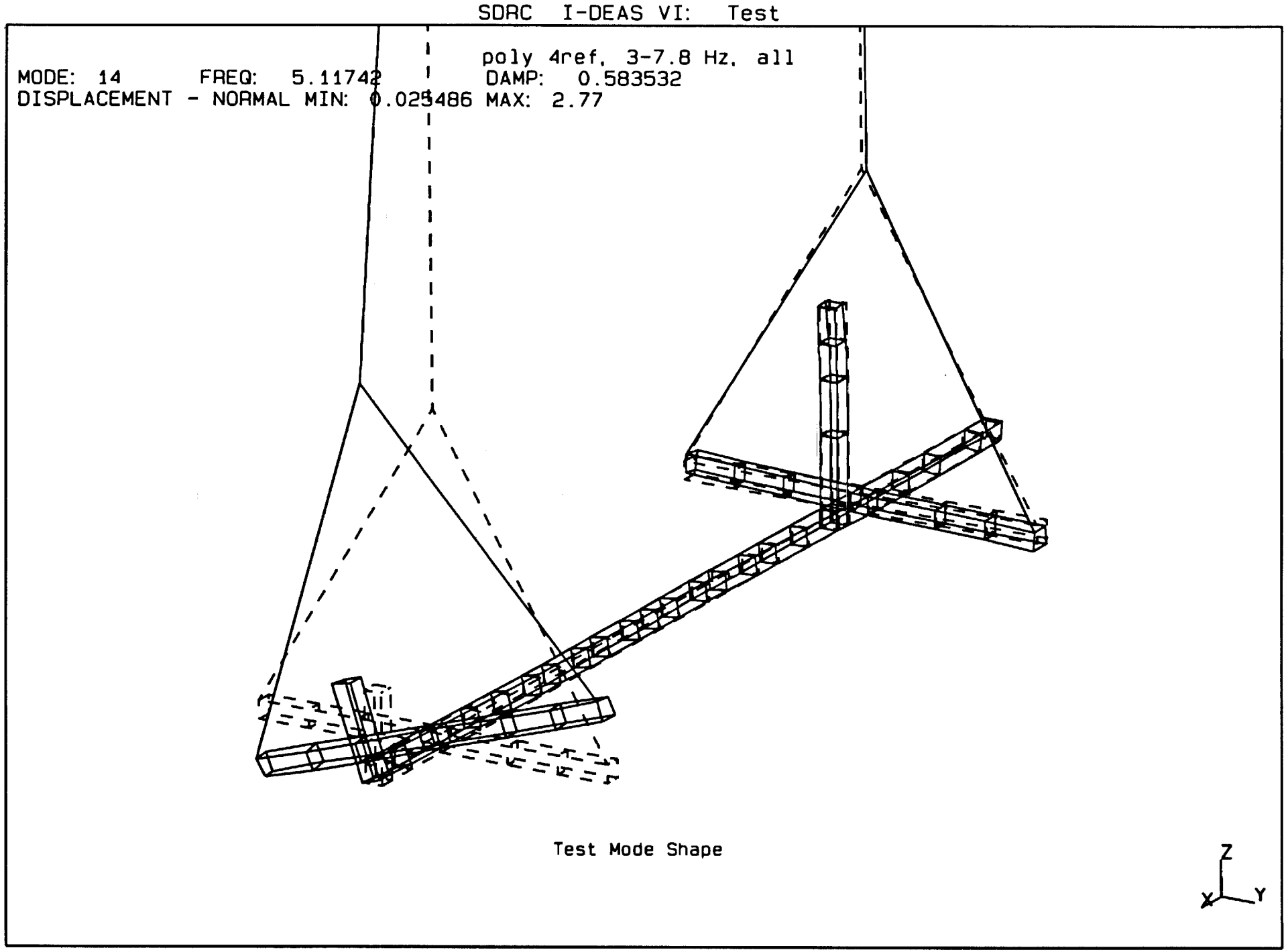
SDRC I-DEAS VI: Test
poly 4ref, 3-7.8 Hz, all
MODE: 14 FREQ: 5.11742 DAMP: 0.583532
DISPLACEMENT - NORMAL MIN: 0.025486 MAX: 2.77
Test Mode Shape
Z
X
Y

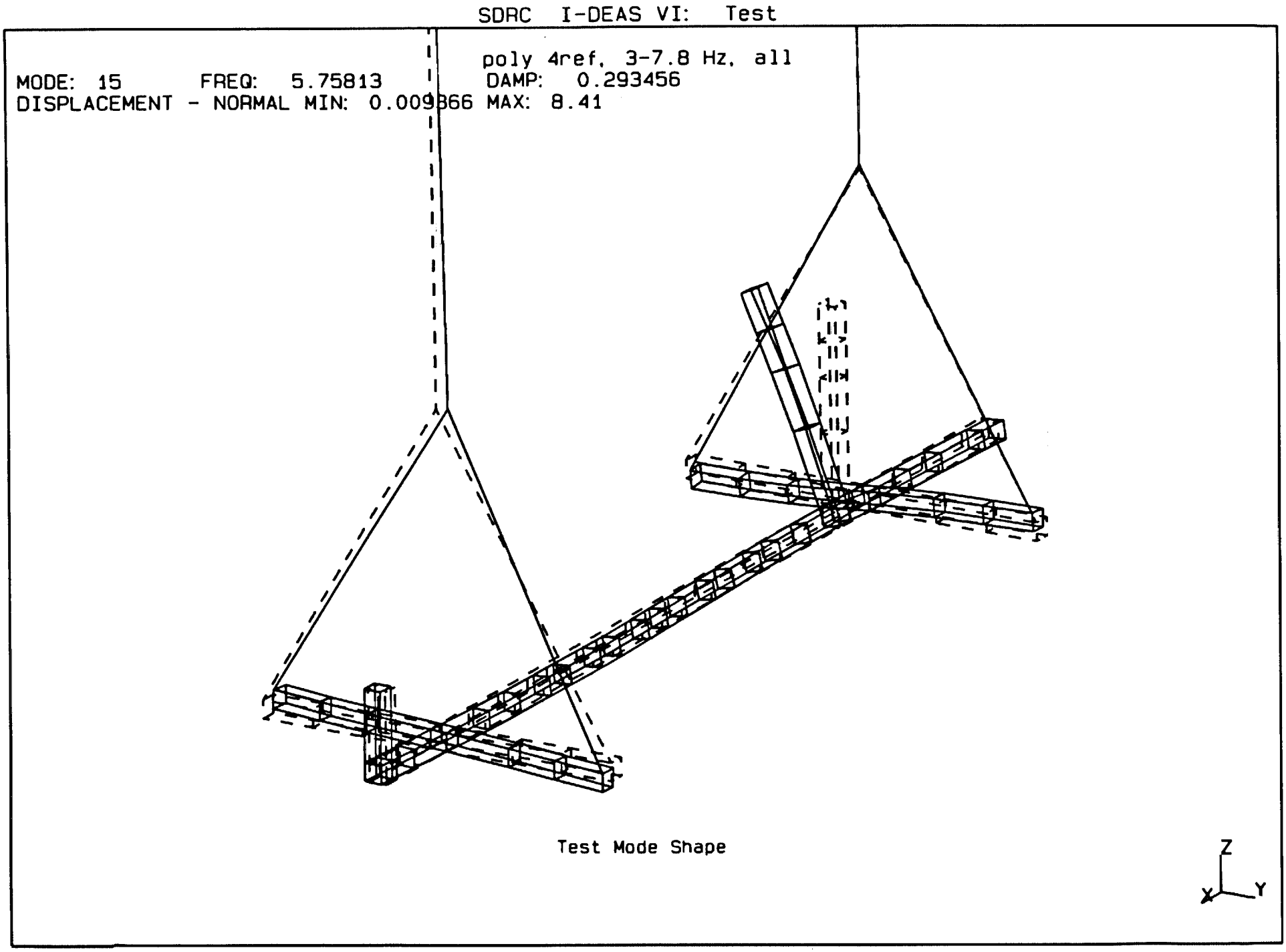
SDRC I-DEAS VI: Test
poly 4ref, 3-7.8 Hz, all
MODE: 15 FREQ: 5.75813
DAMP: 0.293456
DISPLACEMENT - NORMAL MIN: 0.009866 MAX: 8.41
Test Mode Shape
Z
Y
X

SDRC I-DEAS VI: Test

MODE: 17 FREQ: 7.41646
DISPLACEMENT - NORMAL MIN: 0.004629

poly 4ref, 3-7.8 Hz, all
DAMP: 2.75666
MAX: 0.621006

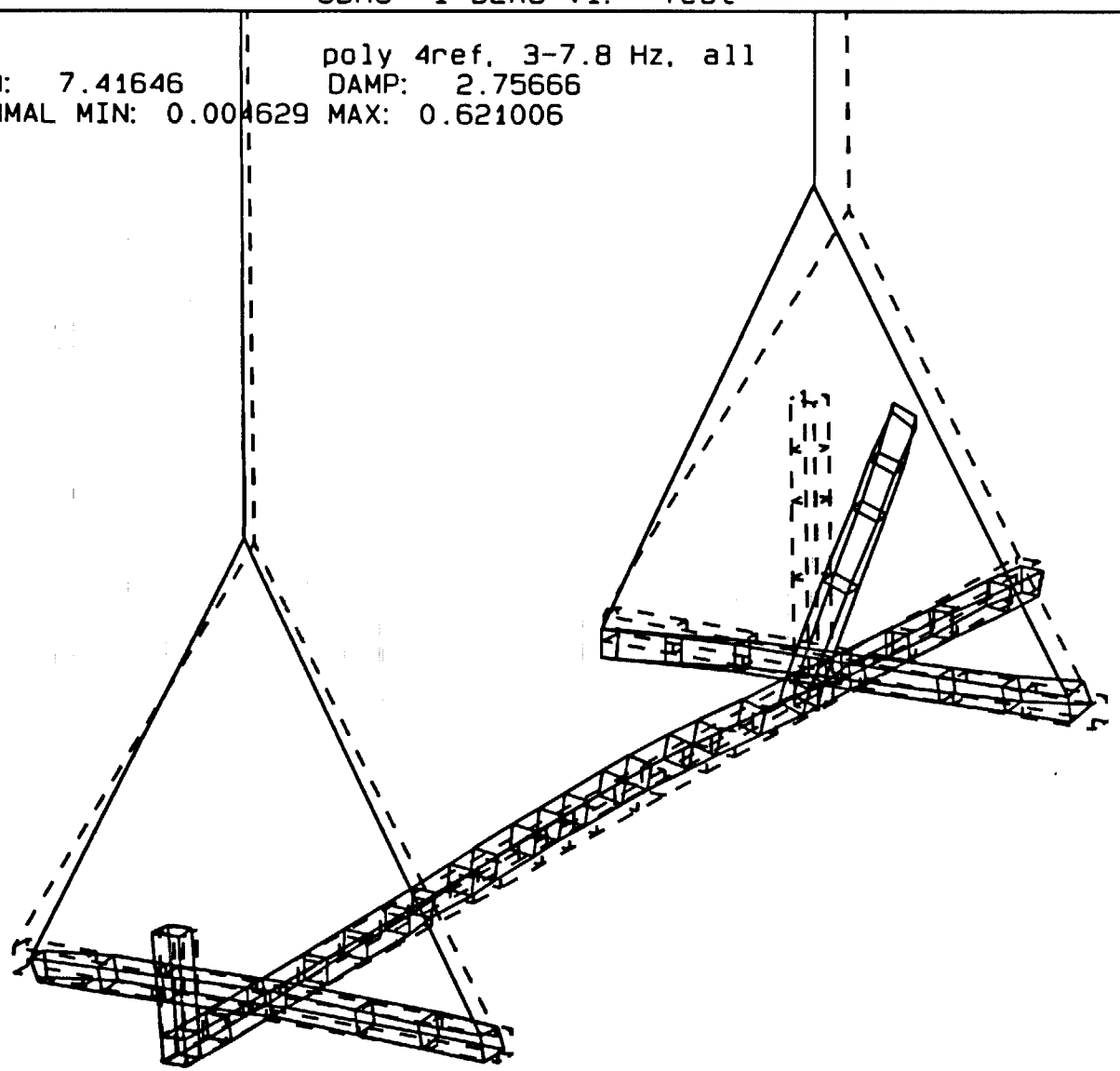

Test Mode Shape

poly 4ref, 3-7.8 Hz, all

MODE: 18 FREQ: 7.5473199 DAMP: 2.82354

DISPLACEMENT - NORMAL MIN: 0.005374 MAX: 2.55

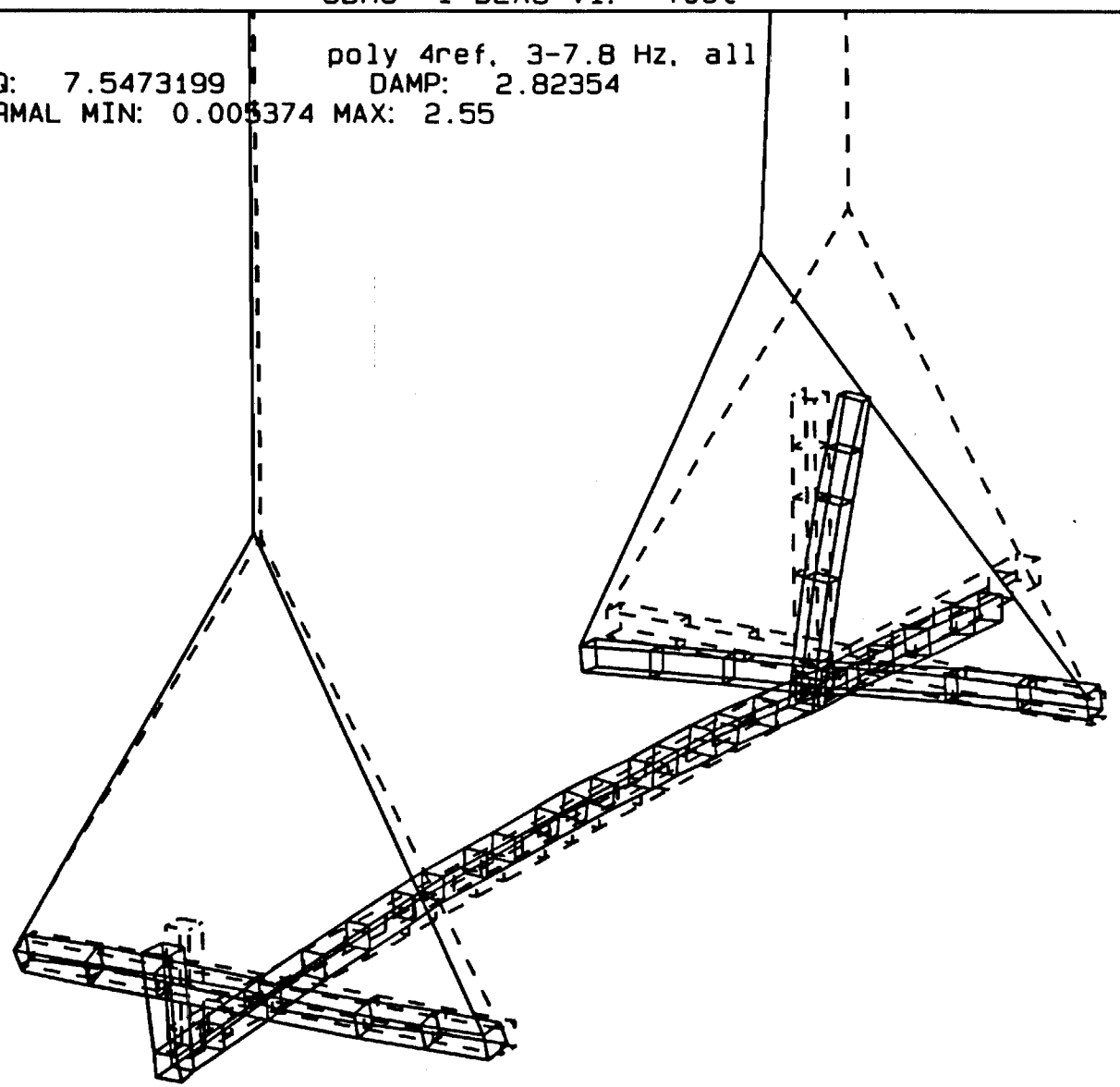

Test Mode Shape

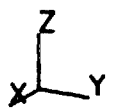

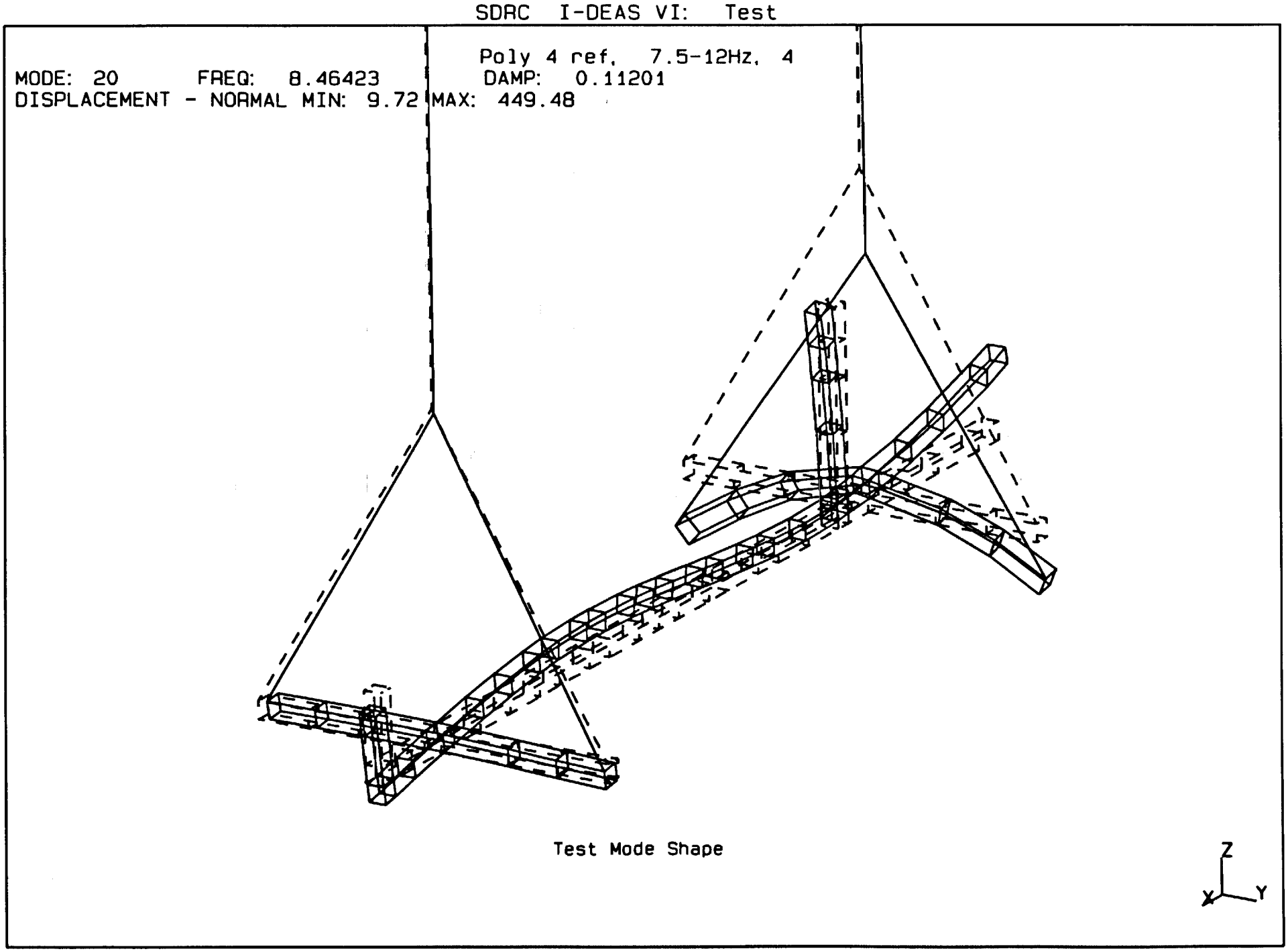
SDRC I-DEAS VI: Test
Poly 4 ref, 7.5-12Hz, 4
MODE: 20 FREQ: 8.46423
DAMP: 0.11201
DISPLACEMENT - NORMAL MIN: 9.72 MAX: 449.48
Test Mode Shape
Z
X
Y

SDRC I-DEAS VI: Test

Poly 4 ref, 7.5-12Hz, 4
MODE: 21 FREQ: 8.64943 DAMP: 0.108741
DISPLACEMENT - NORMAL MIN: 0.079589 MAX: 5.90

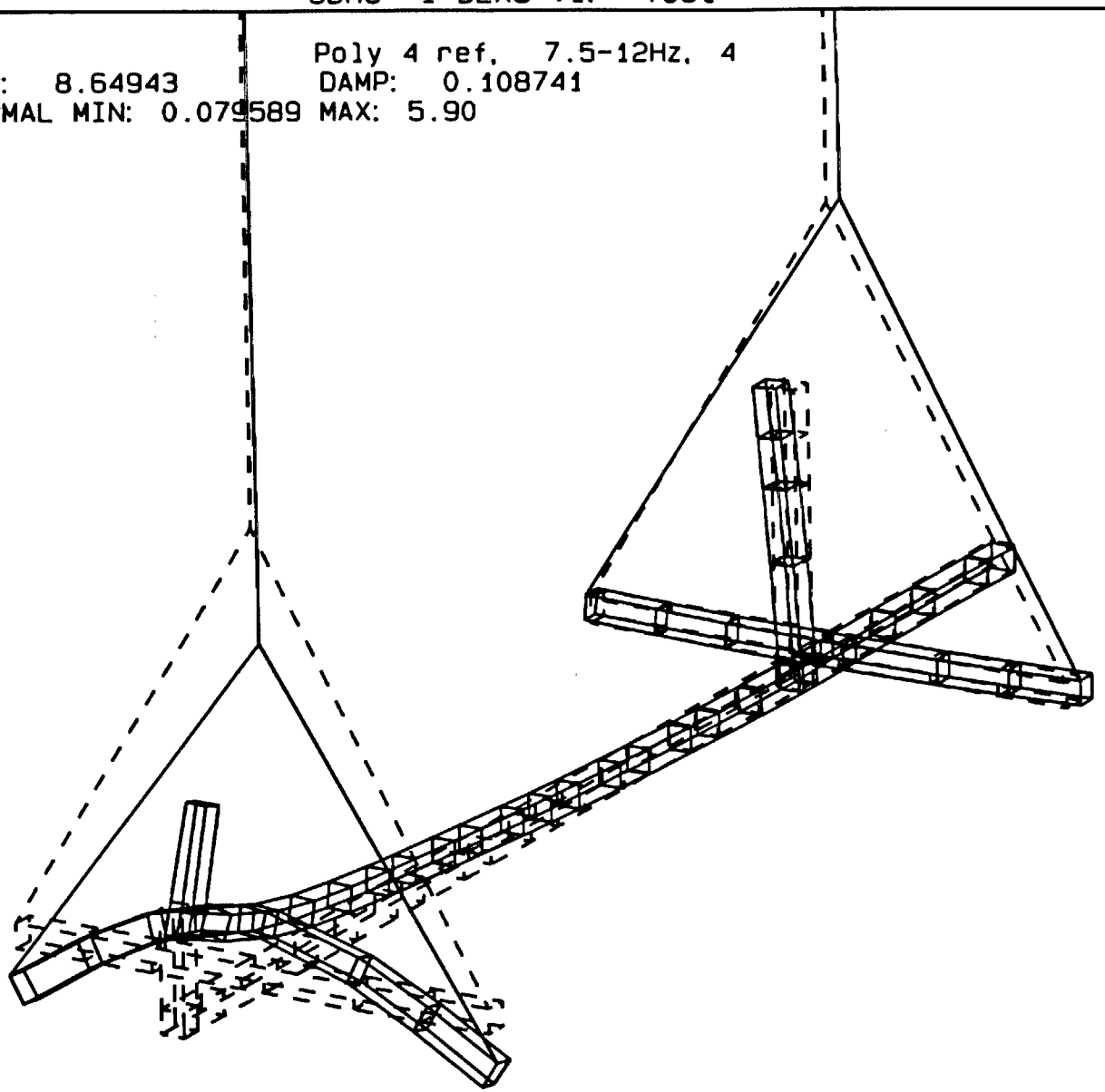

Test Mode Shape

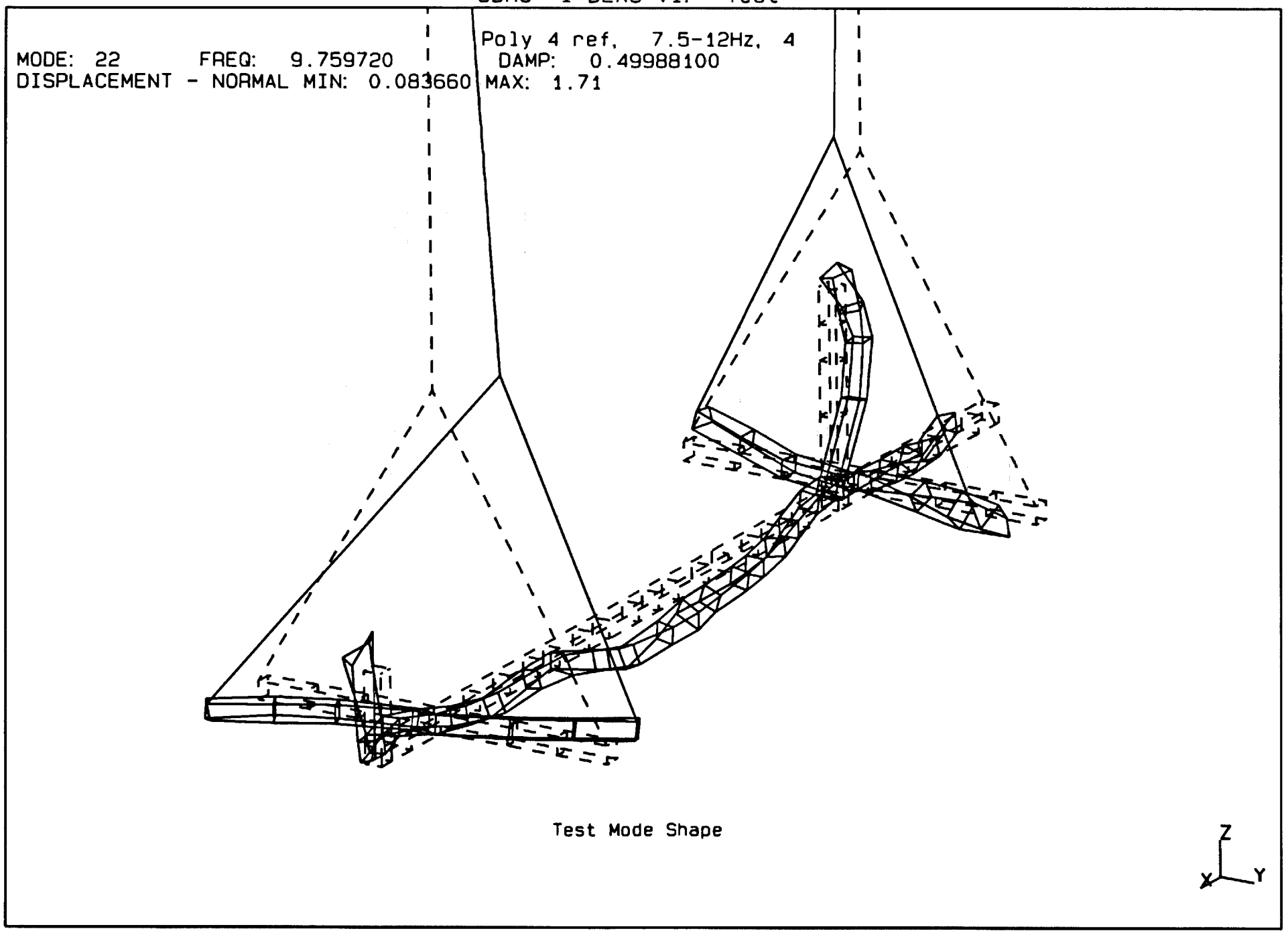
SDRC I-DEAS VI: Test
MODE: 22 FREQ: 9.759720
DISPLACEMENT - NORMAL MIN: 0.083660
Poly 4 ref, 7.5-12Hz, 4
DAMP: 0.49988100
MAX: 1.71
Test Mode Shape
Z
X
Y

SDRC I-DEAS VI: Test

MODE: 23 FREQ: 9.848190
DISPLACEMENT - NORMAL MIN: 0.004121 MAX: 16.31

Poly 4 ref, 7.5-12Hz, 4
DAMP: 0.9480250

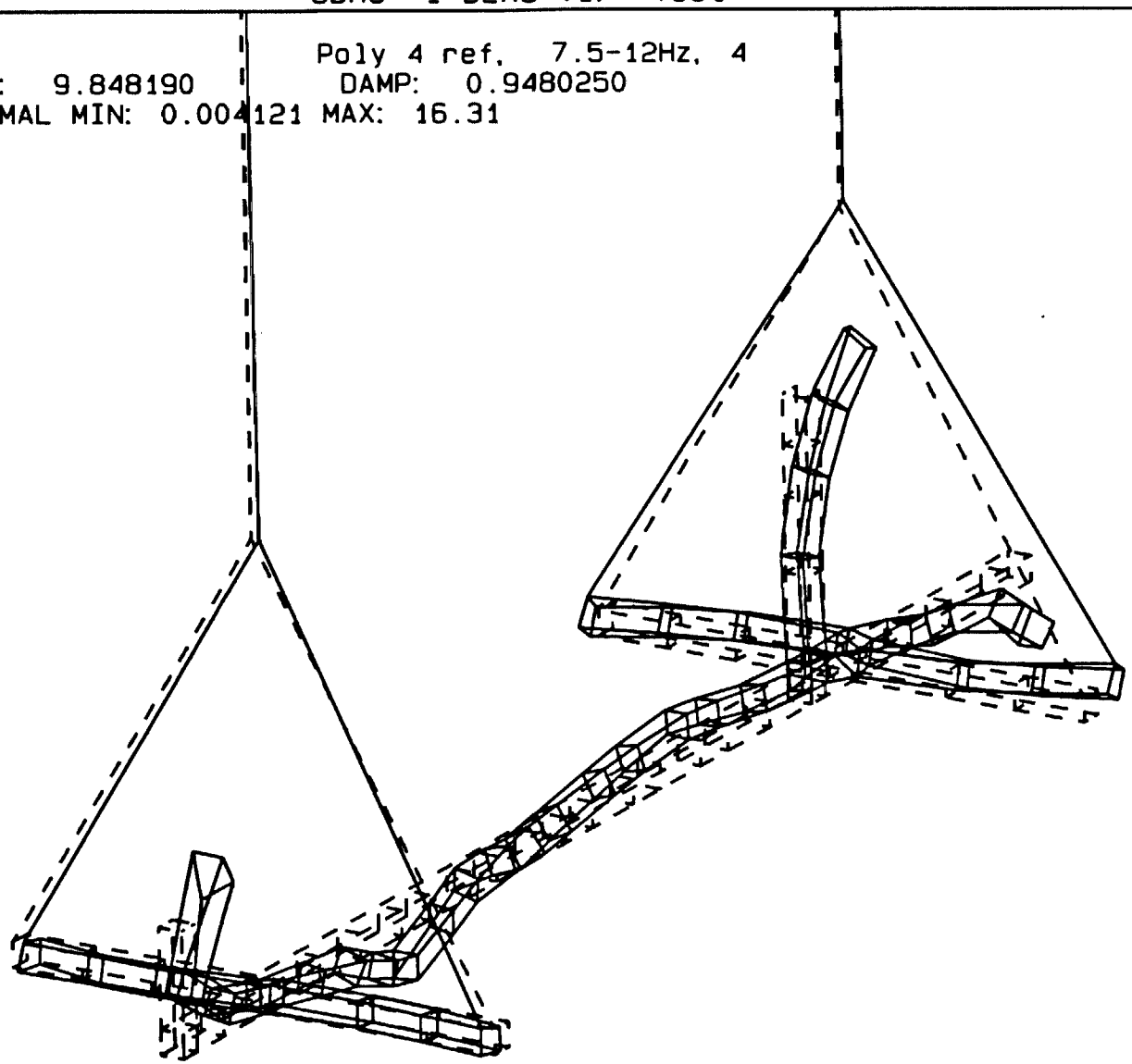

Test Mode Shape

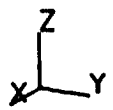

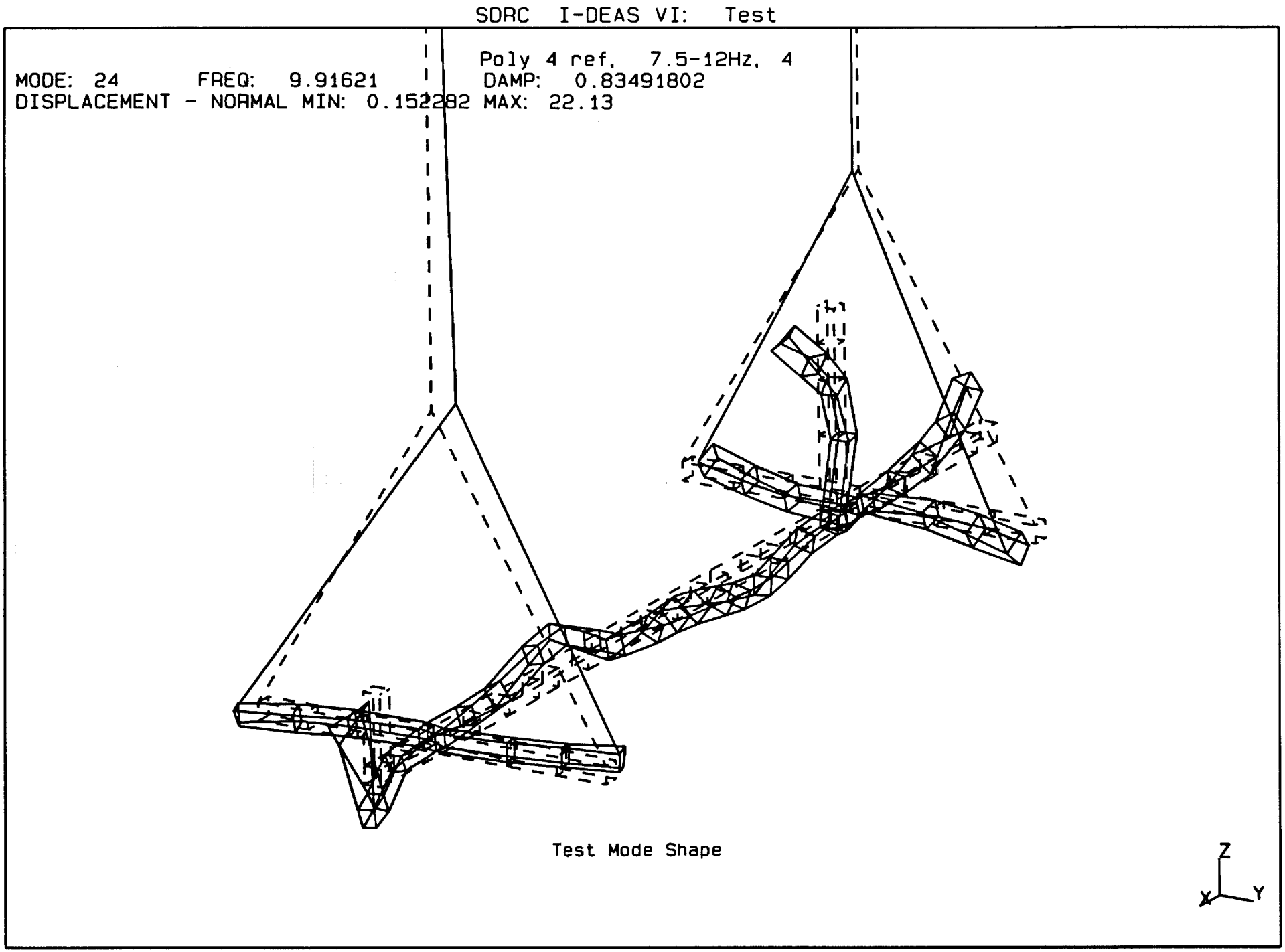
SDRC I-DEAS VI: Test
MODE: 24 FREQ: 9.91621
DISPLACEMENT - NORMAL MIN: 0.152282 MAX: 22.13
Poly 4 ref, 7.5-12Hz, 4
DAMP: 0.83491802
Test Mode Shape
Z
X
Y

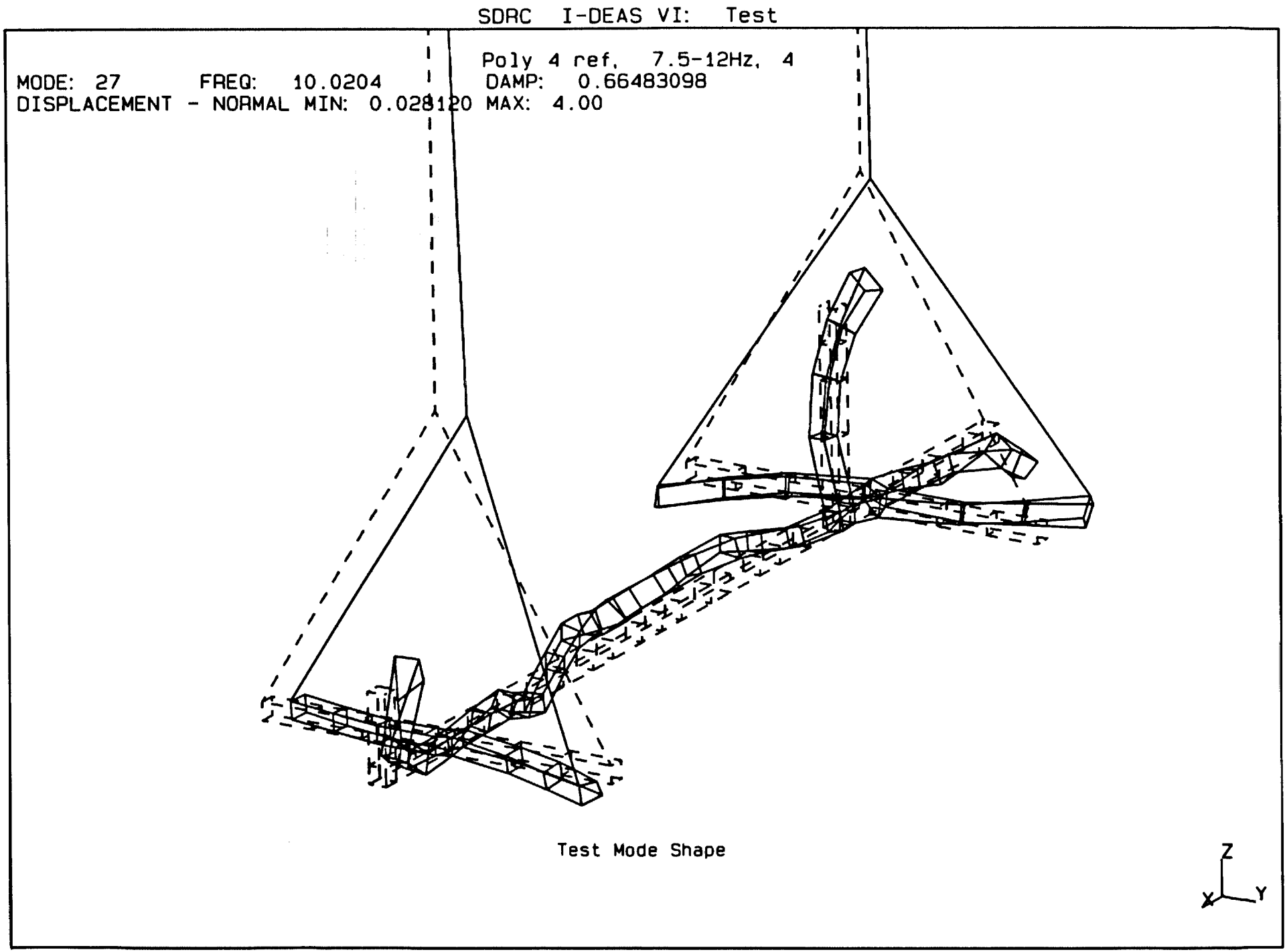
SDRC I-DEAS VI: Test
Poly 4 ref, 7.5-12Hz, 4
MODE: 27 FREQ: 10.0204
DAMP: 0.66483098
DISPLACEMENT - NORMAL MIN: 0.028120 MAX: 4.00
Test Mode Shape
Z
X
Y

SDRC I-DEAS VI: Test

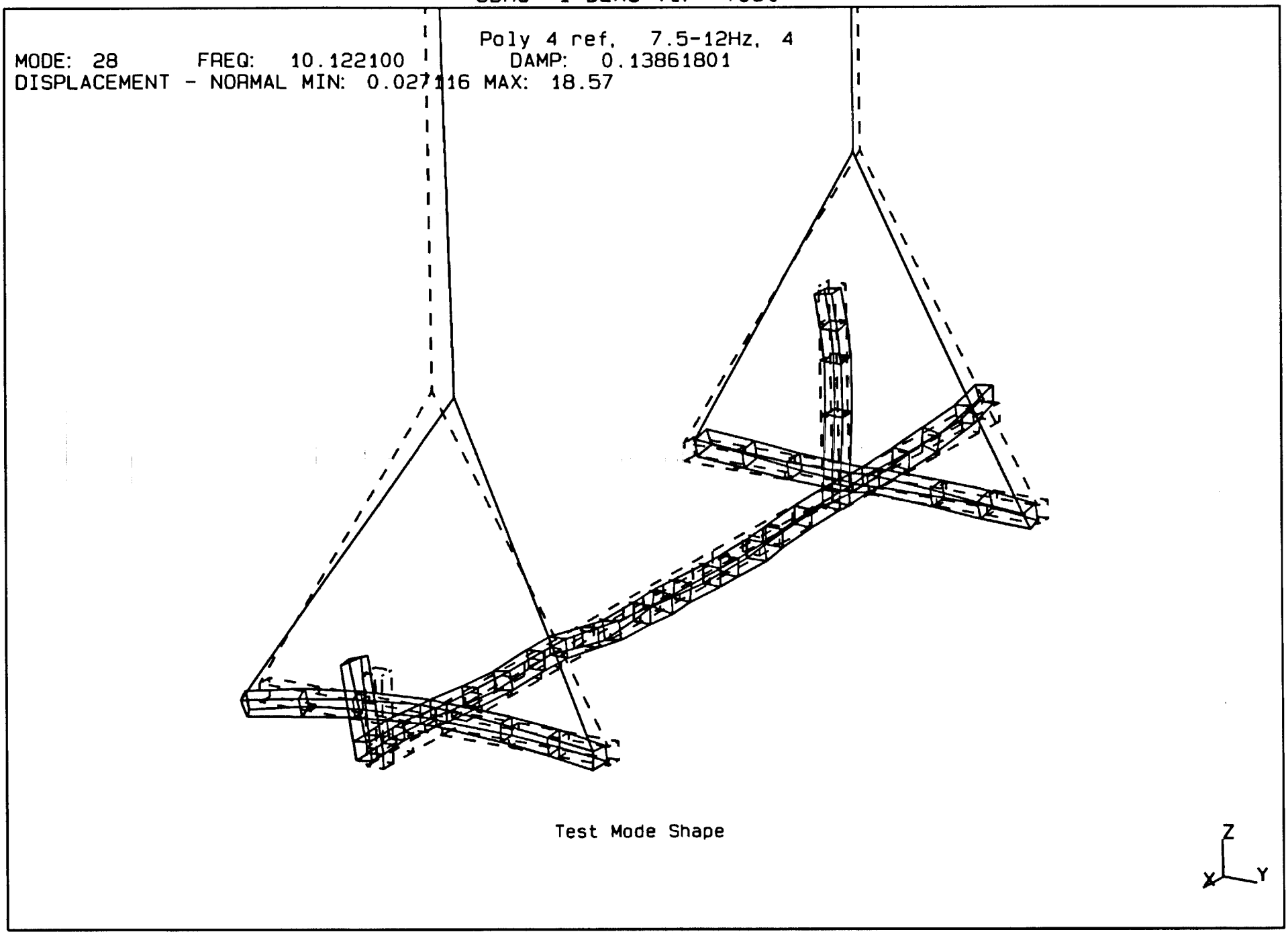

Test Mode Shape

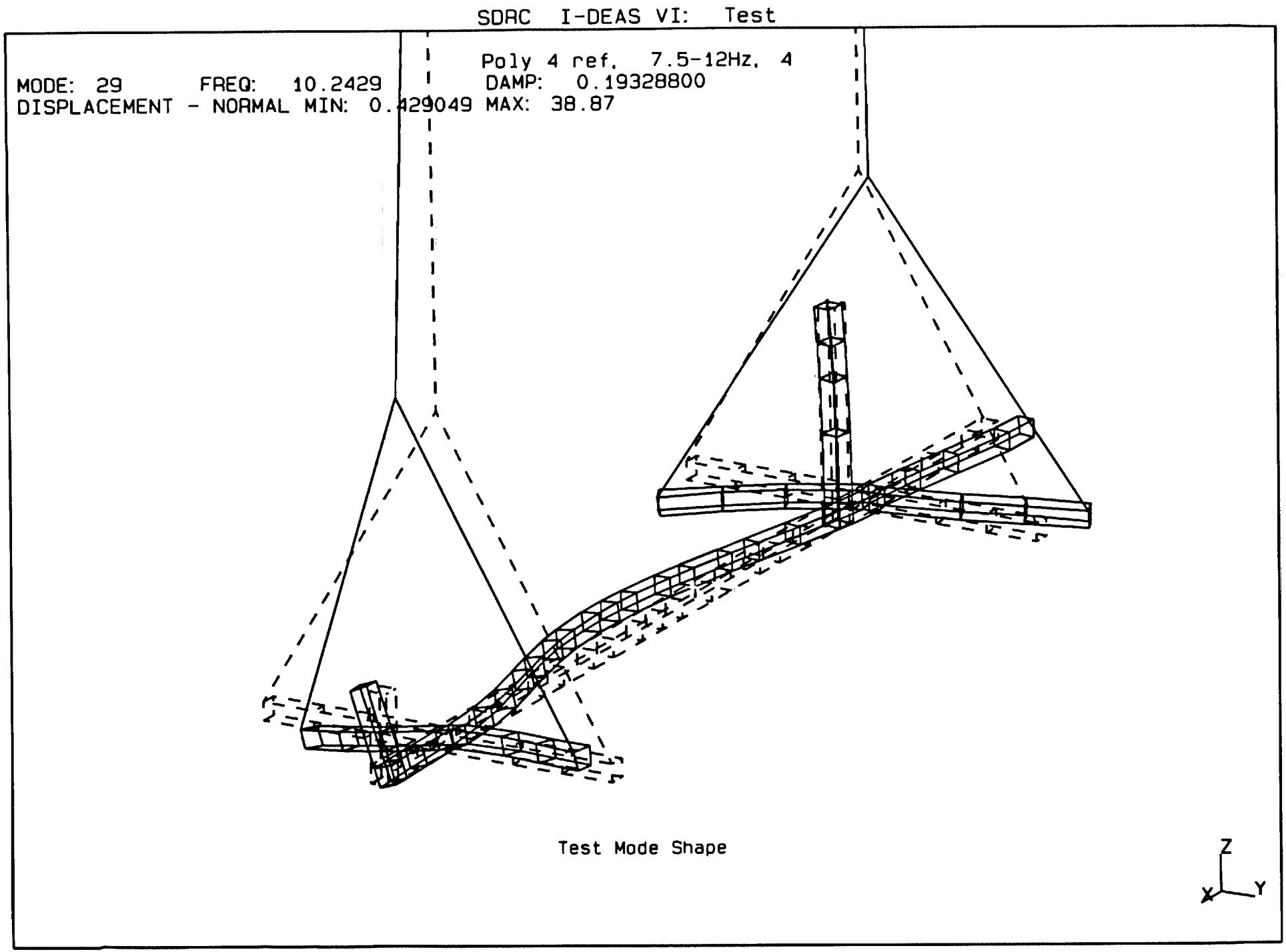
SDRC I-DEAS VI: Test
MODE: 29 FREQ: 10.2429
DISPLACEMENT - NORMAL MIN: 0.429049
Poly 4 ref, 7.5-12Hz, 4
DAMP: 0.19328800
MAX: 38.87
Test Mode Shape
Z
X
Y

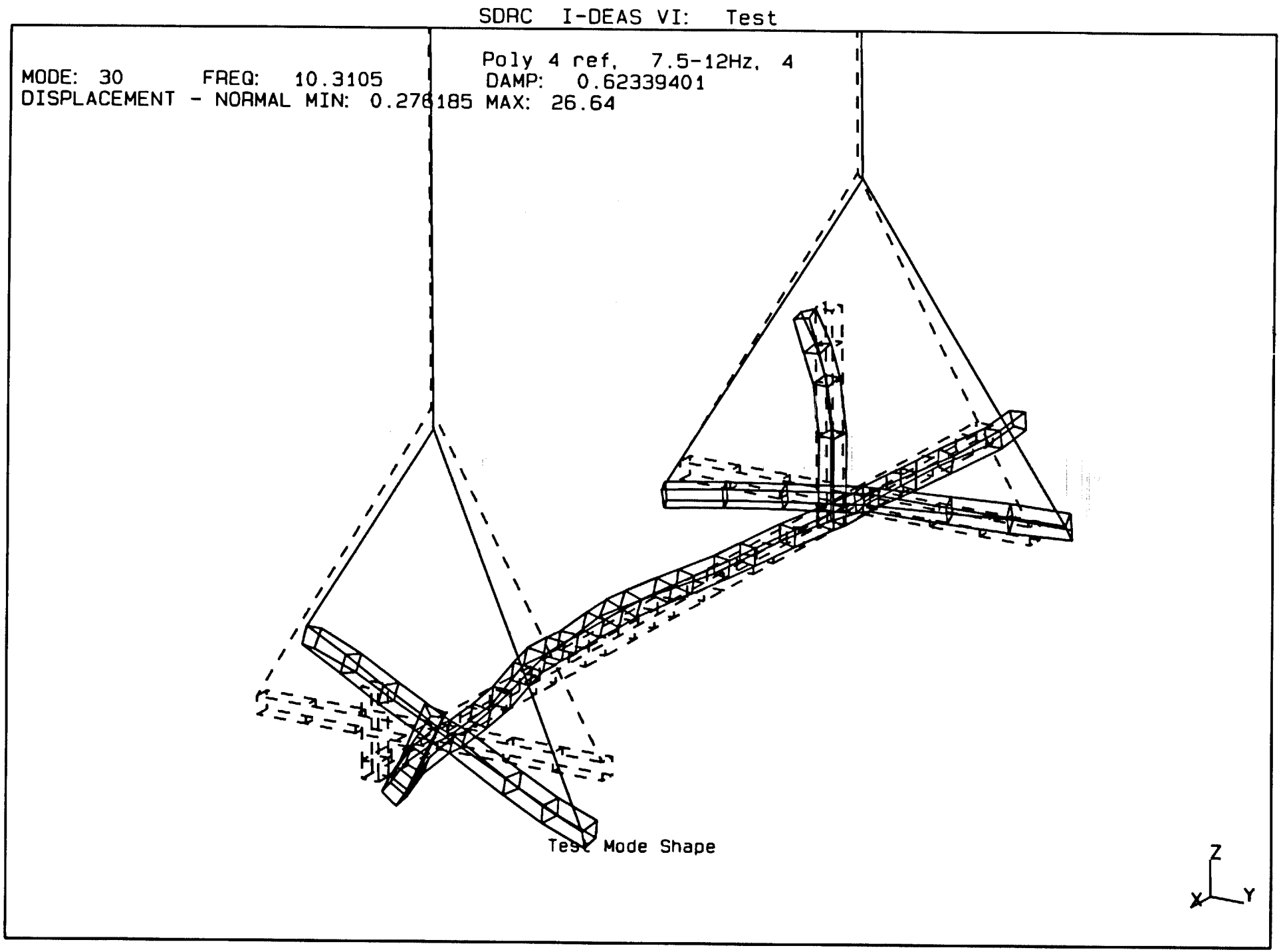
SDRC I-DEAS VI: Test
MODE: 30 FREQ: 10.3105
DISPLACEMENT - NORMAL MIN: 0.276185 MAX: 26.64
Poly 4 ref, 7.5-12Hz, 4
DAMP: 0.62339401
Test Mode Shape
Z
X
Y

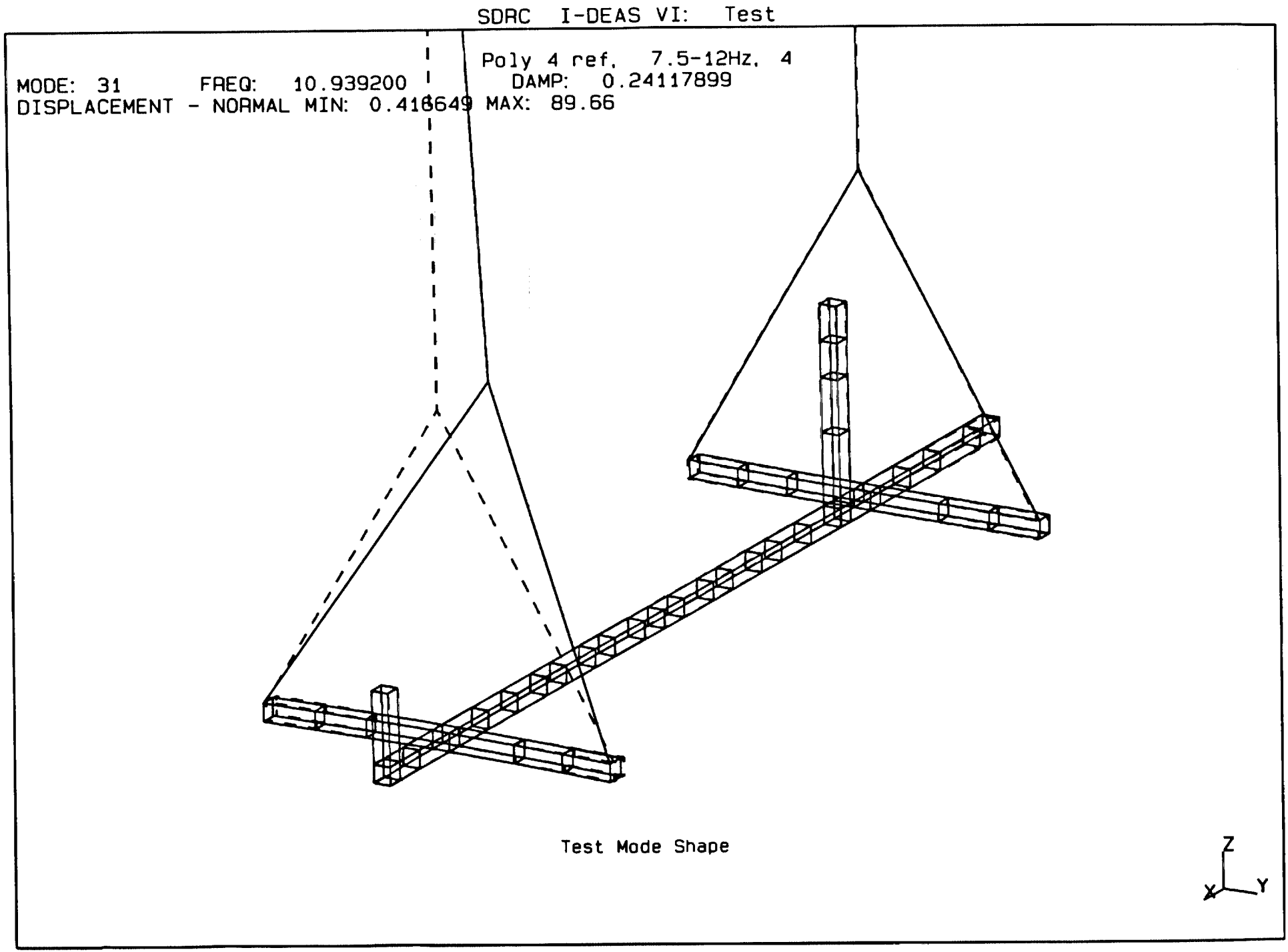
SDRC I-DEAS VI: Test
MODE: 31 FREQ: 10.939200
DISPLACEMENT - NORMAL MIN: 0.416649
Poly 4 ref, 7.5-12Hz, 4
DAMP: 0.24117899
MAX: 89.66
Test Mode Shape
Z
X
Y

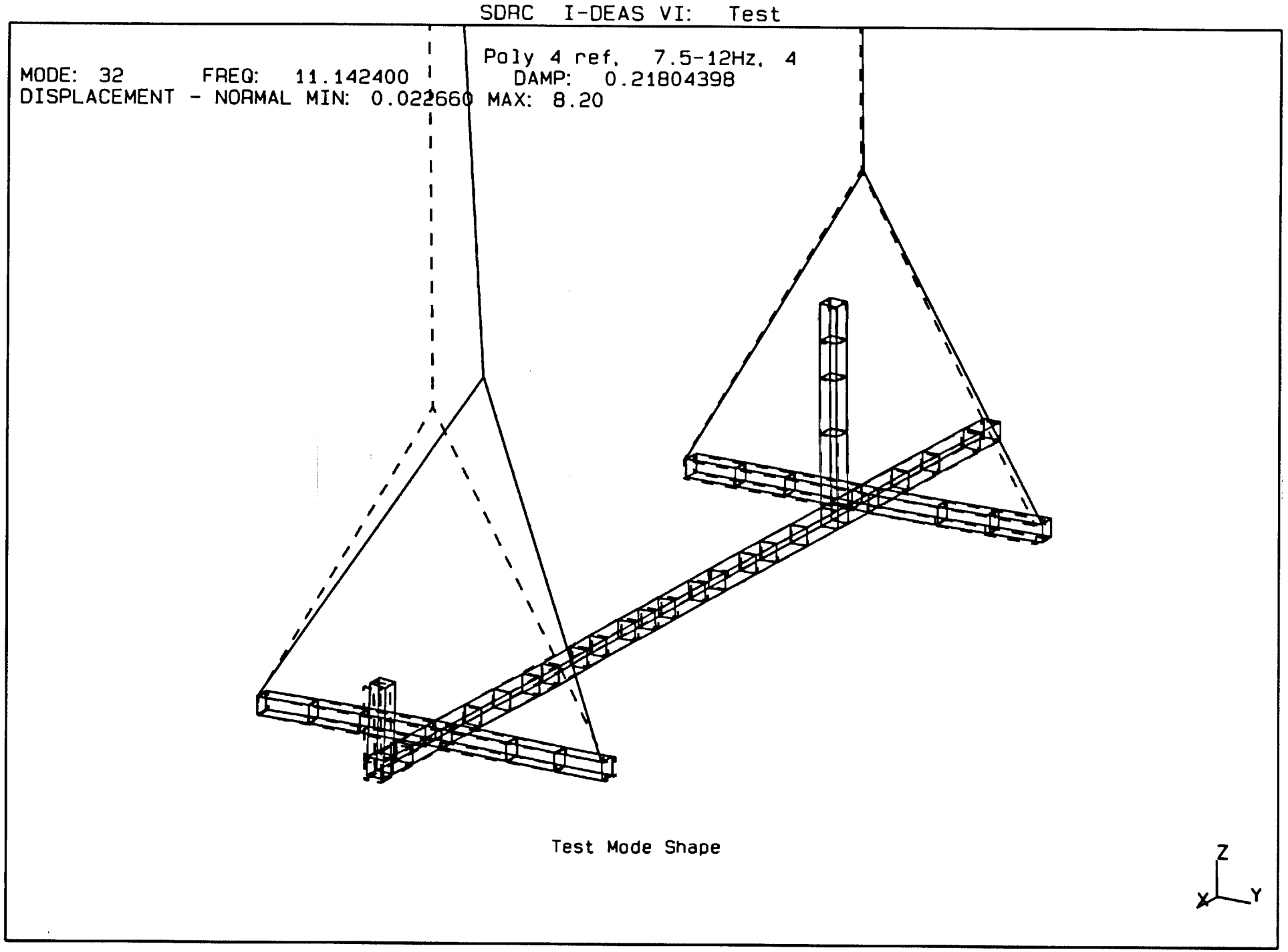
SDRC I-DEAS VI: Test
MODE: 32 FREQ: 11.142400
DISPLACEMENT - NORMAL MIN: 0.022660 MAX: 8.20
Poly 4 ref, 7.5-12Hz, 4
DAMP: 0.21804398
Test Mode Shape
Z
X
Y

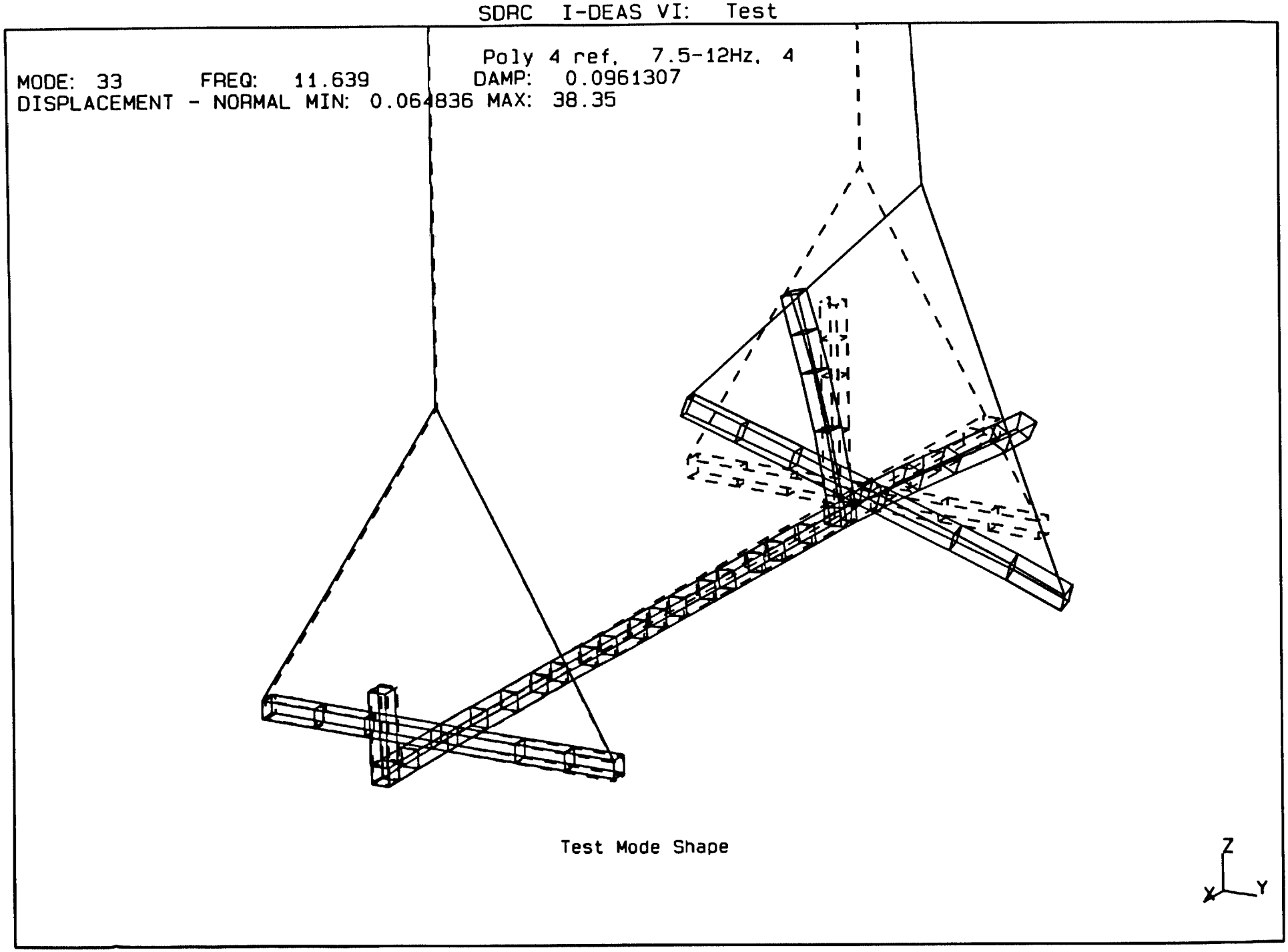
SDRC I-DEAS VI: Test
Poly 4 ref, 7.5-12Hz, 4
MODE: 33 FREQ: 11.639
DAMP: 0.0961307
DISPLACEMENT - NORMAL MIN: 0.064836 MAX: 38.35
Test Mode Shape
Z
X
Y

SDRC I-DEAS VI: Test

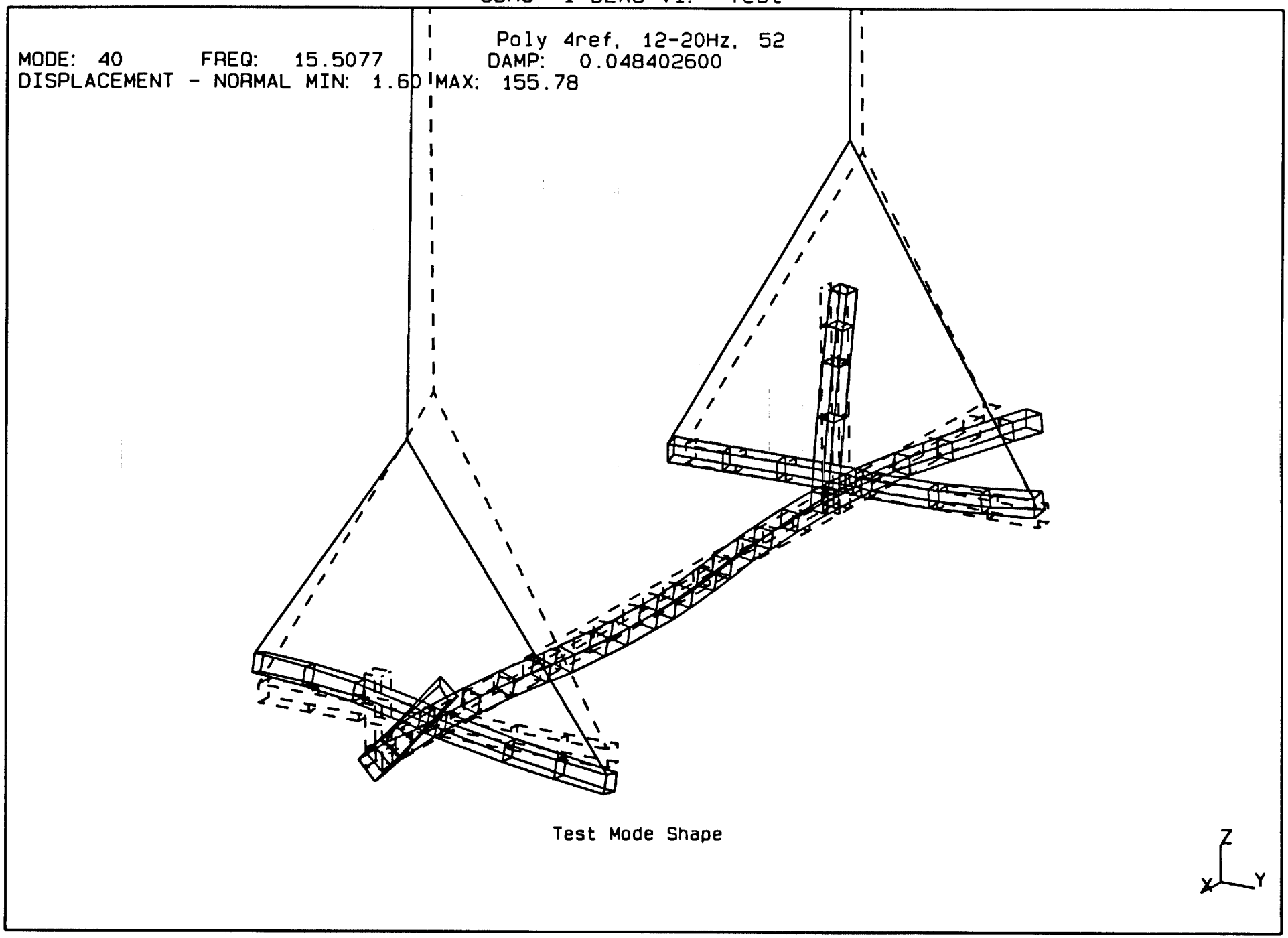

Test Mode Shape

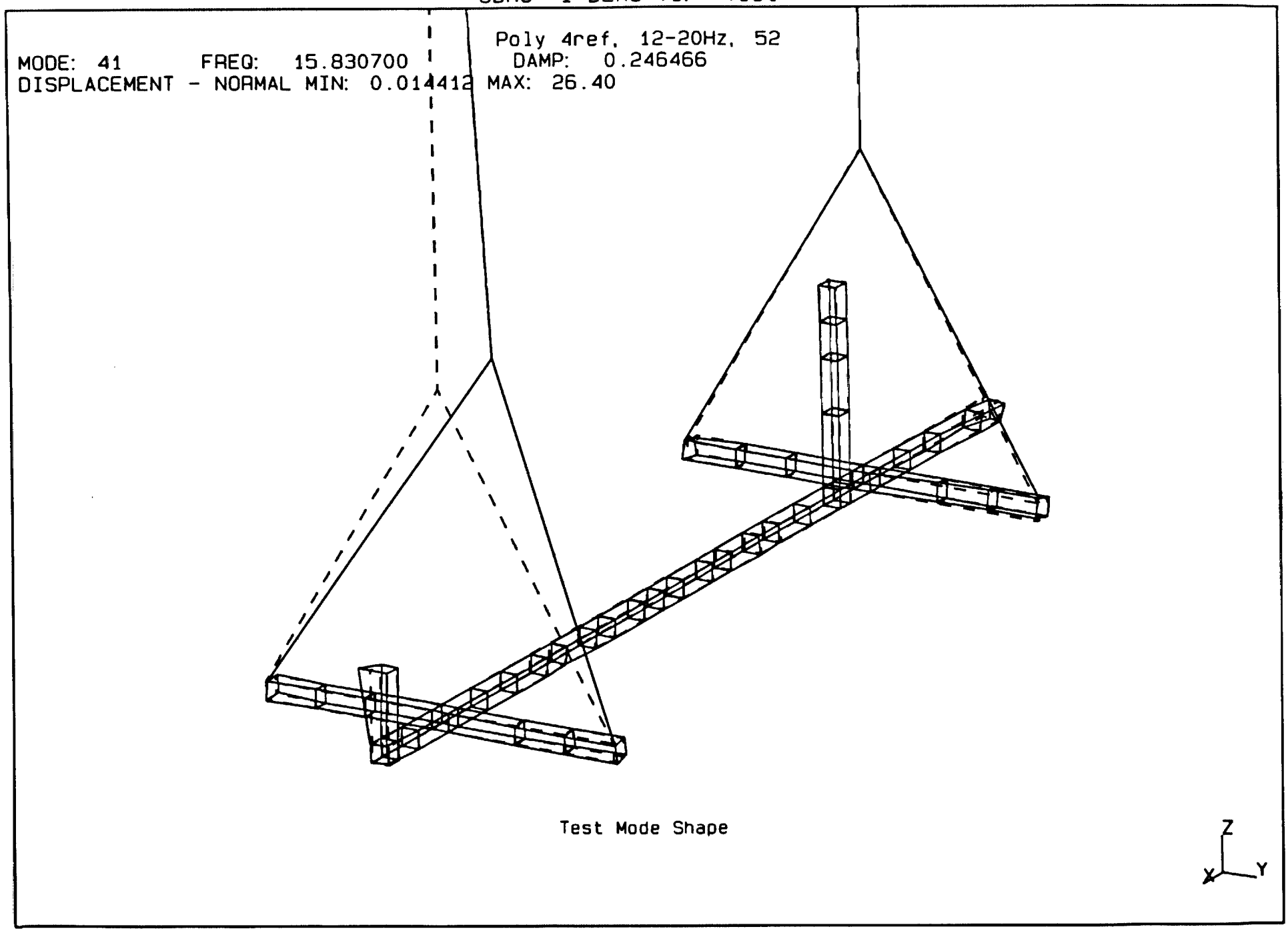
MODE: 41 FREQ: 15.830700
DISPLACEMENT - NORMAL MIN: 0.014412 MAX: 26.40
Poly 4ref, 12-20Hz, 52
DAMP: 0.246466
Test Mode Shape
Z
X
Y

SDRC I-DEAS VI: Test

MODE: 42 FREQ: 17.0271 Poly 4ref, 12-20Hz, 52
DAMP: 0.196211
DISPLACEMENT - NORMAL MIN: 0.137886 MAX: 15.91

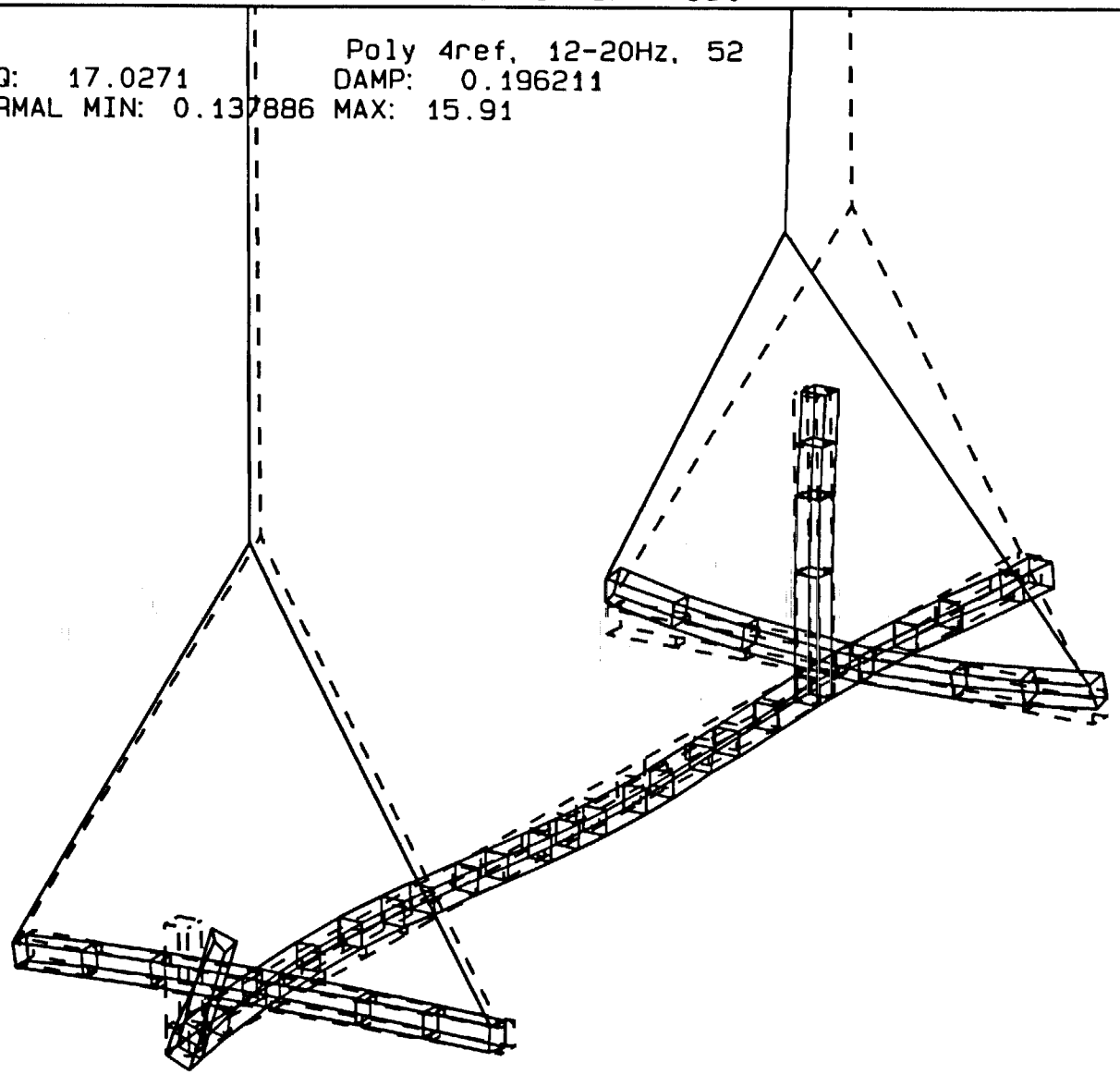

Test Mode Shape

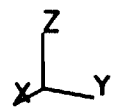

SDRC I-DEAS VI: Test

Poly 4ref, 12-20Hz, 52

MODE: 44 FREQ: 17.570700 DAMP: 0.041060798

DISPLACEMENT - NORMAL MIN: 6.77 MAX: 224.27

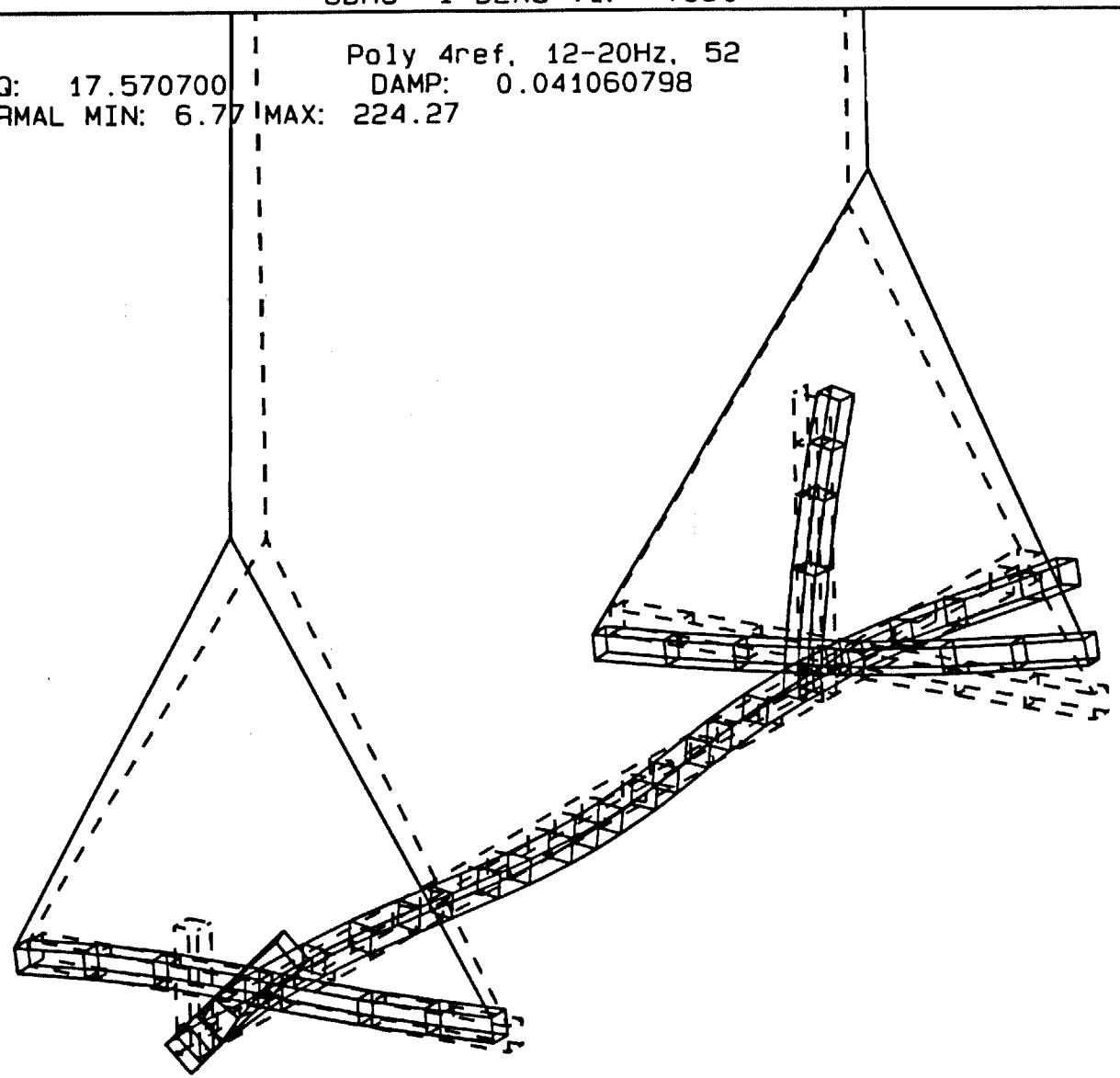

Test Mode Shape

SDRC I-DEAS VI: Test

Poly 4ref, 12-20Hz, 52
MODE: 45 FREQ: 17.9701 DAMP: 0.0977884
DISPLACEMENT - NORMAL MIN: 0.049196 MAX: 29.85

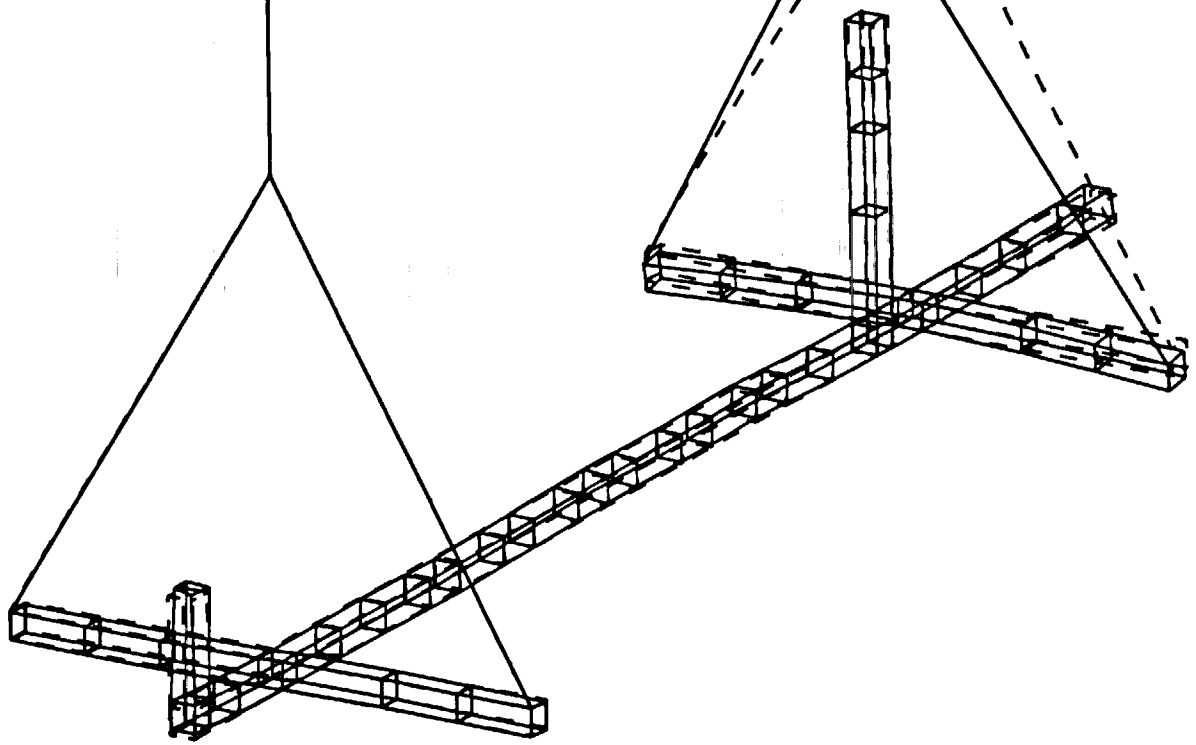

Test Mode Shape

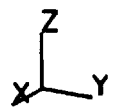

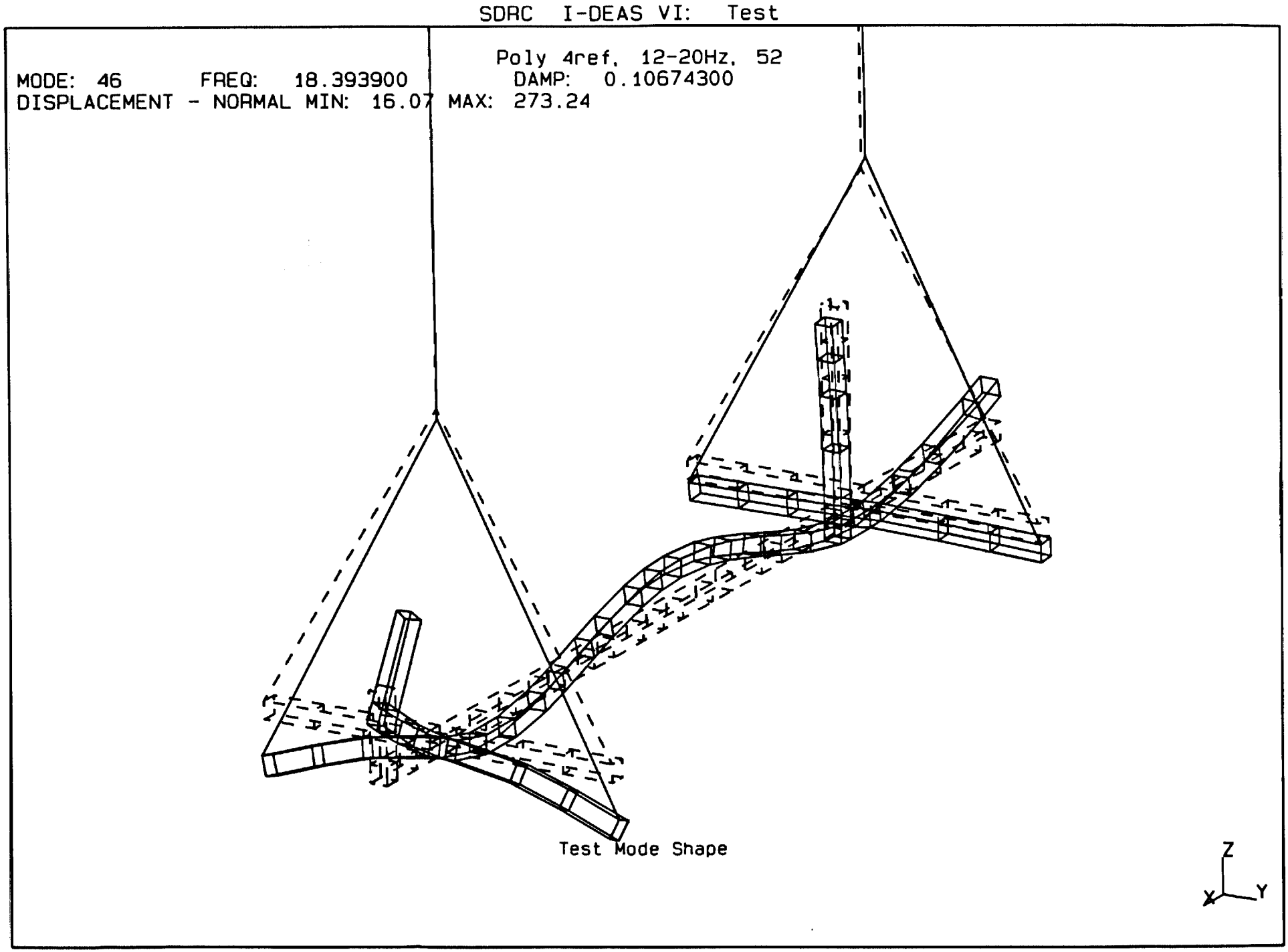
SDRC I-DEAS VI: Test
MODE: 46 FREQ: 18.393900
DISPLACEMENT - NORMAL MIN: 16.07 MAX: 273.24
Poly 4ref, 12-20Hz, 52
DAMP: 0.10674300
Test Mode Shape
Z
X
Y

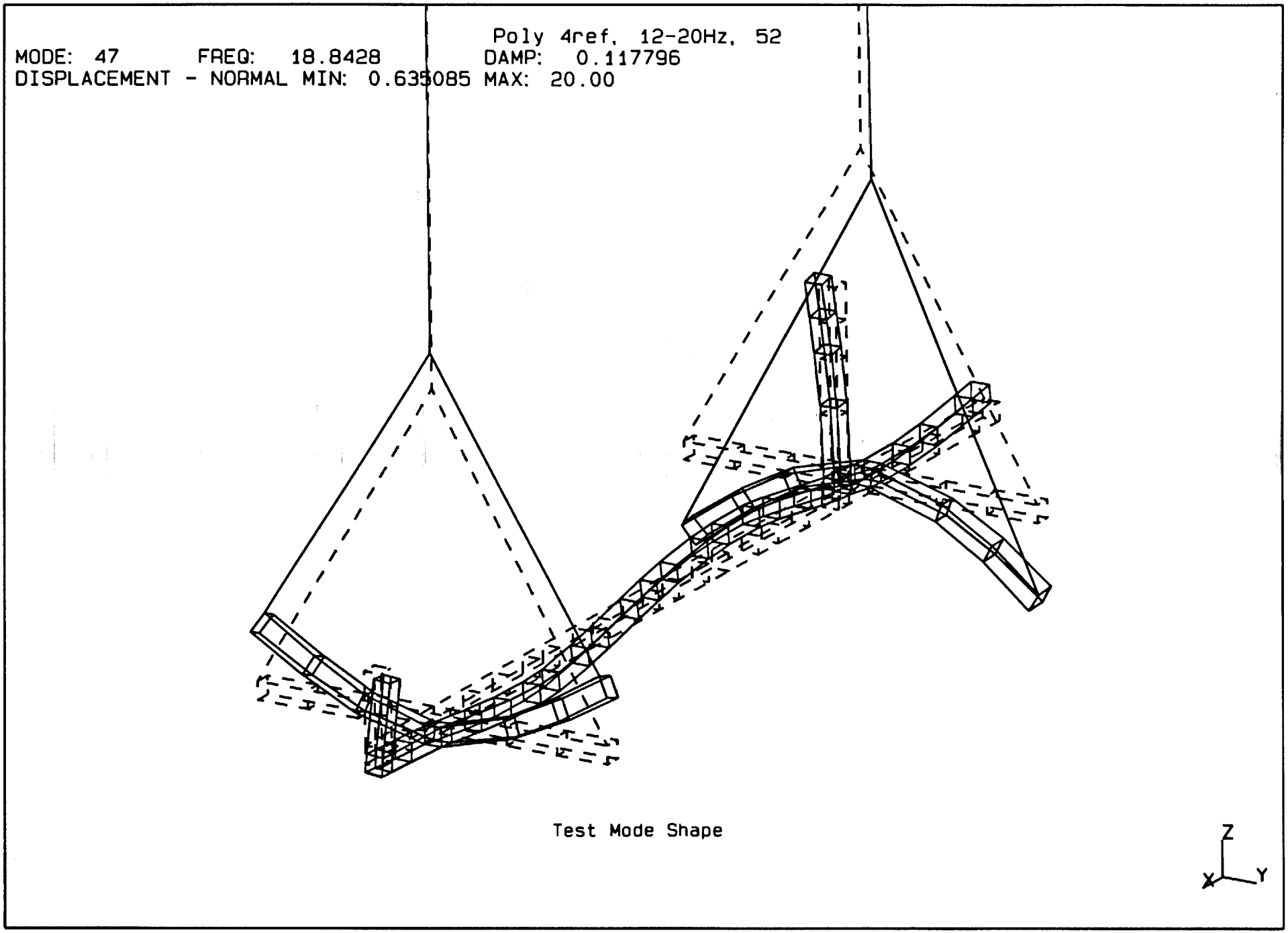
SDRC I-DEAS VI: Test
Poly 4ref, 12-20Hz, 52
MODE: 47 FREQ: 18.8428 DAMP: 0.117796
DISPLACEMENT - NORMAL MIN: 0.635085 MAX: 20.00
Test Mode Shape
Z
X
Y

SDRC I-DEAS VI: Test

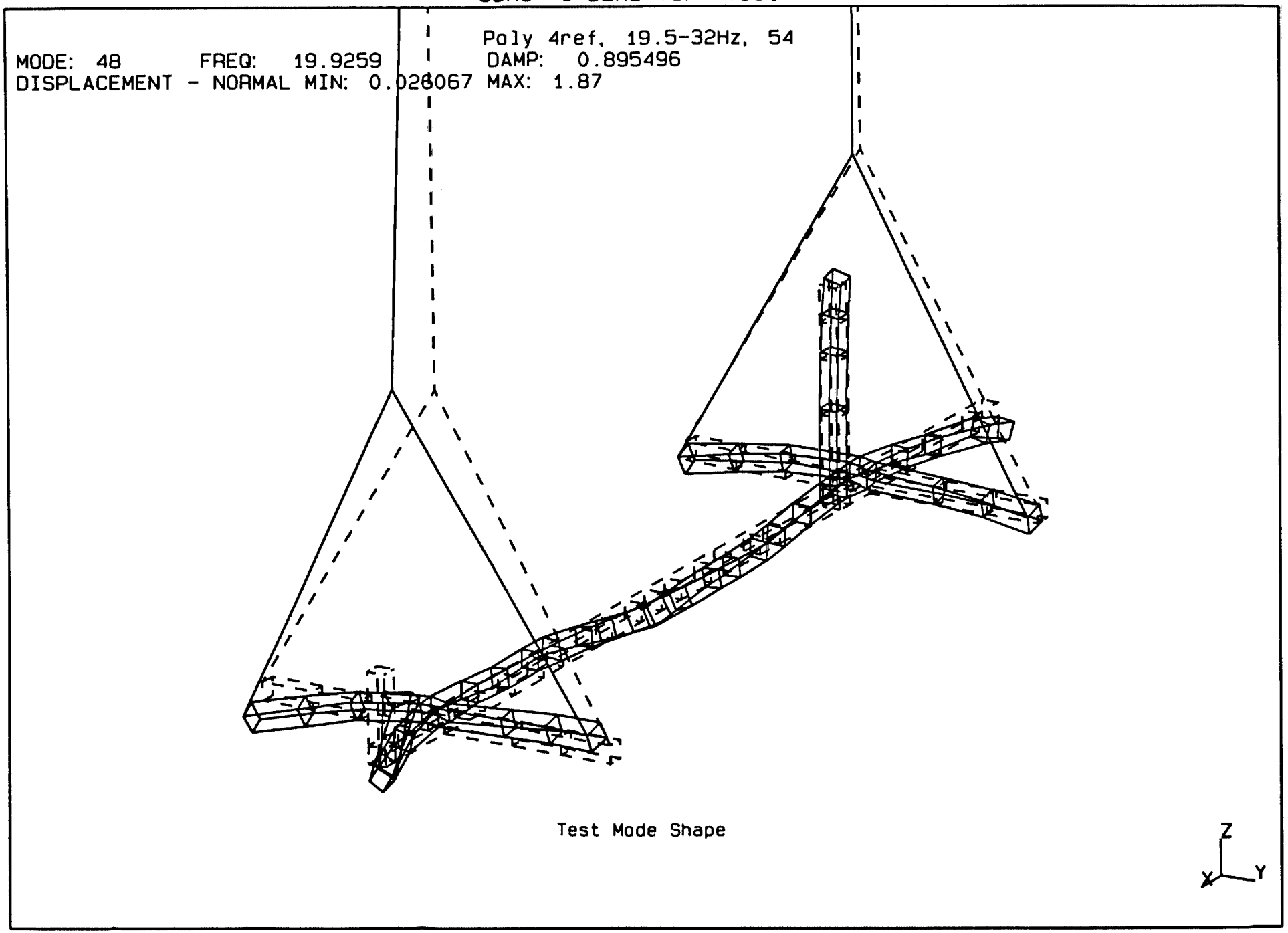

SDRC I-DEAS VI: Test

Poly 4ref, 19.5-32Hz, 54

MODE: 49 FREQ: 20.462500 DAMP: 0.562555

DISPLACEMENT - NORMAL MIN: 0.036271 MAX: 8.35

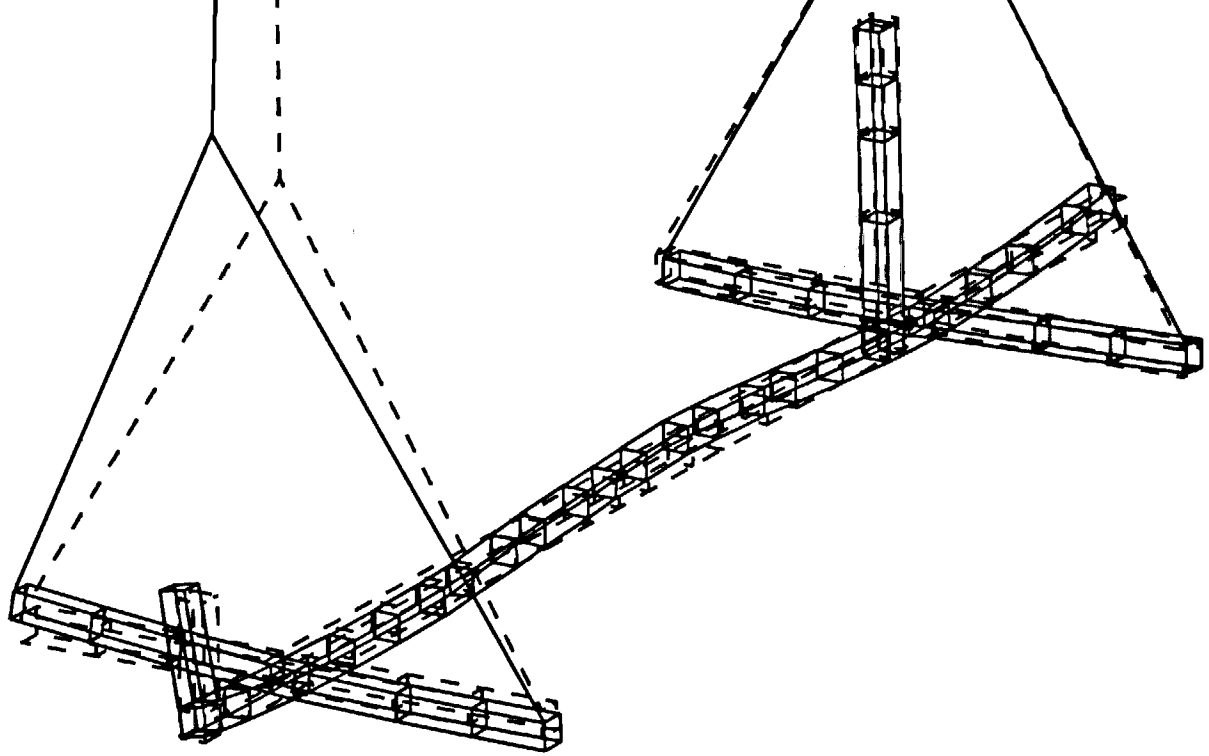

Test Mode Shape

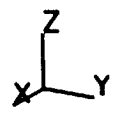

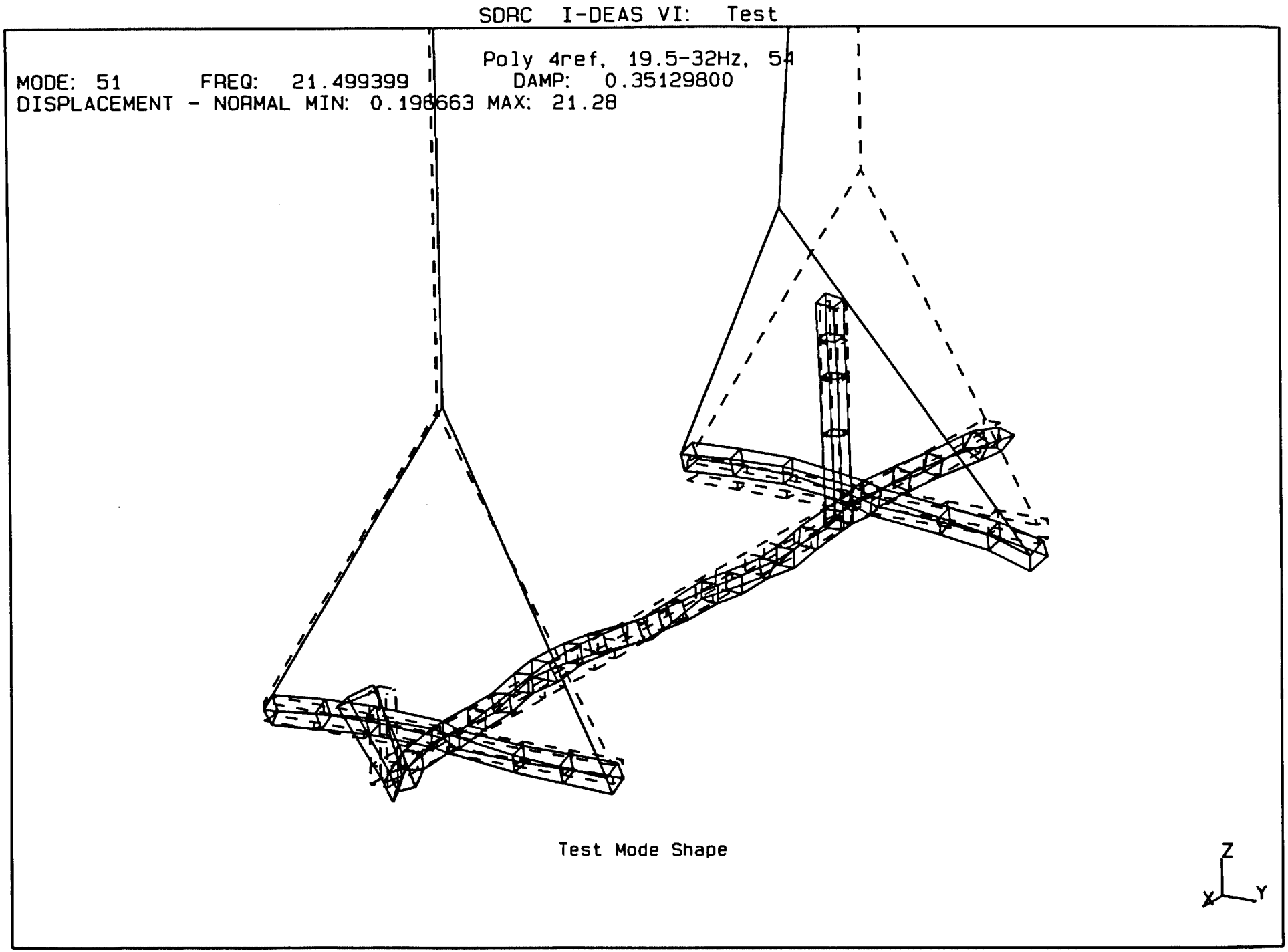
SDRC I-DEAS VI: Test
MODE: 51 FREQ: 21.499399
DISPLACEMENT - NORMAL MIN: 0.196663 MAX: 21.28
Poly 4ref, 19.5-32Hz, 54
DAMP: 0.35129800
Test Mode Shape
Z
X
Y

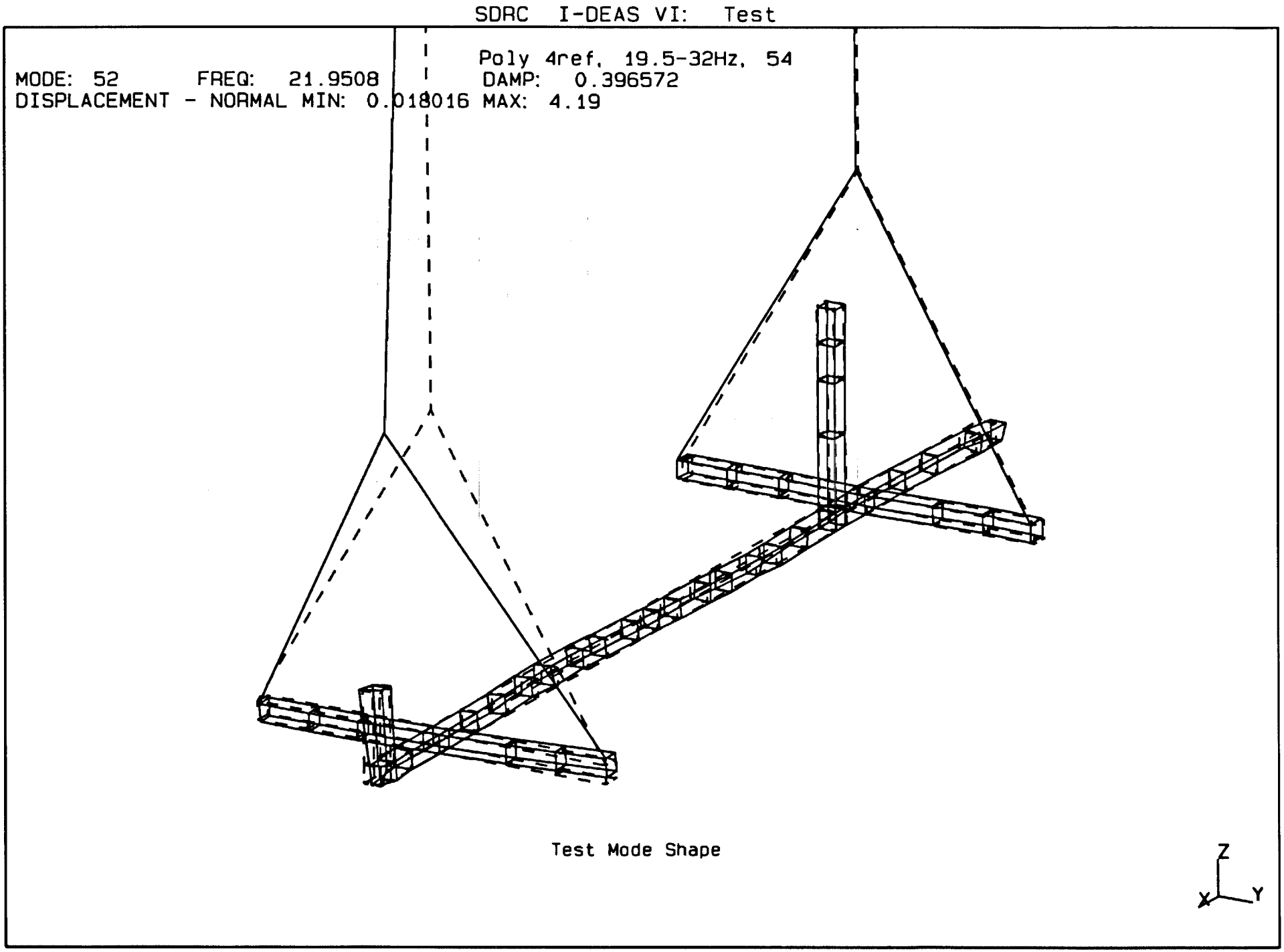
SDRC I-DEAS VI: Test
Poly 4ref, 19.5-32Hz, 54
MODE: 52 FREQ: 21.9508
DAMP: 0.396572
DISPLACEMENT - NORMAL MIN: 0.018016 MAX: 4.19
Test Mode Shape
Z
Y
X

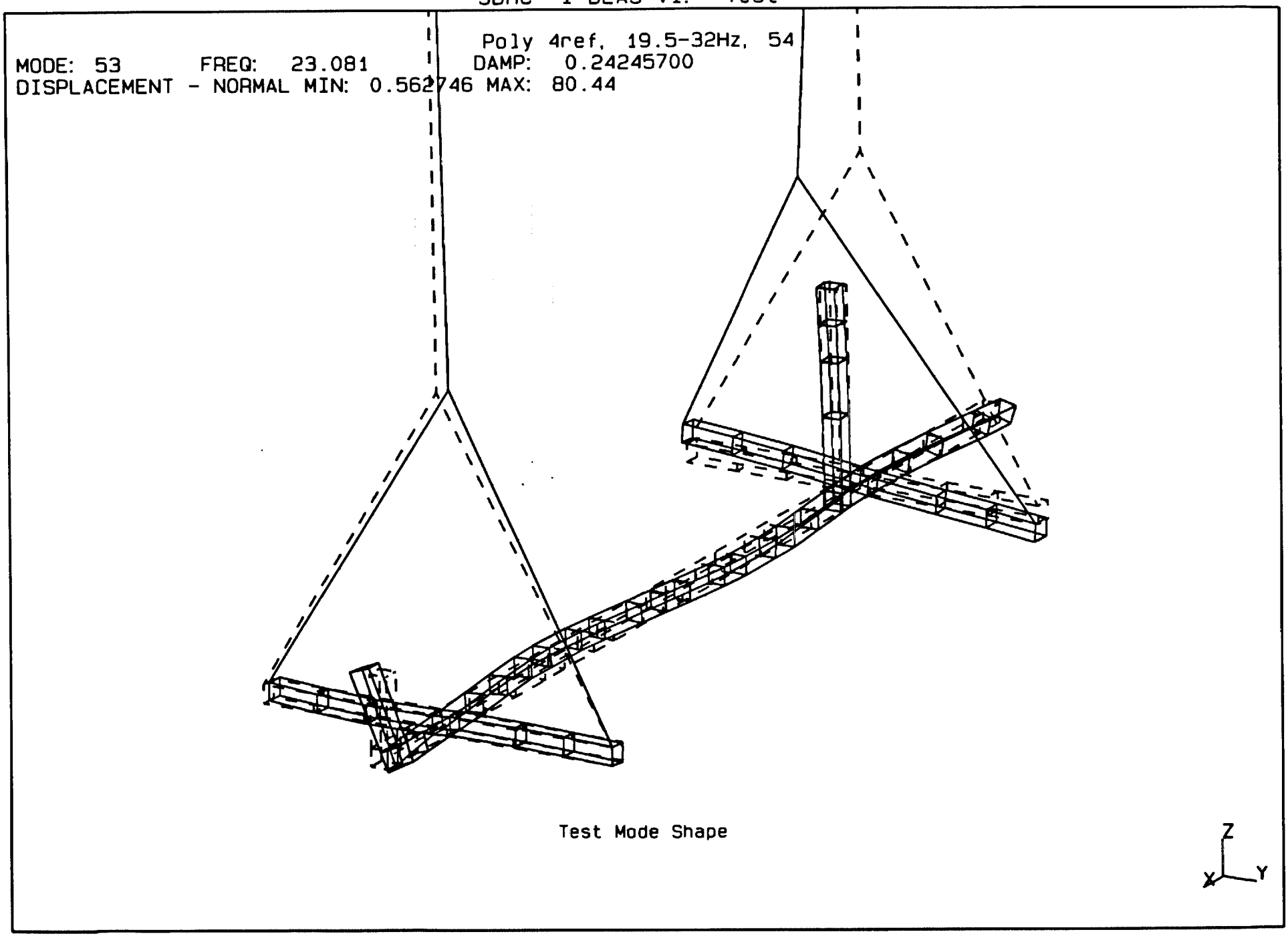
Poly 4ref, 19.5-32Hz, 54
MODE: 53 FREQ: 23.081
DAMP: 0.24245700
DISPLACEMENT - NORMAL MIN: 0.562746 MAX: 80.44
Test Mode Shape
Z
X
Y

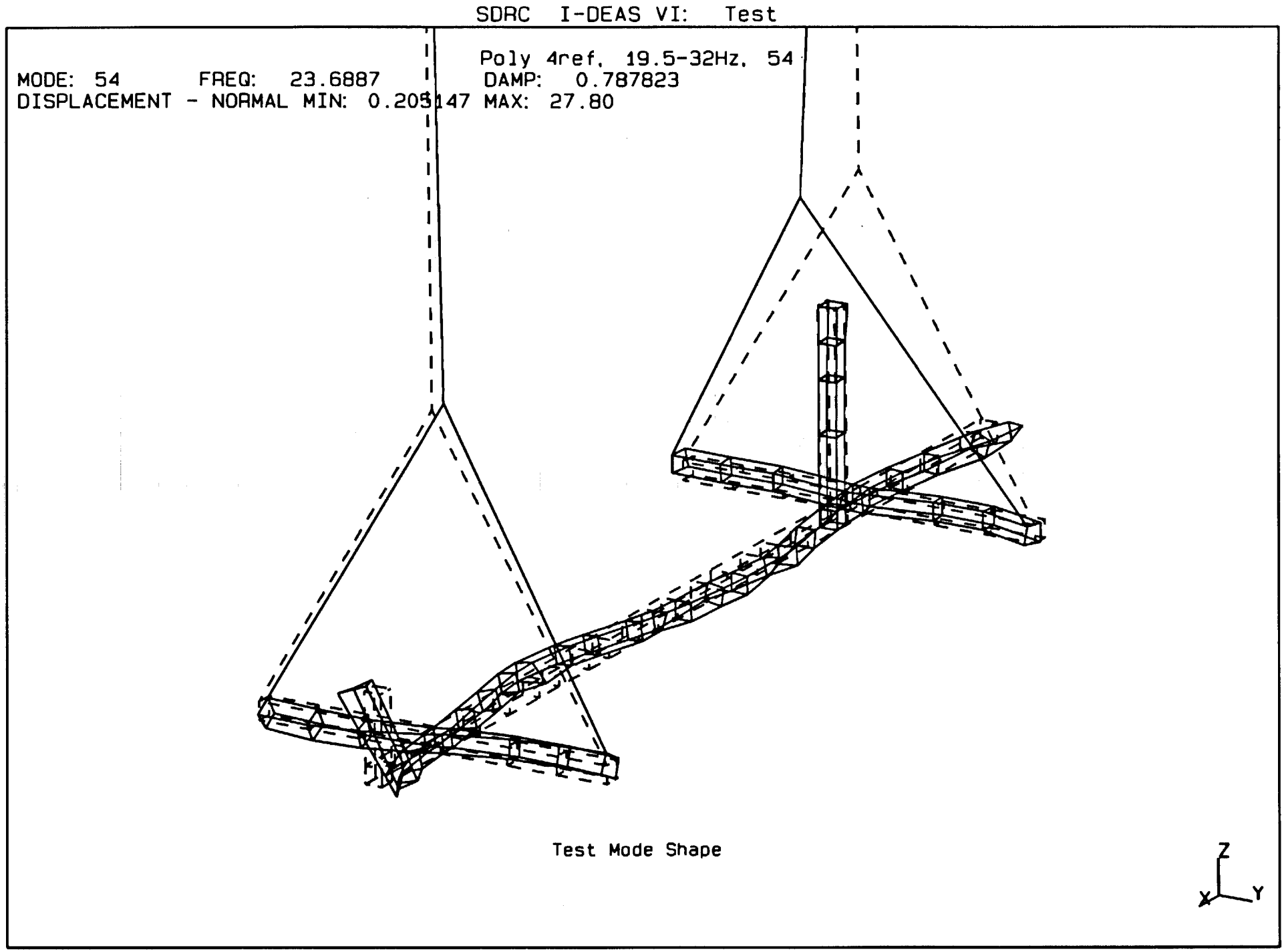
SDRC I-DEAS VI: Test
Poly 4ref, 19.5-32Hz, 54
MODE: 54 FREQ: 23.6887
DAMP: 0.787823
DISPLACEMENT - NORMAL MIN: 0.205147 MAX: 27.80
Test Mode Shape
Z
X
Y

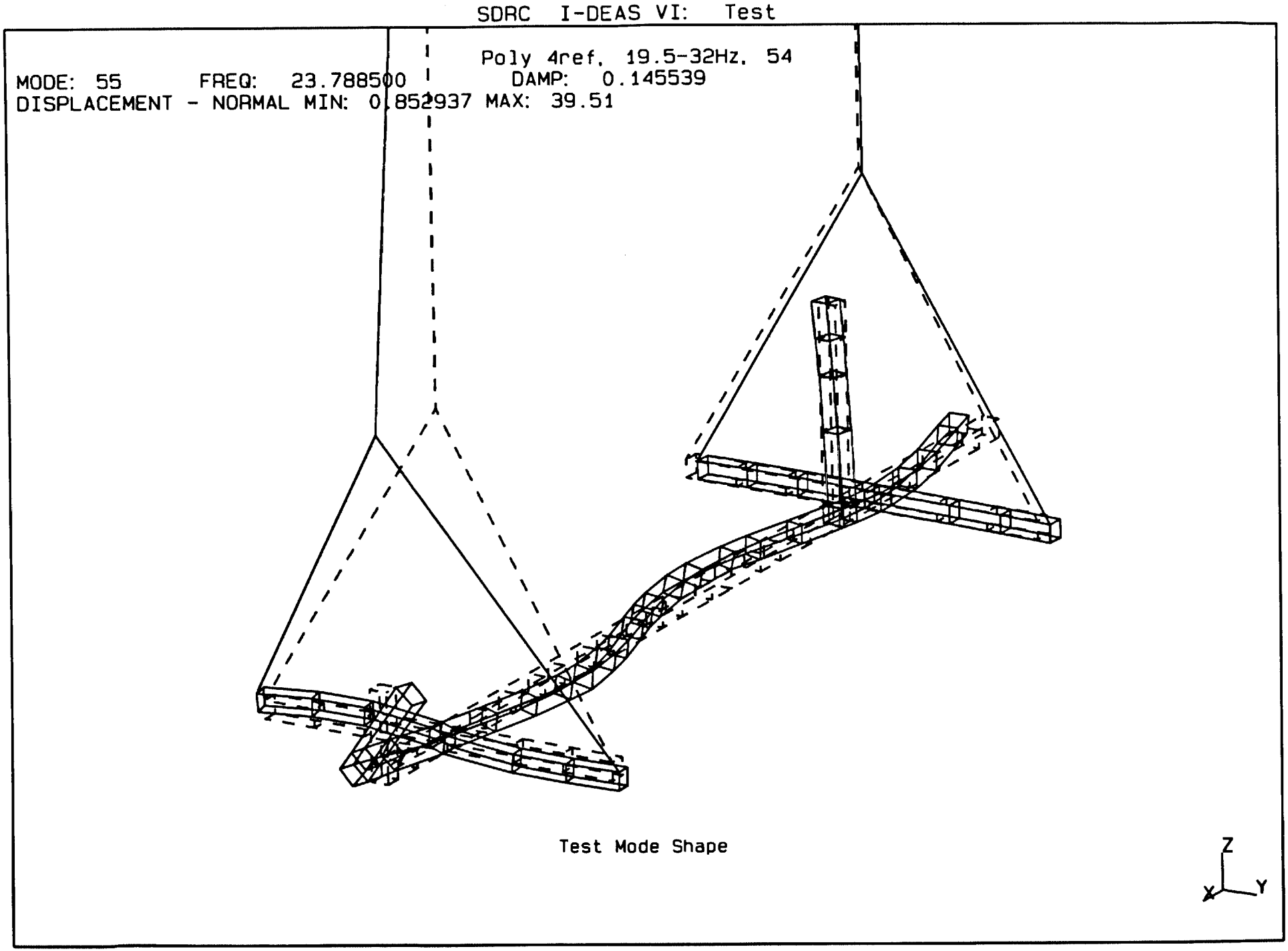
SDRC I-DEAS VI: Test
Poly 4ref, 19.5-32Hz, 54
MODE: 55 FREQ: 23.788500 DAMP: 0.145539
DISPLACEMENT - NORMAL MIN: 0.852937 MAX: 39.51
Test Mode Shape
Z
X
Y

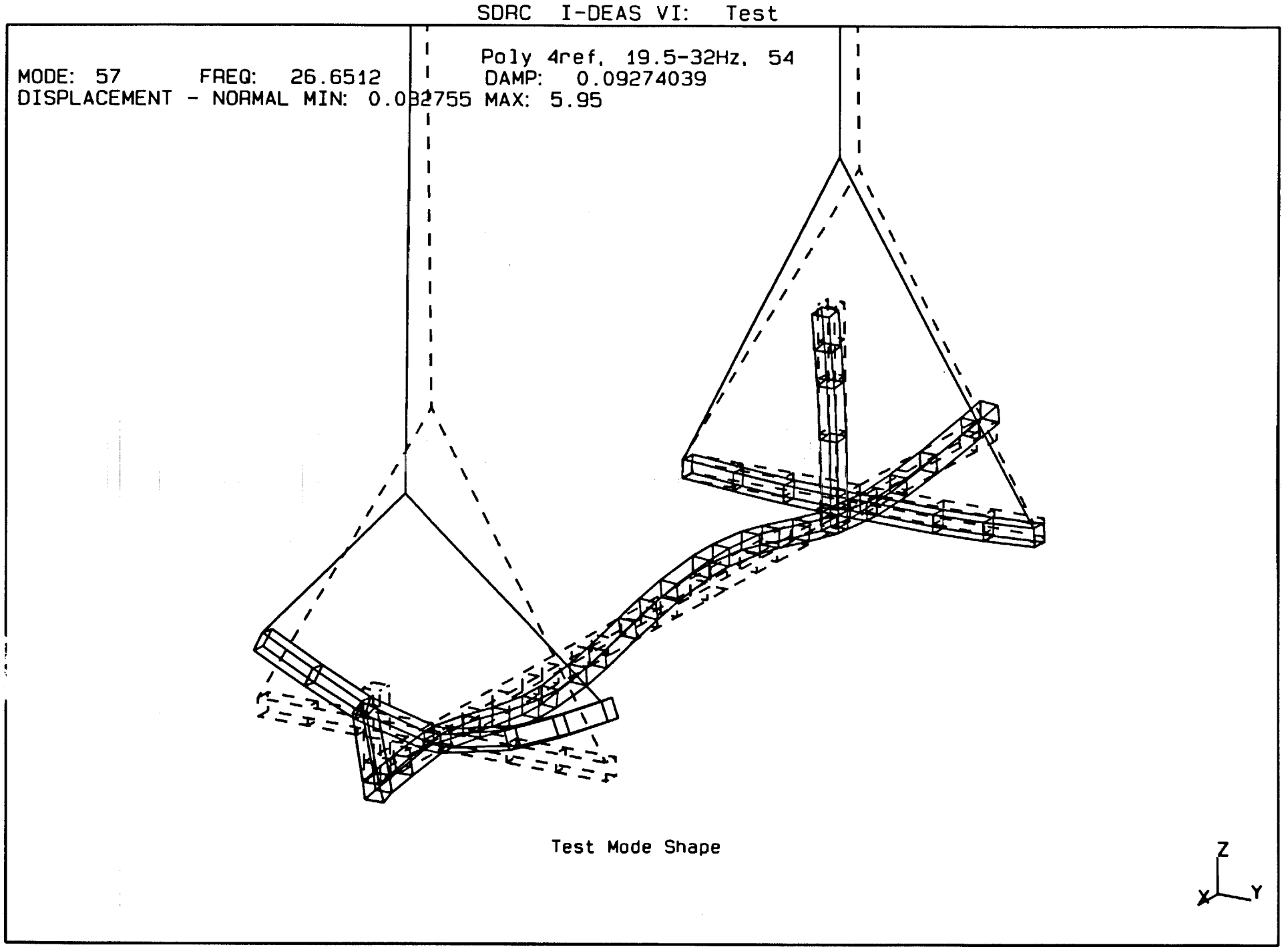
SDRC I-DEAS VI: Test
Poly 4ref, 19.5-32Hz, 54
MODE: 57 FREQ: 26.6512
DAMP: 0.09274039
DISPLACEMENT - NORMAL MIN: 0.032755 MAX: 5.95
Test Mode Shape
Z
X
Y

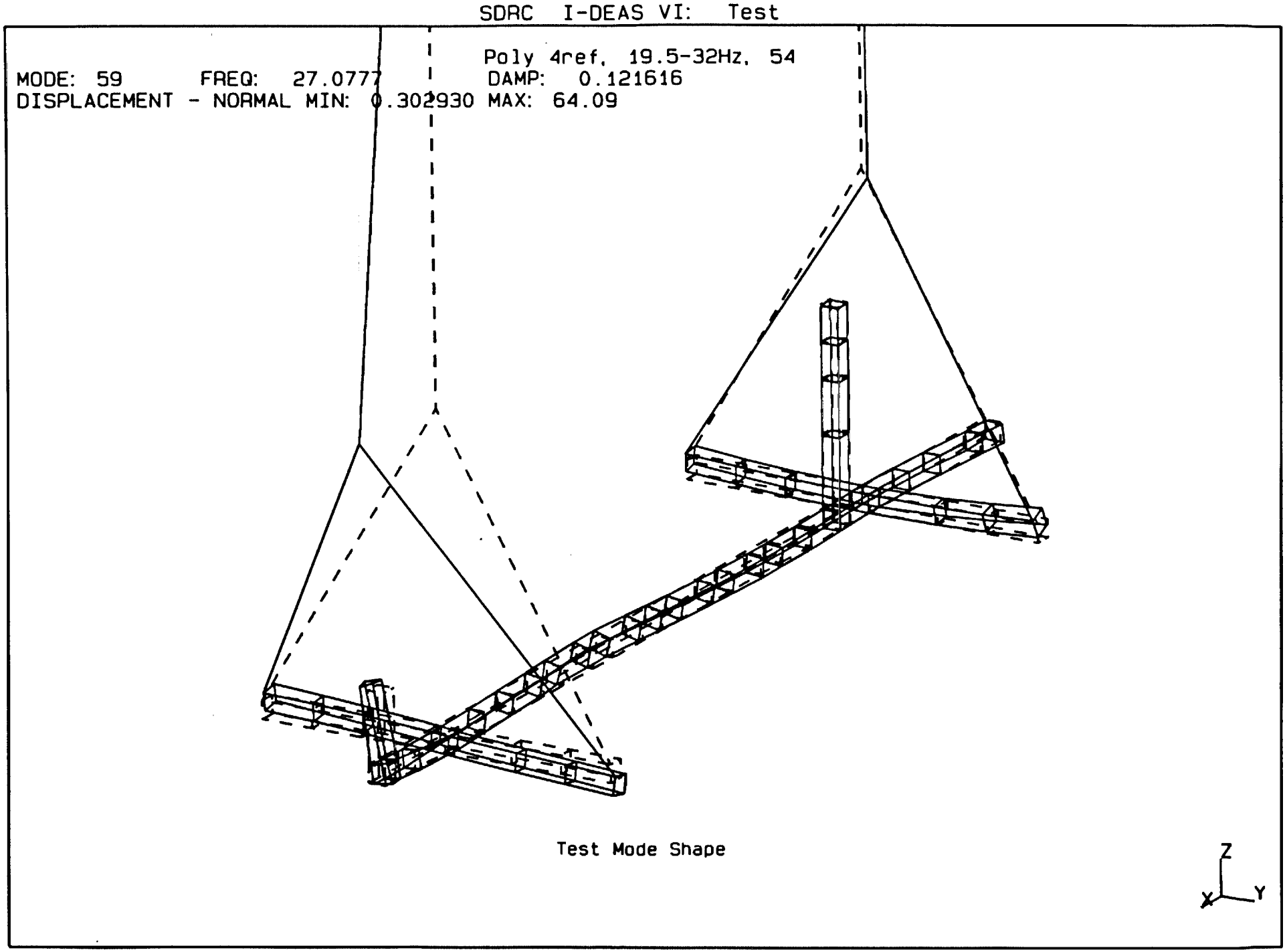
SDRC I-DEAS VI: Test
Poly 4ref, 19.5-32Hz, 54
MODE: 59 FREQ: 27.0777 DAMP: 0.121616
DISPLACEMENT - NORMAL MIN: 0.302930 MAX: 64.09
Test Mode Shape
Z
X
Y

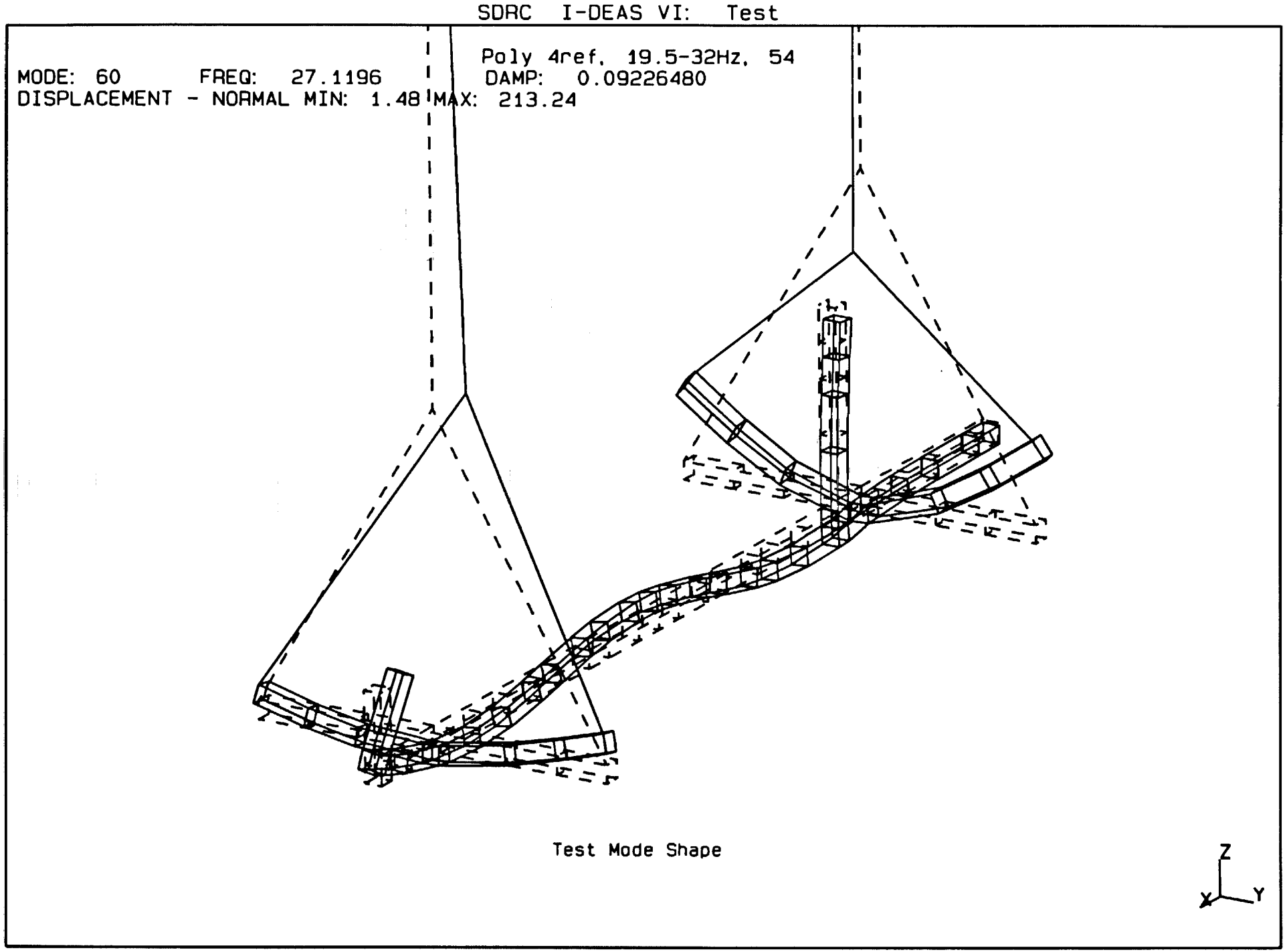
SDRC I-DEAS VI: Test
MODE: 60 FREQ: 27.1196
DISPLACEMENT - NORMAL MIN: 1.48
Poly 4ref, 19.5-32Hz, 54
DAMP: 0.09226480
MAX: 213.24
Test Mode Shape
Z
X
Y

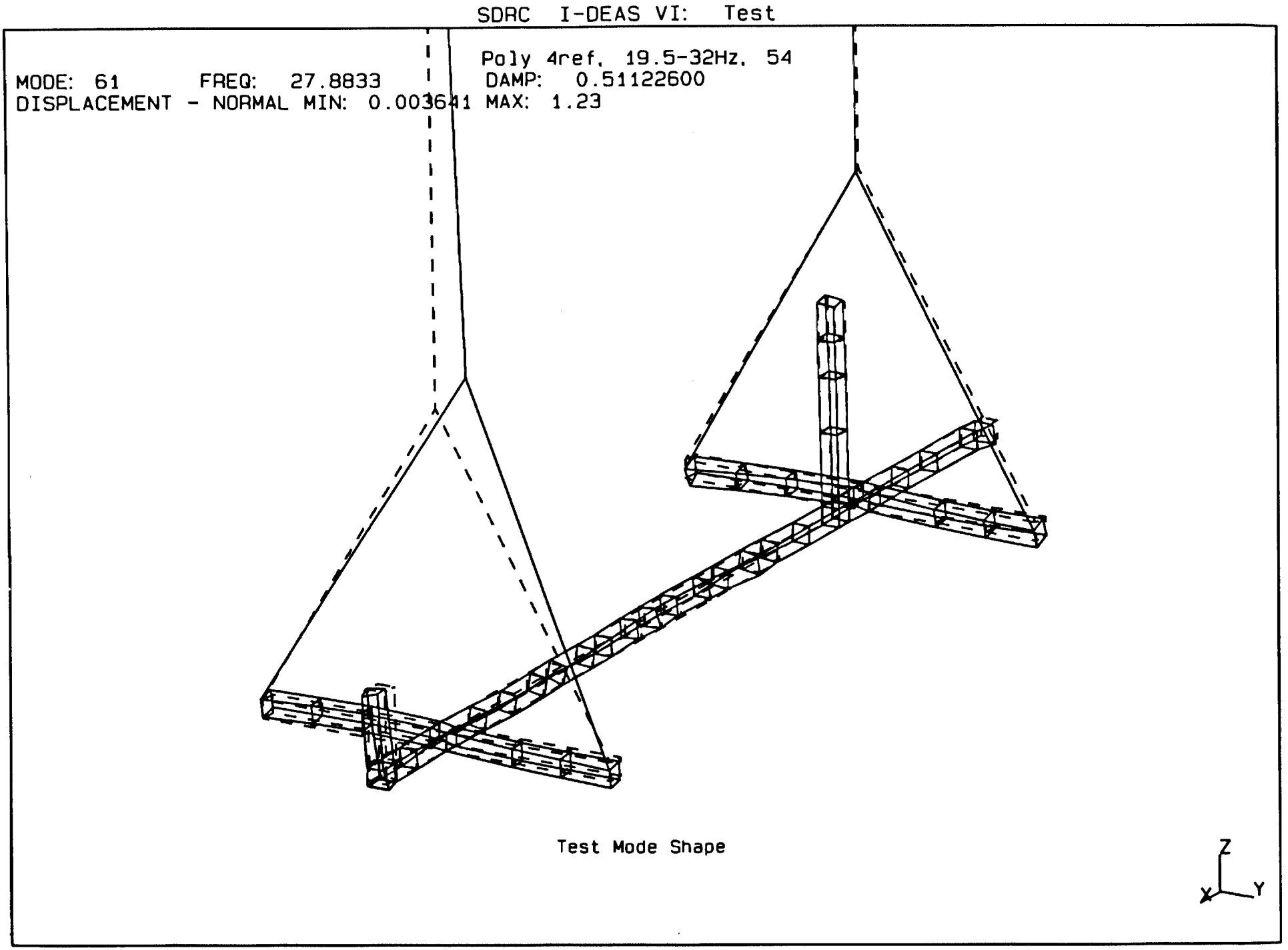
SDRC I-DEAS VI: Test
MODE: 61 FREQ: 27.8833
DISPLACEMENT - NORMAL MIN: 0.003641 MAX: 1.23
Poly 4ref, 19.5-32Hz, 54
DAMP: 0.51122600
Test Mode Shape
Z
X
Y

SDRC I-DEAS VI: Test

Poly 4ref, 19.5-32Hz, 54

MODE: 62 FREQ: 28.8925 DAMP: 0.160828

DISPLACEMENT - NORMAL MIN: 0.051192 MAX: 57.52

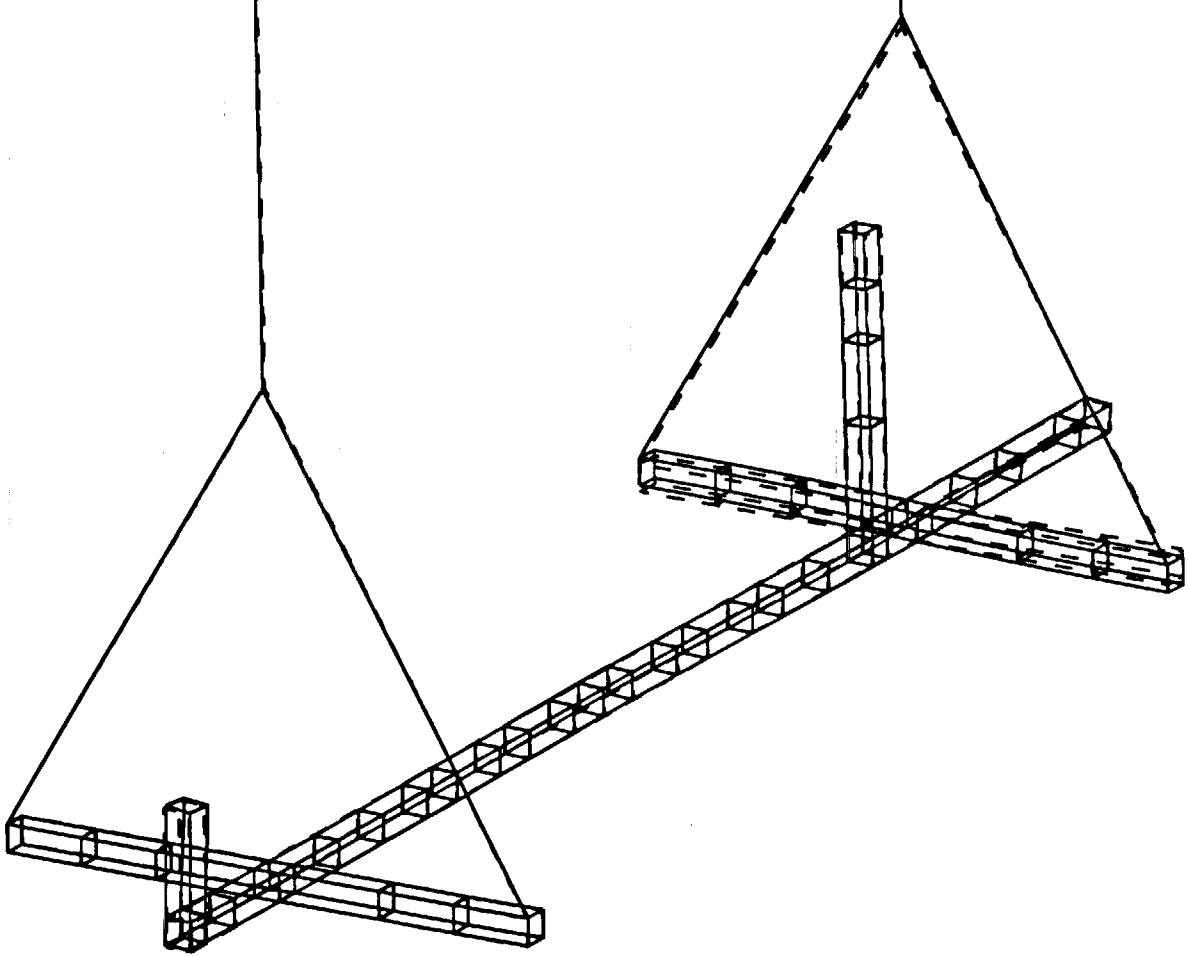

Test Mode Shape

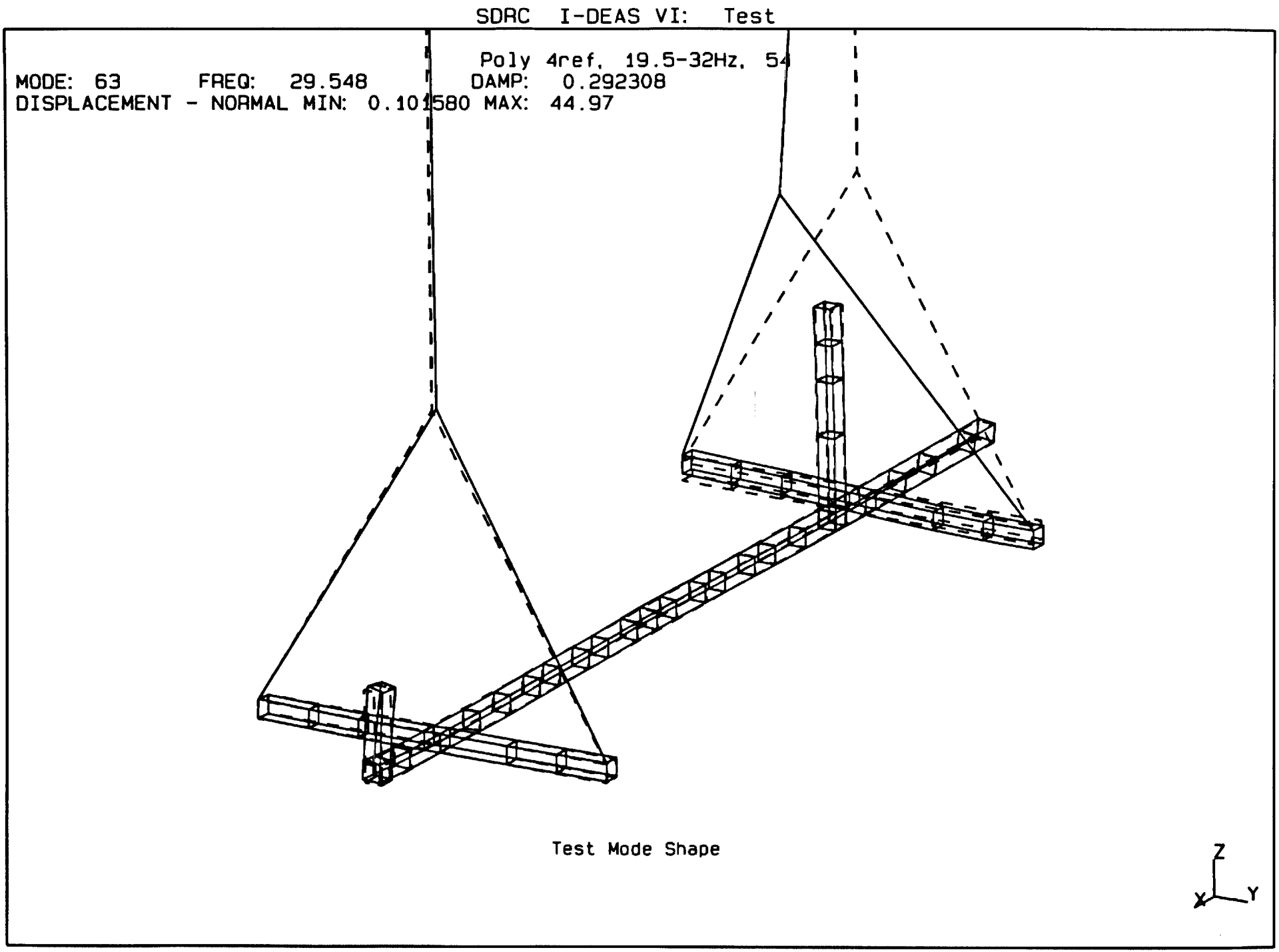
SDRC I-DEAS VI: Test
Poly 4ref, 19.5-32Hz, 54
MODE: 63 FREQ: 29.548
DAMP: 0.292308
DISPLACEMENT - NORMAL MIN: 0.101580 MAX: 44.97
Test Mode Shape
Z
X
Y

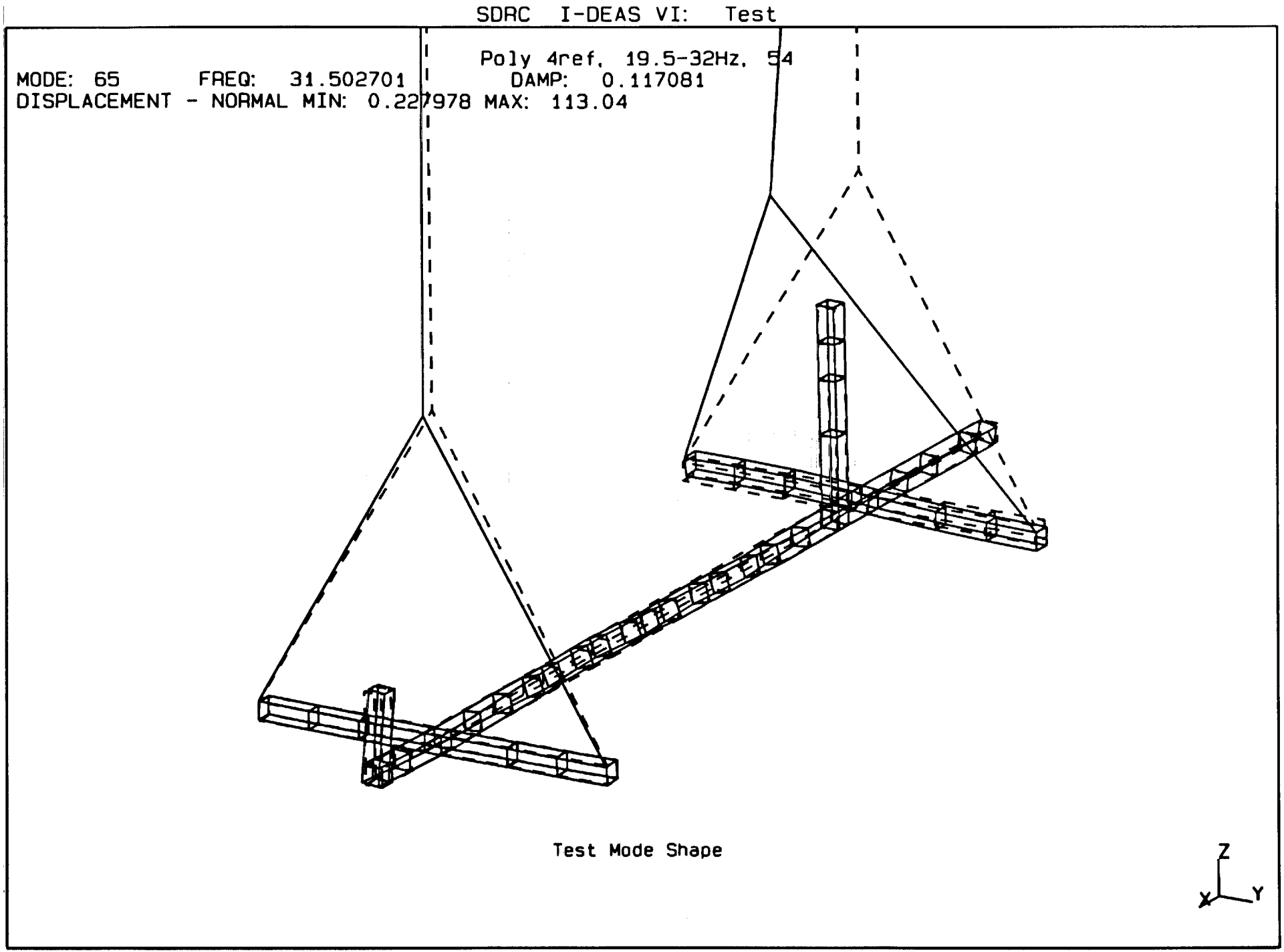
SDRC I-DEAS VI: Test
Poly 4ref, 19.5-32Hz, 54
MODE: 65 FREQ: 31.502701
DAMP: 0.117081
DISPLACEMENT - NORMAL MIN: 0.227978 MAX: 113.04
Test Mode Shape
Z
X
Y

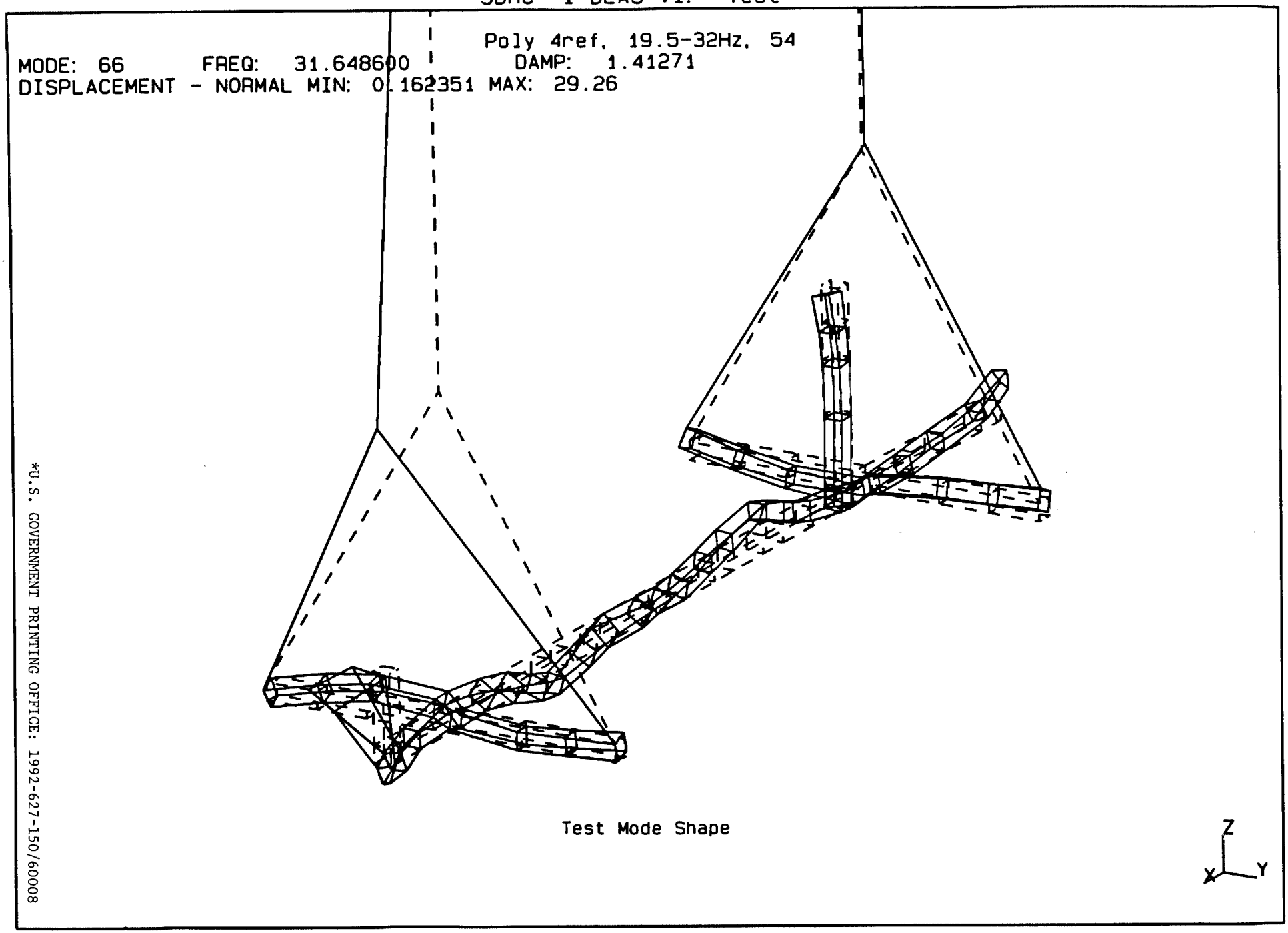

Test Mode Shape

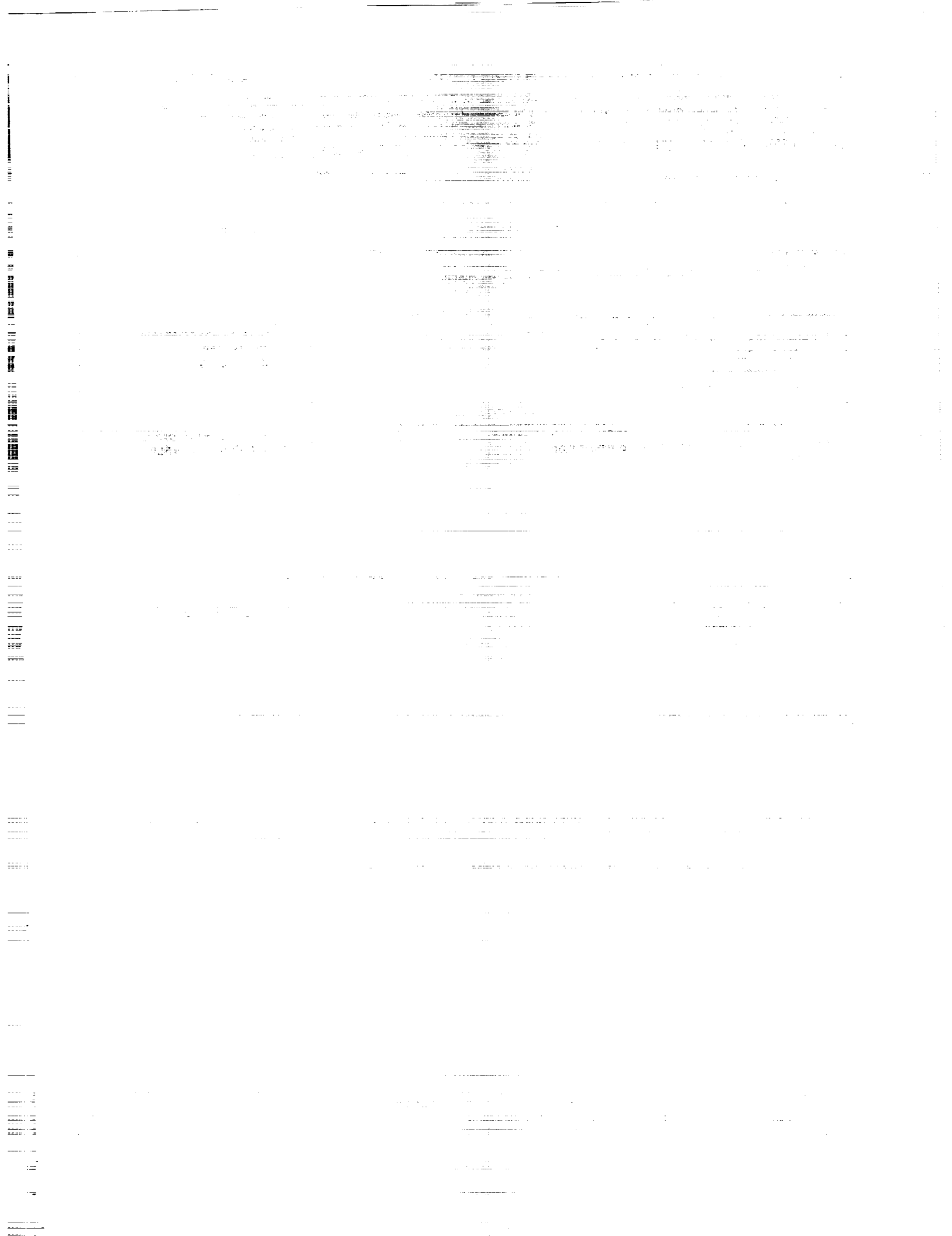

REPORT DOCUMENTATION PAGE

Form Approved
OMB No. 0704-0188

1. AGENCY USE ONLY (*Leave blank*)	2. REPORT DATE	3. REPORT TYPE AND DATES COVERED
	August 1992	Contractor Report

4. TITLE AND SUBTITLE
Design, Analysis, and Testing of the Phase 1 CSI Evolutionary Model Erectable Truss

5. FUNDING NUMBERS
NAS1-19241
WU 590-14-61-01

6. AUTHOR(S)
M. J. Gronet, D. A. Davis, D. H. Kintis, R. D. Brillhart, E. M. Atkins

7. PERFORMING ORGANIZATION NAME(S) AND ADDRESS(ES)
Lockheed Missiles and Space Company, Inc.
Org. 6N-12, Bldg. 579
1111 Lockheed Way
Sunnyvale, CA 94089-3504

8. PERFORMING ORGANIZATION REPORT NUMBER
LMSC/P024859

9. SPONSORING / MONITORING AGENCY NAME(S) AND ADDRESS(ES)
National Aeronautics and Space Administration
Langley Research Center
Hampton, VA 23665-5225

10. SPONSORING / MONITORING AGENCY REPORT NUMBER
NASA CR-4461

11. SUPPLEMENTARY NOTES
Langley Technical Monitor: Rudeen Smith-Taylor
Gronet, Davis, and Kintis: Lockheed Missiles & Space Company, Inc., Sunnyvale, California
Brillhart and Atkins: Structural Dynamics Research Corporation, San Diego, California

12a. DISTRIBUTION / AVAILABILITY STATEMENT
Unclassified - Unlimited
Subject Category 18

12b. DISTRIBUTION CODE

13. ABSTRACT (*Maximum 200 words*)

This report addresses the design, analysis, and testing of the erectable truss structure for the Phase 1 CSI Evolutionary Model (CEM) testbed. The Phase 1 CEM testbed is the second of a series of CEM testbeds that form part of an ongoing program of focused research at NASA/LaRC in the development of Controls-Structures Integration (CSI) technology. The Phase 1 CEM contains the same overall geometry, weight, and sensor locations as the Phase 0 CEM, but is based on an integrated controller and structure design, whereby both structure and controller design variables are sized simultaneously. The Phase 1 CEM design features seven truss sections composed of struts with tailored mass and stiffness properties. A common erectable joint is used and the strut stiffness is tailored by varying the cross-sectional area. To characterize the structure, static tests were conducted on individual struts and 10-bay truss assemblies. Dynamic tests were conducted on 10-bay truss assemblies as well as the fully-assembled CEM truss. The results indicate that the static and dynamic properties of the structure are predictable, well-characterized, and within the performance requirements established during the Phase 1 CEM integrated controller/structure design analysis.

14. SUBJECT TERMS	15. NUMBER OF PAGES
CSI, Erectable Truss, Truss Joint	380
	16. PRICE CODE: A17

17. SECURITY CLASSIFICATION OF REPORT	18. SECURITY CLASSIFICATION OF THIS PAGE	19. SECURITY CLASSIFICATION OF ABSTRACT	20. LIMITATION OF ABSTRACT
Unclassified	Unclassified		